Fossoriality in Snakes:
Perspectives from Morphology and the Fossil Record

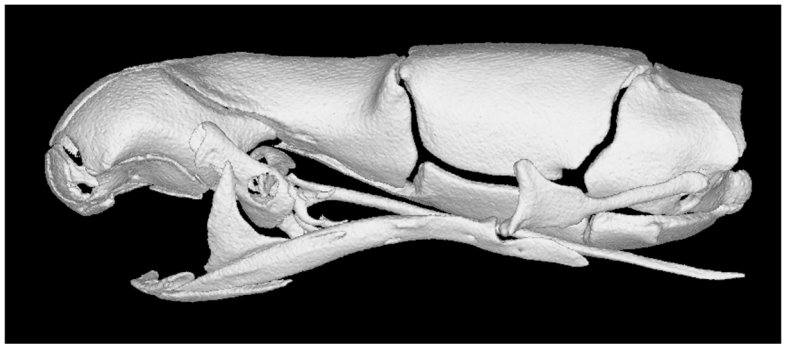

Indotyphlops braminus, skull left lateral

Alexandra Florence Clara Howard

Trinity Hall, Cambridge

Submission Date: 06/2022

This thesis is submitted for the degree of Doctor of Philosophy

Declaration:

- This thesis is the result of my own work and includes nothing which is the outcome of work done in collaboration except as declared in the preface and specified in the text.

- It is not substantially the same as any work that has already been submitted before for any degree or other qualification except as declared in the preface and specified in the text.

- It does not exceed the prescribed word limit (60,000) for the Biology Degree Committee

Word Count: 50,637

Fossoriality in Snakes: Perspectives from Morphology and the Fossil Record

Alexandra Howard

Snakes are a speciose clade of squamates that have diversified into almost all habitats, all with the same elongate limbless body plan. This thesis aims to improve scientific understanding of snake evolution by focusing on novel perspectives using both extant snakes and the fossil record.

1. Alternate phylogenetic positions of fossils affects body size estimates in snakes

Body size is a readily available metric for both extant and extinct snakes. The competing hypothesis of ecological snake origins also predict different outcomes for the evolution of body size in snakes. I used a combination of ancestral state reconstructions, body size estimates of fossils from regression models, and evolutionary rate modelling to examine the evolution of body size in snakes, with a particular focus on early snake evolution. This project showed that snakes achieve a wide range of diversity of body size during the Cretaceous, trends that are not observed when using data from extant taxa.

2. Cranial osteology of Typhlopidae (Serpentes: Scolecophidia)

Scolecophidia are a distinctive group of snakes that occupy the basal most diverging branches of the snake phylogeny. However, due to the small overall size of many taxa, they have been relatively understudied in regards to comparative anatomy. In this project I examined segmented CT scans of 10 different species of Typhlopoidea, the largest clade of Scolecophidia. Using these comparisons I identified variability in several morphological characters not previously thought to be variable in Scolecophidia, as well as the identification of features in large typhlopids such as the lateral wings of the basisphenoid, which were previously thought to be limited only to Alethinophidia.

3. Morphometrics provide evidence for the fossorial origin of snakes

The problem of homoplasy, particularly in relation to adaptation to fossoriality, is potentially responsible for the incongruences between phylogenetic hypothesis of snakes that use either morphological or molecular data. In this project I used CT scans of 73 species of alethinophidian snake and geometric morphometrics to examine morphological correlates to fossoriality. I found that there is a clear morphological signal between the parietal of alethinophidian snakes and ecology. In general, the parietal of fossorial snakes is more elongate with a deep u or v shaped fronto-parietal suture, with an elongated posterior shelf that overlaps the braincase. These projects show how integrative research using both extant and palaeontological data can inform questions about the early evolution of clades, particularly the heavily debated ecological origin of snakes.

Acknowledgements

I would like to thank the Trinity Hall Graduate Studentship for providing the main source of funding for these projects, including academic fees, living expenses, and research costs. In addition, I would also like to thank the Isaac Newton Trust for equipment costs, and the Gans Fund and Society of Vertebrate Paleontology Travel Award for conference travel to present work to my peers.

I am incredibly lucky to have been based at the University Museum of Zoology Cambridge, which granted me access to many of the specimens included in this thesis. In particular I would like to thank: Matt Lowe and Natalie Jones for specimen access. I would also like to thank Keturah Smithson from the Cambridge Biotomography Centre for much of the CT scans contained in this thesis.

I am particularly indebted to all the fellow herpetologists and museum workers who uploaded data to MorphoSource.org, an invaluable resource without which my data collection would have been significantly harder. I would also like to thank Dr Emily Mitchell for her advice and kindness on my academic journey.

No postgraduate exists alone, and so I would like to thank all the other members of the Head Lab, both past and present, who have been with me along this journey, including Dr Kate Criswell, Ben Igielman, and Tom Jameson. Thanks to Abba Parker, for your much needed calm approach. Thanks to Lucy Roberts, you continue to inspire me every day as a fellow scientist and I look forward to our future adventures together. And thanks to all the other members of the museum Creche that have supported me on this journey, including but not limited to: Ellie Bladon, Kate Howlett, Matt Hayes, Michael Pashkevich, Sara Steele.

Of course thanks go to my scaly inspirations, Alfie and Ada, who will never be able to read this but I love them anyway. Thanks to my dad, who has never failed to tell me how proud he is of me. Thanks to my mum for your unending support and kind words, a shoulder to cry on both figuratively and literally. I couldn't have done this without you.

Finally, thanks of course to my supervisor Jason for your continual support. You've taught me how to be a good scientist and not to give up when the going gets tough. Thanks for believing in me and allowing me to learn more about snakes, the most efficient of all animals.

Table Of Contents:

Chapter 1.	Introduction to snake palaeontology	1-25
Chapter 2.	Alternate phylogenetic positions of fossils affects body size estimates in snakes	26-59
	Appendix 1.	59-65
	Appendix 2.	66-74
	Appendix 3.	75-89
Chapter 3.	Cranial osteology of Typhlopidae, with comments on the unique anatomy of the parthenogenic blindsnake, *Indotyphlops braminus*	90-191
Chapter 4.	Morphometric tests of hypotheses of homoplasy provide evidence for the fossorial origin of snakes	192-232
	Appendix 1.	233-238
	Appendix 2.	239-244
	Appendix 3.	245-246
	Appendix 4.	247-248
	Appendix 5.	249-250
	Appendix 6.	251-252
	Appendix 7.	253-327
Chapter 5.	Conclusion: The implications of fossoriality to early snake evolution	328-335

Chapter 1: Introduction to Snake Palaeontology

Abstract

Snakes are a clade of elongate limbless squamates that exhibit a wide range of ecological and dietary specialisations, and occupy an almost global, non-polar distribution. Studies aimed at deciphering early snake evolution, particularly those focussed on the origin of the snake total clade, have been primarily concerned with that of the ancestral ecology which may have facilitated the evolution of the distinctive elongate limbless body plan typical of snakes. Falling into two main hypotheses, fossorial or aquatic, evidence for either ecology has primarily relied on potential evolutionary trajectories of distinctive snake features, such as eye or skull anatomy, and the interpretations of Cretaceous snake fossils that possess both plesiomorphic and derived snake features, confusing their relationships with extant snake clades. The lack of congruence between phylogenetic hypotheses of relatedness for snakes based either on morphological or molecular data also highlights the importance of understanding the potential for homoplasy in certain anatomical characters. This is particularly important in regards to understanding the placement of the aforementioned Cretaceous snakes, and in both understanding the placement of snakes within squamates and in understanding the relationships of extant snake clades to one another. Finally, the development of new analytical techniques has allowed studies into shape change that are quantifiable, and can be used to help predict morphology, and therefore ecology, of fossil snakes. These studies can provide new evidence for the ancestral ecology of snakes, and help in our understanding of early snake evolution.

1. The Origins Debate

Snakes are a speciose clade of squamates that have a non-polar global distribution, and have diversified into almost all known ecologies. Extant snakes number over 3,400 species, and belong to two primary subclades: Scolecophidia and Alethinophidia (Head *et al.* 2020b, 2020a; Uetz *et al.* 2019). For clarity of terms within this thesis, the term Serpentes will be used to refer to the crown group, and Pan-Serpentes to refer to the total-clade. Unless otherwise specified, I use "snake" to refer informally to Serpentes. The term "ancestral snake" refers to the most recent common ancestor of Pan-Serpentes, and "stem snakes" refers to all taxa that are more closely related to crown clade (Serpentes) than the nearest extant sister clades of Iguania, Anguimorpha, or (Iguania + Anguimorpha) (Head 2015). Likewise, I use "Scolecophidia" and scolecophidian to refer to all non-alethinophidian snakes, irrespective of whether this is monophyletic or paraphyletic (see Figure 1). Macrostomata, a clade which is only recovered using morphological data, consists of the following extant clades: Bolyeridae, Boidae, Pythonidae, Tropidophiidae, Xenodermatidae, Acrochordidae, and Colubroidea.

While the relationships of Pan-Serpentes to related squamate clades is still under debate (see section 2), snakes are well-resolved as monophyletic in morphological and molecular analysis, which is supported by numerous morphological characters including but not limited

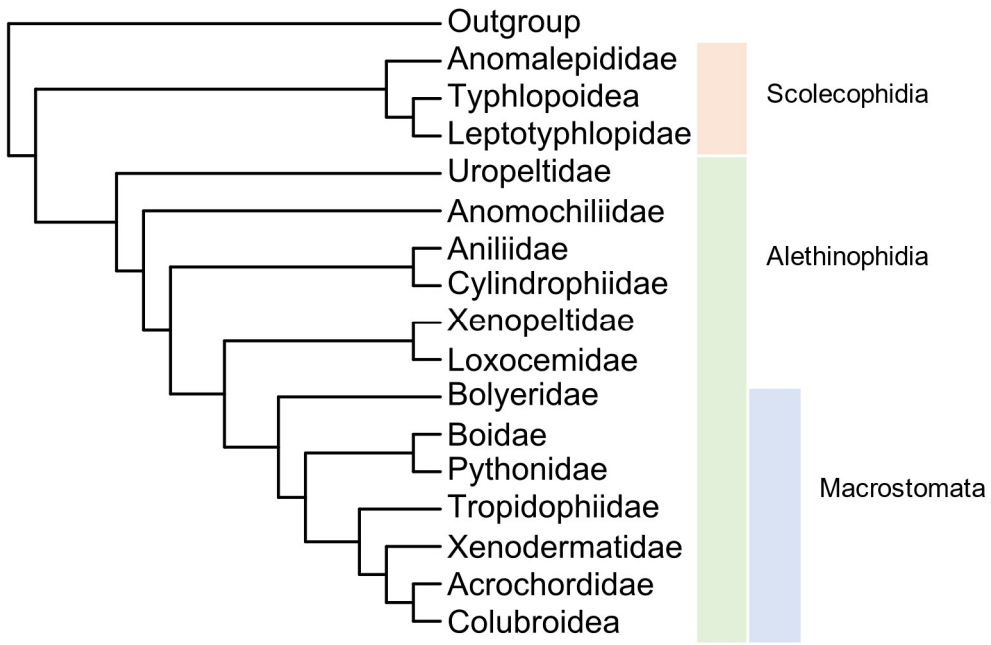

Figure 1. Maximum parsimony Serpentes tree constructed with 610 morphological characters, modified from squamate tree in Gauthier et al. (2012). Major clades of Scolecophidia, Alethinophidia, and Macrostomata are indicated.

to: a platytrabic braincase, anterolateral margin of frontal subolfactory process including the prefrontal process that extends into the socket of the prefrontal, and vertebrae with well-developed zygosphenes (see Head et al, 2020b for full review and other historical perspectives).

Early systematic work that considered the potential ecological origin of snakes by comparing snakes with other squamates first suggested that snakes arose from grass-swimming anguimorph lizards, of which they share an overall similarity in body form that is both elongate and limb-reduced (Camp 1923). More recently, the majority of the debate on the origin of snakes has largely been between two proposed ancestral ecologies for Pan-Serpentes: fossorial (or semi-fossorial/terrestrial) or aquatic. Both of these ecologies are proposed to have facilitated the evolution of the snake-like elongate limbless body form as animals switch from locomotion that uses the limbs for propulsion to locomotion primarily through lateral undulations of the body.

1.1 Evidence from the morphology of extant snakes

The general body plan of snakes comprises of a suite of characters that appear to correlate with fossoriality in squamates. These include the loss of limbs, the loss of an external ear, and the overall elongation of the body (Gans 1975; Rieppel 1988). Limb loss and reduction have evolved repeatedly across squamates, at least 62 times across 53 lineages (Greer 1991; Lee 1998). Almost all limbless squamates, excluding snakes, are fossorial, burrowing in a diverse number of substrates from loose sand as seen in pygopodids and scincids to hard soil that requires more significant tunnelling behaviour as seen in amphisbaenians (Gans 1975). Limbless squamates that do not exhibit fossoriality are limited to “grass-swimming”, characterised by a long tail and relatively short trunk as exemplified in the anguid genera *Anguis* and *Ophisaurus* (Brandley *et al.* 2008; Camaiti *et al.* 2021; Wiens *et al.* 2006). However, no other squamate clade has achieved the diversity of ecologies seen in extant snakes, making the interpretation of the ecology of the ancestral snake difficult to decipher.

Extant snakes exhibit several anatomical features that have been proposed to support a fossorial origin. Early work examining the eye of extant snakes, particularly the absence of oil droplets and the replacement of eyelids with ocular scales, pointed towards an interpretation that the snake eye has undergone degeneration and subsequent re-evolution (Walls 1940). Degeneration of the eye implies adaptation to a low light environment, the most common ecologies of which are nocturnality or fossoriality. In particular, the reduction of the visual system is common in fossorial squamates such as amphisbaenians (Gans 1975). Additionally, the snake ‘spectacle’, or ocular scale, is a clear scale that completely covers the eye to provide

protection from abrasion in the external environment, and acts as a replacement for the eyelids seen in most other squamates. The evolution of this specialised anatomical feature was originally proposed to have required an adaptation to fossoriality (Walls 1940). However, the validity of this interpretation is called into question by highly fossorial extant taxa, including *Anilius,* scolecophidians, and some uropeltids, lacking spectacles; instead the eyes lie beneath the head scales (Gower *et al.* 2022). Nevertheless, a simple transition to nocturnality would not require such a dramatic anatomical shift of lizard eyelid to snake spectacle; the external environment contacting the eye would be similar for both diurnal and nocturnal terrestrial snakes. In contrast, a limbless animal adapting to fossorial habits would encounter more abrasion than a terrestrial one, a scenario where a protective ocular scale would be adaptive. Both of these interpretations of eye anatomy suggest fossoriality in the snake ancestor. Another anatomical feature of the snake eye that supports a hypothesis of a fossorial ancestral ecology is the absence of sclerotic rings, which are also lost in both Dibamidae and Amphisbaenia, both fossorial squamate clades (Atkins & Franz-Odendaal 2016).

However, an obligately fossorial ancestor is not supported by all aspects of eye anatomy. Terrestrial snakes only show the loss of two ancestral visual pigments, with further loss only in taxa that exhibit "dedicated fossoriality" such as scolecophidians and the pipe snake *Anilius scytale* (Simões *et al.* 2015). This supports the hypothesis that snakes never went through a stage of total lost vision, instead a reduction of vision due to adaptation to a low-light environment. This could be suggestive of a semi-fossorial ecology within Pan-Serpentes, one that still relies on visual stimulus and therefore would not support the full loss of visual pigments but would also benefit from the extra protection from abrasion afforded by a clear ocular scale. The hypothesis of further reduction in fully fossorial taxa is supported by the loss of genes associated with alethinophidian photopic phototransduction in the scolecophidians *Anilios bicolor* and *Anilios bituberculatus* (Gower *et al.* 2021).

In contrast to this support for the fossorial origin hypothesis, the eye anatomy of extant snakes has also been suggested to support an aquatic origin for Pan-Serpentes, particularly due to the shared characters of a flattened cornea, thickened corneal margin, and a spherical lens, all of which are characters that extant snakes share with exclusively aquatic or amphibious taxa (Caprette *et al.* 2004). However, this morphology does not exclude the possibility of a fossorial origin, as thick spectacles are present in both fossorial and aquatic extant taxa due to the protection afforded by these structures in potentially abrasive environments (Caprette *et al.* 2004; Da Silva *et al.* 2017).

The anatomy of the snake ear has also been suggested to support the hypothesis of a fossorial origin for Pan-Serpentes. The reduction of the tympanic membrane and tympanic cavity is prevalent across many fossorial squamate clades (Berman & Regal 1967; Rieppel

1988). Snakes have lost both an outer ear and the tympanic middle ear that provides impedance matching hearing in most tetrapods, greatly reducing the frequencies that the snake ear can receive, with hearing in snakes focussed on vibrations transmitted through the substrate rather than airborne sound (Christensen *et al.* 2012). Due to the loss of both the outer and middle ear, the only hearing and balance organ in snakes is the inner ear, although the stapes is retained and transmits vibrations from the environment through an association with the quadrate bone (Yi 2022). Morphology of the inner ear has been found to correlate with ecology in squamates, particularly in distinguishing fossorial species from non-fossorial. Fossorial squamates in general all share a large spherical vestibule and thin semi-circular canals of the inner ear, as opposed to the smaller vestibule and thicker semi-circular canals present in both generalist and aquatic taxa (Yi & Norell 2015). Palci et al (2017) refuted this finding, concluding that a large spherical vestibule (they term 'sacculus') is also observed in semi-aquatic homalopsids *Myron richardsoni* and *Enhydris greyi,* although they did also find a large spherical vestibule in all fossorial taxa. Semi-aquatic in this analysis was defined as squamates that spend considerable amounts of time in the water, but emerge onto land for feeding, reproduction, and basking (Palci *et al.* 2017). The authors also suggest that a mixture of aquatic ancestry and a partial adaptation to a terrestrial ecology (semi-fossorial morphology) could result in the combination of features identified in the inner ear of the stem snake *Dinilysia* (Palci *et al.* 2017).

In addition to both eye and ear anatomy, there are many skeletal characters of snakes that unite them with other fossorial squamates, including the replacement of a metakinetic cranial hinge by a mesokinetic hinge and a reduction or consolidation of a number of cranial bones (Bellairs & Underwood 1951). This consolidation of cranial bones potentially provides greater structure to the braincase during the increased forces experienced when burrowing through a dense substrate. Due to the conflicting interpretations of extant snake anatomy and how it relates to the ancestral ecology of snakes, studies have also focussed on palaeontological evidence.

1.2 Proposed aquatic affinities and relationship to mosasaurs

Examining morphological similarities between snakes and proposed related clades of squamates has the potential for elucidating the early evolution of Pan-Serpentes. Early descriptive anatomical work noted the similarities between snakes and Mosasauroidea, an extinct clade of aquatic squamates, in a clade called Pythonomorpha (Cope 1869). Cope (1869) assigned 20 characters as diagnostic of mosasaurs, ten of which they share with snakes, and five with lacertilians, however some of these characters (such as "lack of fangs on teeth" and

"numerous vertebrae") are of dubious phylogenetic information due to a lack of specificity. Nevertheless, recent work has resurrected Pythonomorpha, and with it support for an aquatic origin of Pan-Serpentes. Recent support for this proposed sister-group relationship between snakes and the mosasaurs is also based on similarities between the skull morphology of the two clades (Caldwell 1999; Lee 1997; Lee & Caldwell 2000). Proposed synapomorphies of the clade Pythonomorpha that unites mosasaurs and snakes include the long posterior process of the septomaxilla, a vertical articulation between the splenial and angular, reduced overlap of the postdentary bones with the dentary, and a reduced splenial-dentary suture (Caldwell 1999). The aquatic hypothesis purports that the elongate limbless body-plan of snakes is due to an adaptation to aquatic locomotion, again utilising lateral undulations of the body as the primary method of locomotion in water over limb-based propulsion seen in many aquatic taxa such as mosasaurs.

For clarity in this section due to the uncertain phylogenetic position of Mosasauroidea, when referring to Pan-Serpentes, I am limiting my description to those fossils that possess unambiguous apomorphies of Pan-Serpentes, which include a well-developed zygosphene-zygantral articulation consisting of a transversely wide zygosphene with dorsolaterally angled articular facets and a medially convex anterior margin, and a deep zygantrum with distinct ventromedially angled articular facts. These characters exclude the known Mosasauroidea, although I concede that should Mosasauroidea be recovered as sister clade to Serpentes in phylogenetic analysis then they can reasonably be termed Pan-Serpentes.

A sister group relationship between Pan-Serpentes and Mosasauroidea is not certain, with many analyses recovering the closest extant clade to mosasaurs as Varanidae (Conrad 2008; Gauthier *et al.* 2012; McDowell & Bogert 1954; Rieppel & Zaher 2000a, 2000b, 2001; Wiens *et al.* 2010). Characters supporting this relationship include the presence of two lacrimal foramina, the vagus nerve passing through the hypoglossal foramen, vertebral centra constricted anterior to condyles (McDowell & Bogert 1954), a strong medial processes of the maxillae behind the nasal process of the premaxilla, weakly inclined anterior margin of the maxillary nasal process, and the splenial not extending anterior to the mid-point of the dentary tooth row (Conrad 2008). Even analyses that propose a similarity between Serpentes and mosasaurs have nested this clade within varanids (Lee *et al.* 1999; Lee & Caldwell 2000). More recent phylogenies using a combined approach with both molecular and morphological data from extant taxa in addition to morphological data from fossil taxa have reunited Serpentes and Mosasauroidea as sister clades (Reeder *et al.* 2015; Simões *et al.* 2018). However a proposed relationship between Serpentes and mosasaurs does not necessarily inform discussions of the ecology of the ancestral snake. As both clades are monophyletic, there is still the possibility that both evolved from a shared terrestrial ancestor, and mosasaurs represent a specialisation to an

aquatic environment independent to whichever ecology influenced body form evolution in Pan-Serpentes. With the context of these conflicting conclusions drawn from the anatomy of extant animals and uncertainty about the closest squamate relation of snakes, there is considerable potential for information from the snake fossil record to elucidate questions about the ecology of the ancestral snake.

1.3 Information from the snake fossil record

Palaeontological evidence for either ecological origin hypothesis has largely focused on the interpretations of ecology and phylogenetic relationships of several species of Cretaceous snakes of which we have complete or near complete skeletal remains. The interpretation of these fossils is not always straightforward, as although their snake affinities are well agreed, the relatedness of these fossils to extant clades is not firmly established.

The clade of marine Cretaceous snakes Simoliophiidae have been suggested to support a marine, aquatic origin of Pan-Serpentes. These fossils often have a mosaic of plesiomorphic and snake characters. These include skull characters that support their assignment to Macrostomata, a derived clade of snakes, as well as the presence of reduced but well-developed hind limbs that are suggestive of a more stemward placement. Nopcsa (1923), when describing the Cretaceous simoliophiid *Pachyophis*, proposed an aquatic origin for Pan-Serpentes on the basis of a combination of plesiomorphic and derived features seen in this fossil. Nopcsa proposed a close relationship between *Pachyophis* and the marine dolichosaurids (a clade of mosasauroids), due to similarity in vertebra construction and pachyostosis of the trunk region (Nopcsa 1923). However, he did not account for the potential of these features resulting from a convergence to a similar marine aquatic ecology. Pachyostosis is a non-pathological osteological specialisation characterised as an increase in bone compactness and/or volume (Houssaye 2009). Pachyostosis is seen across multiple marine amniotes to act as ballast, usually seen in slow swimmers and shallow divers (Taylor 2000). As such, the utility of pachyostosis as a character for phylogenetic reconstruction is questionable, particularly when not distinguishing pachyostosis (increase of bone deposit that increases volume) from osteosclerosis (increase of bone inner compactness) (Houssaye 2009, 2013).

The simoliophiid *Pachyrhachis problematicus* from the Lower Cenomanian of Ein Jabrud is another snake that has been at the centre of the ecological origins debate. Early description of this fossil suggested a marine ecology based on pachyostosis, but did not consider the skull particularly snake-like, rather that it resembled platynotan reptiles, although the vertebrae were noted to resemble the fossil stem snake *Simoliophis* (Haas 1979). Even when united with

Serpentes, the presence of a rudimentary hind-limb suggested a stemward placement for this taxon. The vertebrae of Simoliophiidae possess many plesiomorphic characters, such as the narrow zygosphene, articular facets of zygopophyses strongly inclined on the horizontal, and the lack of prezygopophyseal processes (Rage *et al.* 2016). These features also suggest a stemward placement for this clade. In regards to the ecological origins debate, it is important to distinguish either a crownward or stemward placement of *Pachyrhachis.* The depositional environment of Ein Jabrud is a low energy inter-reef basin, and features such as pachyostosis of vertebrae and ribs and lateral compression of the body indicate that *Pachyrhachis* was an aquatic animal, either a shallow marine swimmer or an inter-reef basin slow swimmer (Scanlon *et al.* 1999). If *Pachyrhachis* is interpreted as an early stem snake, this supports the hypothesis that adaptation to an aquatic ecology occurred early in snake evolution, and that crown snake origins occurred in an aquatic environment.

Later redescription of the skull of *Pachyrhachis* found that this species shares many characters diagnostic of macrostomatan snakes, including the free ending process of the supratemporal and the enlarged posterodorsal process of the dentary (Zaher 1998). The presence of these derived features suggests a crownward placement, as either stem Alethinophidia or stem Macrostomata. Lee (1998) contested some of these character assignments, stating that any *Pachyrhachis*-macrostomatan relationship should be considered dubious, with features such as the presence of the jugal supporting a more stemward placement (Lee 1998), and that many of the proposed derived characters that snakes share with mosasaurs such as the intramandibular joint are present in *Pachyrhachis* (Lee & Caldwell 1998). This stemward position of *Pachyrhachis* was hypothesised to support an aquatic origin for Pan-Serpentes (Caldwell 2000). However, subsequent phylogenetic analysis that includes *Pachyrhachis* and other Simoliophiidae has continued to recover this clade as nested within Serpentes, as stem Macrostomata (Apesteguía & Zaher 2006; Caldwell *et al.* 2015; Conrad 2008; Wiens *et al.* 2010; Wilson *et al.* 2010; Zaher & Rieppel 2002) or nested within Macrostomata (Tchernov *et al.* 2000). Even analysis that recover a stem snake position for Simoliophiidae place them crownward to other stem snakes from terrestrial deposits (Garberoglio *et al.* 2019), again suggesting that Simoliophiidae represent an early diversification of Pan-Serpentes into an aquatic ecology but are not reflective of the ancestral ecology of Pan-Serpentes. If *Pachyrhachis* is recovered as a stem alethinophidian or stem macrostomatan, then its ecology does not provide evidence for either hypothesis of the ecology of the ancestral snake, as *Pachyrhachis* and other simoliophiids would represent a marine derivation of snakes post-origin. This is in contrast to the interpretation of *Pachyrhachis* as the earliest stem snake, where the marine habitat of this species could be interpreted to support an aquatic origin for Pan-Serpentes. Current phylogenetic analysis suggests that Simoliophiidae are not representative of the

morphology of the ancestral Pan-Serpentes. Whether interpreted either as stem Macrostomata or stem Serpentes, terrestrial taxa are recovered as more stemward (Apesteguía & Zaher 2006; Caldwell *et al.* 2015; Garberoglio *et al.* 2019; Tchernov *et al.* 2000; Wiens *et al.* 2010; Wilson *et al.* 2010; Zaher & Rieppel 2002).

Pan-Serpentes fossils from the Cretaceous are not limited to marine deposits (Head *et al.* 2022). Several terrestrial taxa also share the issue of possessing both relatively derived skulls and plesiomorphic axial characters. *Najash rionegrina*, from the Candeleros Formation (Cenomanian-Turonian) in Argentina, was first described in 2006. This taxon possesses a typical snake skull, with a fully enclosed braincase and fused parietals. Additionally, the posterior portion of the braincase is similar to that of fossorial anilioids, with a transversely expanded otico-occipital region as well as dorsal exposure of the prootic between the supratemporal, otooccipital, and supraoccipital (Apesteguía & Zaher 2006). The vertebrae are also distinctly snake-like, with zygosphenal and zygapophyseal facets separated by a non-articular area, divided synapophyses, and three distally forked lymphapophyses (Apesteguía & Zaher 2006). Additionally, *Najash* possesses several plesiomorphic characters, the most obvious being the retention of distinct hind limbs with a clear stylopod and zeugopod, but also including the retention of two sacral vertebrae that separate the trunk region from the caudal region and a pelvis that is functionally connected to the sacral region outside the rib cage (Apesteguía & Zaher 2006; Zaher *et al.* 2009). Several cranial and vertebral features of *Najash* support a potential fossorial ecology, such as the broad stapedial footplate and low neural arch of the vertebrae (Apesteguía & Zaher 2006). However, other researchers have contested this conclusion, citing a similarity in morphology between the vertebrae of *Najash* and that of *Python molurus,* an extant terrestrial python (Palci *et al.* 2013). They also claim that large body size, estimated by Zaher et al (2009) to be approximately 2m, is another reason to reject a fossorial ecology for *Najash* (Palci *et al.* 2013). However, there is no experimental evidence that suggests such a size is impossible for a fossorial animal. The largest burrowing extant snakes can attain body sizes of up to 1.5m (*Xenopeltis unicolor* and *Loxocemus bicolor* (O'Shea 2018)), and it is expected that the density and composition of the substrate will affect the ability of snakes to burrow. As such a size of 2m is not a convincing reason to completely reject a hypothesis of fossoriality. Recent discovery of new skulls and skeletons of *Najash* have allowed further investigation of the anatomy. This discovery include three-dimensional preserved fossils with minimal crushing damage, and allowed the identification of the post-orbital bone as a jugal, homologous to the triradiate element found in many lizards (Garberoglio et al. 2019). Morphological phylogenetic analysis recovers *Najash* either as the basal most stem snake (Apesteguía & Zaher 2006; Caldwell *et al.* 2015; Gauthier *et al.* 2012; Zaher & Scanferla 2012), in

a polytomy with both Scolecophidia and Alethinophidia (Wilson *et al.* 2010), or as a stem snake (Garberoglio *et al.* 2019).

Dinilysia patagonica from the Late Cretaceous of Argentina is another terrestrial fossil stem snake that shows a mosaic of plesiomorphic and derived skull characters. Initial description of this fossil noted its similarity to both Boidae and Ilysidae (an out of date clade comprising the fossorial snake *Anilius scytale*), positing that the skull generally resembles the booid genus *Boa* but with a non-projecting supratemporal and small quadrate more similar to that of *Anilius* (Smith-Woodward 1901). This fossil is clearly assigned to Pan-Serpentes, with features such as the descending lateral flanges of the parietal that enclose the braincase unequivocally confirming its placement in this clade (Estes *et al.* 1970). Plesiomorphic characters include the lateral position of the prefrontal, the absence of a medial vertical flange on the nasals, the basioccipital forming the floor of the recessus scalae tympanae, and a lizard-like contact between the vomer and the palatine (Zaher & Scanferla 2012). Further studies into the cranial anatomy of *Dinilysia* continued to note the similarity in the morphology of certain skull elements between *Dinilysia* and the fossorial snakes *Anilius* and *Cylindrophis*, such as prefrontals with wide interlocking contact with both the frontals and maxillae (Estes *et al.* 1970). Subsequent phylogenetic analysis has recovered *Dinilysia* as either a stem snake (Caldwell *et al.* 2015; Gauthier *et al.* 2012; Scanlon & Lee 2000; Zaher & Scanferla 2012) or a stem alethinophidian (Apesteguía & Zaher 2006; Conrad 2008; Wiens *et al.* 2010; Wilson *et al.* 2010; Zaher & Rieppel 2002).

Madtsoiidae are a clade of snakes that diverged in the mid-Cretaceous and persist in the fossil record until the Late Pleistocene (Rage 1998). These include the genera *Madtsoia* and *Menarana* from the Cretaceous, to the later surviving genera from the Australian Pleistocene, *Wonambi* and *Yurlunggur* (Laduke *et al.* 2010; Mohabey *et al.* 2011; Rieppel *et al.* 2003; Scanlon 1992, 2006; Scanlon & Lee 2000; Vasile *et al.* 2013). Revised anatomy of Pleistocene aged specimens by Scanlon and Lee (2000) found similarities between *Wonambi* and *Dinilysia*, particularly in the large lateral crests of the parietal, and similar morphology of the frontals. Phylogenetic analysis including this material recovered Madtsoiidae as stem snakes, along with Simoliophiidae and *Dinilysia* (Scanlon & Lee 2000). The phylogenetic position of Madtsoiidae however is uncertain, they have variably been recovered as stem snakes (Caldwell *et al.* 2015; Garberoglio *et al.* 2019; Scanlon & Lee 2000), stem Alethinophidia (Wiens *et al.* 2010), and nested within Alethinophidia as stem Macrostomata (Vasile *et al.* 2013; Wilson *et al.* 2010; Zaher & Scanferla 2012). *Wonambi* has also been recovered as stem Boinae, although in an analysis that did not include data from other Madtsoiidae (Apesteguía & Zaher 2006). Regardless of the relationships of Madtsoiidae to extant clades, these taxa represent an early

diversification of Pan-Serpentes with large body sizes in the Late Cretaceous, with the species *Madtsoia madagascariensis* already reaching body sizes of over 8m (Laduke *et al.* 2010).

The fossil record of Pan-Serpentes clearly shows that, by the Late Cretaceous, snakes have already diversified into many different ecologies, and also that the elongate, limb-reduced body plan of snakes is well-adapted to a variety of different habitats without much need for specialised adaptation. A lot of the problems surrounding the phylogenetic placement of fossil taxa stem from issues with the high amount of homoplasy in regards to ecology that is seen in snakes. Further elucidation of the ecology of the ancestral snake will require the discovery of older snake fossils than the current described late Cretaceous taxa. A recent study purported to discover such fossils, claiming that the enigmatic squamate genus *Parviraptor* consists of several genera of snakes from the Middle Jurassic to Lower Cretaceous: *Parviraptor estesi, Diablophis gilmorei*, *Portugalophis lignites*, and *Eophis underwoodi* (Caldwell *et al.* 2015). However, the fragmentary nature of these specimens, that mostly consist of isolated maxilla and vertebrae, and absence of clear snake-like synapomorphies leaves their assignment to Serpentes questionable. In analysis that include these taxa, they are recovered as a large polytomy at the base of Pan-Serpentes, and therefore do not provide much information about early snake evolution (Caldwell *et al.* 2015).

2. Phylogeny Construction and the Problem of Homoplasy

Since the start of the use of molecular data to reconstruct phylogenetic relationships, the relatedness between different clades of snakes, and the position of snakes amongst squamates as a whole, has been unclear. In particular, our understanding of the basally diverging clades has changed considerably since the first attempts to reconstruct the relationships between snake clades. The first major change between phylogenies constructed with morphological data and those constructed with molecular data is the recovery or lack of recovery of a monophyletic Anilioidea. Early work initially united several fossorial clades (Uropeltidae, Aniliidae, Cylindrophiidae, Loxocemidae, and Xenopeltidae) together, with synapomorphies such as reduction or loss of the postorbital bone, solidly united cranial bones, and prefrontals without an anterior process beside the nasal (Romer 1956), or the anterior dentigerous process of the palatine making contact with the vomer (McDowell 1975). Recent phylogenetic analyses using morphological data did not recover a monophyletic Anilioidea, instead finding the fossorial clades as a paraphyletic grade at the base of Macrostomata, but did unite Aniliidae and Cylindrophiidae (Gauthier *et al.* 2012) (See Figure 2A).

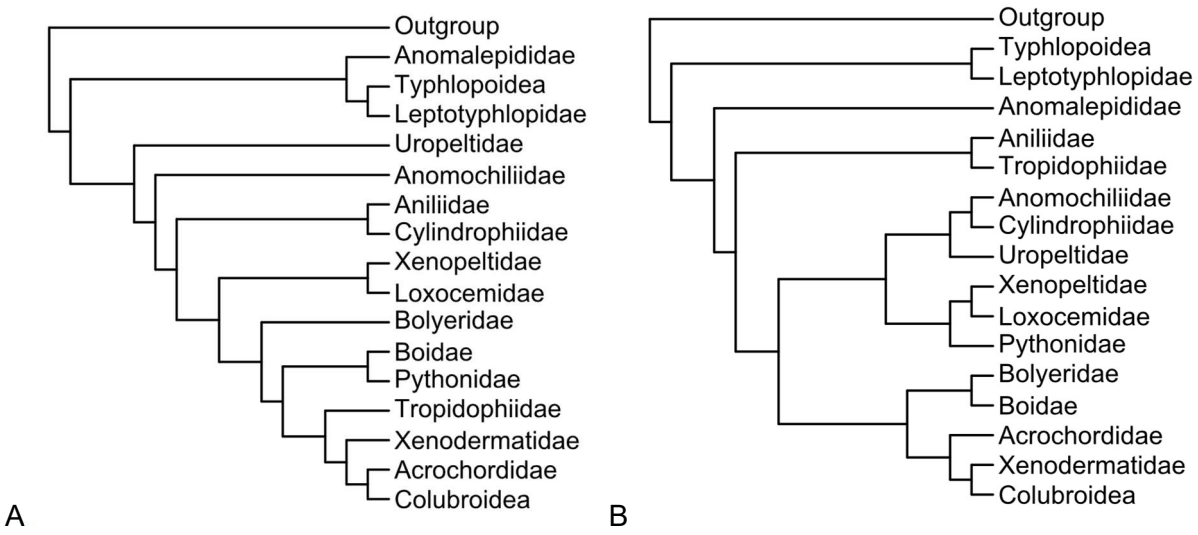

Figure 2. A) Maximum parsimony Serpentes tree constructed with 610 morphological characters, modified from squamate tree in Gauthier et al. (2012). B) Maximum likelihood Serpentes tree constructed from combined matrix (44 genes for 161 species, 12 genes for 4161 species), modified from squamate tree in Zheng & Wiens (2015)

The advent of the utility of molecular data for elucidating phylogeneticrelatedness has led to a significant re-understanding of squamate relationships, including both the relatedness of snakes to other squamate clades and the relationships of the clades within snakes. Early examinations into the relationships between snake clades, using either C-mos and RAG1 genes, or C-mos and 12S rRNA, 16S rRNA and cytochrome b, no longer recovered a monophyletic Anilioidea, and instead united the American pipe snakes Aniliidae, represented by the single taxon *Anilius scytale*, with the dwarf boas, Tropidophiidae, traditionally understood to be macrostomatan (Vidal & David 2004; Vidal & Hedges 2002). This clade was later named Amerophidia, referring to the geographic range of both Aniliidae and Tropidophiidae (Vidal *et al.* 2007).

Phylogenetic analyses of molecular data continue to recover a monophyletic Amerophidia (Burbrink *et al.* 2020; Figueroa *et al.* 2016; Pyron *et al.* 2013a, 2013b; Streicher & Wiens 2016; Wiens *et al.* 2008, 2012; Zheng & Wiens 2016) (See Figure 2B). This relationship is also supported by morphology of soft tissue features, such as a unique cloacal/oviducal junction where there are dorsal projections from the dorso-lateral surface of the urodaeum, the most anterior region of the cloaca (Siegel *et al.* 2011). Combined analysis using both molecular and morphological data either recover a monophyletic Amerophidia (Reeder *et al.* 2015) or find Aniliidae and Tropidophiidae as paraphyletic at the base of the rest of Alethinophidia (Pyron

2017). This repeated discovery of a monophyletic Amerophidia has considerable implications for our understanding of snake adaptation and evolution. As noted in early studies that united this clade, the previously considered 'derived' state of macrostomatan gape cannot be considered to be unaffected by homoplasy (Vidal & Hedges 2002). Instead, macrostomy either appears to have evolved several times across Serpentes, or is the plesiomorphic form of snakes, with multiple specialisations to a fossorial morphology causing the loss of macrostomatan features. It is also possible that both a macrostomatan gape and fossorial morphology evolved from an ancestor possessing an intermediate morphology to the two extremes seen in extant taxa.

The other marked change between phylogenetic hypotheses based on morphological data versus those based on molecular data is whether the clades Typhlopoidea (consisting of Typhlopidae, Gerrhopilidae, Xenotyphlopidae), Leptotyphlopidae, and Anomalepididae form a monophyletic Scolecophidia. The overall skull design of the three clades of Scolecophidia where resistance to the substrate is achieved by an outer bony shell in sutural contact with the outer braincase, achieved by lateral expansions of the premaxilla, the 'outer-shell design' (Cundall & Rossman 1993), superficially supports the monophyly of this clade. All scolecophidians are small, fossorial, and insectivorous, with most specialising in myrmecophagy. Phylogenetic analysis using morphological data routinely supports a monophyletic Scolecophidia (Conrad 2008; Gauthier *et al.* 2012)(see Figure 2A). Although there are no unreserved synapomorphies uniting the Scolecophidia in the Gauthier et al (2012) analysis, they are joined by the combination of a suite of characters, the unambiguous ones of which are: the frontoparietal suture in the medial wall of the orbit vertical or slightly inclined anteriorly; absence of a parietal sagittal crest; anterior end of the septomaxilla not in contact with the maxilla; choanal process of the palatine that narrows to form a curved finger-like process; absence of the lateral extent of the supraoccipital nuchal crest; and a maxillary tooth count between 2 and 5 (Gauthier *et al.* 2012). Early phylogenetic analyses using molecular data that appears to recover a monophyletic Scolecophidia only includes taxa from Leptotyphlopidae and Typhlopoidea, excluding the Anomalepididae (Slowinski & Lawson 2002; Vidal & David 2004).

In contrast to the morphological data, the majority of analyses using molecular data recover a paraphyletic Scolecophidia. These analyses usually unite Typhlopoidea (often reported as Typhlopidae) with Leptotyphlopidae, Scolecophidia *senso stricto* as per Miralles et al (2018), with Anomalepididae either stemward (Figueroa *et al.* 2016; Pyron *et al.* 2013b, 2013a) or closer to Alethinophidia (Burbrink *et al.* 2020; Hsiang *et al.* 2015; Miralles *et al.* 2018; Reeder *et al.* 2015; Wiens *et al.* 2012; Zheng & Wiens 2016)(See Figure 2B). The repeated discoveries of Anomalepididae as a separate clade to the one uniting Typhlopoidea and

Leptotyphlopidae shows an increased importance to decipher anatomical characters that distinguish these three clades from one another.

The repeated recovery of this supposed paraphyly has led to the identification of a number of morphological characters that support a paraphyletic Scolecophidia. Both Typhlopoidea and Leptotyphlopidae share a ramus hyomandibularis of the facial nerve that is enclosed within the juxtastapedial recess, a feature that is not present in *Liotyphlops*, an anomalepid (Rieppel 1979). Uniting the Leptotyphlopidae and Typhlopoidea is supported by several morphological characters even in analyses that recover a monophyletic Scolecophidia. Unique synapomorphies of this clade include: the vomerine process of the palatine passing the vomer lateral to vomer tines (as opposed to medial); the absence of an ectopterygoid; and a paired supraoccipital (Gauthier *et al.* 2012).

This apparent incongruence between phylogenetic hypotheses constructed with either molecular or morphological data leads to considerable issues when attempting to include fossil taxa in phylogenetic analyses. Phylogenies including fossil taxa rely on the inclusion of morphological data, as molecular data is unattainable for extinct organisms. The Conrad (2008) analysis included six fossil snake taxa (*Dinilysia patagonica, Pachyophis woodwardi, Wonambi naracoortensis, Eupodophis descouensi, Haasiophis terrasanctus, Pachyrhachis problematicus)* and the Gauthier et al (2012) analysis included five fossil snake taxa (*Najash rionegrina, Dinilysia patagonica,* and three Simoliophiidae: *Haasiophis terrasanctus, Eupodophis descouensi, Pachyrhachis problematicus*). For taxa that are recovered as stem snakes (*Najash* and *Dinilysia* in Gauthier et al, 2012) or stem alethinophidians (*Dinilysia, Pachyophis, Haasiophis* in Conrad, 2008), placement in a molecular phylogenetic framework is straightforward. However, problems occur when attempting to place fossil taxa when the clades with which they are purported to be related to are no longer recovered. In the Gauthier et al. (2012) and the Conrad (2008) analyses, Simoliophiidae are recovered as stem Macrostomata. This poses an issue for attempts to add fossils to phylogenetic trees constructed with molecular data that do not recover a monophyletic Macrostomata.

That both a monophyletic Anilioidea and Scolecophidia are only found in phylogenies constructed using morphological data suggests that the inclusion of potentially homoplastic characters confuse reconstructions of interrelationships between clades. The repeated adaptation to a fossorial ecology results in a suite of cranial characters appearing across the snake clade, and including these characters in morphological datasets will erroneously lead to these taxa being recovered as related. This leads to a problem with deciphering the ecological origin for snakes, as it is hard to distinguish between characters that are ancestral to snakes and those that result from adaptation to a fossorial ecology, especially if the ancestral snake was fossorial.

In the squamate clade, the repeated evolution of the snake-like body form is often accompanied by a fossorial or grass-swimming ecology, and in morphological analyses of squamates, snakes are often recovered belonging to a "fossorial clade" that includes fossorial lizard clades such as Dibamidae and Amphisbaenia (Conrad 2008; Gauthier *et al.* 2012). A similar trend occurs within snakes, with the recovered monophyly of both Scolecophidia and the 'anilioid' pipe snakes (Conrad 2008; Gauthier *et al.* 2012) uniting fossorial snakes in clades that are not recovered when using molecular data. Therefore, understanding how the snake body form, and snakes themselves, evolved in response to ecology is intwined with deciphering the relationships between snakes.

Fossoriality is associated with a suite of characters, including miniaturisation, body elongation, limb reduction, and the consolidation of cranial bones (Gans 1975; Lee 1998). Limb reduction is a common morphotype in squamates, and often follows the elongation of the body (Greer 1991). Limb reduction and body elongation also have the effect of imposing more mechanical burdens on the head (Gans 1961). This may be especially prevalent in head-first burrowing taxa, where the skull is the primary point of contact with the substrate, and therefore under more mechanical constraints than taxa that primarily use the limbs for locomotion (Wake 1993). Additionally, miniaturisation also has marked effects on the feeding, locomotion, and reproductive biology of an organism, due to the need to maintain these functions at a smaller size (Hanken & Wake 1993). Characters associated with fossoriality must be carefully assessed when included in morphological phylogenies, as their potential to confuse relationships with homoplasy is considerable.

3. New Techniques

The use of new analytical techniques has allowed more complex analysis into snake morphology that may provide insights into our understanding of snake evolution, particularly the heavily debated subject of ecological origins. Recovery of the limbed Cretaceous snakes as nested within extant snakes poses a potential problem when considering the evolution of the snake body plan. No extant snakes possess external limbs, although several clades do retain remnants of pelvic and hind-limb elements (Romer 1956). This means that either snakes lost limbs multiple times, or that the simoliophiids and madtsoiids re-evolved limbs from a limbless snake ancestor. Recent work into the development patterning of snake limbs suggests that this may have been possible. The limb-specific enhancer region of the *Sonic hedgehog* gene has a specific deletion present in snakes that reduces transcription (Leal & Cohn 2016, 2017). Transgenic mice with this enhancer region develop 'serpentinised', with severe limb reduction

(Kvon *et al.* 2016). Limbs can be recovered with synthetic restoration of this deletion, suggesting that the developmental architecture for regaining limbs may still be present in some snakes (Kvon *et al.* 2016). A theoretical mechanism for the maintenance of this enhancer region is pleiotropy between the limb enhancer region and the genital enhancer region, the latter of which is usually under stabilising selection (Leal & Cohn 2017). Therefore, the apparent nested position of limbed Cretaceous snakes within extant clades is explainable through currently understood developmental mechanisms.

A technique that has potential for elucidating the problem of homoplasy of morphological features is geometric morphometrics, which allows quantitative analysis of different shapes that can then be analysed statistically. This technique was used to reconstruct habitat types that correlate with the morphology of the inner ear, particularly in relation to the Cretaceous snake *Dinilysia patagonica*. There are clear morphological similarities between the inner ear of *Dinilysia* and the inner ear of extant burrowing squamates, such as a large spherical vestibule, large foramen ovale, and slender semi-circular canals (Yi & Norell 2015). In the principal component analysis implemented by Yi & Norell (2015), *Dinilysia* clusters with 'modern active burrowers' such as *Loxocemus bicolor* and *Xenopeltis unicolor*. This was confirmed by another study that also analysed the morphology of the inner ear, although not fully supported by the authors (Palci *et al.* 2017). In the Palci et al (2017) principal component analysis of the inner ear, *Dinilysia* again clusters with *L. bicolor* and *X. unicolor*, as well as the fossorial Asian pipe snake *Cylindrophis* on the first principal component axis (Palci *et al.* 2017). Both of these studies support a hypothesis of a fossorial ecology for *Dinilysia*, which therefore either supports a hypothesis of fossorial ecological origin of snakes if *Dinilysia* is recovered as a stem snake, or shows that fossorial adaptations occurred early on in snake evolution. Yi & Norell (2015) also reconstructed the inner ear of a hypothetical ancestor of snakes, which was predicted as fossorial whether or not *Dinilysia* was included in the analysis.

Geometric morphometrics can also be used on whole skull data, rather than individual cranial components. Analysis of both 2D and 3D data found that the two major axes of variation of skull morphology delineate a convergent fossorial skull shape shared by both lizards and snakes, and the most recent common ancestor of Serpentes is recovered as fossorial (Da Silva *et al.* 2018). Recent high-density morphometric analysis of squamate skulls using both landmarks and sliding semi-landmarks found that both diet and habitat have major influences on skull shape evolution (Watanabe *et al.* 2019). This analysis also supported a nonaquatic origin for snakes, due to similarities between the ancestral reconstruction of skull shape with the semi-fossorial lamprophiid *Aparallactus* (Watanabe *et al.* 2019).

Finally, recent analysis of skull roof compactness found that characters associated with fossoriality have evolved independently in over 50 lepidosaur lineages, with the associated

repeated acquisition of characters such as a highly compact skull roof, small skull diameter, and elongate cranium when taxa evolve fossoriality (Ebel *et al.* 2020). On the basis of ancestral state reconstructions of skull roof compactness, the ancestor of snakes is recovered as being fully fossorial (Ebel *et al.* 2020). Many snakes also retain this highly compact skull roof even after reverting to a terrestrial or semi-fossorial lifestyle.

4. Conclusion

Although the ecological origins of snakes is currently unresolved, a number of evidence from different primary sources, as well as recent analytical techniques provide the most support for the hypothesis that early snakes primarily evolved in a fossorial habitat. Analyses of ancestral state reconstructions of inner ear, compactness of skull roof, and total skull shape all independently support a fossorial or semi-fossorial ecology as most likely to have influenced the shape of the ancestral snake skull, and therefore the most likely ecology to have facilitated the early evolution of snakes. Further discoveries of early stem snakes may help elucidate this problem further, as can the development of further analytical techniques.

While individual cranial elements and fossils have been considered in the context of the ecological origins of snakes, as of yet no work has focussed on body size. Body size is a readily available metric for both extinct and extant taxa. Body size, particularly in snakes that show a large variety of extant body sizes, has the potential to influence feeding, reproduction and ecological specialisation. In particular, the different hypotheses of ecological snake origins predict different outcomes for snake body size. I address effects of body size evolution on interpretations of hypotheses of snake origins in chapter 2.

Additionally, with recent molecular phylogenetic analyses repeatedly recovering the Scolecophidia as a paraphyletic grade, it is of vital interest to examine the morphology of these snakes further. Of particular importance is deciphering what morphological characters relate to interrelationships between clades and what morphological characters relate to the shared ecology of fossoriality and miniaturisation. I examine the diversity and variability of Typhlopidae cranial elements, particularly in relation to body size and unique reproductive strategies in chapter 3.

Finally, while the lack of congruence between phylogenetic hypotheses constructed with morphological data and those constructed with molecular data in snakes has been suggested to be a result of homoplasy, little work has been put into identifying what morphological characters of snakes are homoplastic. In cases where there is homoplasy related to ecology, this can also be used to predict the ecology of extinct taxa for which such data is unobtainable. I

examine correlates between ecology and the morphology of the major skull roof bone in snakes, the parietal, to identify if there are morphological characters used in phylogenetics that are potentially homoplastic, and also use this to predict the ecology of the Late Cretaceous snake, *Dinilysia patagonica* in chapter 4.

Bibiliography

Apesteguía, S., & Zaher, H. (2006). A Cretaceous terrestrial snake with robust hindlimbs and a sacrum. *Nature*, **440**(7087), 1037–1040.

Atkins, J. B., & Franz-Odendaal, T. A. (2016). The sclerotic ring of squamates: an evo-devo-eco perspective. *Journal of Anatomy*, **229**(4), 503–513.

Bellairs, A. d'A, & Underwood, G. (1951). The origin of snakes. *Biological Reviews*, **26**, 193–237.

Berman, D. S., & Regal, P. J. (1967). The Loss of the Ophidian Middle Ear. *Evolution*, **21**(3), 641–643.

Brandley, M. C., Huelsenbeck, J. P., & Wiens, J. J. (2008). Rates and patterns in the evolution of snake-like body form in squamate reptiles: Evidence for repeated re-evolution of lost digits and long-term persistence of intermediate body forms. *Evolution*, **62**(8), 2042–2064.

Burbrink, F. T., Grazziotin, F. G., Pyron, R. A., … Zaher, H. (2020). Interrogating Genomic-Scale Data for Squamata (Lizards, Snakes, and Amphisbaenians) Shows no Support for Key Traditional Morphological Relationships. *Systematic Biology*, **69**(3), 502–520.

Caldwell, M. W. (1999). Squamate phylogeny and the relationships of snakes and mosasauroids. *Zoological Journal of the Linnean Society*, **125**(1), 115–147.

Caldwell, M. W. (2000). On the Phylogenetic Relationships of Pachyrhachis within Snakes: A Response to Zaher (1998). *Journal of Vertebrate Paleontology*, **20**(1), 187–190.

Caldwell, M. W., Nydam, R. L., Palci, A., & Apesteguía, S. (2015). The oldest known snakes from the Middle Jurassic-Lower Cretaceous provide insights on snake evolution. *Nature Communications*, **6**, 5996.

Camaiti, M., Evans, A. R., Hipsley, C. A., & Chapple, D. G. (2021). A farewell to arms and legs: a review of limb reduction in squamates. *Biological Reviews*, **96**(3), 1035–1050.

Camp, C. L. (1923). Classification of the lizards. *Bulletin American Museum of Natural History*, **48**, 289–481.

Caprette, C. L., Lee, M. S. Y., Shine, R., Mokany, A., & Downhower, J. F. (2004). The origin of snakes (Serpentes) as seen through eye anatomy. *Biological Journal of the Linnean Society*, **81**(4), 469–482.

Christensen, C. B., Christensen-Dalsgaard, J., Brandt, C., & Madsen, P. T. (2012). Hearing with an atympanic ear: Good vibration and poor sound-pressure detection in the royal python, *Python regius*. *Journal of Experimental Biology*, **215**(2), 331–342.

Conrad, J. L. (2008). Phylogeny and systematics of Squamata (Reptilia) based on morphology. *Bulletin American Museum of Natural History*, **310**, 182.

Cope. (1869). On the reptilian orders Pythonomorpha and Streptosauria. *Proceedings of the Boston Society of Natural History*, **12**, 250–269.

Cundall, D., & Rossman, D. A. (1993). Cephalic anatomy of the rare Indonesian snake *Anomochilus weberi*. *Zoological Journal of the Linnean Society*, **109**(3), 235–273.

Da Silva, F. O., Fabre, A.-C., Savriama, Y., … Di-Poï, N. (2018). The ecological origins of snakes as revealed by skull evolution. *Nature Communications*, **9**(1), 376.

Da Silva, M.-A. O., Heegaard, S., Wang, T., Gade, J. T., Damsgaard, C., & Bertelsen, M. F. (2017). Morphology of the snake spectacle reflects its evolutionary adaptation and development. *BMC Veterinary Research*, **13**, 258.

Ebel, R., Müller, J., Ramm, T., Hipsley, C., & Amson, E. (2020). First evidence of convergent lifestyle signal in reptile skull roof microanatomy. *BMC Biology*, **18**(1), 1–18.

Estes, R., Frazetta, T. H., & Williams, E. E. (1970). Studies on the fossil snake Dinilysia patagonica Woodward: Part I. Cranial Morphology. *Bulletin of the Museum of Comparative Zoology at Harvard College*, **140**(2), 25–74.

Figueroa, A., Mckelvy, A. D., Grismer, L. L., Bell, C. D., & Lailvaux, S. P. (2016). A species-level phylogeny of extant snakes with description of a new colubrid subfamily and genus. *PLoS ONE*, **11**(9), e0161070.

Gans, C. (1961). The feeding mechanism of snakes and its possible evolution. *American Zoologist*, **1**, 217–227.

Gans, C. (1975). Tetrapod Limblessness: Evolution and Functional Corollaries. *American Zoologist*, **15**(2), 455–467.

Garberoglio, F. F., Apesteguía, S., Simões, T. R., … Caldwell, M. W. (2019). New skulls and skeletons of the Cretaceous legged snake *Najash*, and the evolution of the modern snake body plan. *Science Advances*, **5**, eaax5833.

Gauthier, J. A., Kearney, M., Maisano, J. A., Rieppel, O., & Behlke, A. D. B. (2012). Assembling the squamate tree of life : Perspectives from the phenotype and the fossil record. *Bulletin of the Peabody Museum of Natural History*, **53**(1), 3–308.

Gower, D. J., Fleming, J. F., Pisani, D., … Simões, B. F. (2021). Eye-Transcriptome and Genome-Wide Sequencing for Scolecophidia: Implications for Inferring the Visual System of the Ancestral Snake. *Genome Biology and Evolution*, **13**(12), 1–12.

Gower, D. J., Hauzman, E., Simoes, B. F., & Schott, R. K. (2022). Eyes, Vision, and the Origins and Early Evolution of Snakes. In D. J. Gower & H. Zaher, eds., *The Origin and Early Evolutionary History of Snakes*, Cambridge: Cambridge University Press, pp. 316–248.

Greer, A. E. (1991). Limb reduction in squamates: Identification of the lineages and discussion of the trends. *Journal of Herpetology*, **25**(2), 166–173.

Haas, G. (1979). On a new snakelike reptile from the Lower Cenomanian of Ein Jabrud, near Jerusalem. *Bulletin Du Muséum National d'Histoire Naturelle*, **1**(1), 51–64.

Hanken, J., & Wake, D. B. (1993). Miniaturization of body size: Organismal consequences and

evolutionary significance. *Annual Review of Ecology and Systematics*, **24**, 501–519.

Head, J., De Queiroz, K., & Greene, H. (2020a). Pan-Serpentes. In K. de Queiroz, P. D. Cantino, & J. A. Gauthier, eds., *Phylonyms: a companion to the PhyloCode*, 1st edn, Boca Raton: CRC Press, pp. 1093–1096.

Head, J., De Queiroz, K., & Greene, H. (2020b). Serpentes. In K. de Queiroz, P. Cantino, & J. Gauthier, eds., *Phylonyms: a companion to the PhyloCode*, 1st edn, Boca Raton: CRC Press, pp. 1097–1105.

Head, J. J. (2015). Fossil calibration dates for molecular phylogenetic analysis of snakes 1: Serpentes, Alethinophidia, Boidae, Pythonidae. *Palaeontologia Electronica*, **18**(1), 1–17.

Head, J. J., Howard, A. F. C., & Müller, J. (2022). The First 80 Million Years of Snake Evolution: The Mesozoic Fossil Record of Snakes and Its Implications for Origin Hypotheses, Biogeography, and Mass Extinction. In D. J. Gower & H. Zaher, eds., *The Origin and Early Evolutionary History of Snakes*, Cambridge: Cambridge University Press, pp. 26–54.

Houssaye, A. (2009). "Pachyostosis" in aquatic amniotes: a review. *Integrative Zoology*, **4**(4), 325–340.

Houssaye, A. (2013). Palaeoecological and morphofunctional interpretation of bone mass increase: An example in Late Cretaceous shallow marine squamates. *Biological Reviews*, **88**(1), 117–139.

Hsiang, A. Y., Field, D. J., Webster, T. H., … Gauthier, J. A. (2015). The origin of snakes: revealing the ecology, behavior, and evolutionary history of early snakes using genomics, phenomics, and the fossil record. *BMC Evolutionary Biology*, **15**, 87.

Kvon, E. Z., Kamneva, O. K., Melo, U. S., … Visel, A. (2016). Progressive Loss of Function in a Limb Enhancer during Snake Evolution. *Cell*, **167**(3), 633-642.e11.

Laduke, T. C., Krause, D. W., Scanlon, J. D., & Kley, N. J. (2010). A Late Cretaceous (Maastrichtian) Snake Assemblage from the Maevarano Formation, Mahajanga Basin, Madagascar. *Journal of Vertebrate Paleontology*, **30**(1), 109–138.

Leal, F., & Cohn, M. J. (2016). Loss and Re-emergence of Legs in Snakes by Modular Evolution of Sonic hedgehog and HOXD Enhancers. *Current Biology*, **26**(21), 2966–2973.

Leal, F., & Cohn, M. J. (2017). Developmental, genetic, and genomic insights into the evolutionary loss of limbs in snakes. *Genesis*, **56**(1). doi:10.1002/dvg.23077

Lee, M. S. Y. (1997). The phylogeny of varanoid lizards and the affinities of snakes. *Philosophical Transactions of the Royal Society B: Biological Sciences*, **352**(1349), 53–91.

Lee, M. S. Y. (1998). Convergent evolution and character correlation in burrowing reptiles: towards a resolution of squamate relationships. *Biological Journal of the Linnean Society*, **65**, 369–453.

Lee, M. S. Y., & Caldwell, M. W. (1998). Anatomy and relationships of Pachyrhachis

problematicus, a primitive snake with hindlimbs. *Philosophical Transactions of the Royal Society B: Biological Sciences*, **353**(1375), 1521–1552.

Lee, M. S. Y., & Caldwell, M. W. (2000). *Adriosaurus* and the affinities of mosasaurs, dolichosaurs, and snakes. *Journal of Paleontology*, **74**(05), 915–937.

Lee, M. S. Y., Caldwell, M. W., & Scanlon, J. D. (1999). A second primitive marine snake: Pachyophis woodwardi from the Cretaceous of Bosnia-Herzegovina. *Journal of Zoology*, **248**, 509–520.

McDowell, S. B. (1975). A Catalogue of the Snakes of New Guinea and the Solomons, with Special Reference to Those in the Bernice P. Bishop Museum. Part II. Anilioidea and Pythoninae. *Journal of Herpetology*, **9**(1), 1–79.

McDowell, S. B., & Bogert, C. M. (1954). The systematic position of Lanthanotus and the affinities of the anguinomorphan lizards. *Bulletin of the AMNH*, **105**, 1–142.

Miralles, A., Marin, J., Markus, D., Herrel, A., Hedges, S. B., & Vidal, N. (2018). Molecular evidence for the paraphyly of Scolecophidia and its evolutionary implications. *Journal of Evolutionary Biology*. doi:10.1111/jeb.13373

Mohabey, D. M., Head, J. J., & Wilson, J. A. (2011). A new species of the snake Madtsoia from the Upper Cretaceous of India and its paleobiogeographic implications. *Journal of Vertebrate Paleontology*, **31**(3), 588–595.

Nopcsa, F. B. (1923). *Eidolosaurus* und *Pachyophis*: Zwei neue Neocom-Reptilien. *Palaeontographica*, **65**, 96–154.

O'Shea, M. (2018). *The Book of Snakes: a life-size guide to six hundred species from around the world*, London: Ivy Press.

Palci, A., Caldwell, M. W., & Albino, A. M. (2013). Emended diagnosis and phylogenetic relationships of the Upper Cretaceous fossil snake *Najash rionegrina* Apesteguía and Zaher, 2006. *Journal of Vertebrate Paleontology*, **33**(1), 131–140.

Palci, A., Hutchinson, M. N., Caldwell, M. W., & Lee, M. S. Y. (2017). The morphology of the inner ear of squamate reptiles and its bearing on the origin of snakes. *Royal Society Open Science*, **4**, 170685.

Pyron, R. A. (2017). Novel approaches for phylogenetic inference from morphological data and total-evidence dating in squamate reptiles (Lizards, Snakes, and Amphisbaenians). *Systematic Biology*, **66**(1), 38–56.

Pyron, R. A., Burbrink, F. T., & Wiens, J. J. (2013a). A phylogeny and revised classification of Squamata, including 4161 species of lizards and snakes. *BMC Evolutionary Biology*, **13**, 93.

Pyron, R. A., Kandambi, H. K. D., Hendry, C. R., Pushpamal, V., Burbrink, F. T., & Somaweera, R. (2013b). Genus-level phylogeny of snakes reveals the origins of species richness in Sri Lanka. *Molecular Phylogenetics and Evolution*, **66**, 969–978.

Rage, J.-C. (1998). Fossil snakes from the Palaeocene of São José de Itaboraí, Brazil. Part I. Madtsoiidae, Aniliidae. *Palaeovertebrata*, **27**(January 3-4), 109–144.

Rage, J.-C., Vullo, R., & Néraudeau, D. (2016). The mid-Cretaceous snake Simoliophis rochebrunei Sauvage, 1880 (Squamata: Ophidia) from its type area (Charentes, southwestern France): Redescription, distribution, and palaeoecology. *Cretaceous Research*, **58**, 234–253.

Reeder, T. W., Townsend, T. M., Mulcahy, D. G., … Wiens, J. J. (2015). Integrated analyses resolve conflicts over squamate reptile phylogeny and reveal unexpected placements for fossil taxa. *PLoS ONE*, **10**(3), e0118199.

Rieppel, O. (1979). A cladistic classification of primitive snakes based on skull structure. *Journal of Zoological Systematics and Evolutionary Research*, **17**(2).

Rieppel, O. (1988). A review of the origin of snakes. *Evolutionary Biology*, **22**, 37–130.

Rieppel, O., Kluge, A. G., & Zaher, H. (2003). Testing the phylogenetic relationships of the Pleistocene snake Wonambi naracoortensis Smith. *Journal of Vertebrate Paleontology*, **22**(4), 812–829.

Rieppel, O., & Zaher, H. (2000a). The braincases of mosasaurs and Varanus, and the relationships of snakes. *Zoological Journal of the Linnean Society*, **129**, 489–514.

Rieppel, O., & Zaher, H. (2000b). The Intramandibular Joint in Squamates, and the Phylogenetic Relationships of the Fossil Snake *Pachyrhachis problematicus* Haas. *Fieldiana: Geology*, (43), 1–69.

Rieppel, O., & Zaher, H. (2001). Re-building the bridge between mosasaurs and snakes. *Neues Jahrbuch Für Geologie Und Paläontologie - Abhandlungen*, **221**(1), 111–132.

Romer, A. S. (1956). *Osteology of the Reptiles*, Chicago: University of Chicago Press.

Scanlon, J. D. (1992). A new large madtsoiid snake from the Miocene of the Northern Territory. *The Beagle, Records of the Northern Territory Museum of Arts and Sciences*, **9**(1), 49–60.

Scanlon, J. D. (2006). Skull of the large non-macrostomatan snake Yurlunggur from the Australian Oligo-Miocene. *Nature*, **439**(7078), 839–842.

Scanlon, J. D., & Lee, M. S. Y. (2000). The Pleistocene serpent *Wonambi* and the early evolution of snakes. *Nature*, **403**, 416–420.

Scanlon, J. D., Lee, M. S. Y., Caldwell, M. W., & Shine, R. (1999). The palaeoecology of the primitive snake Pachyrhachis. *Historical Biology*, **13**(2–3), 127–152.

Siegel, D. S., Miralles, A., & Aldridge, R. D. (2011). Controversial snake relationships supported by reproductive anatomy. *Journal of Anatomy*, **218**(3), 342–348.

Simões, B. F., Sampaio, F. L., Jared, C., … Gower, D. J. (2015). Visual system evolution and the nature of the ancestral snake. *Journal of Evolutionary Biology*, **28**(7), 1309–1320.

Simões, T. R., Caldwell, M. W., Tałanda, M., … Nydam, R. L. (2018). The origin of squamates revealed by a Middle Triassic lizard from the Italian Alps. *Nature*, **557**(7707), 706–709.

Slowinski, J. B., & Lawson, R. (2002). Snake phylogeny: Evidence from nuclear and mitochondrial genes. *Molecular Phylogenetics and Evolution*, **24**(2), 194–202.

Smith-Woodward, A. (1901). On some Extinct Reptiles from Patagonia, of the Genera Miolania, Dinilysia, and Genyodectes. *Proceedings of the Zoological Society of London*, **70**(2), 169–184.

Streicher, J. W., & Wiens, J. J. (2016). Phylogenomic analyses reveal novel relationships among snake families. *Molecular Phylogenetics and Evolution*, **100**, 160–169.

Taylor, M. A. (2000). Functional significance of bone ballastin in the evolution of buoyancy control strategies by aquatic tetrapods. *Historical Biology*, **14**(1–2), 15–31.

Tchernov, E., Rieppel, O., Zaher, H., Polcyn, M. J., & Jacobs, L. L. (2000). A Fossil Snake with Limbs. *Science*, **287**(5460), 2010–2012.

Uetz, P., Freed, P., & Hosek, J. (2019). The Reptile Database. Retrieved April 22, 2020, from http://www.reptile-database.org

Vasile, Ş., Csiki-Sava, Z., & Venczel, M. (2013). A new madtsoiid snake from the Upper Cretaceous of the Haţeg Basin, western Romania. *Journal of Vertebrate Paleontology*, **33**(5), 1100–1119.

Vidal, N., & David, P. (2004). New insights into the early history of snakes inferred from two nuclear genes. *Molecular Phylogenetics and Evolution*, **31**(2), 783–787.

Vidal, N., Delmas, A.-S., & Hedges, S. B. (2007). The higher-level relationships of alethinophidian snakes inferred from seven nuclear and mitochondrial genes. In *Biology of the Boas and Pythons*, Eagle Mountain Publishing, pp. 27–33.

Vidal, N., & Hedges, S. B. (2002). Higher-level relationships of caenophidian snakes inferred from four nuclear and mitochondrial genes. *C. R. Biologies*, **325**, 987–995.

Wake, M. H. (1993). The skull as a locomotor organ. In J. Hanken & B. K. Hall, eds., *The Skull: Functional and Evolutionary Mechanics*, Chicago: University of Chicago Press.

Walls, G. L. (1940). Ophthalmological implications for the early history of the snakes. *Copeia*, **1940**(1), 1–8.

Watanabe, A., Fabre, A.-C., Felice, R. N., … Goswami, A. (2019). Ecomorphological diversification in squamates from conserved pattern of cranial integration. *Proceedings of National Academy of Sciences*, **July**, e201820967.

Wiens, J. J., Brandley, M. C., & Reeder, T. W. (2006). Why does a trait evolve multiple times within a clade? Repeated evolution of snakelike body form in squamate reptiles. *Evolution*, **60**(1), 123–141.

Wiens, J. J., Hutter, C. R., Mulcahy, D. G., … Reeder, T. W. (2012). Resolving the phylogeny of lizards and snakes (Squamata) with extensive sampling of genes and species. *Biology Letters*, **8**(6), 1043–1046.

Wiens, J. J., Kuczynski, C. A., Smith, S. A., … Reeder, T. W. (2008). Branch lengths, support, and congruence: Testing the phylogenomic approach with 20 nuclear loci in snakes. *Systematic Biology*, **57**(3), 420–431.

Wiens, J. J., Kuczynski, C. A., Townsend, T., Reeder, T. W., Mulcahy, D. G., & Sites, J. W. (2010). Combining phylogenomics and fossils in higher-level squamate reptile phylogeny: Molecular data change the placement of fossil taxa. *Systematic Biology*, **59**(6), 674–688.

Wilson, J. A., Mohabey, D. M., Peters, S. E., & Head, J. J. (2010). Predation upon hatchling dinosaurs by a new snake from the Late Cretaceous of India. *PLoS Biology*, **8**(3). doi:10.1371/journal.pbio.1000322.g001

Yi, H. (2022). Using Adaptive Traits in the Ear to Estimate Ecology of Early Snakes. In D. J. Gower & H. Zaher, eds., *The Origin and Early Evolutionary History of Snakes*, Cambridge: Cambridge University Press, pp. 271–293.

Yi, H., & Norell, M. A. (2015). The burrowing origin of modern snakes. *Science Advances*, **1**(10), e1500743–e1500743.

Zaher, H. (1998). The phylogenetic position of *Pachyrhachis* within snakes (Squamata, Lepidosauria). *Journal of Vertebrate Paleontology*, **18**(1), 1–3.

Zaher, H., Apesteguía, S., & Scanferla, C. A. (2009). The anatomy of the upper cretaceous snake *Najash rionegrina* Apesteguía & Zaher, 2006, and the evolution of limblessness in snakes. *Zoological Journal of the Linnean Society*, **156**(4), 801–826.

Zaher, H., & Rieppel, O. (2002). On the phylogenetic relationships of the Cretaceous snakes with legs, with special reference to Pachyrhachis problematicus (Squamata, Serpentes). *Journal of Vertebrate Paleontology*, **22**(1), 104–109.

Zaher, H., & Scanferla, C. A. (2012). The skull of the Upper Cretaceous snake *Dinilysia patagonica* Smith-Woodward, 1901, and its phylogenetic position revisited. *Zoological Journal of the Linnean Society*, **164**(1), 194–238.

Zheng, Y., & Wiens, J. J. (2016). Combining phylogenomic and supermatrix approaches, and a time-calibrated phylogeny for squamate reptiles (lizards and snakes) based on 52 genes and 4162 species. *Molecular Phylogenetics and Evolution*, **94**, 537–547.

Chapter 2: Alternate phylogenetic positions of fossils affects body size estimates in snakes

Abstract

Attempts to understand the evolution of snakes have primarily concerned the specific ecological habitat that influenced the evolution of the elongate limbless or limb-reduced snake body form. The debate surrounding this potential ecological origin concerns whether the snake body form represents an adaptation to either an aquatic ecology (the 'aquatic hypothesis') or a sub-terranean burrowing ecology (the 'fossorial hypothesis'). Evidence for either side of this debate has used morphological or lithological datasets, but to date no researcher has considered body size trends. In vertebrates, reduction in body size often accompanies a transition to fossorial habits (Lee 1998). However, despite fossoriality being a proposed ecology influencing the early evolution of snakes, the body size at the origin of snakes has not been investigated. To understand body size evolution in snakes using both fossil and extant taxa and to determine whether modelling body size evolution provides greater support to the competing hypotheses of snake ecological origins, I performed ancestral state reconstructions under three different phylogenetic hypotheses of fossil taxa, and using only extant taxa. I estimated rates of body size evolution for the different topologies using BayesTraits, comparing random walk Brownian motion with various tree transformations: delta, kappa, lambda, and variable rates, to find the best fitting model of evolution. I also compared estimates from ancestral state reconstructions with body size estimates of fossil snakes estimated from regression models of isolated vertebrae. The addition of fossils to ancestral state reconstructions greatly increased the estimated body size for the crown snake ancestor, resulting in an estimate of at least double to the estimate recovered when using extant taxa only. The best fit model of body size evolution was consistent across all tested topologies, with the kappa tree transformation model to be the best fit. When comparing estimates from ancestral state reconstructions with estimates from fossil vertebrae regression models, the topologies that included fossil snakes as either stem alethinophidians or both stem snakes and stem alethinophidians were more concordant with fossil estimates. These results do not support the hypothesis that the marine Simoliophiidae are representative of stem snakes, and instead supports the hypothesis that early snake evolution took place in terrestrial environments, with subsequent adaptations to different habitats, including marine ecologies during the Cenomanian. These results also confirm the importance of including fossils in ancestral state reconstructions, even when the precise relationship of fossils to extant clades is uncertain.

1. Introduction

Snakes are a speciose clade of squamates that occupy a wide range of ecologies, encompassing terrestrial, arboreal, aquatic (including both freshwater and marine), and fossorial habits and habitats. Despite this high diversity of habitat preferences seen in extant species, the ecological context of snake origins remains unclear, with conflicting hypotheses posed for the ecological origins of early snakes including fossorial (Tchernov *et al.* 2000; Yi & Norell 2015), aquatic (Caldwell & Lee 1997; Lee 2005), semi-aquatic (Palci *et al.* 2017), terrestrial (Scanlon & Lee 2000), and surface-terrestrial to fossorial in crown snakes (Da Silva *et al.* 2018). These conflicting hypotheses are a result of various interpretations of morphological and lithological datasets, which have resulted in the contention between these alternate ecological contexts of the evolution of the snake body form. The phylogenetic relationships between snakes varies whether using morphological or molecular datasets, which then affects interpretations of the relationships between fossil taxa and extant clades.

The incongruence of molecular and morphological phylogenies in squamates is well-documented (Streicher & Wiens 2016). The discrepancies between these topologies have often been placed on the problems surrounding morphological convergence in primarily fossorial taxa which tends to mask true phylogenetic morphological signals (Cundall & Irish 2008; Lee 1998). These features have historically led to the grouping of snakes with the elongate snake-like fossorial lizard clades such as amphisbaenians and dibamids (Gauthier *et al.* 2012). Internally, the topology of the Serpentes tree obtained from morphological data resulted in the interpretation of snake skull evolution as an increase in complexity of the skull from the small-gaped fossorial taxa such as *Anilius scytale* leading to the wide-gaped snakes, Macrostomata (Gauthier *et al.* 2012). With molecular phylogenies, there are significant changes for the internal topology of the snake tree. Scolecophidia, sister clade to Alethinophidia, while consistently recovered as a monophyletic group from morphological characters (Conrad 2008; Gauthier *et al.* 2012; Romer 1956), are paraphyletic as the stemward most extant snakes in most molecular analysis (Hsiang *et al.* 2015; Pyron *et al.* 2013; Reeder *et al.* 2015; Streicher & Wiens 2016; Wiens *et al.* 2012; Zheng & Wiens 2016). Consequently, the phylogenetic position of many fossil snakes is also under debate, especially those that retain small hindlimbs such as *Eupodophis descouensi* (Rage & Escuillié 2000), *Najash rionegrina* (Zaher *et al.* 2009), and *Pachyrhachis problematicus* (Caldwell & Lee 1997), which have variably been considered to be stem snakes, nested within extant snakes as stem alethinophidians or stem macrostomatans (Caldwell *et al.* 2015; Conrad 2008; Gauthier *et al.* 2012; Rage & Escuillié 2003; Scanlon & Lee 2000; Wiens *et al.* 2010; Wilson *et al.* 2010; Zaher & Scanferla 2012). These alternate positions could have

significant effects on estimates of body size in snakes, particularly for estimates of the body size of the hypothetical snake ancestor.

With these conflicting topologies of snake relationships as context, various morphological evidence has been proposed for the competing hypotheses of the ecological context of snake origins. The anatomy of the snake eye has been variously suggested to support either the aquatic or fossorial hypothesis. There are several morphological characters of the snake eye that suggests a degeneration and subsequent evolution of visual function. The absence of oil droplets, as well as snake cones being derived from rods (low light detecting), in addition to the reduction of visual pigments all support a hypothesis of a fossorial ancestor (Simões *et al.* 2015; Walls 1940). However, a flattened cornea, thickened corneal margin, and spherical lens are all features that snakes share with aquatic vertebrates, which supports a hypothesis of an aquatic ancestor (Caprette *et al.* 2004). Further morphological evidence supporting a fossorial ancestral ecology for snakes has included the absence of a sclerotic ring in the snake eye, and the loss of the tympanic middle ear, both of which are characters that correlate with a fossorial ecology in other squamate clades (Atkins & Franz-Odendaal 2016; Berman & Regal 1967; Rieppel 1988). Further support for a marine ancestral ecology is a proposed sister clade relationship with Mosasauroidea, extinct aquatic squamates that form an monophyletic clade, due to similarities in skull morphology between mosasaurs and snakes (Caldwell 1999; Lee 1997; Lee & Caldwell 2000). While these various morphological characters have been debated in the context of the most probable ancestral snake ecology, currently body size has not been investigated either in extant snakes or in the snake fossil record.

Alternate hypothesis for the ecology of the ancestral snake have different predictions for the effect on snake body size. The fossorial hypothesis of snake origins is complicated by the suite of characters which appear to evolve concurrently with a transition to a fossorial lifestyle, which therefore pose the risk of confusing accurate reconstructions of relationships due to the presence of homoplasy. One of the trends seen in head-first burrowing non-snake squamates is a reduction in body size (Lee 1998). However, interpretation of a reduction in body size is difficult in the context of the overall elongation of the body in snakes relative to lizards. Elongation of the body is also a recurring pattern of body form evolution in fossorial squamates, along with the reduction of digits and limb-loss (Wiens *et al.* 2006; Wiens & Slingluff 2001). Regarding a transition to a marine ecology there is no predicted change in overall body size. Studies into extant snakes, particularly clades such as Elapidae that include both terrestrial members and two clades of marine snakes, show that the cross-sectional body shape of aquatic snakes changes from circular to dorso-ventrally elongated, ie. aquatic species have a higher and taller body than terrestrial species (Brischoux & Shine 2011). Elongation in terrestrial squamates has been shown to also occur for 'grass-swimming', an efficient locomotion style

through long, dense grass (Wiens *et al.* 2006). Terrestrial grass-swimming elongate squamates tend to have relatively longer tails than fossorial elongate squamates (Wiens *et al.* 2006). Examining the traits that are linked to both fossorial, aquatic, and terrestrial lifestyles as well as overall snake evolution is of vital importance to understanding the early evolution of the snake clade particularly in regards to competing hypotheses of snake origins.

The trait that I have chosen to examine, due to its wide applicability to all snakes and the availability of data for both extant and fossil taxa, is body length as a proxy for total body size. Length is a more consistent body metric for snakes than mass, as due to irregular feeding patterns and large prey sizes, body mass can vary considerably in snakes depending on how recently prey was ingested, particularly in pythonids that are able to consume prey over half their own weight (Slip & Shine 1988). Length is also readily available for most extant taxa, and can be estimated for incomplete fossil specimens, allowing greater coverage of the fossil data.

Ancestral state reconstruction is a technique that can been used to estimate trait values for nodes within extant clades. However, results of ancestral state reconstruction are influenced by which taxa are included in analyses. In addition to the importance of widely sampling extant species across modern clades, the inclusion of fossil data can have a profound effect to both the construction of phylogenies (Donoghue *et al.* 1989) and ancestral state reconstructions of body size (Finarelli & Goswami 2013). Fossil taxa represent unique evolutionary histories, and extinct lineages represent periods of evolution that would not be accounted for when using extant taxa alone. While the snake fossil record is mostly comprised of disarticulated isolated skeletal elements, the distinctive elongate body plan of snakes allows length to be estimated using simple regression models, which allows these taxa to be included alongside the examples of complete or near-complete individuals from which body size can be measured. These fossils allow insight into the early processes of snake evolution. This is of particular importance for snakes due to the presence of the three constituent clades of small bodied Scolecophidia (either as a monophyletic clade or paraphyletic grade) in the early branches of the snake phylogeny. Due to the overall reduced size of lizards compared to snakes, this has the potential to bias ancestral state reconstructions.

To examine the history of body size evolution in snakes, I combine ancestral state reconstruction techniques and evolutionary rate modelling to reconstruct the magnitude, tempo, and mode of body size change in the context of alternate phylogenetic hypotheses. I compare these results from ancestral state reconstructions with the temporal pattern of body size change in the standing fossil record for Cretaceous snakes, to examine the congruence between models of body size evolution and observable histories and what these interpretations mean for the different hypotheses of snake ecological origins.

2. Materials and Methods

2.1 Data collection - Body size estimation

I examined maximum total body length (TBL) as a measure of body size, as it is recorded for nearly all species of extant snake and can be readily estimated from vertebral measurements in the fossil record (McCartney *et al.* 2018). Although body mass is typically used as a measure for body size in vertebrates, for animals such as snakes with an elongate body form, length is more informative. Body mass in snakes varies due to a variety of factors such as recency of last meal, seasonal changes, and reproductive status. Maximum length as a measure is a reportedly good proxy for potential size when dealing with animals of indeterminate growth, and is more readily available than mean sizes (Feldman *et al.* 2016).

I obtained maximum lengths for 1260 extant snake species and 22 outgroup squamate species from the extant squamate body size dataset collected by Feldman et al (2016). This dataset is the result of an extensive literature search and supplemented by measures of live individuals and preserved specimens in natural history museums (Feldman *et al.* 2016). As the body sizes of the large constrictor snakes are often overestimated due to their appeal to humans (Murphy & Henderson 1997), I corrected the body sizes reported by Feldman et al. (2016) of the largest snake species; *Eunectes murinus, Python molurus,* and *Malayopython reticulatus,* to the largest verifiable sizes as reported by Murphy & Henderson (1997): *Eunectes murinus* – 7.315m(24ft), *Python molurus* – 5.972m (19ft), and *Malayopython reticulatus* – 8.659m (28ft 6in).

Full body fossils of snakes are rare in the fossil record, instead the majority of taxa are known from isolated vertebrae. To include body sizes of fossil snakes in ancestral state reconstructions, I obtained the reported body sizes and body size estimates for 12 species of extinct snake from the current literature (see Table 1). Of the 12 specimens sampled, three body sizes came from direct measurements of complete or near complete specimens, for the other nine vertebral width or length was used to estimate total body size. These 12 taxa were included in subsequent ancestral state reconstructions.

I conducted a comprehensive literature search for all snake vertebrae from Cretaceous deposits, which amounted to 113 total individual specimens (See Appendix 1 & 2). I calibrated and measured images of specimens from published papers in ImageJ (v. 1.53e) to obtain cotylar width, and then used these measurements to calculate total length. To compare ancestral state reconstructions with the Cretaceous fossil record, I used the regression models constructed from extant snakes from McCartney et al (2018) to estimate the total body length of fossil

Table 1: Fossil specimens used in ancestral state reconstructions and estimated body sizes reported by literature

Species	**Size (mm)**	**Reference**	**Type of Measurement**
Dinilysia patagonica	1800	(Yi & Norell 2015)	Measurement of MACN-RN 976
Eupodophis descouensi	850	(Rage & Escuillié 2003)	Measurement of almost complete specimen Rh-E.F. 9001
Gigantophis garstini	6900	(Rio & Mannion 2017)	Length estimated using the 20 vertebrae of the syntype CGM C.10022 and the body length model of (Head *et al.* 2009)
Haasiophis terrasanctus	880	(Tchernov *et al.* 2000)	Measurement of HUJ-Pal. EJ 695
Madtsoia madagascariensis	8000	(Laduke *et al.* 2010)	Estimate using the largest vertebral specimen MNHN MAH 8 and method of (McCartney 2008)
Menarana nosymena	2400	(Laduke *et al.* 2010)	Estimate using the partial skeleton holotype UA 9684 and method of (McCartney 2008)
Najash rionegrina	2000	(Albino 2011; Apesteguía 2007)	Estimate using vertebral size of specimen
Pachyrhachis problematicus	1500	(Rage & Escuillié 2003)	Estimate from largest specimen
Simoliophis rochebrunei	1500	(Bardet *et al.* 2008)	Estimated by Sauvage,1880
Wonambi barriei	3000	(Scanlon & Lee 2000)	Estimate based on trunk vertebrae width
Wonambi naracoortensis	6130	(Barrie 1990)	Estimate based on average length of vertebrae and estimated number of vertebrae
Yurlunggur sp.	5000	(Scanlon 2006)	Estimate based on maximum vertebral sizes and a simple proportionality method

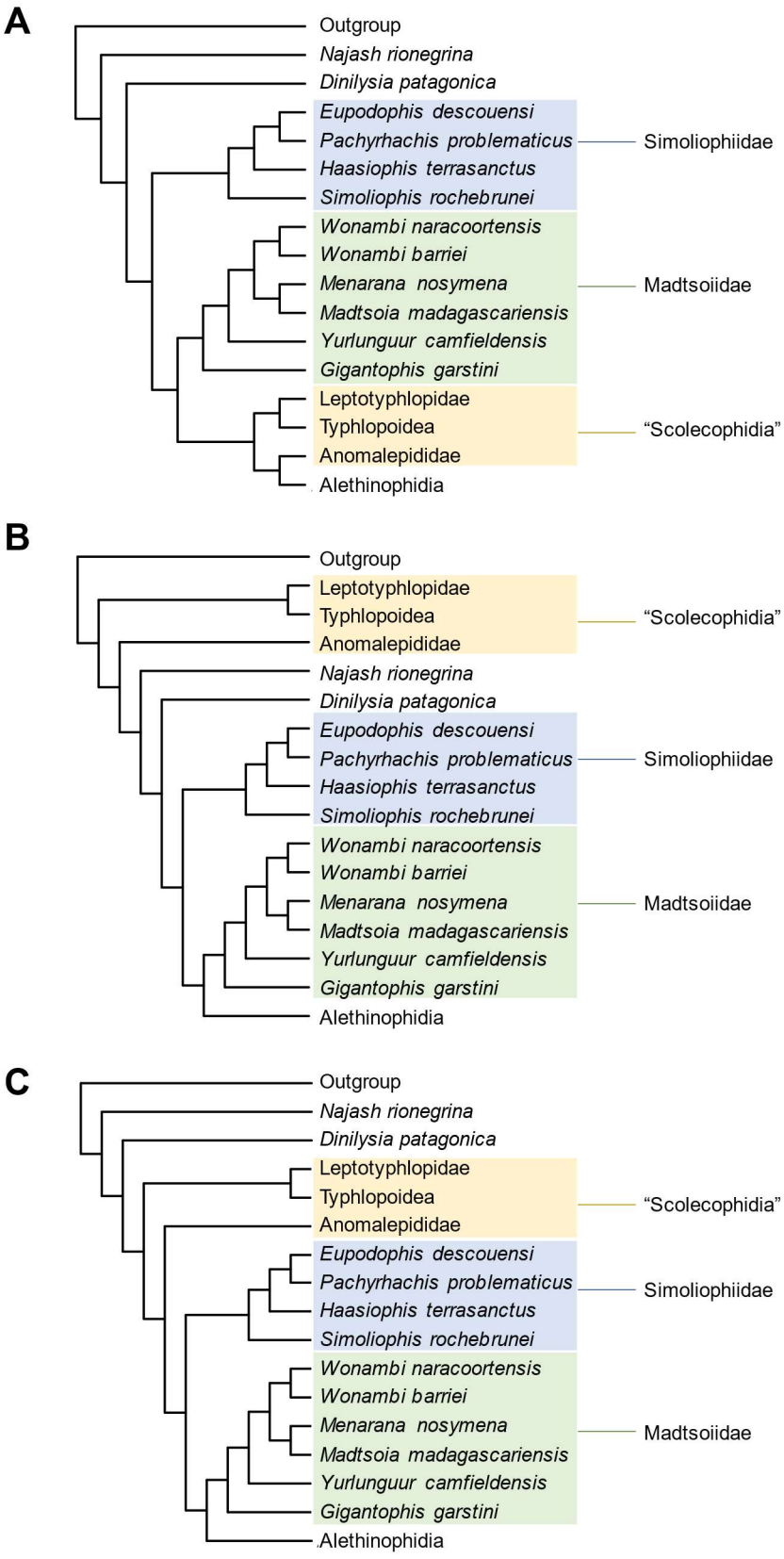

Figure 1: Alternate positions of fossil snakes used in analyses. A. Topology 1 – fossils as stem snakes, B. Topology 2 – fossils as stem Alethinophidia , C. Topology 3 – *Najash rionegrina* and *Dinilysia patagonica* as stem snakes, Madtsoiidae and Simoliophiidae as stem Alethinophidia

snakes from the dimensions of isolated vertebrae. I used the equation calculated by McCartney et al (2018) to estimate body size of 113 fossil snakes from the Cretaceous. This equation estimates body size based on cotylar width using a standard major axis regression of vertebral measurements of 21 extant snakes for which body size is known.
The equation as follows:

$$y = 1.151842x + 5.587911$$

Where x is the natural logarithm of the transverse cotylar width, and y is the natural logarithm of the total length (See Appendix 1).

2.2 Phylogeny Dating

I used the molecular phylogeny reported by Zheng & Wiens (2016) for relationships between extant taxa, as it provides the most comprehensive and most recent dated phylogeny for extant snakes. This phylogeny is constructed using two previously published datasets in an attempt to resolve both higher-level relationships and species-level relationships (Zheng & Wiens 2016). I extracted the Serpentes node and pruned taxa to the species for which body size data was available, consisting of 1260 snake species, with 11 iguanians and 11 anguimorphs as outgroup taxa, for a total of 1282 taxa (see Appendix 3).

Due to the incongruences between phylogenetic topologies recovered using molecular data and those recovered using morphological data, addition of fossils to a molecular phylogeny is difficult to do exactly as reported in the literature as fossil relationships are generally reported using trees constructed with only morphological data. This is due to the conflicting relationships between the 'anilioid' snakes and the Macrostomata. While in phylogenetic hypotheses based on morphological data the macrostomatan snakes appear as a monophyletic group, as are the 'anilioid' snakes (*Anilius*, and Cylindrophiidae), when using molecular data the sister taxa of *Anilius* is recovered as the 'macrostomatan' Tropidophiidae, with the Cylindrophiidae nested within a larger clade that includes both Boidae and Pythonidae. Fossils are unable to be added to trees constructed with molecular data as stem Macrostomata as this clade is no longer recovered, so instead I interpreted fossils recovered as stem Macrostomata in previous morphological analysis as stem Alethinophidia.

I added 12 fossils that have body sizes reported by the literature to the extant phylogeny as reported by Zheng & Wiens (2016) in three alternate positions (See Figure 1). Topology 1: as stem snakes (as reported by: (Apesteguía & Zaher 2006; Caldwell *et al.* 2015; Caldwell & Lee 1997; Rage & Escuillié 2003; Scanlon & Lee 2000)); topology 2: as stem alethinophidians due to aforementioned issue of the macrostomatan clade not being recovered for molecular

phylogenies (fossils nested within Alethinophidia reported by: (Apesteguía & Zaher 2006; Caldwell *et al.* 2015; Rage & Escuillié 2003; Tchernov *et al.* 2000; Vasile *et al.* 2013; Wilson *et al.* 2010; Zaher 1998; Zaher & Rieppel 2002)); topology 3: with *Najash rionegrina* and *Dinilysia patagonica* as stem snakes, and Simoliophiidae and Madtsoiidae as stem alethinophidians (as reported by: (Gauthier *et al.* 2012)) (See Figure 1). I could not include the proposed topology by (Reeder *et al.* 2015) as they recovered the taxa: *Eupodophis descouensi, Haasiophis terrasanctus,* and *Pachyrhachis problematicus*, as stem Tropidophiidae. Given that the divergence age of this clade from *Anilius scytale* in the Zheng & Wiens (2016) analysis is reported as 79.81 mya, which is younger than many fossil appearances of Madtsoiidae and Simoliophiidae, this topology could not be accounted for in the current analysis. Fossils were added to all three topologies as separate branches with *Najash* as the oldest snake as recovered by: (Gauthier *et al.* 2012; Zaher *et al.* 2009; Zaher & Scanferla 2012), the relationships between the madtsoiids as reported by Vasile et al (2013), and the relationships between simoliophiids as reported by Apesteguia & Zaher (2006).

As the age of the internal nodes reported in Zheng & Wiens (2016) are much older than the ages of the fossils, the proposed divergence points of fossil lineages had to be estimated. To date the fossil branches before adding to the molecular informed topology I implemented the 'equal-branch length' method first described by Brusatte *et al.* (2008) using the 'DatePhylo' function from the R package 'strap' (Bell & Lloyd 2015). This function first dates the tree using a basic method where each internal node is the age of its oldest descendent, and then works tip-to-root to assign a share of the time available from the first directly ancestral branch of positive length to any zero length branches encountered, as first implemented by Ruta *et al.* (2006). The size of share used in the 'equal branch' method is equal amount of sharing. This method avoids zero-length branches, which would hinder future analysis on the tree. Once divergence dates were estimated, these branches were manually added to the total Serpentes tree from Zheng & Wiens (2016), in the three alternate topologies.

2.3 Ancestral State Reconstructions

I conducted ancestral state reconstructions using the 'fastAnc' function from the 'phytools' package in R (Revell 2012). This function estimates the maximum likelihood ancestral states for a continuous trait by using Felsenstein's (1985) contrasts algorithm (Felsenstein 1985). This function takes advantage of the fact that when the contrasts algorithm computes the state for the root node, this is also the maximum likelihood estimation for that node. Therefore, this function reroots the tree at all internal nodes and computes the contrasts state at the root each time, which provides the estimates for the ancestral state at each internal node of the tree

(Revell 2012). I ran ancestral state reconstructions for all four topologies using the whole tree from Zheng & Wiens (2016) and the alternate hypothesis of fossil relationships, to estimate body size at ancestral nodes of clades of interest: Scolecophidia *sensu stricto* as per (Miralles *et al.* 2018) (Leptotyphlopidae and Typhlopoidea), Alethinophidia (all extant snakes excluding Typhlopoidea, Leptotyphlopidae, and Anomalepididae), Amerophidia (Tropidophiidae and Aniliidae), Afrophidia (all Alethinophidia excluding Amerophidia), Leptotyphlopidae, Typhlopoidea (Typhlopidae, Xenopeltidae, and Gerrhopilidae as per Miralles et al, 2018), a clade comprising Cylindrophiidae, *Anomochilus* and Uropeltidae, Pythonidae including *Xenopeltis* and *Loxocemus*, Pythonidae, and Boidae. All ancestral state reconstructions used raw body size data.

I compared estimates of body size at ancestral nodes from the four ancestral state reconstructions with estimated body sizes from vertebral measurements of fossils (see section 2.1). I compared the maximum size of fossils at each of the ages within the Cretaceous with corresponding maximum size estimated from ancestral state reconstructions using sum of least squares. I transformed data into comparable datasets using the smooth.spline function in R to fit a cubic smoothing spline, and used the predict function to generate a set of comparable datapoints. I used sum of least squares to compare which of the four ancestral state reconstruction models most closely aligned with estimates of body size from vertebral measurements of fossils.

2.4 Evolutionary Modelling

I quantified rates of body size evolution using BayesTraits version 3, with the random walk Brownian motion model fitted as a null hypothesis, using independent contrasts. To save computational time for variable rates models, I pruned the trees used for the ancestral state reconstructions to reduce number of extant species, removing the speciose clades Viperidae and Colubroidea. The resulting tree after this pruning totalled 341 species for the extant tree and 353 species for the trees including fossils. I then ran evolutionary rate models for the extant tree, and the three alternate hypotheses of fossil placement. All body size data was log normalised before being run through BayesTraits analysis. Log normalising data is standard for body size rates of evolution analysis, as it reduces the over-weighting of large-bodied animals (Benson *et al.* 2022; Haldane 1949).

I compared several different models of the rate of body size evolution, with the random walk model fitted as the null. A number of tree transformations can also be implemented in BayesTraits: Delta, Kappa, and Lambda. Delta transformation scales overall path lengths (distance from root to tip) in a phylogeny, this detects whether the rate of trait evolution has accelerated or slowed over time. Kappa transformation differentially stretches or compresses

individual phylogenetic branch lengths, this tests for punctuated versus gradual mode of trait evolution. The lambda parameter detects whether the phylogeny correctly predicts the patterns of covariance among species of a given trait, to examine if a trait is evolving independently. These different tree transformations were implemented by allowing BayesTraits to estimate the value of Delta, Kappa, and Lambda. Rate models were fitted using 10,100,000 iterations and a burn-in of 100,000. Variable rates models, as they take longer to converge, were fitted using 50,050,000 iterations and a burn-in of 50,000. I compared the null model of random walk with other models (Delta, Kappa, Lambda, and Variable Rates) using a Bayes Factor test, using the marginal likelihoods calculated using stepping-stone sampling with 500 stones for 10,000 iterations. I conducted post processing on all the BayesTraits analysis except variable rates models using the BTRTools package in R. I conducted post processing on variable rates models using the PPPostProcess tool available from www.evolution.reading.ac.uk/VarRatesWebPP/.

3. Results

3.1 Ancestral State Reconstructions

The estimated body size at ancestral nodes varies considerably dependent on the topology used. Estimates for the body size of Serpentes crown node, as well as three major clades of snakes recovered from phylogenies constructed with molecular data: Alethinophidia, and it's subdivisions Amerophidia (Aniliidae and Tropidophiidae) and Afrophidia (all other Alethinophidia) all show substantial variation. When including extant taxa only, the Serpentes node is estimated at 48cm. When adding fossils, the size of the ancestral snake state increases to over double the estimate from using extant taxa only (see Table 2). For topology 1, where fossil snakes are included as stem snakes, the Serpentes node is estimated at 126cm, the largest estimated size for all topologies. Body size estimate of the Serpentes node also increases when most or all fossils are included as stem alethinophidians, nested within snakes, at 102cm for topology 2 and 119cm for topology 3. The estimate of body size for the Alethinophidia node is again smaller for the extant only topology, with a total body length of only 93cm, and increases with addition of fossils. For topology 1, the Alethinophidia node is now an estimated 112cm, which increases to 158cm for topology 2 and 162cm for topology 3. Therefore, the largest estimate for alethinophidian ancestral body size is calculated when *Najash rionegrina* and *Dinilysia patagonica* are included as stem snakes, and Madtsoiidae and Simoliophiidae are included as stem alethinophidians. Body size estimates for the ancestral node of Typhlopoidea + Leptotyphlopidae also increased with the addition of fossils. Using extant taxa only, the ancestor

for this clade is estimated at 44cm. This estimate increases to 108cm for topology 1, 88cm for topology 2, and 102cm for topology 3. Within Typhlopoidea + Leptotyphlopidae, the body size estimates for the ancestral Leptotyphlopidae are 30cm for extant only, 50cm for topology 1, 44cm for topology 2, and 48cm for topology 3. The body size estimates for the ancestral Typhlopoidea are similar to that of Leptotyphlopidae, 32cm for extant only, 52cm for topology 1, 46cm for topology 2, and 50cm for topology 3. For Anomalepididae, the clade of Scolecophidia that Zheng & Wiens (2016) recovered as sister to Alethinophidia, there is also a considerable increase in the estimate of body size from extant to the addition of fossils. Extant only data recovers a body size estimate for the anomalepidid ancestral node as 28cm, whereas addition of fossils recovers a body size estimate of 42cm for topology 1, 40cm for topology 2, and 43cm for topology 3. For both Leptotyphlopidae and Typhlopoidea, the largest body size estimate was recovered for topology 1, whereas the largest body size estimate for Anomalepididae was for topology 3.

For the divisions within Alethinophidia, the results are similar to that recovered for the total clade. When using extant only, body size at the ancestral node of Amerophidia is estimated at 89cm and body size at the ancestral node of Afrophidia is estimated at 101cm. For topology 1, the estimate of body size at the ancestral node of Amerophidia increases to 103cm and the body size at the ancestral node of Afrophidia increases to 114cm, increases of over 10cm in both nodes compared to using extant only. For topology 2 and 3 there are further increases of estimates, estimate of body size at the ancestral node of Amerophidia increases to 137cm and 140cm respectively, and the estimate of body size at the ancestral node of Afrophidia increases to 146cm and 149cm respectively. Both of these topologies share Madtsoiidae and Simoliophiidae as stem alethinophidians, and only differ in position of *Najash rionegrina* and *Dinilysia patagonica*, which are stem alethinophidians in topology 2 and stem snakes in topology 3.

There are also changes in estimates of ancestral nodes of early diverging clades within Afrophidia. The clade comprising Cylindrophiidae (including *Anomochilus*) and Uropeltidae is estimated at a body size of 67cm for extant only taxa, and for fossils the estimate ranges from 68cm for topology 1, 71cm for topology 2, to 72cm for topology 3. For the clade that includes Pythonidae and the two closely related monotypic taxa *Xenopeltis unicolor* and *Loxocemus bicolor*, the body size estimate of the ancestral node is 178cm using extant only. The addition of fossils in topology 1 decreases the estimate of body size to 174cm. For topology 2 and 3, body size estimate increases to 179cm. For Pythonidae, extant only data recovers a body size estimate of 354cm. The addition of fossils decreases the estimate of body size to 333cm for topology 1, and 334cm for topologies 2 and 3. For Boidae, extant only data recovers a body size

Table 2: Estimates of TBL (total body length) at ancestral nodes from ancestral state reconstructions using extant only, and the three topologies of fossil snakes. Size in mm.

Clade	Extant	Topology 1	Topology 2	Topology 3
Serpentes	478.1	1257.8	1018.7	1186.7
Alethinophidia	926.2	1121.5	1577.6	1619.9
Typhlopoidea + Leptotyphlopidae	438.0	1075.2	879.8	1017.1
Amerophidia	891.6	1034.5	1368.3	1399.2
Afrophidia	1007.4	1141.2	1463.8	1493.7
Leptotyphlopidae	302.2	496.3	436.8	478.6
Typhlopoidea	323.8	517.7	458.2	500.0
Anomalepididae	280.2	417.5	401.3	430.6
Cylindrophiidae+ Uropeltidae	671.5	678.6	712.8	715.9
***Xenopeltis* + *Loxocemus* +Pythonidae**	1779.1	1739.5	1788.5	1793.1
Pythonidae	3544.9	3331.4	3336.2	3336.7
Boidae	2380.0	2284.1	2288.5	2288.9

estimate of 238cm. The addition of fossils, as with Pythonidae, decreases the estimate of body size to 228cm for topology 1, and 229cm for topologies 2 and 3.

3.2 Rate of Evolution

Comparing models of the rates of evolution when modelled using random walk showed no change for which model best fits body size data. For all topologies, the kappa-transformed random walk model was the best fit model of rate of body size evolution (See Table 3). This kappa parameter tests for punctuational vs gradual evolution. Estimated kappa values for all topologies were similar (0.24 – extant, 0.27 – topology 1, 0.24 – topology 2, 0,28 – topology 3). A kappa value of less than 1 is interpreted as stasis in longer branches, and implies that changes in body size rate of evolution in snakes is concentrated on shorter branches.

The variable rates models detected rate shifts at particular points of trait evolution. Some of these shifts were consistent in all topologies, including extant-only (See Figure 2-5). Within Scolecophidia, there is an increase in the rate of trait evolution within the Afrotyphlopinae clade, on the branch that leads from *Afrotyphlops obtusus* to the remaining *Afrotyphlops* species. There is also an increase in the rate of evolution within Typhlopinae, particularly an increase in the rate of evolution in the clade including *Typhlops arator – Typhlops*

notorachius, and *Typhlops platycephalus – Typhlops richardi*. Within Alethinophidia, there are several increases in the rate of trait evolution. There is an increase within Tropidophiidae, with *Tropidophis* having a higher rate of trait evolution than *Trachyboa*. There is also an increase in the Pythonidae, with a further increase of trait evolution in the large Pythonidae, including *Malayopython reticulatus*, *Simalia amethistina, Antaresia perthensis,* and *Antaresia stimsoni.* Within Boidae, there are increases in trait evolution on the branches that lead to the Madagascan genera *Sanzinia* and *Acrantophis*, with further increases for *Acrantophis.* There is also an increase in the clade including *Boa, Corallus, Epicrates, Eunectes,* and *Chilabothrus*, with further increases in the *Chilabothrus*. Finally, within Pareadae, there is an increase on the clade leading to *Pareas hamptoni, Pareas carinatus*, and *Pareas nuchalis*, with a further increase in rate of trait evolution in the latter two species.

The different topologies of fossils change how an estimated variable rate of trait evolution is modelled on internal nodes. When using extant taxa only, the rate of trait evolution stays stable from the lizard outgroup to Scolecophidia, only increasing slightly in the branch leading to Alethinophidia. For topology 1, this pattern changes considerably. There is an increase in the rate of trait evolution from lizards to the ancestral node of all snakes. The rate of evolution then returns to low, before increasing again on the branch that leads to Madtsoiidae and the branch that leads to Alethinophidia (See Figure 2). For topology 2, there is a small increase in the rate of trait evolution at the ancestral node of snakes, with a further increase on the branch leading from Anomalepididae to the fossil snakes (See Figure 3). The rate of evolution then returns to the level of the first increase, which is consistent across most internal branches for Alethinophidia. For topology 3, there is a small increase in the rate of trait evolution at the ancestral node of snakes, and also a small increase leading to Leptotyphlopidae and Typhlopidae (See Figure 4). As in topology 2, there is also an increase in rate of evolution on the branch leading from Anomalepididae to the fossil snakes. As in topology 1, there is also an increase in rate of evolution on the branch that leads to Madtsoiidae.

Table 3: Log Bayes Factors of estimated rate of evolution for delta-transformed, kappa-transformed, and lambda-transformed trees compared to random walk for each phylogenetic hypothesis. Estimated mean parameter in brackets.

Model	Extant	Topology 1	Topology 2	Topology 3
Delta	13.36 (2.68)	3.64 (1.20)	5.01 (2.10)	8.05 (1.95)
Kappa	274.18 (0.24)	270.83 (0.27)	275.22 (0.24)	266.44 (0.28)
Lambda	253.20 (0.90)	250.49 (0.94)	247.22 (0.94)	245.12 (0.94)
Best Model	Kappa	Kappa	Kappa	Kappa

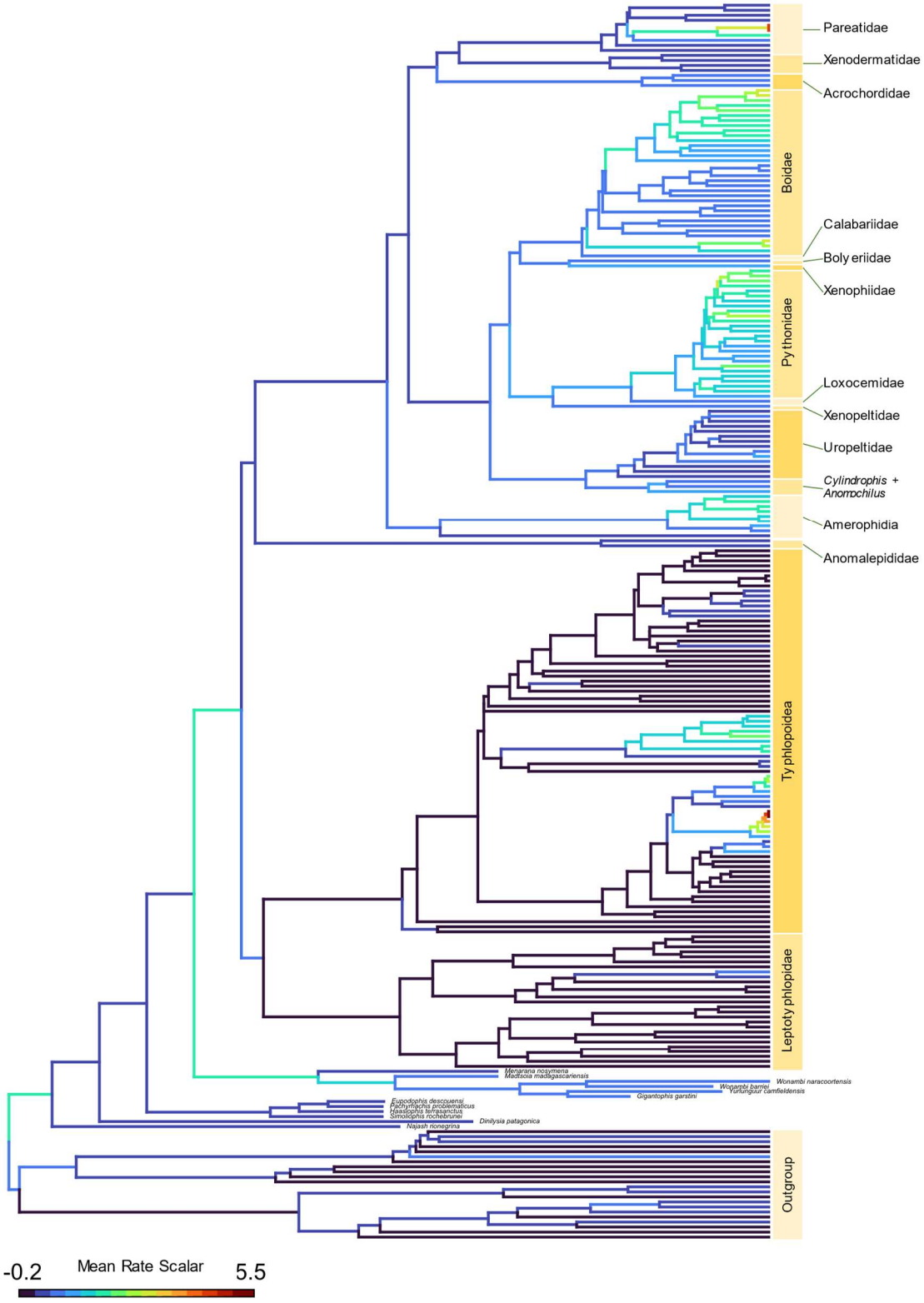

Figure 2: Estimation of rates of body size evolution on time calibrated phylogeny using variable rates model of evolution. Fossils in topology 1, as stem snakes.

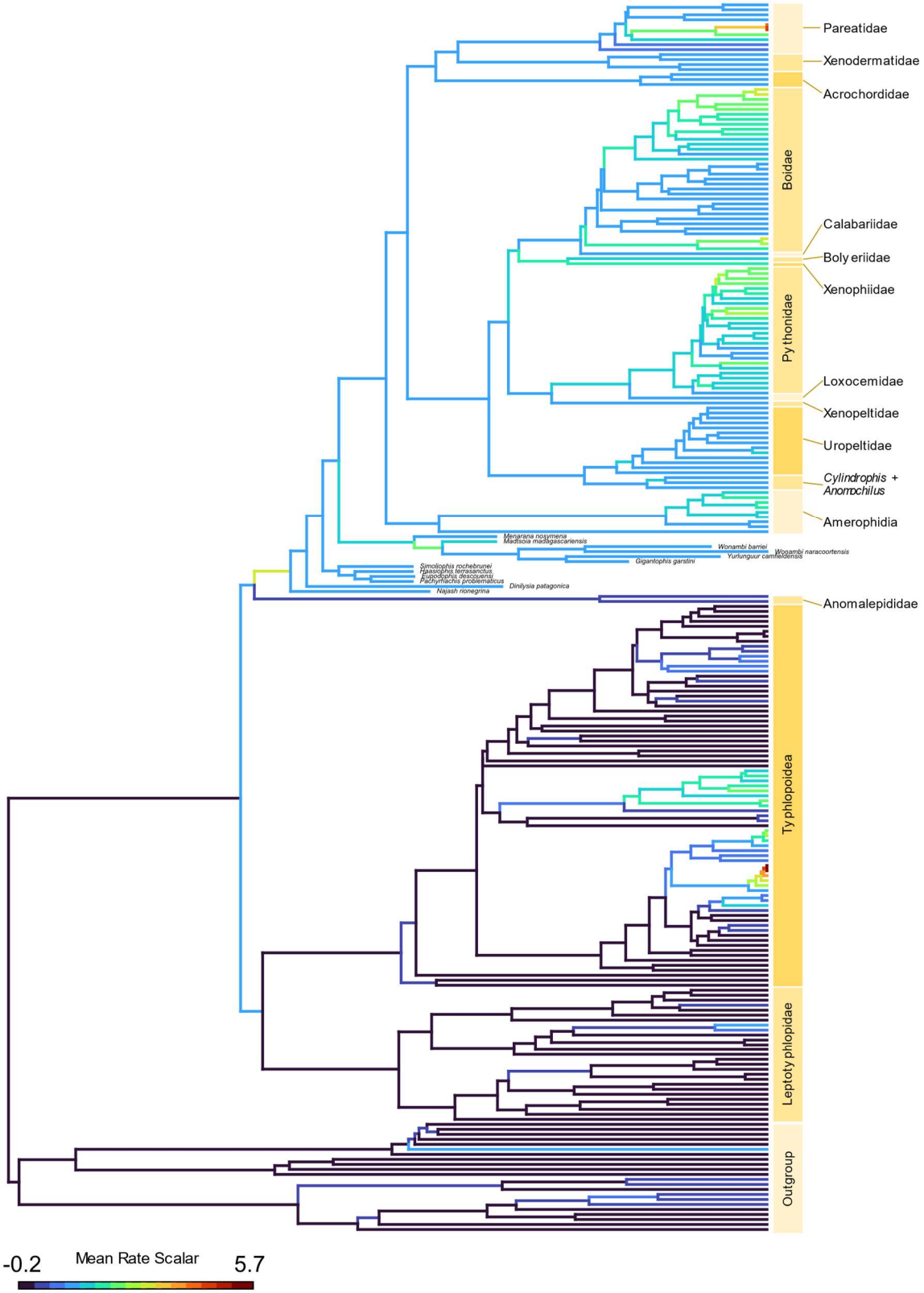

Figure 3: Estimation of rates of body size evolution on time calibrated phylogeny using variable rates model of evolution. Fossils in topology 2, as stem alethinophidians

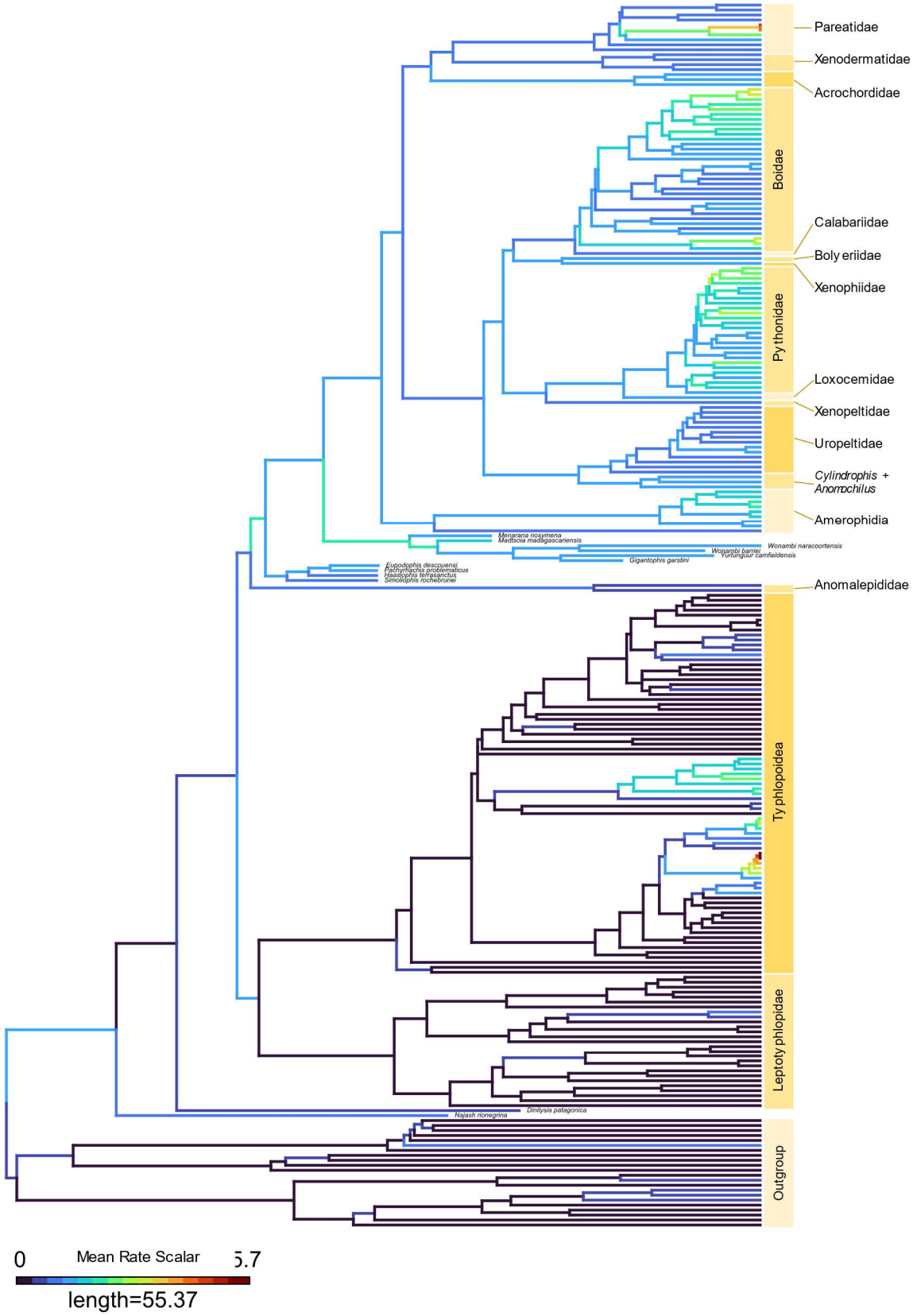

Figure 4: Estimation of rates of body size evolution on time calibrated phylogeny using variable rates model of evolution. Fossils in topology 3, *Najash rionegrina* and *Dinilysia patagonica* as stem snakes, all others as stem alethinophidians.

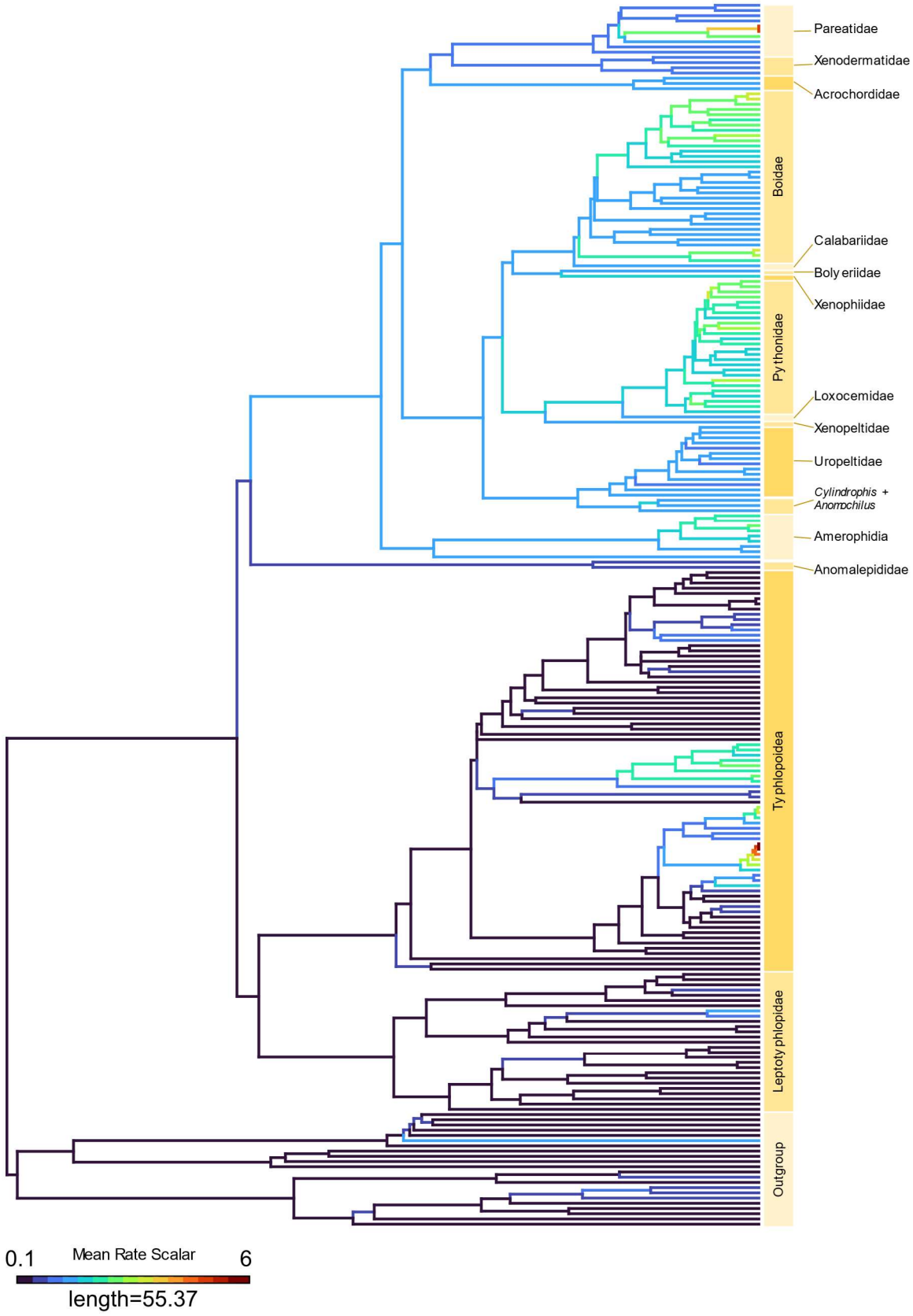

Figure 5: Estimation of rates of body size evolution on time calibrated phylogeny using variable rates model of evolution. Extant only.

3.3 Body size estimates from the standing fossil record and comparison with estimates from ancestral state reconstructions

Body size estimates for fossil snakes based on vertebral measurements vary considerably, from under 15cm long to over 8m, with most taxa under 50cm in length (see Figure 6). In the Albian and Cenomanian (113-93.9mya) body size only just exceeds 2m, represented by three *Norisophis begaa* from Africa (Klein *et al.* 2017). The smallest taxa in these time periods are the *Coniophis* sp. specimens, with estimated body sizes of 39-52cm in the Albian, and 47cm in the Cenomanian. The remaining Cenomanian taxa are predominantly members of Simoliophiidae, mostly from European deposits in France, which are estimated to possess body sizes from 55cm to 1.89m (Rage *et al.* 2016). This 1.89m body size for *Simoliophis rochebrunei* estimated from vertebral morphology is larger than the previously reported maximum size for this taxa of 1.5m (Bardet *et al.* 2008). Only two fossil snakes are reported from the Turonian, both of which are *Coniophis* sp. from North America (Nydam 2013). The estimated body size for these taxa is small (31-34cm). Only one fossil snake is reported from the Coniacian, *Dinilysia patagonica* (Caldwell & Albino 2003), estimated at 1.8m as reported in previous studies (Yi & Norell 2015). There is also *Madtsoia* aff. *madagascariensis*, estimated at 4.2m from the In Beceten formation aged to Coniacian-Santonian (Rage 1981). No fossil snakes are reported from only the Santonian.

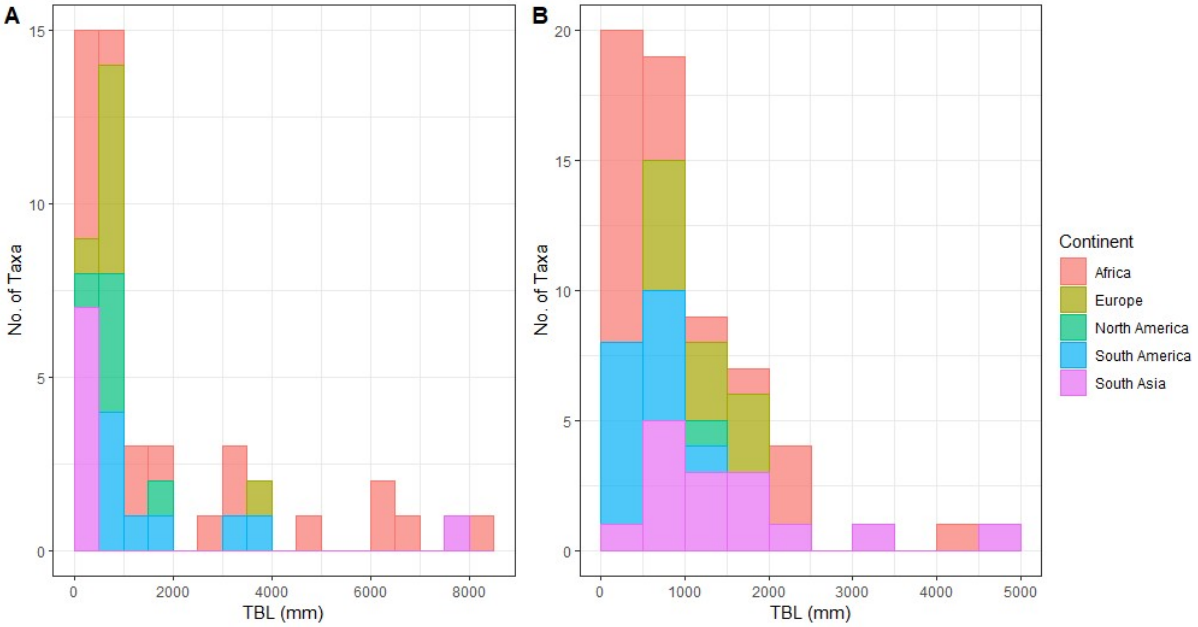

Figure 6: Histogram of total body length in mm of Cretaceous snakes estimated from cotylar width, coloured by continent of origin. A. Maastrichtian, B. Albian-Campanian

In the Campanian, body sizes vary from 11cm to just under 5m. The smallest species are an indeterminate specimen from North America with potential affinity to *Coniophis* (Wick & Shiller 2020), and several indeterminates specimens assigned to Colubridae and *Coniophis* from Africa (Rage & Werner 1999). The largest species at 4.98m and 3.08m are *Dinilysia* sp. from South America (Scanferla & Canale 2007), which also represents the youngest specimen of this genus in the fossil record.

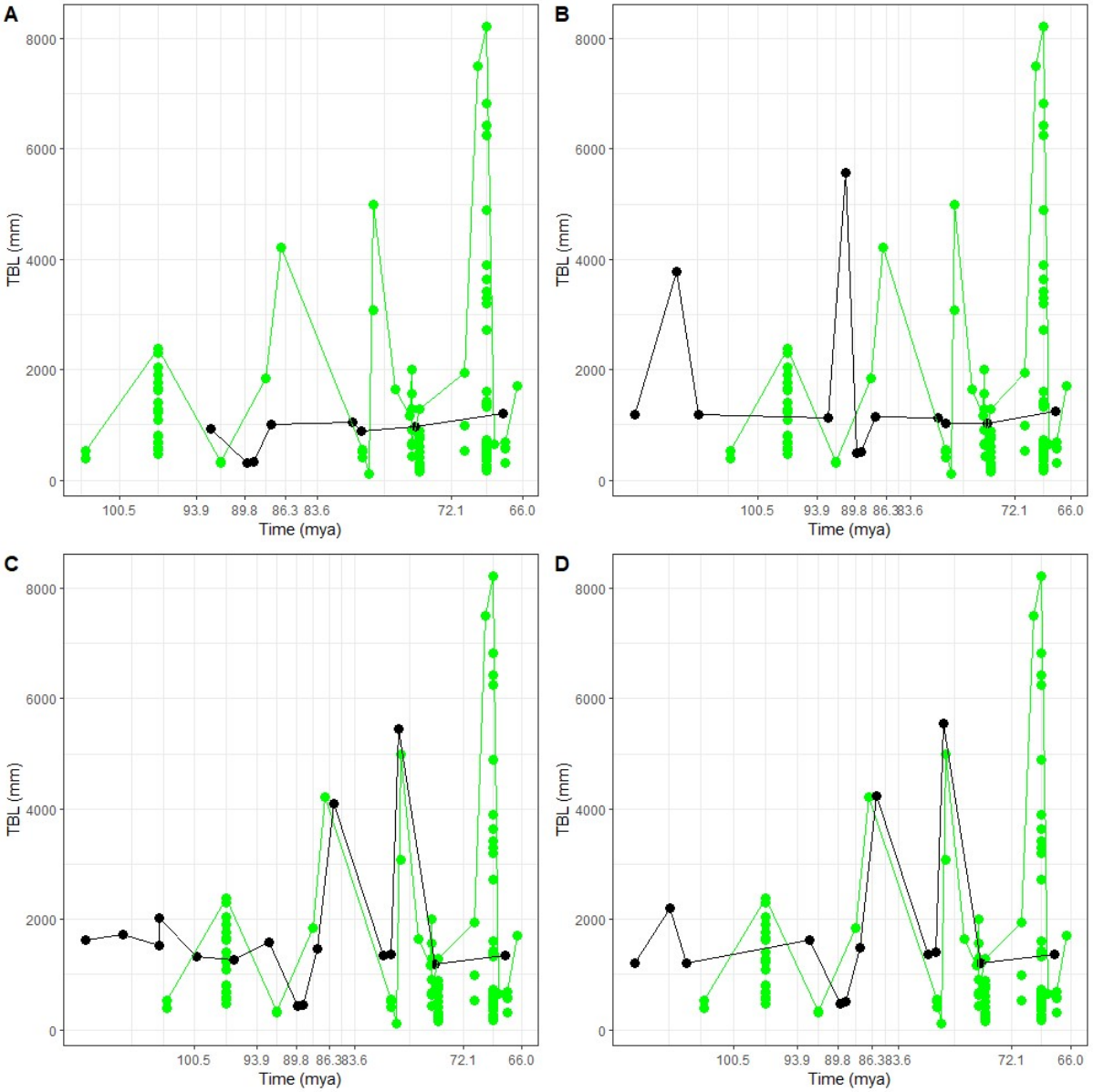

Figure 7: Comparison of total body length (TBL) in mm fossil estimates from isolated vertebrae (green) with ancestral state reconstruction size estimates at nodes (black). Trend line for fossils at maximum size per time period. Ancestral state nodes from 113mya – 66mya (Albian - Maastrichtian), Scolecophidia internal nodes excluded. Length in mm. Tree topology used: A) Extant only, B) Topology 1, C) Topology 2, D) Topology 3

In the Maastrichtian, the size disparity between species is the greatest, with the smallest specimen an estimated 17cm and the largest at 8.2m. The largest taxa in the Maastrichtian are all Madtsoiidae species (*Madtsoia madagascariensis, Madtsoia pisdurensis, Madtsoia laurasiae* and *Eumadtsoia ragei*), with the largest being *Madtsoia madagascariensis* (8.2m) from Africa (Laduke *et al.* 2010). The four largest species represent a global distribution for the large Madtsoiidae by the Maastrichtian, with representatives found in Africa, South Asia, Europe, and South America. The smallest specimen from the Maastrichtian is a Madtsoiidae indet. from South Asia, estimated at a total length of 17cm. The remaining smallest taxa are; *Indophis sahnii* from South Asia (23 to 24cm estimated length) and *Indophis fanambinana* from Africa (27cm estimated length).

Using sum of least squares, the ancestral state size reconstructions using topology 2 (snakes as stem alethinophidians) and topology 3 (*Dinilysia* and *Najash* as stem snakes, the madtsoiids and pachyophiids as stem alethinophidians) most closely aligned with the estimates of body size from fossil vertebrae. The trend of ancestral state reconstructions using topology 2 and 3 also more closely aligns with the trend line of maximum body size of estimates from fossils (See Figure 7).

4. Discussion

4.1 Effects of alternate phylogenetic topologies and addition of fossils to ancestral state reconstructions and models of body size evolution

As expected due to the stemward position of the small Scolecophidia and the relative small size of lizards compared to snakes, the ancestor of snakes when estimated using only extant data was small, estimated at only 48cm. The addition of only 12 fossil snake body size estimates to ancestral state reconstructions greatly increased the estimates of body size of the ancestral snake, which has considerable implications for any ancestral state reconstructions using extant only data. This trend of increased body size in the early diverging snake branches was apparent even when fossils were nested within extant snakes as stem alethinophidians. These results highlight the importance of including fossils even when their relationships to extant taxa are not certain, especially when these fossils potentially represent evolutionary histories that are unrepresented by extant taxa. Ancestral state reconstructions including fossil snakes estimate the crown snake ancestor to be between 102cm to 126cm, a range of body size estimates that are larger than extant scolecophidians. Although the largest taxa within any of the scolecophidian clades, *Afrotyphlops schlegelii* and *Afrotyphlops mucruso,* can reach body lengths of up to 95cm, the majority of extant Scolecophidia are small. The ancestor of the clade which includes all Leptotyphlopidae and Typhlopoidea is estimated at a total length of only 44cm when using extant taxa only. This suggests that the origin of snakes did not include a scolecophidian-like high degree of body size reduction, although does not preclude the possibility of fossoriality as the ancestral ecology of snakes. Fossorial alethinophidians such as *Xenopeltis unicolor* and *Loxocemus bicolor* reach body sizes of over 1m, so the size estimated by the current ancestral state reconstructions does not preclude a fossorial origin for snakes. Instead, the inclusion of fossils in ancestral state reconstructions recovers an evolutionary pattern of increasing body length in the snake stem, preceding a subsequent reduction in overall body size in scolecophidians. This extreme reduction in body size in scolecophidians is potentially a result of adaptation to their distinctive myrmecophagous diet, and the associated skull modifications that occurred concurrently with a more obligately fossorial lifestyle. This scenario matches the trend seen in snake eye evolution. Snakes have a reduced number of opsins than lizards, which implies an adaptation to a low light environment, however fossorial snakes such as Scolecophidia have undergone further loss of visual opsins, which suggests that Scolecophidia are more fossorial than the ancestral snake (Gower *et al.* 2021; Simões *et al.* 2015). The addition of fossils also increases the estimate of the ancestral node of Typhlopoidea

+ Leptotyphlopidae, but the estimated maximum of 50cm is still considerably smaller than estimates for the ancestral node of Serpentes.

When using extant only data, and for topology 2 and 3 with data that includes fossils, the body size estimate at the ancestral node of Alethinophidia increases when compared to the Serpentes node. This increase is approximately 50cm in all three topologies, from 48cm to 93cm for extant only, from 102cm to 158cm for topology 2, and from 119cm to 162cm for topology 3. All three of these scenarios suggest an increase in body length continued to occur subsequent to the initial diversification of snakes. This subsequent increase may be a result of the evolution of a macrostomatan skull structure within Alethinophidia. The macrostomatan skull is characterised by a large gape, usually due to elongation of the supratemporal bone and posterior rotation of the quadrate, which allows macrostomatan snakes to swallow larger prey items than non-macrostomatan snakes (Rieppel 2012). This increase in prey acquisition potential would likely also facilitate the evolution of larger body sizes in snakes. This pattern was found for both scenarios where Madtsoiidae and Simoliophiidae were included as stem Alethinophidia, the former of which achieves considerably large body sizes, for example the largest included in the analysis *Madtsoia madagascariensis* which reaches body sizes of up to 8m (Laduke *et al.* 2010).

The body size estimate for the ancestral node of Typhlopoidea + Leptotyphlopidae also increases with the addition of fossils, with estimates of 108cm, 88cm, and 102cm for topologies 1, 2, and 3 respectively. Interestingly, all of these are around the size or larger than the largest known scolecophidians. This suggests that all three clades, Typhlopoidea, Leptotyphlopidae, and Anomalepididae, all underwent independent reductions in size from a larger ancestor. This is concordant with the disparate jaw architecture in the three clades. While all clades of Scolecophidia are insectivores, with most specialising in a myrmecophagous diet, the three clades differ in which jaw elements facilitate feeding. Typhlopoidea have dentigerous maxilla only, Leptotyphlopidae have dentigerous dentaries only, and Anomalepididae have dentigerous maxilla and a single tooth on each dentary. These disparate jaw architectures, despite a similar diet, support a hypothesis of independent adaptation to myrmecophagy in all three of these clades, a diet which would also support the evolution of body size reduction in snakes where prey is swallowed whole, and where the tongue is primarily a chemosensory organ and can therefore not be co-opted into feeding.

Compared to the ancestral node of Alethinophidia, the body size estimate of the ancestral node of the clade that includes Cylindrophiidae, *Anomochilus*, and Uropeltidae is smaller, at 67cm for extant taxa, and at 68cm, 71cm, and 72cm for topologies 1, 2, and 3 respectively. These taxa are all fossorial, and so this reduction in size relative to the estimate of body size for Alethinophidia is consistent with the hypothesis that adaptation to fossorial habits

cooccurs with reduction in body size (Cundall & Irish 2008; Hanken & Wake 1993; Lee 1998). The clade that unites the fossorial taxa *Xenopeltis unicolor* and *Loxocemus bicolor* with Pythonidae is recovered as relatively large for all ancestral state reconstructions (174cm - 179cm), again implying reduction in body size in both the branch leading to *Xenopeltis unicolor* and in the branch leading to *Loxocemus bicolor*, another instance of reduction in body size as a result of adaptation to fossoriality, although close in size to the largest *X. unicolor* which can reach up to 1.5m (O'Shea 2018). There is a considerable increase of body size estimate at the ancestral node of Pythonidae, with estimates all reaching over 3m (3.54m for extant, 3.33-3.34m for fossils). This is a clade that includes six of the ten largest species of extant snake included in the dataset, including the longest extant snake (*Malayopython reticulatus*). There is also an increase in body size estimate at the ancestral node for Boidae, which includes the second longest snake included in the dataset (*Eunectes murinus*). Large body size is potentially adaptive as snakes that achieve large body size are able to consume a larger range of prey sizes, diversifying diet. This is reflected in studies on extant snakes. A study examining body size evolution in island snakes suggested that snake body size is primarily influenced by the size of prey encountered on islands relative to mainland (Boback 2003). Snakes that change size (either smaller or larger) when adapting to island ecosystems do so as a response to the size of available prey types, particularly seen in the case of colubrids where large size is attained on islands due to predation on nesting seabirds (Boback 2003). The several instances of large body size across snakes, both extant and those examples from the fossil record, perhaps reflect an adaptation to exploit a larger range of prey types. Ecology is not the only predictor of large body size in snakes. In oviparous species, there may be a benefit for females to reach a larger body size, as an increased body size increases the volume of abdominal space to hold the clutch. In viviparous species, there is evidence for a trade-off between body morphology and reproduction. In viviparous garter snakes *Thamnophis marcianus* and *Thamnophis proximus*, there is a marked difference in the trade-off between offspring size and litter size. In the slender species, *T. proximus,* there is a significant negative relationship between number of offspring and size of offspring which gets stronger for smaller females, a relationship that is not seen in the more robust species *T. marcianus* (Ford & Seigel 2015). Therefore there may be a negative relationship between the acquisition of viviparity and reduction in overall body size.

When estimating rates of evolution, all topologies recovered the kappa transformed random walk model to be a better fit of body size evolution than the null model of random walk. The kappa parameter estimated (0.24-0.28) is interpreted as an increase in the rate of evolution on shorter branches relative to longer ones. This may be an artifact of low number of fossils included to break up long internal branches. Breaking up long branches is not always possible,

in particular for the three clades of Scolecophidia where fossils from the Cretaceous are limited to a single specimen (Fachini *et al.* 2020).

Compared to random walk null model, the variable rates model was a better fit, although not as good a fit as the kappa-transformed model. However, using the variable rates model allows shifts in rate of evolution to be detected that reflect changes in body size within snakes. Analyses on all topologies detected an increase on the branches within *Afrotyphlops*, the genus of Typhlopoidea that includes the largest members of Scolecophidia. This increase in the rate of evolution is reflected by an increase in body size relative to the other miniaturised members of this clade. The exact cause of increase in body size in the *Afrotyphlops* lineage has currently not been investigated. It does not appear to be related to diet shifts, as current data suggests that all members of *Afrotyphlops* are still specialised for insectivory, and larger sized species do not consume significantly more prey (Webb *et al.* 2001). Increase in rates of body size evolution is not only limited to clades with increased body size, there is also an increase in the rate of evolution within *Typhlops* in the clade that includes *Typhlops arator* to *Typhlops notorachius,* and the clade that includes *Typhlops platycephalus* to *Typhlops richardi*. This is likely due to these clades consisting of various sized species separated by closely diverging branches. Both of these clades represent diversifications of Typhlopinae onto different islands in the Caribbean, with the former clade found on Cuba, and the latter clade found on the Antilles. The increases in rate of evolution in these clades may also be a response to increased rates of evolution when animals reach previously uninhabited environments such as islands. There are also increases in the rate of evolution within Boidae and Pythonidae that both appear to correspond to the increase in body size in both of these clades. This suggests that the large body size achieved by Boidae and Pythonidae are a result of increases in the rate of evolution.

The four alternate topologies differ in the internal nodes for the variable rates of evolution model. Using extant taxa only, rate of evolution stays stable throughout the early diversification of snakes, only increasing on the branch leading to Alethinophidia. This is inconsistent with the hypothesis that the early evolution of snakes involved elongation of body form and therefore an increase in the rate of evolution of this trait, which would be required for either ecological origins hypothesis. When fossils are added in topology 1, there is an increase in rate of trait evolution in snakes compared to the lizard outgroup, which is more concordant with the hypothesis that the origin of snakes involved a considerable change in body length evolution. For topology 1, there are also increases in both the branch leading to Alethinophidia and the branch leading to Madtsoiidae. These increases in rate of body length evolution are potentially due to further increases in body size in these clades. When fossils are added in topology 2, the increase in rate of trait evolution is still detected at the ancestral node of snakes. This shows that the inclusion of fossils is important to detect early shifts in rates of evolution,

even when the fossils are nested within extant clades. There is also an increase in the rate of evolution in the branch leading from Anomalepididae to the fossil snakes, which likely reflects the relatively small size in anomalepidids compared to fossils and alethinophidians, here an increase in rate of body size evolution is likely linked to a decrease in body size rather than an increase. When fossils are added in topology 3, the relative increase in rate of evolution at the branch that leads from the root to the ancestral node of snakes is less than for topologies 1 and 2, but which still likely reflects the relative increase in body size for snakes when compared to lizards. Interestingly, rate of trait evolution analysis on topology 3 detects an increase in the rate of evolution of the branch leading to the clade comprising Leptotyphlopidae and Typhlopoidea. This likely reflects the decrease in body size of these clades due to their specialisation to fossorial habitats.

4.2 Standing fossil record compared with ancestral state reconstructions

Using vertebral measurements to estimate body length reveals a large diversity of body size attained by snakes in the Cretaceous. The earliest confirmed snake fossils from the Albian are *Coniophis* sp., the largest of which is 52.6cm. This is smaller than ancestral states estimated at these ages for all ancestral state reconstructions. The earliest ancestral states estimated in the Albian (113-100.5mya) are 376.7cm (node age 109mya) for topology 1, 162.3cm (node age 112mya) for topology 2, and 121.6cm (node age 111mya) for topology 3, all of which are larger than the estimated body sizes of Albian *Coniophis* sp. Further discoveries of snake fossils from early Cretaceous deposits may help elucidate the early body size evolution of snakes. Additionally, *Coniophis* likely represents a paraphyletic complex of taxa grouped by plesiomorphic or anilioid characters, and therefore is potentially an early example of snakes reducing in size a result of fossoriality (Fox 1975; Rage *et al.* 2004; Rage 1991).

By the Cenomanian, body size estimates based on vertebral measurements show that snakes already achieve sizes exceeding 2m (*Norisophis begaa*, (Klein *et al.* 2017)). This increase in size exceeds the size estimated from ancestral state reconstructions. While only topology 2 includes nodes that fall within the age range of the Cenomanian, for the other topologies that include fossils, the last Albian node and first Turonian node are similar in estimated TBL. The largest body size estimated for the Cenomanian in topology 2 is 133.1cm (node age 100.3mya), considerably smaller than the estimated size for *Norisophis begaa*.

The earliest estimated node for snakes using extant only data is in the Turonian. This estimate, at 92.6cm (node age 92.7), is much larger than the estimated size of fossils found in this time period (See Figure 7a). This is again likely due to the only fossil snake described from the Turonian being *Coniophis* sp. The estimated sizes during the Turonian for the ancestral state

reconstructions including fossils is considerably larger. Topology 1 recovers a maximum body size of 557.6cm (node age 90.8mya) (See Figure 7b). The estimated sizes for topologies 2 and 3 are smaller than this, but still over a metre in length, with sizes of 157.8cm (node age 92.7mya) and 162.0cm (node age 92.7mya) respectively (See Figure 7c-d).

The Coniacian has an increase in body size estimated from fossil vertebral measurements. The largest snake from the Coniacian-Santonian is *Madtsoia* aff. *madagascariensis* (Rage 1981), estimated at 422cm. This is considerably larger than the ancestral state reconstructions using extant only data, which estimates a maximum size of 100.7cm (node age 87.5mya), or for topology 1, which estimates a maximum size of 114.1cm (node age 87.5mya). Topology 2 and 3 both have larger maximum ages for this time period, 146.4cm (node age 87.5mya) and 149.3cm (node age 87.5mya). Interestingly for these two topologies, there is a node in the early Santonian estimated at over 400cm, 409.3cm (node age 85.8mya) for topology 2 and 424.2cm (node age 85.8mya) for topology 3, which is close to the estimated size of the fossil *Madtsoia* aff. *madagascariensis*.

In the Campanian there is again an increase in body size estimated from fossil vertebral measurements that is reflected by topology 2 and 3. The largest Campanian fossil snake is *Dinilysia* sp. (Scanferla & Canale 2007), estimated at 498.9 cm. The largest ancestral node estimated from the Campanian for extant only is 104.2cm (node age 80.6mya), and for topology 1 is 113.3cm (node age 80.6mya). This is much smaller than the estimated size of *Dinilysia* sp. In contrast, the largest ancestral node estimated from the Campanian for topology 2 and 3 are 545.7cm (node age 79.0mya) and 554.2cm (79.0mya) respectively, which are much closer to size estimated from vertebral measurements.

The largest body sizes for fossil snakes in the Cretaceous are found in the Maastrichtian, with the largest being an 821.7cm *Madtsoia madagascariensis* (Laduke *et al.* 2010). None of the ancestral state reconstructions predict nodes anywhere near this size for the Maastrichtian. For extant only, the largest predicted size is 121.4cm (node age 67.7mya), which is a similar estimated size recovered by topologies 1, 2, and 3, 123.7cm (node age 67.7mya), 134.9cm (node age 67.7mya), and 135.9cm (node age 67.7mya) respectively. The disparities between both methods of ancestral body size estimation show the importance of using multiple sources of data when examining trends in body size evolution over deep time.

5. Conclusion

Comparing trends in body size estimates from ancestral state reconstructions with body size estimates from vertebral measurements of fossils reveals several important patterns when considered in the context of various hypotheses of early snake evolution, particularly the relationships of fossil snakes to extant clades. Using extant only data, inferred ancestral body size during the Cretaceous barely exceeds 1m. This is clearly not reflected by the fossils, which by the Maastrichtian are reaching lengths of over 8m. While all ancestral state reconstructions are better at predicting the presence of large bodied snakes during the Cretaceous, when fossils are included in topology 1, the ancestral state reconstructions predict estimated body lengths for snakes as larger much earlier than what is observed in the fossil record. In contrast, when fossils are included either in topology 2 or topology 3, the ancestral state reconstructions accurately predict a body length for snakes around 4m in the Coniacian-Santonian, and a body length of over 5m in the Campanian, both of which are reflected by fossil vertebrae. Therefore, the range of body sizes estimated using fossil vertebrae supports a hypothesis where many radiations of Cretaceous snakes, including Madtsoiidae and Simoliophiidae, are nested within extant snakes. This does not support the hypothesis that the ecological adaptation to marine habitats shown by Simoliophiidae is typical of stem snakes, and instead that Simoliophiidae represent an early radiation into marine habitats from a terrestrial ancestor. The results of body size evolution are more concordant with hypotheses of an early adaptation to fossoriality, especially when *Najash rionegrina* and *Dinilysia patagonica* are recovered as stem snakes. This, in addition to hypothesised fossorial habitats for *Dinilysia patagonica* (Yi & Norell 2015), supports a hypothesis that the early snake was a large bodied fossorial taxon, and Scolecophidia (Typhlopoidea, Leptotyphlopidae, and Anomalepididae) represent further early specialised adaptation to a fully fossorial and insectivorous lifestyle.

Bibliography

Albino, A. M. (2011). Evolution of Squamata Reptiles in Patagonia based on the fossil record. *Biological Journal of the Linnean Society*, **103**(2), 441–457.

Apesteguía, S. (2007). Lepidosaurios en movimiento: de los lagartos a las serpientes. *Investigacion y Ciencia*, 55–61.

Apesteguía, S., & Zaher, H. (2006). A Cretaceous terrestrial snake with robust hindlimbs and a sacrum. *Nature*, **440**(7087), 1037–1040.

Atkins, J. B., & Franz-Odendaal, T. A. (2016). The sclerotic ring of squamates: an evo-devo-eco perspective. *Journal of Anatomy*, **229**(4), 503–513.

Bardet, N., Houssaye, A., Rage, J. C., & Pereda Suberbiola, X. (2008). The Cenomanian-Turonian (late Cretaceous) radiation of marine squamates (Reptilia): the role of the Mediterranean Tethys. *Bulletin de La Societe Geologique de France*, **179**(6), 605.

Barrie, J. (1990). Skull elements and additional remains of the Pleistocene Boid snake Wonambi naracoortensis. *Memoirs of the Queensland Museum*, **28**(1), 139–151.

Bell, M. A., & Lloyd, G. T. (2015). Strap: An R package for plotting phylogenies against stratigraphy and assessing their stratigraphic congruence. *Palaeontology*, **58**(2), 379–389.

Benson, R. B. J., Godoy, P., Bronzati, M., Butler, R. J., & Gearty, W. (2022). Reconstructed evolutionary patterns for crocodile-line archosaurs demonstrate impact of failure to log-transform body size data. *Communications Biology*, **5**(1), 4–7.

Berman, D. S., & Regal, P. J. (1967). The Loss of the Ophidian Middle Ear. *Evolution*, **21**(3), 641–643.

Boback, S. M. (2003). Body Size Evolution in Snakes : Evidence from Island Populations. *Copeia*, **2003**(1), 81–94.

Brischoux, F., & Shine, R. (2011). Morphological adaptations to marine life in snakes. *Journal of Morphology*, **272**(5), 566–572.

Brusatte, S. L., Benton, M. J., Ruta, M., & Lloyd, G. T. (2008). Superiority, competition, and opportunism in the evolutionary radiation of dinosaurs. *Science*, **321**(5895), 1485–1488.

Caldwell, M. W. (1999). Squamate phylogeny and the relationships of snakes and mosasauroids. *Zoological Journal of the Linnean Society*, **125**(1), 115–147.

Caldwell, M. W., & Albino, A. (2003). Exceptionally Preserved Skeletons of the Cretaceous Snake Dinilysia patagonica Woodward, 1901. *Journal of Vertebrate Paleontology*, **22**(4), 861–866.

Caldwell, M. W., & Lee, M. S. Y. (1997). A snake with legs from the marine Cretaceous of the Middle East. *Nature*, pp. 705–709.

Caldwell, M. W., Nydam, R. L., Palci, A., & Apesteguía, S. (2015). The oldest known snakes from the Middle Jurassic-Lower Cretaceous provide insights on snake evolution. *Nature*

Communications, **6**, 5996.

Caprette, C. L., Lee, M. S. Y., Shine, R., Mokany, A., & Downhower, J. F. (2004). The origin of snakes (Serpentes) as seen through eye anatomy. *Biological Journal of the Linnean Society*, **81**(4), 469–482.

Conrad, J. L. (2008). Phylogeny and systematics of Squamata (Reptilia) based on morphology. *Bulletin American Museum of Natural History*, **310**, 182.

Cundall, D., & Irish, F. (2008). The Snake Skull. In C. Gans, A. S. Gaunt, & K. Adlre, eds., *Biology of the Reptilia. Volume 20. Morphology H. The Skull of Lepidosauria*, Society for the Study of Amphibians and Reptiles, pp. 352–692.

Da Silva, F. O., Fabre, A.-C., Savriama, Y., … Di-Poï, N. (2018). The ecological origins of snakes as revealed by skull evolution. *Nature Communications*, **9**(1), 376.

Donoghue, M. J., Doyle, J. A., Gauthier, J., Kluge, A. G., & Rowe, T. (1989). The importance of fossils in phylogeny reconstruction. *Annual Review of Ecology and Systematics. Vol. 20*, 431–460.

Fachini, T. S., Onary, S., Palci, A., Lee, M. S. Y., Bronzati, M., & Hsiou, A. S. (2020). Cretaceous Blindsnake From Brazil Fills Major Gap in Snake Evolution. *IScience*, **23**(12), 101834.

Feldman, A., Sabath, N., Pyron, R. A., Mayrose, I., & Meiri, S. (2016). Body sizes and diversification rates of lizards, snakes, amphisbaenians and the tuatara. *Global Ecology and Biogeography*, **25**(2), 187–197.

Felsenstein, J. (1985). Phylogenies and the Comparative Method. *The American Naturalist*, **125**(1), 1–15.

Finarelli, J. A., & Goswami, A. (2013). Potential pitfalls of reconstructing deep time evolutionary history with only extant data, a case study using the canidae (mammalia, carnivora). *Evolution*, **67**(12), 3678–3685.

Ford, N. B., & Seigel, R. A. (2015). The influence of female body size and shape on the trade-off between offspring number and offspring size in two viviparous snakes. *Journal of Zoology*, **295**(2), 154–158.

Fox, R. C. (1975). Fossil snakes from the Upper Milk River Formation (Upper Cretaceous), Alberta. *Canadian Journal of Earth Sciences*, **12**, 1557–1563.

Gauthier, J. A., Kearney, M., Maisano, J. A., Rieppel, O., & Behlke, A. D. B. (2012). Assembling the squamate tree of life : Perspectives from the phenotype and the fossil record. *Bulletin of the Peabody Museum of Natural History*, **53**(1), 3–308.

Gower, D. J., Fleming, J. F., Pisani, D., … Simões, B. F. (2021). Eye-Transcriptome and Genome-Wide Sequencing for Scolecophidia: Implications for Inferring the Visual System of the Ancestral Snake. *Genome Biology and Evolution*, **13**(12), 1–12.

Haldane, J. B. (1949). Suggestions as to quantitative measurement of rates of evolution. *Evolution*, **3**(1), 51–56.

Hanken, J., & Wake, D. B. (1993). Miniaturization of body size: Organismal consequences and evolutionary significance. *Annual Review of Ecology and Systematics*, **24**, 501–519.

Head, J. J., Bloch, J. I., Hastings, A. K., … Jaramillo, C. A. (2009). Giant boid snake from the Palaeocene neotropics reveals hotter past equatorial temperatures. *Nature*, **457**(7230), 715–717.

Hsiang, A. Y., Field, D. J., Webster, T. H., … Gauthier, J. A. (2015). The origin of snakes: revealing the ecology, behavior, and evolutionary history of early snakes using genomics, phenomics, and the fossil record. *BMC Evolutionary Biology*, **15**, 87.

Klein, C. G., Longrich, N. R., Ibrahim, N., Zouhri, S., & Martill, D. M. (2017). A new basal snake from the mid-Cretaceous of Morocco. *Cretaceous Research*, **72**, 134–141.

Laduke, T. C., Krause, D. W., Scanlon, J. D., & Kley, N. J. (2010). A Late Cretaceous (Maastrichtian) Snake Assemblage from the Maevarano Formation, Mahajanga Basin, Madagascar. *Journal of Vertebrate Paleontology*, **30**(1), 109–138.

Lee, M. S. Y. (1997). The phylogeny of varanoid lizards and the affinities of snakes. *Philosophical Transactions of the Royal Society B: Biological Sciences*, **352**(1349), 53–91.

Lee, M. S. Y. (1998). Convergent evolution and character correlation in burrowing reptiles: towards a resolution of squamate relationships. *Biological Journal of the Linnean Society*, **65**, 369–453.

Lee, M. S. Y. (2005). Molecular evidence and marine snake origins. *Biology Letters*, **1**(2), 227–230.

Lee, M. S. Y., & Caldwell, M. W. (2000). *Adriosaurus* and the affinities of mosasaurs, dolichosaurs, and snakes. *Journal of Paleontology*, **74**(05), 915–937.

McCartney, J. A. (2008). Body size of the giant Eocene snake, Palaeophis colossaeus (Serpentes: Palaeophiidae) estimated from recently collected material from Mali. *Journal of Vertebrate Paleontology*, **28**(3, supplement), 114A.

McCartney, J. A., Roberts, E. M., Tapanila, L., & O'Leary, M. A. (2018). Large palaeophiid and nigerophiid snakes from Paleogene Trans-Saharan Seaway deposits of Mali. *Acta Palaeontologica Polonica*, **63**(2), 207–220.

Miralles, A., Marin, J., Markus, D., Herrel, A., Hedges, S. B., & Vidal, N. (2018). Molecular evidence for the paraphyly of Scolecophidia and its evolutionary implications. *Journal of Evolutionary Biology*. doi:10.1111/jeb.13373

Murphy, J. C., & Henderson, R. W. (1997). *Tales of Giant Snakes: A Historical Natural History of Anacondas and Pythons*, 1st edn.

Nydam, R. L. (2013). Lizards and snakes from the Cenomanian through Campanian of Southern Utah: Filling the gap in the fossil record of Squamata from the Late Cretaceous of the Western Interior of North America. *At the Top of the Grand Staircase: The Late Cretaceous*

of Southern Utah, 370–423.

O'Shea, M. (2018). *The Book of Snakes: a life-size guide to six hundred species from around the world*, London: Ivy Press.

Palci, A., Hutchinson, M. N., Caldwell, M. W., & Lee, M. S. Y. (2017). The morphology of the inner ear of squamate reptiles and its bearing on the origin of snakes. *Royal Society Open Science*, **4**, 170685.

Pyron, R. A., Burbrink, F. T., & Wiens, J. J. (2013). A phylogeny and revised classification of Squamata, including 4161 species of lizards and snakes. *BMC Evolutionary Biology*, **13**, 93.

Rage, J.-C. (1981). Les continents péri-atlantiques au crétacé supérieur: Migrations des faunes continentales et problèmes paléogéographiques. *Cretaceous Research*, **2**(1), 65–84.

Rage, J.-C., & Escuillié, F. (2000). Un nouveau serpent bipède du Cénomanien (Crétacé). Implications phylétiques. *Comptes Rendus de l'Académie Des Sciences - Series IIA - Earth and Planetary Science*, **330**(7), 513–520.

Rage, J.-C., & Escuillié, F. (2003). The Cenomanian: stage of hindlimbed snakes. *Carnets de Géologie*, **01**, 1–11.

Rage, J.-C., Prasad, G. V. R., & Bajpai, S. (2004). Additional snakes from the uppermost Cretaceous (Maastrichtian) of India. *Cretaceous Research*, **25**(3), 425–434.

Rage, J.-C., Vullo, R., & Néraudeau, D. (2016). The mid-Cretaceous snake Simoliophis rochebrunei Sauvage, 1880 (Squamata: Ophidia) from its type area (Charentes, southwestern France): Redescription, distribution, and palaeoecology. *Cretaceous Research*, **58**, 234–253.

Rage, J.-C., & Werner, C. (1999). Mid-Cretaceous (Cenomanian) snakes from Wadi Abu Hashim, Sudan: The earliest snake assemblage. *Palaeontologia Africana*, **110**(35), 85–110.

Rage, J. C. (1991). Squamate Reptiles from the Early Paleocene of the Tiupampa Area (Santa Lucia Formation), Bolivia. *Fosiles y Facies de Bolivia - Vol. 1 Vertebrados*, 503–508.

Reeder, T. W., Townsend, T. M., Mulcahy, D. G., … Wiens, J. J. (2015). Integrated analyses resolve conflicts over squamate reptile phylogeny and reveal unexpected placements for fossil taxa. *PLoS ONE*, **10**(3), e0118199.

Revell, L. J. (2012). phytools: An R package for phylogenetic comparative biology (and other things). *Methods in Ecology and Evolution*, **3**(2), 217–223.

Rieppel, O. (1988). A review of the origin of snakes. *Evolutionary Biology*, **22**, 37–130.

Rieppel, O. (2012). "Regressed" macrostomatan snakes. *Fieldiana Life and Earth Sciences*, 99–103.

Rio, J. P., & Mannion, P. D. (2017). The osteology of the giant snake Gigantophis garstini from the upper Eocene of North Africa and its bearing on the phylogenetic relationships and biogeography of Madtsoiidae. *Journal of Vertebrate Paleontology*, **37**(4). doi:10.1080/02724634.2017.1347179

Romer, A. S. (1956). *Osteology of the Reptiles*, Chicago: University of Chicago Press.

Ruta, M., Wagner, P. J., & Coates, M. I. (2006). Evolutionary patterns in early tetrapods. I. Rapid initial diversification followed by decrease in rates of character change. *Proceedings of the Royal Society B: Biological Sciences*, **273**(1598), 2107–2111.

Scanferla, C. A., & Canale, J. I. (2007). The youngest record of the Cretaceous snake genus *Dinilysia* (Squamata, Serpentes). *South American Journal of Herpetology*, **2**(1), 76–81.

Scanlon, J. D. (2006). Skull of the large non-macrostomatan snake Yurlunggur from the Australian Oligo-Miocene. *Nature*, **439**(7078), 839–842.

Scanlon, J. D., & Lee, M. S. Y. (2000). The Pleistocene serpent *Wonambi* and the early evolution of snakes. *Nature*, **403**, 416–420.

Simões, B. F., Sampaio, F. L., Jared, C., … Gower, D. J. (2015). Visual system evolution and the nature of the ancestral snake. *Journal of Evolutionary Biology*, **28**(7), 1309–1320.

Slip, D. J., & Shine, R. (1988). Feeding habits of the Diamond Python, *Morelia s. spilota*: Ambush predation by a boid snake. *Journal of Herpetology*, **22**(3), 323–330.

Streicher, J. W., & Wiens, J. J. (2016). Phylogenomic analyses reveal novel relationships among snake families. *Molecular Phylogenetics and Evolution*, **100**, 160–169.

Tchernov, E., Rieppel, O., Zaher, H., Polcyn, M. J., & Jacobs, L. L. (2000). A Fossil Snake with Limbs. *Science*, **287**(5460), 2010–2012.

Vasile, Ş., Csiki-Sava, Z., & Venczel, M. (2013). A new madtsoiid snake from the Upper Cretaceous of the Haţeg Basin, western Romania. *Journal of Vertebrate Paleontology*, **33**(5), 1100–1119.

Walls, G. L. (1940). Ophthalmological implications for the early history of the snakes. *Copeia*, **1940**(1), 1–8.

Webb, J. K., Branch, W. R., & Shine, R. (2001). Dietary habits and reproductive biology of typhlopid snakes from Southern Africa. *Journal of Herpetology*, **35**(4), 558–567.

Wick, S. L., & Shiller, T. A. (2020). New taxa among a remarkably diverse assemblage of fossil squamates from the Aguja Formation (lower Campanian) of West Texas. *Cretaceous Research*, **114**, 104516.

Wiens, J. J., Brandley, M. C., & Reeder, T. W. (2006). Why does a trait evolve multiple times within a clade? Repeated evolution of snakelike body form in squamate reptiles. *Evolution*, **60**(1), 123–141.

Wiens, J. J., Hutter, C. R., Mulcahy, D. G., … Reeder, T. W. (2012). Resolving the phylogeny of lizards and snakes (Squamata) with extensive sampling of genes and species. *Biology Letters*, **8**(6), 1043–1046.

Wiens, J. J., Kuczynski, C. A., Townsend, T., Reeder, T. W., Mulcahy, D. G., & Sites, J. W. (2010). Combining phylogenomics and fossils in higher-level squamate reptile phylogeny:

Molecular data change the placement of fossil taxa. *Systematic Biology*, **59**(6), 674–688.

Wiens, J. J., & Slingluff, J. L. (2001). How Lizards Turn into Snakes : A Phylogenetic Analysis of Body-Form Evolution in Anguid Lizards. *Evolution*, **55**(11), 2303–2318.

Wilson, J. A., Mohabey, D. M., Peters, S. E., & Head, J. J. (2010). Predation upon hatchling dinosaurs by a new snake from the Late Cretaceous of India. *PLoS Biology*, **8**(3). doi:10.1371/journal.pbio.1000322.g001

Yi, H., & Norell, M. A. (2015). The burrowing origin of modern snakes. *Science Advances*, **1**(10), e1500743–e1500743.

Zaher, H. (1998). The phylogenetic position of *Pachyrhachis* within snakes (Squamata, Lepidosauria). *Journal of Vertebrate Paleontology*, **18**(1), 1–3.

Zaher, H., Apesteguía, S., & Scanferla, C. A. (2009). The anatomy of the upper cretaceous snake *Najash rionegrina* Apesteguía & Zaher, 2006, and the evolution of limblessness in snakes. *Zoological Journal of the Linnean Society*, **156**(4), 801–826.

Zaher, H., & Rieppel, O. (2002). On the phylogenetic relationships of the Cretaceous snakes with legs, with special reference to Pachyrhachis problematicus (Squamata, Serpentes). *Journal of Vertebrate Paleontology*, **22**(1), 104–109.

Zaher, H., & Scanferla, C. A. (2012). The skull of the Upper Cretaceous snake *Dinilysia patagonica* Smith-Woodward, 1901, and its phylogenetic position revisited. *Zoological Journal of the Linnean Society*, **164**(1), 194–238.

Zheng, Y., & Wiens, J. J. (2016). Combining phylogenomic and supermatrix approaches, and a time-calibrated phylogeny for squamate reptiles (lizards and snakes) based on 52 genes and 4162 species. *Molecular Phylogenetics and Evolution*, **94**, 537–547.

Appendix 1 – Estimated lengths of Cretaceous snakes based on cotylar width

Species	Clade	Cotylar Width	Estimated Length	Specimen Number	Reference
Adinophis fisaka	Madtsoiidae	4.28	142.60	UA 9941	Pritchard et al, 2014
Adinophis fisaka	Madtsoiidae	4.75	160.78	FMNH PR 2572	Pritchard et al, 2014
aff. *Coniophis* indet.	Serpentes	0.481	11.50	TMM 45947-554	Wick & Shiller, 2020
Alamitophis argentinus	Madtsoiidae	3.087	97.87	MACN-PV RN 1053	Martinelli & Forasiepi, 2004
Alamitophis argentinus	Madtsoiidae	4.192	139.23	MPEF-PV 643	Albino, 2000
Alamitophis argentinus	Madtsoiidae	2.9	91.08	MACN-RN 27	Albino, 1986
Alamitophis elongatus	Madtsoiidae	3.935	129.44	MLP 88-111-31-1	Albino, 1994
Alamitophis elongatus	Madtsoiidae	4.64	156.50	MACN-RN 38	Albino, 1994
Alethinophidia indet.	Alethinophidia	1.944	57.46	?	Longrich et al, 2012b
Australophis anilioides	Anilioidea	3.907	128.38	MML-PV181	Gomez et al, 2008
Boidae indet.	Boidae	0.693	17.51	MACN-M 22	Gonzalez Riga, 1999
Boipeba tayasuensis	Scolecophidia	4.835	164.10	MPMA 16-0008-08	Fachini et al, 2020
Cerberophis robustus	Alethinophidia	5.001	170.61	UCMP 130696	Longrich et al, 2012b
Colubridae incertae sedis	Colubridae	0.617	15.32	Vb-1057	Rage & Werner, 1999
Colubridae incertae sedis	Colubridae	0.617	15.32	Vb-1061	Rage & Werner, 1999
Colubridae incertae sedis	Colubridae	0.642	16.04	Vb-1056	Rage & Werner, 1999
Coniophis* cf. *C. dabiebus	Serpentes	0.619	15.38	Vb-674	Rage & Werner, 1999
Coniophis cosgriffi	Serpentes	3.605	117.02	MNA Pl. 1612	Armstrong-Ziegler, 1978

Coniophis dabiebus	Serpentes	0.914	24.09	Vb-673	Rage & Werner, 1999
Coniophis dabiebus	Serpentes	0.979	26.07	Vb-674	Rage & Werner, 1999
Coniophis precedens	Serpentes	1.106	30.01	AMNH 26999	Longrich et al, 2012a
Coniophis precedens	Serpentes	1.955	57.83	YPM-PU 16845	Longrich et al, 2012a
Coniophis precedens	Serpentes	1.997	59.26	AMNH 26833	Longrich et al, 2012a
Coniophis precedens	Serpentes	2.291	69.42	USNM 2143	Longrich et al, 2012a
***Coniophis* sp.**	Serpentes	1.343	37.53	VPL/JU/1500	Rage et al, 2004
***Coniophis* sp.**	Serpentes	1.425	40.18	UMNH VP 19250	Nydam, 2013
***Coniophis* sp.**	Serpentes	1.48	41.97	UMNH VP 19237	Nydam, 2013
***Coniophis* sp.**	Serpentes	1.766	51.44	UMNH VP 19249	Nydam, 2013
***Coniophis* sp.**	Serpentes	1.873	55.05	UMNH VP 19248	Nydam, 2013
***Coniophis* sp.**	Serpentes	2.102	62.87	UMNH VP 19238	Nydam, 2013
***Coniophis* sp.**	Serpentes	2.2	66.25	UMNH VP 18061	Nydam, 2013
***Coniophis* sp.**	Serpentes	1.129	30.73	UMNH VP 19243	Nydam, 2013
***Coniophis* sp.**	Serpentes	1.224	33.72	MNA V10375	Nydam, 2013
***Coniophis* sp.**	Serpentes	1.62	46.57	MNA V9102	Nydam, 2013
***Coniophis* sp.**	Serpentes	1.4	39.37	OMNH 33251	Gardner & Cifelli, 1999
***Coniophis* sp.**	Serpentes	1.8	52.58	OMNH 33250	Gardner & Cifelli, 1999
Dinilysia patagonica	Dinilysiidae	5.331	183.64	MLP 26-410	Caldwell & Albino, 2003
***Dinilysia* sp.**	Dinilysiidae	8.362	308.43	MAU-Pv-PR-457	Filippi & Garrido, 2012
***Dinilysia* sp.**	Dinilysiidae	12.697	498.99	MACN-N 26	Scanferla & Canale, 2007
Eumadtsoia ragei	Madtsoiidae	9.155	342.36	MPEF-PV 2380	Gomez et al, 2019
Eumadtsoia ragei	Madtsoiidae	9.664	364.37	MPEF-PV 2378	Gomez et al, 2019

Eupodophis descouensi	Simoliophiidae	3.735	121.90	Rh-E.F 9003	Rage & Escuillie, 2000
Herensugea caristiorum	Madtsoiidae	2.205	66.43	MCNA 5387	Rage, 1996
Indophis fanambinana	Nigerophiidae	1.015	27.18	UA 9942	Pritchard et al, 2014
Indophis fanambinana	Nigerophiidae	1.261	34.90	FMNH PR 3057	Pritchard et al, 2014
Indophis fanambinana	Nigerophiidae	1.566	44.79	FMNH PR 3048	Pritchard et al, 2014
Indophis sahnii	Nigerophiidae	0.88	23.06	VPL/JU/502	Rage & Prasad, 1992
Indophis sahnii	Nigerophiidae	0.882	23.12	VPL/JU/501	Rage & Prasad, 1992
Indophis sahnii	Nigerophiidae	0.889	23.33	VPL/JU/500	Rage & Prasad, 1992
Indophis sahnii	Nigerophiidae	0.912	24.03	VPL/JU/503	Rage & Prasad, 1992
Indophis sahnii	Nigerophiidae	1.308	36.40	VPL/JU/1501	Rage et al, 2004
Kelyophis hechti	Nigerophiidae	1.334	37.24	UA 9682	LaDuke et al, 2010
Kelyophis hechti	Nigerophiidae	1.391	39.07	FMNH PR 2539	LaDuke et al, 2010
Kelyophis hechti	Nigerophiidae	1.746	50.77	FMNH 3058	Pritchard et al, 2014
Krebsophis thobanus	Russellophiidae	0.827	21.47	Vb-681	Rage & Werner, 1999
Krebsophis thobanus	Russellophiidae	1.149	31.35	Vb-682	Rage & Werner, 1999
Lapparentophiidae indet. A.	Lapparentophiidae	3.889	127.70	Vb-671	Rage & Werner, 1999
Lunaophis aquaticus	Serpentes	4.218	140.22	MNCN-1827-A	Albino et al, 2016
Madtsoia* aff. *madagascariensis	Madtsoiidae	10.987	422.40	?	Rage, 1981
Madtsoia laurasiae	Madtsoiidae	10.251	389.98	MCNA 5337	Rage, 1996
Madtsoia madagascariensis	Madtsoiidae	12.497	489.94	FMNH PR 2555	LaDuke et al, 2010
Madtsoia madagascariensis	Madtsoiidae	15.436	624.89	FMNH PR 2546	LaDuke et al, 2010

Madtsoia madagascariensis	Madtsoiidae	15.835	643.53	FMNH PR 2554	LaDuke et al, 2010
Madtsoia madagascariensis	Madtsoiidae	16.663	682.44	FMNH PR 2549	LaDuke et al, 2010
Madtsoia madagascariensis	Madtsoiidae	19.579	821.75	FMNH PR 2551	LaDuke et al, 2010
Madtsoia pisdurensis	Madtsoiidae	18.089	750.14	225/GSI/PAL/CR/10	Mohabey et al, 2011
Madtsoiidae indet.	Madtsoiidae	0.686	17.31	VPL/JU/1519	Rage et al, 2004
Madtsoiidae indet.	Madtsoiidae	2.138	64.11	MHNC 8586	Gayet et al, 2001
Madtsoiidae indet.	Madtsoiidae	2.169	65.18	PSMUBB V 407	Folie & Codrea,2005
Madtsoiidae indet.	Madtsoiidae	5.576	193.39	MACN-PV RN 1052	Martinelli & Forasiepi, 2004
Madtsoiidae indet.	Madtsoiidae	2.02	60.05	Vb-668	Rage & Werner, 1999
Menarana nosymena	Madtsoiidae	4.028	132.97	UA 9687-1	LaDuke et al, 2010
Menarana nosymena	Madtsoiidae	7.501	272.14	UA 9684-2	LaDuke et al, 2010
Menarana nosymena	Madtsoiidae	8.612	319.07	UA 9684-1	LaDuke et al, 2010
Najash rionegrina	Serpentes	2.012	59.78	MPCA 418	Garberoglio et al, 2019
Najash rionegrina	Serpentes	2.616	80.88	MPCA 390-398	Apesteguia & Zaher, 2006
Nidophis insularis	Madtsoiidae	1.501	42.65	LPB (FGGUB) v.547/27	Vasile et al, 2013
Nidophis insularis	Madtsoiidae	1.792	52.31	LPB (FGGUB) v.547/3	Vasile et al, 2013
Nidophis insularis	Madtsoiidae	1.917	56.54	LPB (FGGUB) v.547/7	Vasile et al, 2013
Nidophis insularis	Madtsoiidae	2.043	60.84	LPB (FGGUB) v.547/1	Vasile et al, 2013
Nidophis insularis	Madtsoiidae	2.098	62.73	LPB [FGGUB] v.547/1	Vasile et al, 2013
Norisophis begaa	Serpentes	5.151	176.52	FSAC-KK 7001	Klein et al, 2017
Norisophis begaa	Serpentes	5.835	203.78	FSAC-KK 7004	Klein et al, 2017

Norisophis begaa	Serpentes	6.483	230.06	FSAC-KK 7005	Klein et al, 2017
Norisophis begaa	Serpentes	6.667	237.59	FSAC-KK 7002	Klein et al, 2017
Nubianophis afaahus	Nigerophiidae	0.803	20.75	Vb-1054	Rage & Werner, 1999
Nubianophis afaahus	Nigerophiidae	1.084	29.32	Vb-1044	Rage & Werner, 1999
Nubianophis afaahus	Nigerophiidae	1.748	50.84	Vb-1041	Rage & Werner, 1999
Nubianophis afaahus	Nigerophiidae	2.421	73.98	Vb-1045	Rage & Werner, 1999
Nubianophis* cf. *N. afaahus	Nigerophiidae	1.008	26.96	Vb-1055	Rage & Werner, 1999
Palaeophiidae indet.	Palaeophiidae	2.597	80.21	Vb-688	Rage & Werner, 1999
***Palaeophis* sp.**	Palaeophiidae	8.872	330.19	?	Rage & Wouters, 1979
Patagoniophis parvus	Madtsoiidae	1.813	53.02	MACN-PV RN 1049	Martinelli & Forasiepi, 2004
Patagoniophis parvus	Madtsoiidae	2.175	65.39	MACN-RN 33	Albino, 1986
Rionegrophis madtsoiodes	Madtsoiidae	5.744	200.12	MACN-RN 32	Albino, 1986
Serpentes incertae sedis	Serpentes	1.281	35.54	UA 9943	Pritchard et al, 2014
Serpentes incertae sedis	Serpentes	2.395	73.06	MPEF-PV 642	Albino, 2000
Serpentes indet.	Serpentes	1.449	40.96	Vb-689	Rage & Werner, 1999
Serpentes indet.	Serpentes	2.812	87.90	MPM 21522	Novas et al, 2019
Simoliophis rochebrunei	Simoliophiidae	1.893	55.72	MA BZN 11	Rage et al, 2016
Simoliophis rochebrunei	Simoliophiidae	2.228	67.23	MNHN.R.RND 12b	Rage et al, 2016
Simoliophis rochebrunei	Simoliophiidae	2.277	68.93	MA TLM 12	Rage et al, 2016
Simoliophis rochebrunei	Simoliophiidae	2.576	79.46	MA SNA 1	Rage et al, 2016
Simoliophis rochebrunei	Simoliophiidae	2.596	80.17	MA RND 6	Rage et al, 2016

Simoliophis rochebrunei	Simoliophiidae	3.361	107.95	lost specimens from Rochebrune, 1880	Rage et al, 2016
Simoliophis rochebrunei	Simoliophiidae	3.906	128.35	MA RND 23	Rage et al, 2016
Simoliophis rochebrunei	Simoliophiidae	3.934	129.41	MA SNA 4	Rage et al, 2016
Simoliophis rochebrunei	Simoliophiidae	4.78	161.95	MA SNA 2	Rage et al, 2016
Simoliophis rochebrunei	Simoliophiidae	4.914	167.19	MA RND 11	Rage et al, 2016
Simoliophis rochebrunei	Simoliophiidae	5.489	189.92	lost specimens from Rochebrune, 1880	Rage et al, 2016

Appendix 2 – Locality of Cretaceous snakes

Species	Clade	Formation	Country	Specimen Number	Age	Reference
Adinophis fisaka	Madtsoiidae	Maevarano Formation	Madagascar	UA 9941	Maastrichtian	Pritchard et al, 2014
Adinophis fisaka	Madtsoiidae	Maevarano Formation	Madagascar	FMNH PR 2572	Maastrichtian	Pritchard et al, 2014
aff. *Coniophis* indet.	Serpentes	Aguja Formation	Texas, USA	TMM 45947-554	Lower Campanian	Wick & Shiller, 2020
Alamitophis argentinus	Madtsoiidae	Bajo de Santa Rosa, Allen Formation	Argentina	MACN-PV RN 1053	Late Campanian - Early Maastrichtian	Martinelli & Forasiepi, 2004
Alamitophis argentinus	Madtsoiidae	La Colonia Formation	Argentina	MPEF-PV 643	Maastrichtian	Albino, 2000
Alamitophis argentinus	Madtsoiidae	Los Alamitos Formation	Argentina	MACN-RN 27	Late Campanian-Early Maastrichtian	Albino, 1986
Alamitophis elongatus	Madtsoiidae	Los Alamitos Formation	Argentina	MLP 88-111-31-1	Late Campanian-Early Maastrichtian	Albino, 1994
Alamitophis elongatus	Madtsoiidae	Los Alamitos Formation	Argentina	MACN-RN 38	Late Campanian-Early Maastrichtian	Albino, 1994
Alethinophidia indet.	Alethinophidia	Lance Formation	Wyoming, USA	?	Upper Maastrichtian	Longrich et al, 2012b
Australophis anilioides	Anilioidea	Bajo Trapalcó, Allen Formation	Argentina	MML-PV181	Late Campanian - Early Maastrichtian	Gomez et al, 2008
Boidae indet.	Boidae	Loncoche Formation	Argentina	MACN-M 22	Upper Cretaceous	Gonzalez Riga, 1999

Boipeba tayasuensis	Scolecophidia	Adamantina Formation	Brazil	MPMA 16-0008-08	Campanian-Maastrichtian	Fachini et al, 2020
Cerberophis robustus	Alethinophidia	Hell Creek Formation	Montana, USA	UCMP 130696	Upper Cretaceous	Longrich et al, 2012b
Colubridae incertae sedis	Colubridae	Wadi Abu Hashim Member, Wadi Milk Formation	Sudan	Vb-1057	Campanian-Maastrichtian	Rage & Werner, 1999
Colubridae incertae sedis	Colubridae	Wadi Abu Hashim Member, Wadi Milk Formation	Sudan	Vb-1061	Campanian-Maastrichtian	Rage & Werner, 1999
Colubridae incertae sedis	Colubridae	Wadi Abu Hashim Member, Wadi Milk Formation	Sudan	Vb-1056	Campanian-Maastrichtian	Rage & Werner, 1999
Coniophis* cf. *C. dabiebus	Serpentes	Wadi Abu Hashim Member, Wadi Milk Formation	Sudan	Vb-674	Campanian-Maastrichtian	Rage & Werner, 1999
Coniophis cosgriffi	Serpentes	Fruitland Formation	New Mexico, USA	MNA Pl. 1612	Campanian	Armstrong-Ziegler, 1978
Coniophis dabiebus	Serpentes	Wadi Abu Hashim Member, Wadi Milk Formation	Sudan	Vb-673	Campanian-Maastrichtian	Rage & Werner, 1999
Coniophis dabiebus	Serpentes	Wadi Abu Hashim Member, Wadi Milk Formation	Sudan	Vb-674	Campanian-Maastrichtian	Rage & Werner, 1999
Coniophis precedens	Serpentes	Lance Formation	Wyoming, USA	AMNH 26999	Upper Maastrichtian	Longrich et al, 2012a
Coniophis precedens	Serpentes	Lance Formation	Wyoming, USA	YPM-PU 16845	Upper Maastrichtian	Longrich et al, 2012a
Coniophis precedens	Serpentes	Lance Formation	Wyoming, USA	AMNH 26833	Upper Maastrichtian	Longrich et al, 2012a

Coniophis precedens	Serpentes	Lance Formation	Wyoming, USA	USNM 2143	Upper Maastrichtian	Longrich et al, 2012a
***Coniophis* sp.**	Serpentes	Naskal	India	VPL/JU/1500	Maastrichtian	Rage et al, 2004
***Coniophis* sp.**	Serpentes	Wahweap Formation	Utah, USA	UMNH VP 19250	Campanian	Nydam, 2013
***Coniophis* sp.**	Serpentes	Kaiparowits Formation	Utah, USA	UMNH VP 19237	Campanian	Nydam, 2013
***Coniophis* sp.**	Serpentes	Wahweap Formation	Utah, USA	UMNH VP 19249	Campanian	Nydam, 2013
***Coniophis* sp.**	Serpentes	Wahweap Formation	Utah, USA	UMNH VP 19248	Campanian	Nydam, 2013
***Coniophis* sp.**	Serpentes	Kaiparowits Formation	Utah, USA	UMNH VP 19238	Campanian	Nydam, 2013
***Coniophis* sp.**	Serpentes	Kaiparowits Formation	Utah, USA	UMNH VP 18061	Campanian	Nydam, 2013
***Coniophis* sp.**	Serpentes	John Henry Member, Straight Cliffs Formation	Utah, USA	UMNH VP 19243	Turonian	Nydam, 2013
***Coniophis* sp.**	Serpentes	MNA 995	Utah, USA	MNA V10375	Turonian	Nydam, 2013
***Coniophis* sp.**	Serpentes	Dakota Formation	Utah, USA	MNA V9102	Cenomanian	Nydam, 2013
***Coniophis* sp.**	Serpentes	OMNH locality V867, Cedar Mountain Formation	Utah, USA	OMNH 33251	Upper Albian to Lower Cenomanian	Gardner & Cifelli, 1999
***Coniophis* sp.**	Serpentes	OMNH locality V695, Cedar Mountain Formation	Utah, USA	OMNH 33250	Upper Albian to Lower Cenomanian	Gardner & Cifelli, 1999
Dinilysia patagonica	Dinilysiidae	Boca de la Carpa Member, Rio	Argentina	MLP 26-410	Coniacian	Caldwell & Albino, 2003

		Colorado Formation				
***Dinilysia* sp.**	Dinilysiidae	Anacleto Formation	Argentina	MAU-Pv-PR-457	Early-Middle Campanian	Filippi & Garrido, 2012
***Dinilysia* sp.**	Dinilysiidae	Anacleto Formation	Argentina	MACN-N 26	Early-Middle Campanian	Scanferla & Canale, 2007
Eumadtsoia ragei	Madtsoiidae	La Colonia Formation	Argentina	MPEF-PV 2380	Maastrichtian - Danian	Gomez et al, 2019
Eumadtsoia ragei	Madtsoiidae	La Colonia Formation	Argentina	MPEF-PV 2378	Maastrichtian - Danian	Gomez et al, 2019
Eupodophis descouensi	Simoliophiidae	Al Nammoura	Lebanon	Rh-E.F 9003	Cenomanian	Rage & Escuillie, 2000
Herensugea caristiorum	Madtsoiidae	Laño, Basque Country	Spain	MCNA 5387	Maastrichtian	Rage, 1996
Indophis fanambinana	Nigerophiidae	Maevarano Formation	Madagascar	UA 9942	Maastrichtian	Pritchard et al, 2014
Indophis fanambinana	Nigerophiidae	Maevarano Formation	Madagascar	FMNH PR 3057	Maastrichtian	Pritchard et al, 2014
Indophis fanambinana	Nigerophiidae	Maevarano Formation	Madagascar	FMNH PR 3048	Maastrichtian	Pritchard et al, 2014
Indophis sahnii	Nigerophiidae	Naskal	India	VPL/JU/502	Maastrichtian	Rage & Prasad, 1992
Indophis sahnii	Nigerophiidae	Naskal	India	VPL/JU/501	Maastrichtian	Rage & Prasad, 1992
Indophis sahnii	Nigerophiidae	Naskal	India	VPL/JU/500	Maastrichtian	Rage & Prasad, 1992
Indophis sahnii	Nigerophiidae	Naskal	India	VPL/JU/503	Maastrichtian	Rage & Prasad, 1992
Indophis sahnii	Nigerophiidae	Anjar	India	VPL/JU/1501	Maastrichtian	Rage et al, 2004

Kelyophis hechti	Nigerophiidae	Maevarano Formation	Madagascar	UA 9682	Maastrichtian	LaDuke et al, 2010
Kelyophis hechti	Nigerophiidae	Maevarano Formation	Madagascar	FMNH PR 2539	Maastrichtian	LaDuke et al, 2010
Kelyophis hechti	Nigerophiidae	Maevarano Formation	Madagascar	FMNH 3058	Maastrichtian	Pritchard et al, 2014
Krebsophis thobanus	Russellophiidae	Wadi Abu Hashim Member, Wadi Milk Formation	Sudan	Vb-681	Campanian-Maastrichtian	Rage & Werner, 1999
Krebsophis thobanus	Russellophiidae	Wadi Abu Hashim Member, Wadi Milk Formation	Sudan	Vb-682	Campanian-Maastrichtian	Rage & Werner, 1999
Lapparentophiidae indet. A.	Lapparentophiidae	Wadi Abu Hashim Member, Wadi Milk Formation	Sudan	Vb-671	Campanian-Maastrichtian	Rage & Werner, 1999
Lunaophis aquaticus	Serpentes	La Aguada Member, La Luna Formation	Venezuela	MNCN-1827-A	Cenomanian	Albino et al, 2016
Madtsoia* aff. *madagascariensis	Madtsoiidae	In Beceten Formation	Niger	?	Late Cretaceous	Rage, 1981
Madtsoia laurasiae	Madtsoiidae	Laño, Basque Country	Spain	MCNA 5337	Maastrichtian	Rage, 1996
Madtsoia madagascariensis	Madtsoiidae	Maevarano Formation	Madagascar	FMNH PR 2555	Maastrichtian	LaDuke et al, 2010
Madtsoia madagascariensis	Madtsoiidae	Maevarano Formation	Madagascar	FMNH PR 2546	Maastrichtian	LaDuke et al, 2010
Madtsoia madagascariensis	Madtsoiidae	Maevarano Formation	Madagascar	FMNH PR 2554	Maastrichtian	LaDuke et al, 2010
Madtsoia madagascariensis	Madtsoiidae	Maevarano Formation	Madagascar	FMNH PR 2549	Maastrichtian	LaDuke et al, 2010

Madtsoia madagascariensis	Madtsoiidae	Maevarano Formation	Madagascar	FMNH PR 2551	Maastrichtian	LaDuke et al, 2010
Madtsoia pisdurensis	Madtsoiidae	Lameta Formation	India	225/GSI/PAL/CR/10	Maastrichtian	Mohabey et al, 2011
Madtsoiidae indet.	Madtsoiidae	Kelapur	India	VPL/JU/1519	Maastrichtian	Rage et al, 2004
Madtsoiidae indet.	Madtsoiidae	Pajcha Pata Locality, El Molino Formation	Bolivia	MHNC 8586	Middle Maastrichtian	Gayet et al, 2001
Madtsoiidae indet.	Madtsoiidae	Sânpetru Formation	Romania	PSMUBB V 407	Early Maastrichtian	Folie & Codrea,2005
Madtsoiidae indet.	Madtsoiidae	Bajo de Santa Rosa, Allen Formation	Argentina	MACN-PV RN 1052	Late Campanian - Early Maastrichtian	Martinelli & Forasiepi, 2004
Madtsoiidae indet.	Madtsoiidae	Wadi Abu Hashim Member, Wadi Milk Formation	Sudan	Vb-668	Campanian-Maastrichtian	Rage & Werner, 1999
Menarana nosymena	Madtsoiidae	Maevarano Formation	Madagascar	UA 9687-1	Maastrichtian	LaDuke et al, 2010
Menarana nosymena	Madtsoiidae	Maevarano Formation	Madagascar	UA 9684-2	Maastrichtian	LaDuke et al, 2010
Menarana nosymena	Madtsoiidae	Maevarano Formation	Madagascar	UA 9684-1	Maastrichtian	LaDuke et al, 2010
Najash rionegrina	Serpentes	LBPA, Candeleros Formation	Argentina	MPCA 418	Cenomanian	Garberoglio et al, 2019
Najash rionegrina	Serpentes	Rio Negro Province	Argentina	MPCA 390-398	Cenomanian	Apesteguia & Zaher, 2006
Nidophis insularis	Madtsoiidae	Densuş-Ciula Formation	Romania	LPB (FGGUB) v.547/27	Maastrichtian	Vasile et al, 2013
Nidophis insularis	Madtsoiidae	Densuş-Ciula Formation	Romania	LPB (FGGUB) v.547/3	Maastrichtian	Vasile et al, 2013

Nidophis insularis	Madtsoiidae	Densuş-Ciula Formation	Romania	LPB (FGGUB) v.547/7	Maastrichtian	Vasile et al, 2013
Nidophis insularis	Madtsoiidae	Densuş-Ciula Formation	Romania	LPB (FGGUB) v.547/1	Maastrichtian	Vasile et al, 2013
Nidophis insularis	Madtsoiidae	Densuş-Ciula Formation	Romania	LPB [FGGUB] v.547/1	Maastrichtian	Vasile et al, 2013
Norisophis begaa	Serpentes	Kem Kem beds	Morocco	FSAC-KK 7001	Cenomanian	Klein et al, 2017
Norisophis begaa	Serpentes	Kem Kem beds	Morocco	FSAC-KK 7004	Cenomanian	Klein et al, 2017
Norisophis begaa	Serpentes	Kem Kem beds	Morocco	FSAC-KK 7005	Cenomanian	Klein et al, 2017
Norisophis begaa	Serpentes	Kem Kem beds	Morocco	FSAC-KK 7002	Cenomanian	Klein et al, 2017
Nubianophis afaahus	Nigerophiidae	Wadi Abu Hashim Member, Wadi Milk Formation	Sudan	Vb-1054	Campanian-Maastrichtian	Rage & Werner, 1999
Nubianophis afaahus	Nigerophiidae	Wadi Abu Hashim Member, Wadi Milk Formation	Sudan	Vb-1044	Campanian-Maastrichtian	Rage & Werner, 1999
Nubianophis afaahus	Nigerophiidae	Wadi Abu Hashim Member, Wadi Milk Formation	Sudan	Vb-1041	Campanian-Maastrichtian	Rage & Werner, 1999
Nubianophis afaahus	Nigerophiidae	Wadi Abu Hashim Member, Wadi Milk Formation	Sudan	Vb-1045	Campanian-Maastrichtian	Rage & Werner, 1999
Nubianophis* cf. *N. afaahus	Nigerophiidae	Wadi Abu Hashim Member, Wadi Milk Formation	Sudan	Vb-1055	Campanian-Maastrichtian	Rage & Werner, 1999
Palaeophiidae indet.	Palaeophiidae	Wadi Abu Hashim Member, Wadi Milk Formation	Sudan	Vb-688	Campanian-Maastrichtian	Rage & Werner, 1999
***Palaeophis* sp.**	Palaeophiidae	?	Morocco	?	Maastrichtian	Rage & Wouters, 1979

Patagoniophis parvus	Madtsoiidae	Bajo de Santa Rosa, Allen Formation	Argentina	MACN-PV RN 1049	Late Campanian - Early Maastrichtian	Martinelli & Forasiepi, 2004
Patagoniophis parvus	Madtsoiidae	Los Alamitos Formation	Argentina	MACN-RN 33	Late Campanian-Early Maastrichtian	Albino, 1986
Rionegrophis madtsoiodes	Madtsoiidae	Los Alamitos Formation	Argentina	MACN-RN 32	Late Campanian-Early Maastrichtian	Albino, 1986
Serpentes incertae sedis	Serpentes	Maevarano Formation	Madagascar	UA 9943	Maastrichtian	Pritchard et al, 2014
Serpentes incertae sedis	Serpentes	La Colonia Formation	Argentina	MPEF-PV 642	Maastrichtian	Albino, 2000
Serpentes indet.	Serpentes	Wadi Abu Hashim Member, Wadi Milk Formation	Sudan	Vb-689	Campanian-Maastrichtian	Rage & Werner, 1999
Serpentes indet.	Serpentes	Chorillo Formation	Argentina	MPM 21522	Upper Campanian - Lower Maastrichtian	Novas et al, 2019
Simoliophis rochebrunei	Simoliophiidae	Charentes	France	MA BZN 11	Cenomanian	Rage et al, 2016
Simoliophis rochebrunei	Simoliophiidae	Charentes	France	MNHN.R.RND 12b	Cenomanian	Rage et al, 2016
Simoliophis rochebrunei	Simoliophiidae	Charentes	France	MA TLM 12	Cenomanian	Rage et al, 2016
Simoliophis rochebrunei	Simoliophiidae	Charentes	France	MA SNA 1	Cenomanian	Rage et al, 2016
Simoliophis rochebrunei	Simoliophiidae	Charentes	France	MA RND 6	Cenomanian	Rage et al, 2016

Simoliophis rochebrunei	Simoliophiidae	Aix Island	France	lost specimens from Rochebrune, 1880	Cenomanian	Rage et al, 2016
Simoliophis rochebrunei	Simoliophiidae	Charentes	France	MA RND 23	Cenomanian	Rage et al, 2016
Simoliophis rochebrunei	Simoliophiidae	Charentes	France	MA SNA 4	Cenomanian	Rage et al, 2016
Simoliophis rochebrunei	Simoliophiidae	Charentes	France	MA SNA 2	Cenomanian	Rage et al, 2016
Simoliophis rochebrunei	Simoliophiidae	Charentes	France	MA RND 11	Cenomanian	Rage et al, 2016
Simoliophis rochebrunei	Simoliophiidae	Sillac	France	lost specimens from Rochebrune, 1880	Cenomanian	Rage et al, 2016

Appendix 3 – Body sizes of extant taxa
From Feldman et al 2016

Taxa	Size (mm)
Abronia frosti	110
Acalyptophis peronii	1230
Acanthophis antarcticus	1000
Acanthophis praelongus	700
Achalinus meiguensis	405
Achalinus rufescens	450
Acrantophis dumerili	1708
Acrantophis madagascariensis	3200
Acrochordus arafurae	2500
Acrochordus granulatus	1220
Acrochordus javanicus	2900
Acutotyphlops kunuaensis	373
Acutotyphlops subocularis	394
Adelophis foxi	430
Adelphicos quadrivirgatum	390
Afronatrix anoscopus	750
Afrotyphlops angolensis	660
Afrotyphlops bibronii	484
Afrotyphlops congestus	765
Afrotyphlops fornasinii	180
Afrotyphlops lineolatus	640
Afrotyphlops obtusus	372
Afrotyphlops punctatus	660
Afrotyphlops schlegelii	900
Agama spinosa	126
Agkistrodon bilineatus	1380
Agkistrodon contortrix	1350
Agkistrodon piscivorus	1892
Agkistrodon taylori	960
Ahaetulla fronticincta	980
Ahaetulla nasuta	2000
Ahaetulla pulverulenta	1730
Aipysurus apraefrontalis	600
Aipysurus duboisii	700
Aipysurus eydouxii	1000
Aipysurus fuscus	600
Aipysurus laevis	2000
Alluaudina bellyi	447
Alsophis antiguae	700
Alsophis antillensis	930
Alsophis rijgersmaei	790
Alsophis rufiventris	920
Amastridium veliferum	725
Amblyodipsas dimidiata	515
Amblyodipsas polylepis	1120
Amerotyphlops brongersmianus	325
Amerotyphlops reticulatus	522
Amphiesma stolatum	800
Amplorhinus multimaculatus	630
Anguis fragilis	291
Anilios ammodytes	252
Anilios australis	500
Anilios bicolor	420
Anilios bituberculatus	450
Anilios diversus	350
Anilios endoterus	400
Anilios ganei	335
Anilios grypus	450
Anilios guentheri	400
Anilios hamatus	420
Anilios howi	210
Anilios kimberleyensis	296
Anilios leptosomus	400
Anilios ligatus	500
Anilios longissimus	268
Anilios pilbarensis	370
Anilios pinguis	550
Anilios polygrammicus	395
Anilios splendidus	512
Anilios troglodytes	402
Anilios unguirostris	700
Anilios waitii	600
Anilius scytale	1200
Anniella geronimensis	165
Anomochilus leonardi	228
Antaresia childreni	1000
Antaresia maculosa	1000
Antaresia perthensis	600
Antaresia stimsoni	1000
Aparallactus capensis	400
Aparallactus guentheri	470
Aparallactus modestus	650
Aparallactus werneri	360
Aplopeltura boa	840
Apostolepis albicollaris	497

Apostolepis assimilis	500
Apostolepis cearensis	255
Apostolepis cearensis2	255
Apostolepis dimidiata	634
Apostolepis flavotorquata	500
Archelaphe bella	800
Arizona elegans	1780
Arrhyton dolichura	249
Arrhyton procerum	207
Arrhyton redimitum	250
Arrhyton supernum	255
Arrhyton taeniatum	448
Arrhyton tanyplectum	306
Arrhyton vittatum	207
Aspidelaps scutatus	750
Aspidites melanocephalus	2500
Aspidites ramsayi	2700
Aspidomorphus lineaticollis	400
Aspidomorphus muelleri	660
Aspidomorphus schlegeli	425
Aspidura ceylonensis	500
Aspidura drummondhayi	200
Aspidura guentheri	160
Aspidura trachyprocta	383
Asthenodipsas vertebralis	760
Atheris barbouri	369
Atheris ceratophora	550
Atheris chlorechis	700
Atheris desaixi	700
Atheris hispida	735
Atheris nitschei	750
Atheris squamigera	780
Atractaspis bibronii	700
Atractaspis boulengeri	700
Atractaspis corpulenta	600
Atractaspis irregularis	660
Atractaspis microlepidota	670
Atractaspis micropholis	920
Atractus albuquerquei	772
Atractus badius	430
Atractus elaps	631
Atractus flammigerus	400
Atractus reticulatus	437
Atractus schach	421
Atractus trihedrurus	1085
Atractus wagleri	541
Atractus zebrinus	649
Atractus zidoki	300
Atretium schistosum	1000
Atretium yunnanensis	750
Atropoides nummifer	870
Atropoides occiduus	795
Atropoides olmec	770
Atropoides picadoi	1202
Austrelaps labialis	870
Austrelaps superbus	1700
Azemiops feae	925
Balanophis ceylonensis	500
Bamanophis dorri	995
Basiliscus vittatus	225
Bitia hydroides	718
Bitis arietans	1850
Bitis atropos	550
Bitis caudalis	600
Bitis cornuta	750
Bitis gabonica	1800
Bitis nasicornis	1200
Bitis peringueyi	330
Bitis rubida	420
Bitis worthingtoni	560
Bitis xeropaga	650
Boa constrictor	4500
Boaedon fuliginosus	1300
Boaedon lineatus	800
Boaedon olivaceus	900
Boaedon virgatus	900
Bogertophis rosaliae	1520
Bogertophis subocularis	1680
Boiga barnesii	600
Boiga beddomei	1232
Boiga ceylonensis	1320
Boiga cynodon	2765
Boiga dendrophila	2500
Boiga forsteni	2313
Boiga irregularis	2200
Boiga kraepelini	1520
Boiga multomaculata	1900
Boiga trigonata	1250
Boiruna maculata	1800
Borikenophis portoricensis	923
Bothriechis aurifer	1000
Bothriechis bicolor	1000
Bothriechis lateralis	1000
Bothriechis marchi	968

Bothriechis nigroviridis	937
Bothriechis rowleyi	970
Bothriechis schlegelii	820
Bothriechis thalassinus	1000
Bothrochilus albertisii	2440
Bothrochilus boa	1730
Bothrocophias campbelli	1230
Bothrocophias hyoprora	830
Bothrocophias microphthalmus	1162
Bothrolycus ater	702
Bothrophthalmus brunneus	1200
Bothrophthalmus lineatus	1300
Bothrops alcatraz	505
Bothrops alternatus	1690
Bothrops ammodytoides	1000
Bothrops asper	2500
Bothrops atrox	1532
Bothrops bilineata	965
Bothrops brazili	1400
Bothrops caribbaeus	2000
Bothrops chloromelas	1000
Bothrops cotiara	1000
Bothrops diporus	1100
Bothrops erythromelas	850
Bothrops fonsecai	1079
Bothrops insularis	1180
Bothrops itapetiningae	570
Bothrops jararaca	1600
Bothrops jararacussu	2200
Bothrops lanceolatus	2000
Bothrops leucurus	1950
Bothrops marajoensis	1500
Bothrops moojeni	2300
Bothrops neuwiedi	1000
Bothrops pictus	600
Bothrops pulchra	764
Bothrops punctatus	1400
Bothrops taeniata	1360
Brachyophidium rhodogaster	210
Brachyurophis semifasciatus	400
Buhoma depressiceps	440
Buhoma procterae	520
Bungarus bungaroides	1400
Bungarus caeruleus	1750
Bungarus candidus	1600
Bungarus ceylonicus	1350
Bungarus fasciatus	2250
Bungarus flaviceps	1850
Bungarus multicinctus	1354
Bungarus niger	1295
Bungarus sindanus	1800
Caaeteboia amarali	386
Cacophis squamulosus	750
Calabaria reinhardtii	1030
Calamaria pavimentata	490
Calamaria yunnanensis	362
Calamodontophis paucidens	416
Calliophis bivirgata	1850
Calliophis melanurus	350
Calloselasma rhodostoma	1045
Candoia aspera	1000
Candoia bibroni	1460
Candoia carinata	720
Cantoria violacea	1250
Caraiba andreae	700
Carphophis amoenus	350
Casarea dussumieri	1500
Causus defilippii	420
Causus resimus	750
Causus rhombeatus	950
Celestus haetianus	98
Cemophora coccinea	828
Cerastes cerastes	890
Cerastes gasperettii	860
Cerastes vipera	480
Cerberus australis	737
Cerberus microlepis	1046
Cerberus rynchops	1270
Cerrophidion godmani	822
Cerrophidion petlalcalensis	467
Cerrophidion tzotzilorum	500
Charina bottae	840
Chilabothrus angulifer	4000
Chilabothrus chrysogaster	1310
Chilabothrus exsul	810
Chilabothrus fordii	860
Chilabothrus inornatus	2700
Chilabothrus monensis	1230
Chilabothrus striatus	2220
Chilabothrus subflavus	2300
Chilomeniscus stramineus	285
Chionactis occipitalis	432

Chironius bicarinatus	1800
Chironius carinatus	2054
Chironius exoletus	1545
Chironius flavolineatus	1200
Chironius fuscus	1597
Chironius grandisquamis	2718
Chironius laevicollis	1800
Chironius laurenti	2152
Chironius monticola	1500
Chironius multiventris	2611
Chironius quadricarinatus	1200
Chironius scurrulus	2430
Chrysopelea ornata	1750
Chrysopelea paradisi	1500
Chrysopelea taprobanica	1000
Clelia clelia	2500
Clonophis kirtlandii	622
Coelognathus erythrurus	1680
Coelognathus flavolineatus	1800
Coelognathus helena	1680
Coelognathus radiatus	2300
Coelognathus subradiatus	1200
Coluber constrictor	1911
Coluber flagellum	2600
Coluber taeniatus	1830
Coluber zebrinus	650
Compsophis albiventris	504
Compsophis boulengeri	353
Compsophis infralineatus	933
Compsophis laphystius	622
Coniophanes fissidens	795
Conophis lineatus	1170
Conopsis biserialis	377
Conopsis nasus	385
Contia tenuis	483
Corallus annulatus	1725
Corallus caninus	1945
Corallus hortulanus	1887
Coronella austriaca	800
Coronella girondica	800
Crisantophis nevermanni	1007
Crotalus adamanteus	2515
Crotalus aquilus	678
Crotalus atrox	2337
Crotalus atrox2	2337
Crotalus basiliscus	2045
Crotalus catalinensis	847
Crotalus cerastes	840
Crotalus durissus	1800
Crotalus enyo	890
Crotalus horridus	1892
Crotalus intermedius	570
Crotalus lepidus	840
Crotalus mitchellii	1370
Crotalus molossus	1370
Crotalus oreganus	1625
Crotalus polystictus	1000
Crotalus pricei	670
Crotalus pusillus	682
Crotalus ravus	700
Crotalus ruber	1650
Crotalus scutulatus	1400
Crotalus simus	1800
Crotalus tancitarensis	410
Crotalus tigris	910
Crotalus totonacus	1800
Crotalus transversus	465
Crotalus triseriatus	683
Crotalus viridis	1650
Crotalus willardi	670
Crotaphopeltis tornieri	630
Cryophis hallbergi	725
Cryptophis nigrescens	1200
Cubophis cantherigerus	1120
Cubophis vudii	840
Cyclophiops major	1200
Cylindrophis maculatus	350
Cylindrophis ruffus	1000
Daboia deserti	1600
Daboia mauritanica	1810
Daboia palaestinae	1500
Daboia russelii	1850
Dasypeltis atra	1100
Dasypeltis confusa	1000
Dasypeltis fasciata	1150
Dasypeltis gansi	1020
Dasypeltis sahelensis	620
Dasypeltis scabra	1160
Deinagkistrodon acutus	1490
Demansia papuensis	1650
Demansia psammophis	1000
Demansia vestigiata	1200
Dendrelaphis bifrenalis	900
Dendrelaphis caudolineatus	1800

Dendrelaphis caudolineolatus	1500
Dendrelaphis schokari	735
Dendrelaphis tristis	1690
Dendroaspis angusticeps	2500
Dendroaspis polylepis	4250
Dendrophidion dendrophis	1183
Dendrophidion percarinatum	1175
Denisonia devisi	600
Diadophis punctatus	870
Dinilysia patagonica	1800
Diploglossus pleii	160
Dipsadoboa unicolor	1280
Dipsas albifrons	590
Dipsas articulata	712
Dipsas catesbyi	705
Dipsas indica	1028
Dipsas neivai	680
Dipsas pratti	670
Dipsas variegata	912
Dipsina multimaculata	500
Dispholidus typus	1850
Ditypophis vivax	304.8
Dolichophis caspius	2500
Dolichophis jugularis	2500
Dolichophis schmidti	1600
Drepanoides anomalus	837
Dromicodryas bernieri	1100
Dromicodryas quadrilineatus	1200
Drymarchon corais	2630
Drymobius rhombifer	1270
Drymoluber brazili	1000
Drymoluber dichrous	1300
Dryocalamus nympha	535
Drysdalia coronoides	450
Drysdalia mastersii	400
Duberria lutrix	450
Duberria variegata	400
Echinanthera melanostigma	770
Echinanthera undulata	480
Echiopsis curta	600
Echis carinatus	800
Echis coloratus	900
Echis jogeri	300
Echis leucogaster	870
Echis ocellatus	670
Echis omanensis	800
Echis pyramidum	850
Eirenis aurolineatus	480
Eirenis barani	492
Eirenis collaris	403
Eirenis coronelloides	334
Eirenis decemlineatus	807
Eirenis eiselti	400
Eirenis levantinus	462
Eirenis lineomaculatus	316
Eirenis medus	310
Eirenis modestus	600
Eirenis persicus	1080
Eirenis punctatolineatus	600
Eirenis rothii	350
Eirenis thospitis	540
Elaphe bimaculata	800
Elaphe carinata	2500
Elaphe climacophora	2000
Elaphe davidi	960
Elaphe dione	1000
Elaphe quadrivirgata	1500
Elaphe quatuorlineata	2000
Elaphe sauromates	2000
Elaphe schrenckii	1700
Elapognathus coronatus	690
Elapomorphus quinquelineatus	1000
Elapsoidea nigra	600
Elapsoidea semiannulata	600
Elapsoidea sundevallii	1000
Emydocephalus annulatus	900
Enhydris enhydris	972
Enhydris innominata	175
Enhydris jagorii	515
Enhydris longicauda	803
Ephalophis greyae	500
Epicrates cenchria	2200
Epictia albipuncta	355
Epictia columbi	180
Epictia goudotii	185
Eristicophis macmahoni	719
Erpeton tentaculatum	770
Erythrolamprus aesculapii	927
Erythrolamprus almadensis	660
Erythrolamprus atraventer	455
Erythrolamprus breviceps	607

Erythrolamprus ceii	524
Erythrolamprus epinephelus	800
Erythrolamprus jaegeri	676
Erythrolamprus juliae	458
Erythrolamprus miliaris	684
Erythrolamprus mimus	1000
Erythrolamprus poecilogyrus	700
Erythrolamprus pygmaeus	247
Erythrolamprus reginae	810
Erythrolamprus typhlus	853
Eryx colubrinus	900
Eryx conicus	1000
Eryx elegans	690
Eryx jaculus	800
Eryx jayakari	640
Eryx johnii	1000
Eryx miliaris	910
Eryx tataricus	720
Eunectes murinus	7315
Eunectes notaeus	4000
Eupodophis descouensi	850
Euprepiophis conspicillata	1200
Euprepiophis mandarinus	1740
Exiliboa placata	467
Farancia abacura	2070
Farancia erytrogramma	1733
Ficimia streckeri	483
Fordonia leucobalia	1000
Furina diadema	400
Furina ornata	700
Garthius chaseni	690
Geophis carinosus	276
Geophis godmani	401
Gerarda prevostiana	525
Gerrhonotus parvus	84.5
Gerrhopilus hedraeus	134
Gerrhopilus mirus	130
Gigantophis garstini	6900
Gloydius blomhoffii	675
Gloydius brevicaudus	710
Gloydius halys	750
Gloydius intermedius	790
Gloydius saxatilis	740
Gloydius shedaoensis	990
Gloydius strauchi	547
Gloydius tsushimaensis	600
Gloydius ussuriensis	650
Gomesophis brasiliensis	336
Gonionotophis brussauxi	450
Gonionotophis capensis	1750
Gonionotophis nyassae	650
Gonionotophis poensis	1400
Gonionotophis stenophthalmus	760
Gonyosoma boulengeri	1380
Gonyosoma frenatus	1500
Gonyosoma jansenii	2300
Gonyosoma oxycephalum	2400
Gonyosoma prasinus	1200
Grayia ornata	1065
Grayia smithii	700
Grayia tholloni	1200
Gyalopion canum	384
Haasiophis terrasanctus	880
Haitiophis anomalus	2743
Hapsidophrys lineatus	1100
Hapsidophrys principis	1150
Hapsidophrys smaragdina	1100
Hebius craspedogaster	635
Hebius sauteri	401
Helicops angulatus	1025
Helicops carinicaudus	1010
Helicops gomesi	1007
Helicops hagmanni	945
Helicops infrataeniatus	1000
Heloderma suspectum	362
Hemachatus haemachatus	1500
Hemerophis socotrae	1480
Hemiaspis damelii	600
Hemiaspis signata	700
Hemibungarus calligaster	519
Hemirhagerrhis hildebrandtii	630
Hemirhagerrhis kelleri	390
Hemirhagerrhis viperina	300
Hemorrhois algirus	1145
Hemorrhois hippocrepis	2000
Hemorrhois nummifer	1275
Hemorrhois ravergieri	1391.5
Heterodon nasicus	1540
Heterodon platirhinos	1156
Heterodon simus	610
Heteroliodon occipitalis	325
Hierophis gemonensis	1280

Hierophis viridiflavus	1600
Homalopsis buccata	1400
Homoroselaps lacteus	650
Hoplocephalus bitorquatus	800
Hormonotus modestus	850
Hydrelaps darwiniensis	500
Hydrodynastes bicinctus	1500
Hydrodynastes gigas	2750
Hydromorphus concolor	797
Hydrophis atriceps	1200
Hydrophis brooki	1040
Hydrophis caerulescens	820
Hydrophis curtus	1100
Hydrophis cyanocinctus	2750
Hydrophis czeblukovi	1200
Hydrophis elegans	2000
Hydrophis kingii	1500
Hydrophis lapemoides	1050
Hydrophis macdowelli	800
Hydrophis major	1300
Hydrophis melanocephalus	1230
Hydrophis ornatus	1115
Hydrophis pacificus	1400
Hydrophis parviceps	1250
Hydrophis platurus	880
Hydrophis schistosus	1200
Hydrophis semperi	700
Hydrophis spiralis	2750
Hydrophis stokesii	2000
Hydrops triangularis	712
Hypnale hypnale	550
Hypnale nepa	387
Hypnale zara	407
Hypsiglena affinis	310
Hypsiglena chlorophaea	600
Hypsiglena jani	660
Hypsiglena ochrorhyncha	660
Hypsiglena slevini	560
Hypsiglena torquata	660
Hypsirhynchus callilaemus	465
Hypsirhynchus ferox	773
Hypsirhynchus funereus	479
Hypsirhynchus parvifrons	557
Hypsirhynchus polylepis	455
Hypsiscopus matannensis	563
Hypsiscopus plumbea	560
Ialtris dorsalis	990
Ialtris haetianus	305
Iguana iguana	580
Imantodes cenchoa	1554
Imantodes gemmistratus	880
Imantodes inornatus	1035
Imantodes lentiferus	1200
Indotyphlops albiceps	302
Indotyphlops braminus	180
Indotyphlops pammeces	145
Inyoka swazicus	900
Ithycyphus miniatus	1700
Ithycyphus oursi	1568
Lachesis muta	3600
Lachesis stenophrys	3900
Lampropeltis alterna	1471
Lampropeltis californiae	2000
Lampropeltis calligaster	1427
Lampropeltis elapsoides	686
Lampropeltis extenuata	654
Lampropeltis getula	2083
Lampropeltis holbrooki	1829
Lampropeltis mexicana	605
Lampropeltis nigra	1473
Lampropeltis pyromelana	1088
Lampropeltis ruthveni	800
Lampropeltis splendida	1524
Lampropeltis triangulum	1900
Lampropeltis webbi	306
Lampropeltis zonata	1230
Lamprophis aurora	620
Lamprophis fiskii	400
Lamprophis fuscus	760
Lamprophis guttatus	620
Langaha madagascariensis	1000
Lanthanotus borneensis	400
Laticauda colubrina	1420
Laticauda guineai	1457
Laticauda laticaudata	1100
Laticauda saintgironsi	1090
Leiocephalus barahonensis	84
Leioheterodon geayi	1400
Leioheterodon madagascariensis	1500
Leioheterodon modestus	1200
Leiolepis guttata	250
Leiosaurus bellii	110
Leptodeira annulata	1038

Leptodeira bakeri	691
Leptodeira frenata	715
Leptodeira maculata	630
Leptodeira nigrofasciata	581
Leptodeira punctata	523
Leptodeira rubricata	700
Leptodeira septentrionalis	1055
Leptodeira splendida	888
Leptodeira uribei	542
Leptophis ahaetulla	2250
Leptotyphlops conjunctus	191
Leptotyphlops distanti	240
Leptotyphlops nigricans	200
Leptotyphlops nigroterminus	193
Leptotyphlops scutifrons	280
Leptotyphlops sylvicolus	126
Letheobia feae	330
Letheobia newtoni	400
Liasis fuscus	3000
Liasis mackloti	2500
Liasis olivaceus	4000
Liasis papuana	4270
Lichanura trivirgata	1120
Liolaemus ceii	90
Liophidium chabaudi	490
Liophidium mayottensis	978
Liophidium rhodogaster	600
Liophidium therezieni	726
Liophidium torquatum	700
Liophidium vaillanti	620
Liopholidophis dimorphus	1072
Liopholidophis dolicocercus	1426
Liopholidophis sexlineatus	1385
Liotyphlops albirostris	223
Loxocemus bicolor	1530
Lycodon aulicus	800
Lycodon capucinus	780
Lycodon carinatus	600
Lycodon fasciatus	895
Lycodon laoensis	560
Lycodon osmanhilli	545
Lycodon paucifasciatus	763
Lycodon rufozonatus	1350
Lycodon ruhstrati	1055
Lycodon semicarinatus	1700
Lycodon zawi	480
Lycodonomorphus inornatus	1300
Lycodonomorphus laevissimus	1200
Lycodonomorphus rufulus	850
Lycodonomorphus whytii	660
Lycodryas citrinus	705
Lycodryas granuliceps	1020
Lycodryas inopinae	619
Lycodryas inornatus	647
Lycodryas maculatus	867
Lycodryas pseudogranuliceps	710
Lycognathophis seychellensis	1200
Lycophidion capense	580
Lycophidion laterale	480
Lycophidion nigromaculatum	400
Lycophidion ornatum	590
Lygophis anomalus	760
Lygophis elegantissimus	745
Lygophis flavifrenatus	755
Lygophis lineatus	737
Lygophis meridionalis	649
Lygophis paucidens	496
Lytorhynchus diadema	440
Macrelaps microlepidotus	1200
Macropisthodon rudis	1156
Macroprotodon abubakeri	464
Macroprotodon cucullatus	550
Macrovipera lebetina	2140
Macrovipera schweizeri	1070
Madagascarophis colubrinus	1060
Madagascarophis meridionalis	870
Madatyphlops arenarius	220
Madtsoia madagascariensis	8000
Magliophis exiguum	360.5
Malayopython reticulatus	8659
Malayopython timoriensis	3000
Malayotyphlops luzonensis	260
Malayotyphlops ruber	225
Malpolon monspessulanus	1400
Manolepis putnami	717
Mastigodryas bifossatus	1700
Mastigodryas boddaerti	1505
Mastigodryas melanolomus	2000

Melanophidium punctatum	560
Menarana nosymena	2400
Micrelaps bicoloratus	330
Microlophus tigris	105
Micropechis ikaheka	2000
Micropisthodon ochraceus	700
Micruroides euryxanthus	660
Micrurus albicinctus	573
Micrurus altirostris	1310
Micrurus baliocoryphus	1449
Micrurus brasiliensis	1513
Micrurus corallinus	987
Micrurus decoratus	670
Micrurus diastema	895
Micrurus dissoleucus	650
Micrurus frontalis	1418
Micrurus fulvius	1213
Micrurus hemprichii	917
Micrurus ibiboboca	1330
Micrurus lemniscatus	1390
Micrurus mipartitus	1130
Micrurus narduccii	1157
Micrurus psyches	910
Micrurus pyrrhocryptus	1747
Micrurus spixii	1602
Micrurus surinamensis	1325
Mimophis mahfalensis	1000
Mitophis asbolepis	156
Mitophis leptipileptus	156
Mitophis pyrites	165
Mixcoatlus barbouri	510
Mixcoatlus melanurus	578
Montivipera albizona	780
Montivipera bornmuelleri	740
Montivipera raddei	1100
Montivipera wagneri	950
Montivipera xanthina	1300
Morelia bredli	3000
Morelia carinata	2000
Morelia spilota	4000
Morelia viridis	2000
Mussurana bicolor	825
Myriopholis adleri	135
Myriopholis algeriensis	285
Myriopholis blanfordi	240
Myriopholis boueti	205
Myriopholis longicauda	255
Myriopholis macrorhyncha	269
Myriopholis rouxestevae	180
Myron richardsonii	600
Myrrophis chinensis	810
Naja annulata	2700
Naja annulifera	2130
Naja ashei	2700
Naja atra	1650
Naja haje	2600
Naja kaouthia	2300
Naja katiensis	1400
Naja mandalayensis	828
Naja melanoleuca	2700
Naja mossambica	1500
Naja multifasciata	800
Naja naja	2200
Naja nigricollis	2700
Naja nivea	1860
Naja nubiae	1480
Naja pallida	1500
Naja siamensis	1600
Naja sumatrana	1600
Najash rionegrina	2000
Namibiana occidentalis	322
Natriciteres olivacea	540
Natrix maura	800
Natrix natrix	2000
Natrix tessellata	1000
Nerodia cyclopion	1295
Nerodia erythrogaster	1636
Nerodia fasciata	1588
Nerodia floridana	1880
Nerodia harteri	902
Nerodia rhombifer	1753
Nerodia sipedon	1500
Nerodia taxispilota	1766
Ninia atrata	450
Notechis scutatus	2000
Nothopsis rugosus	433
Oligodon arnensis	700
Oligodon barroni	450
Oligodon chinensis	496
Oligodon cinereus	730
Oligodon cruentatus	410
Oligodon cyclurus	940
Oligodon formosanus	750
Oligodon maculatus	299

Oligodon ocellatus	852
Oligodon octolineatus	700
Oligodon planiceps	255
Oligodon splendidus	830
Oligodon sublineatus	300
Oligodon taeniatus	440
Oligodon taeniolatus	590
Oligodon theobaldi	437
Oligodon torquatus	300
Oocatochus rufodorsatus	205
Opheodrys aestivus	1159
Opheodrys vernalis	810
Ophiophagus hannah	5850
Ophryacus undulatus	700
Opisthotropis cheni	430
Opisthotropis guangxiensis	455
Opisthotropis lateralis	500
Opisthotropis latouchii	577
Oreocryptophis porphyraceus	1250
Orientocoluber spinalis	570
Orthriophis cantoris	1960
Orthriophis hodgsoni	2100
Orthriophis moellendorffi	2500
Orthriophis taeniurus	2700
Ovophis monticola	1250
Ovophis okinavensis	1000
Ovophis tonkinensis	561
Ovophis zayuensis	580
Oxybelis aeneus	1524
Oxybelis fulgidus	2160
Oxyrhabdium leporinum	685
Oxyrhopus clathratus	800
Oxyrhopus formosus	1027
Oxyrhopus guibei	1080
Oxyrhopus melanogenys	1018
Oxyrhopus petolarius	2200
Oxyrhopus rhombifer	900
Oxyrhopus trigeminus	860
Oxyuranus microlepidotus	2500
Oxyuranus scutellatus	3360
Pachyophis woodwardi	400
Pachyrhachis problematicus	1500
Pantherophis alleghaniensis	2565
Pantherophis bairdi	1575
Pantherophis emoryi	1530
Pantherophis guttatus	1830
Pantherophis obsoletus	2565
Pantherophis slowinskii	1500
Pantherophis spiloides	2140
Pantherophis vulpinus	1791
Parahydrophis mertoni	500
Paraphimophis rusticus	1850
Parastenophis betsileanus	1290
Parasuta monachus	460
Parasuta spectabilis	400
Pareas boulengeri	610
Pareas carinatus	600
Pareas formosensis	682
Pareas hamptoni	705
Pareas margaritophorus	480
Pareas margaritophorus2	480
Pareas monticola	610
Pareas nuchalis	715
Paroplocephalus atriceps	569
Phalotris lativittatus	800
Phalotris lemniscatus	570
Phalotris mertensi	1262
Phalotris nasutus	950
Philodryas aestivus	1000
Philodryas agassizii	500
Philodryas argentea	1335
Philodryas baroni	1500
Philodryas georgeboulengeri	790
Philodryas mattogrossensis	1500
Philodryas nattereri	1065.5
Philodryas olfersii	1476
Philodryas patagoniensis	1550
Philodryas psammophidea	1000
Philodryas viridissima	1200
Philothamnus angolensis	1200
Philothamnus carinatus	850
Philothamnus girardi	910
Philothamnus heterodermus	960
Philothamnus hoplogaster	960
Philothamnus natalensis	1300
Philothamnus nitidus	930
Philothamnus semivariegatus	1300
Philothamnus thomensis	900
Phimophis guerini	1038
Phyllorhynchus decurtatus	510
Phytolopsis punctata	450
Pituophis catenifer	2790

Pituophis deppei	1790
Pituophis lineaticollis	2100
Pituophis melanoleucus	2286
Pituophis ruthveni	1784
Pituophis vertebralis	1530
Plagiopholis styani	396
Platyceps collaris	1000
Platyceps florulentus	1000
Platyceps karelini	1000
Platyceps karelini2	1000
Platyceps najadum	1300
Platyceps rhodorachis	1400
Platyceps ventromaculatus	1260
Pogona minor	170
Polemon acanthias	560
Polemon collaris	860
Polemon notatus	310
Polychrus femoralis	108
Porthidium dunni	542
Porthidium lansbergii	900
Porthidium nasutum	635
Porthidium ophryomegas	800
Porthidium porrasi	700
Porthidium yucatanicum	550
Proatheris superciliaris	600
Prosymna greigerti	360
Prosymna janii	310
Prosymna meleagris	370
Prosymna ruspolii	300
Prosymna visseri	350
Protobothrops cornutus	696
Protobothrops elegans	1320
Protobothrops flavoviridis	2400
Protobothrops jerdonii	1090
Protobothrops kaulbacki	1410
Protobothrops mangshanensis	2030
Protobothrops mucrosquamatus	1280
Protobothrops sieversorum	1255
Protobothrops tokarensis	1500
Protobothrops xiangchengensis	889
Psammodynastes pictus	550
Psammodynastes pulverulentus	770
Psammophis angolensis	500
Psammophis biseriatus	1000
Psammophis condanarus	1075
Psammophis crucifer	822
Psammophis jallae	1200
Psammophis leightoni	1000
Psammophis leopardinus	1400
Psammophis lineatus	1200
Psammophis lineolatus	1047
Psammophis mossambicus	1800
Psammophis notostictus	1000
Psammophis orientalis	1400
Psammophis phillipsi	1740
Psammophis praeornatus	550
Psammophis punctulatus	1900
Psammophis rukwae	1300
Psammophis schokari	1500
Psammophis sibilans	1500
Psammophis subtaeniatus	1400
Psammophis sudanensis	1200
Psammophis tanganicus	1000
Psammophis trigrammus	1200
Psammophylax acutus	1060
Psammophylax rhombeatus	1400
Psammophylax tritaeniatus	930
Psammophylax variabilis	1400
Pseudalsophis biserialis	1005
Pseudalsophis elegans	1020
Pseudaspis cana	2400
Pseudechis australis	2750
Pseudechis butleri	1600
Pseudechis colletti	1500
Pseudechis guttatus	1500
Pseudechis papuanus	2440
Pseudechis porphyriacus	2000
Pseudelaphe flavirufa	1650
Pseudoboa coronata	1076
Pseudoboa neuwiedii	1217
Pseudoboa nigra	1261
Pseudoboodon lemniscatus	965
Pseudocerastes fieldi	890
Pseudocerastes persicus	1080
Pseudoeryx plicatilis	1070
Pseudoferania polylepis	800
Pseudoficimia frontalis	502
Pseudoleptodeira latifasciata	688
Pseudonaja modesta	600
Pseudonaja textilis	2200

Pseudorabdion oxycephalum	282
Pseudotomodon trigonatus	450
Pseudotyphlops philippinus	430
Pseudoxenodon bambusicola	530
Pseudoxenodon karlschmidti	1730
Pseudoxenodon macrops	1400
Pseudoxyrhopus ambreensis	423
Psomophis genimaculatus	450
Psomophis joberti	301
Psomophis obtusus	455
Ptyas korros	2680
Ptyas mucosa	3700
Ptychophis flavovirgatus	495
Python brongersmai	3000
Python curtus	2000
Python molurus	5791
Python regius	1500
Python sebae	5500
Pythonodipsas carinata	800
Ramphotyphlops acuticaudus	243
Ramphotyphlops lineatus	480
Regina alleni	705
Regina grahami	1194
Regina rigida	797
Regina septemvittata	922
Rena dulcis	283
Rena humilis	410
Rhabdophis nuchalis	620
Rhabdophis subminiatus	800
Rhabdophis tigrinus	1013
Rhachidelus brazili	1311
Rhadinaea flavilata	403
Rhadinaea fulvivittis	565
Rhagerhis moilensis	1890
Rhamphiophis oxyrhynchus	1600
Rhamphiophis rubropunctatus	2500
Rhinechis scalaris	1600
Rhinobothryum lentiginosum	1605
Rhinocheilus lecontei	1520
Rhinophis blythii	350
Rhinophis dorsimaculatus	350
Rhinophis drummondhayi	300
Rhinophis homolepis	275
Rhinophis oxyrhynchus	430
Rhinophis philippinus	270
Rhinophis travancoricus	180
Rhinoplocephalus bicolor	450
Rhinotyphlops lalandei	350
Rodriguesophis iglesiasi	444
Salvadora mexicana	1615
Sanzinia madagascariensis	1910
Scaphiodontophis annulatus	900
Scaphiophis albopunctatus	1600
Seminatrix pygaea	555
Senticolis triaspis	1600
Siagonodon septemstriatus	300
Sibon nebulatus	1013
Sibynomorphus mikanii	580
Sibynomorphus neuwiedi	660
Sibynomorphus turgidus	610
Sibynomorphus ventrimaculatus	577
Sibynophis bistrigatus	300
Sibynophis chinensis	694
Sibynophis collaris	850
Sibynophis subpunctatus	460
Sibynophis triangularis	700
Simalia amethistina	8500
Simalia boeleni	2440
Simalia oenpelliensis	4300
Simoliophis rochebrunei	1500
Simoselaps anomalus	250
Simoselaps bertholdi	300
Sinomicrurus japonicus	600
Sinomicrurus kelloggi	800
Sinomicrurus macclellandi	840
Sinonatrix aequifasciata	1420
Sinonatrix annularis	941
Sinonatrix percarinata	1100
Siphlophis cervinus	1022
Siphlophis compressus	1431
Siphlophis longicaudatus	525.5
Siphlophis pulcher	803
Sistrurus catenatus	1030
Sistrurus miliarius	803
Sonora semiannulata	480
Sordellina punctata	496
Spalerosophis diadema	2000
Spalerosophis microlepis	1430
Spilotes pullatus	3600
Spilotes sulphureus	2752

Stenorrhina freminvillei	700
Stoliczkia borneensis	750
Storeria dekayi	527
Storeria occipitomaculata	410
Subsessor bocourti	1230
Suta fasciata	620
Suta suta	600
Sympholis lippiens	535
Tachymenis peruviana	660
Taeniophallus affinis	712
Taeniophallus brevirostris	505
Taeniophallus nicagus	465
Tantalophis discolor	620
Tantilla melanocephala	450
Telescopus fallax	1200
Tetracheilostoma breuili	113
Tetracheilostoma carlae	104
Thalesius viridis	1600
Thamnodynastes hypoconia	650
Thamnodynastes lanei	648
Thamnodynastes pallidus	450
Thamnodynastes rutilus	641
Thamnodynastes strigatus	800
Thamnophis atratus	1070
Thamnophis brachystoma	559
Thamnophis butleri	737
Thamnophis chrysocephalus	450
Thamnophis couchii	1200
Thamnophis cyrtopsis	1145
Thamnophis elegans	1090
Thamnophis eques	2000
Thamnophis exsul	463
Thamnophis fulvus	652
Thamnophis gigas	1650
Thamnophis godmani	520
Thamnophis hammondii	1068
Thamnophis marcianus	1080
Thamnophis melanogaster	864
Thamnophis mendax	710
Thamnophis ordinoides	960
Thamnophis proximus	1230
Thamnophis radix	1095
Thamnophis rufipunctatus	1120
Thamnophis sauritus	1016
Thamnophis scaliger	420
Thamnophis sirtalis	1400
Thamnophis sumichrasti	756
Thamnophis valida	1096
Thamnosophis epistibes	917
Thamnosophis infrasignatus	920
Thamnosophis lateralis	828
Thamnosophis martae	893
Thamnosophis stumpffi	711
Thelotornis capensis	1400
Thermophis baileyi	590
Thermophis zhaoermii	917
Thrasops jacksonii	2300
Tomodon dorsatum	645
Toxicocalamus loriae	690
Toxicocalamus preussi	765
Toxicodryas pulverulenta	1250
Trachischium monticola	640
Trachyboa boulengeri	430
Trachyboa gularis	320
Tretanorhinus nigroluteus	885
Tretanorhinus variabilis	800
Tricheilostoma bicolor	185
Trilepida macrolepis	400
Trimeresurus albolabris	1000
Trimeresurus andersonii	1100
Trimeresurus borneensis	874
Trimeresurus cantori	1232
Trimeresurus erythrurus	1050
Trimeresurus fasciatus	509
Trimeresurus flavomaculatus	1100
Trimeresurus gracilis	479
Trimeresurus gramineus	1135
Trimeresurus hageni	1300
Trimeresurus insularis	930
Trimeresurus kanburiensis	667
Trimeresurus macrops	720
Trimeresurus malabaricus	1050
Trimeresurus malcolmi	1330
Trimeresurus popeiorum	1050
Trimeresurus puniceus	860
Trimeresurus purpureomaculatus	1050
Trimeresurus schultzei	1300
Trimeresurus septentrionalis	730
Trimeresurus sumatranus	1600
Trimeresurus tibetanus	722
Trimeresurus trigonocephalus	1200

Trimeresurus venustus	680
Trimetopon gracile	300
Trimorphodon biscutatus	1750
Tropidechis carinatus	1000
Tropidoclonion lineatum	570
Tropidodipsas sartorii	857
Tropidodryas serra	830
Tropidodryas striaticeps	678
Tropidolaemus wagleri	920
Tropidophis feicki	448
Tropidophis greenwayi	380
Tropidophis haetianus	552
Tropidophis melanurus	957
Tropidophis pardalis	287
Tropidophis wrighti	488
Typhlophis squamosus	225
Typhlops agoralionis	193
Typhlops anchaurus	240
Typhlops anousius	197
Typhlops arator	460
Typhlops biminiensis	363
Typhlops capitulatus	267
Typhlops catapontus	265
Typhlops caymanensis	260
Typhlops contorhinus	316
Typhlops dominicanus	385
Typhlops elegans	420
Typhlops eperopeus	281
Typhlops granti	210
Typhlops hectus	237
Typhlops hypomethes	270
Typhlops jamaicensis	445
Typhlops lumbricalis	257
Typhlops monastus	258
Typhlops notorachius	301
Typhlops platycephalus	337
Typhlops pusillus	226
Typhlops richardi	342
Typhlops rostellatus	222
Typhlops schwartzi	326
Typhlops sulcatus	319
Typhlops sylleptor	214
Typhlops syntherus	209
Typhlops titanops	216
Ungaliophis continentalis	762
Uromacer catesbyi	830
Uromacer frenatus	930
Uromacer oxyrhynchus	1500
Uromastyx ornata	210
Uropeltis ceylanicus	450
Uropeltis liura	320
Uropeltis melanogaster	300
Uropeltis phillipsi	200
Varanus griseus	625
Varanus tristis	305
Vermicella calonotus	300
Vermicella intermedia	605
Vipera ammodytes	1100
Vipera aspis	850
Vipera barani	590
Vipera berus	752
Vipera berus2	752
Vipera dinniki	590
Vipera eriwanensis	510
Vipera kaznakovi	700
Vipera latastei	720
Vipera lotievi	600
Vipera renardi	710
Vipera seoanei	700
Vipera ursinii	600
Virginia striatula	348
Viridovipera gumprechti	1280
Viridovipera medoensis	677
Viridovipera stejnegeri	1045
Viridovipera vogeli	1300
Viridovipera yunnanensis	1233
Walterinnesia aegyptia	1400
Wonambi barriei	3000
Wonambi naracoortensis	6130
Xenocalamus transvaalensis	470
Xenochrophis asperrimus	890
Xenochrophis flavipunctatus	1200
Xenochrophis piscator	1750
Xenochrophis punctulatus	630
Xenochrophis vittatus	700
Xenodermus javanicus	700
Xenodon dorbignyi	800
Xenodon guentheri	800
Xenodon histricus	345
Xenodon matogrossensis	441
Xenodon merremi	1000
Xenodon nattereri	442
Xenodon neuwiedii	800
Xenodon pulcher	700

Xenodon semicinctus	600
Xenodon severus	2000
Xenopeltis unicolor	1330
Xenophidion schaeferi	263
Xenopholis scalaris	354
Xenopholis undulatus	465
Xenosaurus grandis	120
Xenotyphlops grandidieri	284
Xerotyphlops vermicularis	400
Yurlunguur camfieldensis	5000
Zamenis hohenackeri	760
Zamenis lineata	1700
Zamenis longissimus	2000
Zamenis persica	1200
Zamenis situla	1000

Chapter 3: Cranial osteology of Typhlopidae, with comments on the unique anatomy of the parthenogenic blindsnake, *Indotyphlops braminus*

Abstract

Accurate descriptions of the highly specialised and distinctive cranial osteology of miniaturised, fossorial Scolecophidia are limited. Recent developments in computed tomography for biological specimens have allowed researchers to isolate individual cranial elements for detailed analysis and description. Accurate descriptions are important in light of conflicting results of the disparity between phylogenetic reconstructions of snakes based on either molecular or morphological data. These conflicting topologies require high degrees of homoplasy, either morphological or molecular, when considering snake evolution from other squamates. This is especially relevant when considering the potential paraphyly of Scolecophidia, reported by multiple studies using molecular data to reconstruct relationships, as opposed to the monophyly consistently recovered when morphological data is used for such analyses. Here I provide the first detailed descriptions of individual cranial elements of representative species of Typhlopidae. the largest clade of Scolecophidia and the only clade of snakes that possess teeth solely on the upper jaw. All specimens were CT scanned, and individual elements were segmented to allow detailed observations and comparisons between taxa. Several features may be important for the further understanding of the relationships between different Typhlopidae taxa, including the presence of a paired parietal, the presence or absence of the splenial, and the fusion between the various bones of the otic component of the skull. Features previously thought to be unique to Alethinophidia were found present in the largest typhlopids, *Afrotyphlops schlegelii* and *Afrotyphlops mucruso*, most prominently the dorsally projecting lateral wings of the basisphenoid. Additionally, this study has revealed previously unappreciated unique anatomy of the parthenogenic typhlopid *Indotyphlops braminus*, including large fissures between the cranial bones of adult specimens, and the fused otic region. These findings highlight the previously unappreciated diversity of anatomy that can be found in this understudied clade of fossorial snakes.

1. Introduction

Scolecophidia is a highly specialised clade or grade of fossorial snakes with a sub-tropical and tropical terrestrial distribution, and over 600 currently described species (Uetz *et al.* 2019). Scolecophidia are a distinctive snake clade or grade that show a combination of both specialised features that allow their highly fossorial lifestyle, such as a short tail and reduction of neural spines of the vertebrae, as well as plesiomorphic lizard features including the distinct proatlas, three separate elements comprising the atlas, and the presence of remnants of the pelvic girdle (List 1966). This combination of both primitive and highly derived features, as well as the recovery of a stemward position of the three clades as a paraphyletic grade relative to other snakes in molecular phylogenetic hypotheses, makes reconstructing the evolutionary relationships of snakes difficult, as it is hard to distinguish characters that are plesiomorphic for snakes and ones that are apomorphic for Scolecophidia. This problem highlights the importance of understanding the unique morphology of Scolecophidia, particularly as it relates to differences in body size and diet.

Convergent morphologies have the capability to confound phylogenetic reconstructions when relying solely on morphological data to hypothesise relatedness between taxa. Due to the distinctive cranial morphologies observed in scolecophidians, traditional morphological phylogenies consistently recover Scolecophidia as a monophyletic sister clade to Alethinophidia, the clade including all other extant snakes (Gauthier *et al.* 2012). In contrast, recent molecular phylogenies tend to recover Scolecophidia as paraphyletic at the base of the snake phylogeny (Figueroa *et al.* 2016; Miralles *et al.* 2018; Pyron *et al.* 2013; Streicher & Wiens 2016; Wiens *et al.* 2008; Zaher *et al.* 2019; Zheng & Wiens 2016). Recently Typhlopoidea, previously known as Typhlopidae, has been further divided into Typhlopidae, Gerrhopilidae (including the genus *Gerrhopilus*), and Xenotyphlopidae (including the monospecific genus *Xenotyphlops*) (Adalsteinsson *et al.* 2009; Miralles *et al.* 2018; Vidal *et al.* 2010). The incongruence of the proposed relatedness between species as a result of using either molecular or morphological data could be influenced by convergence in skull shape due to similar adaptations to a fossorial environment, a shared myrmecophagous diet, or reduction in overall body size. As the majority of characters used in snake phylogenetics are cranial (Lee & Scanlon 2002; Scanlon 2006), it is important to understand when morphological similarity in the cranium is homologous or homoplastic. This requires investigation of individual cranial elements to a greater specificity than previously established.

Scolecophidia are so easily distinguished from all other snakes that their assignment as snakes was initially contested by anatomists (McDowell & Bogert 1954). Although features such as the Jacobson's organ being enclosed by a bony capsule formed by the vomer and septomaxilla

and the descending processes of the parietal meeting the prootic and the basisphenoid to fully enclose the braincase confirm their placement as snakes (Underwood 1967), the morphology of Scolecophidia is still considerably distinct from all other snakes. Scolecophidia in general are characterised by a suite of characters such as a lack of a prokinetic joint, frontals lacking mesial frontal flanges, and a mandible shorter than the combined length of the braincase and snout (see Cundall & Irish, 2008 for full review). They also are the only snakes known whose vertebrae completely lack neural spines (Underwood 1967). This is a feature known to correlate with fossoriality in squamates, as reduction in neural spines is seen also in amphisbaenids, a fossorial clade of squamates (List 1966). Despite the considerable number of shared morphological features of the clade, the recovery hypothesis of phylogenetic relatedness constructed using molecular data that suggest the clades of Scolecophidia are paraphyletic highlights the importance of understanding the morphology of the different clades of Scolecophidia, particularly in deciphering morphological characters that define clades.

There are some aspects of scolecophidian morphology than support the hypothesis of paraphyly. This is most apparent when examining the differing jaw morphology between the three main clades of Scolecophidia; Typhlopoidea Leptotyphlopidae, and Anomalepididae. Although all clades share both a fossorial lifestyle and a diet predominantly made of small arthropods (Webb & Shine 1993), the jaw apparatuses of the three main clades are modified in distinct ways. In Leptotyphlopidae the maxilla is fixed and toothless, whereas in Typhlopoidea and Anomalepididae the maxilla is a rotatable short, toothed bone that is the primary means of prey manipulation and transport (Cundall & Irish 2008). In contrast, the dentary of Typhlopoidea is edentulous, whereas in Leptotyphlopidae the toothed dentary is instead the primary means of prey manipulation and transport in a unique behaviour known as 'mandibular raking' (Kley & Brainerd 1999). The dentary of Anomalepididae possesses only one or two teeth, that appear to not serve much function during feeding (Rieppel *et al.* 2009). All three configurations allow Scolecophidia to engage in a 'binge-feeding' method, where many small items of prey are taken in a single feeding event, usually the larvae or adults of eusocial insects such as ants or termites (Gans 1961). This is in stark contrast to the other extant clade of Serpentes, Alethinophidia, which instead show considerable morphological specialisations to eat a single prey item in a feeding event such as an elongated jaw suspensorium (supratemporal and quadrate) seen in macrostomatan clades and the pterygoid walk method of intraoral prey manipulation. The unique feeding methods of Scolecophidia are thought to have evolved in order to minimise the amount of time spent feeding, likely due to the aggressive nature of their preferred prey animals, ants and termites, which are known to exhibit vigorous nest-defending behaviours and toxic bites (Kley 2001). As all three clades of Scolecophidia have adapted to the

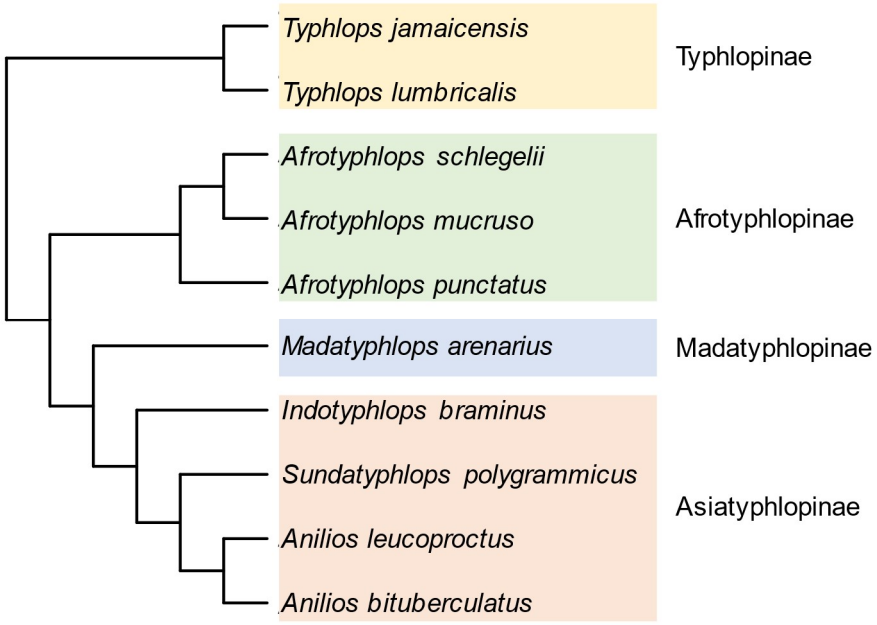

Figure 1: Relationships of examined taxa, based on Zheng & Wiens (2016). *Anilios leucoproctus* was not included in Zheng & Wiens (2016), and so was instead considered to be the closest relative to *Anilios bituberculatus*, as according to Hedges *et al.* (2014) and Pyron & Wallach (2014).

same ecological stimulus (the quick feeding on small prey) albeit using different bones of the jaw, this lends considerable support to the presence of convergence in other areas of the skull.

The majority of Scolecophidia are small in overall body size. The small size of individuals has made detailed descriptions of their cranial anatomy historically difficult to successfully complete. Previous studies include: The general patterns of cranial anatomy of Leptotyphlopidae, Typhlopidae, and Anomalepididae reviewed in Cundall & Irish (2008) and List (1966); Anomalepids including *Anomalepis aspinosus* (Haas 1968), *Liotyphlops albirostris* (Haas 1964), and *Liotyphlops albirostris* by Rieppel et al (2009), which includes comparisons to the typhlopid *Typhlops jamaicensis,* the leptotyphlopid *Leptotyphlops dulcis*, and the anomalepid *Typhlophis squamosus*; Leptotyphlopids including *Leptotyphlops dulcis* (Kley 2006) and *Trilepida salgueiroi* (Pinto *et al.* 2015); Typhlopoidea including the typhlopid *Typhlops jamaicensis* (Evans 1955), and the xenotyphlopid *Xenotyphlops grandidieri* (Chretien *et al.* 2019; Wallach & Ineich 1996). There is also an extensive comparative study of Scolecophidia composed by List (1966), although this work contains detailed anatomical drawings of individual species, the descriptions do not go into detail for individual species and are instead overall descriptions of the three main scolecophidian clades (List 1966). Recent micro-CT data allows more comprehensive descriptions to be completed, especially for miniaturised taxa that are difficult to examine through visual observations alone, as seen in recent descriptions of the taxa

Afrotyphlops punctatus (Deolindo *et al.* 2021), *Madatyphlops eudelini* (Hawlitschek *et al.* 2021), and *Amerotyphlops brongersmianus* and *Amerotyphlops reticulatus* (Lira & Martins 2021). These new techniques allow for detailed understanding of morphology and have the potential to elucidate interpretations of convergence and homoplasy.

This study aims to contribute to our understanding of scolecophidian anatomy by providing detailed descriptions of the cranial osteology of several species of Typhlopidae, the largest clade of Scolecophidia. The species examined include two Typhlopinae: *Typhlops jamaicensis, Typhlops lumbricalis;* three Afrotyphlopinae: *Afrotyphlops schlegelii, Afrotyphlops punctatus;* one Madatyphlopinae*: Madatyphlops arenarius*; and four Asiatyphlopinae: *Indotyphlops braminus, Sundatyphlops polygrammicus, Anilios bituberculatus,* and *Anilios leucoproctus*. These species span the phylogenetic breadth of Typhlopidae, with species from all geographical regions where the clade is located, and including four of the primary divisions within Typhlopidae (See Figure 1). The aim of this study is to identify features which may be either systematically useful, or aid in understanding the evolution and development of these distinctive taxa.

2. Methods

2.1 Data Collection and Scanning Parameters

I examined 10 species of Typhlopidae, representing the four major subclades: Typhlopinae, Afrotyphlopinae, Madatyphlopinae, and Asiatyphlopinae. Specimens were obtained from the University Museum of Zoology, Cambridge, the Natural History Museum, London, and the digital repository MorphoSource (See Table 1). No information about the age of specimens was available so all individuals were assumed to be adults. The following specimens were scanned at the Cambridge Biotomography Centre (CBC) at the University Museum of Zoology, Cambridge, with the Nikon Metrology XT H 225 ST High Resolution CT scanner: *Sundatyphlops polygrammicus* (UMZC R1.10-2, *Typhlops polygrammicus*), *Afrotyphlops mucruso* (UMZC R1.6-1), *Afrotyphlops schlegelii* (BMNH 1948.1.1.80), *Anilios leucoproctus* (UMZC 5R1.16-1). The parameters used were: 100kV and 105uA. The following specimens were obtained from the digital repository MorphoSource: *Typhlops jamaicensis* (USNM: Amphibians & Reptiles: 12378, ark:/87602/m4/M98645, *Typhlops jamaicensis*; oUTCT provided access to these data originally appearing in Gauthier et al., 2012, with data collection funded by NSF EF-0334961 and data upload to MorphoSource funded by DBI-1902242. The files were downloaded from www.MorphoSource.org, Duke University); *Afrotyphlops punctatus* (UMMZ:herps:61189, ark:/87602/m4/M76245, *Typhlops punctatus*; University of Michigan Museum of Zoology provided access to these data, the collection of which was funded by oVert TCN. The files were downloaded from www.MorphoSource.org, Duke University); and *Madatyphlops arenarius* (UMMZ:herps:241854, doi:10.17602/M2/M70130, *Typhlops arenarius;* University of Michigan Museum of Zoology provided access to these data, the collection of which was funded by oVert TCN. The files were downloaded from www.MorphoSource.org, Duke University).

2.2 Data Rendering

The data was rendered in Avizo Lite 9.3 (Thermo Scientific). Data volumes were rotated to position the skull along three orthogonal axes. Skull material was isolated using the 'threshold' tool, and individual bones were segmented using the 'brush' and 'magic wand' tools, highlighting along clear joins visible in the scans that demarcate the contact points between bones. After segmentation, data was resampled to reduce computation time and converted into 3D volumes for imaging. Descriptions were made by examining and comparing 3D ply files of individual bones of multiple taxa in the 3D modelling software MeshLab v2020.12 (Cignoni *et al.* 2008).

Table 1. Species examined, specimen numbers and skull length (tip of premaxilla to occipital condyle). Max total length recorded for species from (Feldman *et al.* 2016). Institutional abbreviations used: BMNH, Natural History Museum, London, UK; UMMZ, University of Michigan Museum of Zoology, USA; UMZC, University Museum of Zoology, Cambridge, UK; USNM, Smithsonian Institution, National Museum of Natural History, USA.

Species	**Specimen Number**	**Skull Length (mm)**	**Max Length (mm) of species**
Typhlops jamaicensis	USNM 12378	7.58	445
Typhlops lumbricalis	UMZC R1.11-1	7.03	257
Afrotyphlops mucruso	UMZC R1.6-1	10.8	950
Afrotyphlops schlegelii	BMNH 1948.1.1.80	14.67	900
Afrotyphlops punctatus	UMMZ 61189	13.5	660
Madatyphlops arenarius	UMMZ 241854	4.59	220
Indotyphlops braminus	UMZC R1.12-1, R1.12-2, R1.12-3	4.28	180
Sundatyphlops polygrammicus	UMZC R1.10-2	7.23	395
Anilios leucoproctus	UMZC 5R1.16-1	4.4	250
Anilios bituberculatus	UMZC R1.16-1	5.4	450

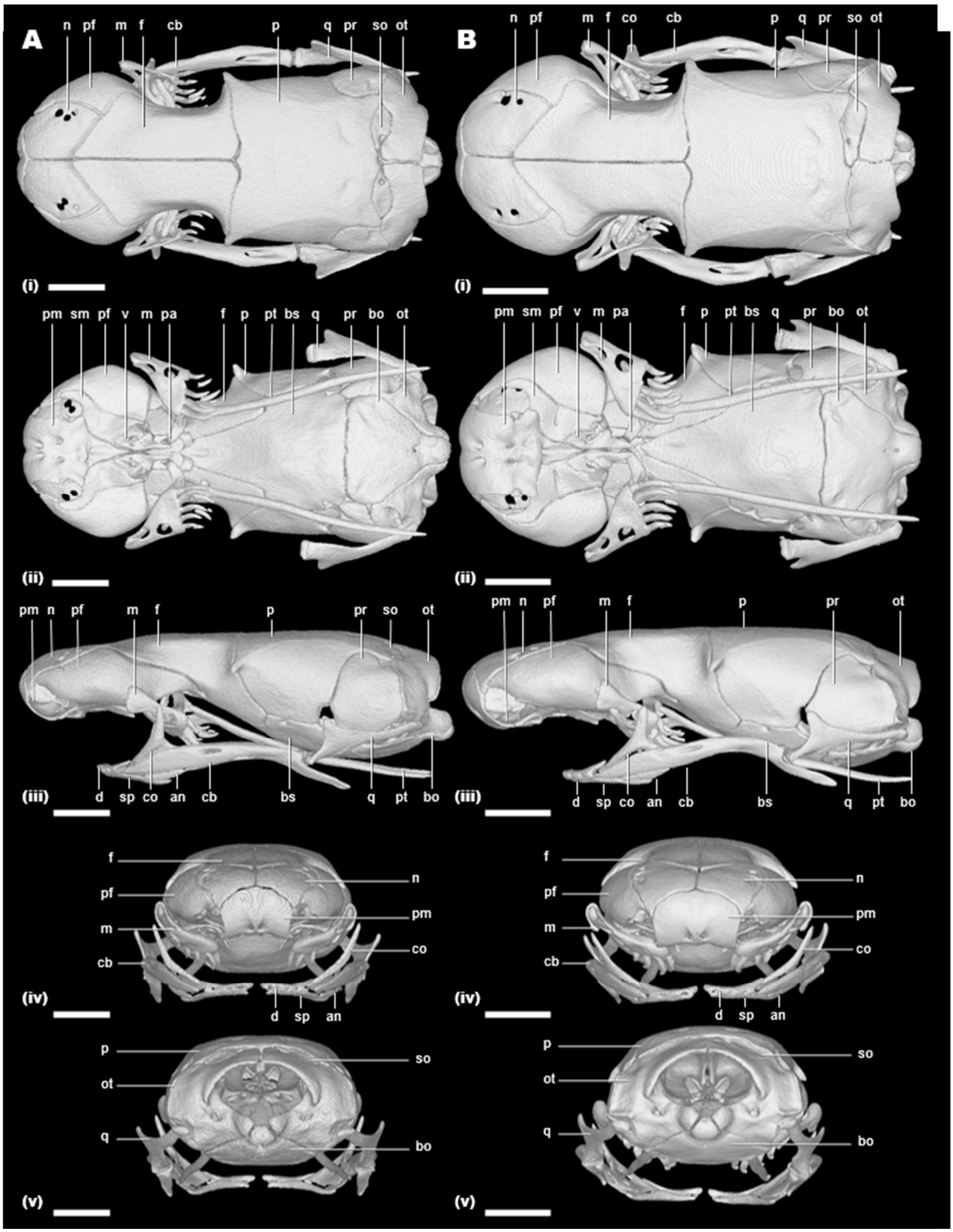

Figure 2. Whole skull (A) *Typhlops jamaicensis*; (B) *Typhlops lumbricalis*; (i) Dorsal, (ii) Ventral, (iii) Lateral, (iv) Anterior, (v) Posterior. Abbreviations: an – angular, bo – basioccipital, bs – basisphenoid, cb – compound bone, co - coronoid d – dentary, f – frontal, m – maxilla, n – nasal, ot – otooccipitals, p – parietal, pf – prefrontal, pm – premaxilla, pr – prootic, pt – pterygoid, q – quadrate, sm – septomaxilla, so – supraoccipital, sp – splenial, v - vomer

Scale bar = 1mm

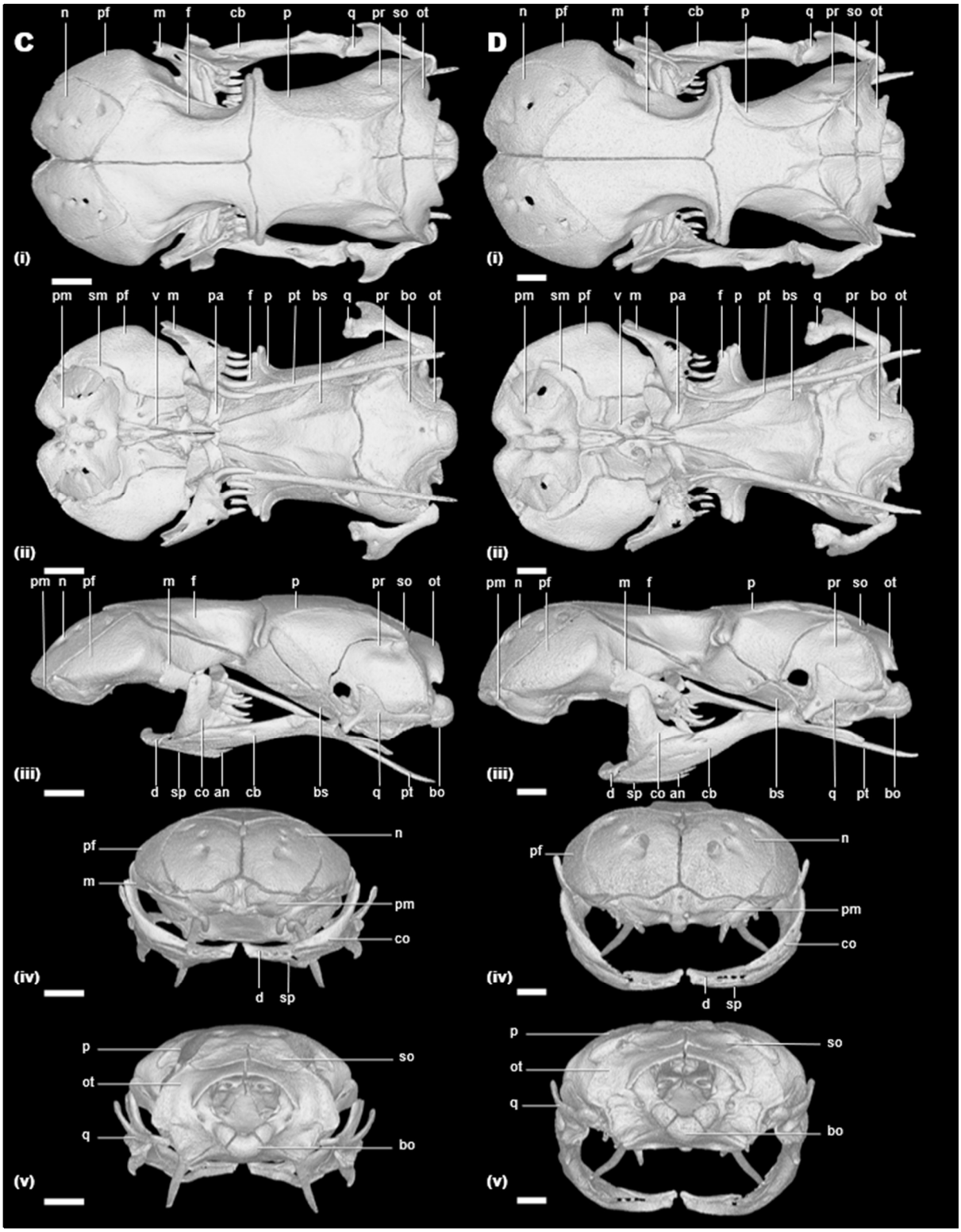

Figure 2 cont. (C) *Afrotyphlops mucruso,* (D) *Afrotyphlops schlegelii*; (i) Dorsal, (ii) Ventral, (iii) Lateral, (iv) Anterior, (v) Posterior. Abbreviations: an – angular, bo – basioccipital, bs – basisphenoid, cb – compound bone, co - coronoid d – dentary, f – frontal, m – maxilla, n – nasal, ot – otooccipitals, p – parietal, pf – prefrontal, pm – premaxilla, pr – prootic, pt – pterygoid, q – quadrate, sm – septomaxilla, so – supraoccipital, sp – splenial, v - vomer

Scale bar =1mm

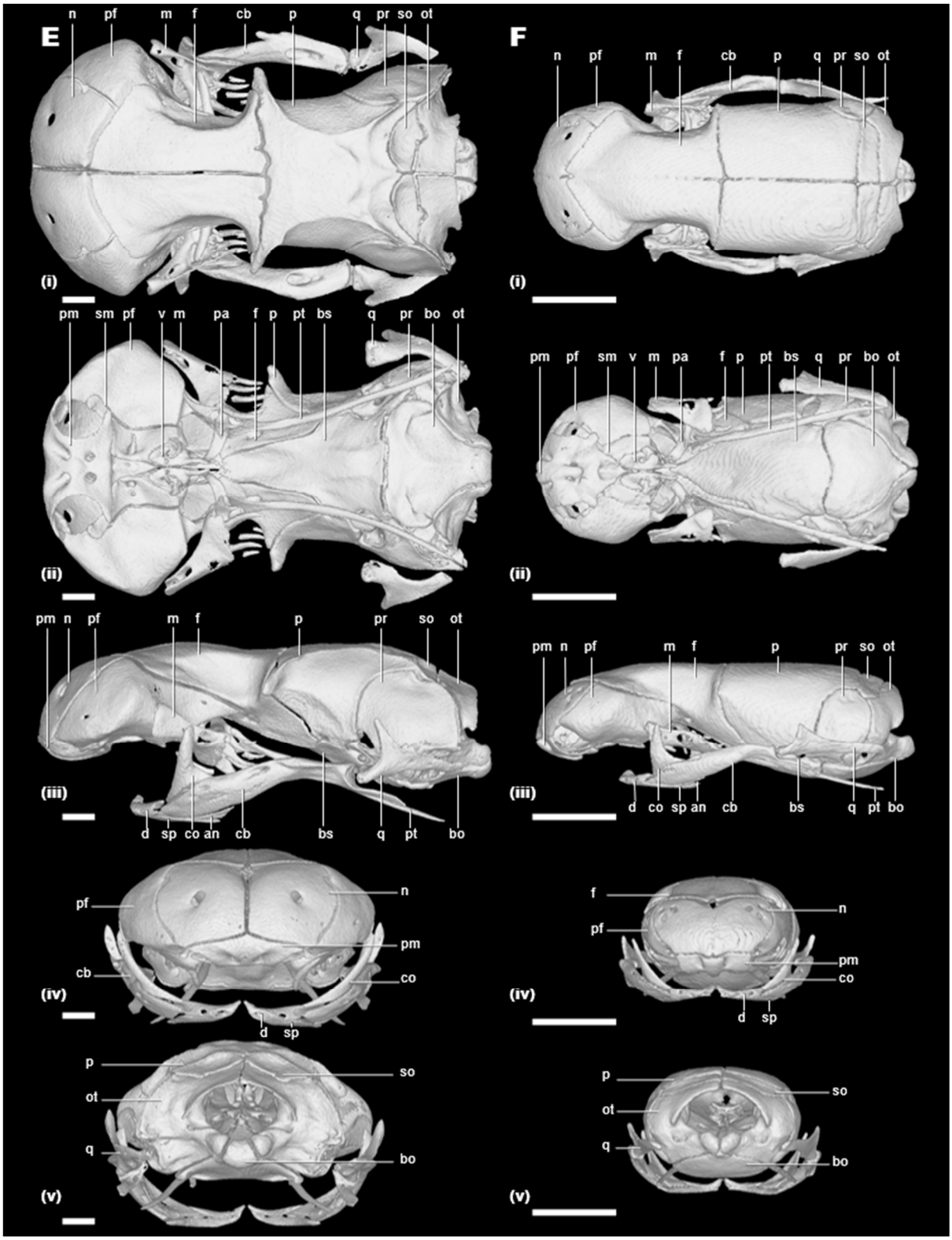

Figure 2 cont. (E) *Afrotyphlops punctatus,* (F) *Madatyphlops arenarius*; (i) Dorsal, (ii) Ventral, (iii) Lateral, (iv) Anterior, (v) Posterior. Abbreviations: an – angular, bo – basioccipital, bs – basisphenoid, cb – compound bone, co - coronoid d – dentary, f – frontal, m – maxilla, n – nasal, ot – otooccipitals, p – parietal, pf – prefrontal, pm – premaxilla, pr – prootic, pt – pterygoid, q – quadrate, sm – septomaxilla, so – supraoccipital, sp – splenial, v - vomer

Scale bar =1mm

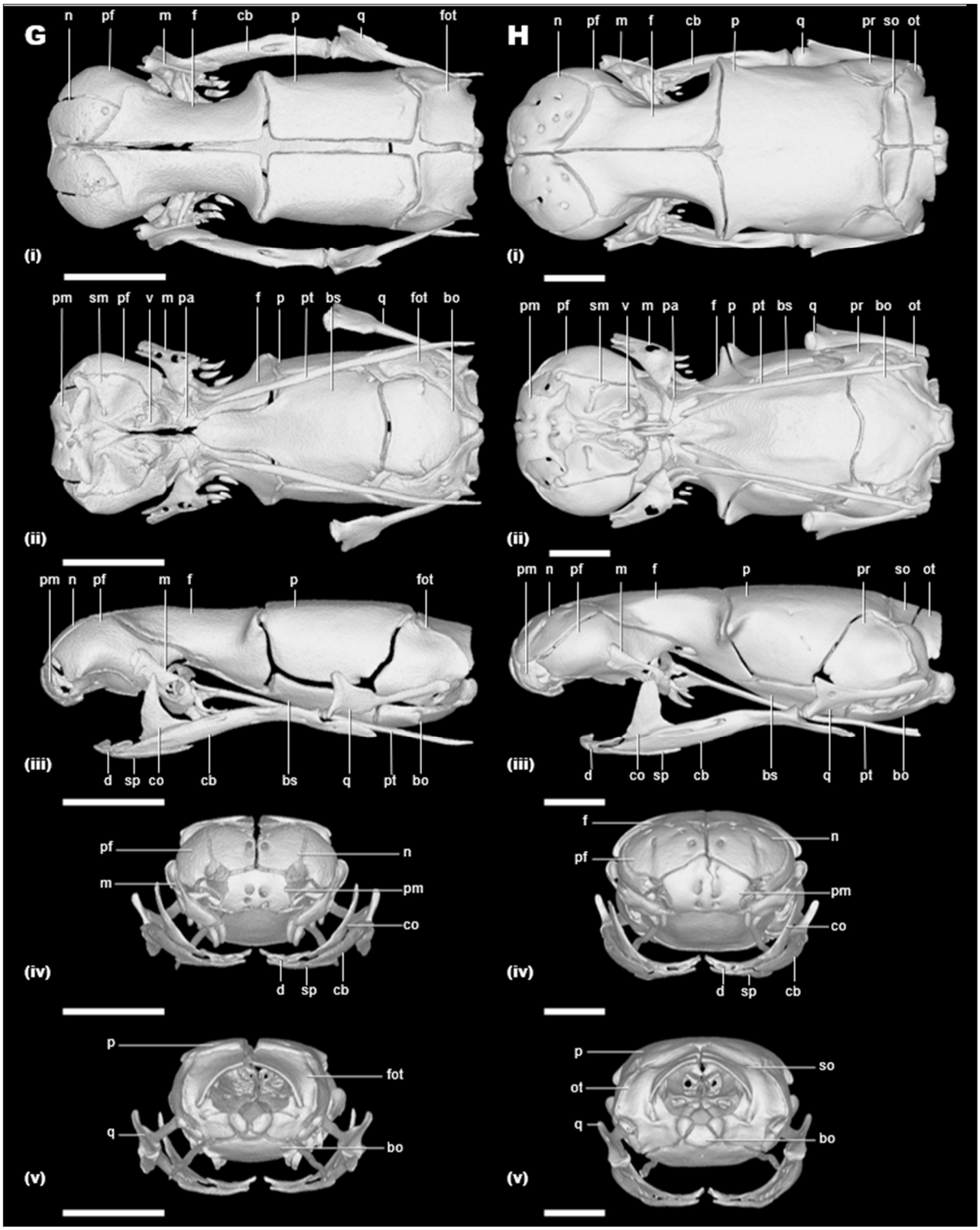

Figure 2 cont. (G) *Indotyphlops braminus,* (H) *Sundatyphlops polygrammicus*; (i) Dorsal, (ii) Ventral, (iii) Lateral, (iv) Anterior, (v) Posterior. Abbreviations: an – angular, bo – basioccipital, bs – basisphenoid, cb – compound bone, co - coronoid d – dentary, f – frontal, fot – fused otic, m – maxilla, n – nasal, ot – otooccipitals, p – parietal, pf – prefrontal, pm – premaxilla, pr – prootic, pt – pterygoid, q – quadrate, sm – septomaxilla, so – supraoccipital, sp – splenial, v - vomer

Scale bar =1mm

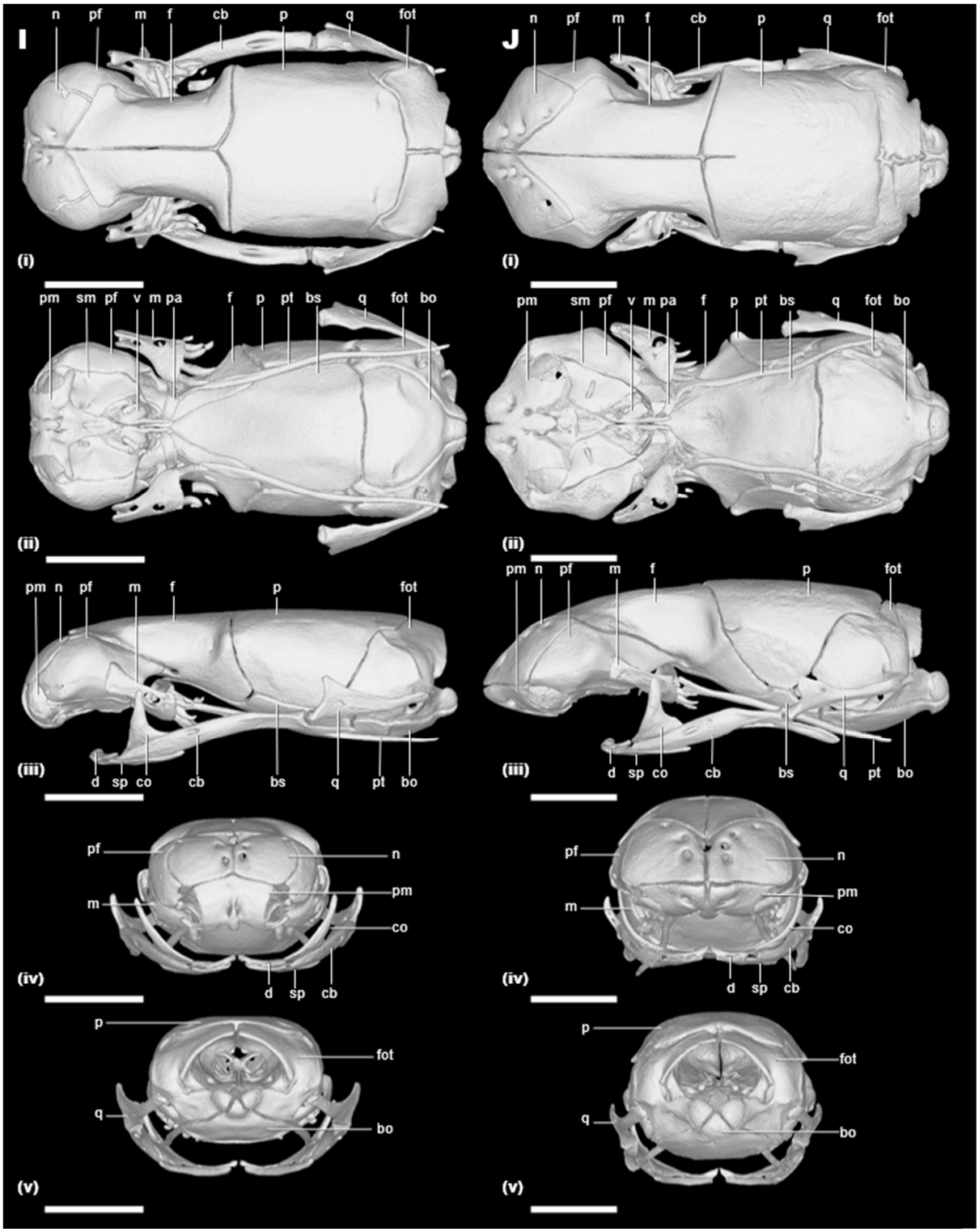

Figure 2 cont. (I) *Anilios leucoproctus,* (J) *Anilios bituberculatus*; (i) Dorsal, (ii) Ventral, (iii) Lateral, (iv) Anterior, (v) Posterior. Abbreviations: an – angular, bo – basioccipital, bs – basisphenoid, cb – compound bone, co - coronoid d – dentary, f – frontal, fot – fused otic m – maxilla, n – nasal, p – parietal, pf – prefrontal, pm – premaxilla, pt – pterygoid, q – quadrate, sm – septomaxilla, sp – splenial, v – vomer

Scale bar =1mm

3. Results

3.1 General Form – Figure 2

The general form of the skull of Typhlopidae represent the overall expanded "outer shell design" typical to scolecophidians, where resistance to deformation during burrowing is achieved by enlarging the dermal snout bones through lateral expansions of the premaxilla to meet the nasals and septomaxillae (Cundall & Rossman 1993). This is considered to be an adaptation to fossoriality in this group. Although superficially similar in morphology, individual species differ in proportions of parts of the skull relative to one another. In *Indotyphlops braminus* and *Sundatyphlops polygrammmicus* the rostrum is expanded slightly in comparison to the cranium compared to examined *Typhlops* and *Anilios*, where the rostrum and cranium reach similar widths. This expansion is seen to a greater extent in *Afrotyphlops punctatus* and taken to the extreme in the two largest species of typhlopid, *Afrotyphlops schlegelii* and *Afrotyphlops mucruso*. The prefrontals of *Indotyphlops braminus* contribute more to the anterior surface of the snout than observed in other species, and the skull is overall shallower.

3.2 The Snout Complex

The snout complex of all Typhlopidae examined are composed of a premaxilla, paired nasals, paired septomaxillae, paired vomers, and paired prefrontals. In general the snout is expanded compared to the rest of the braincase, either of equal size or larger, the greatest extent of which in the giant blind snakes, *Afrotyphlops mucruso* and *Afrotyphlops schlegelii*. The snout of *Anilios bituberculatus* is unique to all other species examined in that the dorsal edge of the nares is composed of the premaxilla and prefrontals, with the nasals excluded by a contact between these two bones. In all other species examined, a small portion of the lateral surface of the nasals forms part of the dorsal edge of the nares.

3.2.1 Premaxilla – Figures 3-5

The premaxilla is a single, edentulous element. It is confined to the anterior and dorsal face of the skull, and contributes to the medial and ventral edges of the nares. The premaxilla makes contact with the same bones in all species. The anterior edge abuts the nasals dorsally, and the posterior edge forms a broad contact with the septomaxillae. The anteroventral edge and face forms the ventral portion of the snout and curves medially to form the medial margins of the nares, which then expands to a triangular process that meets the lateroventral projections of the septomaxilla, the septomaxillary process. The posterior of the premaxilla is a triangular projection that extends past the medial edges of the septomaxilla to meet the vomers, the vomerine process. In the examined *Typhlops* and the examined asiatyphlopines excluding

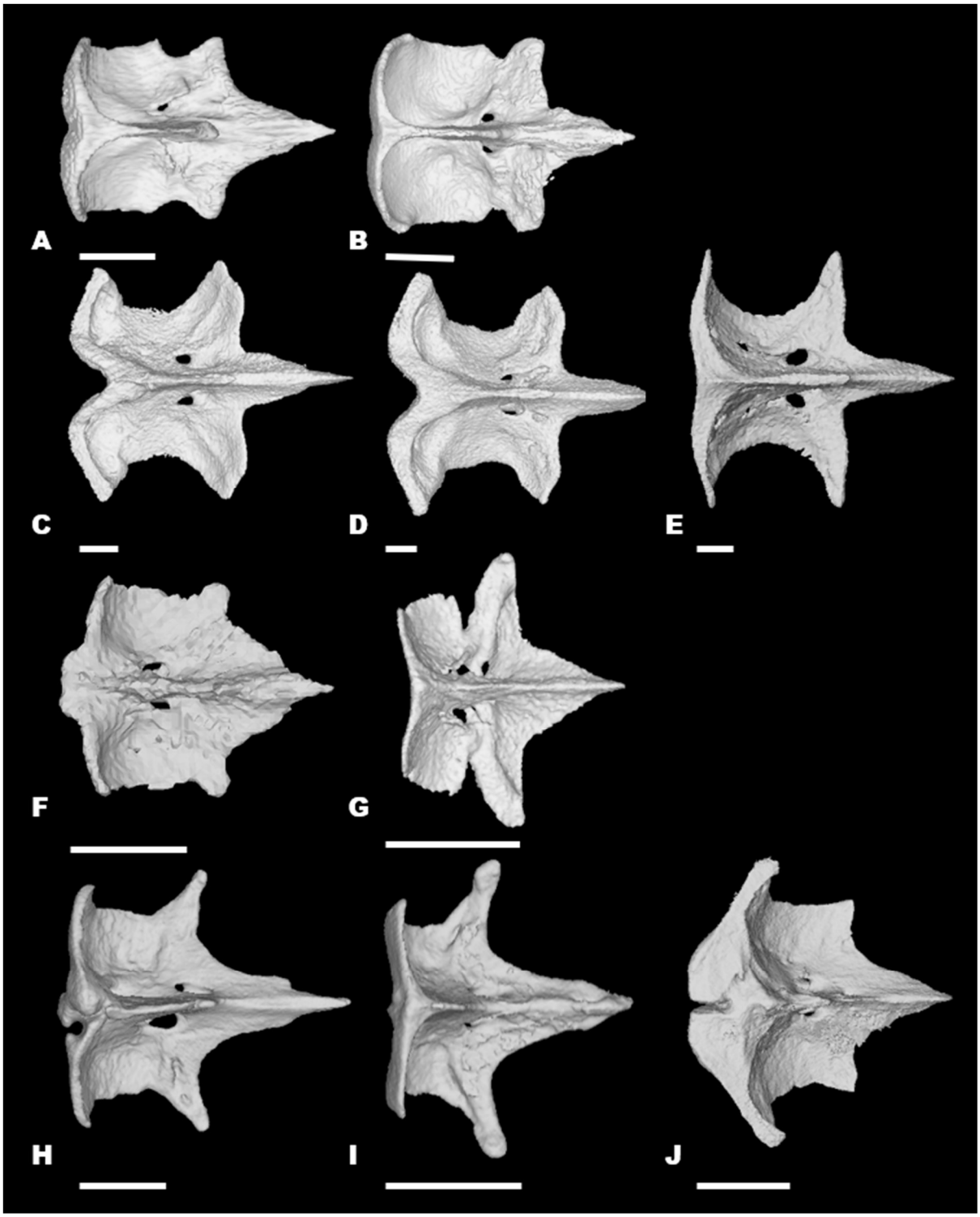

Figure 3. Premaxilla, Dorsal (A) *Typhlops jamaicensis*, (B) *Typhlops lumbricalis*, (C) *Afrotyphlops mucruso*, (D) *Afrotyphlops schlegelii*, (E) *Afrotyphlops punctatus,* (F) *Madatyphlops arenarius,* (G) *Indotyphlops braminus*, (H) *Sundatyphlops polygrammicus,* (I) *Anilios leucoproctus*, (J) *Anilios bituberculatus*.

Scale bar = 0.5mm

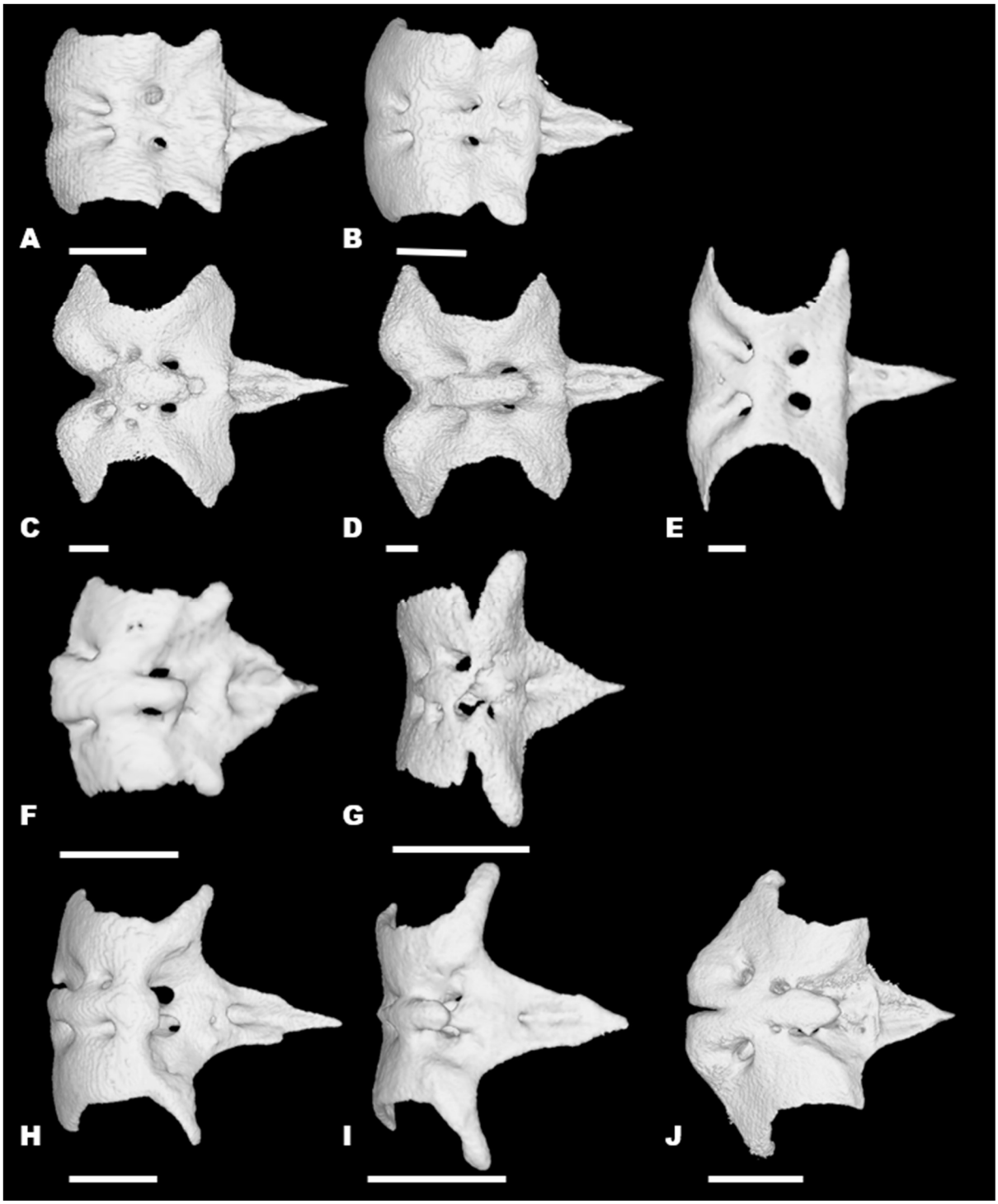

Figure 4. Premaxilla, Ventral (A) *Typhlops jamaicensis*, (B) *Typhlops lumbricalis*, (C) *Afrotyphlops mucruso*, (D) *Afrotyphlops schlegelii*, (E) *Afrotyphlops punctatus,* (F) *Madatyphlops arenarius,* (G) *Indotyphlops braminus*, (H) *Sundatyphlops polygrammicus,* (I) *Anilios leucoproctus*, (J) *Anilios bituberculatus*.

Scale bar = 0.5mm

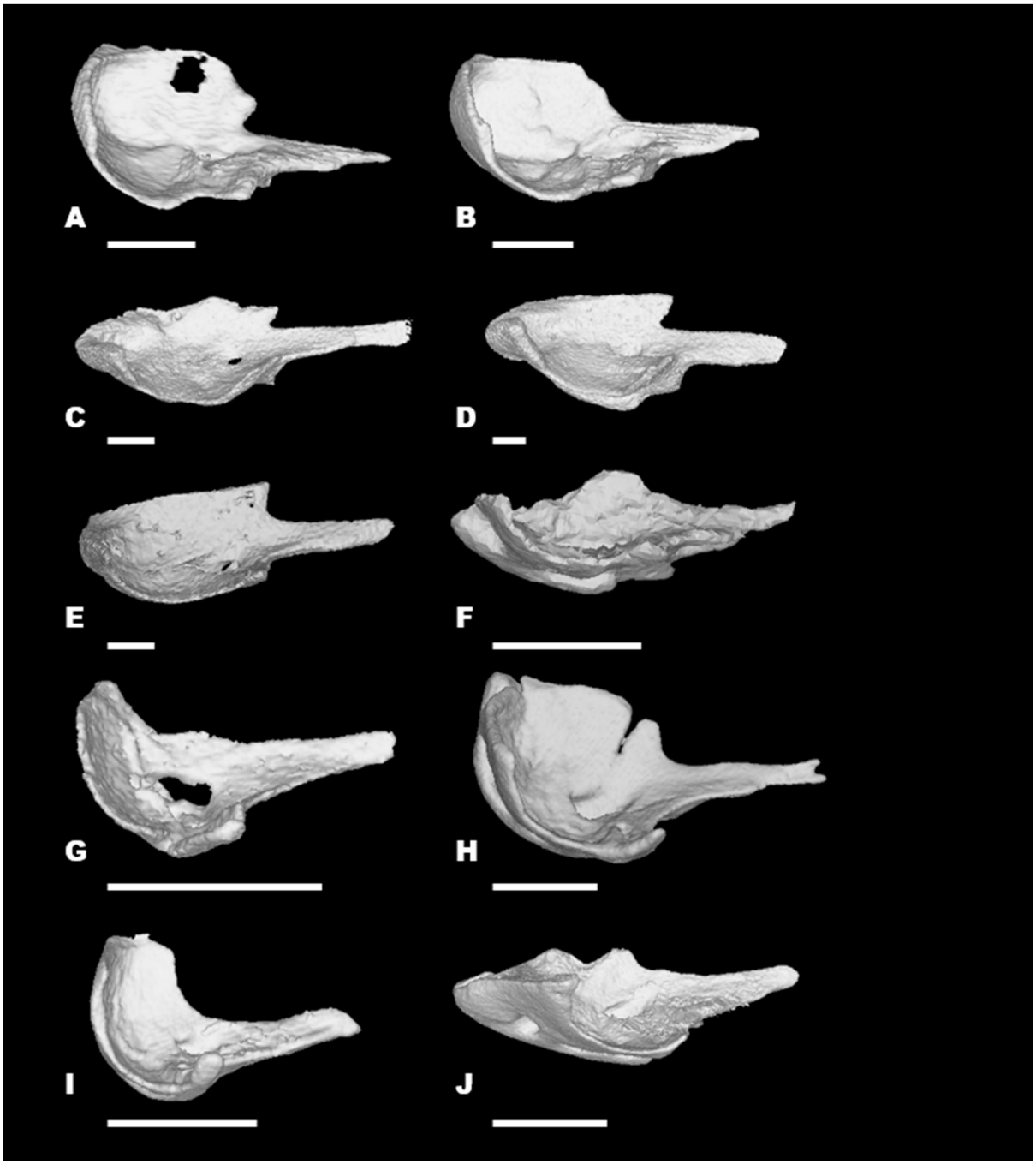

Figure 5. Premaxilla, Left Lateral (A) *Typhlops jamaicensis*, (B) *Typhlops lumbricalis*, (C) *Afrotyphlops mucruso*, (D) *Afrotyphlops schlegelii*, (E) *Afrotyphlops punctatus,* (F) *Madatyphlops arenarius,* (G) *Indotyphlops braminus*, (H) *Sundatyphlops polygrammicus,* (I) *Anilios leucoproctus*, (J) *Anilios bituberculatus*.

Scale bar = 0.5mm

Anilios bituberculatus, the premaxilla forms over half of the anteroventral face of the snout, contacting the nasals in a curved suture in *Typhlops* and a pointed suture in asiatyphlopines. The premaxilla forms half of the anteroventral face of the snout in *Madatyphlops arenarius.* In the examined *Afrotyphlops* species and *A. bituberculatus*, the more wedge-shaped snout results in the premaxilla mainly forming the ventral edge, with the majority of the anteroventral face comprising of the nasals.

In dorsal view the morphology of the premaxilla is highly variable (See Figure 3). In examined *Typhlops,* the lateral edges of the premaxilla project posteriorly perpendicular to the anterior edge, with a small medial notch lateral to the posterior paired foramen. The septomaxillary process projects laterally but does not exceed the lateral extent of the rest of the premaxilla. In the examined *Afrotyphlops*, the lateral edges of the premaxilla are curved medially from the anterior edge to the septomaxillary process. In *Afrotyphlops schlegelli* and *Afrotyphlops mucruso*, the anterior edge of the premaxilla contributes to an unusual morphology seen in the snout, where the anterior face, rather than being curved, possesses at the mid-line a posteriorly projecting triangular notch. Such a notch is not present in the smaller species, *Afrotyphlops punctatus*. The dorso-anterior edge that forms a contact with the nasals is broader in the examined *Afrotyphlops* than in the other species (with the exception of *Anilios bituberculatus*). Additionally, the vomerine process of examined *Afrotyphlops* is narrower than other species.

The morphology of the premaxilla of *Madatyphlops arenarius* is similar to examined *Typhlops*, with relatively straight lateral edges and a small septomaxillary process. However it is shorter along the anterior-posterior axis than seen in examined *Typhlops*. Additionally, in *M. arenarius* the midline of the anterior edge of the premaxilla protrudes slightly anteriorly in a shallow rectangular process. The overall shape of the element in *Indotyphlops braminus* is more compact than in other species examined. The anterior face is more vertically oriented than in other species, contributing to a larger portion of the anterior snout face. The lateral edges run perpendicular to the anterior edge, projecting posteroventrally, until meeting a distinct medially projecting notch immediately anterior to the septomaxillary process. This septomaxillary process reaches a greater lateral extent than the anterior edge of the premaxilla. In *Sundatyphlops polygrammicus* and *Anilios leucoproctus*, the anterior face of the premaxilla is more vertically oriented than in the examined *Typhlops* and *Afrotyphlops*, but not to the extent seen in *I. braminus*. The lateral edges are slightly medially curved in *S. polygrammicus, A. leucoproctus,* and *I. braminus*, projecting laterally to a narrow triangular septomaxillary process, that extends passed the extent of the anterior edge. The vomerine process is also wider than in examined *Afrotyphlops*. The premaxilla of *Anilios bituberculatus* is distinctly dissimilar to the other species of *Anilios* examined. The anterior edge of the premaxilla forms a rounded point, with a distinct notch at the midpoint. The dorsal contact with the nasals is widest at the

midpoint, to a greater extent than seen in any other species. The lateral edges project medially on the anterior face, and the ventral lateral edges then run posteriorly to septomaxillary processes that form a right angle with the edge of the vomerine process.

All premaxilla possesses several foramina that transmit the ventral branches of the medial ophthalmicus profundus (V_1) nerve (Haas 1964; Rieppel *et al.* 2009). The number of foramina is highly variable (See Figure 4). There are six foramina in *Typhlops jamaicensis,* five foramina in *Typhlops lumbricalis,* nine foramina in *Afrotyphlops mucruso,* six foramina in *Afrotyphlops schlegelii*, five foramina in *Afrotyphlops punctatus*, five foramina in *Madatyphlops arenarius*, seven foramina in *Indotyphlops braminus*, seven foramina in *Sundatyphlops polygrammicus*, five foramina in *Anilios leucoproctus*, and eight foramina in *Anilios bituberculatus*. The anterior foramina are paired either side of a thick bony septum, and the posterior most foramina projects posteriorly, at the midline of where the vomerine process meets the rest of the premaxilla. In *A. mucruso*, *A. schlegelii*, and *A. bituberculatus* another foramen is positioned at the midline of the bony septum, which also projects posteriorly.

There is also considerable morphological variation when comparing the premaxilla in lateral view with respect to the medial septum on the dorsal surface which forms the ventral portion of the nasal septum (See Figure 5). This septum generally extends posteriorly from the anterodorsal edge of the premaxilla until the end of the contact with the ventral nasal septum and the beginning of the vomerine process, where it decreases in height as a step-like margin. In *Typhlops lumbricalis*, the nasal septum continues until the vomerine process. The angle of this step-like aspect of the medial septum is acute in *Typhlops jamaicensis* and examined *Afrotyphlops*, but more vertically oriented in *Madatyphlops arenarius*, examined *Anilios,* and *Sundatyphlops polygrammicus,* with the medial septum of *Anilios leucoproctus* appearing curved in lateral view. The exception to the general shape of the medial septum morphology is *Indotyphlops braminus*, where this septum is of a generally small height throughout the premaxilla, and the nasal septum is in contact for the anterior half.

3.2.2 Nasal – Figure 6

The nasals are paired and contribute to the anterior and dorsal portion of the snout (See Figure 6). The nasals meet the premaxilla anteroventrally and the prefrontals laterally. They contribute to the anterior and dorsal margins of the external nares, the exception being *Anilios bituberculatus,* where contact between the prefrontals and the premaxilla excludes the nasals from the margin of the nares. In dorsal view these bones are roughly ovaloid, meeting at a straight suture in the midline. In lateral view, there is a descending laminae from the medial margin, which forms an internasal septum which separates the two olfactory chambers.

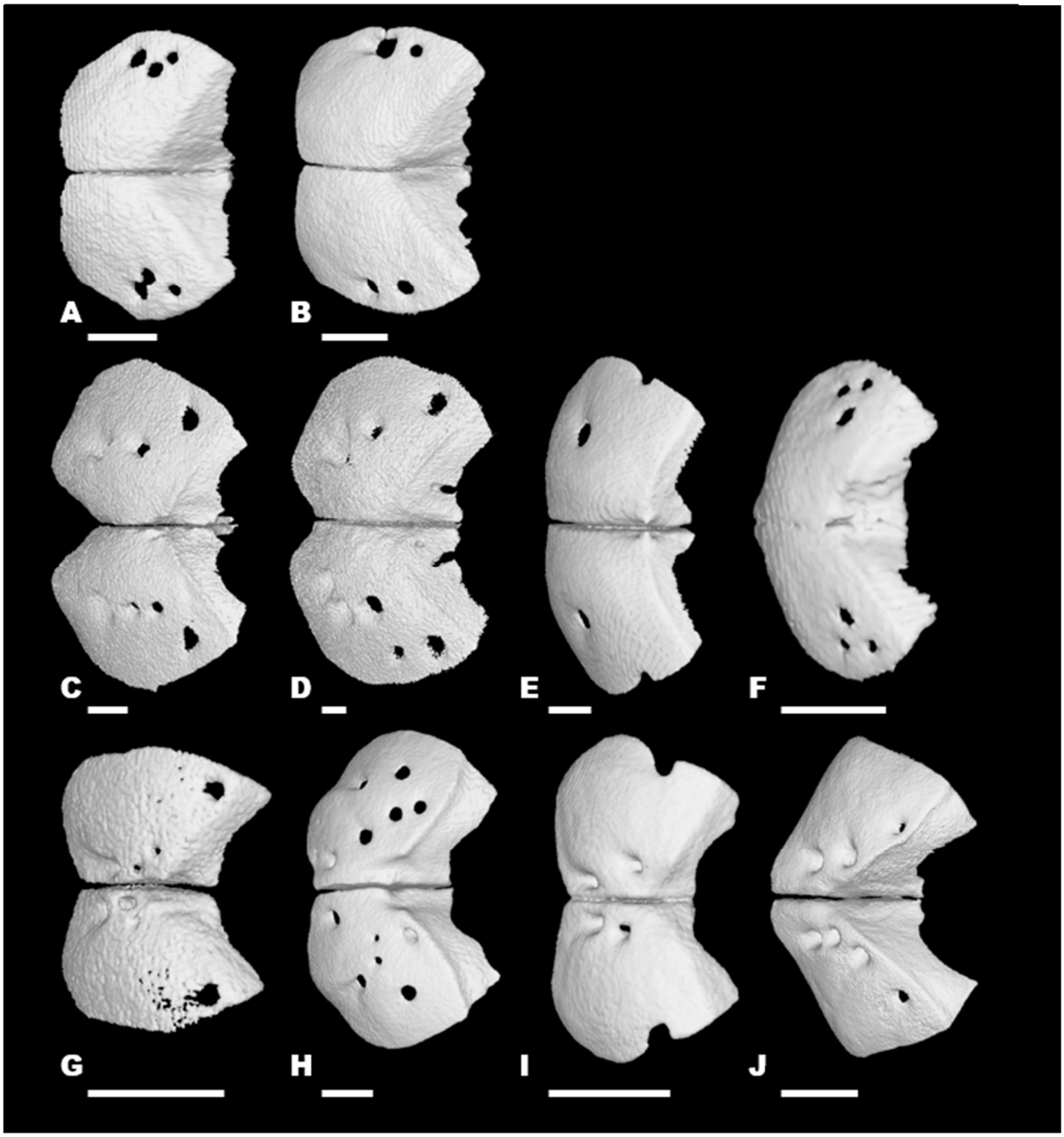

Figure 6. Nasals, Dorsal (A) *Typhlops jamaicensis*, (B) *Typhlops lumbricalis*, (C) *Afrotyphlops mucruso*, (D) *Afrotyphlops schlegelii*, (E) *Afrotyphlops punctatus,* (F) *Madatyphlops arenarius,* (G) *Indotyphlops braminus*, (H) *Sundatyphlops polygrammicus,* (I) *Anilios leucoproctus*, (J) *Anilios bituberculatus*.

Scale bar = 0.5mm

Posteriorly, the nasals meet the frontals in a V-shaped suture, where a short posterior projection contacts the anterior edge of the laterally descending frontal flange.

Interspecific variation in the number of nasal foramina ranges from one in each nasal seen in *Afrotyphlops punctatus* (although a notch in the lateral edge of the nasals could also be interpreted as another), to six in each seen in *Sundatyphlops polygrammicus.* This feature also varies by individual, as the multiple individuals of *Indotyphlops braminus* examined possess either three or four foramina per nasal. There is considerable asymmetry and variation in the position and number of foramina in the species examined. In *Typhlops jamaicensis,* the three foramina are positioned on the lateral edge of the nasals, with the middle one slightly more medially positioned. The two anteriormost foramina of the left nasal are not fully subdivided by bone. In *Typhlops lumbricalis,* there are two foramina on each nasal, positioned at the lateral edge. The lateral bony wall of the anteriormost foramen of the right nasal is not fully complete. In *Afrotyphlops mucruso*, the left nasal contains four foramina and the right nasal contains three. The posterior most foramen is positioned more laterally, near the suture of the nasals, frontals and prefrontals. The anterior most foramina are positioned in the middle of each nasal, more medially than seen in examined *Typhlops*. In *Afrotyphlops schlegelii* the left nasal possesses five foramina whereas the right nasal possesses only three. As in *Afrotyphlops mucruso*, the posterior most foramen is positioned anterior to the suture of the nasals, frontals and prefrontals. The remaining foramina are roughly positioned diagonally towards the midline suture of the two nasals. In *Afrotyphlops punctatus,* the single foramen is positioned in the middle of each nasal. The notch that is potentially a second foramen is in the middle of the suture between the nasals and prefrontals. In *Madatyphlops arenarius*, the cluster of three foramina are positioned anterior to the suture with the frontals and prefrontals. In *Indotyphlops braminus*, there is also a foramen positioned anterior to the suture point of the nasals, frontals and prefrontals. The remaining three foramina are positioned along the midline suture between the nasals, although they are small and irregular in positioning, not symmetrical along the midline of the animal. In *S. polygrammicus* the position and size of the six foramina differs slightly on each nasal. In both, the anterior-most foramen is positioned just lateral to the anterior-most point of the nasal suture. There is a foramen anterior to the midpoint of the suture with the frontals. There are two foramina in the middle of the bone, one more posterior towards the suture between the nasals, frontals and prefrontals. All of these four foramina are of equal size on both nasals. On the left nasal, the remaining two foramina on the left nasal are half the diameter, and positioned centrally to the other foramina. The remaining two foramina of the right nasal are equal in size to the other foramina on this nasal, and are positioned more along the anterior-posterior axis, forming a diagonal line with the anterior-most foramen and the foramen at the middle of the nasal-frontal suture. In *Anilios bituberculatus*, there are four foramina on the left nasal and three

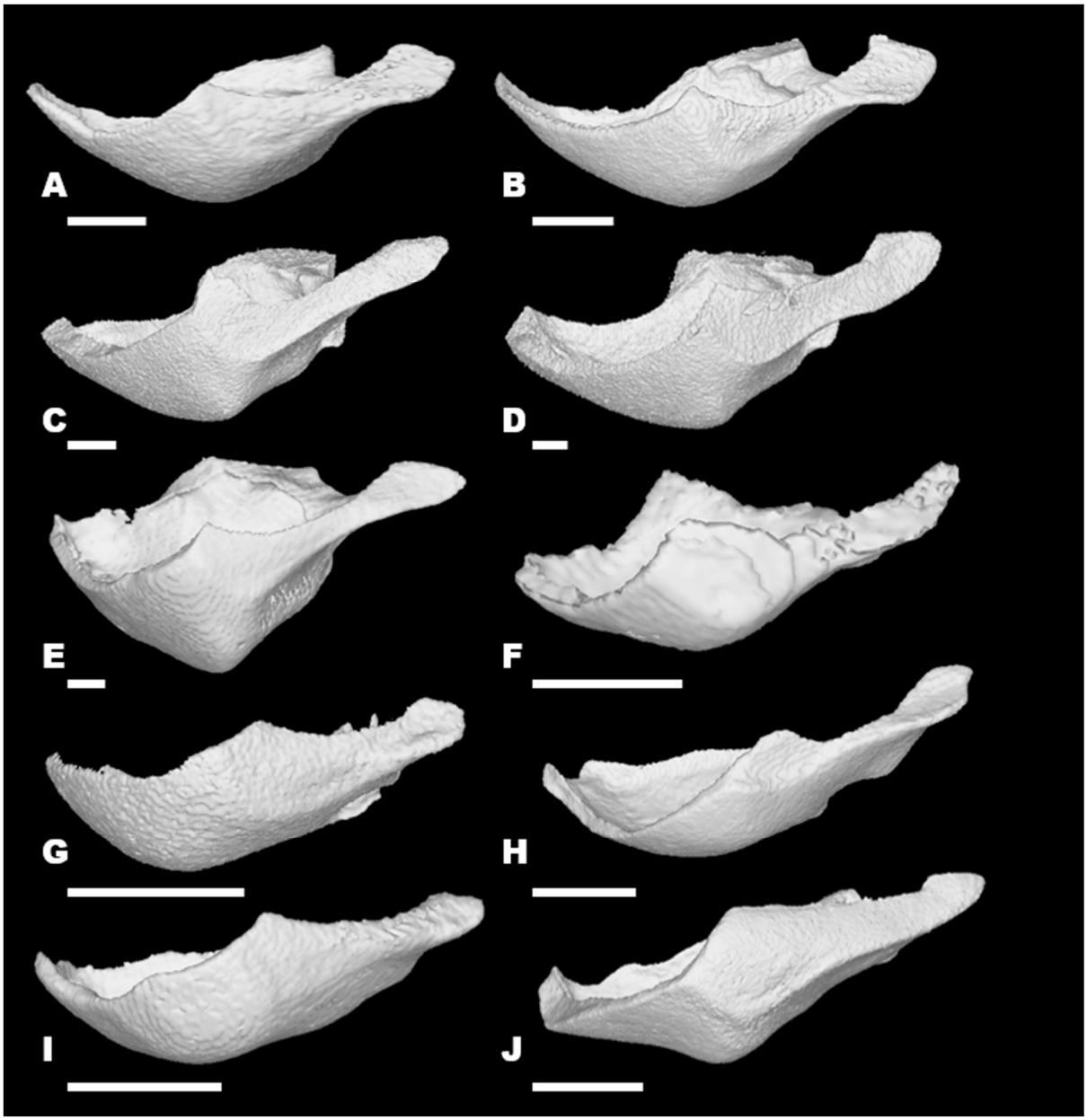

Figure 7. Left Prefrontal, Dorsal (A) *Typhlops jamaicensis*, (B) *Typhlops lumbricalis*, (C) *Afrotyphlops mucruso*, (D) *Afrotyphlops schlegelii*, (E) *Afrotyphlops punctatus,* (F) *Madatyphlops arenarius,* (G) *Indotyphlops braminus*, (H) *Sundatyphlops polygrammicus,* (I) *Anilios leucoproctus*, (J) *Anilios bituberculatus*.

Scale bar = 0.5mm

on the right. All these foramina are of equal size. The anterior most foramina (two on left, one on right) are positioned laterally to the posterior of the nasal suture. The remaining two foramina are positioned at equal distances anterior to the suture with the nasals. In *Anilios leucoproctus* there are two foramina positioned either side of the nasal suture. There is also a notch on the lateral edge of the nasals where the nasals contact the prefrontals, as seen in *Afrotyphlops punctatus,* which is possibly the edge of another foramen. The foramina of both *Anilios* are pointed posteriorly, so the anterior wall of the foramen is visible in dorsal view. In all species, these foramina transmit the afferent nerve bundles originating from the trigeminal, to supply the sense organs located in the snout (Rieppel *et al.* 2009). The medial edges of the nasals descend laterally where they contact each other, forming the nasal septum that connects ventrally with the medial septum of the premaxilla. The posterior edge of the nasals projects postero-ventrally to form a wide contact with the frontals. This is seen to greatest extend in *A. bituberculatus*, where the nasals connect to the frontals in a deep v-shaped suture.

3.2.3 Prefrontal – Figure 7

The prefrontals are paired convex bones which form the lateral walls of the snout complex and contribute to the dorsal margin of the external nares (See Figure 7). They are sutured anteroventrally with the premaxilla, dorsolaterally with the nasals, ventromedially with the septomaxillae. The dorsal edge of the prefrontals expands medially, continuing the broad contact with the frontals that starts medially with the posterior edge of the nasals. In general the prefrontals contribute more to the lateral and ventral portion of the snout, except in *Indotyphlops braminus*, where the prefrontals contribute to a larger portion of the dorsal snout, with the nasals contributing little to the lateral profile of the snout. In all the species, the lateral edge of the prefrontals posterior to the expanded midsection possesses a notch leading towards the lateral edge of the element. In *I. braminus* this notch is now a full foramen.

3.2.4 Septomaxilla – Figure 8-9

The septomaxillae are relatively large elements that make up much of the ventral portion of the snout complex. Laterally the septomaxillae are in contact with the medial edges of the ventral extent of the prefrontals. In dorsal view the septomaxillae are concealed by the nasals, prefrontals, and frontals, and laterally by the prefrontals. The overall shape of these bones is a large flat plate that makes up the ventral surface of the snout, with internally a dorsally projecting smooth-walled vomeronasal cupola that encloses the vomeronasal organ and the mushroom body (Rieppel *et al.* 2008, 2009). This projection channels several nerves to the braincase via several foramina to the large opening on the anteroventral face of the paired frontals. The anteromedial extent of this vomeronasal cupola contacts the medial most points of

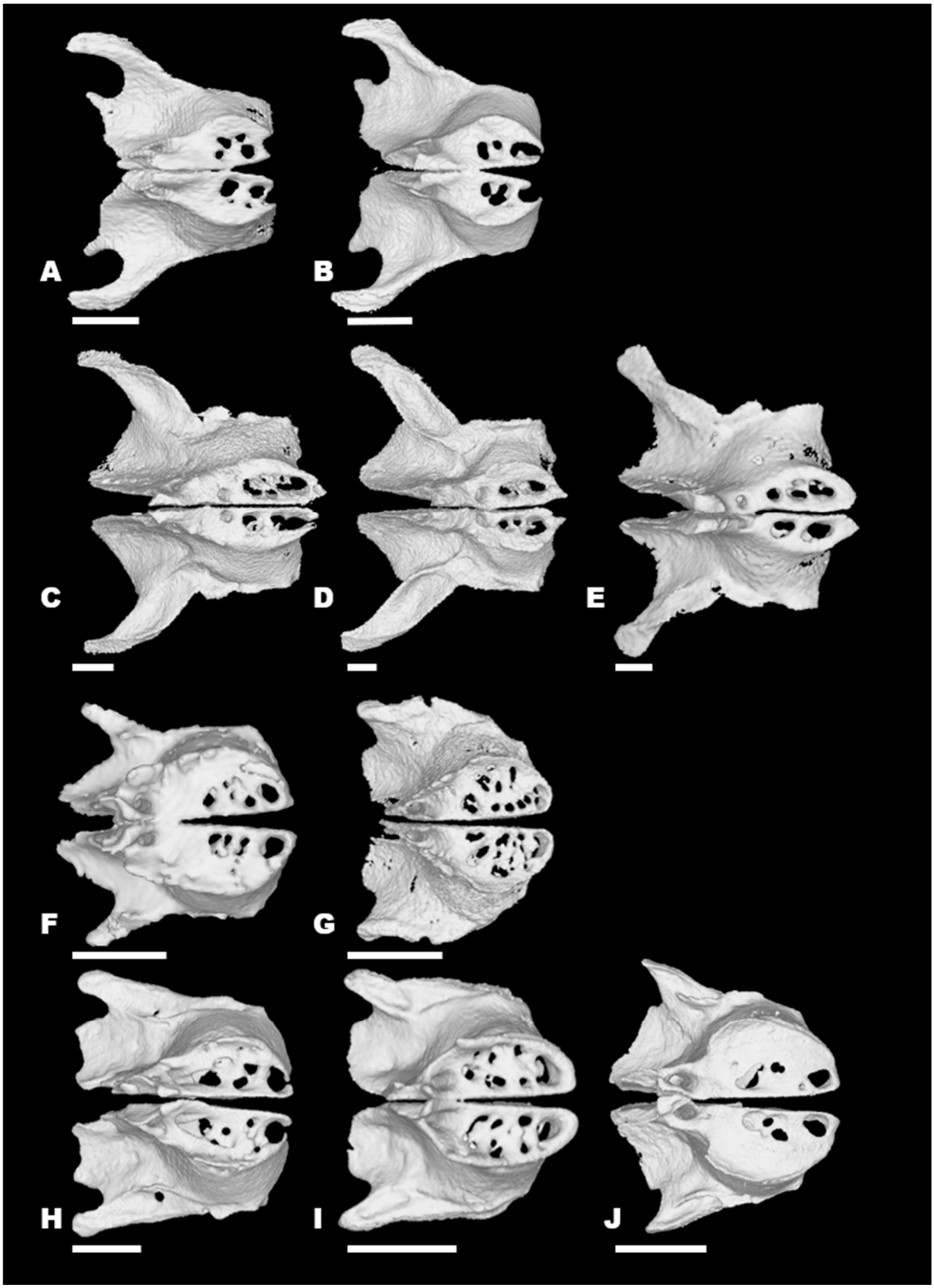

Figure 8. Septomaxillae, Dorsal (A) *Typhlops jamaicensis*, (B) *Typhlops lumbricalis*, (C) *Afrotyphlops mucruso*, (D) *Afrotyphlops schlegelii*, (E) *Afrotyphlops punctatus,* (F) *Madatyphlops arenarius,* (G) *Indotyphlops braminus*, (H) *Sundatyphlops polygrammicus,* (I) *Anilios leucoproctus*, (J) *Anilios bituberculatus*.

Scale bar = 0.5mm

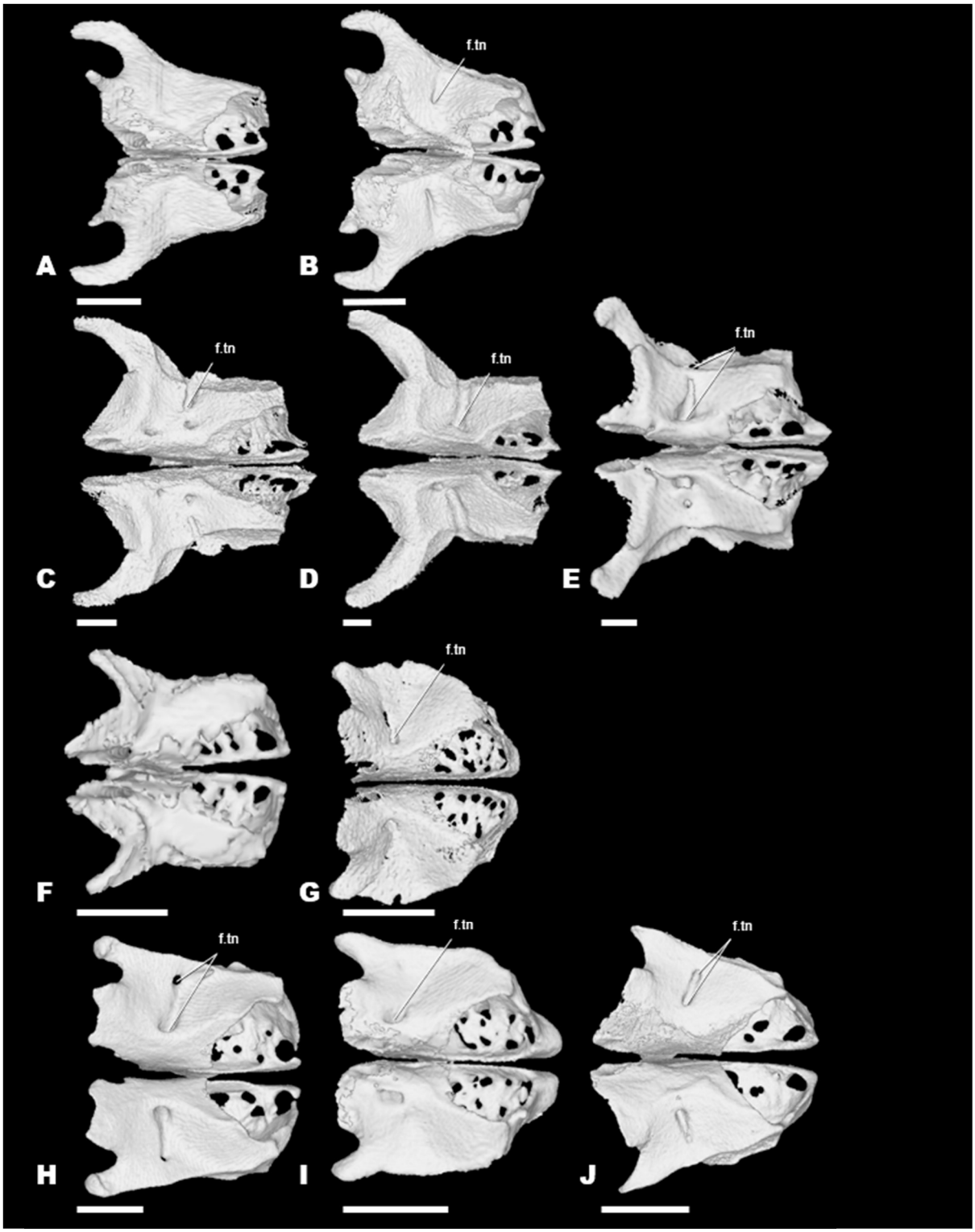

Figure 9. Septomaxillae, Ventral (A) *Typhlops jamaicensis*, (B) *Typhlops lumbricalis*, (C) *Afrotyphlops mucruso*, (D) *Afrotyphlops schlegelii*, (E) *Afrotyphlops punctatus,* (F) *Madatyphlops arenarius,* (G) *Indotyphlops braminus*, (H) *Sundatyphlops polygrammicus,* (I) *Anilios leucoproctus*, (J) *Anilios bituberculatus*. Abbreviations: f.tn – foramen for trigeminal nerve

Scale bar = 0.5mm

the posterior ventrally descending laminae of the nasals. In ventral view, the dorsal extent of the septomaxillae are overlapped by the posterior extent of the premaxilla.

The foramen that transmit nerves from the vomeronasal cupola vary in number between species (See Figure 8). In the *Typhlops* examined *Typhlops jamaicensis* have five foramina on each and *Typhlops lumbricalis* also have five foramina, although some of these are not fully separated by bony septums. In *Afrotyphlops mucruso,* there are at least three foramina, the posteriormost of which may be many fused together. In *Afrotyphlops schlegelii* there are six foramina on the left vomeronasal cupola but only four on the right. In *Afrotyphlops punctatus*, there are three on the left and five on the right. In *Madatyphlops arenarius*, there are five foramina on each. *Indotyphlops braminus* has many foramina, at least fifteen on each but some may be fused with one another. In *Sundatyphlops polugrammicus* there are at least five foramina on each, but they have irregular shape and orientation. In *Anilios bituberculatus* there are five on each, and in *Anilios leucoproctus* there are at least eight foramina on each of irregular shape and orientation. The anterior-most foramina in examined *Typhlops* are at the anterior of the dorsal extent of the septomaxilla, forming channels along the vomeronasal cupola. In all other species, all foramina are positioned on the dorsal surface of the septomaxilla. The dorsal extent of the vomeronasal cupola is relatively smaller in examined *Typhlops* and *Afrotyphlops*, but takes up relatively more of the snout in *M. arenarius* and asiatyphlopines, almost contacting the lateral flanges of the prefrontals in *I. braminus* and *A. bituberculatus*.

There is considerable variation between species in the extent of the lateral projection of the ventral plate of the septomaxillae (See Figure 9). This projection follows the medial edge of the ventral surface of the prefrontals, which is roughly straight in examined asiatyphlopines. The projection is more laterally directed in *Madatyphlops arenarius*, although not to the extent seen in examined *Typhlops* and *Afrotyphlops*. The anterior edges of septomaxillae in examined *Typhlops* is slightly anteriorly directed, with the medial point where the septomaxillae meet more posterior. The lateral part of the ventral edge is curved into a claw-like projection, with the more medial 'claw' pointing dorsally whereas the lateral most projection is horizontally oriented. For the largest typhlopids, *Afrotyphlops mucruso* and *Afrotyphlops schlegelii*, the medial points of the anterior edges are more anterior, then the edge directs posterolateral, before curving anteriorly to the anteriorly projecting lateral edges, which are straight rather than curved. *Afrotyphlops punctatus* is similar to the other *Afrotyphlops* examined, but the medial anterior edge is slightly concave, and the lateral extent is slightly bulbous. The medial points of the anterior edge of the septomaxilla of *M. arenarius* are more anteriorly projected than the lateral edges, otherwise the shape is similar to that of *A. mucruso* and *A. schlegelii*. In *Indotyphlops braminus*, the medial anterior edge is more posterior than the lateral projection. Then there is a v-shaped notch before the small lateral projection. In *Sundatyphlops*

polygrammicus and *Anilios leucoproctus*, the anterior edge is straight, positioned along the medio-lateral axis, before a large u-shaped notch and then a small lateral projection. In *Anilios bituberculatus*, the medial anterior edge is more anterior, leading posterior as the edge moves laterally, then a small u-shaped notch. The lateral projection is small and triangular, as opposed to the round-ended lateral projections of the other species.

The other variation observable is the position and presence of the groove and foramen that transmit the trigeminal nerve, which when present is on the ventral surface of the septomaxilla posterior to the lateral projection of the ventral plate (See Figure 9). In *Typhlops lumbricalis* the groove starts on the mid-point of the ventral surface of the septomaxilla, and a small foramen projects into the bone medially. There is no foramen or groove present on the ventral edge of the septomaxilla of *Typhlops jamaicensis*. In *Afrotyphlops schlegelii* the groove starts at the lateral edge, becoming a foramen when the groove turns anteriorly into the bone. There is a foramen that opens into this internal tube. The morphology is similar in *Afrotyphlops mucruso*, but the groove ends more lateral, and there are two foramina that open into the tube. In *Afrotyphlops punctatus*, the groove/foramen begins on the lateral edge of the septomaxilla. The right septomaxilla projection has two foramen that open on the dorsal surface, whereas the left septomaxilla instead has a large groove. In *Madatyphlops arenarius* there is a small notch on the lateral edge of the septomaxilla, and a small foramen at the medial point. *Indotyphlops braminus* and *Anilios leucoproctus* have a similar morphology to *T. lumbricalis*, where the foramen is more medially positioned before exiting at the most anterior medial point of the septomaxilla. *Sundatyphlops polygrammicus* and *Anilios bituberculatus* have foramen that begin on the dorsal side of the septomaxilla, before emerging on the ventral side along a shallow groove and re-entering the septomaxilla medially.

3.2.5 Vomer – Figures 10-11

The vomers are small elements with a complex topology, that form part of the ventral and posteromedial closure of the vomeronasal cupola (See Figure 10). In ventral view the vomers have a flat anterior triangular expansion that curves posteriorly into a hook and which projects into the vomeronasal foramen (See Figure 11). The posterior part of the vomer expands laterally to a lobe, before narrowing to a slender process that projects slightly ventrally to meet the most lateral extent of the curved palatine. There is a large foramen dorsal to this projection, except in *Madatyphlops arenarius* where this foramen is relatively smaller. The anterior end of the vomers is triangular, in contact with the posterior opening of the ventral lamina of the septomaxillae. Medially, dorsal projections of the vomers enter the vomeronasal cupola, providing extra support to this structure. In all species examined except *M. arenarius*,

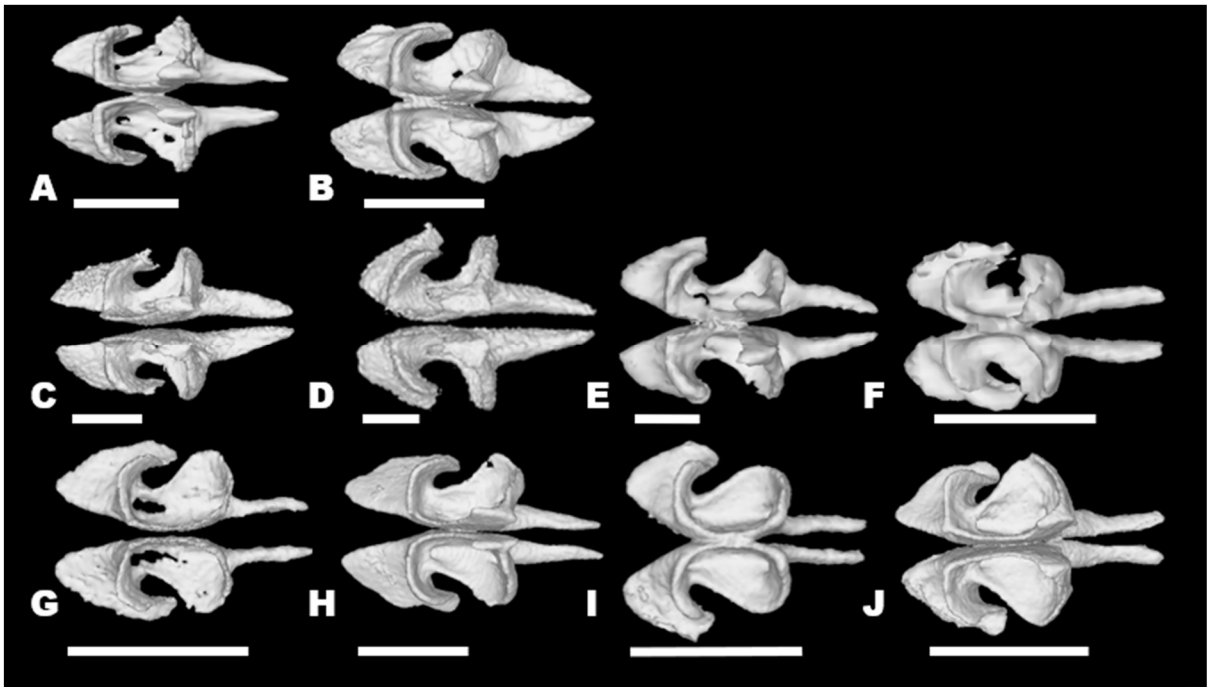

Figure 10. Vomer, Dorsal (A) *Typhlops jamaicensis*, (B) *Typhlops lumbricalis*, (C) *Afrotyphlops mucruso*, (D) *Afrotyphlops schlegelii*, (E) *Afrotyphlops punctatus,* (F) *Madatyphlops arenarius,* (G) *Indotyphlops braminus*, (H) *Sundatyphlops polygrammicus,* (I) *Anilios leucoproctus*, (J) *Anilios bituberculatus*.

Scale bar = 0.5mm

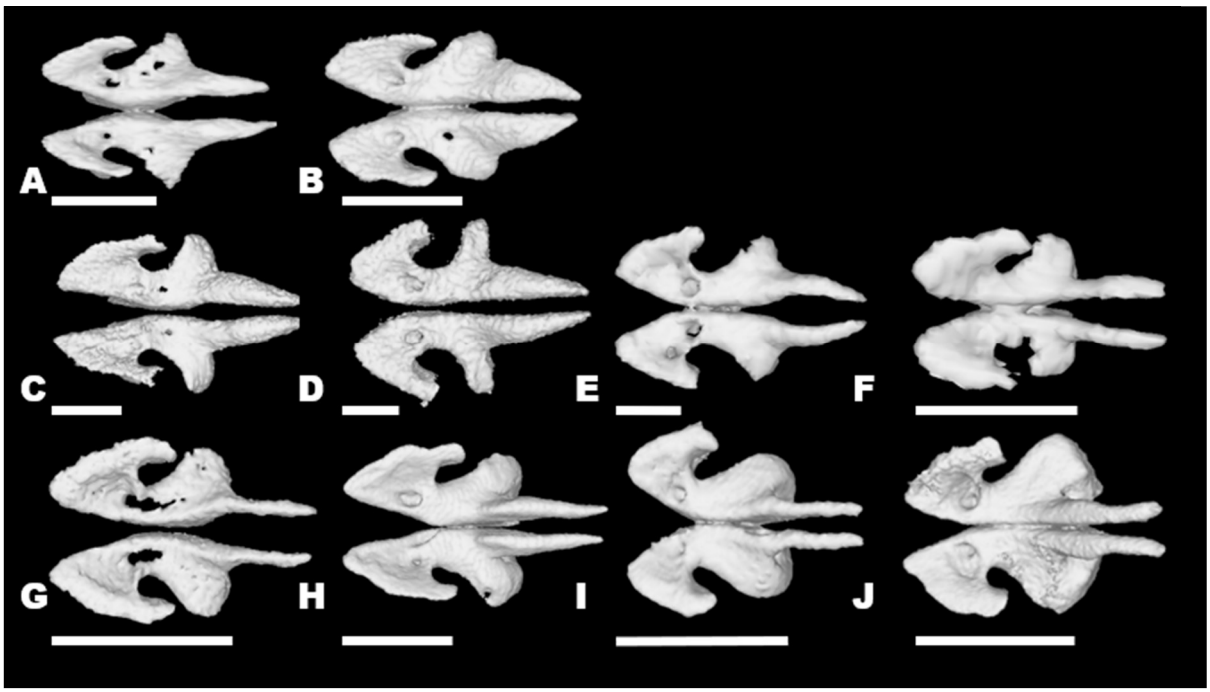

Figure 11. Vomer, Ventral (A) *Typhlops jamaicensis*, (B) *Typhlops lumbricalis*, (C) *Afrotyphlops mucruso*, (D) *Afrotyphlops schlegelii*, (E) *Afrotyphlops punctatus,* (F) *Madatyphlops arenarius,* (G) *Indotyphlops braminus*, (H) *Sundatyphlops polygrammicus,* (I) *Anilios leucoproctus*, (J) *Anilios bituberculatus*.

Scale bar = 0.5mm

the vomer also possesses a small foramen in the anterior portion of the bone, lateral to the beginning of the curved hook-like expansion. The overall topology of the vomers is consistent in all the species examined.

3.3 Dorsal Jaw Complex and Palate

The dorsal jaw complex and palate are composed of paired pterygoid, palatine, and maxilla. As previously described for Typhlopidae, the ectopterygoid is absent, likely fused with the pterygoid (Cundall & Irish 2008).

3.3.1 Pterygoid – Figure 12

The pterygoid is a long and rod-like edentulous bone, with a y-shaped anterior end (See Figure 12). The pterygoid connects to the rest of the dorsal jaw complex in an articulation between the y-shaped anterior end of the pterygoid and the medially curving process of the palatine, and is not in contact with any other bone. The long rod-like extension of the pterygoid projects posteriorly along the ventral aspect of the skull. The posterior process is much separated from the quadrate, no articulation is visible. The y-shaped anterior end splits into two processes, the dorsolateral of which is rod-shaped and the ventromedial is laminar. The morphology of these two processes differs slightly between species, but in general the laminar ventral process is larger than the dorsal rod-shaped process, and follows the ventrally projecting process of the palatine. The medial process of the y-shaped anterior process of *Indotyphlops braminus* is expanded at the anterior end, not rod-shaped as in the other species examined, due to a slightly more ventrally positioned articulation with the palatine.

3.3.2 Palatine – Figure 13

The palatine is a triradiate element, much reduced to its medial choanal processes. The lateral part of the palatine forms a slender bar of bone that meets the large foramen of the maxilla. Medially, the palatines meet the ventral tips of the vomers, and then curve dorsally over the choanal tubes. There is a ventral projection positioned halfway along the element with a small posteriorly deflected spur that articulates with the pterygoid (See Figure 13). In most species, this spur is a continuation of the dorsal curve of the medial portion of the palatine, and the y-shaped anterior end of the pterygoid articulates with this projection, with the more lateral shorter end of the 'y' articulating dorsally, and the longer end of the 'y' articulating ventrally and continuing along the ventral projection. The exception to this general morphology is seen in *I. braminus*, where the posteriorly projecting spur is ventral to the dorsal curve of the palatine. The pterygoid articulates to this spur and the dorsal curve, hence the expanded shape of the pterygoid anterior end.

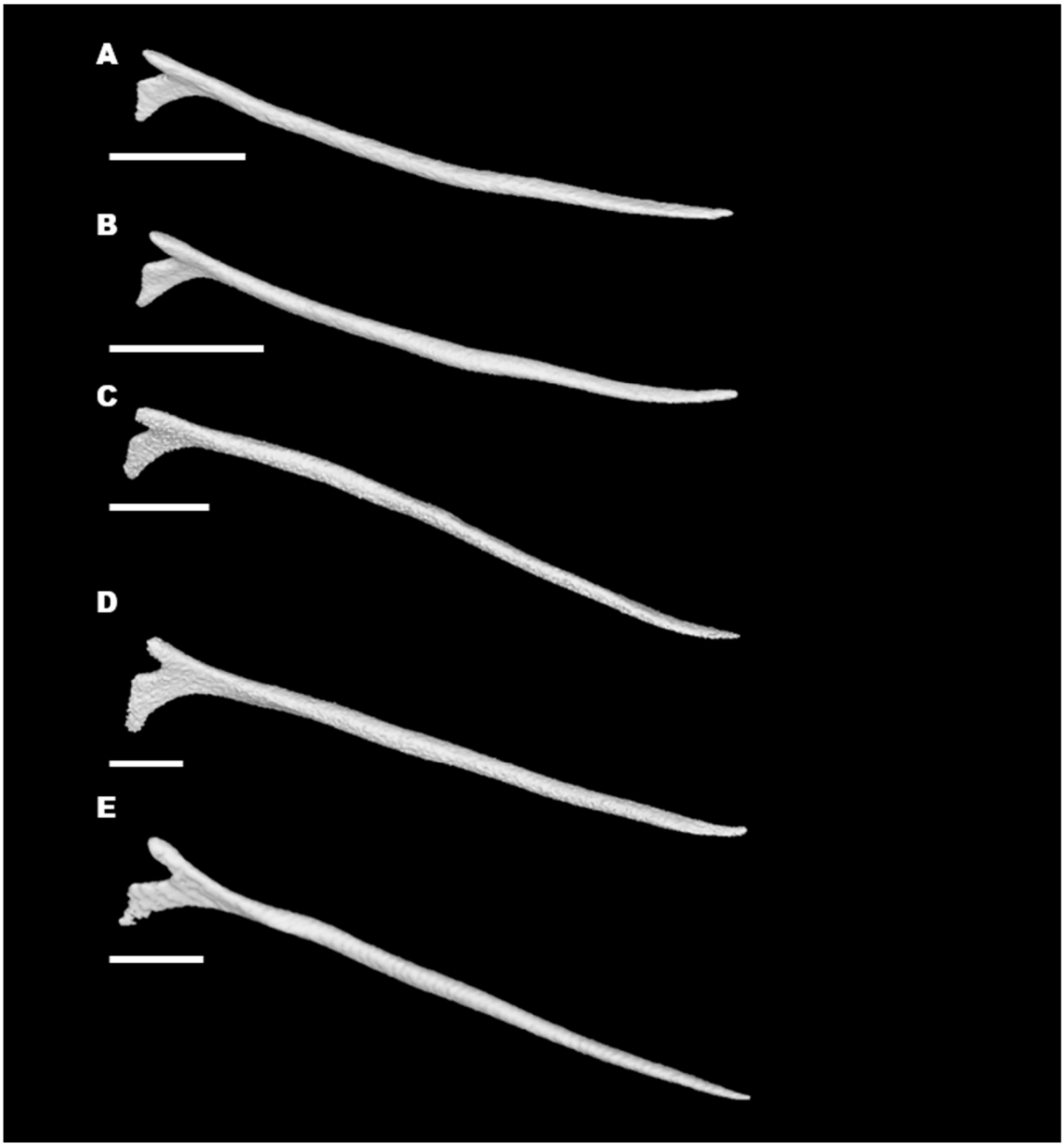

Figure 12. Pterygoid, Lateral (A) *Typhlops jamaicensis*, (B) *Typhlops lumbricalis*, (C) *Afrotyphlops mucruso*, (D) *Afrotyphlops schlegelii*, (E) *Afrotyphlops punctatus,* (F) *Madatyphlops arenarius,* (G) *Indotyphlops braminus*, (H) *Sundatyphlops polygrammicus,* (I) *Anilios leucoproctus*, (J) *Anilios bituberculatus*.

Scale bar = 1mm

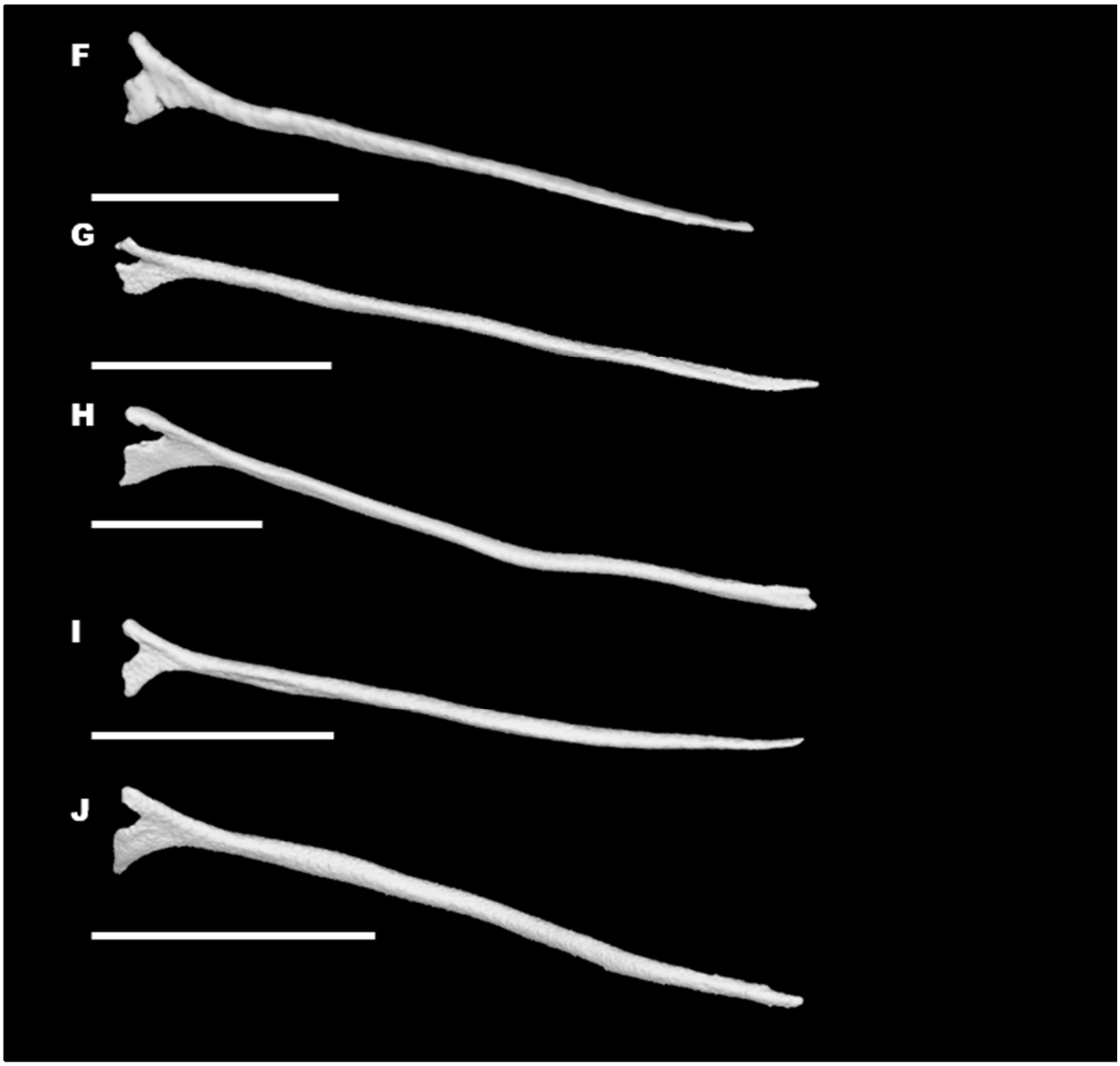

Figure 12 cont. Pterygoid, Lateral (A) *Typhlops jamaicensis*, (B) *Typhlops lumbricalis*, (C) *Afrotyphlops mucruso*, (D) *Afrotyphlops schlegelii*, (E) *Afrotyphlops punctatus,* (F) *Madatyphlops arenarius,* (G) *Indotyphlops braminus*, (H) *Sundatyphlops polygrammicus,* (I) *Anilios leucoproctus*, (J) *Anilios bituberculatus*.

Scale bar = 1mm

3.3.3 Maxilla – Figure 14

Unique among snakes, the maxilla are the only tooth-bearing bones in the skull of Typhlopidae (Cundall & Irish 2008; List 1966). At rest, these elements are oriented horizontally, although they are highly mobile and can be rotated considerably during feeding, through angles of 60° to 90°. For sake of clarity, the tooth-bearing end will be referred to as 'posterior', and the rostral

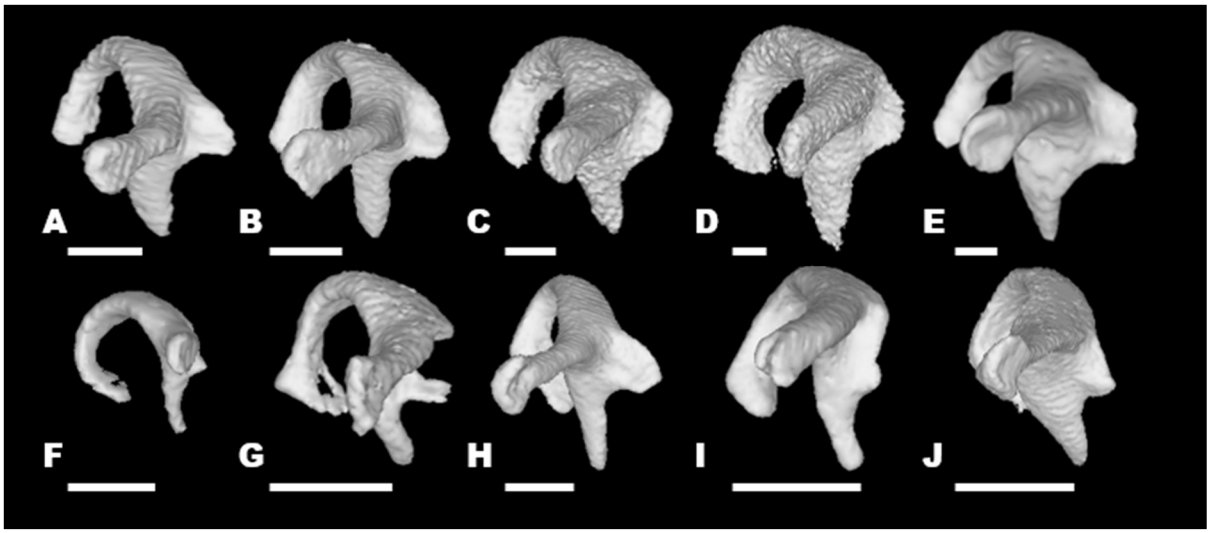

Figure 13. Palatine, Lateral (A) *Typhlops jamaicensis*, (B) *Typhlops lumbricalis*, (C) *Afrotyphlops mucruso*, (D) *Afrotyphlops schlegelii*, (E) *Afrotyphlops punctatus,* (F) *Madatyphlops arenarius,* (G) *Indotyphlops braminus*, (H) *Sundatyphlops polygrammicus,* (I) *Anilios leucoproctus*, (J) *Anilios bituberculatus*.

Scale bar = 0.25mm

end as 'anterior'. The maxilla does not directly articulate with the skull, the anterior end is indirectly attached to the prefrontals and premaxilla by a premaxillomaxillary ligament (Cundall & Irish 2008). The maxilla is largely flat and roughly triangular, with a large foramen at the dorsal part of the tooth-bearing end where the maxilla articulates with the palatine (See Figure 14). This large palatine foramen is a unique feature of typhlopoids (Chretien *et al.* 2019). Unlike as reported by Chretien et al (2019) and Cundall & Irish (2008), a palatine foramen is visible in the maxilla of both *Afrotyphlops mucruso* and *Afrotyphlops punctatus.* There is a large foramen, known as the keyhole foramen, that runs from midway up the shaft to the anterior end, resulting in a v-shaped end to the maxilla shaft. Tooth number appears to vary slightly between species, with possible replacement teeth visible in scans. The teeth are large and recurved, and decrease in size from the largest at the ventral edge of the maxilla.

3.4 Orbit

The shallow orbit is composed posteriorly of the lateral margin of the frontal, and anteriorly the posterolateral margin of prefrontals in all the species examined.

3.5 Braincase

The braincase is always composed of paired frontals, a basisphenoid and a basioccipital. The parietal is either a single element or paired, as in *Indotyphlops braminus* and *Madatyphlops arenarius*. The otic complex is composed of three sets of paired elements that are variably fused

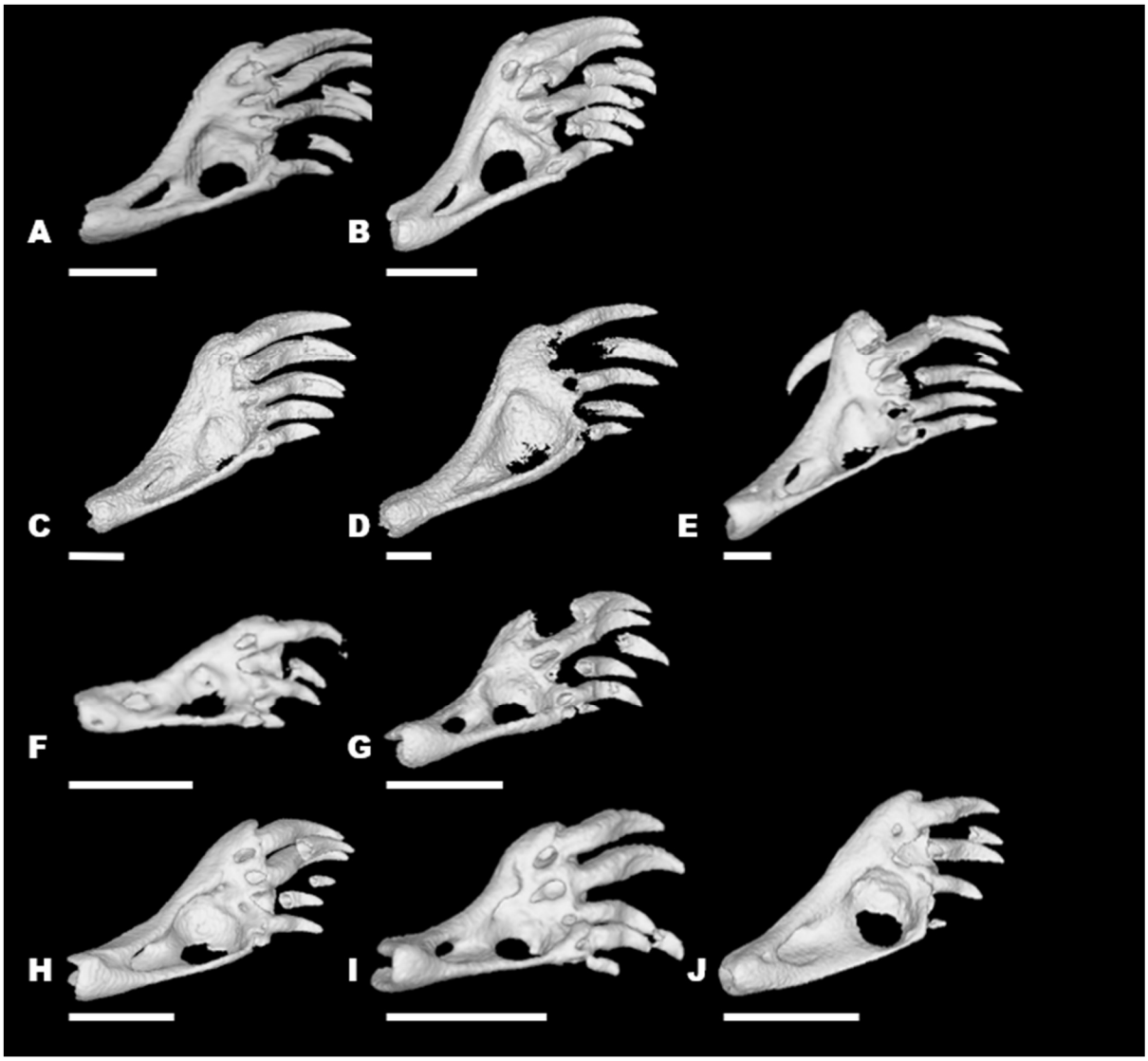

Figure 14. Maxilla, dorsal (A) *Typhlops jamaicensis*, (B) *Typhlops lumbricalis*, (C) *Afrotyphlops mucruso*, (D) *Afrotyphlops schlegelii*, (E) *Afrotyphlops punctatus,* (F) *Madatyphlops arenarius,* (G) *Indotyphlops braminus*, (H) *Sundatyphlops polygrammicus,* (I) *Anilios leucoproctus*, (J) *Anilios bituberculatus*.

Scale bar = 0.5mm

among species, the paired otooccipitals, paired prootics, and paired supraoccipitals. The supraoccipitals are absent in *I. braminus, Anilios bituberculatus* and *Anilios leucoproctus*. As opposed to reported in List (1966) the prootics of *I. braminus* are not present as separate elements in any of the three individuals examined, and are instead fused with the rest of the otic complex. It is unclear whether the prootics and supraoccipitals are fused with the otooccipitals or absent, as there are no visible lines of fusion. In *A. leucoproctus* and *A. bituberculatus*, the supraoccipitals appear to be fused with the parietal.

3.5.1 Frontal – Figures 15-18

The frontals are large, paired elements comprising the anterior portion of the braincase. In dorsal view, the anterior edge of the frontals contact the nasals and the prefrontals, and the posterior edge of the frontals expand laterally to meet the anterior edge of the parietal (See Figure 15-16). This posterior edge is generally straight, with a small amount of variation among species. In the *Typhlops* examined, the posterior edge of the frontal projects slightly posteriorly just medial to the mid-line suture, resulting in an m-shaped suture between the two frontals and the parietal. In *Afrotyphlops mucruso* and *Afrotyphlops schlegelii*, the posterior edge of the frontals curves very slightly anteriorly, resulting in a v-shaped suture between the frontals and the parietal. Contrary to other species examined, the posterior edges of the frontals of *Afrotyphlops punctatus* are not smooth, instead both frontals possess a notch on this posterior edge lateral to the medial suture between the frontals. In *Madatyphlops arenarius* and *Indotyphlops braminus* the posterior edge is mostly straight, with the lateral edges curving slightly anteriorly. The frontals of *I. braminus* do not contact one another in a suture as in other species, but instead contact in a 'fissure', as termed by Rieppel et al (2009), where adjacent bones do not immediately contact one another. Presumably in life the bones are connected across this fissure by ligamentous connections. The frontals of *Anilios bituberculatus* contact the parietal by a straight edge, the lateral extent of which is slightly posteriorly deflected. In contrast the posterior edge of the frontals of *Anilios leucoproctus* are laterally straight and then curve anteriorly at the mid-point, in a similar morphology as seen in the *Typhlops* examined.

In dorsal view, the unusual morphology of the examined *Afrotyphlops* is also visible. In all other species the lateral walls of the frontals project ventrally before wrapping around the braincase. However in the *Afrotyphlops* examined, after projecting ventrally these walls expand laterally, forming a shelf that forms a contact with the dorsal surface of the posterior edge of the prefrontals. The examined *Afrotyphlops* also differ from the other species examined in that the lateral extent of the anterior dorsal edge is wider than the lateral extent of the posterior dorsal edge. In all other species, the anterior edge is slightly more medially positioned than the posterior edge. The posterior ventral edge is visible in dorsal view in all species except *Indotyphlops braminus*, but is seen to most extreme extent in the examined *Afrotyphlops*, where the contact between the ventral edges of the paired frontals is also visible in dorsal view. In *I. braminus*, in contrast, the ventral edges are barely visible.

The frontals surround the braincase and then meet ventrally above the basisphenoid. There is variation between the species in the amount of contact the ventral edges of the frontals make with one another. In most species examined the frontals contact one another, whereas in *Madatyphlops arenarius* and *Indotyphlops braminus* the frontals approach but do not form a

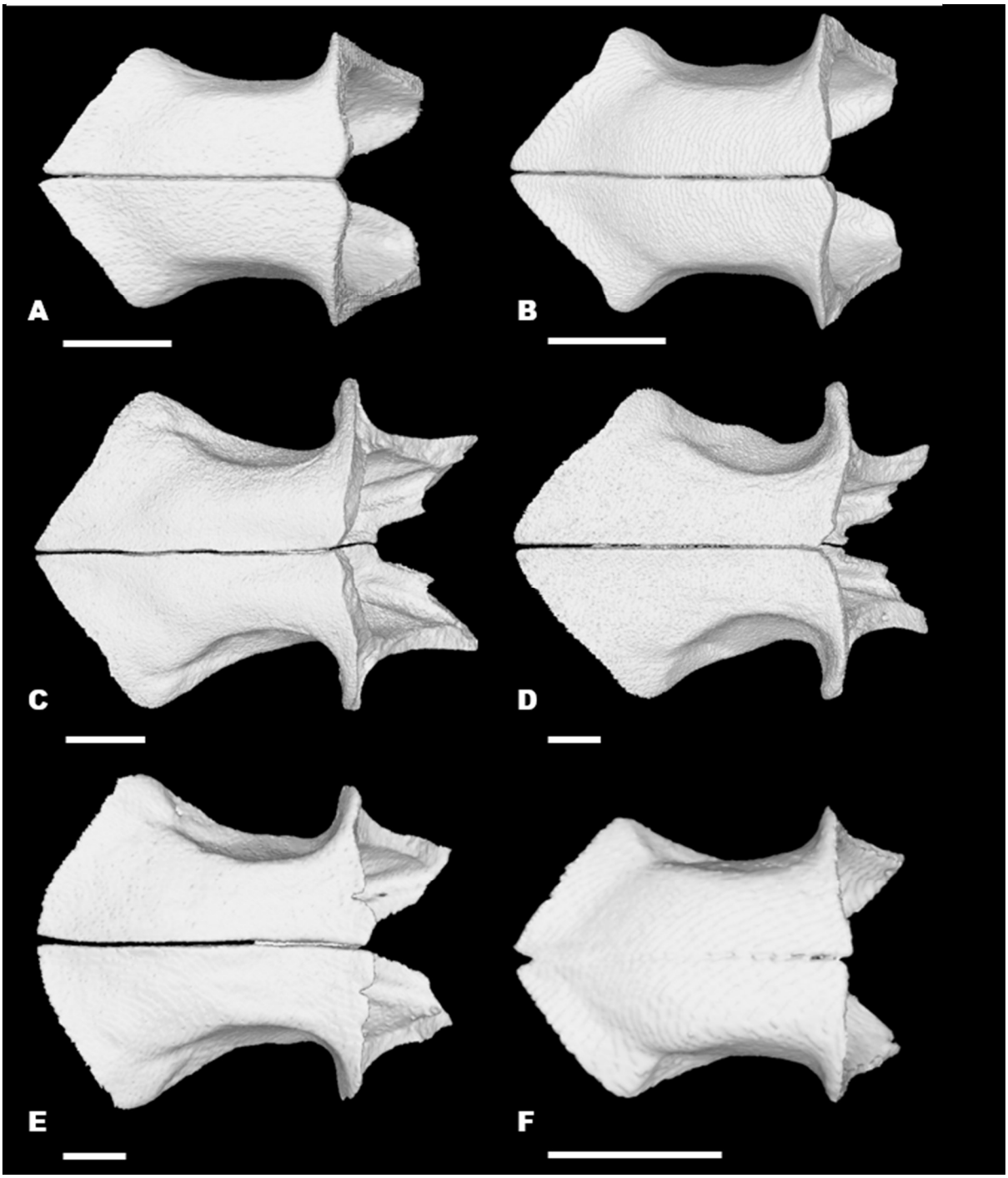

Figure 15. Frontal, Dorsal (A) *Typhlops jamaicensis*, (B) *Typhlops lumbricalis*, (C) *Afrotyphlops mucruso*, (D) *Afrotyphlops schlegelii*, (E) *Afrotyphlops punctatus,* (F) *Madatyphlops arenarius,* (G) *Indotyphlops braminus*, (H) *Sundatyphlops polygrammicus,* (I) *Anilios leucoproctus*, (J) *Anilios bituberculatus*.

Scale bar = 1mm

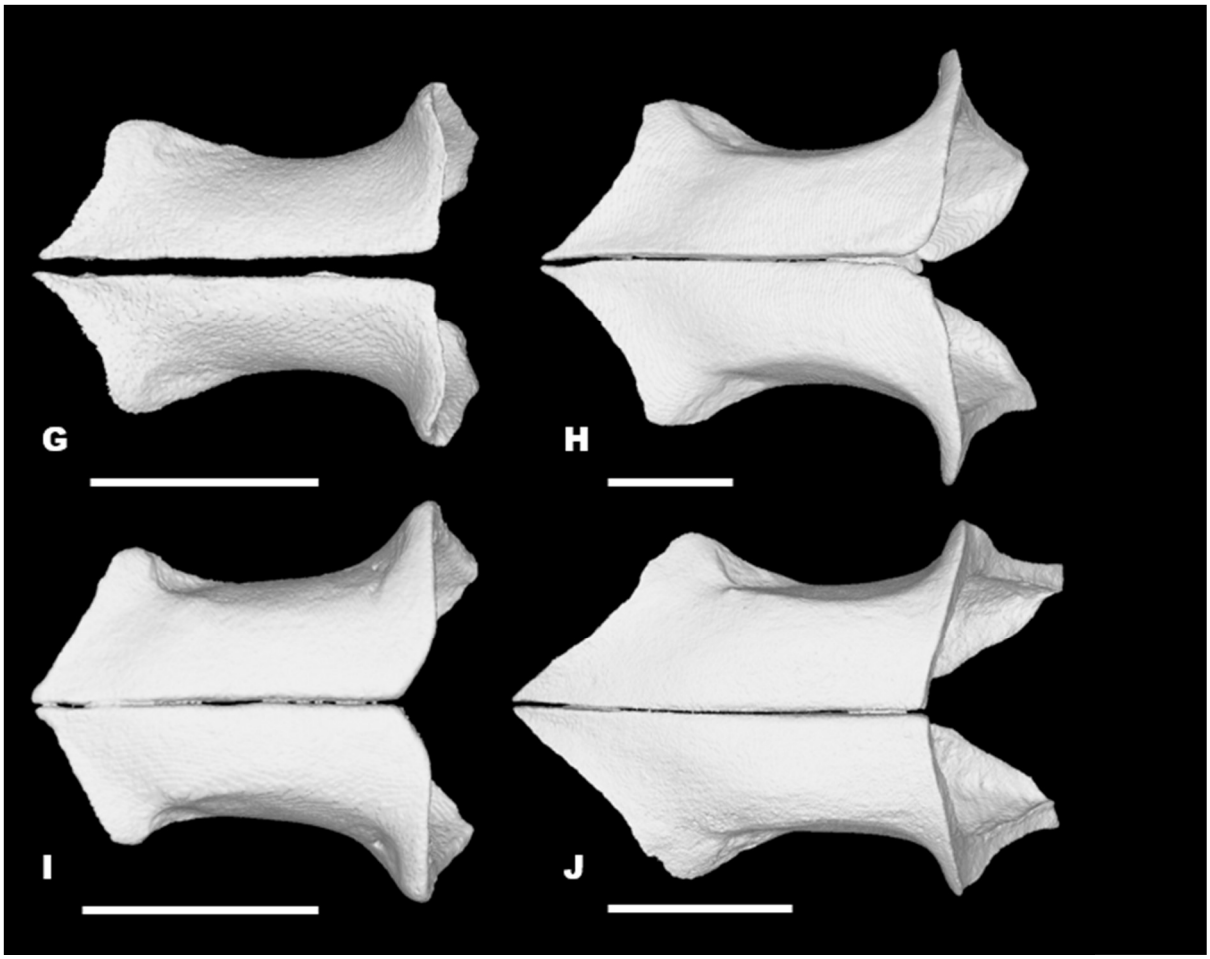

Figure 15 cont. Frontal, Dorsal (A) *Typhlops jamaicensis*, (B) *Typhlops lumbricalis*, (C) *Afrotyphlops mucruso*, (D) *Afrotyphlops schlegelii*, (E) *Afrotyphlops punctatus,* (F) *Madatyphlops arenarius,* (G) *Indotyphlops braminus*, (H) *Sundatyphlops polygrammicus,* (I) *Anilios leucoproctus*, (J) *Anilios bituberculatus*.

Scale bar = 1mm

contact. In ventral view these contacts are overlapped by the anterior extent of the basisphenoid.

The interior of the frontals are smooth, but there is considerable variation in the position of the foramina which transmit the optic nerve and the trigeminal nerve along the ventral projections of the frontals. In posterior view, the trajectory of these nerves can be interpreted from examining the grooves on the dorsal surface of the ventral projections of the frontals (See Figure 18). In *Typhlops jamaicensis* a large foramen that transmits both the optic and the trigeminal nerve is positioned lateral to the contact between the two frontals. The optic nerve immediately exits the braincase laterally, and the trigeminal nerve continues anteriorly, exiting the frontals ventral to the anterior of the ventral contact of the frontals. In *Typhlops lumbricalis*, the trajectory of the optic nerve is the same as in *T. jamaicensis*, but the trigeminal

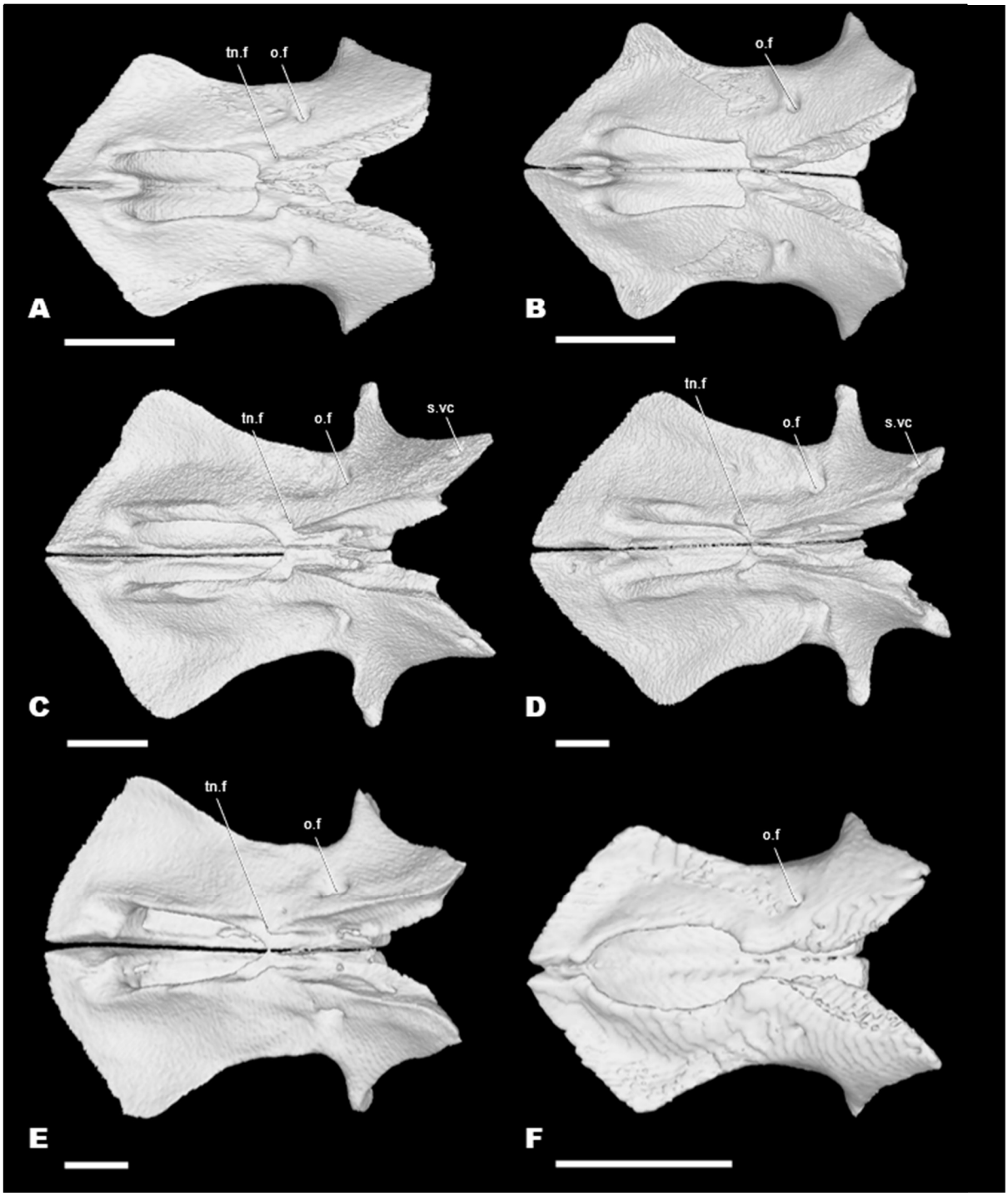

Figure 16. Frontal, Ventral (A) *Typhlops jamaicensis*, (B) *Typhlops lumbricalis*, (C) *Afrotyphlops mucruso*, (D) *Afrotyphlops schlegelii*, (E) *Afrotyphlops punctatus,* (F) *Madatyphlops arenarius,* (G) *Indotyphlops braminus*, (H) *Sundatyphlops polygrammicus,* (I) *Anilios leucoproctus*, (J) *Anilios bituberculatus*. Abbreviations: tn.f – foramen for trigeminal nerve, o.f – optic foramen, s.vc – secondary opening of Vidian canal

Scale bar = 1mm

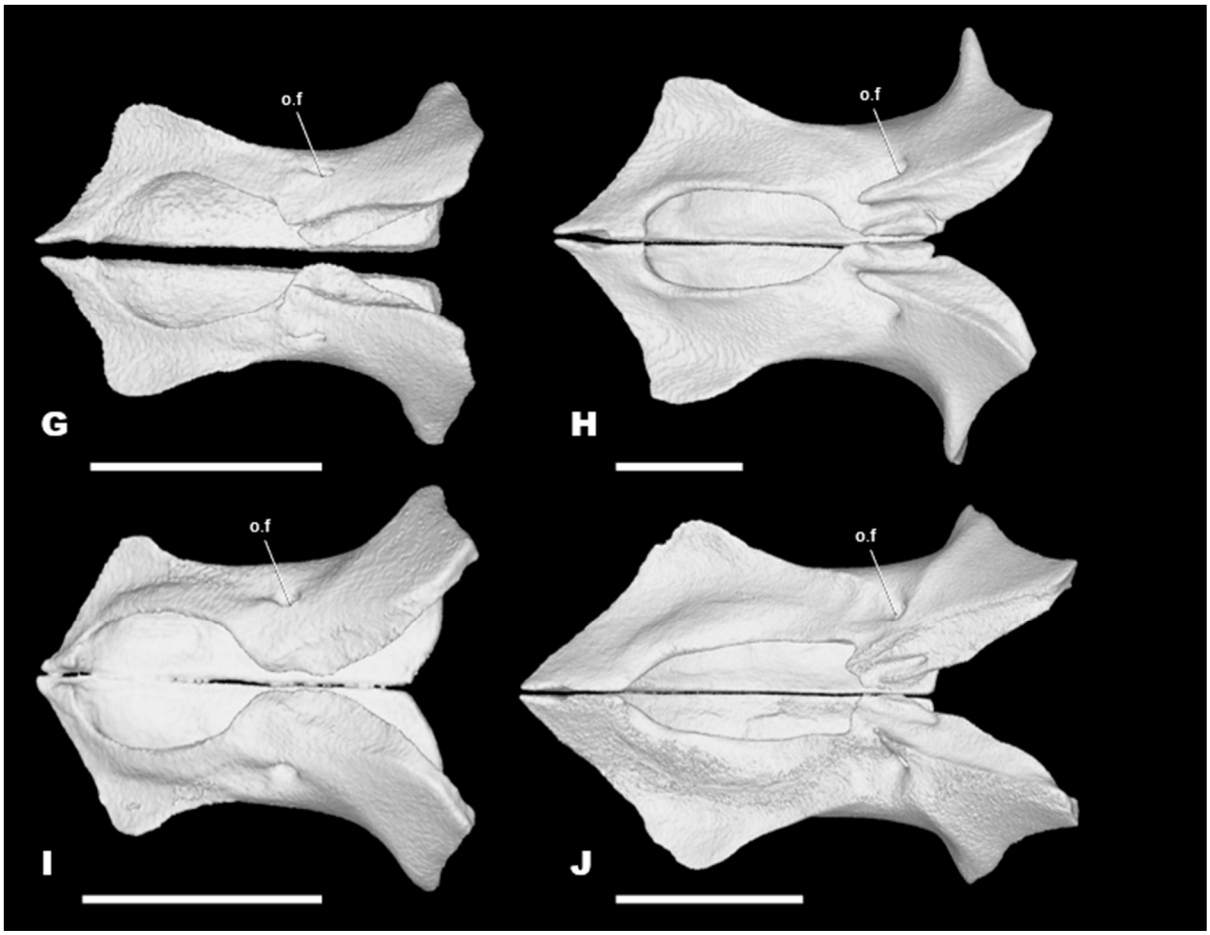

Figure 16 cont. Frontal, Ventral (A) *Typhlops jamaicensis*, (B) *Typhlops lumbricalis*, (C) *Afrotyphlops mucruso*, (D) *Afrotyphlops schlegelii*, (E) *Afrotyphlops punctatus,* (F) *Madatyphlops arenarius,* (G) *Indotyphlops braminus*, (H) *Sundatyphlops polygrammicus,* (I) *Anilios leucoproctus*, (J) *Anilios bituberculatus*. Abbreviations: o.f – optic foramen

Scale bar = 1mm

nerve is more dorsally positioned, so that rather than a foramen, this nerve travels along a groove in the dorsal surface of the bone, exiting the braincase lateral to the ventral contact of the frontals. In both *Afrotyphlops mucruso* and *Afrotyphlops schlegelii*, the groove which carries these nerves starts at the posterior most point of the ventral projections of the frontals, before entering the bone lateral to the midpoint of the ventral contact between the frontals. The optic nerve again exits immediately lateral to this entry foramen, and the trigeminal continues lateral to the ventral contact, exiting the braincase ventral to the anterior point of this contact. The medial wall of this foramen is completed by the dorsal surface of the basisphenoid. In *Afrotyphlops punctatus*, the morphology is similar to the other species of *Afrotyphlops* examined, except the foramen that carries the trigeminal nerve is more dorsally positioned, so the dorsal surface of the right frontal. Less of the medial wall of this foramen is completed by

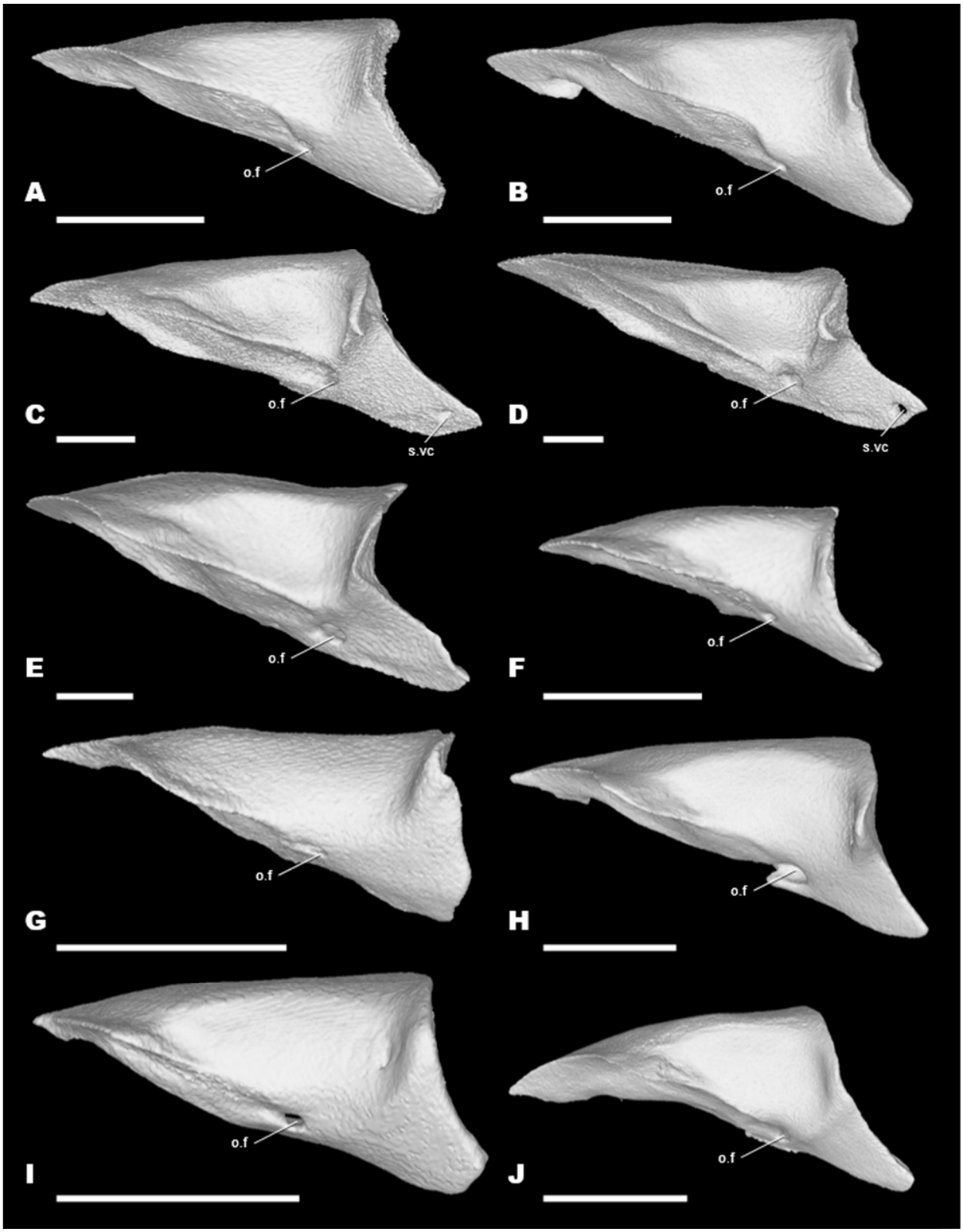

Figure 17. Frontal, Ventral (A) *Typhlops jamaicensis*, (B) *Typhlops lumbricalis*, (C) *Afrotyphlops mucruso*, (D) *Afrotyphlops schlegelii*, (E) *Afrotyphlops punctatus,* (F) *Madatyphlops arenarius,* (G) *Indotyphlops braminus*, (H) *Sundatyphlops polygrammicus,* (I) *Anilios leucoproctus*, (J) *Anilios bituberculatus*. Abbreviations: o.f – optic foramen, s.vc – secondary opening of Vidian canal

Scale bar = 1mm

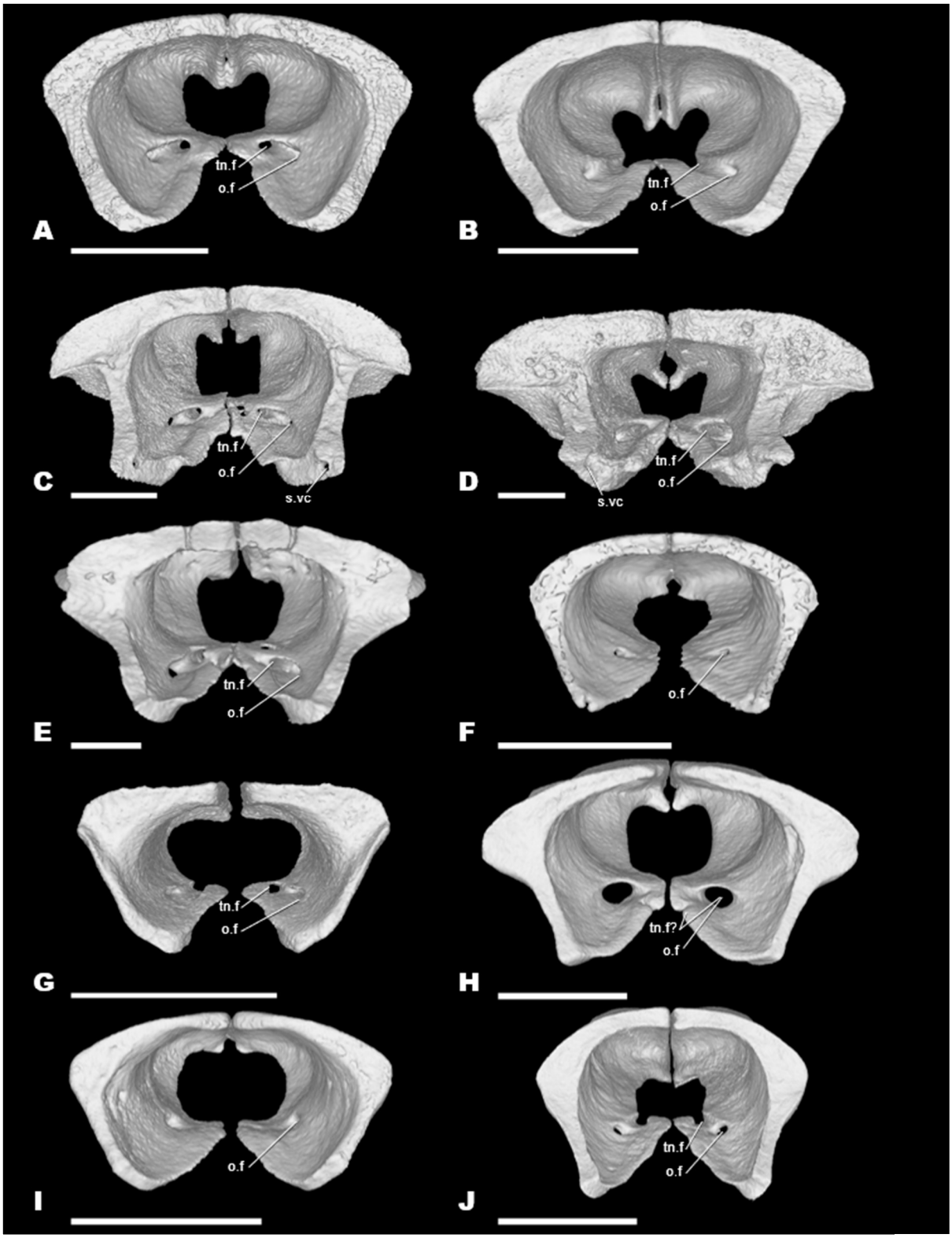

Figure 18. Frontal, Posterior (A) *Typhlops jamaicensis*, (B) *Typhlops lumbricalis*, (C) *Afrotyphlops mucruso*, (D) *Afrotyphlops schlegelii*, (E) *Afrotyphlops punctatus,* (F) *Madatyphlops arenarius,* (G) *Indotyphlops braminus*, (H) *Sundatyphlops polygrammicus,* (I) *Anilios leucoproctus*, (J) *Anilios bituberculatus*. Abbreviations: tn.f – foramen for trigeminal nerve, o.f – optic foramen, s.vc – secondary opening of Vidian canal

Scale bar = 1mm

the dorsal surface of the basisphenoid than in *A. schlegelii* and *A. mucruso*. In contrast, *Madatyphlops arenarius* shows very little indicators of nerve trajectory, the only foramen visible is positioned in the middle of the ventral projections, and presumably transmits the optic nerve. As the frontals do not fully make contact ventrally, it is possible that the trigeminal nerve exits the braincase through the suture between the frontals and the basisphenoid. In Indotyphlops braminus the morphology is similar to that of *T. lumbricalis*, with a lateral exit of the optic nerve and a groove transmitting the trigeminal nerve anteriorly. The position of the optic nerve foramen is more anteriorly positioned than seen in *T. lumbricalis*. Additionally, in the right frontal the groove turns into a full foramen just before the nerve exits the bone on its anterior edge. In *Sundatyphlops polygrammicus*, either both the optic nerve and the trigeminal nerve are transmitted through the same large foramen that exits the braincase lateral to the ventral contact between the frontals, or the trigeminal nerve runs along a groove on the ventral surface of this contact. In *Anilios leucoproctus*, the morphology is similar to *M. arenarius*, with only a single foramen visible that transmits the optic nerve laterally, positioned in the middle of the ventral approaches of the frontals. There is no visible groove or foramen for the trigeminal nerve, which presumably exits the braincase between the suture of the frontals and the basisphenoid. In *Anilios bituberculatus* the morphology is similar to that of *T. lumbricalis*, although the exit of the optic nerve is more anteriorly positioned in *A. bituberculatus* than in *T. lumbricalis*. The frontals of *A. mucruso* and left frontal of *A. schlegelii* also possess small foramen on the posterolateral most points of the ventral projections, which presumably is the secondary opening of the Vidian canal, that transmits the maxillary branch of the trigeminal nerve. Examination of the internal surface of the frontals also shows that the interior footprint of the frontals is relatively consistent, with the lateral flanges of the examined *Afrotyphlops* and examined asiatyphlopines resulting in thicker walls of the frontals, to the most extreme extent in the giant typhlopids *A. schlegelii* and *A. mucruso*.

3.5.2 Parietal - Figures 19-21

The parietal is a large element that is either paired or single. The anterior edge of the parietal contacts the posterior edges of the frontal, following the morphology of the ventral projections. The lateral projections of the parietal curve ventrally to contact the lateral edges of the basisphenoid, forming the side walls of the braincase, a typical feature of snakes and some fossorial lizards (List, 1966). The posterior edge contacts the bones comprising the back of the braincase, variably the supraoccipital, prootic, and otooccipital. The parietal is a single bone in *Typhlops jamaicensis*, *Afrotyphlops schlegelii*, *Afrotyphlops punctatus*, *Sundatyphlops polygrammicus*, and *Anilios leucoproctus*. In *Indotyphlops braminus* and *Madatyphlops arenarius*,

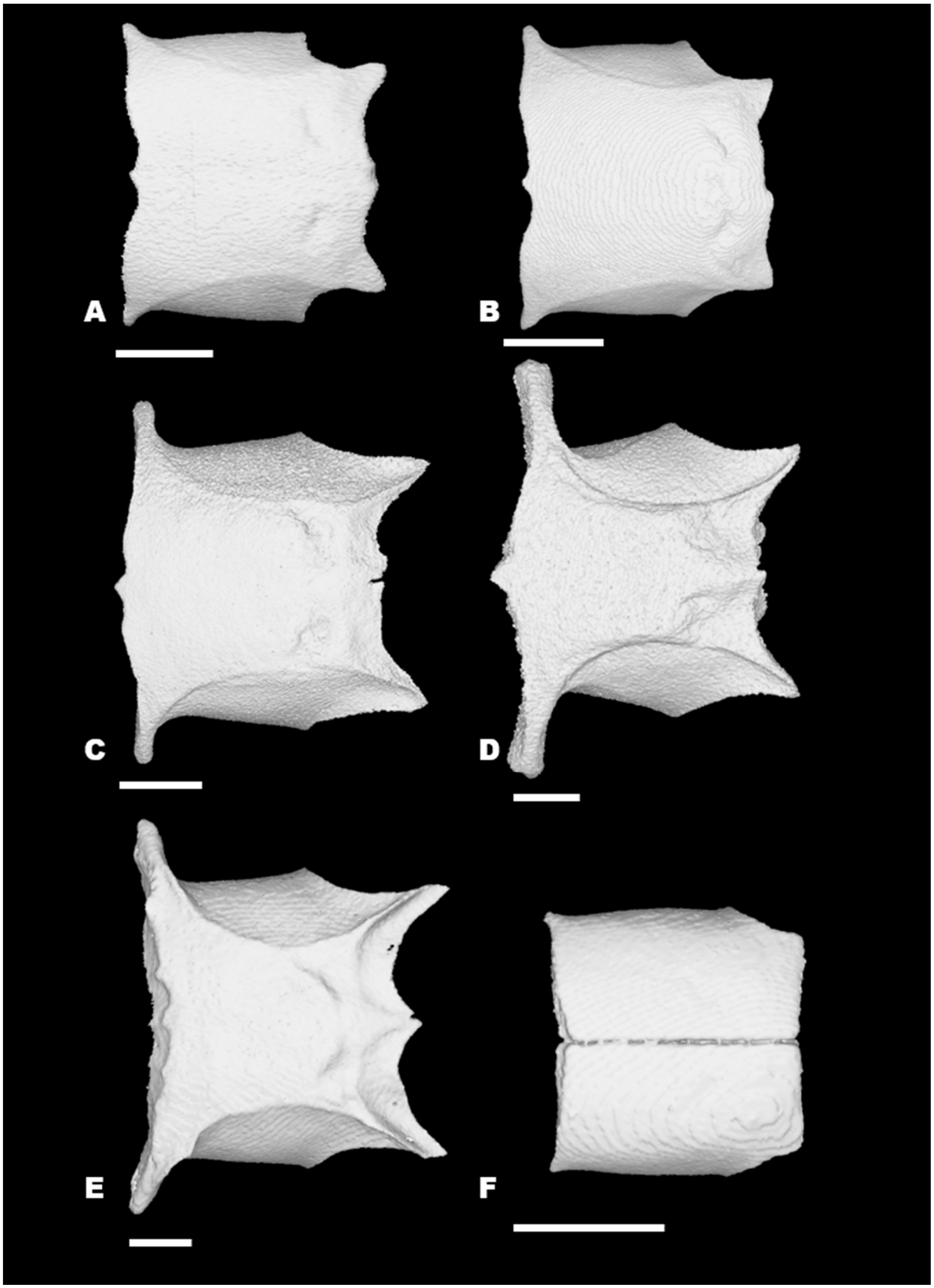

Figure 19. Parietal, Dorsal (A) *Typhlops jamaicensis*, (B) *Typhlops lumbricalis*, (C) *Afrotyphlops mucruso*, (D) *Afrotyphlops schlegelii*, (E) *Afrotyphlops punctatus,* (F) *Madatyphlops arenarius,* (G) *Indotyphlops braminus*, (H) *Sundatyphlops polygrammicus,* (I) *Anilios leucoproctus*, (J) *Anilios bituberculatus*.

Scale bar = 1mm

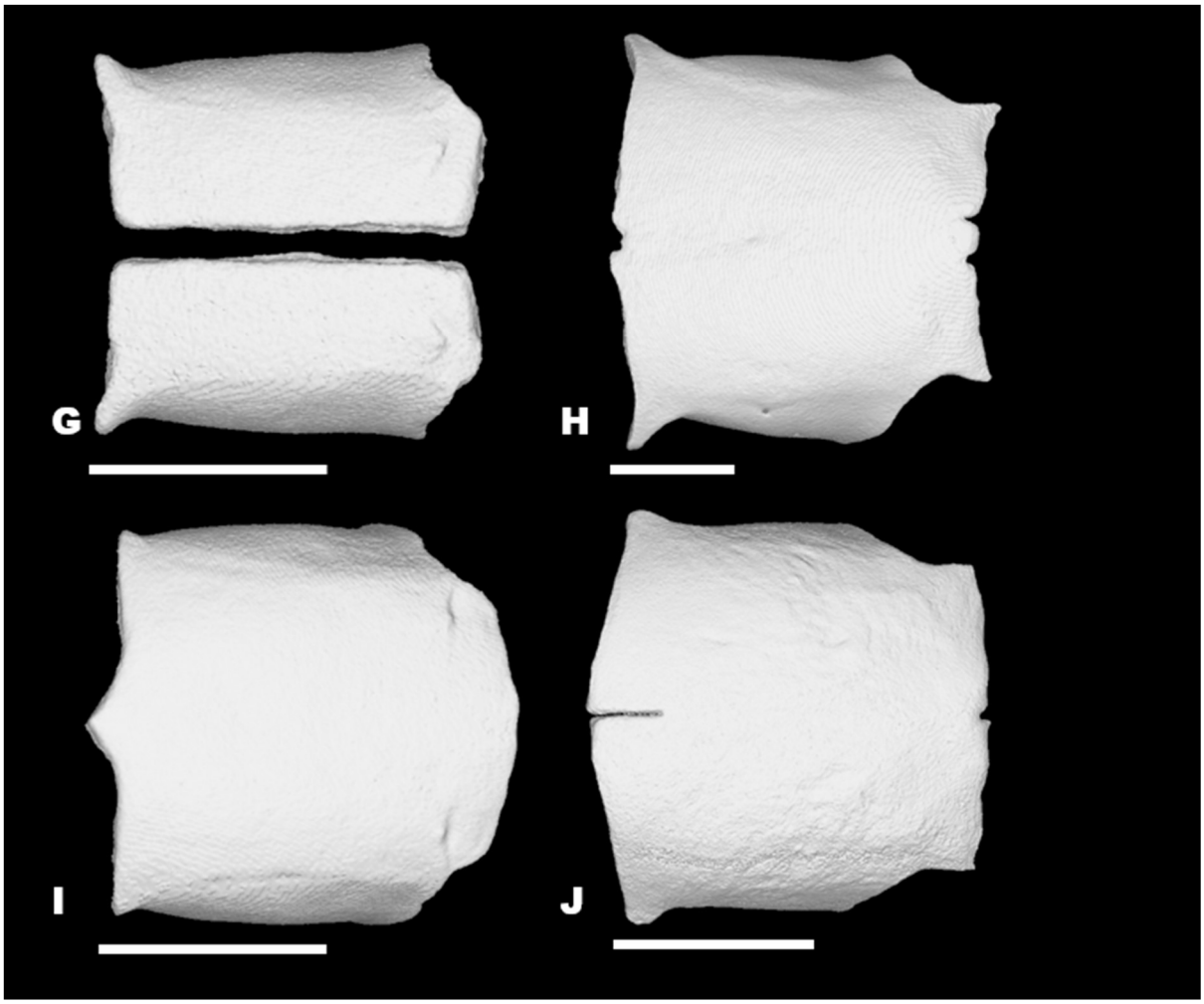

Figure 19 cont. Parietal, Dorsal (A) *Typhlops jamaicensis*, (B) *Typhlops lumbricalis*, (C) *Afrotyphlops mucruso*, (D) *Afrotyphlops schlegelii*, (E) *Afrotyphlops punctatus,* (F) *Madatyphlops arenarius,* (G) *Indotyphlops braminus*, (H) *Sundatyphlops polygrammicus,* (I) *Anilios leucoproctus*, (J) *Anilios bituberculatus*.
Scale bar = 1mm

the parietal is a paired element, which meet at a distinct suture in *M. arenarius*, but are separated by a 'fissure' in *I. braminus* (See Figure 19).

The morphology of the parietal varies between the clades of Typhlopidae. In the examined *Typhlops*, the anterior edge in dorsal view is roughly w-shaped, matching the m-shaped edge of the frontals. The parietal has small projections on this anterior edge that project more laterally than the frontals, that are triangular in cross section. In the examined *Typhlops*, the lateral walls of the parietal are separated slightly from the dorsal surface by a ridge, which in dorsal view curve medially before reaching the posterior dorsal extent of the lateral parietal walls. The dorsal surface of the parietal protrudes past the extent of the lateral walls, forming a shelf above the otic complex. The posterior edge of this shelf also follows a rough w-shape, with

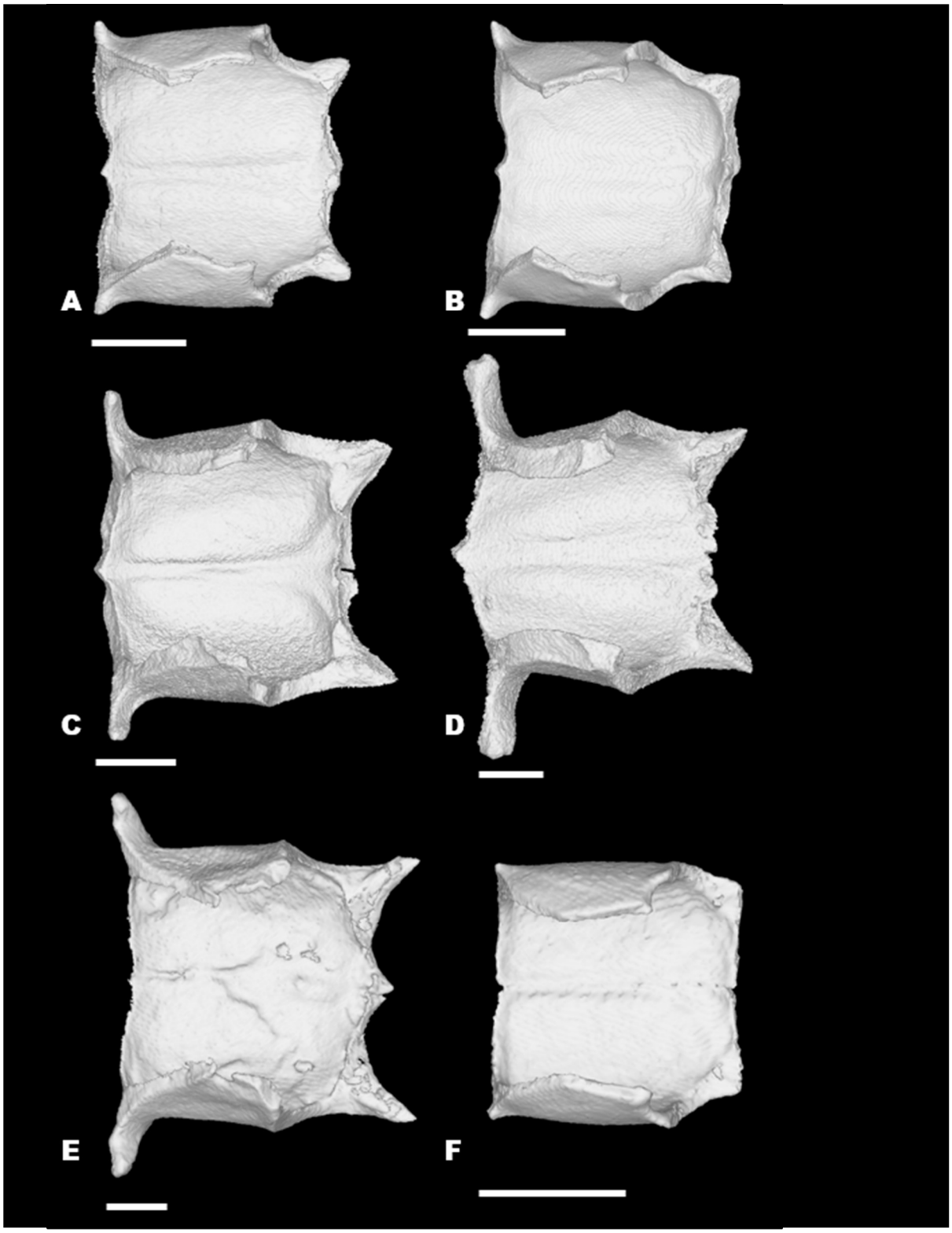

Figure 20. Parietal, Ventral (A) *Typhlops jamaicensis*, (B) *Typhlops lumbricalis*, (C) *Afrotyphlops mucruso*, (D) *Afrotyphlops schlegelii*, (E) *Afrotyphlops punctatus,* (F) *Madatyphlops arenarius,* (G) *Indotyphlops braminus*, (H) *Sundatyphlops polygrammicus,* (I) *Anilios leucoproctus*, (J) *Anilios bituberculatus*.

Scale bar = 1mm

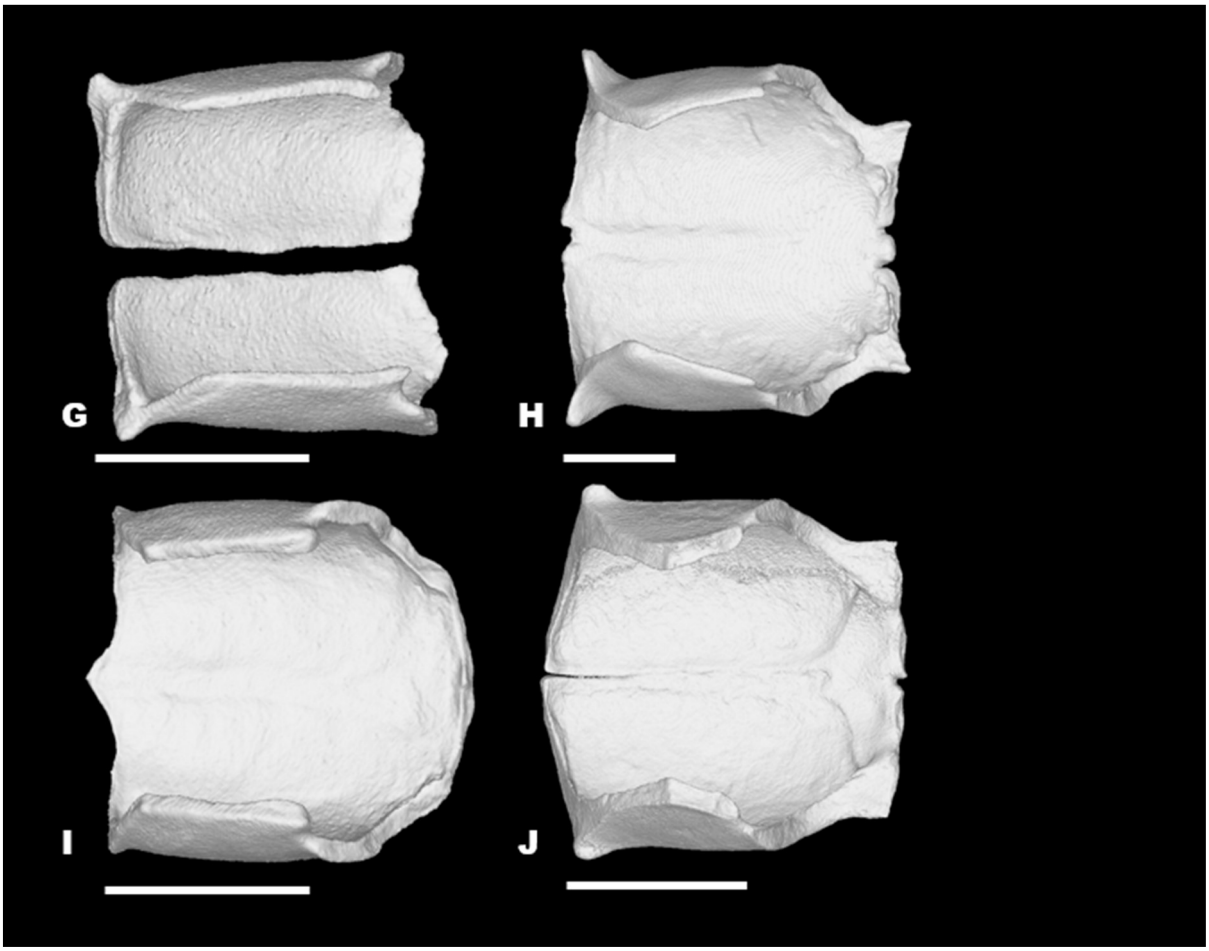

Figure 20 cont. Parietal, Ventral (A) *Typhlops jamaicensis*, (B) *Typhlops lumbricalis*, (C) *Afrotyphlops mucruso*, (D) *Afrotyphlops schlegelii*, (E) *Afrotyphlops punctatus,* (F) *Madatyphlops arenarius,* (G) *Indotyphlops braminus*, (H) *Sundatyphlops polygrammicus,* (I) *Anilios leucoproctus*, (J) *Anilios bituberculatus*.

Scale bar = 1mm

the lateral projections slightly triangular. The posterior edge is less of a w-shape in *Typhlops lumbricalis*, possibly due to the unusual supraoccipital morphology of this specimen. At the ventral extent of the posterior edge of the lateral wall there is a semi-circular notch that forms the anterior edge of the trigeminal foramen.

In the examined *Afrotyphlops*, the anterior edge projects slightly anteriorly at the midline, following the posterior edge of the frontals. The lateral edges of this anterior edge project considerably, and in *Afrotyphlops schlegelii* are slightly expanded at the end. The ridge that separates the lateral walls from the dorsal surface begins from the posterior edge of the dorsal surface of these projections, and then curves medially before projecting laterally to the posterior most lateral point of the dorsal surface. This posterior edge of the parietal of examined *Afrotyphlops* is also w-shaped, more so than seen in examined *Typhlops* due to more posteriorly projecting lateral edges of the dorsal surface. There are also two additional ridges

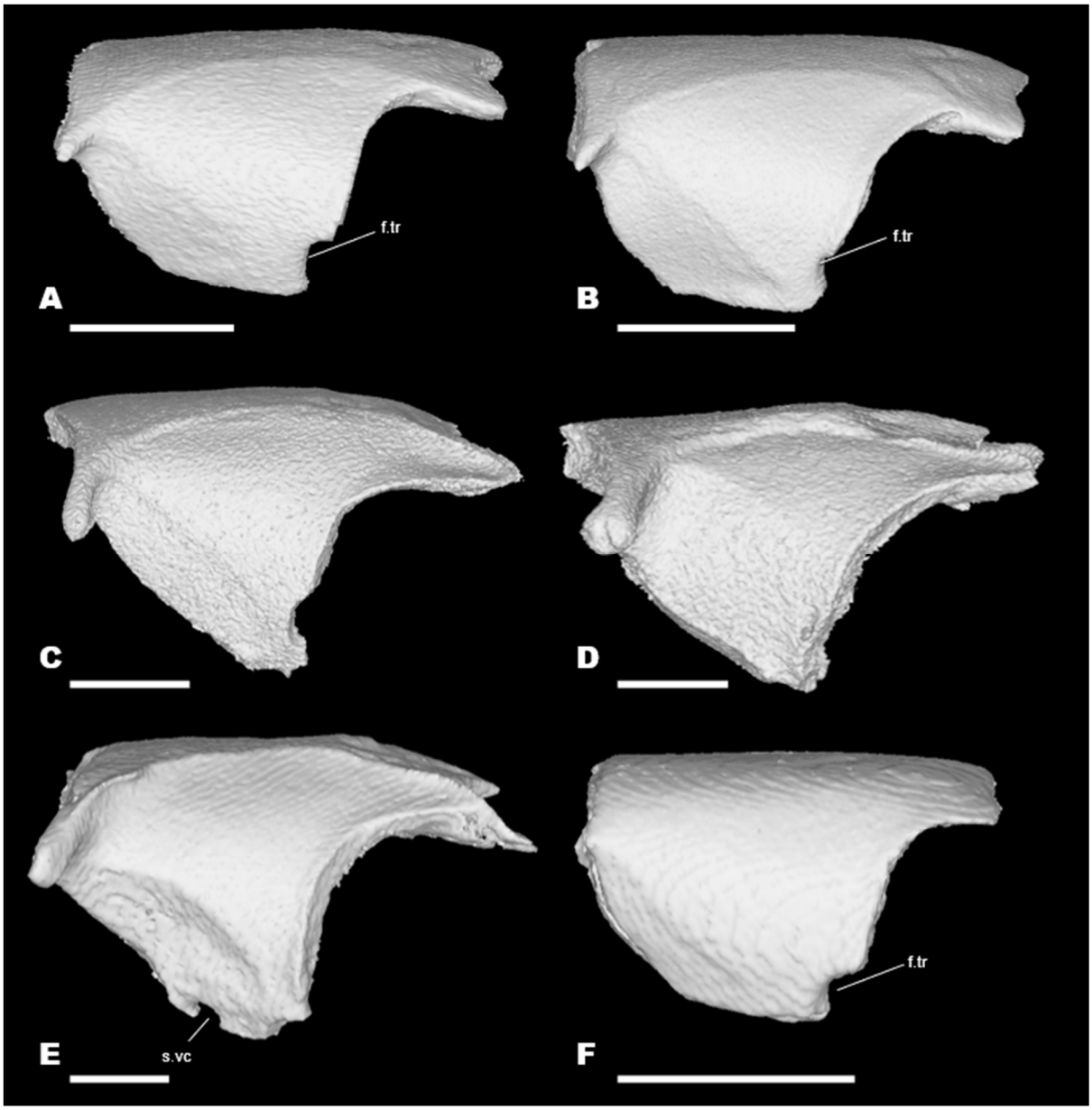

Figure 21. Parietal, Lateral (A) *Typhlops jamaicensis*, (B) *Typhlops lumbricalis*, (C) *Afrotyphlops mucruso*, (D) *Afrotyphlops schlegelii*, (E) *Afrotyphlops punctatus,* (F) *Madatyphlops arenarius,* (G) *Indotyphlops braminus*, (H) *Sundatyphlops polygrammicus,* (I) *Anilios leucoproctus*, (J) *Anilios bituberculatus*. Abbreviations: f.tr – trigeminal foramen, s.vc – secondary opening of Vidian canal.

Scale bar = 1mm

anterior to the posterior edge in *Afrotyphlops punctatus*, that reach the posterior edge at the mid point. In *A. schlegelii,* there are no ridges, but the dorsal surface of the parietal does decrease slightly in the same position as the ridges in *A. punctatus*. The lateral walls of the examined *Afrotyphlops* parietal contribute to much less of the lateral profile of the braincase, due to the ventral projections of the frontal that almost completely exclude the parietal from the suture with the basisphenoid. These lateral walls of the parietal also have a ridge where the lateral walls project more medially. In *A. schlegelii* and *A. mucruso*, this ridge begins at the same point

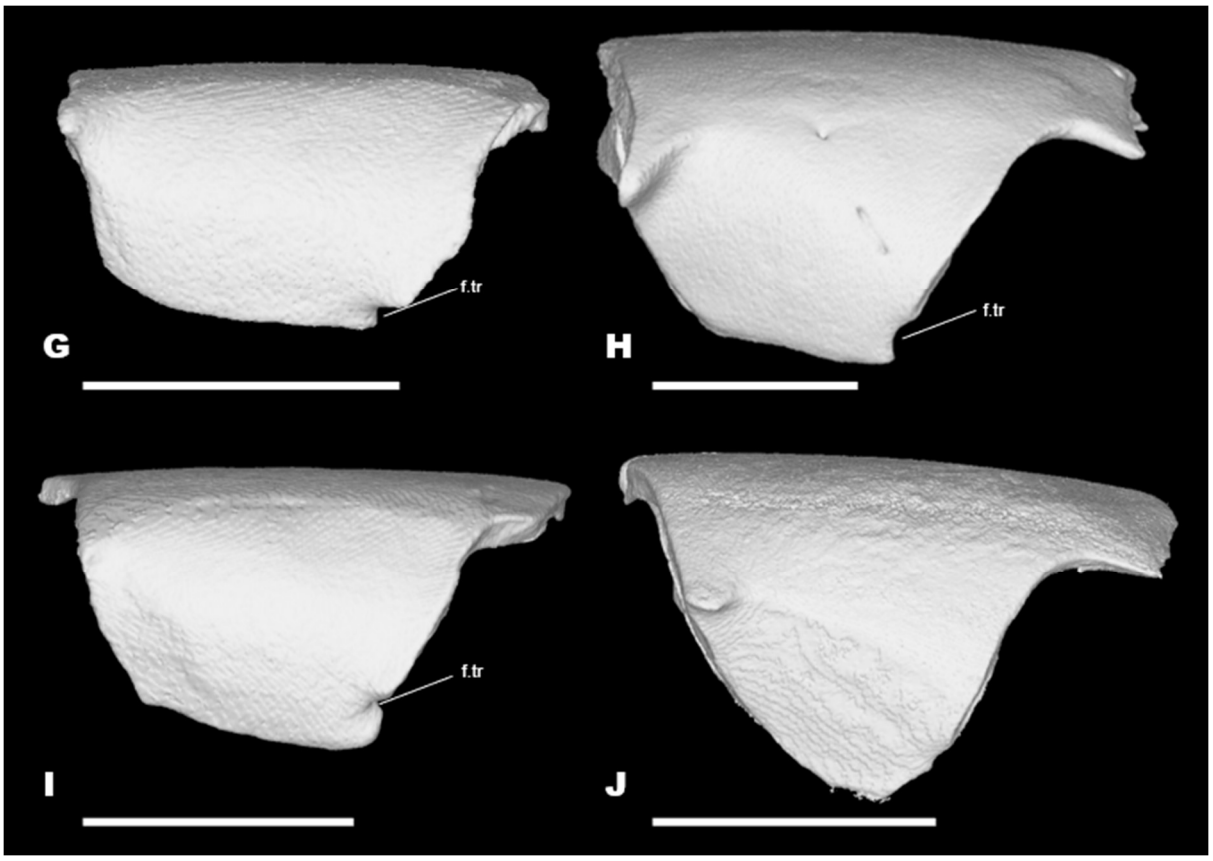

Figure 21 cont. Parietal, Lateral (A) *Typhlops jamaicensis*, (B) *Typhlops lumbricalis*, (C) *Afrotyphlops mucruso*, (D) *Afrotyphlops schlegelii*, (E) *Afrotyphlops punctatus,* (F) *Madatyphlops arenarius,* (G) *Indotyphlops braminus*, (H) *Sundatyphlops polygrammicus,* (I) *Anilios leucoproctus*, (J) *Anilios bituberculatus*. Abbreviations: f.tr – trigeminal foramen.

Scale bar = 1mm

that the dorsolateral ridge begins, before projecting diagonally posteroventrally, more pronounced at its' anterior end. In *A. punctatus*, this ridge begins ventral to the lateral projections of the anterior edge, and projects downwards to the posteroventral corner of the lateral wall. In contrast to the other species examined, the posterior edge of the lateral wall of the parietal of *A. punctatus* does not contribute to any part of the trigeminal foramen. In *A. punctatus*, there is a semi-circular notch on the ventral edge of the lateral wall that is the dorsal edge of the secondary opening of the Vidian canal.

In *Madatyphlops arenarius*, the parietal is paired, meeting at a close suture at the midline that is also visible on the interior of the bone. Both the anterior and the posterior edges are straight, and there is no distinct ridge between the dorsal surface and the lateral walls. There are very small lateral projections on the anterior edge that follow downwards from the dorsal surface, but these projections are much smaller than seen in the other species. As in the examined *Typhlops*, at the ventral extent of the posterior edge of the lateral wall there is a small notch that contributes to the anterior edge of the trigeminal foramen.

The parietal of *Indotyphlops braminus* is also paired, but uniquely the two parietals are not connected at the midline, instead are separated by what has been termed a 'fissure' by Rieppel et al (2009). The anterior edges of the parietals are mostly straight, projecting slightly anteriorly at the small lateral projections, which are similar in size to seen in the examined *Typhlops*. There are no distinct ridges between the dorsal surface and the lateral walls. There is also very little of the dorsal surface that extends posterior past the extent of the lateral walls.

In *Sundatyphlops polygrammicus*, the anterior edge of the parietal does not fully follow the posterior edges of the frontals, instead at the midline there is a slight notch in the parietal that results in a lack of contact between both frontals and the parietal. The anterior edge also has small lateral projections, that are larger than seen in examined *Typhlops*, but not to the extent seen in examined *Afrotyphlops*. The posterior edge of the lateral wall is more diagonally oriented than the vertical orientation seen in other species, and there is a distinct dorsal shelf at the posterior of the parietal. The posterior edge of the dorsal extent is slightly concave, with the lateral points protruding slightly laterally. There are two small notches either side of the midline of this edge. In contrast to *S. polygrammicus*, the anterior edge of the parietal of *Anilios leucoproctus* follows the posterior edges of the frontal, projecting anteriorly at the midline in a v-shaped projection. The lateral projections of this anterior edge are minimal, mostly just forming a triangular corner in anterior view. The posterior dorsal edge is curved, and there is a slight ridge where the lateral wall meets the dorsal shelf that does not project all the way to the midline. The posterior edge of the lateral wall possesses a small notch ventrally positioned that contributes to the anterior edge of the trigeminal foramen.

The parietal of *Anilios bituberculatus* is unique among the species examined in that it shows partial fusion, with a suture visible at the midline of the anterior end of the parietal and a small notch on the posterior edge. This suture is visible on the interior of the bone until the dorsal shelf. The anterior edge is slightly v-shaped, following the shape of the frontals by the mid-point being slightly anteriorly positioned relative to the lateral edges. The posterior edge is straight. Although a small portion of the posterior edge of the lateral wall of the parietal contributes to the anterior edge of the trigeminal foramen, there is no corresponding notch in the parietal, the edge is straight.

3.5.3 Basisphenoid – Figures 22-24

The basisphenoid is the main element that forms the ventral surface of the skull. It is largely broad and rectangular in its posterior half, meeting the basioccipital and paired otooccipitals at the posterior edge, and the parietals laterally. The anterior portion of the bone is a triangular process that extends between the ventral edges of the paired frontals, and approaches the posterior extent of the vomers. This anterior portion underlies the medial

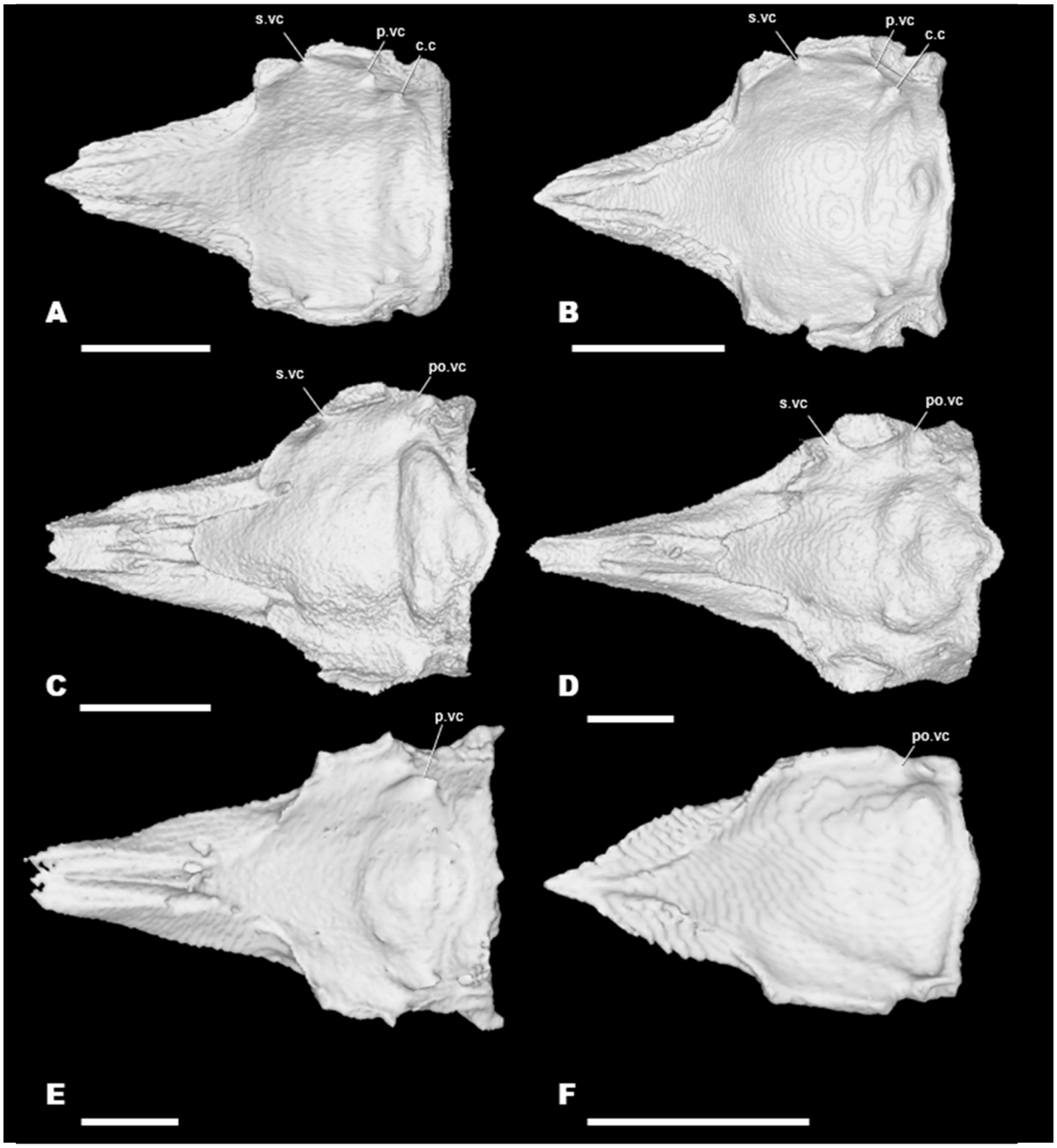

Figure 22. Basisphenoid, Dorsal (A) *Typhlops jamaicensis*, (B) *Typhlops lumbricalis*, (C) *Afrotyphlops mucruso*, (D) *Afrotyphlops schlegelii*, (E) *Afrotyphlops punctatus,* (F) *Madatyphlops arenarius,* (G) *Indotyphlops braminus*, (H) *Sundatyphlops polygrammicus,* (I) *Anilios leucoproctus*, (J) *Anilios bituberculatus*. Abbreviations: c.c – cerebral carotid, p.vc – primary anterior opening of Vidian canal, s.vc – secondary anterior opening of Vidian canal

Scale bar = 1mm

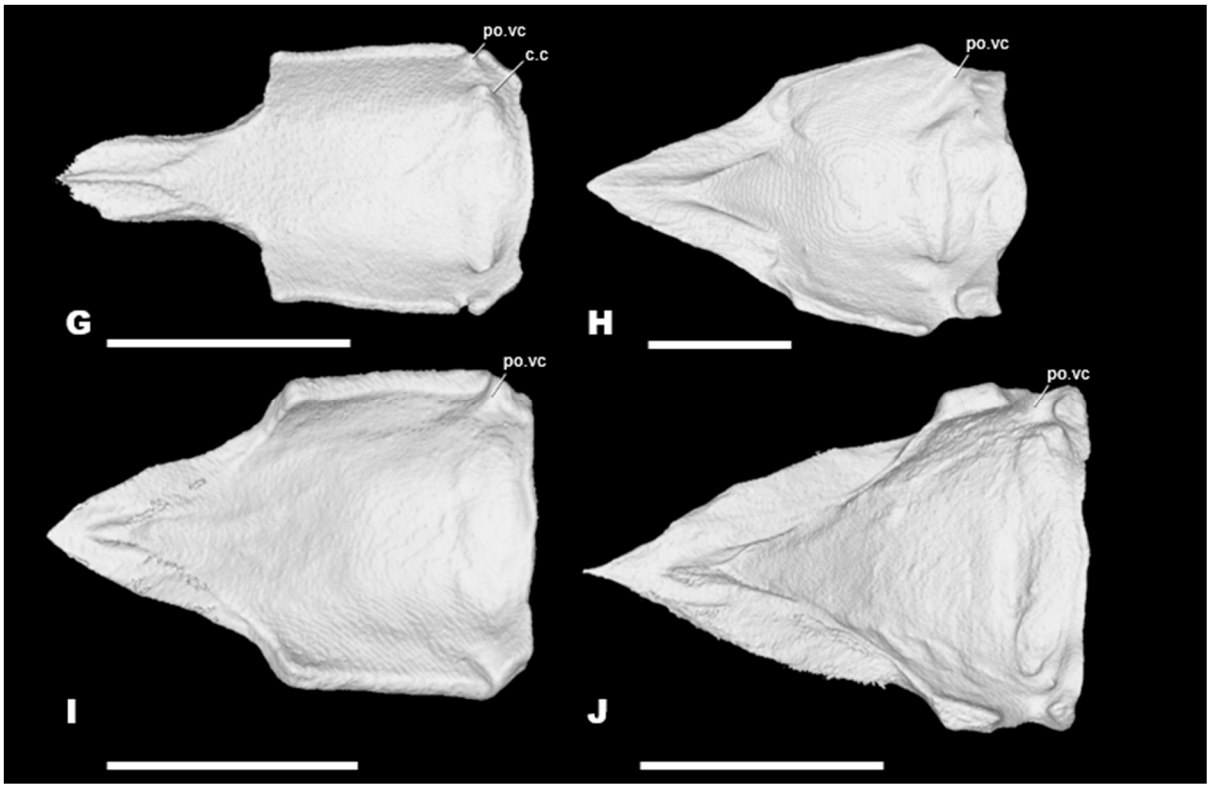

Figure 22 cont. Basisphenoid, Dorsal (A) *Typhlops jamaicensis*, (B) *Typhlops lumbricalis*, (C) *Afrotyphlops mucruso*, (D) *Afrotyphlops schlegelii*, (E) *Afrotyphlops punctatus,* (F) *Madatyphlops arenarius,* (G) *Indotyphlops braminus*, (H) *Sundatyphlops polygrammicus,* (I) *Anilios leucoproctus*, (J) *Anilios bituberculatus*. Abbreviations: c.c – cerebral carotid, po.vc – posterior opening of Vidian canal

Scale bar = 1mm

extensions of the frontals. In previous discussions of the basisphenoid of Scolecophidia, the Vidian canal is observed as being a poorly defined groove on the dorsal surface or lateral margin of the basisphenoid (Cundall & Irish 2008; Rieppel 1979a). This canal transmits the palatine branch of the facial nerve, as well as the cerebral carotid artery. Contrary to previous discussions of characters that unite Scolecophidians citing this feature, the presence and topology of the Vidian canal varied greatly between species examined here (See Figure 22-23).

In the examined *Typhlops*, the Vidian canal is short, as in lizards and the fossorial alethinophidians *Anilius scytale* and *Cylindrophis rufus* (Rieppel 1979b). The posterior opening of the Vidian canal in examined *Typhlops* is a foramen on the posterior lateral edge of the basisphenoid. In *Typhlops jamaicensis* this foramen is positioned ventral to the posterior edge of the trigeminal foramen, with the prootic contributing to the medial edge of the foramen. In *Typhlops lumbricalis*, this entry foramen is positioned posterior to the trigeminal foramen. The prootic contributes to the medial edge, and also meets the basisphenoid both anteriorly and posteriorly to the foramen, forming part of the tube. In both species, the dorsal (internal) surface of the basisphenoid is observable when examining this foramen externally. Continuing

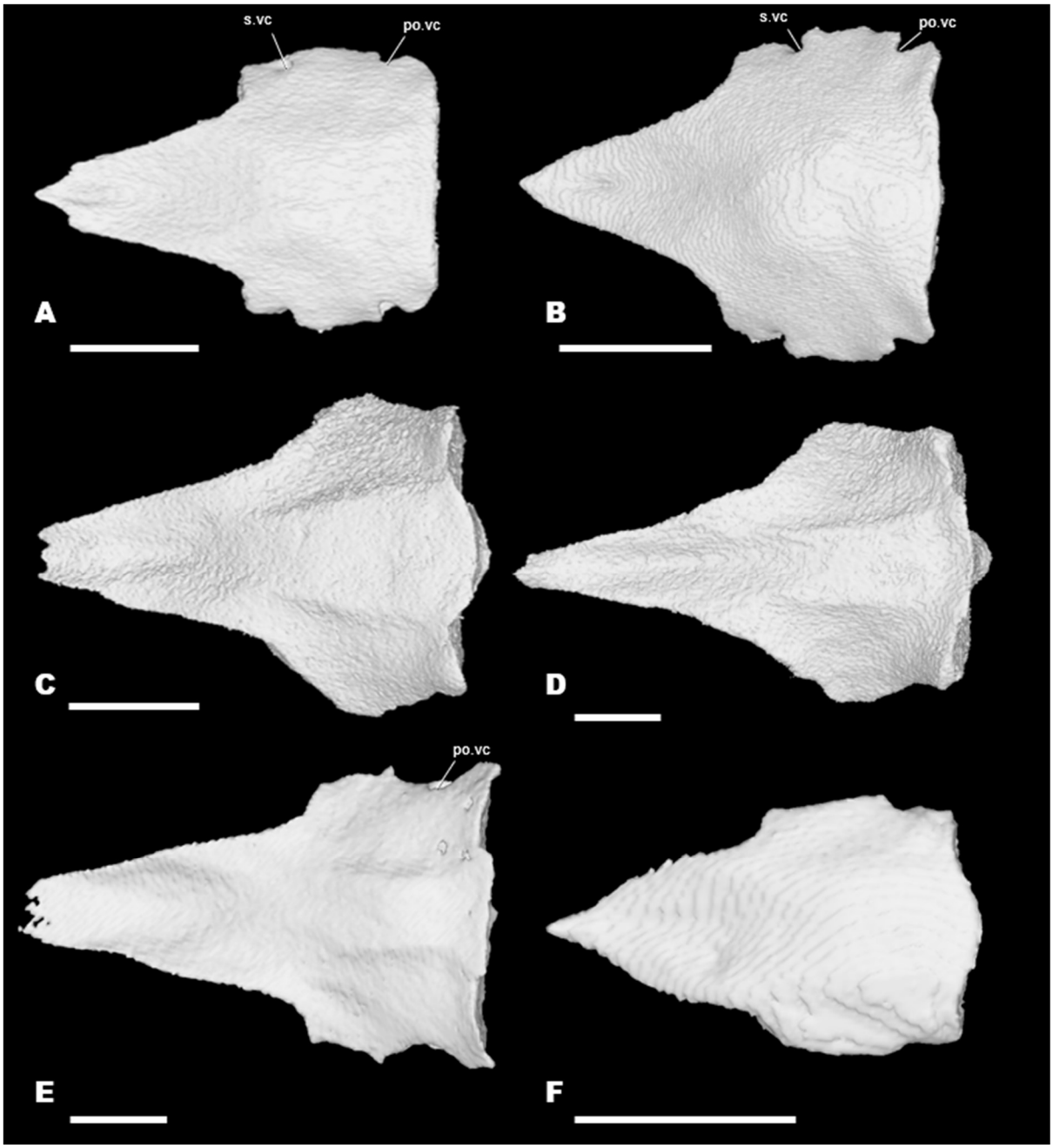

Figure 23. Basisphenoid, Ventral (A) *Typhlops jamaicensis*, (B) *Typhlops lumbricalis*, (C) *Afrotyphlops mucruso*, (D) *Afrotyphlops schlegelii*, (E) *Afrotyphlops punctatus,* (F) *Madatyphlops arenarius,* (G) *Indotyphlops braminus*, (H) *Sundatyphlops polygrammicus,* (I) *Anilios leucoproctus*, (J) *Anilios bituberculatus*. Abbreviations: po.vc – posterior opening of Vidian canal, s.vc – secondary anterior opening of Vidian canal

Scale bar = 1mm

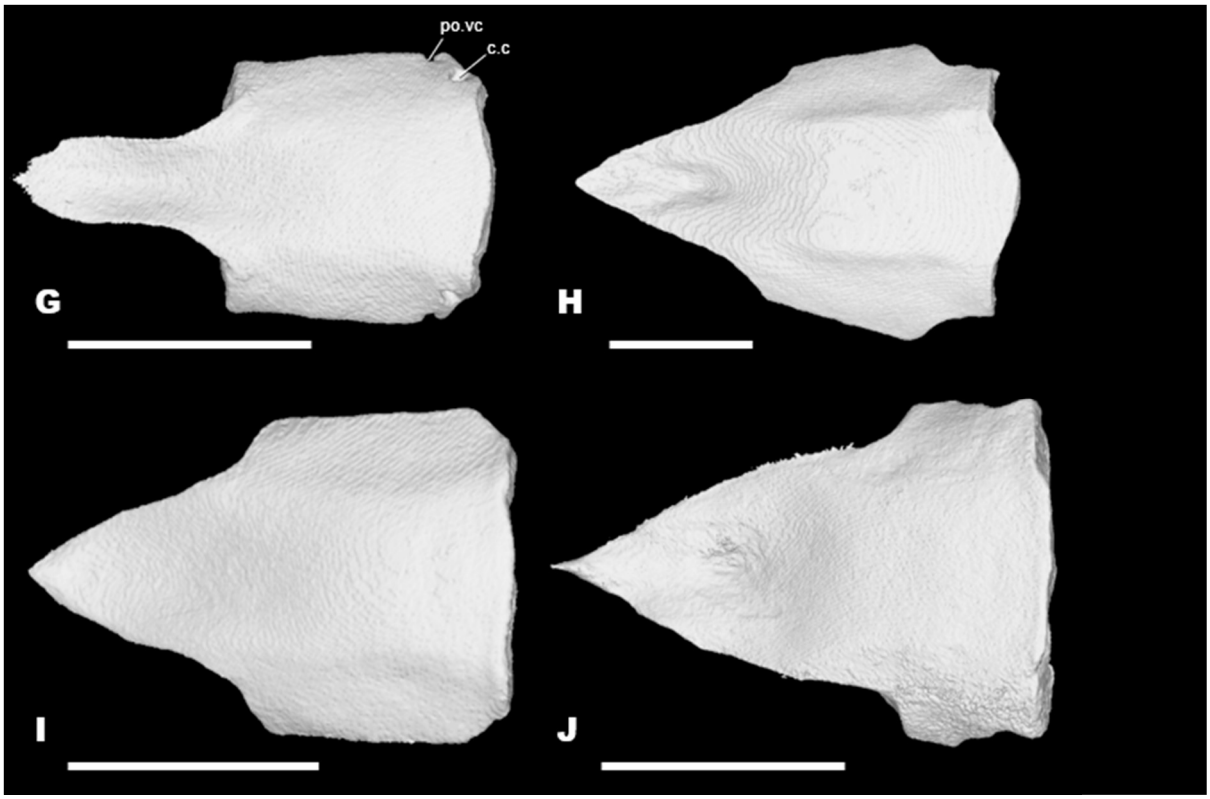

Figure 23 cont. Basisphenoid, Ventral (A) *Typhlops jamaicensis*, (B) *Typhlops lumbricalis*, (C) *Afrotyphlops mucruso*, (D) *Afrotyphlops schlegelii*, (E) *Afrotyphlops punctatus,* (F) *Madatyphlops arenarius,* (G) *Indotyphlops braminus*, (H) *Sundatyphlops polygrammicus,* (I) *Anilios leucoproctus*, (J) *Anilios bituberculatus*. Abbreviations: c.c – cerebral carotid, po.vc – posterior opening of Vidian canal

Scale bar = 1mm

the trajectory of the nerves transmitted by the Vidian canal, the cerebral carotid enters the braincase through a medially positioned foramen, the palatine branch of the facial nerve enters the braincase via the primary anterior opening of the Vidian canal. The palatine branch of the facial nerve then presumably travels anteriorly, following a shallow groove along the lateral edge of the basisphenoid, before exiting the braincase via the secondary anterior opening of the Vidian canal, which is positioned halfway along the contact between the parietal and the basisphenoid, the dorsal edge of which is completed by the ventral edge of the parietal. This condition is seen in both *T. lumbricalis* and the right side of the basisphenoid of *T. jamaicensis.* However in the left side of the basisphenoid of *T. jamaicensis* the exit foramen for the facial nerve is slightly ventrally positioned, completely enclosed by the basisphenoid.

The condition of the Vidian canal in *Afrotyphlops schlegelii* and *Afrotyphlops mucruso*, is as previously understood for Scolecophidia, being a shallow groove on the dorsal surface of the basisphenoid. The posterior opening of the Vidian canal is positioned on the lateral edge of the basisphenoid, now mostly composed of the prootic, positioned ventrally to the trigeminal foramen, with only the ventral edge of the foramen being composed of the internal surface of

the basisphenoid, as such is not visible from external view of the braincase. The secondary anterior opening of the Vidian canal through which the palatine branch of the facial nerve exits the braincase is internally composed ventrally by the basisphenoid and dorsally by the posterior edges of the frontals. Externally the exit of this foramen is composed completely of the frontals, except in the right foramen of *A. schlegelii*, where the basisphenoid contributes to the ventral edge of the foramen throughout its trajectory.

In contrast, in *Afrotyphlops punctatus*, the posterior opening of the Vidian canal is large, positioned ventral to the trigeminal foramen. The cerebral carotid enters the braincase via an anteromedially positioned foramen in the posterior portion of the basisphenoid. The primary anterior opening of the Vidian canal is composed ventrally of the basisphenoid and dorsally of the prootic and a small portion of the parietal. The secondary anterior opening of the Vidian canal in *A. punctatus,* in contrast to the other *Afrotyphlops* examined, is a foramen composed of a notch in the ventral edge of the parietal and the anterior most extent of the lateral edge of the posterior part of the basisphenoid.

In *Madatyphlops arenarius* the prootic and the parietal do not contact each other above the basisphenoid, instead the posterior opening of the Vidian canal is positioned below and partially fused to the trigeminal foramen. As such, the posterior opening of the Vidian canal is composed ventrally of the basisphenoid, posteriorly the prootic, and anteriorly by the parietal, with the dorsal open to the trigeminal foramen. There is no distinct groove of the Vidian canal on the internal surface of the basisphenoid. The secondary anterior opening of the Vidian canal is a very small foramen that is mostly composed of the frontals, closed ventrally by the basisphenoid on the left, and completely enclosed by the frontals on the right.

In *Indotyphlops braminus* the posterior opening of the Vidian canal appears to be separate to the entrance to the cerebral carotid. For the cerebral carotid, the foramen is composed completely by the basisphenoid, ventral to the posterior extent of the trigeminal foramen. There is also a notch on the marginal edge of the basisphenoid just anterior to the anterior extent of the trigeminal foramen which I interpreted as the posterior opening of the Vidian canal. The Vidian canal is completely absent on the internal surface of the basisphenoid. There is no distinct secondary opening for the Vidian canal, but due to the lack of direct contact between the basisphenoid and adjacent bones possible that the facial nerve exits through the large gap between the basisphenoid and the parietal, or the basisphenoid and the frontals.

In the remaining asiatyphlopines examined, the Vidian canal is greatly reduced. In *Sundatyphlops polygrammicus* the posterior opening for the Vidian canal is ventrally composed of a medially projecting notch in the basisphenoid. As in *Madatyphlops arenarius*, the dorsal part of the opening is fused with the ventral extent of the trigeminal foramen. Again there is no visible groove for the Vidian canal on the dorsal surface of the basisphenoid or clear secondary

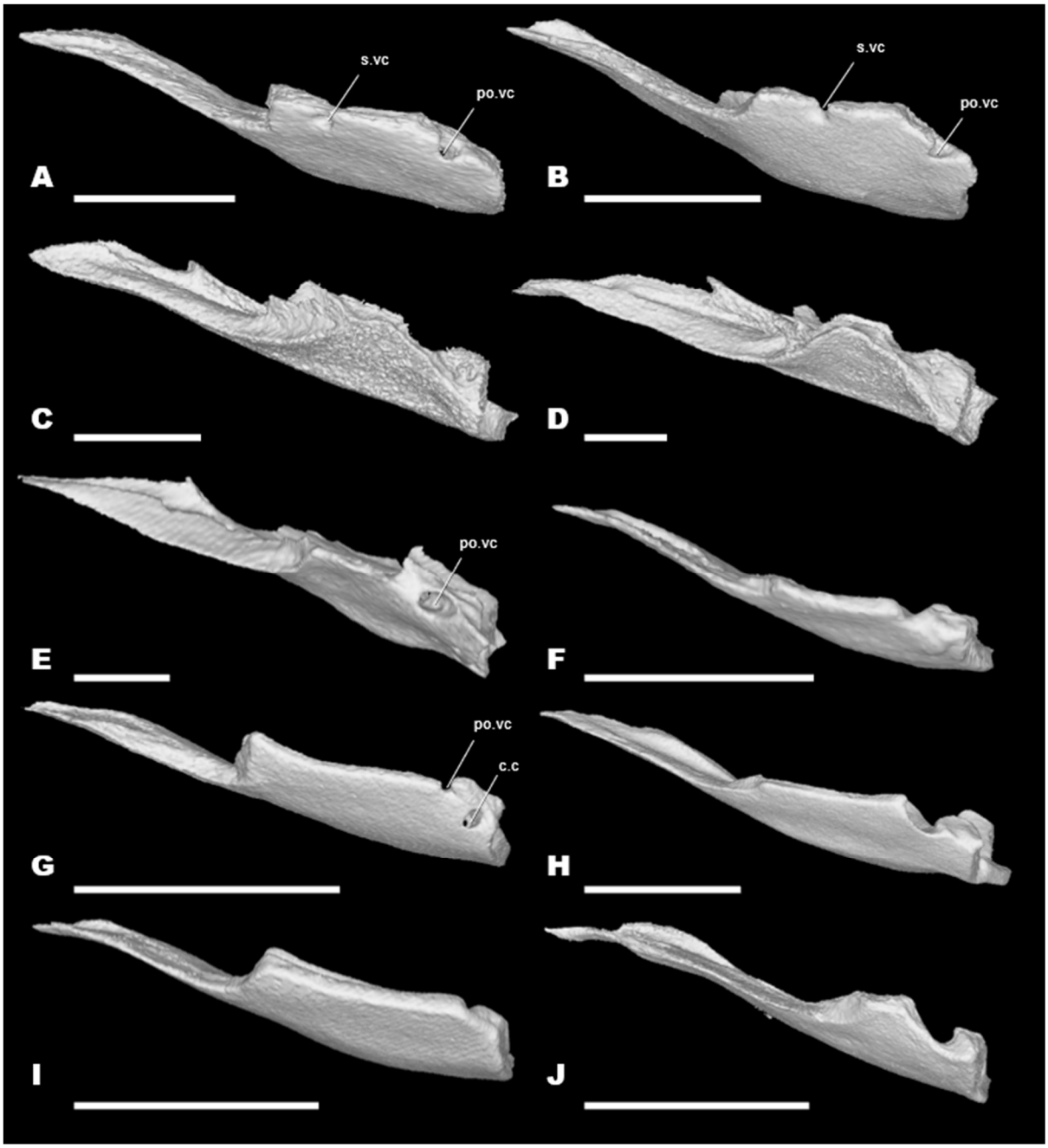

Figure 24. Basisphenoid, Lateral (A) *Typhlops jamaicensis*, (B) *Typhlops lumbricalis*, (C) *Afrotyphlops mucruso*, (D) *Afrotyphlops schlegelii*, (E) *Afrotyphlops punctatus,* (F) *Madatyphlops arenarius,* (G) *Indotyphlops braminus*, (H) *Sundatyphlops polygrammicus,* (I) *Anilios leucoproctus*, (J) *Anilios bituberculatus*. Abbreviations: c.c – cerebral carotid, po.vc – posterior opening of Vidian canal, s.vc – secondary anterior opening of Vidian canal

Scale bar = 1mm

opening. The facial nerve likely exits in the gap between the parietal and the basisphenoid. In *Anilios leucoproctus* the posterior opening for the Vidian canal is a triangular shaped foramen ventral to the trigeminal foramen, formed at the meeting point between the basisphenoid, parietal, and the fused otic complex. There is again no visible groove for the Vidian canal on the dorsal surface of the basisphenoid. In *Anilios bituberculatus* the posterior opening of the Vidian canal is a foramen ventral to the trigeminal foramen composed of the basisphenoid, parietal, and fused otic complex. There is no observable secondary opening, so the facial nerve likely exits via the gap between the parietal and the basisphenoid.

The overall morphology of the basisphenoid also differs in the species examined (See Figure 23). In the examined *Typhlops*, the anterior portion of the basisphenoid is triangular. The tip of this anterior process is slightly dented medially in *Typhlops jamaicensis.* The posterior portion of the bone is sub-rectangular, that begins from the end of the anterior portion and expands laterally to meet the point of contact between the frontals, parietal, and basisphenoid. The lateral edge of the basisphenoid then projects slightly dorsolaterally, following the ventral edge of the frontal, until the point of contact between the prootic, parietal, and basisphenoid, then projects slightly medial until the basisphenoid meets the basioccipital. In both examined *Typhlops* the posterior edge of the basisphenoid is straight. In general shape the anterior portion of the basisphenoid is slightly convex, with the middle of the bone slightly dorsally projected. The posterior portion is flat in its middle, but curves up to meet the lateral walls of the braincase, although no distinct ridges are visible.

In most taxa the basisphenoid is a largely flat bone, however in the examined *Afrotyphlops,* the dorsal surface of the middle of the anterior portion is considerably dorsally projected than the lateral edges (See Figure 24). As such a large part of the dorsal surface of the anterior portion of the basisphenoid is overlaid by the ventral extents of the frontals. Additionally, the lateral edge of the basisphenoid also curves dorsally to a larger extent than seen in the other species examined, with a distinct ridge separating the flat middle surface with the lateral edges. This results in the basisphenoid contributing greater to the formation of the lateral edges of the skull. The posterior edge of the basisphenoid is not straight, with the flat rectangular portion of the basisphenoid projection more posteriorly than the posterior edges of the lateral raised sides. The internal surface is also thicker at this posterior edge. Immediately anterior to this ridge is a roughly triangular shaped depression, which is most pronounced in *Afrotyphlops mucruso*. In *A. schlegelii* and *A. mucruso*, there is less of a distinct separation between the anterior portion of the basisphenoid and the posterior portion. The lateral edges of the anterior portion curve laterally diagonally to the point where the basisphenoid contacts the parietals and the frontals, following the extended ventral posterior projections of the frontals. The tip of the anterior portion is not pointed, instead is wavy (*A. mucruso*) or subtriangular (*A.*

schlegelii). Due to the extended ventral posterior projections of the frontals, very little of the parietal contacts the basisphenoid. Only the anterior most portion of the lateral edges of the basisphenoid contacts the parietal, the rest contacts the prootic. Overall the shape of the basisphenoid of *Afrotyphlops punctatus* is similar to that of the other *Afrotyphlops* examined, but there is a more distinct lateral curve at the transition from anterior triangular portion to posterior rectangular portion.

In *Madatyphlops arenarius*, the anterior portion of the basisphenoid is much wider at the base, and tapers in to a point. The bone is much flatter than seen in the examined *Afrotyphlops* and *Typhlops*, although the anterior portion is still slightly concave. The lateral edges of the posterior portion of the basisphenoid rise very slightly to meet the ventral edge of the parietal, but there is no distinct ridge between the flat middle portion.

The anterior portion of the basisphenoid in *Indotyphlops braminus* is less triangular than in other species. Instead, the lateral walls of this projection are largely straight, only curving towards the midline at the very anterior-most portion. The posterior portion is rectangular with straight lateral edges, only curving medially at the posterior corners where the foramen for the cerebral carotid and facial nerve are located. The posterior edge is very slightly curved, with the midpoint slightly more posteriorly projected. As with many of the bones of *I. braminus* braincase, the basisphenoid does not directly connect to the adjacent bones.

The basisphenoid of *Sundatyphlops polygrammicus,* is more triangular than the other species examined. The anterior portion is broadly triangular, following the ventral edges of the frontals until the meeting point with the lateral walls of the parietal. Unlike the other basisphenoids examined, the lateral edges of the posterior portion of the basisphenoid of *S. polygrammicus* continue to expand laterally along the ventral edge of the parietal, although at more acute angle than the anterior portion. The posterior edge of the basisphenoid begins straight laterally, with the middle part of the edge projecting posteriorly in a shallow rounded process. In *Anilios leucoproctus* the anterior portion is similar to that of *Sundatyphlops polygrammicus*, but the posterior portion is more rectangular, with the lateral edges following the straight ventral edges of the parietal. The posterior edge of the basisphenoid curves slightly posteriorly at the lateral corners, and then is mostly straight. In *Anilios bituberculatus*, the anterior portion of the basisphenoid is larger than the posterior portion, and is largely triangular with a more pointed end than seen in the other examined asiatyphlopines.

3.5.4 Basioccipital – Figures 25-26

The basioccipital is roughly triangular or trapezoidal in shape, with the posterior tip articulating with the hypocentrum of the atlas and forming the ventral portion of the occipital condyle. The posterior tip is dorsally expanded, creating a strong connection to the posterior

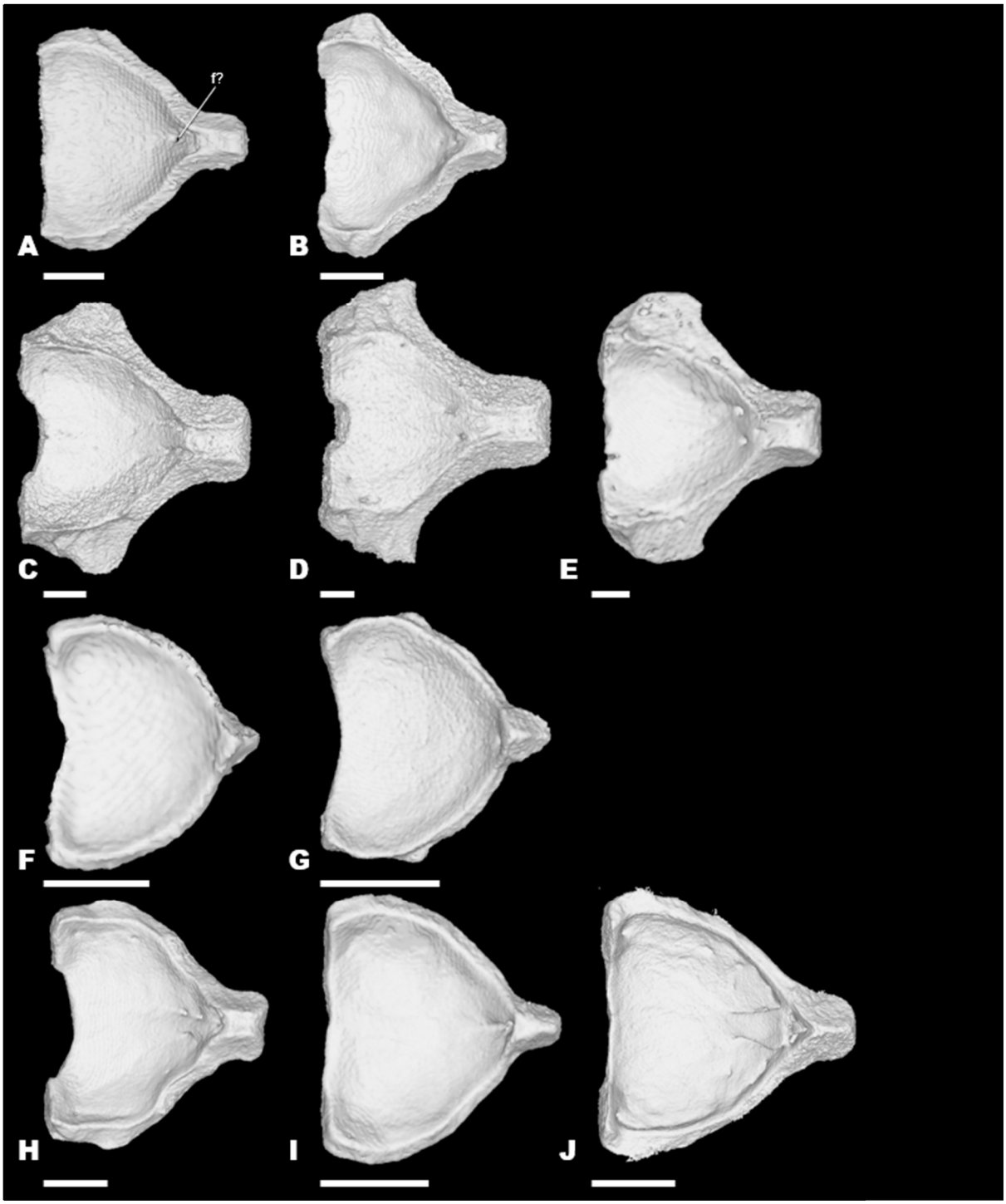

Figure 25. Basioccipital, Dorsal (A) *Typhlops jamaicensis*, (B) *Typhlops lumbricalis*, (C) *Afrotyphlops mucruso*, (D) *Afrotyphlops schlegelii*, (E) *Afrotyphlops punctatus,* (F) *Madatyphlops arenarius,* (G) *Indotyphlops braminus*, (H) *Sundatyphlops polygrammicus,* (I) *Anilios leucoproctus*, (J) *Anilios bituberculatus*. Abbreviations: f? – unknown foramen

Scale bar = 0.5mm

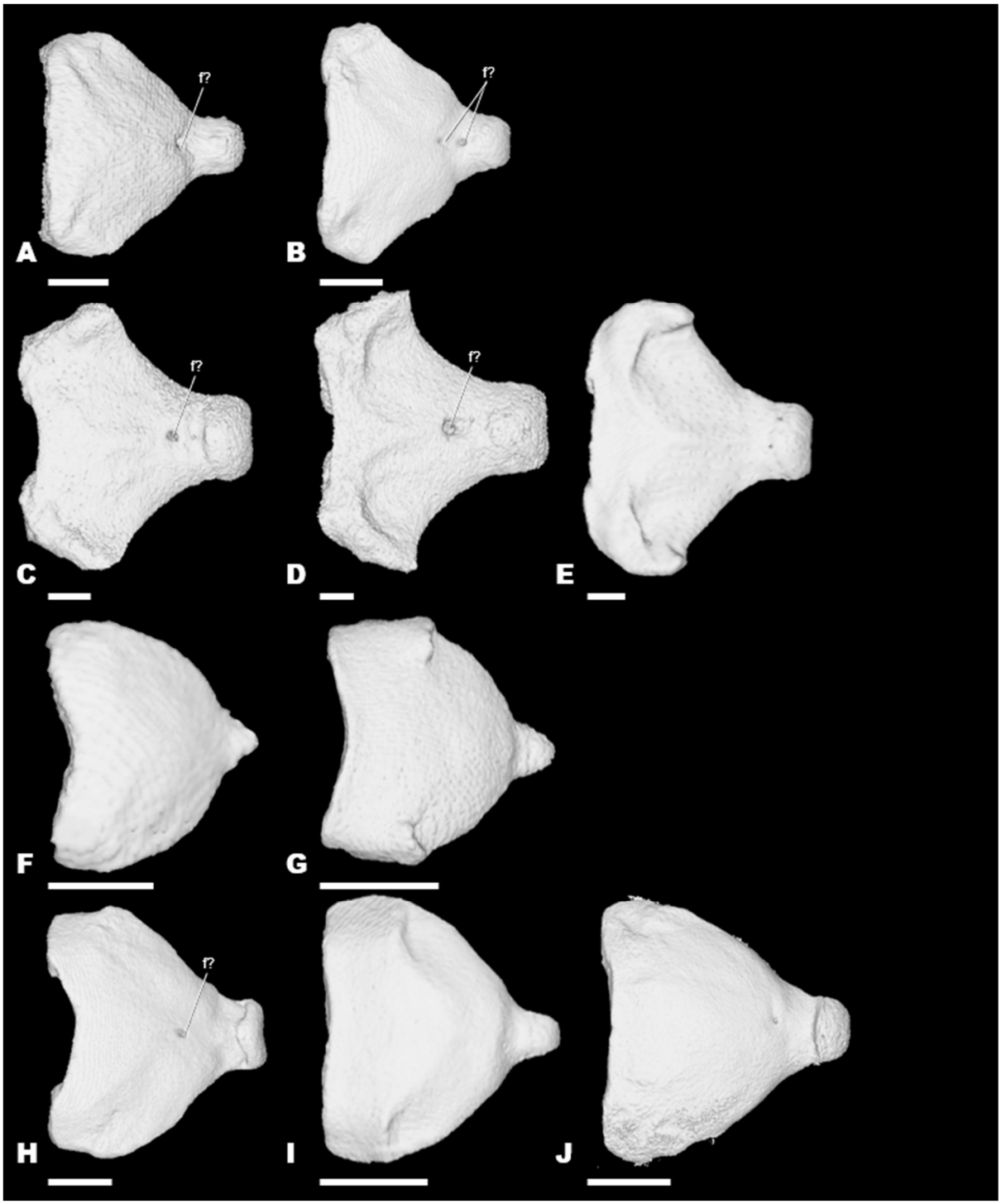

Figure 26. Basioccipital, Ventral (A) *Typhlops jamaicensis*, (B) *Typhlops lumbricalis*, (C) *Afrotyphlops mucruso*, (D) *Afrotyphlops schlegelii*, (E) *Afrotyphlops punctatus,* (F) *Madatyphlops arenarius,* (G) *Indotyphlops braminus*, (H) *Sundatyphlops polygrammicus,* (I) *Anilios leucoproctus*, (J) *Anilios bituberculatus*. Abbreviations: f? – unknown foramen

Scale bar = 0.5mm

ventral tips of the paired otooccipitals or fused otic complex dorsally. The anterior edge of the basioccipital contacts the posterior edge of the basisphenoid, and the lateral edges contact the paired otooccipitals and prootic when present, or fused otic complex.

In the examined *Typhlops*, the basioccipital has a straight anterior edge, with short laterally projecting sides that then project medially to the posterior tip of the basioccipital. The posterior tip is rounded, and is expanded both ventrally and dorsally. There is also a small foramen medial to the point where the posterior projection begins, which appears to pierce through the bone in *Typhlops jamaicensis*, but does not in *Typhlops lumbricalis*. *T. lumbricalis* has an additional foramen anterior to the first foramen.

Contrary to the conditions seen in the examined *Typhlops*, where the basioccipital is not wider than the widest part of the basisphenoid, in examined *Afrotyphlops* the basioccipital is wider, contributing more to the ventral surface of the braincase. The anterior edge follows the irregular edge of the basisphenoid. The lateral edges first expand into a lateral process, and then the posterior half of the lateral edges curves slightly medially to the posterior edge of the occipital condyle, which is largely straight. The lateral processes are more rounded in *Afrotyphlops punctatus* than in the other two species examined. In the examined *Afrotyphlops*, particularly *Afrotyphlops schlegelii* and *Afrotyphlops mucruso*, the lateral edges of the basioccipital are much thicker than the middle of the bone. In *A. schlegelii* and *A. punctatus*, to a lesser extent in *A. mucruso*, the ventral surface of the basioccipital is interrupted by two semicircular ridges that begin at the tips of the lateral processes, and then curve anteriorly before meeting in the middle at a less-defined midline ridge. Only the lateral most part of these ridges is visible in *A. mucruso*. As in the examined *Typhlops* there is a midline foramen in the posterior part of the basioccipital, although it is slightly more anteriorly positioned, especially in *A. schlegelii*. In neither of the specimens examined does the foramen pierce through the bone. No similar foramen is visible in *A. punctatus*.

The basioccipital of *Madatyphlops arenarius* has a rounded anterior edge that is slightly concave at the mid point. The lateral edges, as opposed to the other species examined, curve from the antero-lateral points to just anterior to the posterior tip, which is triangular in ventral view. There are no visible ridges on the ventral surface, or foramen.

In *Indotyphlops braminus*, the basioccipital has a slightly curved anterior edge. The lateral edges are straight in the anterior portion of the element, and then curve medially until the posterior projection that forms the base of the occipital condyle. At the point where the lateral edges transition from straight to curved, there are two ridges on the ventral surface that project medially but not all the way across the element. There are no foramina visible on the ventral surface, but the dorsal surface has a small foramen on the posterior projection that does not fully pierce the bone.

In *Sundatyphlops polygrammicus*, the anterior edge follows the wavy posterior edge of the basisphenoid. The lateral edges are straight, before projecting medially in a roughly straight line. At the posterior extent, the lateral edges project posteriorly to form a rectangular process that forms the bottom of the occipital condyle. The very posterior extent of this process projects ventrally to form a lip. There is also a foramen at the midpoint of the triangular posterior portion of the bone.

In *Anilios leucoproctus*, the basioccipital lateral edges are more rounded, similar to that of *Madatyphlops arenarius*. The posterior projection that forms the underside of the occipital condyle is rounded, but thinner than seen in *Sundatyphlops polygrammicus* or *Anilios bituberculatus*. There are also two small ridges that begin medial to the midpoint of the lateral edge, and then curve posteriorly. These ridges are more distinct at their lateral extents. There are also no foramen visible on the external ventral surface, but there appears to be a foramen internal to the occipital condyle posterior projection.

Unlike the rest of the asiatyphlopines examined, and similar to the examined *Afrotyphlops,* the basioccipital of *Anilios bituberculatus* is wider than the basisphenoid, although the overall shape is more similar to that of *Anilios leucoproctus* and *Sundatyphlops polygrammicus*. The basioccipital contributes to a larger portion of the ventral surface of the skull. The lateral edges of the basioccipital are gently curved in a subtriangular shape. Similar to *S. polygrammicus*, the posterior projection that forms the ventral part of the occipital condyle expands ventrally to form a lip. There are no visible foramen on the ventral external surface, however several foramen are visible on the dorsal internal surface. The midpoint of the posterior projection is raised on the internal surface, nerves are potentially funnelled beneath this raised portion of the bone, although the resolution of the scans means that this is not fully confirmable.

3.5.5 Otic Complex

In most species, the back of the braincase is formed by three sets of paired elements: the otooccipitals, the prootics, and the supraoccipitals. The otooccipitals form the postero-dorsal and lateral portion of the posterior braincase, the supraoccipitals contribute to the dorsal surface, and prootics the lateral surface. Internally, the lateral walls of the otooccipitals, along with the prootics and the supraoccipitals, house the otic complex. Anteriorly these bones contact the posterior edges of the dorsal and lateral sides of the parietal, and the ventral edges are in contact with the broad ventral edges of the basioccipital. The antero-ventral edge of the prootic also contacts the dorsal edge of the basisphenoid.

The location and position of the foramen of the otic capsule are similar in most species, and as follows. The endolymphatic foramen is present on the inner surface of the supraoccipital.

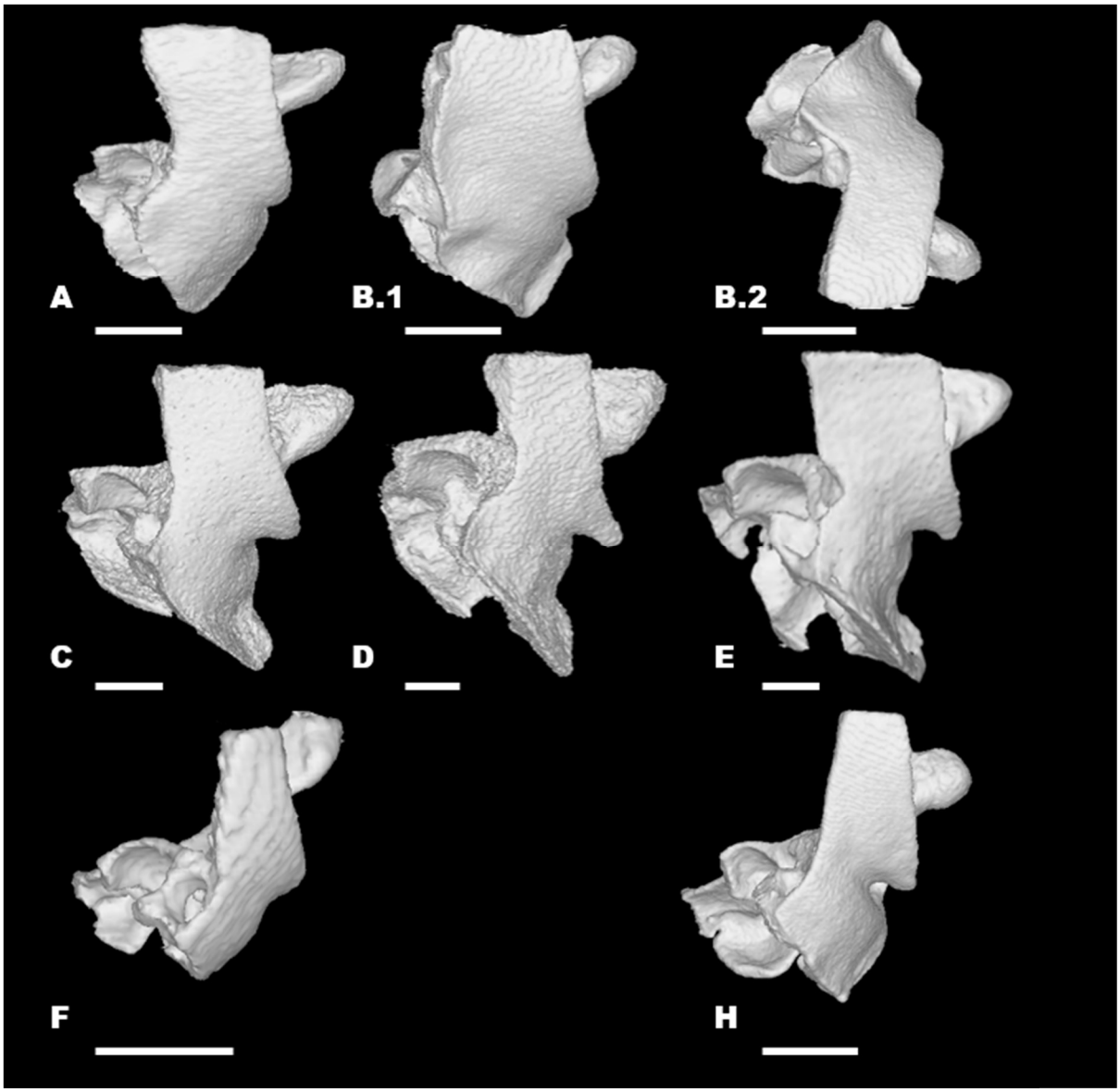

Figure 27. Left otooccipital, dorsal (A) *Typhlops jamaicensis*, (B.1) *Typhlops lumbricalis*, left, (B.2) *Typhlops lumbricalis,* right (C) *Afrotyphlops mucruso*, (D) *Afrotyphlops schlegelii*, (E) *Afrotyphlops punctatus,* (F) *Madatyphlops arenarius,* (H) *Sundatyphlops polygrammicus*

Scale bar = 0.5mm

The acoustic foramen which transmit the auditory nerves are located in the posterior most corner of the prootic, ventral to the endolymphatic foramen. The comissura praefacialis, the interior opening of the trigeminal foramen, is present as the most anterior foramen on the prootic. In the otooccipital, the anterior-most foramina, close to the suture with the basioccipital, are the recessus scalae tympanae, and the perilymphatic foramen. Immediately posterior to these are the jugular foramen and the opening for the vagus nerve, at the bottom of the dorsal metotic fissure.

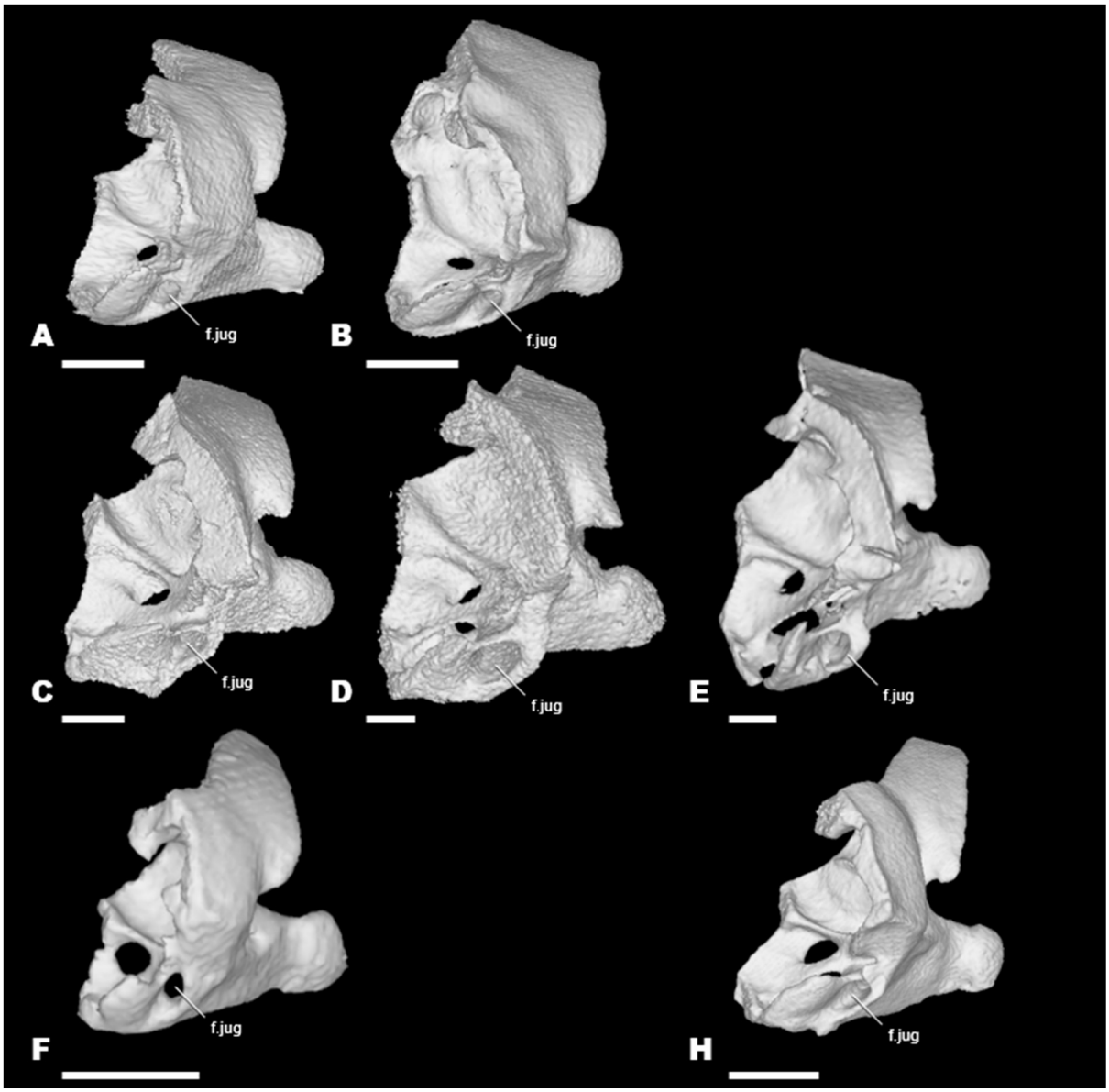

Figure 28. Left otooccipital, lateral (A) *Typhlops jamaicensis*, (B) *Typhlops lumbricalis* (C) *Afrotyphlops mucruso*, (D) *Afrotyphlops schlegelii*, (E) *Afrotyphlops punctatus,* (F) *Madatyphlops arenarius,* (H) *Sundatyphlops polygrammicus*. Abbreviations: f.jug – jugular foramen

Scale bar = 0.5mm

The trigeminal foramen also differs considerably between species. In examined *Typhlops*, the trigeminal foramen is usually located at the intersection between the parietal, the prootic, and the basisphenoid. However in examined *Afrotyphlops,* the anterior edge of the trigeminal foramen is almost completely enclosed by the anterior edge of the prootic, seen to the greatest extent in *Afrotyphlops schlegelii* where the prootic completely surrounds the foramen, meeting at a distinct suture. In *Afrotyphlops punctatus*, the parietal still slightly contributes to the anterior edge. In the examined asiatyphlopines, *Anilios bituberculatus* and *Anilios leucoproctus*, the basisphenoid is excluded from the trigeminal foramen by an extension

of the prootic, but the parietal still contributes to the anterior edge. The condition seen in these taxa approaches that seen in the xenotyphlopid *Xenotyphlops grandidieri,* where the trigeminal foramen is completely enclosed by the fused otooccipital and prootic (Chretien *et al.* 2019).

3.5.6 Otooccipitals - Figures 27-29

The otooccipitals are paired, and are large, complex bones that form the back of the skull and house much of the inner ear cavity. The otooccipitals are in contact with the supraoccipitals, parietal (variably), and the prootic. Together with the basioccipital, the posterior projections of this bone are rounded and expanded to form the occipital condyle. The lateral wall of the otooccipital, ventral to the contact with the prootic, contains two large foramen. The ventral is the jugular foramen, and the dorsal is the vestibular window, through which projects the small shaft of the stapes. The dorsal extensions of the otooccipitals form the roof of the posterior braincase, meeting at a straight suture at the midline. Internally, the inner wall of the otooccipital is pierced by several foramina, including the dorsal metotic foramen, the perilymphatic foramen, the jugular foramen, and the recessus scalae tympanae, the positions of which varies slightly between species. Generally, the dorsal metotic foramen is positioned at the dorsal extent of the dorsal metotic fissure, with a large opening at the ventral extent of the fissure that is composed posteriorly of the large internal opening of the jugular foramen, and anteriorly the perilymphatic foramen and the recessus scalae tympanae. These three foramen are separated by small struts of bone, with the divisions between them internal to the large opening. The internal foramen for the hypoglossal nerve, when observable, is found posterior to this opening. Due to the differing resolution of scans obtained from the digital repository Morphosource and the relatively small aperture of this foramen, it is possible that despite the apparent absence of the hypoglossal foramen, it is present in the specimen just not observable at the current resolution. The external entrance foramen for the hypoglossal nerve is found lateral to the occipital condyle and projections ventro-anteriorly into the otooccipital. This relatively large channel runs along the lateral side of the braincase, opening in the internal wall of the jugular foramen. A medial projection halfway along this channel transmits the hypoglossal nerve into the braincase.

In examined *Typhlops*, the dorsal surface of the otooccipitals contact the parietal medial to the dorsal contact with the prootic. This is more evident in *Typhlops jamaicensis*, where the supraoccipitals are not externally in contact with the prootic at all. The otooccipital also approach the parietal lateral to the midline, separating the two paired supraoccipitals. In *Typhlops lumbricalis*, due to the absence of the left supraoccipital (see supraoccipitals section), the anterior dorsal edge of the left otooccipital forms a contact with the left posterior edge of the dorsal surface of the parietal. The lateral anterior edge of the otooccipitals forms a contact

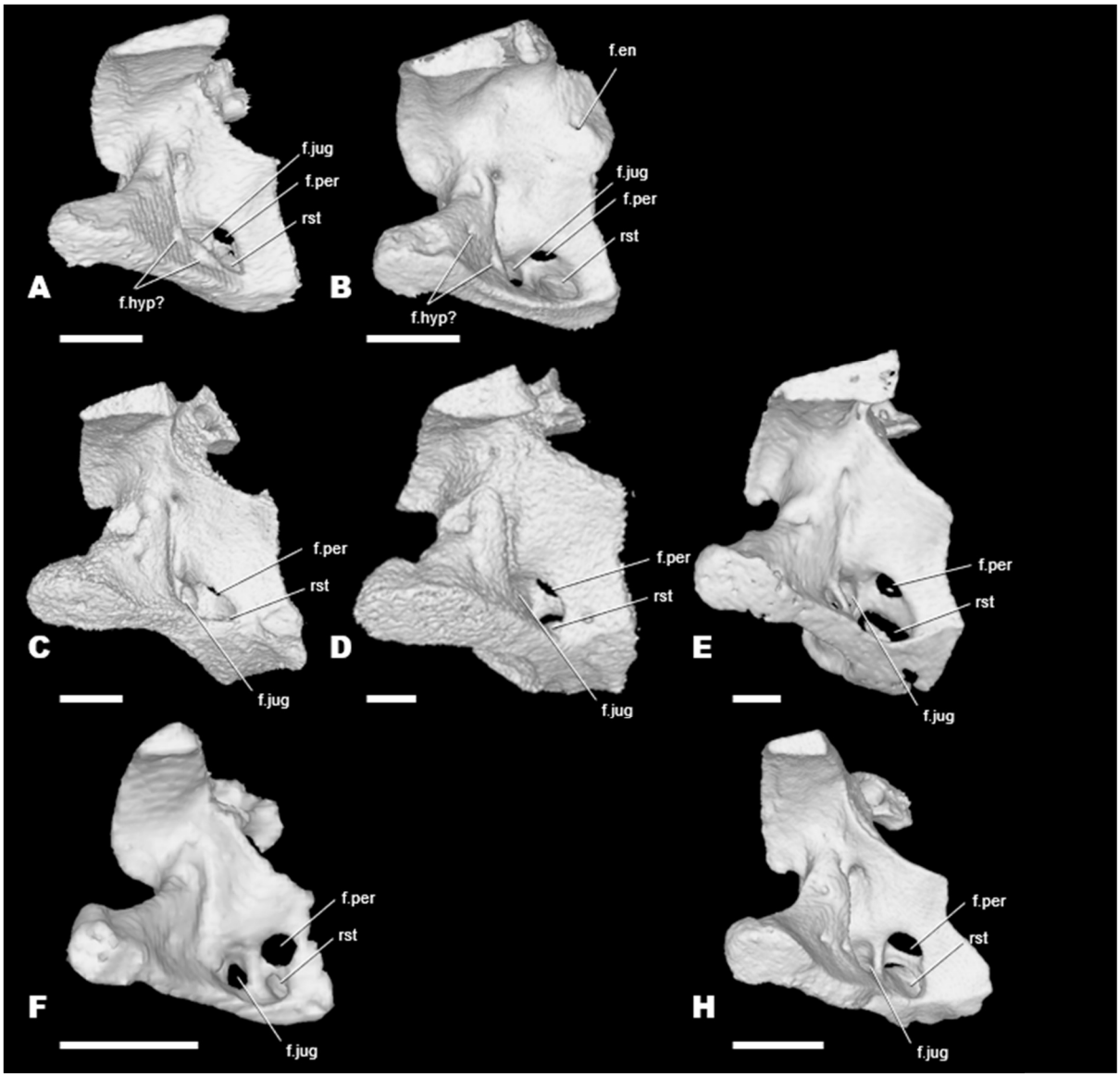

Figure 29. Left otooccipital, medial (A) *Typhlops jamaicensis*, (B) *Typhlops lumbricalis*, (C) *Afrotyphlops mucruso*, (D) *Afrotyphlops schlegelii*, (E) *Afrotyphlops punctatus,* (F) *Madatyphlops arenarius,* ((H) *Sundatyphlops polygrammicus*. Abbreviations: f.en – endolymphatic foramen, f.hyp – foramen for hypoglossal nerve, f.jug – jugular foramen, f.per – perilymphatic foramen, rst – recessus scalae tympani

Scale bar = 0.5mm

with the posterior edge of the prootic. Halfway down the otooccipitals there is a horizontal ridge. Ventral to this ridge is the large jugular foramen, and the large vestibular window, which is mostly composed of the anterior edge of the otooccipital. The anterior edge of the vestibular window is completed by the posterior edge of the prootic. The stapes is visible through this window in lateral view. Internally, the dorsal metotic fissure separates the posterior projecting aspect of the otooccipital that forms the occipital condyle, with the internal surface that surrounds the otic capsule. At the ventral extent of the dorsal metotic fissure is the internal

projection of the jugular foramen. This foramen is more anteriorly directed in comparison to *Madatyphlops arenarius* and the examined asiatyphlopines. A dorsally projecting foramen, which is laterally subdivided by a slim projection of horizontal bone separates the perilymphatic foramen (dorsally) and the recessus scalae tympanae (ventrally). There are a couple of foramina posterior to these large foramen, two in *T. jamaicensis* and three in the left otooccipital of *T. lumbricalis*, and either two or one foramen in the right otooccipital. One of these foramen likely transmits cranial nerve XII, the hypoglossal nerve. As the left supraoccipital is absent in this *T. lumbricalis* specimen, the internal component of the otic capsule wall that is usually composed of the internal surface of the supraoccipital is composed of the otooccipital. The endolymphatic foramen is in the same position, but smaller than the endolymphatic foramen present on the right supraoccipital.

In the examined *Afrotyphlops*, the otooccipitals are contacted anteriorly by the prootics and supraoccipitals, with minimal contact with the lateral extent of the dorsal shelf of the parietal. The dorsal laminae of the otooccipitals that form the dorsal edge of the foramen magnum are more pointed than in other species, projecting laterally in a triangular shaped process. Additionally, the increased relative contribution of the prootic to the lateral side of the braincase results in a reduced contribution of the otooccipitals. The lateral edges of the otooccipitals curve posteriorly along the posterior edge of the prootic, forming a distinct ridge with these bones. Internally, the dorsal metotic foramen in *Afrotyphlops schlegelii* and *Afrotyphlops mucruso*, is positioned slightly anterior to the dorsal metotic fissure. No internal foramen for the hypoglossal nerve is visible in either of these species, however in *Afrotyphlops punctatus*, there are two foramen visible posterior to the jugular foramen, one of which likely transmits the hypoglossal nerve.

In *Madatyphlops arenarius*, the dorsal lamina of the otooccipitals contact the supraoccipitals, with no contact with the parietal. In comparison to the other species examined, the two projections of the otooccipitals that form the occipital condyle contact each other medially, excluding the basioccipital from the dorsal portion of the occipital condyle. The scan of *M. arenarius* was of a lower resolution than the others examined. As such, the absence of an internal opening for the dorsal metotic foramen or the hypoglossal nerve foramen is either a true absence or a result of low resolution scans.

Sundatyphlops polygrammicus is the only asiatyphlopine examined in which the otic capsule is not a single fused element. The otooccipitals are similar in contribution to the braincase as in examined *Typhlops*, but the dorsal lamina that project posteriorly over the foramen magnum are more defined, with a distinct groove separating the lateral walls of the otic capsule and the dorsal lamina. The ventroposterior corners of this dorsal lamina are square, rather than rounded as seen in examined *Typhlops* and *Madatyphlops arenarius*, or pointed as

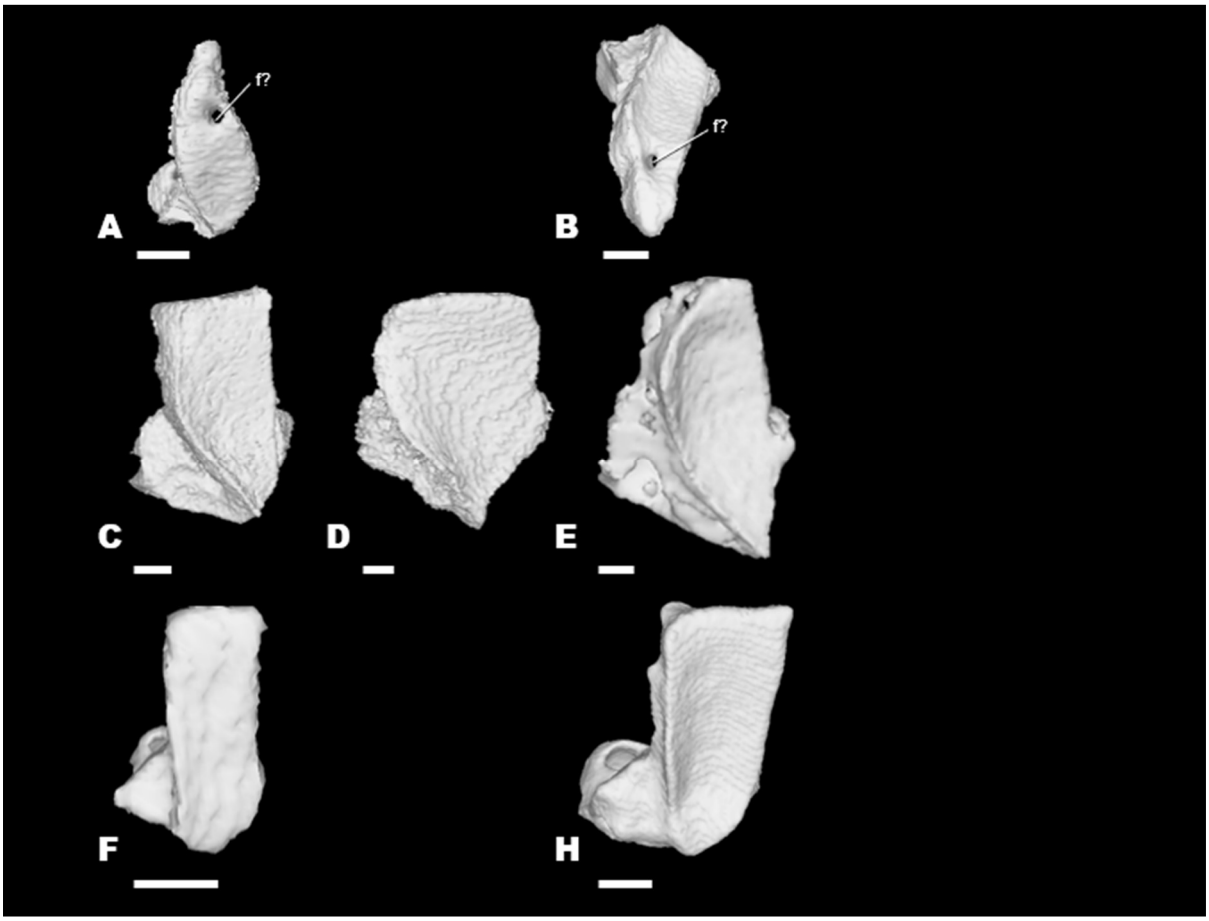

Figure 30. Left supraoccipital, dorsal (A) *Typhlops jamaicensis*, (B.2) *Typhlops lumbricalis,* right (C) *Afrotyphlops mucruso*, (D) *Afrotyphlops schlegelii*, (E) *Afrotyphlops punctatus,* (F) *Madatyphlops arenarius,* (H) *Sundatyphlops polygrammicus*. Abbreviations: f? – unknown foramen

Scale bar = 0.5mm

seen as in examined *Afrotyphlops*. The ventral projections form the lateral walls of the occipital condyle and do not touch in the midline. Internally, the dorsal metotic foramen is well defined at the dorsal extent of the dorsal metotic fissure. There are also two foramina posterior to the dorsal metotic fissure. An indentation posterior to the dorsal extent of the dorsal metotic fissure does not appear to pierce the bone through. Of the two foramina, one is positioned mid way between the dorsal metotic fissure and the occipital condyle, and the other is immediately posterior to the ventral extent of the dorsal metotic fissure. Both of these foramina pierce through to the channel that runs from the entrance of the hypoglossal nerve foramen to the jugular foramen opening, and so either could transmit the hypoglossal nerve.

3.5.7 Supraoccipitals - Figures 30-32

The supraoccipitals are small paired elements that contribute to a small part of the posterior braincase, housing part of the semicircular canals and otic nerves. The dorsal extents

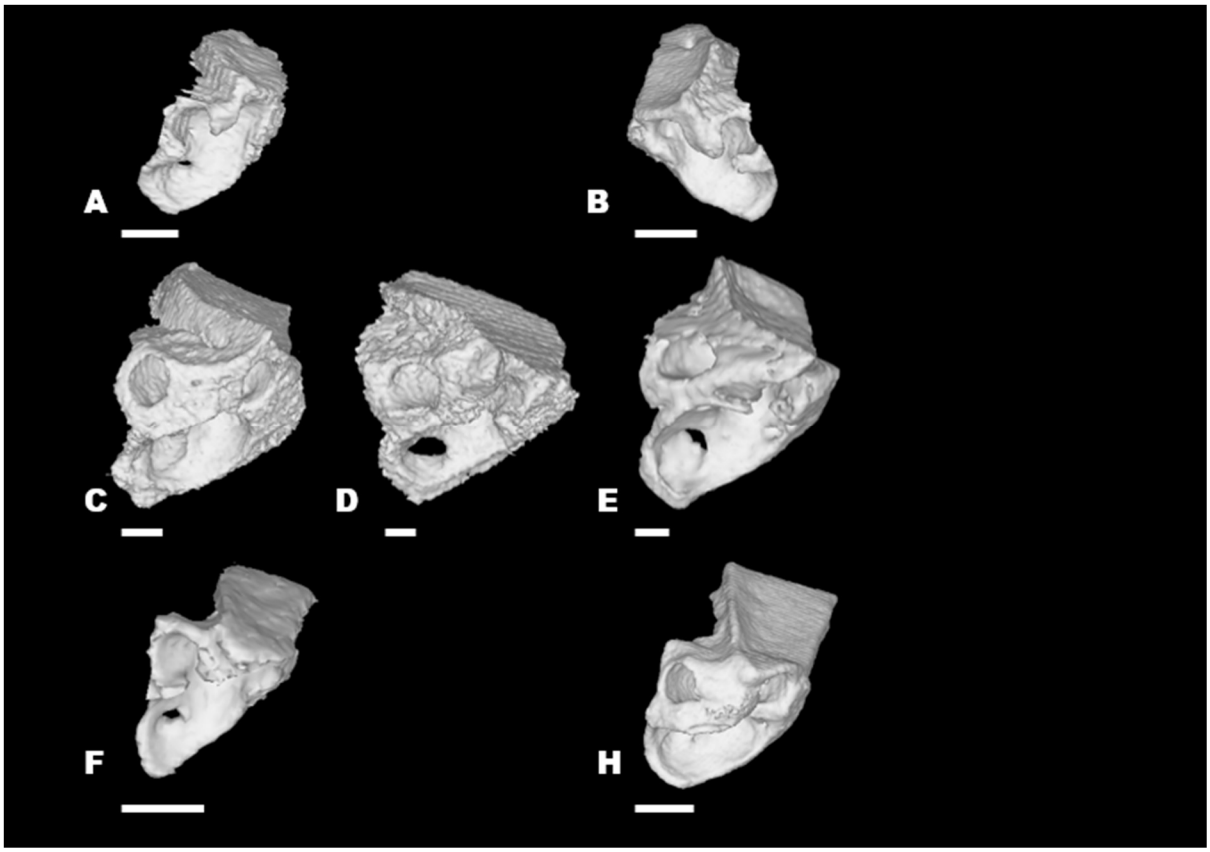

Figure 31. Left supraoccipital, lateral (A) *Typhlops jamaicensis*, (B.2) *Typhlops lumbricalis,* right (C) *Afrotyphlops mucruso*, (D) *Afrotyphlops schlegelii*, (E) *Afrotyphlops punctatus,* (F) *Madatyphlops arenarius,* (H) *Sundatyphlops polygrammicus*

Scale bar = 0.25mm

of the supraoccipitals form a small part of the dorsal surface of the braincase, in anterior contact with the posterior edge of the parietal, and in posterior contact with the anterior edge of the dorsal shelf of the otooccipitals. Additionally the internal part which houses the semicircular canals projects more anteriorly than the dorsal extents, overlapped by the posterior dorsal extents of the parietal.

In the examined *Typhlops*, the supraoccipitals are greatly reduced in external view. In *Typhlops jamaicensis*, the supraoccipitals in dorsal view appear ovaloid. They do not contact at the midline externally, and only approach one another internally. There is also a small foramen on the dorsal surface of the supraoccipital, positioned lateral to the medial tip of the left supraoccipital. The foramen on the right supraoccipital is more posteriorly positioned, as such the otooccipital forms the posterior edge of this foramen. In *Typhlops lumbricalis*, only one supraoccipital is present. However, rather than being an unpaired element, this appears to be the right supraoccipital, with the left supraoccipital absent in this specimen. As only one individual *T. lumbricalis* was available to study, it is unclear but possible that this is a

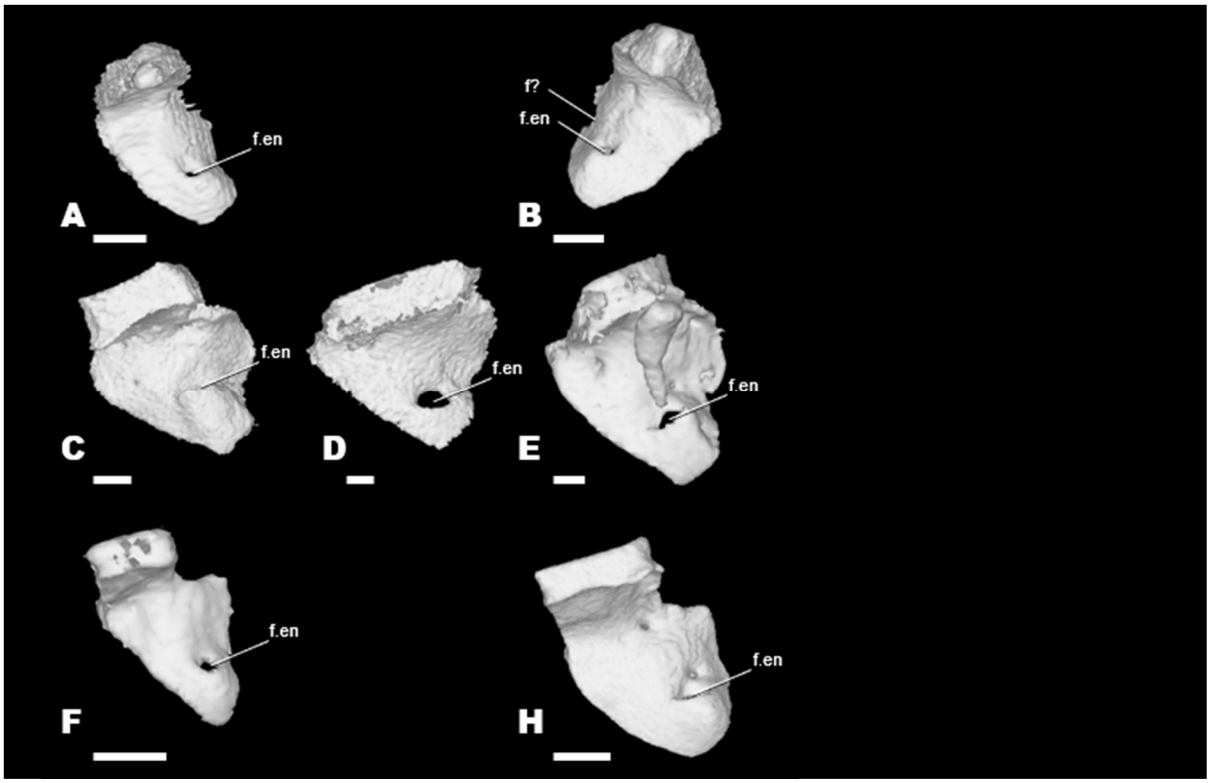

Figure 32. Left supraoccipital, medial (A) *Typhlops jamaicensis*, (B) *Typhlops lumbricalis,* right (C) *Afrotyphlops mucruso*, (D) *Afrotyphlops schlegelii*, (E) *Afrotyphlops punctatus,* (F) *Madatyphlops arenarius,* (H) *Sundatyphlops polygrammicus*. Abbreviations: f.en – endolymphatic foramen, f? – unknown foramen

Scale bar = 0.5mm

developmental anomaly for the specific individual studied. The dorsal extent of the supraoccipital of *T. lumbricalis* is also larger than in *T. jamaicensis*, extending from the contact point between the parietal, prootic, and otooccipital, to just passed the meeting point between the two otooccipitals. This supraoccipital also has a small foramen, slightly more anteriorly positioned than the ones in *T. jamaicensis*. Internally, the posterior edge of the supraoccipital contacts the internal surface of the otooccipital, and the anterior edge contacts the prootic. The internal surface of the supraoccipital only extends halfway down the braincase. Dorsal to the contact point between the internal surfaces of the supraoccipital, prootic, and otooccipital is the endolymphatic foramen. This foramen projects dorsally. In the single supraoccipital of *T. lumbricalis*, there appears to be an additional foramen in the supraoccipital in the dorsal part of the contact between the internal surfaces of the supraoccipital and prootic. This foramen is of unknown function, and is not present in *T. jamaicensis*.

Compared to the other species examined, the supraoccipitals of the examined *Afrotyphlops* contribute to much more of the dorsal surface of the braincase, the largest supraoccipitals being present in *Afrotyphlops schlegelii*. Externally, the supraoccipitals meet the parietal anteriorly and the otooccipitals posteriorly. In *A. schlegelii*, the very lateral points of the

supraoccipitals meet the dorsal tips of the prootics, excluding the parietal from contact with the otooccipitals. In contrast, in both *Afrotyphlops mucruso* and *Afrotyphlops punctatus*, the supraoccipitals are excluded from dorsal contact with the prootic by a small contact between the dorsal surfaces of the parietals and otooccipitals. Additionally, the posterior edge of the dorsal surface is not smooth in both *A. schlegelii* and *A. punctatus*, instead the edge is wavy. In *A. punctatus* the medial portion of this edge possibly possesses a small foramen, although this may be an artefact of scan quality.

The supraoccipitals of *Madatyphlops arenarius* are rectangular in dorsal view, contacting the parietal anteriorly and the otooccipitals posteriorly, with a small lateral contact with the prootic. The supraoccipitals of *Sundatyphlops polygrammicus* are most similar to that of *M. arenarius*, only the medial contact between the two supraoccipitals is wider than the lateral extents of these bones. Internally there are two foramen in addition to the typical endolymphatic foramen. One is just ventral to the dorsal lamina of the supraoccipital. The second is immediately dorsal to the endolymphatic foramen, on the lateral wall into the braincase. The function of these two foramen is unknown.

3.5.8 Prootic – Figures 33-35

The prootic are large curved elements that form the side of the back of the braincase. They form the anterior of the hollow otic complex that houses the semicircular canals and the anterior ampulla. Externally, the posterior edge of the prootic contacts the otooccipitals, and the anterior edge contacts the parietal. The ventral edge contacts the basioccipital posteriorly, and the basioccipital anteriorly. Internally, the prootic also contacts the anterior edge of the internal component of the supraoccipital. Internally, the prootics also contain the two foramen that transmit the anterior and posterior auditory nerves, which are positioned ventral to the internal contact with the supraoccipitals.

In the examined *Typhlops*, the prootics are a relatively large component of the lateral walls of the posterior braincase. The ventral extent of the anterior edge of the prootic forms the posterior edge of the trigeminal foramen. In *Typhlops jamaicensis*, the external surface of the prootic projects dorso-laterally but does not recontact the prootic. In *Typhlops lumbricalis* this external projection connects back to the ventral anterior tip of the prootic. Ventral to this projection is a small channel that likely funnels the cerebral carotid into the braincase. Immediately interior to the opening for the trigeminal foramen is a rounded depression which forms the comissura praefacialis. On the internal surface of the prootic, ventral to the contact with the supraoccipital, are two foramen that channel the anterior and posterior auditory nerves (nerve VIII). In *T. lumbricalis* there is an additional foramen ventral to this.

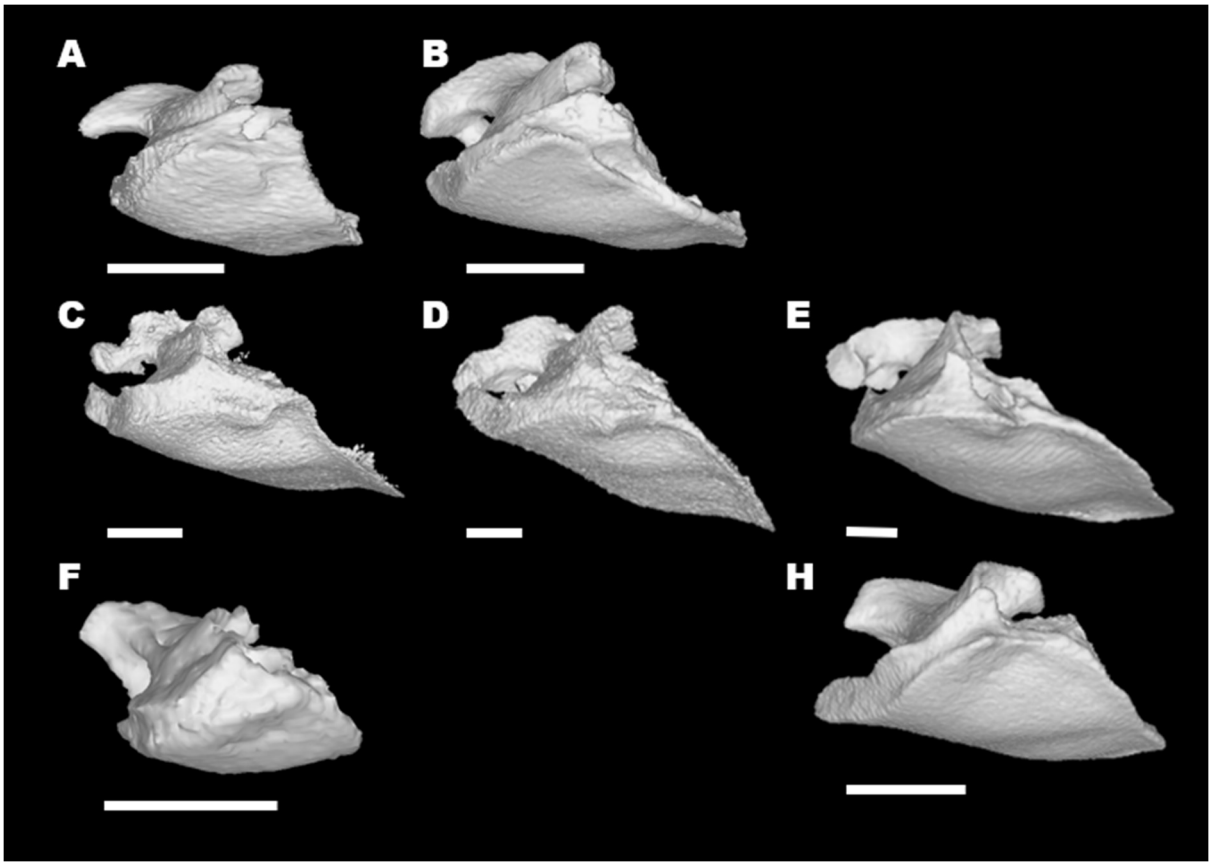

Figure 33. Left prootic, dorsal (A) *Typhlops jamaicensis*, (B) *Typhlops lumbricalis* (C) *Afrotyphlops mucruso*, (D) *Afrotyphlops schlegelii*, (E) *Afrotyphlops punctatus,* (F) *Madatyphlops arenarius,* (H) *Sundatyphlops polygrammicus*

Scale bar = 0.5mm

The prootics of the examined *Afrotyphlops* contribute to relatively more of the posterior braincase than in the other species examined. The posterior edge of the prootic meets the lateral edge of the otooccipitals in a posteriorly projecting ridge. The anterior edge of the prootics contacts the parietal, with the prootic contributing to much more of the edge of the trigeminal foramen. In *Afrotyphlops mucruso* and *Afrotyphlops punctatus*, the anterior edge of the prootic projects ventrally, and the ventral portion of the prootic projects anteriorly to form the dorsal, ventral, and posterior edges of the trigeminal foramen, with only a small part of the anterior edge being composed of the posterior edge of the parietal. The condition in *Afrotyphlops schlegelii* is the extreme of this, with the ventrally projecting anterior edge and the anteriorly projecting ventral portion of the prootic meeting at a distinct suture, excluding the parietal from the trigeminal foramen completely. The prootic of examined *Afrotyphlops* is also more involved with the transmission of the cerebral carotid into the braincase. In *A. punctatus*, the ventral projection of the prootic forms the dorsal edge of the channel for the entrance of the

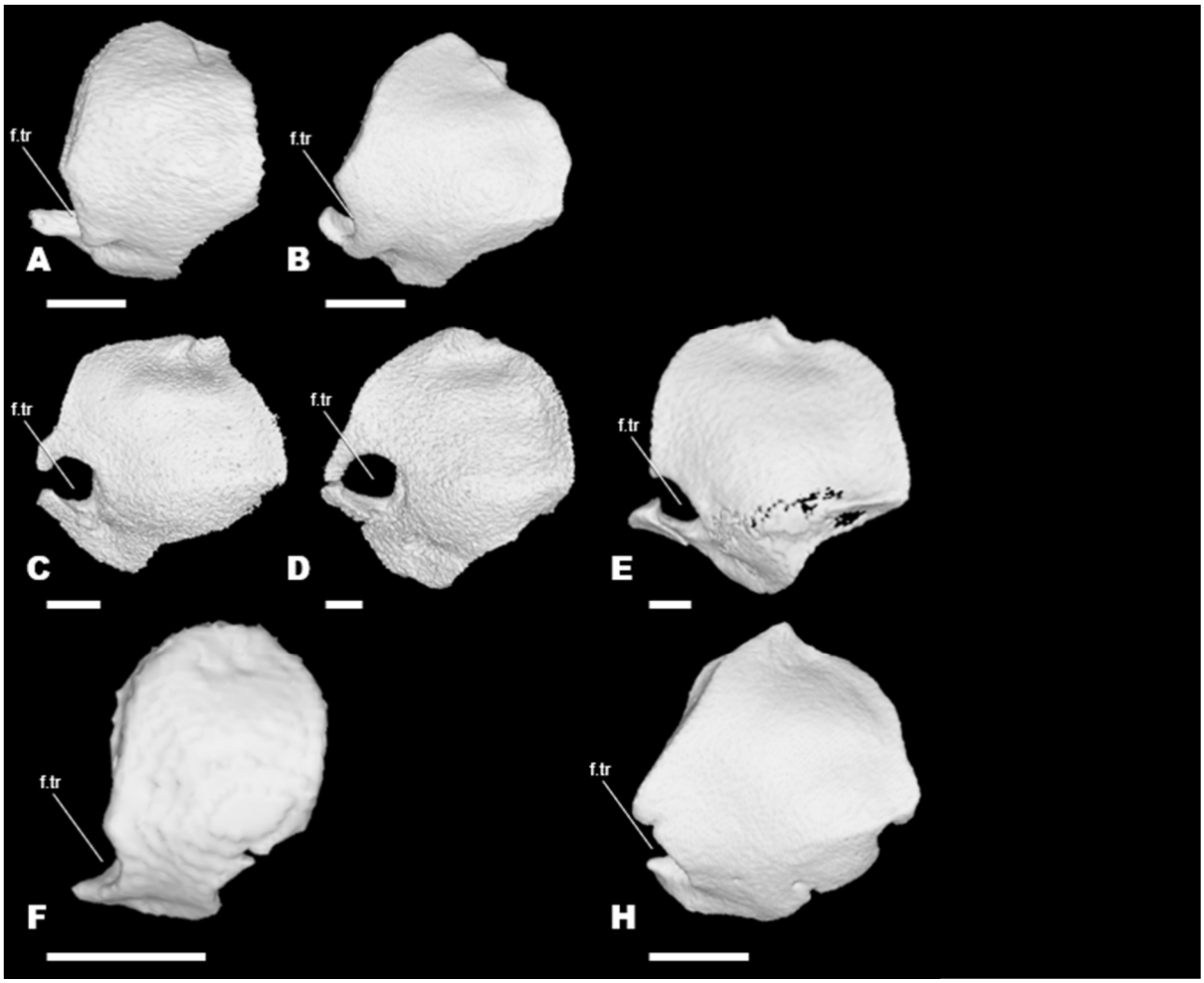

Figure 34. Left prootic, lateral (A) *Typhlops jamaicensis*, (B) *Typhlops lumbricalis* (C) *Afrotyphlops mucruso*, (D) *Afrotyphlops schlegelii*, (E) *Afrotyphlops punctatus,* (F) *Madatyphlops arenarius,* (H) *Sundatyphlops polygrammicus*. Abbreviations: f.tr – trigeminal foramen

Scale bar = 0.5mm

cerebral carotid. In *A. mucruso* and *A. schlegelii*, the entrance of the cerebral carotid into the braincase is completely enclosed by the prootic. In *A. mucruso*, the cerebral carotid enters the braincase ventral to the posterior edge of the trigeminal foramen. In *A. schlegelii*, the cerebral carotid enters posterior to the ventral edge of the trigeminal foramen, opening onto the postero-ventral extent of the trigeminal foramen before projecting ventrally towards the basisphenoid. Internally, the foramen for the auditory nerves is much more substantial, with the internal strut separating the two foramen more internal to the prootic in *A. mucruso* and *A. schlegelii*, and completely absent in *A. punctatus*, where instead the auditory nerves all pass through a large undivided foramen. In addition to the usual foramina located on the prootic, all three species of *Afrotyphlops* examined have a small foramen positioned ventral to the internal contact between the supraoccipital and the prootic, about halfway along this contact.

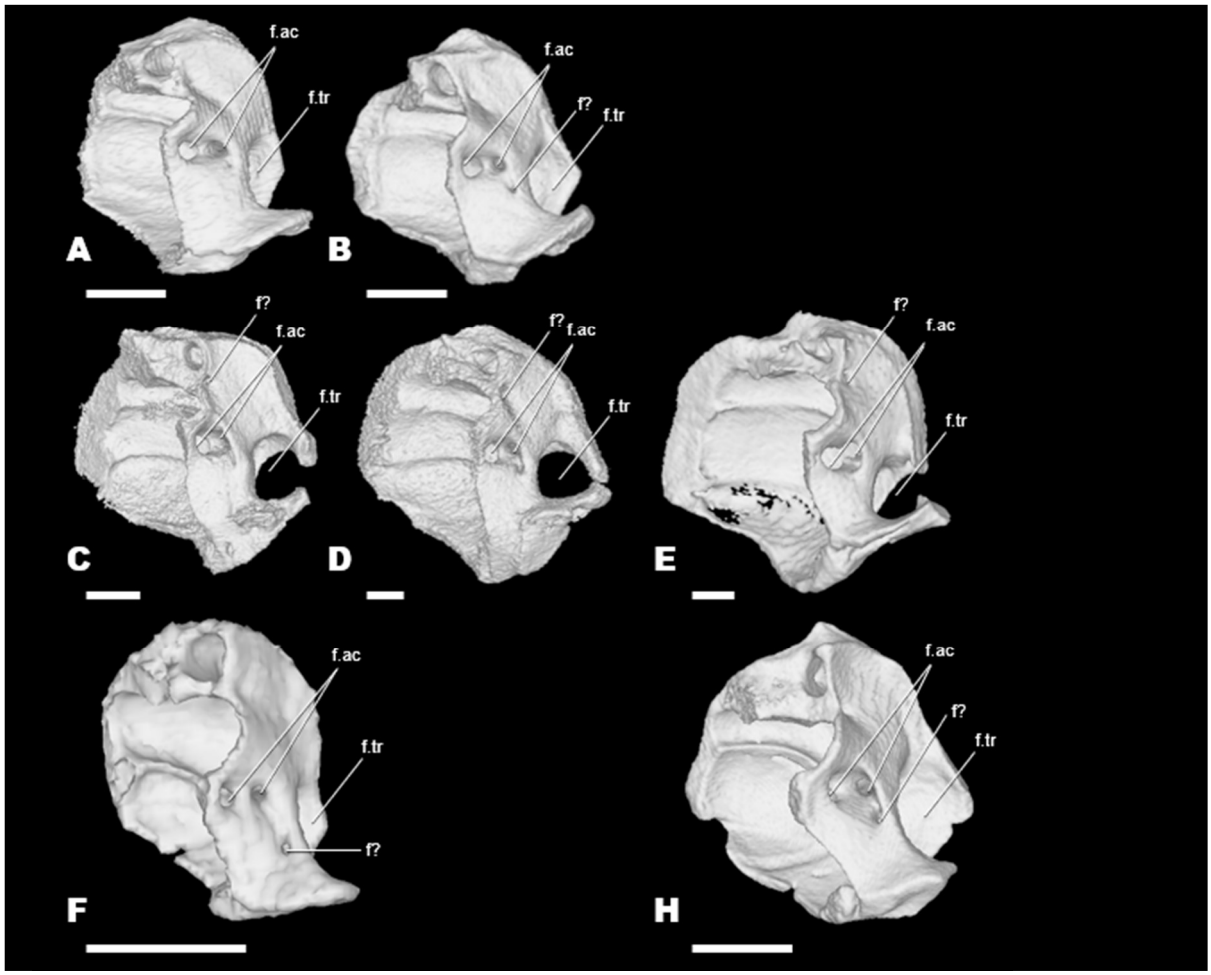

Figure 35. Left prootic, medial (A) *Typhlops jamaicensis*, (B) *Typhlops lumbricalis* (C) *Afrotyphlops mucruso*, (D) *Afrotyphlops schlegelii*, (E) *Afrotyphlops punctatus,* (F) *Madatyphlops arenarius,* (H) *Sundatyphlops polygrammicus*. Abbreviations: f. ac – acoustic foramen, f.tr – trigeminal foramen, f? – unknown foramen

Scale bar = 0.5mm

The prootics of *Madatyphlops arenarius* are smaller in lateral view than the prootics of the other species examined. The ventral part of the anterior edge of the prootic forms the posterior half of the oval-shaped trigeminal foramen. The ventral projection of the prootic is slightly indented, channelling the cerebral carotid into the notch formed by the basisphenoid, ventral to the trigeminal foramen. Internally there are the typical two foramina for the auditory nerves.

The prootics of *Sundatyphlops polygrammicus* are similar in their extent of contribution to the lateral part of the braincase as in the examined *Typhlops*. The ventral extents of the prootics do not extend as far anteriorly, resulting in the trigeminal foramen not being completely separated from the entrance foramen for the cerebral carotid. This ventral projection contacts the posterior most corner of the basisphenoid. Internally, there are several foramina in addition to the auditory nerve foramina. A foramen ventral to the anterior auditory

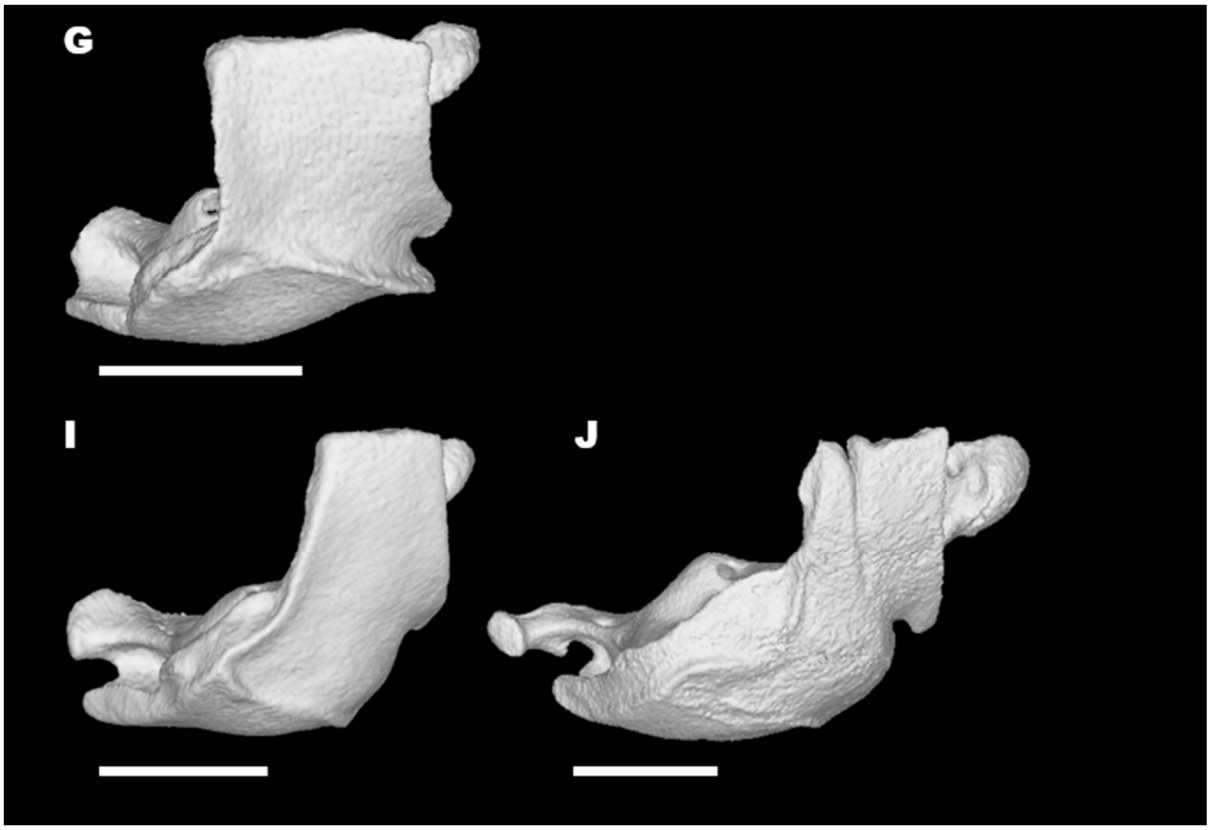

Figure 36. Fused otic, dorsal (G) *Indotyphlops braminus*, (I) *Anilios leucoproctus,* (J) *Anilios bituberculatus*
Scale bar = 0.5mm

nerve foramen pierces the side of the auditory meatus and enters the vestibular window. Another foramen pierces the otooccipital dorsal to the auditory meatus, anterior to the contact with the supraoccipital.

Some species possess additional foramina on the internal surface of the vestibular window, forming a lateral aperture opening into the juxstastapedial recess. One foramen is visible on each of the prootics of *Afrotyphlops mucruso*, and two present in both *Afrotyphlops shlegelii* and *Afrotyphlops punctatus.* The prootics of *Sundatyphlops polygrammicus* have three foramen, the dorsal most two of which are both in the same small depression.

3.5.9 Fused element: Otooccipitals + Prootic + Supraoccipital – Figures 36-38

Although the typical condition in Typhlopoidea is the presence of all three pairs of bones as separate elements, there is considerable variation in the species examined. In *Anilios leucoproctus, Anilios bituberculatus*, and *Indotyphlops braminus* the otooccipitals, prootics and supraoccipitals are all fused into a single element. In all three of these species the entirety of the otic complex is housed within this single bone. This is similar to the fusion of the prootics and otooccipitals seen in the anomalepid *Liotyphlops albirostris*, denoted as the 'otico-occipital' by

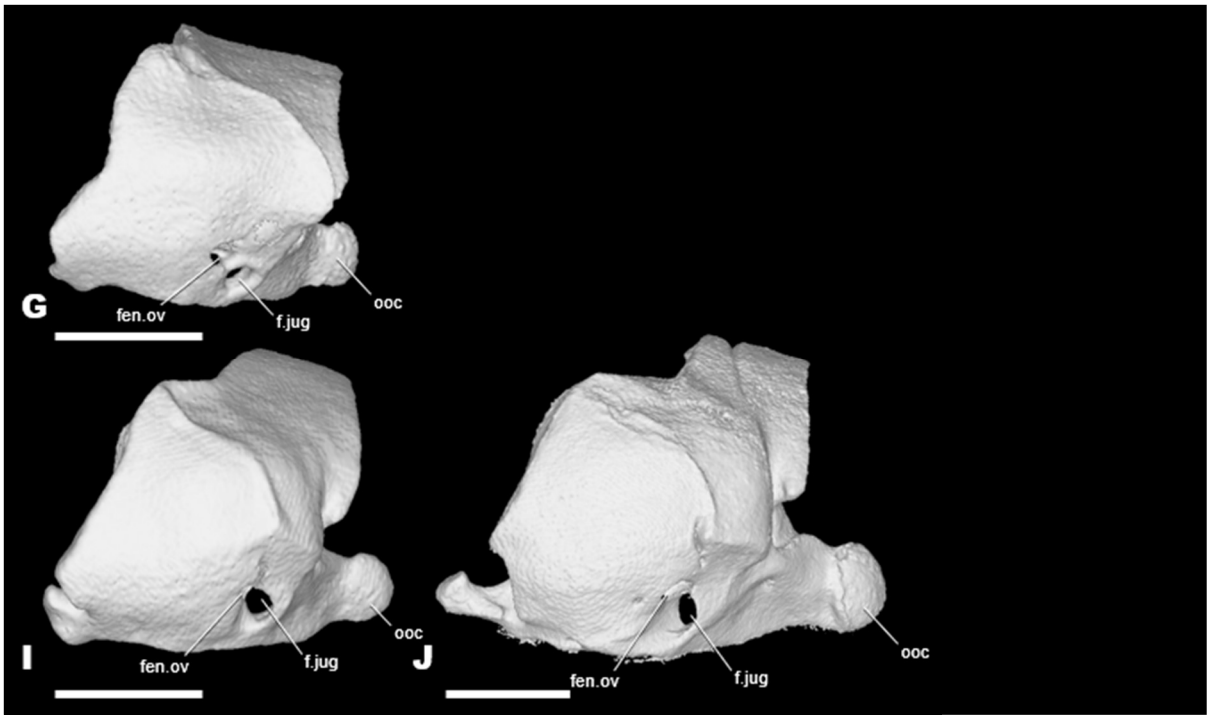

Figure 37. Fused lateral, dorsal (G) *Indotyphlops braminus*, (I) *Anilios leucoproctus,* (J) *Anilios bituberculatus*. Abbreviations: f.jug – jugular foramen, fen.ov – fenestra ovalis, ooc – occipital condyle

Scale bar = 0.5mm

Rieppel et al (2009), however this element excludes the unpaired supraoccipital. This fusion of the otic bones seen in *I. braminus* is contrary to the condition reported in List (1966), where the prootic was listed as present (species reported as *Typhlops braminus*). Previous description of all three otic bones in *Anilios australis* (Laver *et al.* 2021) shows that the fusion of the otic complex is variable in this genus.

The fused otic complex of *Indotyphlops braminus,* as with the other bones in this species, does not form direct contacts with the adjacent bones. Unlike other species, the parietal does not overlap with any part of the otic complex. The ventral anterior corner of the otic complex approaches the posterior lateral corner of the basisphenoid, forming the posterior wall of the trigeminal foramen. Similar to the shape of the otic complex in the examined *Afrotyphlops*, the lateral edges of the otic complex form distinct posteriorly projecting ridges. Additionally, the jugular foramen is not bounded by a crista tubularis, instead pierces the braincase as a simple foramen. Internally, most foramen are in the same position as they would be in the non-fused otic complex of other species. The dorsal metotic foramen is more ventrally positioned than in other species, about midway down the metotic fissure. The two foramen that transmit the auditory nerves are very large, with the bony strut that separates the auditory meatus barely captured by the scans.

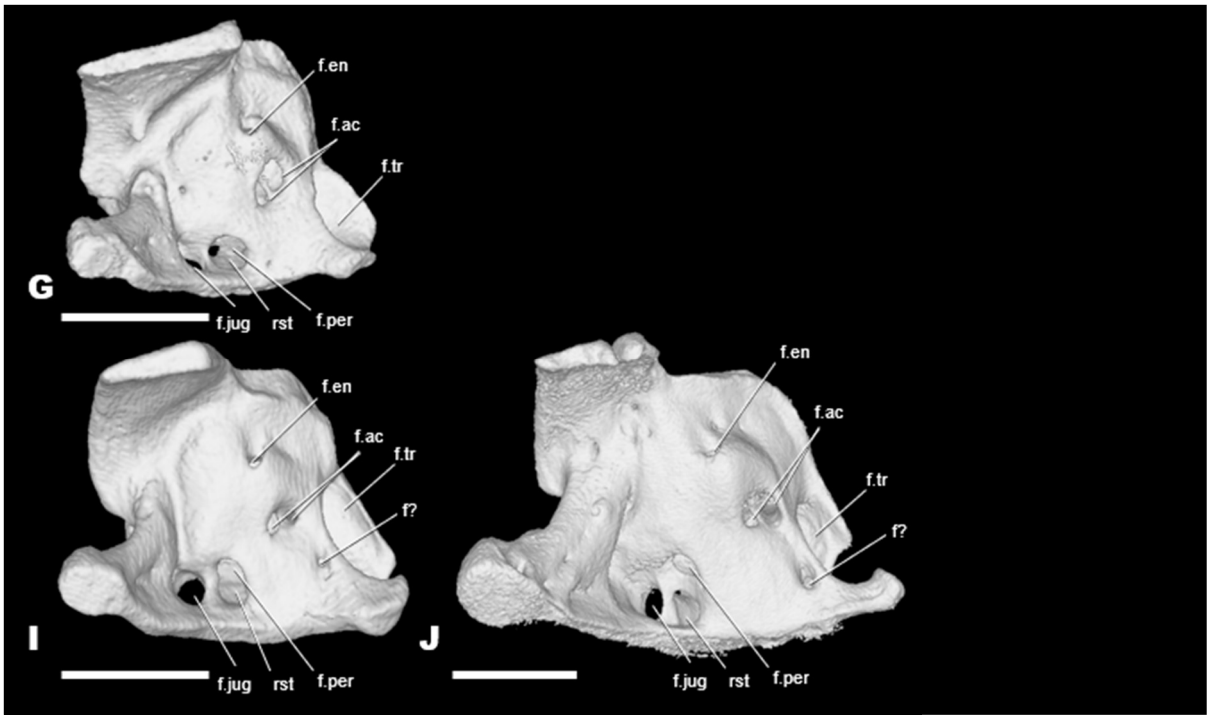

Figure 38. Fused otic, dorsal (G) *Indotyphlops braminus*, (I) *Anilios leucoproctus,* (J) *Anilios bituberculatus*. Abbreviations: f.ac – acoustic foramen, f.en – endolymphatic foramen, f.hyp – foramen for hypoglossal nerve, f.jug – jugular foramen, f.per – perilymphatic foramen, f.tr – trigeminal foramen, f? – unknown foramen, rst – recessus scalae tympani

Scale bar = 0.5mm

The fused otic complex of *Anilios leucoproctus* is similar in overall shape to *Sundatyphlops polygrammicus.* Unusually, the fused otic complex of *Anilios bituberculatus* is more similar in overall shape to that of the examined *Typhlops* rather than either the fused complex of *Indotyphlops braminus* or the unfused otic complex of *Sundatyphlops polygrammicus*. Although completely fused, the dorsal lamina of the left fused element of *A. bituberculatus* shows a notch and groove that are in a corresponding position to where the dorsal lamina of the supraoccipital would separate from the dorsal lamina of the otoocipital. In *A. leucoproctus,* the ventral anterior projection of the fused complex contacts the postero-lateral corner of the basisphenoid, and the ventral corner of the lateral walls of the parietal. The trigeminal foramen is smaller in lateral view, with the anterior edge composed of a notch in the lateral wall of the parietal, and the posterior edge composed of a larger notch in the fused element. There is a distinct triangular gap at the meeting point of the basisphenoid, parietal, and the fused element, where presumably the cerebral carotid enters the braincase. In contrast to this, the ventral anterior projection of the fused complex of *A. bituberculatus* is more similar to the ventral anterior projection of the prootic of *A. punctatus*. Both the dorsal and ventral edges of the trigeminal foramen are composed of the fused element, with only the anterior edge being

composed of a slightly curved portion of the posterior edge of the lateral wall of the parietal. The cerebral carotid appears to pass via a groove on the ventral lateral edge of the fused element, before entering the braincase via a notch in the basisphenoid, ventral to the projection of the fused element. On the right side of the specimen there is a foramen on the ventral projection that opens into the ventral wall of the trigeminal foramen. This foramen is more laterally positioned on the left side, forming a notch rather than a full foramen. In addition to the usual foramina present internally, there are also two additional foramina present in *A. bituberculatus* and one additional foramen in *A. leucoproctus*. In both species there is a small foramen of unknown function immediately posterior to the vestibular window. In *A. bituberculatus*, there is another foramen positioned dorsally to the anterior extent of the endolymphatic foramen.

As with the prootics of the examined *Afrotyphlops* and *Sundatyphlops polygrammicus*, there are additional foramina of unknown function located within the vestibular window, piercing through into the juxtastapedial recess. Both *Indotyphlops braminus* and *Anilios bituberculatus* have two foramina in each vestibular window, and *Anilios leucoproctus* has one in the right vestibular window, and two in the left vestibular window.

3.5.10 Stapes

The rod of the stapes is small in all taxa examined and barely extends through the fenestra ovalis. The expanded stapedial foot plate is contained completely within the otic capsule, and is in contact with the otooccipital. The stapes and the fenestra ovalis are concealed in lateral view by the quadrate.

3.6 Suspensorium and Mandible

The mandible of typhlopoids functions primarily as a passive scoop during feeding (Cundall & Irish 2008). The structure of the mandible is highly similar across all Typhlopidae examined. The mandible articulates with the rest of the skull via the quadrate, which is suspended from the otooccipitals.

3.6.1 Quadrate – Figure 39

The quadrate is a complex bone that projects anteriorly from the braincase towards the rest of the lower jaw. There is no visible articulation with the braincase, so presumably the lower jaw is attached to the rest of the skull with cartilage. The overall morphology is largely the same between species. The quadrate has a posterior rod-like process, which presumably attaches the quadrate to the braincase, and expands to a sub-triangular anterior process from the mid-point. The relatively short mandible typical of typhlopoids requires the quadrate to be

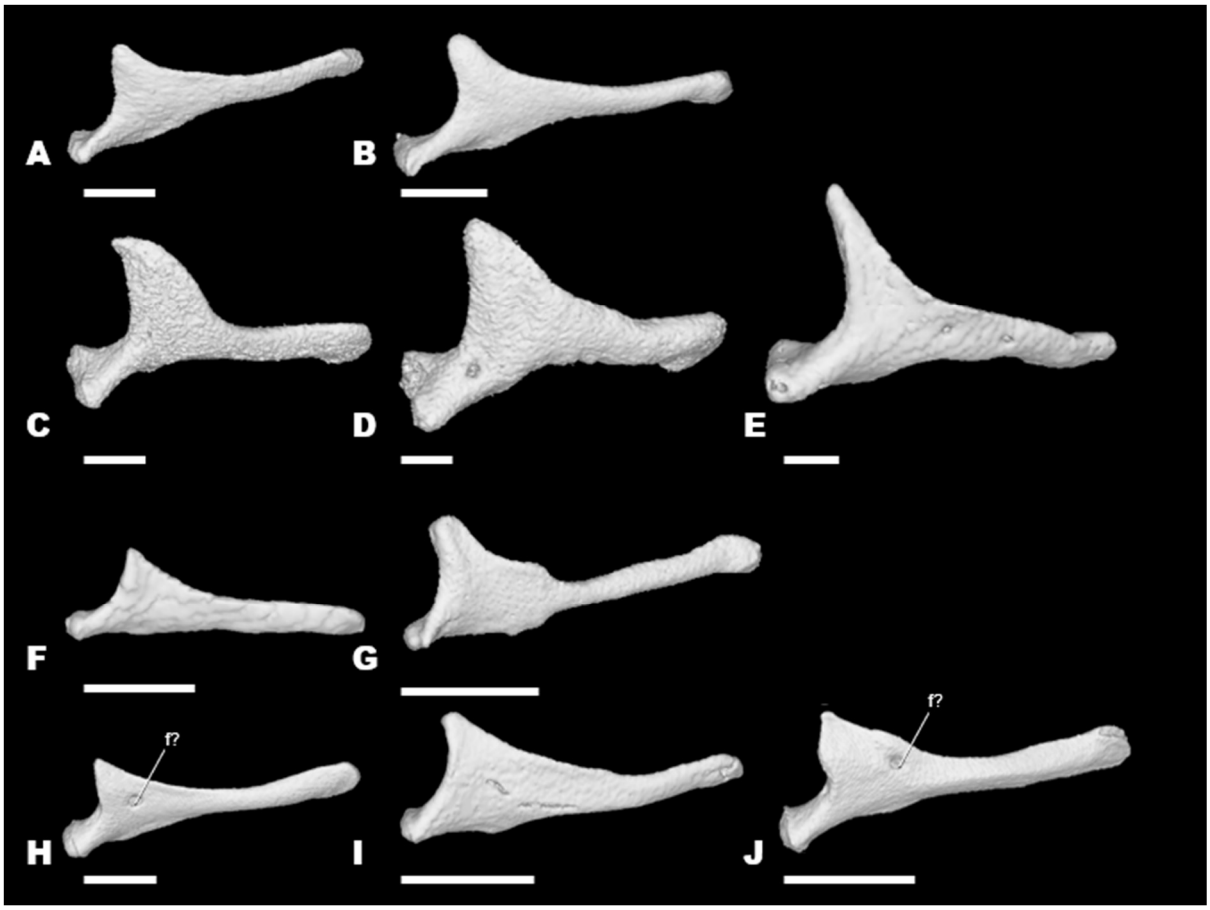

Figure 39. Quadrate, lateral (A) *Typhlops jamaicensis*, (B) *Typhlops lumbricalis*, (C) *Afrotyphlops mucruso*, (D) *Afrotyphlops schlegelii*, (E) *Afrotyphlops punctatus,* (F) *Madatyphlops arenarius,* (G) *Indotyphlops braminus*, (H) *Sundatyphlops polygrammicus,* (I) *Anilios leucoproctus*, (J) *Anilios bituberculatus*. Abbreviations: f? – unknown foramen

Scale bar = 0.5mm

directed anteriorly from the otic region to the articulation with the mandible, as opposed to the vertical or posteriorly directed quadrates of alethinophidians (List 1966). The anterior end of the quadrate is expanded in a triangular shape, with the prominent anterodorsal (cephalic) projection posterior to the articulation with the compound bone. This process extends laterally to the maxillary retractor muscle and originates the caudalmost mandibulae externus profundus (Cundall & Irish 2008). The quadrate is mostly medio-laterally flattened, except at the anterior articulation contact with the compound, which is expanded both medially and laterally.

Morphological variation between species is seen in the anterior process. In the examined *Typhlops* and *Madatyphlops arenarius*, the cephalic process is triangular and points perpendicular to the long edge of the quadrate. The tip of this triangular process is slightly

rounded. When viewed laterally, this triangular cephalic process reaches its peak slightly anterior to the anterior edge of the prootic.

In the examined *Afrotyphlops*, the quadrate is relatively shorter, not extending past the anterior edge of the prootic in lateral view. The posterior rod-like process is also reduced in length. The anterior cephalic process is much more prominent in all species, though of different morphology. In *Afrotyphlops mucruso* this process is pointed anteriorly, with the posterior edge of the process forming a curve, whereas the anterior edge is almost completely vertical relative to the long edge of the quadrate. In contrast, in *Afrotyphlops schlegelii*, the cephalic process is large and triangular. In *Afrotyphlops punctatus* the process is still triangular but forms a thinner triangle when viewed laterally. In all three species, the dorsal extent of this process exceeds the dorsal edge of the trigeminal foramen, not seen in any other species.

In *Sundatyphlops polygrammicus, Anilios leucoproctus*, and *Anilios bituberculatus*, the anterior process is more pointed, as well as being more anteriorly positioned, resulting in a shorter mandibular process. The morphology of the anterior process of *Indotyphlops braminus* is unique compared to all other species examined. Instead of the triangular anterior process continuing from the dorsal and ventral edges of the quadrate, the posterior process continues in same thickness, and meets the anterior process with a sharp widening. The anterior process is more rectangular, although the cephalic process is still slightly triangular.

The presence of foramen in the quadrate is variable between species. The only visible foramen for *Indotyphlops braminus* is visible from medial view in the centre of the anterior process, the foramen does not extend all the way through the bone. No foramen were visible on the quadrates of *Typhlops jamaicensis, Typhlops lumbricalis, Afrotyphlops punctatus*, *Madatyphlops arenarius* or *Anilios leucoproctus*,. The anterior process of the quadrate of *Sundatyphlops polygrammicus, Afrotyphlops schlegelii*, and *Anilios bituberculatus* possesses a foramen only visible from lateral view which does not pierce through the bone.

3.6.2 Compound – Figures 40-41

As in all snakes, the main bone of the lower jaw is the compound bone. This bone is composed of the fused articular, surangular and prearticular elements (Cundall & Irish 2008). In lateral view, the compound bone of typhlopids is curved downwards. The retroarticular process extends posteriorly from the articulation with the quadrate about half the length of the quadrate, but does not exceed the back of the braincase. The anterior portion of the bone is blade-like and medio-laterally flattened. In medial view, the Meckelien canal runs anteriorly from the mandibular fossa that is positioned anterior medial to the articulation with the quadrate, forward to exit medially between the compound and the ventral projection of the

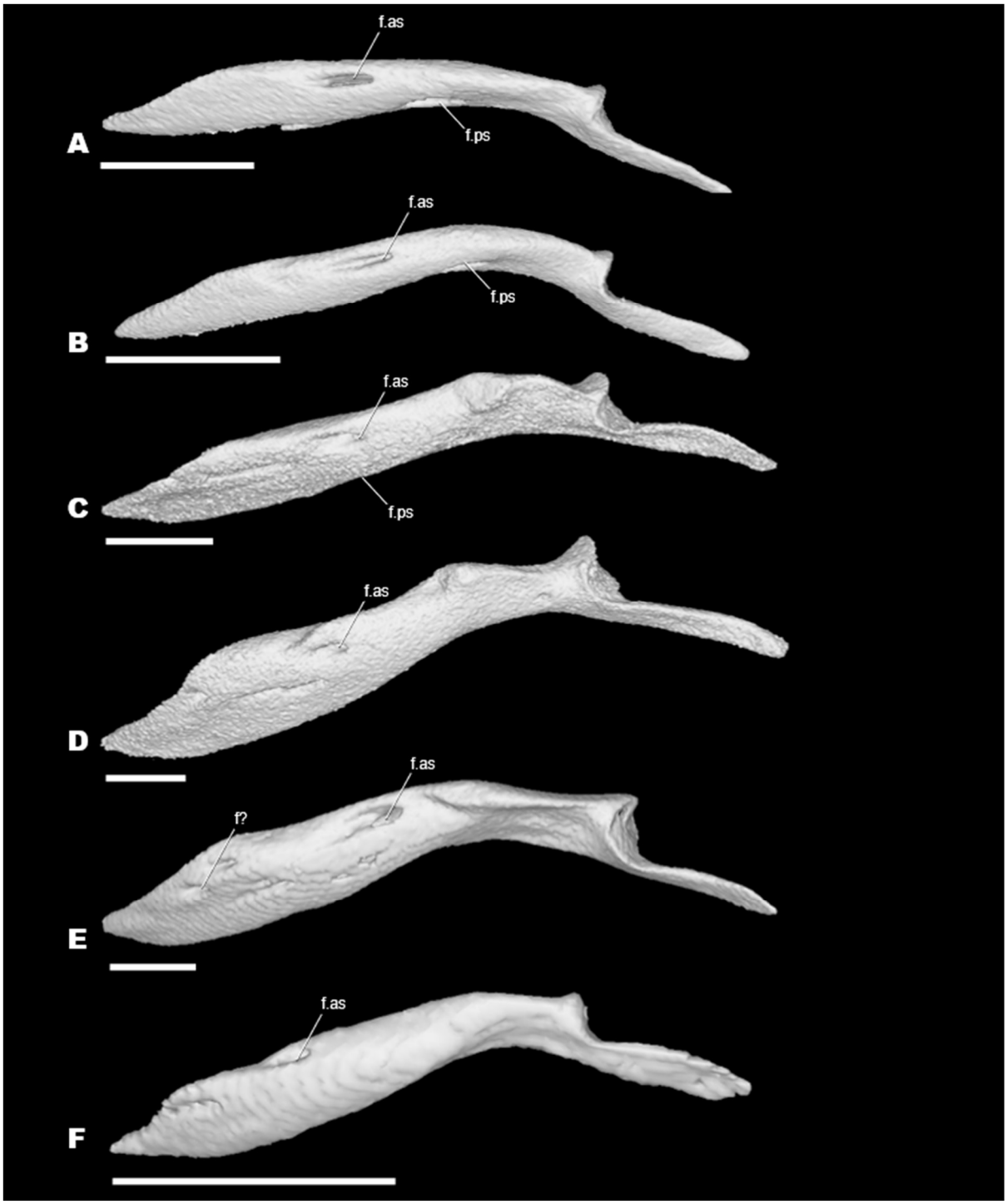

Figure 40. Compound, lateral (A) *Typhlops jamaicensis*, (B) *Typhlops lumbricalis*, (C) *Afrotyphlops mucruso*, (D) *Afrotyphlops schlegelii*, (E) *Afrotyphlops punctatus,* (F) *Madatyphlops arenarius,* (G) *Indotyphlops braminus*, (H) *Sundatyphlops polygrammicus,* (I) *Anilios leucoproctus*, (J) *Anilios bituberculatus*. Abbreviations: f? – unknown foramen, f.as – anterior surangular foramen, f.ps – posterior surangular foramen

Scale bar = 1mm

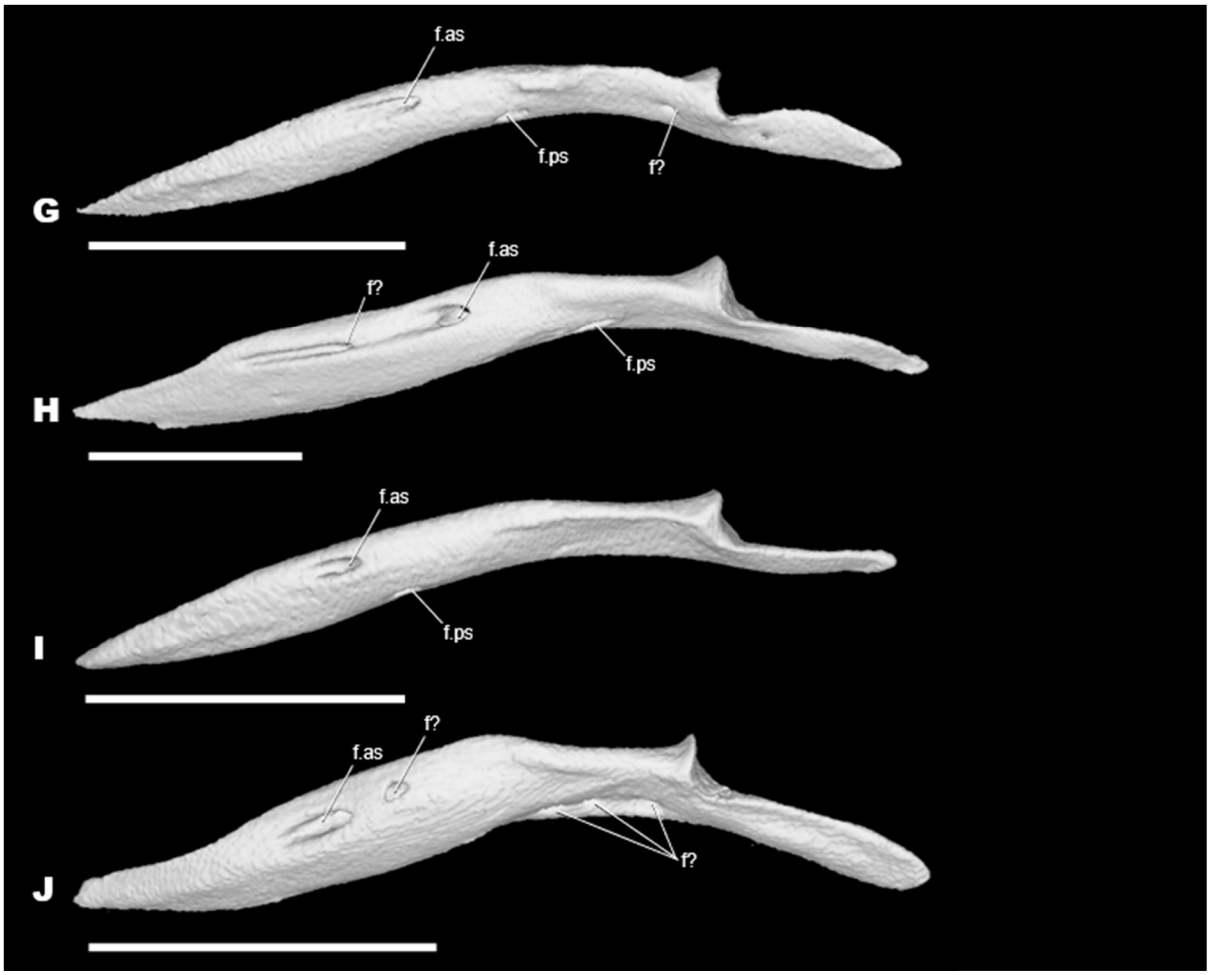

Figure 40 cont. Compound, lateral (A) *Typhlops jamaicensis*, (B) *Typhlops lumbricalis*, (C) *Afrotyphlops mucruso*, (D) *Afrotyphlops schlegelii*, (E) *Afrotyphlops punctatus,* (F) *Madatyphlops arenarius,* (G) *Indotyphlops braminus*, (H) *Sundatyphlops polygrammicus,* (I) *Anilios leucoproctus*, (J) *Anilios bituberculatus*. Abbreviations: f? – unknown foramen, f.as – anterior surangular foramen, f.ps – posterior surangular foramen

Scale bar = 1mm

coronoid. In lateral view, there are usually two foramina, but the position of these varies, these are the anterior surangular foramen and the posterior surangular foramen. The anterior process of the compound approaches the dentary but does not make contact. The compound is in contact ventrally with the angular and variably the splenial when present. The compound also possesses several foramina along the lateral surface, variable among the species examined

In the examined *Typhlops*, there is a small ventral projection of the posterior edge of the compound that runs ventral to the Meckelian canal, which is not present in other species. The anterior surangular foramen is located about half way along the anterior blade, dorsally oriented, whereas the posterior surangular foramen is ventrally oriented, immediately posterior to the anterior foramen. There is no visible foramen for the chorda tympani nerve.

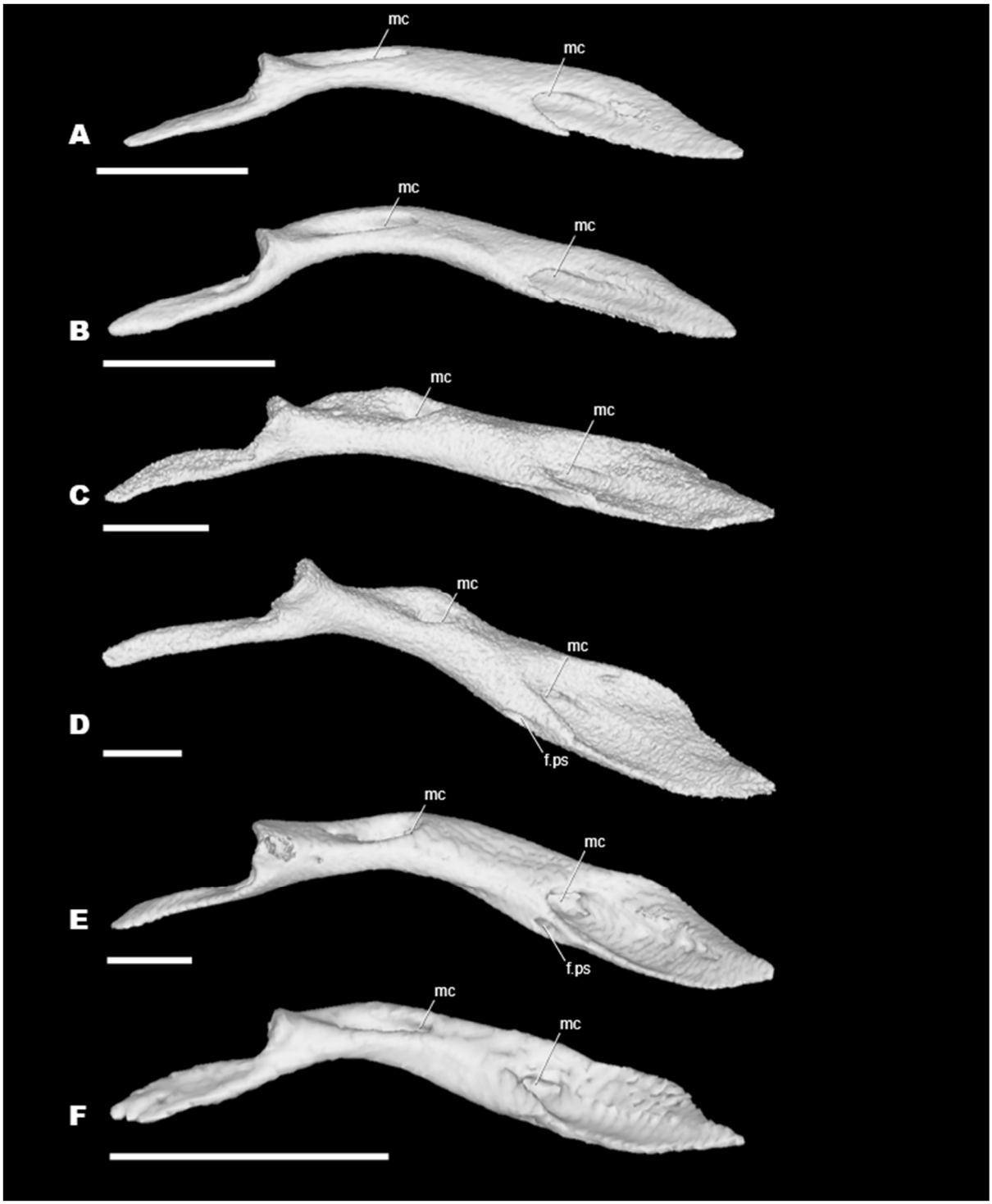

Figure 41 . Compound, medial (A) *Typhlops jamaicensis*, (B) *Typhlops lumbricalis*, (C) *Afrotyphlops mucruso*, (D) *Afrotyphlops schlegelii*, (E) *Afrotyphlops punctatus,* (F) *Madatyphlops arenarius,* (G) *Indotyphlops braminus*, (H) *Sundatyphlops polygrammicus,* (I) *Anilios leucoproctus*, (J) *Anilios bituberculatus*. Abbreviations: f.ps – posterior surangular foramen, mc – Meckelian canal

Scale bar = 1mm

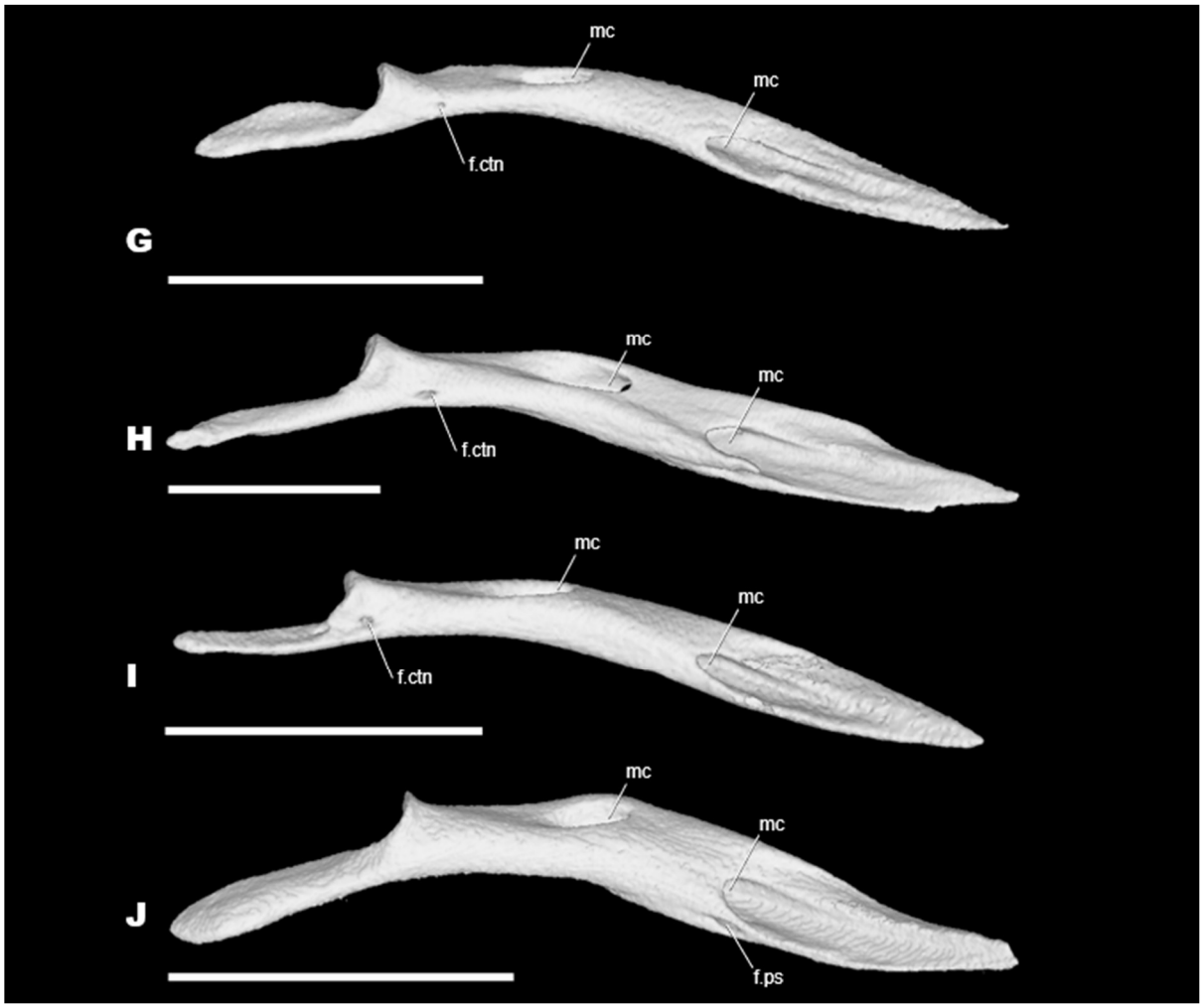

Figure 41 cont. Compound, medial (A) *Typhlops jamaicensis*, (B) *Typhlops lumbricalis*, (C) *Afrotyphlops mucruso*, (D) *Afrotyphlops schlegelii*, (E) *Afrotyphlops punctatus,* (F) *Madatyphlops arenarius,* (G) *Indotyphlops braminus*, (H) *Sundatyphlops polygrammicus,* (I) *Anilios leucoproctus*, (J) *Anilios bituberculatus*. Abbreviations: f.ctn – foramen for chorda tympani nerve, f.ps – posterior surangular foramen, mc – Meckelian canal

Scale bar = 1mm

In the examined *Afrotyphlops*, the anterior blade is more ventrally directed, and wider than in other species. The foramina on the lateral side of the compound are small and difficult to identify. In *Afrotyphlops schlegelii* and *Afrotyphlops mucruso*, the foramen I identified as the anterior surangular foramen is halfway along the anterior dorsal edge, and the foramen I identified as the posterior surangular foramen is immediately ventral to this. In *A. mucruso* there is a groove anterior to the anterior surangular foramen, that inserts into the bone before exiting at a foramen located on the anterior edge. This is of unknown function, and may transmit a blood vessel. A similar groove and foramen is present in *A. schlegelii* in a different position, the posterior extent of the groove is ventral to the anterior surangular foramen. Also, the groove does not enter the bone, the anterior foramen appears to belong to a separate structure. The

compound of *Afrotyphlops punctatus* contains several foramina of unknown function. The largest on the anterior edge is positioned halfway along the extent of the compound, and due to a similar location in the other *Afrotyphlops* examined it is probable that this is the anterior surangular foramen. However, the identity of the posterior surangular foramen is less clear. The ventral-most foramen is anterior to the supposed anterior surangular foramen, located just ventral to the anterior opening of the Meckelian canal. On the left compound there are six additional foramina visible laterally, two ventral to the anterior surangular foramen, two antero-ventral, and two anterior. The right compound has an unusual morphology. There is a process positioned dorsal to the anterior surangular foramen. Additionally, there are four foramina of unknown function positioned anterior to this foramen. The ventral-most foramen (possible posterior surangular foramen) is positioned the same as in the left compound. The resolution of the scans of *Madatyphlops arenarius* are not high enough to identify any foramina medially other than those transmitting the Meckelian canal. Laterally, only the anterior surangular foramen is identifiable, halfway along the compound blade

In *Indotyphlops braminus*, the two largest foramina visible laterally are the two surangular foramina, in similar position to the *Typhlops* examined. There are two possible foramina ventral to the articulation of the quadrate on the left compound, but neither appear to pierce the bone or are visible on the right compound. As such they may be artefacts of preservation. Medially, a small foramen is visible antero-ventral to the articulation with the quadrate, which probably transmits the chorda tympani nerve.

In *Sundatyphlops polygrammicus*, the anterior surangular foramen is positioned dorsally half way along the compound. In the left compound, this foramen pierces all the way through the bone, connecting with the passage for the Meckelian canal. In both compounds, there is a groove anterior to this foramen, with another foramen into the compound halfway along the groove. The posterior surangular foramen is positioned ventrally, halfway between the anterior surangular foramen and the articulation with the quadrate. Medially, the chorda tympani nerve foramen is visible.

In *Anilios leucoproctus*, the anterior surangular foramen is half way along the dorsal edge of the compound, with the posterior surangular foramen positioned ventrally, just posterior to the anterior foramen. The foramen for the chorda tympani nerve is more ventrally positioned than in previous taxa, appearing ventral to the articulation with the quadrate.

In *Anilios bituberculatus*, there are several foramina present on the lateral surface of the compound. There are two dorsally positioned, the anterior of which is more ovoid in shape, and is likely the exit for the anterior surangular foramen. The posterior foramen appears to pierce into this channel. On the left compound, there are three ventrally positioned foramina antero-ventral to the articulation of the quadrate, one of which is likely the posterior surangular

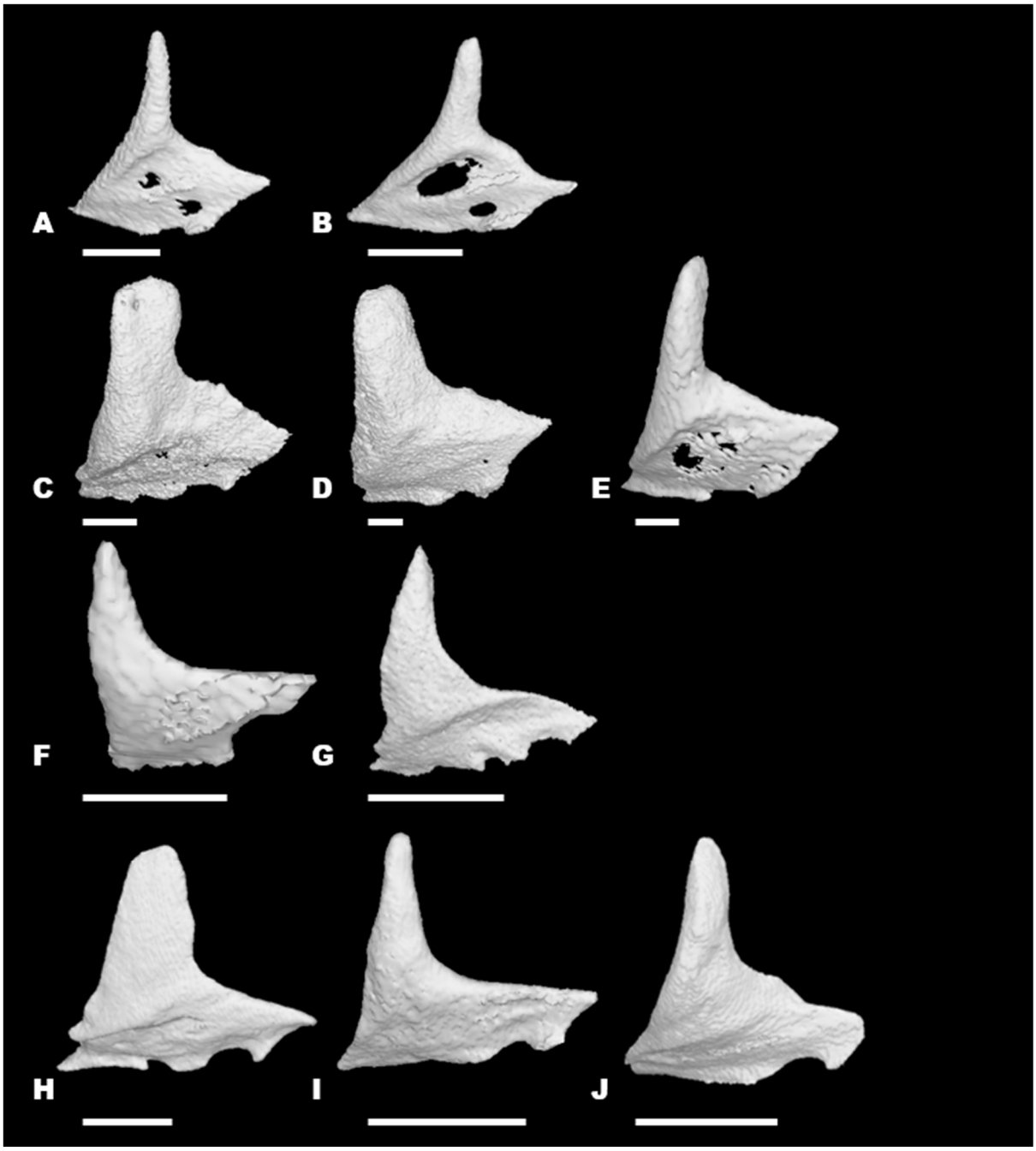

Figure 42. Coronoid, lateral (A) *Typhlops jamaicensis*, (B) *Typhlops lumbricalis*, (C) *Afrotyphlops mucruso*, (D) *Afrotyphlops schlegelii*, (E) *Afrotyphlops punctatus,* (F) *Madatyphlops arenarius,* (G) *Indotyphlops braminus*, (H) *Sundatyphlops polygrammicus,* (I) *Anilios leucoproctus*, (J) *Anilios bituberculatus*.

Scale bar = 0.5mm

foramen. On the right compound, the foramina are less visible, but there appears to be two, in the same positions as the left compound. The anterior of this foramen is an elongated groove. There is no visible foramen for the chorda tympani nerve on the medial surface of either compound.

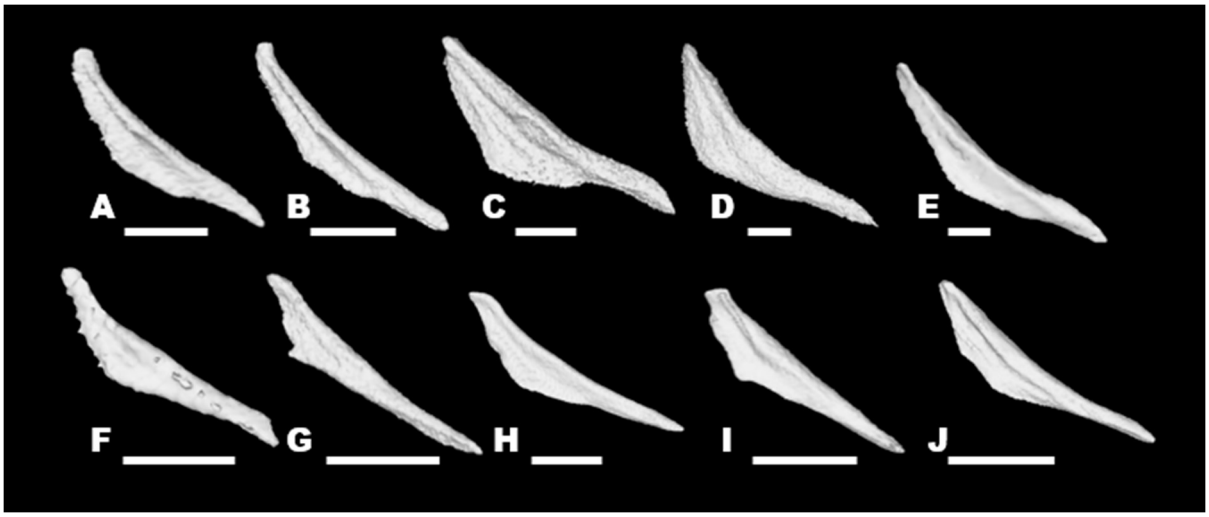

Figure 43. Splenial, dorsal (A) *Typhlops jamaicensis*, (B) *Typhlops lumbricalis*, (C) *Afrotyphlops mucruso*, (D) *Afrotyphlops schlegelii*, (E) *Afrotyphlops punctatus,* (F) *Madatyphlops arenarius,* (G) *Indotyphlops braminus*, (H) *Sundatyphlops polygrammicus,* (I) *Anilios leucoproctus*, (J) *Anilios bituberculatus*.

Scale bar = 0.5mm

3.6.3 Coronoid – Figure 42

The coronoid is a triangular laterally-compressed laminar bone that lies medially inside the lower jaw, the dorsal portion of which curves posteriorly. The ventral portion of the coronoid contacts medially with the anterior end of the compound bone and the posterior end of the splenial, bridging both elements. The dorsally projecting coronoid process approaches the maxilla laterally when the jaw is closed. The dorsal coronoid process differs among species. In *Typhlops jamaicensis* and *Typhlops lumbricalis*, this dorsal process is rod-like. In the largest examined species, *Afrotyphlops schlegelii* and *Afrotyphlops mucruso*, the dorsal process is more laterally expanded, with a flat edge at the dorsal most point. In contrast the dorsal process of *Afrotyphlops punctatus* is more rod like, but more posteriorly projected than seen in examined *Typhlops*. In *Madatyphlops arenarius* and *Indotyphlops braminus* the dorsal process is acuminate, more posteriorly projected in *I. braminus*. The dorsal process of *Sundatyphlops polygrammicus* is similar to that seen in *A. schlegelii* and *A. mucruso*, whereas the dorsal process of *Anilios leucoproctus* is again more rod-like, with the dorsal process of *Anilios bituberculatus* a between morphology. Additionally, the ventral edge of the asiatyphlopines is more posteroventrally expanded than seen in other species.

3.6.4 Splenial – Figures 43-44

The splenial is a triangular element that lines the ventral edge of the anterior portion of the jaw, in contact with the dentary anteriorly, the compound, and the angular when present.

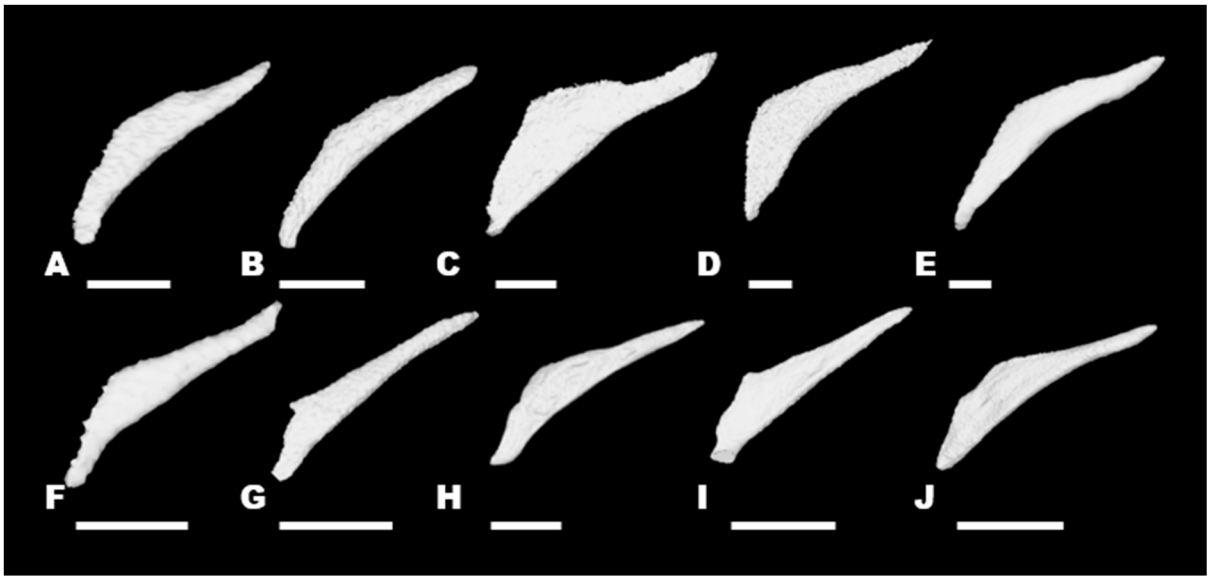

Figure 44. Splenial, ventral (A) *Typhlops jamaicensis*, (B) *Typhlops lumbricalis*, (C) *Afrotyphlops mucruso*, (D) *Afrotyphlops schlegelii*, (E) *Afrotyphlops punctatus,* (F) *Madatyphlops arenarius,* (G) *Indotyphlops braminus*, (H) *Sundatyphlops polygrammicus,* (I) *Anilios leucoproctus*, (J) *Anilios bituberculatus*.

Scale bar = 0.5mm

This bone is almost laminar, except the ventral edge is slightly thicker, tapering to the dorsal edges. The dorso-anterior edge of the splenial contacts the dentary, with the apex of the triangle at the contact point between the dentary and compound as visible in lateral view. The posterior edge of this triangular bone is variable of length, approximately equal to the anterior edge in the examined *Typhlops*, but longer than the anterior edge in the other species. The greatest difference is seen in *Indotyphlops braminus*, where the posterior edge is approximately twice the length of the anterior edge. The splenial underlies the Meckelian canal before the canal enters the ventral portion of the coronoid.

3.6.5 Angular – Figure 45

The angular, when present, is a small bone positioned between the compound and the posterior portion of the splenial. Of the specimens examined, the angular is present in the typhlopines *Typhlops jamaicensis* and *Typhlops lumbricalis,* and the afrotyphlopines *Afrotyphlops schlegelii, Afrotyphlops mucruso* and *Afrotyphlops punctatus*. It is a rod-like element in *T. jamaicensis, A. mucruso* and *A. schlegelii* and a triangular element in *T. lumbricalis* and *A. punctatus.* In *Madatyphlops arenarius* , the angular is a tiny sliver of bone. The angular is absent in *Indotyphlops braminus, Sundatyphlops polygrammicus, Anilios bituberculatus* and *Anilios leucoproctus*.

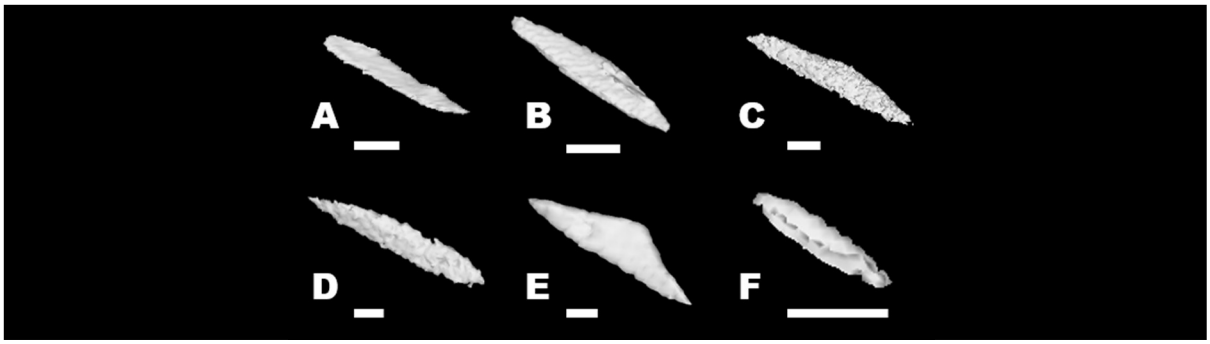

Figure 45. Angular, ventral (A) *Typhlops jamaicensis*, (B) *Typhlops lumbricalis*, (C) *Afrotyphlops mucruso*, (D) *Afrotyphlops schlegelii*, (E) *Afrotyphlops punctatus,* (F) *Madatyphlops arenarius*

Scale bar = 0.25mm

3.6.6 Dentary – Figures 46-47

As is diagnostic of the Typhlopoidea, the dentary is small and edentulous and comprises the anterior portion of the lower jaw. The bone is slightly dorsoventrally flattened, and ventrally contains a groove for the Meckelian canal where the canal runs between the splenial and the dentary. Ventrally the dentary is in contact with the anterior portion of the angular bone. The dentary is hollow, and forms an incomplete tube. The anterior edge contains a varying number of foramina, even within individuals. There are three to four in *Typhlops jamaicensis,* two to three in *Typhlops lumbricalis,* four in *Afrotyphlops mucruso*, three to four in *Afrotyphlops schlegelii*, two in *Afrotyphlops punctatus*, three in *Madatyphlops arenarius*, two in *Indotyphlops braminus*, two to three in *Sundatyphlops polygrammicus*, one to two in *Anilios leucoproctus* (although some of these foramina are not fully surrounded by bone, and instead appear as notches in the dorsal surface of the dentary), and one large foramen in *Anilios bituberculatus*. The exact function of these foramina is unknown. The dorsal surface of the dentary extends posteriorly to contact the coronoid. The medial tips of the dentaries curve inwards, pointing slightly posteriorly into the mouth, presumably as they function as a 'scoop' for the Typhlopoidea rapid feeding method of maxillary raking.

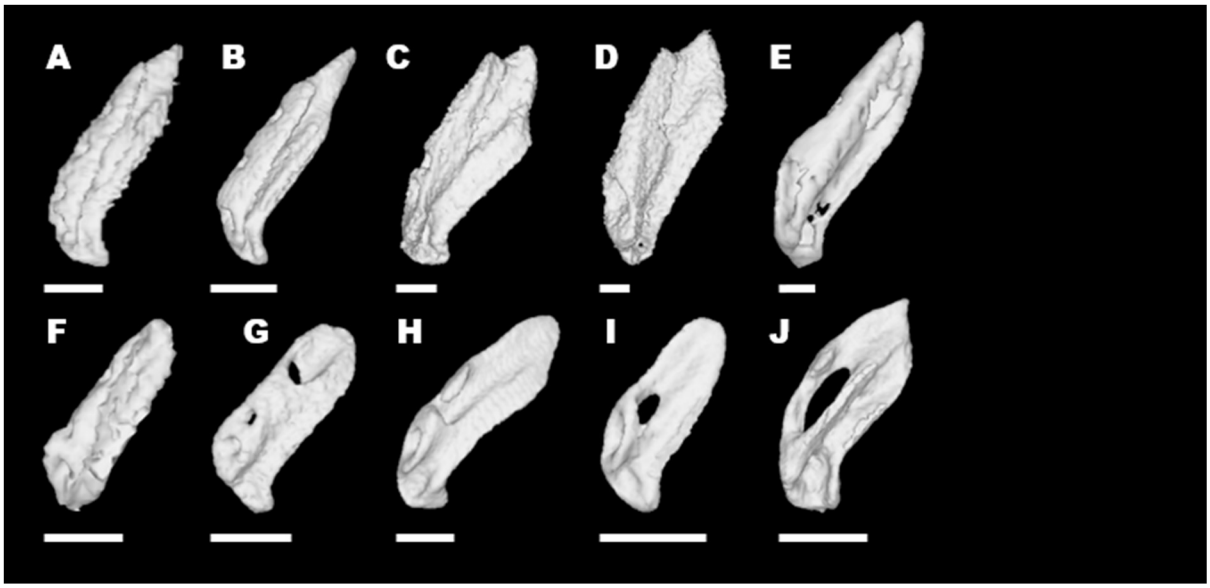

Figure 46. Dentary, dorsal (A) *Typhlops jamaicensis*, (B) *Typhlops lumbricalis*, (C) *Afrotyphlops mucruso*, (D) *Afrotyphlops schlegelii*, (E) *Afrotyphlops punctatus,* (F) *Madatyphlops arenarius,* (G) *Indotyphlops braminus*, (H) *Sundatyphlops polygrammicus,* (I) *Anilios leucoproctus*, (J) *Anilios bituberculatus*.

Scale bar = 0.25mm

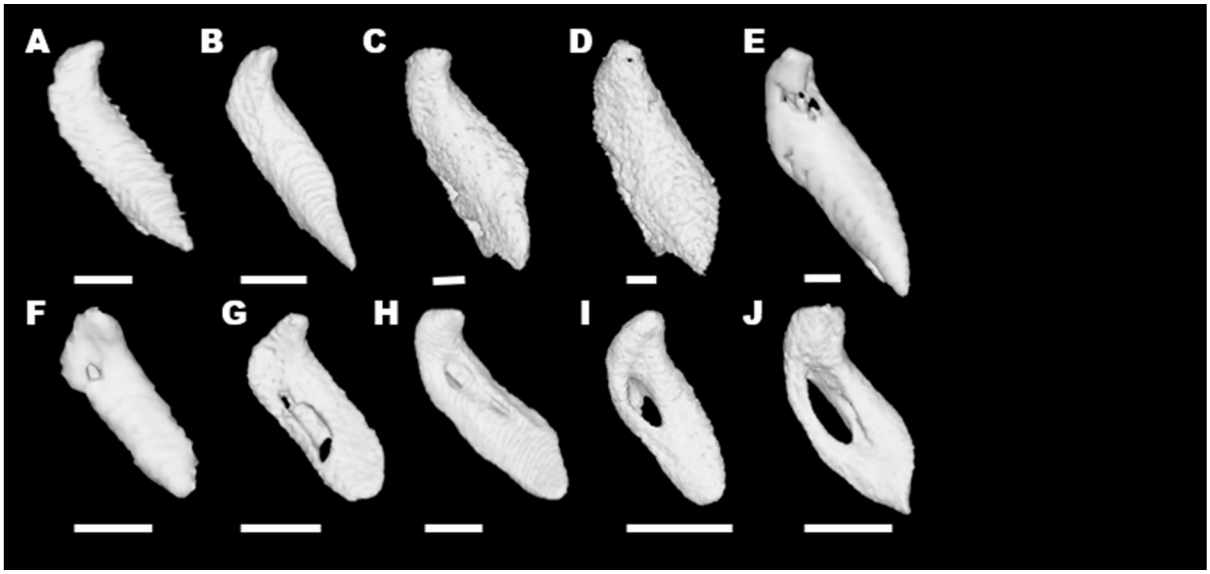

Figure 47. Dentary, ventral (A) *Typhlops jamaicensis*, (B) *Typhlops lumbricalis*, (C) *Afrotyphlops mucruso*, (D) *Afrotyphlops schlegelii*, (E) *Afrotyphlops punctatus,* (F) *Madatyphlops arenarius,* (G) *Indotyphlops braminus*, (H) *Sundatyphlops polygrammicus,* (I) *Anilios leucoproctus*, (J) *Anilios bituberculatus*.

Scale bar = 0.25mm

4. Discussion

Recent advances in microCT and digital disarticulation has allowed the examination of the distinct anatomical features of Scolecophidia to a greater degree than ever before (Bell *et al.* 2021). As the most speciose clade of Scolecophidia, Typhlopidae show a remarkable amount of morphological variation, particularly for a group of snakes that all share a specialised insectivorous diet and fossorial ecology. There are several different ecological traits that likely influence the diversity of morphology seen in the examined species. Although all species are fossorial and insectivorous, there is considerable diversity in size and geographical location that likely impact morphology in the various clades of Typhlopidae, particularly extremes of small body size.

The reduction of overall body size is known to have a significant effect on anatomy, such as resulting in overall changes in body plan, promoting novel morphological relationships, and/or increasing morphological homoplasy (Hanken & Wake 1993). Most Scolecophidia have a small body size, there are many taxa that have taken this to an extreme. One of the clades of Scolecophidia, Leptotyphlopidae, includes the smallest snake species discovered, *Leptotyphlops carlae,* which reaches a maximum body length of 104mm (Hedges 2008). In addition to the morphological changes that occur with miniaturisation, the cranium of Scolecophidia is also under adaptational constraint due to the specific needs of actively locomoting in a completely subterranean environment (Wake 1993). These two processes are also not separate, as reduction in body size often follows a transition to fossoriality (Lee 1998), therefore it can be difficult to parse out adaptations that are associated with fossoriality versus those associated with overall body size reduction. Ecology is not the only factor that places constraints on the skull. The jaw apparatus of Typhlopidae are under further constraints due to the need to maintain the fast prey transport of small invertebrate prey via maxillary raking (Kley 2001). Due to these additional constraints on the skull, it is useful to compare large and small species of Typhlopidae to examine the specific changes that occur with a further reduction in body size from an already size reduced form.

In comparison to Alethinophidia, Typhlopidae show considerable differences in their cranial anatomy. The most striking of which are the complete absence of bones from the skull, including the ectopterygoid, postfrontals, and supratemporals. Additionally, the connections between bones are much more substantial in Typhlopidae, likely due to the increased need for consolidation between bones to resist the forces during head-first burrowing. The changes in skull structure due to miniaturisation are even more noticeable in typhlopids that achieve an even smaller size than the average size of the clade. By comparing the smallest specimen examined, *Madatyphlops arenarius*, with other species of typhlopid, I have identified numerous

features that may be a result of the constraints of small size, although these features may also be a result of *Madatyphlops arenarius* being the only *Madatyphlops* included in the present study. The lateral extents of the prootic are greatly reduced in *M. arenarius* in comparison to the other species that also possess a separated prootic. This unusual morphology is perhaps a function of eventual fusion of these bones. No information about the age of specimens was available, as such all individuals were assumed to be adults. However, a recent study describing the newly discovered *Madatyphlops eudelini* found fusion of the otic region to be variable in this species, with separated bones in a smaller specimen compared to a fused otic region in a larger specimen (Hawlitschek *et al.* 2021). By comparing the examined specimen of *Madatyphlops arenarius* with this smaller specimen of *Madatyphlops eudelini,* I also identify a similar morphology of the frontals, along with an overall shallower skull profile in lateral view, that supports the hypothesis that the included specimen of *Madatyphlops arenarius* may be a juvenile. This finding highlights the importance of understanding how ontogeny affects morphology in miniaturised taxa, and the need for more growth series of different species of Scolecophidia.

Understanding how fusion of bones changes through ontogeny appears to be of considerable importance for Typhlopidae. Though many Typhlopidae examined here possess the typical three components that contribute to the posterior aspect of the skull that houses the otic capsule (the paired supraoccipitals, prootics, and otooccipitals comprising of a fused exoccipital and opisthotic), in several species these bones are fused into a single otic complex which shows the variability of this feature across the clade. In *Indotyphlops braminus*, *Anilios leucoproctus*, and *Anilios bituberculatus*, the otic capsule is completely enclosed in a single bony element comprised of all three otic elements with no visible sutures, in contrast to the three separate elements as seen in the examined *Typhlops*, *Afrotyphlops*, and *Madatyphlops arenarius.* The precise function of a fused otic region relative to separate elements in Typhlopidae is unknown, although fusion of separate skull elements is a common trait among fossorial squamates. In fossorial taxa, the fusion of skull bones is suggested to be a method to reinforce the skull against the increased pressures of pushing the skull through a dense substrate. Further ecological information may inform whether this increased amount of fusion in the rear braincase allows these Typhlopidae species to burrow through denser soils and potentially access different prey species.

Additional information about ontogeny can be obtained through comparison of the examined *Afrotyphlops punctatus* with a recent description by Deolindo et al (2021), which shows the potential hidden morphological diversity in assigned species groups. While the size of the specimens examined by Deolindo et al (2021) were not explicitly mentioned in the text, the specimen ZFMK 78817 in figure 1 has a skull length of 9.9mm. This is considerably smaller than

the *A. punctatus* examined in the present study, which possesses a skull length of 13.5mm, which suggests that the specimen included in the study by Deolindo et al (2021) was a juvenile. As no geographic information was available for either specimen, these differences may be due to interspecific variation between populations. However, the hypothesis that the Deolindo et al (2021) specimen is a juvenile is supported by the presence of a small unfused section in the posterior extent of the dorsal surface of the parietal in the Deolindo et al (2021) specimen. There are considerable differences between the two descriptions. The rostral region of the examined specimen in the current study is expanded considerably, and the distinct dorsal ridges of the parietal and posteriorly projecting prootic crest are absent in the Deolindo et al (2021) specimen. This supports the hypothesis that these morphological features are only present in the largest Typhlopidae, and that their absence in most Scolecophidia is reflective of the small overall size, and that care must be taken to include ontogenetic series when discussing morphological characters that distinguish species from one another. The morphology of the septomaxilla of the two specimens is also different, with less marked lateral expansions of the ventral plate in the smaller Deolindo et al (2021) specimen compared to the larger examined specimen in the present study, again suggesting that this morphological character seen in the examined *Afrotyphlops* is a result of their larger body size.

The similarities between *Afrotyphlops punctatus* specimens also allow a greater understanding of features that are species specific, rather than indicative of size or age dependent variation. Interestingly, the position of the nasal foramina, a highly variable feature in the Typhlopidae examined in the current study, are consistent between the examined *A. punctatus* and the right nasal of the Deolindo et al. (2021) specimen, with a large foramen at the centre of the nasal, and a smaller one positioned at the lateral edge as a notch in the nasal. That the left nasal of the Deolindo et al. (2021) specimen has three foramina highlights the variability of this feature even within a single individual. The position of the trigeminal foramen, also shown to be highly variable in Typhlopidae, is in the same position in both the large specimen examined here and the small Deolindo et al. (2021) specimen. Additionally, the morphology of the premaxilla where the lateral edges of the premaxilla curve medially from the anterior edge to the septomaxillary process in a smooth curve, and the step-like medial septum, are consistent between both the examined specimen and the Deolindo et al. (2021) specimen. These comparisons between previously described specimens and the examined specimens in the current work show the importance of understanding ontogenetic changes when identifying morphological characters that distinguish species from one another.

4.1 Parietal – Paired or Singular

Another character that may result from paedomorphosis is the presence of paired parietals in snakes. The presence of paired parietal bones is a plesiomorphic feature for snakes and appears variably across Scolecophidia (List 1966). Previous studies have identified a paired parietal in the anamolepidids *Liotyphlops albirostris* (List 1966; Rieppel *et al.* 2009) and *Typhlophis squamosus* (Rieppel *et al.* 2009), the leptotyphlopid *Leptotyphlops emini* (List 1966) and in some Typhlopidae: *Indotyphlops braminus* (reported as *Typhlops braminus*), *Typhlops flaviventer*, *Typhlops pusillus*, *Typhlops boettgeri* (List 1966), and in *Xerotyphlops luristanicus* (Torki 2017). A recent study also identified the presence of a paired parietal in *Madatyphlops comorensis* and the newly described *Madatyphlops eudelini* (Hawlitschek *et al.* 2021). I have also identified a paired parietal in the examined *Madatyphlops arenarius*, suggesting that this is a feature shared amongst all *Madatyphlops* species. In all the taxa with paired parietals the parietals contact at a distinct suture, except for *I. braminus*, where the parietals are separated by a distinct gap or 'fissure'.

The presence of a paired parietal may be an indication of heterochrony, particularly the process of paedomorphosis where an adult individual retains juvenile characteristics, as a paired parietal is sometimes observed in juveniles of species that possess a single parietal as an adult. The parietal is paired in juveniles and fused in the adult in the typhlopid *Anilios bicolor* (Palci *et al.* 2016). Additionally, a study examining 19 specimens of *Typhlops jamaicensis* found that of these, the four smallest individuals possessed a paired parietal, which if body size is taken as a proxy for specimen age, suggests that paired parietals are more likely to be found in juveniles (Evans 1955). In this current study, three *Indotyphlops braminus* were examined, and all possessed paired parietals, as has been previously reported for this species (Mookerjee & Das 1932). Only one individual *Madatyphlops arenarius* was examined, leaving the possibility that the specimen studied was a juvenile, in addition to the previously mentioned characters of an unfused otic region and morphology of the frontals. However the recent descriptions of the newly discovered species *Madatyphlops eudelini* and its closely related species *Madatyphlops comorensis* reported paired parietals in both of these taxa, including small and large individuals of the same species (Hawlitschek *et al.* 2021). This suggests that the presence of paired parietals may be a diagnostic character of the genus *Madatyphlops*. Further description of the species within this genus will help confirm this diagnosis.

Both *Madatyphlops arenarius* and *Indotyphlops braminus* were among the smallest specimens examined, with skull lengths of 4.59mm and 4.28mm respectively. However, another small specimen examined, *Anilios leucoproctus,* that has a skull length of 4.4mm showed no suture line in the midpoint of the parietal, indicating that there is not a clear link between size of

a species and the presence of a paired parietal. Additionally there is a partially divided parietal present in *Anilios bituberculatus*, which has a skull length of 5.4mm, larger than that of the smaller species in the same genus, *A. leucoproctus*. Again the presence of a partially fused parietal in *A. bituberculatus* may be indicative of this specimen being a juvenile, or may be a developmental anomaly in the individual specimen.

Again, further study specifically comparing juvenile Typhlopidae with adult forms will help to elucidate whether all juvenile Typhlopidae share a paired parietal that variably fuses in the adult, particularly data from embryonic specimens. More comprehensive analysis of CT data of adults compared with overall body size would also help to inform whether the presence of a paired parietal is a factor of overall body size.

4.2 *Indotyphlops braminus* - Parthenogenesis, a possible source for unique anatomies

The unique reproductive habits of *Indotyphlops braminus*, that of obligate parthenogenesis, as well as its global habitat range have dominated discussions of this species. Although parthenogenesis is seen in a variety of different snake species (Booth *et al.* 2012; Booth & Schuett 2016; Groot *et al.* 2003; Kinney *et al.* 2013; Reynolds *et al.* 2012) as well as other squamates (Andrewartha *et al.* 2010; Lutes *et al.* 2011; MacCulloch *et al.* 1997; Sinclair *et al.* 2010; Tokarskaya *et al.* 2001; Watts *et al.* 2006), *I. braminus* is the only known snake to reproduce solely by parthenogenesis (Booth & Schuett 2016; McDowell 1974; Wynn *et al.* 1987). As of time of writing, no study has looked into what effect this reproductive strategy may have on the skeletal morphology of the adult animals.

Indotyphlops braminus, the only obligately parthenogenic snake, also possesses a range of unique anatomies when compared with other members of Typhlopidae. Most strikingly in comparison to the other species examined, most of the bones in the braincase are not in contact with one another, instead separated by fissures between the bones. These bones are likely connected by cartilage in the living animal, but these structures were not visible in CT scans that capture only bone. An increased reliance on cartilage to connect skull bones may be a factor of the small size of this species, however this is not seen in other miniaturised taxa. Instead, this increased reliance on cartilaginous connections may be an artefact of the low genetic diversity that obligately parthenogenic taxa, as non-adaptive traits have the potential to become fixed in such populations.

Due to the ability of this snake to reproduce through parthenogenesis, *Indotyphlops braminus* is thought to have one of the largest ranges of any terrestrial snake, with a worldwide distribution within subtropical and tropical regions (Afroosheh *et al.* 2010; Buden 2008; Cagle

1946; Clements *et al.* 2019; De Pous & Dingemans 2009; Fields & Horrocks 2011; Goldberg *et al.* 2005; Jesus *et al.* 2013; Kamosawa & Ota 1996; Lieberman & Lieberman 1970; McDowell 1974; Nussbaum 1980; Rato *et al.* 2015; Yokoyama 2012), likely through accidental introductions due the exotic plant trade (Nussbaum 1980; Wynn *et al.* 1987; Zamora-Camacho 2017). Although there has been some work into the external morphology of *I. braminus*, (Ota *et al.* 1991), little attention has been paid to the osteology of this interesting species, and the potential impact that their unique reproductive strategy may have on their morphology. Previous authors have noted extensive uniformity in the scale characters of *I. braminus*, and attributed this to low genetic diversity due to parthenogenesis (Ota *et al.* 1991). It is possible that low genetic diversity may also have similar effects in restricting morphological diversity of individual cranial bones, as well as contribute to the extensive fusion of the otic region and the increased space between cranial bones.

There are numerous characters present in the skull of *Indotyphlops braminus* that distinguish this species from the other species examined and could be useful in species diagnosis. Some of these characters relate to the overall contributions of bones to the different parts of the skull. The premaxilla contributes relatively more to the anterior face of the skull, and the prefrontals contribute to a larger portion of the dorsal snout. These features alter the overall profile of the skull of *I. braminus*. The premaxilla in particular has a distinctive morphology, including the medially projecting notch at the anterior edge and a reduced medial septum, both of which are characters not present in the other typhlopids examined. The functional importance of these characters are not clear, as the overall profile of the snout throughout typhlopids does not appear to alter with differences in size. Additional changes in the contribution of bones to portions of the skull is seen in the braincase. *I. braminus* possesses a much shorter posterior shelf of the parietal relative to the rest of typhlopids examined. This posterior shelf of the parietal does not overlap the otic complex, and likewise the dorsal lamina of the fused otic complex contributes to a larger portion of the braincase. The anterior portion of the braincase also differs in composition, with a reduced dorsal extent of the frontals and ventrally the straight edges of the anterior portion of the basisphenoid rather than triangular as seen in other examined typhlopids. The differences in the contribution of individual cranial elements in *I. braminus* relative to the other examined typhlopids highlights the plasticity of form in Typhlopidae, despite their previously understood conserved morphology.

I have also identified a couple of potential diagnostic characters that distinguish *Indotyphlops braminus* from other typhlopids. The ventrally positioned posteriorly projecting spur of the palatine and the horizontal ridges of the basioccipitals, in addition to the previously described unusual morphology of the premaxilla are not seen in any other species examined. Further examination of how these characters vary across individual *I. braminus* may help

confirm whether these characters are useful as diagnostic of the species. Further study should also include closely related species of *Indotyphlops*, as it is possible that the features identified as unique to *I. braminus* in the current study are characteristic of the genus rather than diagnostic of the species.

Previous work has suggested a diagnostic character of *Indotyphlops braminus* shared only with *Rhinotyphlops flaviventer*, is the lack of participation of the basioccipital in the occipital condyle (Wallach 2020). However in the specimen examined in the current study I find that the basioccipital does contribute to the occipital condyle, although not to the extent seen in the other asiatyphlopines, *Typhlops*, and *Afrotyphlops*. The basioccipital of examined *Madatyphlops arenarius* contributes to less of the occipital condyle than in *I. braminus*, which suggests that this character is dependent on size and not a reliable diagnostic character.

4.3 Giant Typhlopidae – *Afrotyphlops schlegelii* and *Afrotyphlops mucruso*

Although Typhlopidae are known for their small size, a few sub-Saharan African taxa of the genus *Afrotyphlops* have the ability to reach a relatively substantial body size. The largest Typhlopidae currently recorded are the Schlegel's Beaked Blind Snake, *Afrotyphlops schlegelii*, and the Zambezi Blind Snake, *Afrotyphlops mucruso*. These taxa can reach sizes of 900mm and 950mm respectively (Feldman *et al.* 2016; Hedges *et al.* 2014). While little is known about the ecology of these taxa, especially with regards to likely changes in habit corresponding to phenological shifts as taxa grow larger with age, it is possible that this larger size releases these species from the morphological constraints associated with miniaturisation. When comparing *A. mucruso* and *A. schlegelii* with their closest relative examined here, *Afrotyphlops punctatus*, there are considerable differences observable, despite the individual *A. punctatus* being of intermediate size between the specimen of *A. mucruso* and *A. schlegelii*. The most obvious difference is the overall shape of the skull, where the snout is wider than the braincase to a greater extent in both *A. schlegelii* and *A. mucruso*. This expanded rostral region may be due to increasing the main contact surface used during burrowing. The burrowing forces of Typhlopidae are higher than burrowing alethinophidians (Herrel *et al.* 2021), and so there are likely anatomical changes necessary with an overall increase in skull size.

Of the *Afrotyphlops* examined, both *Afrotyphlops schlegelii* and *Afrotyphlops mucruso* share a distinct notch between the two nasals, which is not present in *Afrotyphlops punctatus*, despite that particular specimen possessing a skull of intermediate size. The function of this notch in *A. schlegelii* and *A. mucruso* is unknown. It is not visible in observations of the external morphology, and as is present in both species it is unlikely to be a developmental abnormality.

Presumably in the living animal this space is filled with cartilage, although confirmation of this hypothesis would require dissection of specimens which is beyond the scope of this study. It may also have a function in supporting the 'beak' that facilitates burrowing in both of these species, possibly serving to cushion the braincase from the forces experienced when pushing through compact substrate. This also highlights that similar morphologies seen in both *A. schlegelii* and *A. mucruso* may be due to these species being sister taxa rather than a factor of body size. Further clarification of this will require a more careful examination of ontogenetic series within species of *Afrotyphlops*.

The parietal of the *Afrotyphlops* examined is distinct from the rest of the examined Typhlopidae in possessing prominent lateral projections along the anterior edge. There are also prominent lateral ridges that run from these projections to the back of the skull. These are presumably for the attachment of jaw adductor muscles. The presence of a laterally projecting anterior edge of the parietal and distinct adductor ridges show the parietal of *Afrotyphlops* approaching the morphology of the alethinophidian parietal. The need for increased attachment surfaces for jaw adductor muscles is unlikely due to a change in diet in these taxa. Previous diet studies into *Afrotyphlops* has shown that diet in these taxa does not differ considerably from small typhlopids, the giant blindsnakes *Afrotyphlops mucruso* and *Afrotyphlops schlegelii* also consume the larvae of eusocial insects such as ants and termites (Webb *et al.* 2001). Therefore it is unlikely that the large body size and distinct parietal anatomy achieved by these two species is due to a different dietary specialisation.

Additionally, a notable feature of the skulls of both *Afrotyphlops mucruso* and *Afrotyphlops schlegelii* is the apparent presence of dorsally projecting lateral wings of the basisphenoid. This feature has been interpreted in alethinophidians as an expanded basipterygoid process that has fused with the epipterygoid, providing an increased surface for the attachment of muscles such as the protractor pterygoideus and the retractor pterygoideus (McDowell 1967). Interestingly, this feature has previously been reported as absent in the Scolecophidian skull (McDowell 1967; Rieppel 1979a). The presence of these lateral wings in the basisphenoid of the largest extant typhlopids perhaps suggests that this character is more a function of size rather than a true character distinguishing scolecophidians from alethinophidians. Testing this would again require a more careful study of ontogenetic series within Typhlopidae, as well as comparisons of the morphology of species from a range of body sizes.

5. Conclusion

Digital disarticulation of 3D models generated from CT data opens up the potential for detailed descriptions of miniaturised taxa that are difficult to dissect and examine with the naked eye. These new techniques will allow the further exploration of anatomical changes, relating to size, ontogeny, and help to support phylogenetic hypotheses constructed with molecular data with morphological characters.

This study has identified numerous variable features in the skull of Typhlopidae, which were previously not thought to possess variation. In the giant blindsnakes, *Afrotyphlops schlegelii* and *Afrotyphlops mucruso*, the presence of distinct lateral processes of the parietal and the lateral wings of the basisphenoid shows that characters previously thought to be limited to alethinophidians can be present in scolecophidians when the individual species reach a large enough body size. Additionally, there are several unique characteristics of the parthenogenic blindsnake *Indotyphlops braminus* that deserve further study. These include the large fissures between the bones, the presence of a ventral projecting spur on the palatine, and the greater contribution of the otic complex to the dorsal surface of the skull.

This study has shown that, although considered to be morphologically conserved, the skulls of Typhlopidae are variable to a degree not previously appreciated. Future work focussing on interspecific variation in relation to size and age may help elucidate further complexities in the anatomy of these miniaturised snakes.

Bibliography

Adalsteinsson, S. A., Branch, W. R., Trape, S., Vitt, L. J., & Hedges, S. B. (2009). Molecular phylogeny, classification, and biogeography of snakes of the Family Leptotyphlopidae (Reptilia, Squamata). *Zootaxa*, **2244**, 1–50.

Afroosheh, M., Rastegar-Pouyani, N., Rajabizadeh, M., & Kami, H. G. (2010). The brahminy blind snake, *Ramphotyphlops braminus* (Daudin, 1803), a newcomer to iran (Ophidia: typhlopidae). *Zoology in the Middle East*, **50**(1), 135–137.

Andrewartha, S. J., Mitchell, N. J., & Frappell, P. B. (2010). Does Incubation Temperature Fluctuation Influence Hatchling Phenotypes in Reptiles? A Test Using Parthenogenetic Geckos. *Physiological and Biochemical Zoology*, **83**(4), 597–607.

Bell, C. J., Daza, J. D., Stanley, E. L., & Laver, R. J. (2021). Unveiling the elusive: X-rays bring scolecophidian snakes out of the dark. *The Anatomical Record*, (June), 1–8.

Booth, W., & Schuett, G. W. (2016). The emerging phylogenetic pattern of parthenogenesis in snakes. *Biological Journal of the Linnean Society*, **118**(2), 172–186.

Booth, W., Smith, C. F., Eskridge, P. H., Hoss, S. K., Iii, R. M., & Schuett, G. W. (2012). Facultative parthenogenesis discovered in wild vertebrates. *Biology Letters*, **8**, 983–985.

Buden, D. W. (2008). The Reptiles of Nauru. *Pacific Science*, **62**(4), 499–507.

Cagle, F. R. (1946). *Typhlops braminus* in the Marianas Islands. *Copeia*, **1946**(2), 101.

Chretien, J., Wang-Claypool, C. Y., Glaw, F., & Scherz, M. D. (2019). The bizarre skull of Xenotyphlops sheds light on synapomorphies of Typhlopoidea. *Journal of Anatomy*. doi:10.1111/joa.12952

Cignoni, P., Callieri, M., Corsini, M., Dellepiane, M., Ganovelli, F., & Ranzuglia, G. (2008). MeshLab: and Open-Source Mesh Processing Tool. In *Sixth Eurographics Italian Chapter Conference*, pp. 129–136.

Clements, S. L., Catania, S. V. L., & Searcy, C. A. (2019). Non-native species dominate herpetofaunal community patterns in both native and non-native habitat patches in urban Miami-Dade County. *Biological Invasions*, **21**(5), 1775–1788.

Cundall, D., & Irish, F. (2008). The Snake Skull. In C. Gans, A. S. Gaunt, & K. Adlre, eds., *Biology of the Reptilia. Volume 20. Morphology H. The Skull of Lepidosauria*, Society for the Study of Amphibians and Reptiles, pp. 352–692.

Cundall, D., & Rossman, D. A. (1993). Cephalic anatomy of the rare Indonesian snake *Anomochilus weberi*. *Zoological Journal of the Linnean Society*, **109**(3), 235–273.

De Pous, P. E., & Dingemans, D. J. (2009). The first record of Ramphotyphlops braminus from the Isle of Pines, New Caledonia. *Applied Herpetology*, **6**(4), 401–402.

Deolindo, V., Koch, C., & Joshi, M. (2021). To move or not to move ? Skull and lower jaw

morphology of the blindsnake Afrotyphlops punctatus (Leach, 1819) (Serpentes, Typhlopoidea, Typhlopidae) with comments on its previously advocated cranial kinesis. *The Anatomical Record*, (January), 1–13.

Evans, H. E. (1955). The osteology of a worm snake, Typhlops jamaicensis (Shaw). *The Anatomical Record*, **122**(3), 554–555.

Feldman, A., Sabath, N., Pyron, R. A., Mayrose, I., & Meiri, S. (2016). Body sizes and diversification rates of lizards, snakes, amphisbaenians and the tuatara. *Global Ecology and Biogeography*, **25**(2), 187–197.

Fields, A., & Horrocks, J. A. (2011). The Herpetofauna of Barbados: Anthropogenic impacts and conservation status. In A. Hailey, B. S. Wilson, & J. A. Horrocks, eds., *Conservation of Caribbean Island Herpetofaunas Volume 2: Regional Accounts of the West Indies*, Brill, pp. 89–104.

Figueroa, A., Mckelvy, A. D., Grismer, L. L., Bell, C. D., & Lailvaux, S. P. (2016). A species-level phylogeny of extant snakes with description of a new colubrid subfamily and genus. *PLoS ONE*, **11**(9), e0161070.

Gans, C. (1961). The feeding mechanism of snakes and its possible evolution. *American Zoologist*, **1**, 217–227.

Gauthier, J. A., Kearney, M., Maisano, J. A., Rieppel, O., & Behlke, A. D. B. (2012). Assembling the squamate tree of life : Perspectives from the phenotype and the fossil record. *Bulletin of the Peabody Museum of Natural History*, **53**(1), 3–308.

Goldberg, S. R., Bursey, C. R., & Telford, S. R. (2005). Metazoan Endoparasites of Four Species of Lizards, Gehyra mutilata, Hemidactylus frenatus (Gekkonidae), Mabuya cumingi, Mabuya multifasciata (Scincidae), and One Species of Snake, Ramphotyphlops braminus (Typhlopidae), from the Philippine Islands. *Comparative Parasitology*, **72**(1), 88–101.

Groot, T. V. M., Bruins, E., & Breeuwer, J. A. J. (2003). Molecular genetic evidence for parthenogenesis in the Burmese python, Python molurus bivittatus. *Heredity*, **90**(2), 130–135.

Haas, G. (1964). Anatomical observations on the head of *Liotyphlops albirostris* (Typhlopidae, Ophidia). *Acta Zoologica*, **45**(1–2), 1–62.

Haas, G. (1968). Anatomical observations on the head of *Anomalepis aspinosus* (Typhlopidae, Ophidia). *Acta Zoologica*, **49**(1–2), 63–139.

Hanken, J., & Wake, D. B. (1993). Miniaturization of body size: Organismal consequences and evolutionary significance. *Annual Review of Ecology and Systematics*, **24**, 501–519.

Hawlitschek, O., Scherz, M. D., Webster, K. C., Ineich, I., & Glaw, F. (2021). Morphological, osteological, and genetic data support a new species of Madatyphlops (Serpentes: Typhlopidae) endemic to Mayotte Island, Comoros Archipelago. *Anatomical Record*,

(January), 1–15.

Hedges, S. B. (2008). At the lower size limit in snakes: two new species of threadsnakes (Squamata: Leptotyphlopidae: *Leptotyphlops*) from the Lesser Antilles. *Zootaxa*, **30**, 1–30.

Hedges, S. B., Marion, A. B., Lipp, K. M., Marin, J., & Vidal, N. (2014). A taxonomic framework for typhlopid snakes from the Caribbean and other regions (Reptilia , Squamata). *Caribbean Herpetology*, **49**, 1–61.

Herrel, A., Lowie, A., Miralles, A., … Tolley, K. A. (2021). Burrowing in blindsnakes: A preliminary analysis of burrowing forces and consequences for the evolution of morphology. *Anatomical Record*, **304**(10), 2292–2302.

Jesus, J., Gonçalves, R., Spínola, C., & Brehm, A. (2013). First record of Ramphotyphlops braminus (Daudin, 1803) on Madeira island (Portugal). *Herpetozoa*, **26**(1/2), 106–109.

Kamosawa, M., & Ota, H. (1996). Reproductive Biology of the Brahminy Blind Snake (Ramphotyphlops braminus) from the Ryukyu Archipelago, Japan. *Journal of Herpetology*, **30**(1), 9–14.

Kinney, M. E., Wack, R. F., Grahn, R. A., & Lyons, L. (2013). Parthenogenesis in a brazilian rainbow Boa (Epicrates cenchria cenchria). *Zoo Biology*, **32**(2), 172–176.

Kley, N. J. (2001). Prey transport mechanisms in blindsnakes and the evolution of unilateral feeding systems in snakes. *American Zoologist*, **41**(6), 1321–1337.

Kley, N. J. (2006). Morphology of the lower jaw and suspensorium in the Texas blindsnake, Leptotyphlops dulcis (Scolecophidia: Leptotyphlopidae). *Journal of Morphology*, **267**, 494–515.

Kley, N. J., & Brainerd, E. L. (1999). Feeding by mandibular raking in a snake. *Nature*, **402**(November), 369–370.

Laver, R. J., Daza, J. D., Ellis, R. J., Stanley, E. L., & Bauer, A. M. (2021). Underground Down Under: Skull anatomy of the southern blind snake *Anilios australis* Gray, 1845 (Typhlopidae: Serpentes: Squamata). *Anatomical Record*, **304**(10), 2215–2242.

Lee, M. S. Y. (1998). Convergent evolution and character correlation in burrowing reptiles: towards a resolution of squamate relationships. *Biological Journal of the Linnean Society*, **65**, 369–453.

Lee, M. S. Y., & Scanlon, J. D. (2002). Snake phylogeny based on osteology, soft anatomy and ecology. *Biological Reviews of the Cambridge Philosophical Society*, **77**, 333–401.

Lieberman, D. D., & Lieberman, M. E. (1970). Record of the Brahminy blind snake, *Typhlops braminus*, from the island of Hawaii. *Pacific Science*, **24**(4), 528.

Lira, I., & Martins, A. (2021). Digging into blindsnakes' morphology: Description of the skull, lower jaw, and cervical vertebrae of two Amerotyphlops (Hedges et al., 2014) (Serpentes, Typhlopidae) with comments on the typhlopoidean skull morphological diversity. *The*

Anatomical Record, 1–17.

List, J. C. (1966). Comparative osteology of the snake families Typhlopidae and Leptotyphlopidae. *Illinois Biological Monographs*, **36**(36), 1–112.

Lutes, A. A., Baumann, D. P., Neaves, W. B., & Baumann, P. (2011). Laboratory synthesis of an independently reproducing vertebrate species. *Proceedings of the National Academy of Sciences*, **108**(24), 9910–9915.

MacCulloch, R. D., Murphy, R. W., Kupriyanova, L. A., & Darevsky, I. S. (1997). The Caucasian rock lizard Lacerta rostombekovi: A monoclonal parthenogenetic vertebrate. *Biochemical Systematics and Ecology*, **25**(1), 33–37.

McDowell, S. B. (1967). Osteology of the Typhlopidae and Leptotyphlopidae : A Critical Review. *Copeia*, **1967**(3), 686–692.

McDowell, S. B. (1974). A catalogue of the snakes of New Guinea and the Solomons, with special reference to those in the Bernice P. Bishop Museum. Part I. Scolecophidia. *Journal of Herpetology*, **8**(1), 1–57.

McDowell, S. B., & Bogert, C. M. (1954). The systematic position of Lanthanotus and the affinities of the anguinomorphan lizards. *Bulletin of the AMNH*, **105**, 1–142.

Miralles, A., Marin, J., Markus, D., Herrel, A., Hedges, S. B., & Vidal, N. (2018). Molecular evidence for the paraphyly of Scolecophidia and its evolutionary implications. *Journal of Evolutionary Biology*. doi:10.1111/jeb.13373

Mookerjee, H. K., & Das, G. M. (1932). Occurrence of a paired parietal bone in a snake. *Nature*, **130**, 629.

Nussbaum, R. A. (1980). The Brahminy Blind Snake (*Ramphotyphlops braminus*) in the Seychelles Archipelago: Distribution, variation, and further evidence for parthenogenesis. *Herpetologica*, **36**(3), 215–221.

Ota, H., Hikida, T., Matsui, M., Mori, A., & Wynn, A. H. (1991). Morphological variation, karyotype and reproduction of the parthenogenic blind snake, Raphotyphlops braminus, from the insular region of East Asia and Saipan. *Amphibia-Reptilia*, **12**, 181–193.

Palci, A., Lee, M. S. Y., & Hutchinson, M. N. (2016). Patterns of postnatal ontogeny of the skull and lower jaw of snakes as revealed by micro-CT scan data and three-dimensional geometric morphometrics. *Journal of Anatomy*, **229**(6), 723–754.

Pinto, R. R., Martins, A. R., Curcio, F., & Ramos, L. de O. (2015). Osteology and cartilaginous elements of *Trilepida salgueiroi* (Amaral, 1954) (Scolecophidia: Leptotyphlopidae). *The Anatomical Record*, **298**, 1722–1747.

Pyron, R. A., Burbrink, F. T., & Wiens, J. J. (2013). A phylogeny and revised classification of Squamata, including 4161 species of lizards and snakes. *BMC Evolutionary Biology*, **13**, 93.

Pyron, R. A., & Wallach, V. (2014). *Systematics of the blindsnakes (Serpentes: Scolecophidia:*

Typhlopoidea) based on molecular and morphological evidence. *Zootaxa*, Vol. 3829. doi:10.11646/zootaxa.3829.1.1

Rato, C., Silva-Rocha, I., Gonzalez-Miras, E., Rodriguez-Luque, F., Farina, B., & Carretero, M. A. (2015). A molecular assessment of European populations of Indotyphlops braminus (Daudin, 1803). *Herpetozoa*, **27**(3/4), 179–182.

Reynolds, R. G., Booth, W., Schuett, G. W., Fitzpatrick, B. M., & Burghardt, G. M. (2012). Successive virgin births of viable male progeny in the checkered gartersnake, Thamnophis marcianus. *Biological Journal of the Linnean Society*, **107**(3), 566–572.

Rieppel, O. (1979a). The braincase of *Typhlops* and *Leptotyphlops* (Reptilia: Serpentes). *Zoological Journal of the Linnean Society*, **65**, 161–176.

Rieppel, O. (1979b). The evolution of the basicranium in the Henophidia (Reptilia: Serpentes). *Zoological Journal of the Linnean Society*, **66**, 411–431.

Rieppel, O., Gauthier, J., & Maisano, J. (2008). Comparative morphology of the dermal palate in squamate reptiles, with comments on phylogenetic implications. *Zoological Journal of the Linnean Society*, **152**(1), 131–152.

Rieppel, O., Kley, N. J., & Maisano, J. A. (2009). Morphology of the skull of the white-nosed blindsnake, *Liotyphlops albirostris* (Scolecophidia: Anomalepididae). *Journal of Morphology*, **270**(5), 536–557.

Scanlon, J. D. (2006). Skull of the large non-macrostomatan snake Yurlunggur from the Australian Oligo-Miocene. *Nature*, **439**(7078), 839–842.

Sinclair, E. A., Pramuk, J. B., Bezy, R. L., Crandall, K. A., & Sites, J. W. (2010). Dna evidence for nonhybrid origins of parthenogenesis in natural populations of vertebrates. *Evolution*, **64**(5), 1346–1357.

Streicher, J. W., & Wiens, J. J. (2016). Phylogenomic analyses reveal novel relationships among snake families. *Molecular Phylogenetics and Evolution*, **100**, 160–169.

Tokarskaya, O. N., Kan, N. G., Petrosyan, V. G., … Ryskov, A. P. (2001). Genetic variation in parthenogenetic Caucasian rock lizards of the genus Lacerta (L. dahli, L. armeniaca, L. unisexualis) analyzed by DNA fingerprinting. *Molecular Genetics and Genomics*, **265**(5), 812–819.

Torki, F. (2017). A new species of blind snake, Xerotyphlops, from Iran. *Herpetological Bulletin*, (140), 1–5.

Uetz, P., Freed, P., & Hosek, J. (2019). The Reptile Database. Retrieved April 22, 2020, from http://www.reptile-database.org

Underwood, G. (1967). *A contribution to the classification of snakes*, London: British Museum.

Vidal, N., Marin, J., Morini, M., … Hedges, S. B. (2010). Blindsnake evolutionary tree reveals long history on Gondwana. *Biology Letters*, **6**(4), 558–561.

Wake, M. H. (1993). The skull as a locomotor organ. In J. Hanken & B. K. Hall, eds., *The Skull: Functional and Evolutionary Mechanics*, Chicago: University of Chicago Press.

Wallach, V. (2020). How to easily identify the flowerpot blindsnake, Indotyphlops braminus (Daudin, 1803), with proposal of a new genus (Serpentes: Typhlopidae). *Podarcis*, **11**(1).

Wallach, V., & Ineich, I. (1996). Redescription of a Rare Malagasy Blind Snake, Typhlops grandidieri Mocquard, with Placement in a New Genus (Serpentes: Typhlopidae). *Journal of Herpetology*, **30**(3), 367–376.

Watts, P. C., Buley, K. R., Sanderson, S., Boardman, W., Ciofi, C., & Gibson, R. (2006). Parthenogenesis in Komodo dragons. *Nature*, **444**(7122), 1021–1022.

Webb, J. K., Branch, W. R., & Shine, R. (2001). Dietary habits and reproductive biology of typhlopid snakes from Southern Africa. *Journal of Herpetology*, **35**(4), 558–567.

Webb, J. K., & Shine, R. (1993). Dietary habits of Australian blindsnakes (Typhlopidae). *Copeia*, **1993**(3), 762–770.

Wiens, J. J., Kuczynski, C. A., Smith, S. A., … Reeder, T. W. (2008). Branch lengths, support, and congruence: Testing the phylogenomic approach with 20 nuclear loci in snakes. *Systematic Biology*, **57**(3), 420–431.

Wynn, A. H., Cole, C. J., & Gardner, A. L. (1987). Apparent Triploidy in the Unisexual Brahminy Blind Snake , *Ramphotyphlops braminus*. *American Museum Novitates*, (2868), 1–7.

Yokoyama, M. (2012). Reptiles and Amphibians Introduced on St. Martin, Lesser Antilles. *IRCF Reptiles et Amphibians*, **19**(4), 271–279.

Zaher, H., Murphy, R. W., Arredondo, J. C., … Grazziotin, F. G. (2019). *Large-scale molecular phylogeny, morphology, divergence-time estimation, and the fossil record of advanced caenophidian snakes (Squamata: Serpentes)*. *Plos One*, Vol. 14. doi:10.1371/journal.pone.0216148

Zamora-Camacho, F. J. (2017). On the role of plant nurseries introducing Indotyphlops braminus (Daudin, 1803), in Spain. *Herpetozoa*, **30**(1), 69–72.

Zheng, Y., & Wiens, J. J. (2016). Combining phylogenomic and supermatrix approaches, and a time-calibrated phylogeny for squamate reptiles (lizards and snakes) based on 52 genes and 4162 species. *Molecular Phylogenetics and Evolution*, **94**, 537–547.

Chapter 4: Morphometric tests of hypotheses of homoplasy provide evidence for the fossorial origin of snakes.

Abstract

The discrepancy between phylogenetic hypotheses of relatedness for snakes constructed with either morphological or molecular data is well documented. One possible explanation for this discrepancy that has been postulated is the prevalence of homoplasy in snake morphology, particularly when species specialise to fossoriality. Understanding the correlation between certain morphologies and a fossorial ecology is therefore important for a further understanding of snake relationships. Here I use geometric morphometrics on the largest skull bone in snakes, the parietal, to analyse how shape relates to ecology. The parietal was chosen due to its importance in the snake skull, as well as its high morphological diversity across extant snakes. The parietal is also preserved in fossil taxa, including the Late Cretaceous stem-snake *Dinilysia patagonica*, which has been variably hypothesised to be fossorial and thus evidence of a fossorial origin for snakes. I segmented and landmarked the parietal of 73 species of extant snake in addition to *Dinilysia.* I conducted a principal component analyses on rescaled landmarks of all species. I also conducted a phylogenetically corrected principal component analysis using both a molecular hypothesis of relatedness between snakes and a morphological hypothesis of relatedness between snakes, to examine phylogenetic non-independence of shape change. Principal component analysis of parietal shape reveals a clear morphological difference between the parietals of fossorial taxa and the parietals of terrestrial taxa. Linear discriminant analysis of all principal components shows a clear separation of morphology by ecology. The parietal of *Dinilysia* appears in the morphospace most close to the fossorial taxa *Loxocemus bicolor* and *Xenopeltis unicolor*, suggesting a similar ecology for *Dinilysia*. This is confirmed by linear discriminant analysis, which predicted a fossorial ecology for *Dinilysia* after being trained on data from extant taxa. While previous studies on the inner ear morphology of snakes have disagreed on the estimated ecology of *Dinilysia*, this study provides clear support for a fossorial ecology for *Dinilysia* based on parietal morphology. This also shows the utility of geometric morphometrics in detecting potentially homoplastic characters, and has implications for the use of such characters when reconstructing patterns of relatedness between snakes, and how these homoplastic characters can be useful for deciphering the ecology of extinct organisms, particularly where fossilised material is fragmentary.

1. Introduction

Snakes are a speciose clade of squamates that have specialised into a variety of different ecologies, using the same specialised elongate limbless body plan. Due to this lack of limbs, locomotion in snakes is primarily through lateral undulation, with some species also able to perform other locomotive styles such as concertina, rectilinear, and side-winding (Lillywhite, 2014). Limblessness is known to correlate with many morphological features in tetrapods, including an elongate body, and increased cranial bracing (Gans, 1975). When such an animal adapts to fossoriality, there is a high probability that morphological adaptation will be concentrated on the skull. As the skull is also used in feeding, there are also likely to be trade-offs between morphological adaptation in order to maintain feeding ability. This limited ability to adapt differently to similar ecologies increases the likelihood of convergent evolution and therefore homoplasy. Additionally, convergent evolution, where organisms appear morphologically similar due to ecological specialisation rather than close phylogenetic relatedness, provides information about the role of adaptation in processes of evolution (Currie, 2013; Stayton, 2015). The specialised body plan of snakes, in combination with the wide range of ecological specialisations seen in this clade, make them an ideal study system for examining morphological convergence.

Convergent evolution can result in homoplastic morphological characters. The presence of homoplasy is particularly concerning for phylogenetic hypotheses constructed with morphological data as homoplastic characters have the potential to confuse our understanding of phylogenetic relationships. In squamates in general and snakes in particular, the discrepancies between phylogenies constructed with morphological or molecular data are well documented (Wiens et al., 2010), with several well established clades from phylogenies using morphological data not appearing when using molecular data. These include the Macrostomata and the Anilioidea (a clade uniting the fossorial pipe snakes, Aniliidae and Cylindrophiidae) that appear only in phylogenetic hypothesis constructed with morphological data (Romer, 1956; McDowell, 1975; Conrad, 2008; Gauthier et al., 2012). The discrepancies between phylogenetic hypotheses constructed with either morphological or molecular data may result from the inclusion of homoplastic characters in character lists, as these characters can confound attempts to reconstruct accurate phylogenetic relationships, particularly those characters associated with adaptation to fossoriality such as limblessness and miniaturisation (Gans, 1961, 1975; Greer, 1991; Hanken and Wake, 1993; Wake, 1993; Lee, 1998). There is therefore considerable benefit to examining the morphological convergence present in the snake skull as it relates to specialisation to different habitat types.

The snake-like elongate limbless body form has evolved over 25 times in non-snake squamates, and is almost always accompanied by a transition to a fossorial or semi-fossorial ecology (Wiens et al., 2006). Additionally, one of the theorised ecological origins for the evolution of the elongate limbless body plan in snakes is a fossorial habitat (Hsiang et al., 2015; Simões et al., 2015; Yi and Norell, 2015). Therefore, in the light of questions about the origin of snakes that concern the ecological habits that led to the evolution of the snakelike body as well as the correlation between the snake-like elongate body form and fossoriality, there is considerable importance to understanding morphological correlates with fossoriality.

While previous studies have focussed on linking ecology to the morphology of whole skull specimens (Palci et al., 2016; Da Silva et al., 2018; Watanabe et al., 2019), in my study I concentrated on a single skull bone. The parietal bone is the major skull roof bone in snakes. It connects the rostrum with the back of the braincase and the lateral edges of the bone project downwards and enclose the ophthalmic and eye-muscle nerves within the bony braincase. This unique morphology is a diagnostic character of snakes (Underwood, 1967). As this bone is a major component of the snake skull, it is probable that any changes in overall skull shape of snakes relating to ecological specialisation will be clear in the shape change of the parietal bone. Focussing on a single bone has considerable benefits over analyses using entire skull morphology. Due to the highly kinetic nature of the snake skull, specimens have a high likelihood of deformation, even when the bones themselves are undamaged. Focus on a single bone also allows more careful examination of the extent of sutures, including internal morphology and features that may be overlayed by other bones when looking at the skull as a whole. Focusing on a single bone also allows direct comparisons between taxa with very disparate overall skull shapes, and may help to identify distinct patterns of convergence that can influence future attempts to reconstruct relatedness based on morphological characters.

Characters describing the morphology of the parietal is a used in many morphological datasets that aim to inferring the phylogenetic relationships of higher-order snake clades, and the relationships of extant taxa to key Cretaceous fossils (Tchernov et al., 2000; Scanlon, 2005, 2006; Gauthier et al., 2012). It is therefore vital to understand what characters of the skull are homoplastic, and have the potential to confuse reconstructions of relationships, particularly in light of the importance of these fossils to future understanding of the ecological habitats that influenced snake origins.

In studies on convergence, it is important to compare like with like (Currie, 2013; Stayton, 2015). For this reason, I chose to exclude any representatives of the purported paraphyletic “Scolecophidia” from the current analysis. These snakes, which appear basal to all other extant snakes in phylogenetic analyses as either a monophyletic clade (when using morphological data), or a paraphyletic grade (as repeatedly recovered by molecular data), are a

highly specialised group of fossorial snakes. Their exclusion is justified by their considerable morphological divergence from all other known snakes. All three clades of Scolecophidia (Typhlopoidea, Leptotyphlopidae, and Anomalepididae) have adapted to an insectivorous fossorial life, with adaptations to the skull that facilitate these two important aspects of their ecology. The adaptation to insectivory, particularly myrmecophagy, where large numbers of small prey are ingested rapidly during one feeding event is unique to Scolecophidia, and the jaw architecture of the three main clades suggests that this was somewhat independent in the three clades. These techniques are maxillary raking in Typhlopoidea (with teeth only present on the maxilla) and Anomalepididae (with teeth present on the maxilla and dentary), and mandibular raking in Leptotyphlopidae (with teeth present only on the dentary) (Kley and Brainerd, 1999; Mizuno and Kojima, 2015). This is completely different to the strategy seen in all other extant snakes where a single prey item is swallowed whole in a single feeding event, (with only few exceptions, such as the crab-eating Homalopsidae, *Fordonia leucobalia* and *Gerarda prevostiana* which eat one prey item in multiple parts (Jayne et al., 2018), and the fish egg-eating sea snakes *Aipysurus eydouxii* and *Emydocephalus annulatus*, which eat entire clutches of fish eggs at once (Voris and Voris, 1983; Li et al., 2005)). Scolecophidia also actively burrow to a greater extent than seen in other burrowing snakes. When correcting for body size, Typhlopidae produce on average greater residual push force in N when compared to burrowing Alethinophidia (Herrel et al., 2021). Due to their considerable morphological uniqueness they were not included in this analysis, as the focus of the current study was on how repeated colonisations of fossorial habitats from multiple different terrestrial lineages affects parietal shape evolution.

Geometric morphometric analyses also has the potential to elucidate the ecological designations for specimens of which the ecology is unknown. Recent studies using geometric morphometrics to examine the inner ear morphology of extant snakes in relation to ecology have attempted to extrapolate the ecology of the Cretaceous snake *Dinilysia patagonica* (Yi and Norell, 2015; Palci et al., 2017). This fossil has most recently been recovered as a stem snake (Scanlon and Lee, 2000; Gauthier et al., 2012; Zaher and Scanferla, 2012; Caldwell et al., 2015), and therefore the ecology of this animal has considerable implications for our understanding of snake origins. Yi & Norrell (2015) concluded a fossorial ecology for *Dinilysia*, however Palci et al (2017) disagreed, claiming that the large spherical vestibule is also found in semi-aquatic taxa, despite using the same methods as Yi & Norrell (2015). By examining the parietal of *Dinilysia* I can determine if there is any independent evidence for a correlation between cranial morphology and ecology for this fossil snake.

2. Methods

2.1 Data Collection

Burrowing in snakes is a common ecology. As well as the typical fossorial taxa included in comparative studies such as aniliids and uropeltids, many caenophidian clades include fossorial taxa alongside terrestrial relatives, potentially representing repeated instances of the evolution of fossoriality. Due to the widespread instances of fossoriality across snakes, I included extant taxa from across the Serpentes clade to capture the diversity of snake skull morphology. Many of these clades, such as Elapidae, Lamprophiidae, and Colubridae, possess both terrestrial and fossorial members (See Table 1 for full species list). These clades are also reliably recovered as monophyletic in phylogenetic hypotheses constructed with either morphological or molecular data. Including both terrestrial and fossorial members of clades that are recovered as monophyletic whether using molecular or morphological data is important to identify any potential homoplastic characters present in the bone of interest. Sampling of caenophidians focussed on identification of fossorial taxa, along with closely related terrestrial species as per Zheng & Wiens (2016).

I quantified morphology of the parietal using computed tomography (CT) scans of alcohol-preserved specimens housed in museum collections. CT scans of snake skulls were obtained for 73 specimens, spanning 67 species. For specimens housed at the Museum of Zoology at Cambridge and the Natural History Museum of London, specimens were scanned at the Cambridge Biotomography Centre, Department of Zoology, University of Cambridge (CBC). The scanner is a Nikon XTEK H 225 ST MicroCT scanner that can achieve resolution of up to 3 microns. Other specimens were obtained from the digital repository MorphoSource at Duke University Research Computing from various sources. See Appendix 1 and 2 for full details of specimens including ARK number for specimens obtained from MorphoSource and full specimen numbers.

I processed the CT scans from stacks of TIFF files into 3D models using the 3D visualization software Avizo Lite (FEI Visualization Sciences Group, Oregon, USA). Initially scans were imported as TIFF stacks, and then segmented using the segmentation tools in the Avizo software. First I set a threshold that captured the density of bone in the scans. Then I used the 'magic wand' and 'paint brush' tools to manually segment scans further, as automatic tools do not pick up the distinction between adjacent bones. I first separated the skull from any associated vertebrae present in the scans, and then separated the parietal from the rest of the skull, with care taken to accurately separate along sutures with the adjacent bones visible in the scans.

Table 1. Specimens included in data analysis. Institutional Abbreviations: AMNH, American Museum of Natural History, New York, USA; BMNH, Natural History Museum, London, UK; CAS, California Academy of Sciences, San Francisco, USA; CBC, Cambridge Biotomography Centre; FRIM, Forest Research Institute Malaysia, Kuala Lumpur, Malaysia; FMNH, Field Museum of Natural History, Chicago, USA; KUNHM, Kansas University Natural History Museum, Lawrence, USA; LSUMZ, Louisiana State Museum of Natural History, Baton Rouge, USA; MVZ, Museum of Vertebrate Zoology, University of California, Berkeley, USA; UMMZ, University of Michigan Museum of Zoology, Ann Arbor, USA; UMZC, University Museum of Zoology Cambridge, Cambridge, UK; YPM, Yale Peabody Museum, New Haven, USA.

Species	Clade	Specimen Number	CT Scan Source
Anilius scytale	Aniliidae	BMNH 1855.5.28.23	CBC
Anilius scytale	Aniliidae	BMNH 1923.11.7.6	CBC
Anomochilus leonardi	Anomochilidae	frim:0026	MorphoSource
Candoia bibroni	Boidae	BMNH 1967.771	CBC
Casarea dussumieri	Boidae	ummz:herps:190285	MorphoSource
Epicrates cenchria	Boidae	UMZC R3.51-1	CBC
Exiliboa placata	Boidae	MVZ 137126	CBC
Sanzinia madagascariensis	Boidae	ku:kuh:183837	MorphoSource
Boiga irregularis	Colubridae: Colubrinae	ummz:herps:170417	MorphoSource
Coluber constrictor	Colubridae: Colubrinae	ummz:herps:225480	MorphoSource
Dasypeltis gansi	Colubridae: Colubrinae	ummz:herps:FS1352	MorphoSource
Drymarchon corais	Colubridae: Colubrinae	ku:kuh:289805	MorphoSource
Lampropeltis getula	Colubridae: Colubrinae	ummz:herps:218638	MorphoSource
Oligodon arnensis	Colubridae: Colubrinae	ummz:herps:65634	MorphoSource
Pantherophis guttatus	Colubridae: Colubrinae	lsumz:herps:88802	MorphoSource
Platyceps najadum	Colubridae: Colubrinae	ummz:herps:127487	MorphoSource
Ptyas mucosa	Colubridae: Colubrinae	ummz:herps169877	MorphoSource
Senticolis triaspis	Colubridae: Colubrinae	ummz:herps:111096	MorphoSource
Carphophis amoenus	Colubridae: Dipsadinae	ummz:herps:209970	MorphoSource
Elapomorphus quinquelineatus	Colubridae: Dipsadinae	ummz:herps:65879	MorphoSource
Phalotris mertensi	Colubridae: Dipsadinae	ummz:herps:63022	MorphoSource
Philodryas patagoniensis	Colubridae: Dipsadinae	ummz:herps:108987	MorphoSource
Pseudoboa coronata	Colubridae: Dipsadinae	ummz:herps:246839	MorphoSource
Xenodon neuwiedii	Colubridae: Dipsadinae	ummz:herps:63002	MorphoSource
Natrix natrix	Colubridae: Natricinae	ummz:herps:65465	MorphoSource
Nerodia sipedon	Colubridae: Natricinae	ummz:herps:205025	MorphoSource
Thamnophis rufipunctatus	Colubridae: Natricinae	ummz:herps:172510	MorphoSource
Cylindrophis lineatus	Cylindrophiidae	BMNH 1901.5.17-1	CBC
Cylindrophis melanotus	Cylindrophiidae	BMNH 1872.4.6.123	CBC
Cylindrophis ruffus	Cylindrophiidae	UMZC R4.12-1	CBC

Cylindrophis ruffus	Cylindrophiidae	UMZC R4.12-2	CBC
Cylindrophis ruffus	Cylindrophiidae	UMZC R4.12-3	CBC
Bungarus fasciatus	Elapidae	ummz:herps:201916	MorphoSource
Calliophis maculiceps	Elapidae	UMZC R9.221-1	CBC
Furina diadema	Elapidae	ummz:herps:83498	MorphoSource
Micruroides euryxanthus	Elapidae	ummz:herps:200295	MorphoSource
Micrurus fulvius	Elapidae	fmnh:amphibians and reptiles:39479	MorphoSource
Micrurus nigrocinctus	Elapidae	ummz:herps:131984	MorphoSource
Naja naja	Elapidae	UMZC R9.177-3	CBC
Notechis scutatus	Elapidae	ummz:herps:65874	MorphoSource
Oxyuranus scutellatus	Elapidae	lsumz:herps:94344	MorphoSource
Simoselaps bertholdi	Elapidae	ummz:herps:244197	MorphoSource
Vermicella annulata	Elapidae	UMZC R9.239-1	CBC
Amblyodipsas polylepis hildebrantii	Lamprophiidae: Aparallactinae	cas:herp:173555	MorphoSource
Aparallactus capensis	Lamprophiidae: Aparallactinae	cas:herp:11683	MorphoSource
Aparallactus modestus	Lamprophiidae: Aparallactinae	cas:herp:111865	MorphoSource
Aparallactus niger	Lamprophiidae: Aparallactinae	amnh:herpetology:r-142406	MorphoSource
Polemon christyi	Lamprophiidae: Aparallactinae	cas:herp:147905	MorphoSource
Homoroselaps lacteus	Lamprophiidae: Atractaspidinae	cas:herp:173258	MorphoSource
Boaedon fuliginosus	Lamprophiidae: Lamprophiinae	cas:herp:85747	MorphoSource
Psammophylax variabilis	Lamprophiidae: Psammophiinae	ummz:herps:61233	MorphoSource
Pseudaspis cana	Lamprophiidae: Pseudaspidinae	lsumz:herps:54361	MorphoSource
Duberria lutrix	Lamprophiidae: Pseudoxyrhophiinae	cas:herp:201763	MorphoSource
Heteroliodon occipitalis	Lamprophiidae: Pseudoxyrhophiinae	ummz:herps:229038	MorphoSource
Langaha madagascariensis	Lamprophiidae: Pseudoxyrhophiinae	ummz:herps:209371	MorphoSource
Lycodryas granuliceps	Lamprophiidae: Pseudoxyrhophiinae	ummz:herps:209566	MorphoSource
Loxocemus bicolor	Loxocemidae	BMNH 1988.354	CBC
Loxocemus bicolor	Loxocemidae	BMNH 1988.355	CBC
Aspidites melanocephalus	Pythonidae	fmnh:amphibians and reptiles:97055	MorphoSource

Malayopython reticulatus	Pythonidae	UMZC R3.24-4	CBC
Morelia spilota	Pythonidae	UMZC R3.22-4	CBC
Morelia spilota	Pythonidae	ummz:herps:227833	MorphoSource
Python molurus	Pythonidae	UMZC R3.25-7	CBC
Trachyboa boulengeri	Tropidophiidae	BMNH 1923.10.12.9	CBC
Tropidophis melanurus	Tropidophiidae	BMNH 1932.11.11.33	CBC
Plectrurus perroteti	Uropeltidae	UMZC R5.56-1	CBC
Rhinophis philippinus	Uropeltidae	UMZC R5.7-1	CBC
Teretrurus sanguineus	Uropeltidae	cas:herp:244362	MorphoSource
Uropeltis melanogaster	Uropeltidae	ummz:herps:96275	MorphoSource
Crotalus atrox	Viperidae	ummz:herps:11004	MorphoSource
Vipera aspis	Viperidae	ummz:herps:116957	MorphoSource
Xenopeltis unicolor	Xenopeltidae	BMNH 1912.6.26.3	CBC
Xenopeltis unicolor	Xenopeltidae	UMZC R6.1-2	CBC
Dinilysia patagonica	Fossil	MACN RN-1013	MorphoSource

2.2 Ecological designations

Applying a single signifier of ecology to a species is difficult, especially with snakes, where the elongate limbless body allows snakes to traverse a variety of different environments with ease (Lillywhite, 2014). Fossorial is a term to describe a sub-terranean burrowing ecology, where animals retreat under the ground for a variety of activities including hunting, refuge, and reproduction. As the difference between fossorial and semi-fossorial designations does not appear to have an agreed definition in the literature, all taxa that are reported as either fossorial or semi-fossorial in the literature were classed as fossorial in the current analysis. The clades Aniliidae, Xenopeltidae, Loxocemidae were classed as fossorial as per (O'Shea, 2018). *Anomochilus leonardi* was classed as fossorial as per (Gower et al., 2005). Uropeltidae were classed as fossorial as per (Olori and Bell, 2012). Within Colubridae: Dipsadinae, *Elapomorphus quinquelineatus* and *Phalotris mertensi* were classified as fossorial as per (O'Shea, 2018). Within Elapidae, the genera *Micrurus, Micruroides,* and *Calliophis* were classed as fossorial due to the reporting of *Micrurus fulvius* as fossorial (Jackson and Franz, 1981), *Simoselaps bertholdi* was classed as fossorial as per (How and Shine, 1999), and *Vermicella annulata* was classed as fossorial as per (Shine, 1980; Greenlees et al., 2005). Within Lamprophiidae, Amparallactinae and Atractaspidinae were classed as fossorial as per (Maritz and Alexander, 2009). Any taxa reported as either terrestrial, arboreal, or generalist were all designated as terrestrial in this analysis. See Appendix 1 for full list of species and associated ecological designations.

Figure 1. Parietal of *Dinilysia patagonica* MACN-RN1013 in context of rest of the skull fragment. A) Dorsal, B) Left Lateral. Scale bar =5mm

2.3 *Dinilysia patagonica*

This analysis also compared the parietal morphology of extant snakes with one fossil specimen. I segmented out the parietal of the Late Cretaceous snake, *Dinilysia patagonica* from an available scan of MACN-RN 1013, a partial braincase which includes an almost complete parietal (MACN-RN 1013, oUTCT provided access to these data originally appearing in Gauthier et al., 2012, with data collection funded by NSF EF-0334961 and data upload to MorphoSource funded by DBI-1902242. The files were downloaded from www.MorphoSource.org, Duke University.). During the segmentation process, I referenced Zaher & Scanferla (2012) in order to accurately identify the parietal from adjacent bones. This was necessary due to the breaks present in the specimen, which can be misidentified in the scans as suture lines. The suture lines were faint, and I identified them by reducing the threshold to a more narrow filter, which highlighted areas of higher density more likely to belong to the bone. The gaps between these regions of higher density were then identified as sutures between bones. This allowed me to identify and capture the distinct interdigitated anterior edge of the parietal previously identified in *Dinilysia* (Zaher and Scanferla, 2012).

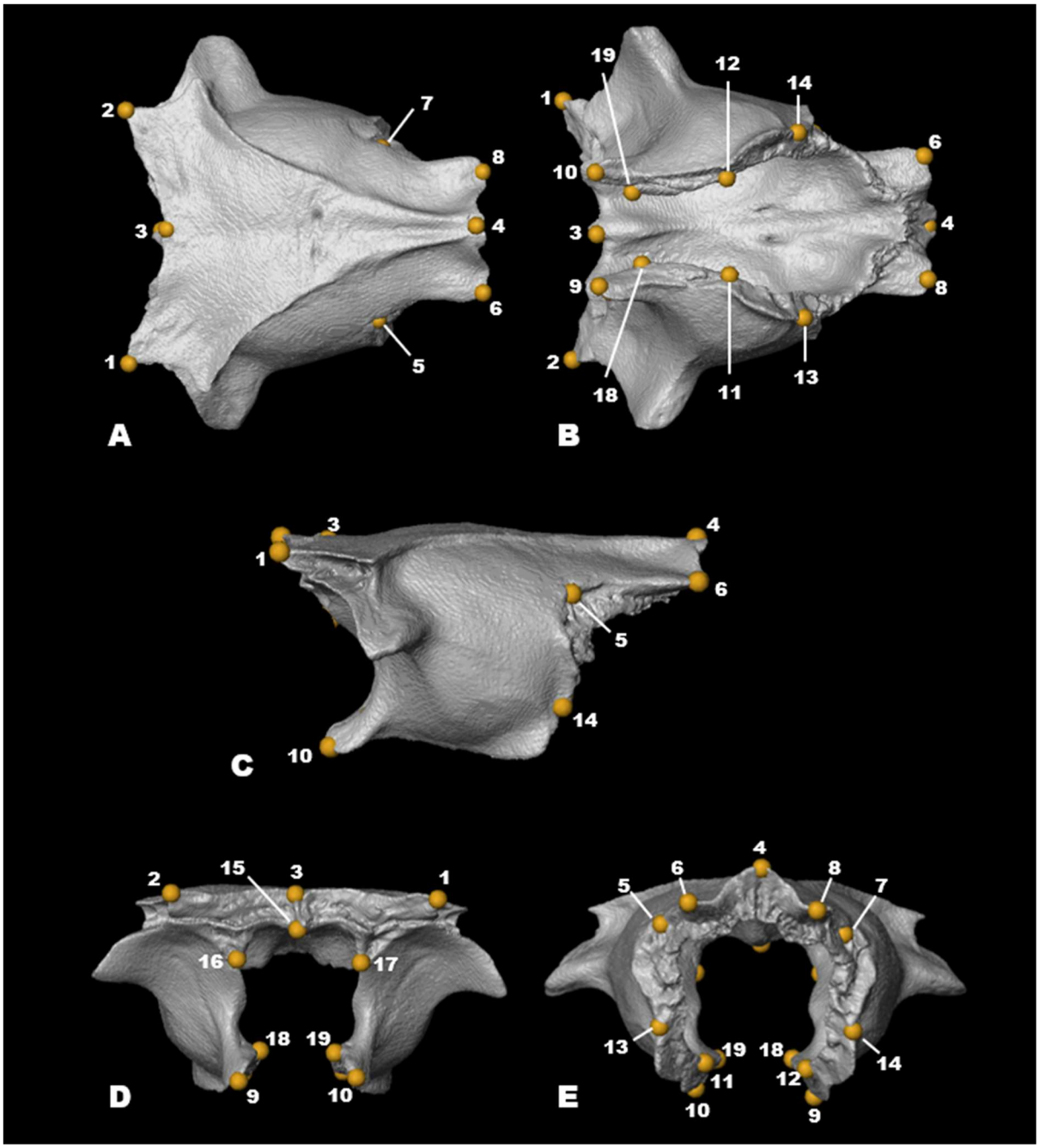

Figure 2. Landmark placement scheme on *Naja naja* (UMZC R9.177-3). A) Dorsal, B) Ventral, C) Left Lateral, D) Anterior, E) Posterior. See Table 2 for landmark descriptions.

2.4 Geometric morphometrics

I applied and extracted digital landmarks using the 'landmark editor' tool in project view of the Avizo Lite software. (See Table 2). Landmarks were chosen that best represented the overall shape of the parietal, and that were present in every species. Landmarks 1-3 relate to the anterior edge to capture variation between the straight anterior edge and the u-shaped/v-shaped anterior edge. Landmark 4 relates to the posterior extent of the midline of the parietal, which captures information about the overall length of the parietal. Landmarks 5-8 capture information about the overall extent of the posterior parietal shelf, particularly how the extent of the posterior shelf relates to the main body of the parietal. Landmarks 9-14 capture information about the ventral extent of the parietal, including how far the parietal wraps around the braincase. Landmarks 15-17 capture information about how the parietal sutures with the frontal, including the depth of the frontoparietal suture, and how far ventrally the contact between the frontals and the parietal extends. Landmarks 18-19 capture the extent to which the ventral edge of the anterior end of the parietal extends medially, which also varies considerably in snakes, with these two landmarks almost contacting one another in some taxa.

One feature not able to be captured by my landmark set is the extent of the lateral postorbital processes, which contribute to much of the overall triangular dorsal shape seen in terrestrial snake parietals. This was necessary to capture the shape change between fossorial and terrestrial snakes. Many prominent fossorial taxa, the uropeltids and *Anilius scytale* lack postorbitals which could signpost a homologous landmark in these taxa.

All subsequent analysis was conducted in R. Landmark coordinates were aligned using General Procrustes Analysis (GPA) using the function gpagen from the package *geomorph* v4.0 (Adams and Otárola-Castillo, 2013; Baken et al., 2021). GPA superimposes specimens to a common coordinate system, accounting for differences in size, orientation and position. These rescaled landmarks can then be utilised for further analyses. Using these rescaled landmark coordinates from all 73 extant species and the one fossil, I conducted a principal component analysis (PCA) using the gm.prcomp function in *geomorph*. This function performs a standard PCA based on ordinary least-squares centring and projection of input data. A principal component analysis extracts major axis of shape variation as variables called principal components. I produced warp grids for individual species that appear at the extremes of principal component values for PC1 and PC2 using the online gmShiny v0.1.1 tool. I used the package *ggplot2* to visualise results from PCA.

Table 2. Landmarks used for principal component analysis

No.	Description
1	Left lateral anterodorsal tip of frontoparietal suture on the parietal
2	Right lateral anterodorsal tip of frontoparietal suture on the parietal
3	Anterodorsal midpoint of frontoparietal suture on the parietal
4	Posterodorsal midpoint of supraoccipital suture on the parietal
5	Contact point of anterodorsal extent of left prootic
6	Left lateral tip of posterodorsal process (supratemporal process) of the parietal
7	Contact point of anterodorsal extent of right prootic
8	Right lateral tip of posterodorsal process (supratemporal process) of the parietal
9	Anterior tip of extent of right parietal downgrowth
10	Anterior tip of extent of left parietal downgrowth
11	Posterior tip of extent of right parietal downgrowth
12	Posterior tip of extent of left parietal downgrowth
13	Point of contact of parietal with basisphenoid and right prootic
14	Point of contact of parietal with basisphenoid and left prootic
15	Anteroventral midpoint of frontoparietal suture on the parietal
16	Anteroventral tip of suture with right frontal
17	Anteroventral tip of suture with left frontal
18	Most medial extent of the anterior tip of the left parietal downgrowth
19	Most medial extent of the anterior tip of the right parietal downgrowth

2.5 Phylogenetically informed geometric morphometrics

Due to the phylogenetic non-independence of morphological data from animals, it is important to consider trends of trait variation most independent from variation resulting from phylogenetic relatedness. To investigate phylogenetic signal I conducted a phylogenetically corrected PCA (pPCA), which corrects for non-independence in traits due to phylogenetic signal (Revell, 2009). There are many competing phylogenetic hypotheses for the interrelationships of snakes and the noncongruence between phylogenies constructed with either molecular or morphological data are well documented. For the phylogenetically informed analyses herein, I used two phylogenetic hypotheses that represent these differing results. For the phylogeny constructed using molecular data, I modified the large time-calibrated squamate tree from Zheng & Wiens (2016). This tree was constructed using combined phylogenomic and supermatrix methods and utilised two published datasets; one based on 44 genes for 161

species and one based on 12 genes for 4161 species (Zheng and Wiens, 2016). This tree was chosen due to its large taxonomic coverage, necessary when matching phylogenetic hypothesis with the available dataset for 3D skulls. The Serpentes clade was extracted from the total squamate clade and pruned to the number of taxa in this analysis. Where scanned taxa were not present in the Zheng & Wiens (2016) tree, they were added as bifurcating branches on clades of the same genus (ie. *Aparallactus niger* was added as sister taxon to *Aparallactus modestus + Aparallactus capensis*). Taxa with multiple specimens were added as polytomies (See Figure 3). For the morphologically informed hypothesis, I used the topology of the squamate tree recovered by Gauthier et al. (2012). This tree was constructed using 192 species and 610 phenotypic characters (Gauthier et al., 2012). Due to the lower number of snakes included, the topology of the tree was constructed so that their higher level relationships between clades represent those recovered by the Gauthier et al (2012) tree, but relationships between individual species within monophyletic clades remained the same as in Zheng & Wiens (2016) tree (See Figure 4). Using these phylogenetic hypotheses as input data, I implemented a phylogenetically corrected principal component analysis using the previously described geometric morphometric protocol. For both phylogenetic hypothesis I added *Dinilysia* as the earliest stem snake, as this fossil is recovered as either a stem snake (Scanlon and Lee, 2000; Gauthier et al., 2012; Zaher and Scanferla, 2012; Caldwell et al., 2015) or a stem alethinophidian (Zaher and Rieppel, 2002; Apesteguía and Zaher, 2006; Conrad, 2008; Wiens et al., 2010; Wilson et al., 2010)

2.6 Testing relationship between ecology and morphology

The relationships between the first ten principal components (which represent over 90% of the variation of shape) and ecology were analysed by a Student's t-test using the t.test function available in R, after testing for normality using a Shapiro-Wilk test, which tests whether a given dataset is from a normally distributed population. A t-test is used for normally distributed data, and determines whether the means of two datasets differ statistically. I tested the relationship further using linear discriminant analysis, which finds a linear combination of features that separates data based on inputted categories. Linear discriminant analysis using the package MASS was performed on the principal components to assess how shape relates to ecological designation. The values of the principal components were used as predictor variables for the linear discriminant analyses, with the ecological designations of 'terrestrial' and 'fossorial' used as categories. I first used extant taxa to test ability of the model to predict ecology of extant taxa. Afterwards I predicted the ecology of *Dinilysia* using the linear discriminant analyses values of the extant taxa as training data.

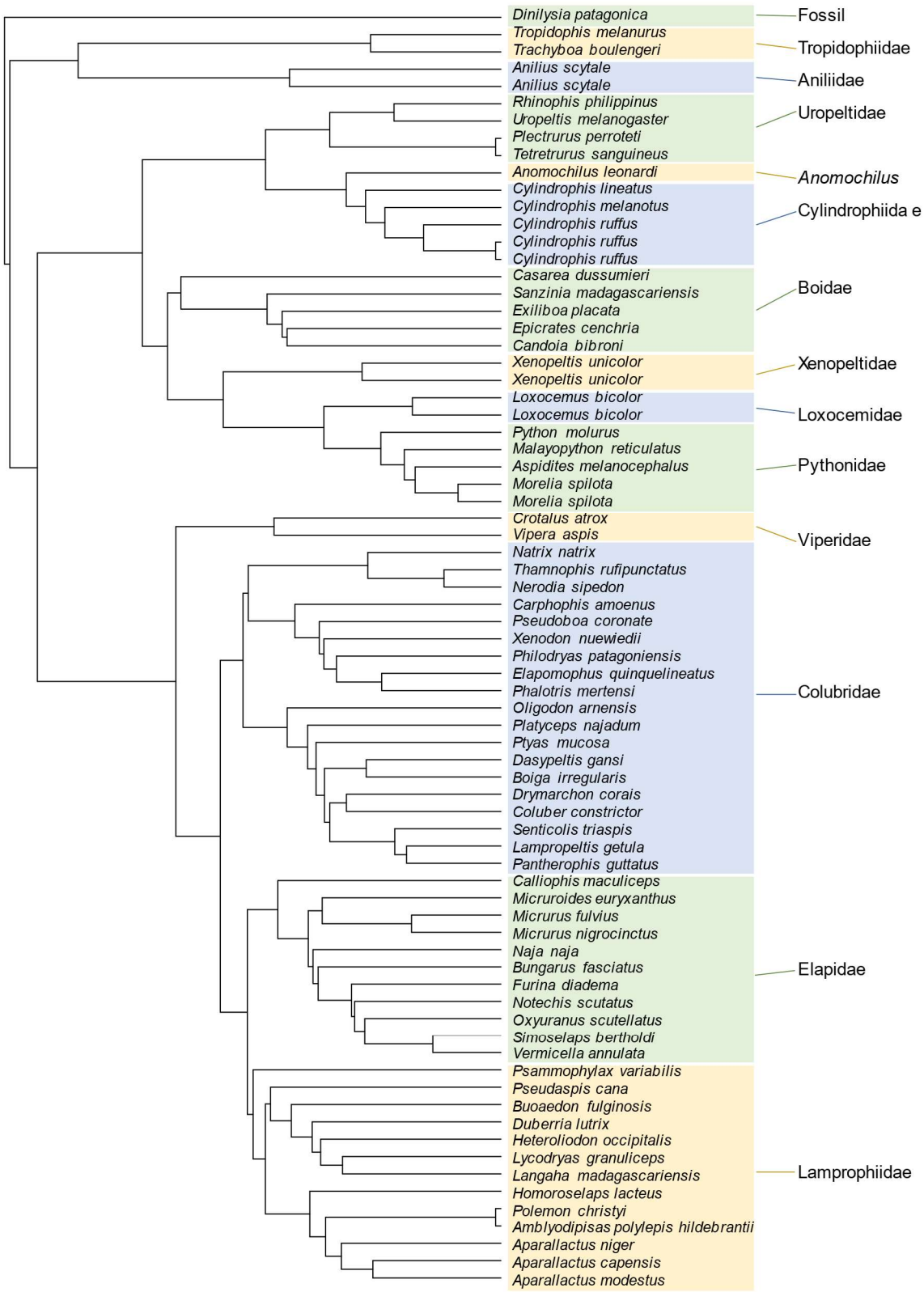

Figure 3. Phylogenetic relatedness of taxa based on molecular data, modified from Zheng & Wiens (2016)

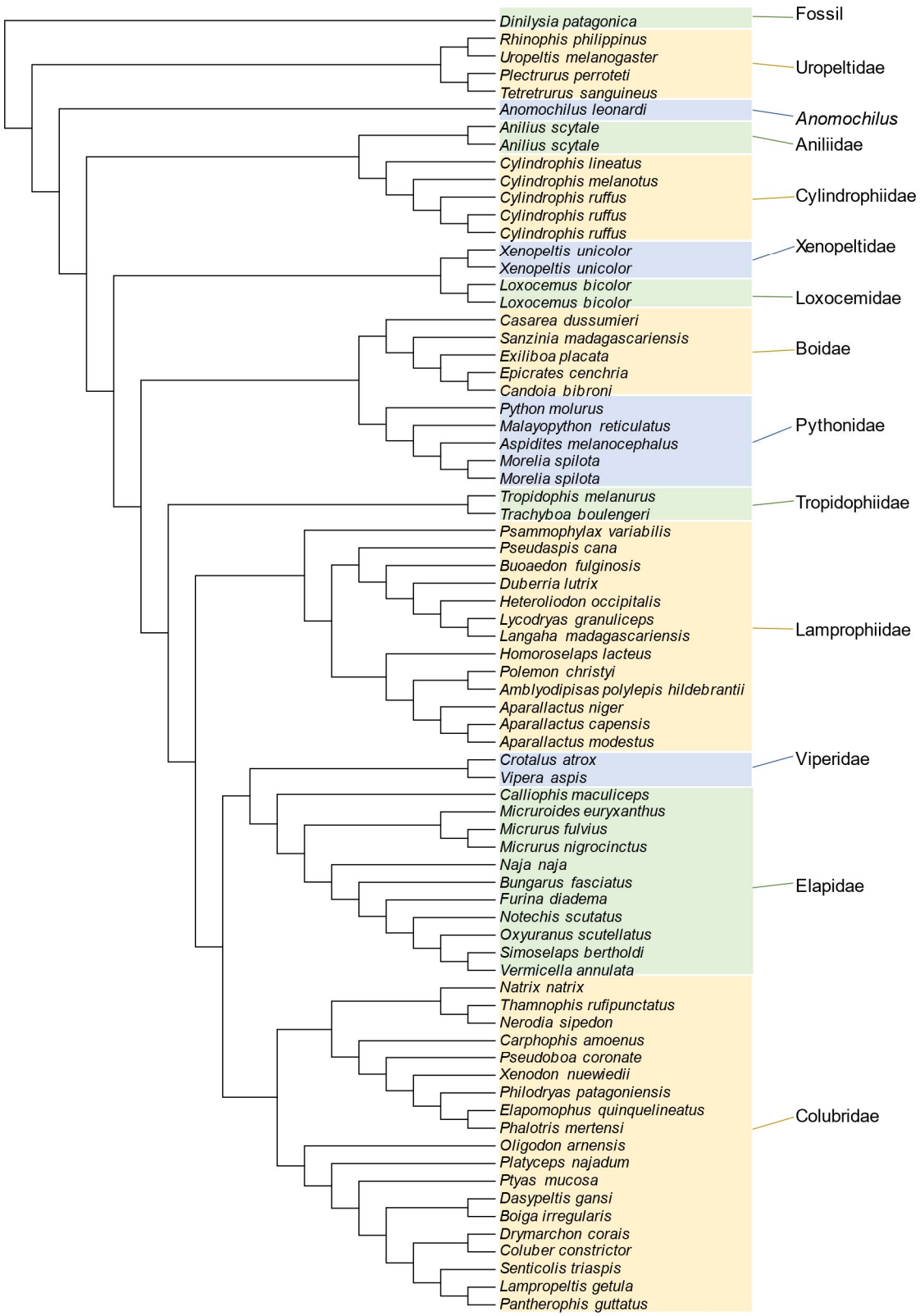

Figure 4. Phylogenetic relatedness of higher level clades based on morphological data, modified from Gauthier et al (2012). Interrelatedness between species based on Zheng & Wiens (2016)

3. Results

3.1 Parietal morphology

See Appendix 7 for figures of parietals in all views.

3.1.1 *Anilius scytale*

The parietal of *Anilius scytale* (Appendix 7 Figures 1-2) is elongate, greatly extending the postorbital portion of the braincase relative to other alethinophidians. In dorsal view, the parietal meets the frontals anteriorly in a deep v-shaped suture, the lateral supraorbital processes bounding the posterior extent of the frontals. The posterior shelf of the parietal extends over the otic complex in two large triangular processes, which extend both laterally and posteriorly further than the mid-point of the posterior edge of the parietal. The parietal of *Anilius* also possesses a sagittal crest, that begins at the anterior edge and increases in height towards the posterior edge. The lateral descending walls of the parietal curve medially at the ventral extent, forming a tube like structure. These lateral descending walls contact at the anterior end. The posterior edge of these lateral descending walls also possesses a small triangular process that projects posteriorly, positioned ventral to the posterior shelf of the parietal. In anterior view, the parietal of *Anilius scytale* (BMNH 1923.11.7.6) is more dorso-laterally flattened than the parietal of *Anilius scytale* (BMNH 1855.5.28.23). The parietal of the 1923 specimen also possesses a straighter profile in lateral view. These differences appear to be interspecific variation, as both specimens are of similar size.

3.1.2 Tropidophiidae

The parietal of tropidophiids (Appendix 7 Figures 3-4) is overall triangular in dorsal view, meeting the frontals in a shallow u-shaped suture that projects slightly anteriorly at the midline. Lateral to the contact with the frontals, the anterior edge makes contact with the postorbitals, forming a slightly posteriorly projecting triangular postorbital process. Of the two species examined, only *Tropidophis melanurus* possesses a small sagittal crest, that begins medial to the posterior edge of the lateral walls of the parietal, only on the posterior shelf of the parietal. The contact with the prootic is formed be a medial projection of the posterior edge of the lateral wall of the parietal, as well as a ventral projection of the dorsal shelf. In both taxa examined, the posterior shelf of the parietal is roughly triangular in shape. In *Trachyboa boulengeri* there is a small anteriorly projecting notch at the midline of this posterior shelf.

3.1.3 *Cylindrophis*

The morphology of the parietal of all *Cylindrophis* examined (Appendix 7 Figures 5-9) are broadly similar to that of *Anilius,* with an overall elongate shape and pronounced supraorbital processes that enclose the frontals. However there are some morphological differences that supports the molecular phylogenetic hypothesis. The morphology of the suture with the frontals varies between species. *Cylindrophis melanotus* has a deep v-shaped suture, whereas the suture in *Cylindrophis lineatus* shows some interdigitation, as seen in fossorial lizards. The three specimens of *Cylindrophis ruffus* vary in size, and therefore likely represent an ontogenetic series, particularly as all specimens were collected at the same time. In the smaller two specimens (UMZC R4.12-2 and UMZC R4.12-3), the frontoparietal suture is u-shaped, whereas in the largest of the specimens (UMZC R4.12-1) the suture is v-shaped. The supraorbital processes of specimen R4.12-1 are also considerably longer than in the other two specimens. The extent of the sagittal crest also varies between species. In *C. lineatus* and *C. melanotus* the sagittal crest begins halfway, extending to the posterior edge. In *C. ruffus*, the sagittal crest begins at the anterior edge in the two largest specimens, more prominent in the largest specimen. No sagittal crest is present in the smallest specimen, suggesting that the sagittal crest develops with age and/or size. The posterior shelf forms a less triangular process than seen in *Anilius*. In *C. lineatus,* the posterior edge of the shelf is w-shaped, with a small notch at the midline, a condition also seen in the two smallest *C. ruffus* specimens. In contrast, the posterior edge of the shelf in *C.ruffus* and *C. melanotus* has straight edges. In *C. melanotus,* this edge possesses a triangular notch on the right lateral extent, and a small semi-circular notch on the left lateral extent alongside a small foramen. In *C. ruffus*, the right lateral extent is straight, and the left lateral extent possesses a large triangular notch, the apex of which is closest to the midline of the parietal. In all species the lateral projections of the posterior shelf do project laterally from the anterior extent, but do not project past the posterior extent of the midline of the parietal as seen in *Anilius*. In all species, the ventral edges of the lateral walls of the parietal project medially, and contact one another in the largest *C. ruffus* specimen, as in *Anilius*.

3.1.4 *Anomochilus leonardi*

The parietal of *Anomochilus leonardi* (See Appendix 7 Figure 10) is similar in morphology to the smallest *Cylindrophis ruffus* specimen examined, sharing both a u-shaped frontoparietal suture and no sagittal crest. In contrast to *C. ruffus*, *Anomochilus* possesses a short, rectangular posterior shelf. The ventral edges of the lateral walls project medially only at the anterior extent of the parietal, and do not form a contact.

3.1.5 Uropeltidae

The parietal of uropeltids (See Appendix 7 Figures 11-14) have a distinctive morphology compared to all other alethinophidians, where the anterior part of the parietal is both lateromedially and dorsoventrally reduced compared to the posterior extent, which contributes to the triangular shaped skull of this clade. The supraorbital processes are thin and pointed, forming an almost square-shaped frontoparietal suture. Also uniquely, these supraorbital processes do not form part of the lateral wall of the parietal, instead meeting the anterior edge of the parietal at a right angle. Due to the pointed nature of uropeltid skulls, in dorsal view the lateral edges of the parietal become wider towards the posterior. The parietal shelf forms a generally wide u-shaped process. In *Plectrurus perroteti*, there is a small u-shaped notch at the midline of the shelf, and in *Rhinophis philippinus* there is a small triangular-shaped notch at the midline. The posterior shelf of *Teretrurus sanguineus* is more expanded at the lateral extents, forming a more m-shaped process. The posterior shelf of *Uropeltis melanogaster* has an irregular edge, but this may be due to scan quality. There is a small ridge present in the posterior midline of the parietals of *Plecturus perroteti* and *Teretrurus sanguineus*, that may relate to the attachment of jaw adductor muscles. These two species were also the largest of the four examined, and so this feature may be related to size. Unlike in most other species examined, the posterior edge of the lateral wall of the parietal does not project medially.

3.1.6 *Xenopeltis*

The parietal of *Xenopeltis unicolor* (Appendix 7 Figures 15-16) possess a u-shaped frontoparietal suture. The ridges that form the attachment for the jaw adductor muscles are more laterally positioned than in Cylindrophiidae, so while the midline of the parietal is raised it does not form a crest. This raised portion is thinner in the larger of the two specimens examined (BMNH 1912.6.26.3), suggesting that this feature is affected by ontogeny. The posterior shelf expands posterolaterally, and has a m-shaped posterior edge that is more distinct in the smaller specimen (UMZC R6.1-2). The supraorbital processes that form the frontoparietal suture are more distinct an anteriorly projected in the larger specimen, as well as possessing a small laterally projecting crest that is not present in the smaller specimen. The medial extents of the ventral edges also project slightly anteriorly.

3.1.7 *Loxocemus*

The parietal of *Loxocemus bicolor* (Appendix 7 Figures 17-18) is similar in overall morphology to *Xenopeltis unicolor*. The supraorbital processes of the parietal enclose the frontals in a u-shaped frontoparietal suture. The parietal shelf is more rectangular in dorsal view than seen in *X. unicolor*, with the lateral extents of the posterior shelf in line with the

anterior edge. There is also a triangular notch at the midline of the posterior edge, creating a m-shaped suture with the back of the braincase. The sagittal crest begins just anterior to this posterior shelf, and projects to the midline of the posterior edge. The medial extents of the ventral edge of the lateral walls approach one another to a greater extent than seen in *Xenopeltis*, but do not contact.

3.1.8 Pythonidae

The parietal of Pythonidae examined vary considerably in morphology (Appendix 7 Figures 19-23). In both *Morelia spilota* examined and *Aspidites melanocephalus,* there is a distinct sagittal crest that begins just posterior to the anterior edge. In *A. melanocephalus*, the front-parietal suture is u-shaped, with the ventral edge of the dorsal anterior edge projecting anteriorly in a triangular shaped process. The postorbital processes meet the post-orbitals in a triangular shaped suture. The parietal shelf in this taxa also has a complect morphology, consisting of the aforementioned sagittal crest, and two second processes lateral to this crest. The posterior shelf expands laterally from its projection from the parietal and then continues posteriorly. In *M. spilota* the anterior edge of the dorsal surface of the parietal is much wider than the posterior edge, and meets the frontals in a shallow v-shaped suture. The postorbital processes also meet the postorbitals in a triangular shaped suture, but this is less pronounced than seen in *A. melanocephalus*. The posterior shelf of both *Morelia spilota* examined projects posteriorly from its projection from the parietal. In *M. spilota* (UMMZ.HERPS.227833) the midline of the parietal that also possesses the sagittal crest projects posteriorly passed the lateral extents of the posterior shelf. In *M. spilota* (UMZC R3.22-4) the midline of the parietal posterior edge is in line with the lateral extents of the posterior shelf. The small size of both *Python molurus* (UMZC R3.24-4) and *Malayopython reticulatus* (UMZC R3.25-7) relative to estimated adult sizes of these species means it is probable that both these individuals are juveniles. Compared to the specimens of both *A. melanocephalus* and *M. spilota*, there are several clearly observable morphological differences. The anterior edge is much shallower, forming an almost straight edge in *P. molurus*, and the postorbital processes are greatly reduced. The overall braincase is more rounded in both presumed juvenile specimens. The sagittal crest is also greatly reduced. As in *M. spilota*, the posterior shelf of both *M. reticulatus* and *P. molurus* projects posteriorly from the body of the parietal in a straight edge. The posterior edge of this shelf has a triangular notch either side of the midline in *M. reticulatus*, and two u-shaped notches at the lateral edges in *P. molurus*.

3.1.9 Boidae

The morphology of the parietal of Boidae (Appendix 7 Figures 24-28) is similar to that of the Pythonidae. The parietal of *Candoia bibroni* and *Sanzinia madagascariensis* have a wide and shallowly curved frontoparietal suture, similar to that seen in the pythonid *Morelia spilota*. The sagittal crest begins halfway along the braincase, rather than beginning at the anterior edge as in pythonids, and has a greater dorsal extent in *S. madagascariensis*. In *Epicrates cenchria* this sagittal crest is greatly reduced, and the anterior edge forms a shallow u-shaped frontoparietal suture that has a small anterior projection at the midline. The parietal is raised at the posterior midline in both *Casarea dussumieri* and *Exiliboa placata*, but does not form a distinct crest. The frontoparietal suture in both of these taxa is m-shaped, formed by an anteriorly projecting midline, that is more pronounced in *C. dussumieri*. The postorbital processes of *C. dussumieri* and *E. placata* are also greatly reduced compared to the other boids examined. The posterior shelf of both *C. bibroni* and *S. madagascariensis* projects posteriorly from the body of the parietal in a straight edge. The midline of the parietal and sagittal crest project beyond the lateral extents of the posterior shelf. In *E. cenchria*, the posterior shelf is more triangular shaped on the right lateral extent, although the left lateral extent projects more. The morphology of the right lateral extent may be an artefact of scan quality, or individual variation. In *C. dussumieri*, the posterior shelf has an unusual morphology, where there are two posteriorly projecting triangular processes either side of the midline. In contrast, the posterior shelf of *E. placata* forms a v-shaped suture with the back of the braincase.

3.1.10 Colubridae

Three clades of Colubridae were included in this study: Colubrinae (Appendix 7 Figures 26-35), Dipsadinae (Appendix 7 Figures 36-41), and Natricinae (Appendix 7 Figures 42-44). The overall shape of colubrines is relatively conserved except for in *Boiga irregularis*. In the species *Coluber constrictor, Dasypeltis gansi, Drymarchon corais, Lampropeltis getula, Oligodon arnensis, Pantherophis guttatus, Platyceps najadum, Ptyas mucosa,* and *Senticolis triaspis*, the ridges that form the attachment for the adductor muscles are laterally positioned. The anterior edge forms a very shallow u-shaped frontoparietal suture. Laterally, this anterior edge curves posteriorly in a contact with the postorbitals, which ends just before the beginning of the lateral downgrowths. In most taxa the adductor ridges are visible. They begin ventral to the postorbital processes, and project posteriorly in a straight line, either to the posterior edge of the posterior shelf or forming a sagittal crest. A sagittal crest is visible in *Pantherophis gutattus* and *Senticolis triaspis*. The posterior shelf in all taxa is short, either rectangular or u-shaped, with an exception in *Pantherophis guttatus* where the midline of the parietal and sagittal crest projects posteriorly to the lateral extents of the posterior shelf. In contrast to other colubrines, the parietal of *Boiga*

irregularis is more triangular in shape, approaching the morphology of the larger boids. The adductor ridges begin just posterior to the lateral extents of the anterior edge, and project posteromedially to the midline of the parietal, forming the sagittal crest. In the specimen examined, the left of the parietal possesses a prominent postorbital process that contacts the postorbitals in an m-shaped suture. The right process of the specimen examined is broken, but as this process is not capture by the landmarks this would not affect the morphometric interpretation of this specimen.

In contrast Dipsadinae show considerable morphological diversity. The dipsadines, *Philodryas patagoniensis, Pseudoboa coronata*, and *Xenodon neuwiedii* all share a relatively short parietal in lateral view, with a u-shaped frontoparietal suture in dorsal view. In *P. patagoniensis* and *X. neuwiedii*, there are prominent laterally projecting postorbital processes that begin posterior to the anterior edge of the parietal. The postorbital processes of *P. coronata* is much reduced in comparison to these two other taxa. In both *P. coronata* and *X. neuwiedii*, the adductor ridges begin posterior to the postorbital processes and project posteriorly to the mid-point of the posterior edge in *P. coronata* and the lateral point of the posterior edge in *X. neuwiedii*. In *P. patagoniensis*, the adductor ridges begin anterior to the postorbital processes, and project to the mid-point of the posterior edge. An unusual morphology of the suture with the frontals is present in *P. patagoniensis*, where the ventral extents of this suture projects medially to contact at the midline. In contrast to the short parietals seen in the other dipsadines, the parietals of *Elapomorphus quinquelineatus* and *Phalotris mertensi* are elongated. The anterior edge forms a deep u-shaped frontoparietal suture. The posterior shelf is elongated, projecting considerably past the posterior edge of the lateral downgrowths of the parietal. This shelf is u-shaped in *E. quinquelineatus*, and wide with a straight posterior edge in *P. mertensi. P. mertensi* also possesses a prominent sagittal crest that begins halfway along the parietal. In contrast to the other dipsadines, the parietal of *Carphophis amoenus* has a distinctive morphology. The frontoparietal suture is u-shaped, although not to the extent seen in *E. quinquelineatus* and *P. mertensi*. There is also a small notch at the midline of the anterior edge, which possibly represents an unfused portion of the parietal. The overall parietal is relatively short, with a short u-shaped posterior shelf. No adductor ridges are visible, although there is a distinct ridge demarcating the dorsal surface from the lateral walls. No sagittal crest or postorbital processes are present.

The morphology of the natricines is most similar to that of *X. neuwiedii*. This includes the u-shaped frontoparietal suture with a small projection at the midline as well as the prominent postorbital processes that project posterior to the anterior edge. The adductor ridges begin either posterior or on the dorsal surface of these processes, and project to the midline to form a small sagittal crest in *Nerodia sipedon* and *Thamnophis rufipunctatus*. In *Natrix natrix*, the

adductor ridges end lateral to the midline. Relative to the other natricines examined, the parietal of *T. rufipunctatus* is more elongated, with longer lateral walls and a shorter anterior edge.

3.1.11 Elapidae

The morphology of the parietal of Elapidae also varies considerably (Appendix 7 Figures 48-58). Both *Bungarus fascuatus* and *Furina diadema* have overall short and rounded parietals, where the anterior edge and posterior edge are roughly the same width. The frontoparietal suture is u-shaped, from the edges of which project the postorbital processes. The adductor ridges project from the anterior edge in *F. diadema* and the midpoint of the postorbital processes in *B. fasciatus*. The posterior shelf in both of these taxa is short, u-shaped in *F. diadema* and rectangular in *B. fasciatus.* The coral snakes, *Calliophis maculiceps, Micruroides euryxanthus, Micrurus fulvius,* and *Micrurus nigrocinctus,* all have an elongate parietal. The frontoparietal suture is shallowly curved in *C. maculiceps*, but forms a u-shape in *Micrurus* and *Micruroides*. The posterior shelf is similar in morphology in *C. maculiceps*, *M. euryxanthus*, and *M. nigrocinctus*, forming a u-shaped process. By contrast, the posterior shelf of *M. fulvius* is a pointed triangular process. This species is also the only coral snake examined to possess a sagittal crest and adductor ridges, the latter of which begin on the postorbital processes and project posteromedially to the mid-point, where the sagittal crest continues to the posterior edge of the parietal. The parietal of *M. fulvius* is also more elongate than the other coral snakes examined, and the u-shaped process is more pronounced. The parietal of the larger elapids examined, *Naja naja*, *Notechis scutatus*, and *Oxyuranus scutellatus*, are similar in morphology. The frontoparietal suture is shallowly curved. Both *N. naja* and *N. scutatus* possess prominent laterally projecting postorbital processes, which are absent in *Oxyuranus scutellatus*. The adductor ridges of *N.naja* and *N. scutatus* project from the midpoint of the postorbital processes to just lateral to the midpoint of the posterior edge. These ridges are more prominent in *N. naja.* The posterior shelf of *N. naja* is rectangular, with a slight w-shaped morphology at the midline. By contrast the posterior shelf of *N. scutatus* projects anteriorly in a u-shaped notch. No adductor ridges are visible in *O. scutellatus*, but there is a small sagittal crest that projects along the midline of the u-shaped posterior shelf. Both *Simoselaps bertholdi* and *Vermicella annulata* have a u-shaped frontoparietal suture, although *S. bertholdi* has an anteriorly projecting triangular process at the midline. The postorbital processes are more pronounced in *S. bertholdi* than *V. annulata*. The posterior shelf of both of these taxa is u-shaped. As with the coral snakes, the parietal is more elongate than in other elapids, to a greater extent in *V. annulata*. Adductor ridges are faintly visible on *S. bertholdi*, but absent on *V. annulata.*

3.1.12 Lamprophiidae

The parietal of the lamprophiids was also highly variable (Appendix 7 Figures 59-71). *Amblyodipsas polylepis hildebrantii*, *Aparallactus capensis*, *Aparallactus modestus*, and *Aparallactus niger*, all possess an elongate parietal with no sagittal crest. The frontoparietal suture of these taxa has a deep u-shape, with short, posteriorly projecting postorbital processes. The adductor ridges are short, and begin midway along the parietal, ending at the lateral edges of the posterior shelf. The parietals of *Polemon christyi* and *Homoroselaps lacteus* are even more elongated, also possessing a u-shaped frontoparietal suture and a u-shaped posterior shelf, although there is a small anteriorly projecting triangular notch in *P. christyi*. Both of these taxa also possess small but distinct sagittal crests that begin just posterior to the anterior edge, and project along the parietal to the posterior edge. The other lamprophiids examined (*Boaedon fulginosus, Psammophylax variabilis, Pseudaspis cana, Duberria lutrix, Heteroliodon occipitalis, Langaha madagascariensis,* and *Lycodryas granuliceps*) all possess short parietals. The frontoparietal suture is either straight or very shallowly curved, and there are short laterally projecting postorbital processes. The adductor ridges begin at the lateral extents of the anterior edge in *B. fulginosus, P. variabilis,* and *L. granuliceps*, and at the midpoint of the postorbital processes in *L. madagascariensis.* The posterior shelf in all of these taxa is u-shaped, and only *B. fulginosus* has a sagittal crest. The parietal of *P. cana* has an irregular anterior and posterior edge, and the posterior shelf is much reduced. The parietal of *D. lutrix* has a flat dorsal surface, with a laterally projecting ridge that surrounds the whole parietal.

3.1.13 Viperidae

The two viperids included differ in morphology (Appendix 7 Figures 72-73). The frontoparietal suture is straight in both taxa examined, *Crotalus atrox* and *Vipera aspis*. The parietal of *C. atrox* is wider than *V. aspis,* with large posteriorly projecting lateral postorbital processes. The adductor ridges begin posterior to these processes, and project in a curve to the anterior extent of the posterior shelf. The dorsal surface of the parietal projects laterally. The posterior shelf is triangular, with a anteriorly projecting triangular notch at the mid-point. In contrast there are no visible adductor ridges in *V. aspis* or lateral processes of the dorsal surface. The posterior shelf is u-shaped, with no notch visible, and the postorbital processes are short.

3.1.14 *Dinilysia patagonica*

The parietal of *Dinilysia patagonica* is almost complete, although enough of the bone is present to assign homologous landmarks. There is a breakage line that separates the anterior portion from the rest of the parietal, but there is no distortion. The parietal is elongate in dorsal view, with a prominent sagittal crest that begins from the anterior edge. The frontoparietal

suture is largely straight, with some interdigitation at the midline. There are no visible adductor ridges. The posterior shelf is expanded at the posterior edge, and appears to form a slight u-shaped edge although breakages in the specimen make this difficult to ascertain. The parietal of *Dinilysia patagonica* also possesses a shelf-like lateral process, which does not appear to be present in any other extant species. This feature has previously been noted in *Dinilysia* (Estes et al., 1970; Caldwell and Albino, 2003; Zaher and Scanferla, 2012) and in the madtsoiid *Wonambi naracoortensis* (Scanlon, 2005)

3.2 Geometric Morphometrics

PCA of parietal shape produced 50 principal components, the first 10 of which correspond to over 90% of total variance in shape (See Table 3). The main axis of variation, principal component 1 (PC1) accounts for 43.3% of total variance in parietal shape. PC1 corresponds to overall elongation of the parietal, expansion of the posterior parietal shelf, and the deep v or u-shaped anterior edge of the parietal. Comparison of the warps of *Anilius scytale* (lowest value of PC1 -0.3087) and *Pseudaspis cana* (highest value of PC1 0.2569) reveals specific morphological characters that relate to the extremes of this principal component (See Figure 6). Relative to the mean shape, the warp for PC1 of *Anilius*, and therefore the shape component that is represented by negative values of PC1, is narrower. This is seen both in the X,Y dimension (corresponding to mediolateral narrowing) and the Y,Z dimension (corresponding to dorsoventral narrowing). At the negative extreme of PC1, landmarks 1 and 2 are anteriorly projected, representing the pronounced u-shaped anterior edge in taxa with negative PC1 values. Additionally in the Y,Z warp grid, the overall profile of the parietal of *Anilius* is narrower, particularly at the anterior end. This corresponds to an overall narrowing of the snout complex in taxa with negative PC1 values.

Table 3. Eigenvalues of first 10 principal components

Principal Component	**PC1**	**PC2**	**PC3**	**PC4**	**PC5**
Eigenvalues	0.018831	0.004938	0.004154	0.003565	0.00215
Proportion of Variance	0.432722	0.113464	0.095451	0.081923	0.049399
Cumulative Proportion	0.432722	0.546186	0.641637	0.72356	0.772959

Principal Component	**PC6**	**PC7**	**PC8**	**PC9**	**PC10**
Eigenvalues	0.001901	0.001467	0.001033	0.000886	0.000811
Proportion of Variance	0.043694	0.033722	0.023736	0.020367	0.018629
Cumulative Proportion	0.816654	0.850375	0.874111	0.894478	0.913107

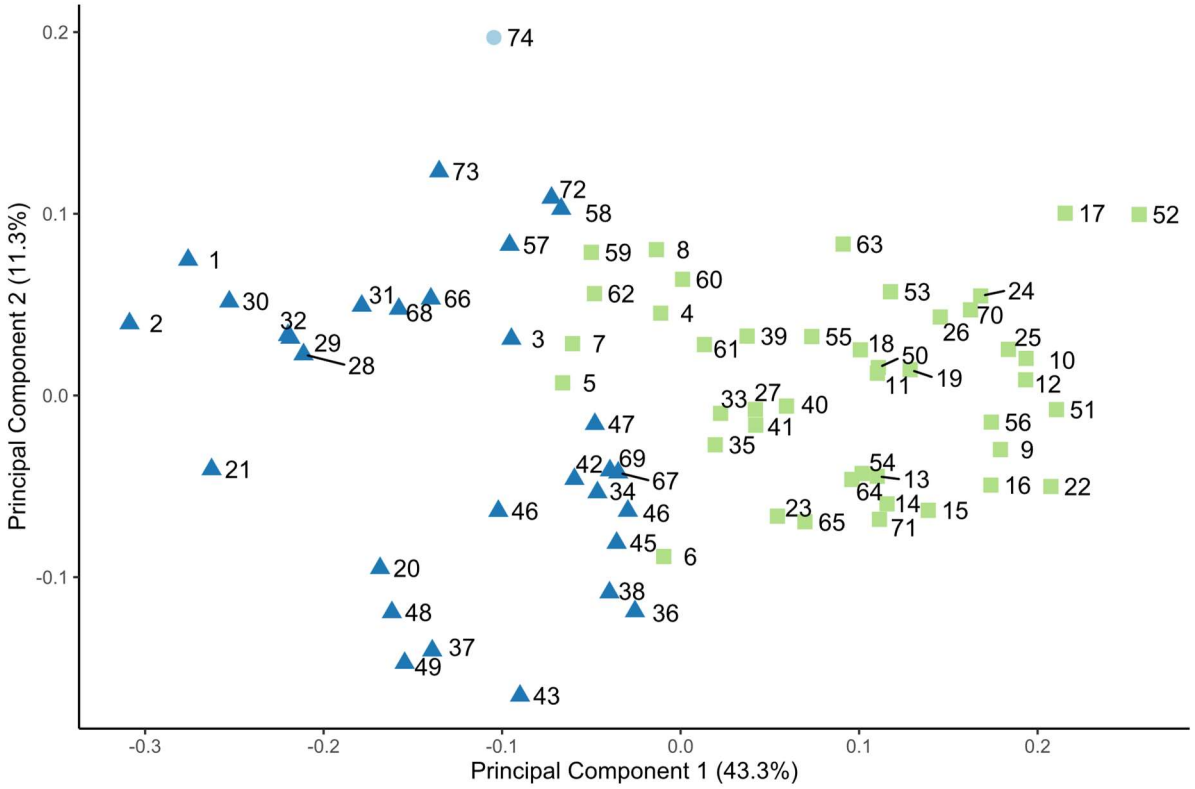

Figure 5. Principal component analysis. Principal component 1 (43.5% of variation) and principal component 2 (11.3%). Colours and shapes by ecological category: Dark blue triangles – Fossorial, Light green squares – Terrestrial, Light blue circle - Fossil. See Appendix 1 for specimen numbers

Species: 1 Anilius scytale, 2 Anilius scytale, 3 Anomochilus leonardi, 4 Candoia bibroni, 5 Casarea dussumieri, 6 Epicrates cenchria, 7 Exiliboa placata, 8 Sanzinia madagascariensis, 9 Boiga irregularis, 10 Coluber constrictor, 11 Dasypeltis gansi, 12 Drymarchon corais, 13 Lampropeltis getula, 14 Oligodon arnensis, 15 Pantherophis guttatus, 16 Platyceps najadum, 17 Ptyas mucosa, 18 Senticolis triaspis, 19 Carphophis amoenus, 20 Elapomorphus quinquelineatus, 21 Phalotris mertensi, 22 Philodryas patagoniensis, 23 Pseudoboa coronata, 24 Xenodon neuwiedii, 25 Natrix natrix, 26 Nerodia sipedon, 27 Thamnophis rufipunctatus, 28 Cylindrophis lineatus, 29 Cylindrophis melanotus, 30 Cylindrophis ruffus, 31 Cylindrophis ruffus, 32 Cylindrophis ruffus, 33 Bungarus fasciatus, 34 Calliophis maculiceps, 35 Furina diadema, 36 Micruroides euryxanthus, 37 Micrurus fulvius, 38 Micrurus nigrocinctus. 39 Naja naja, 40 Notechis scutatus, 41 Oxyuranus scutellatus, 42 Simoselaps bertholdi, 43 Vermicella annulata, 44 Amblyodipsas polylepis hildebrantii, 45 Aparallactus capensis, 46 Aparallactus modestus, 47 Aparallactus niger, 48 Polemon christyi, 49 Homoroselaps lacteus, 50 Boaedon fuliginosus, 51 Psammophylax variabilis, 52 Pseudaspis cana, 53 Duberria lutrix, 54 Heteroliodon occipitalis, 55 Langaha madagascariensis, 56 Lycodryas granuliceps, 57 Loxocemus bicolor, 58 Loxocemus bicolor, 59 Aspidites melanocephalus, 60 Malayopython reticulatus, 61 Morelia spilota, 62 Morelia spilota, 63 Python molurus, 64 Trachyboa boulengeri, 65 Tropidophis melanurus, 66 Plectrurus perroteti, 67 Rhinophis philippinus, 68 Teretrurus sanguineus, 69 Uropeltis melanogaster, 70 Crotalus atrox, 71 Vipera aspis, 72 Xenopeltis unicolor, 73 Xenopeltis unicolor, 74 Dinilysia patagonica

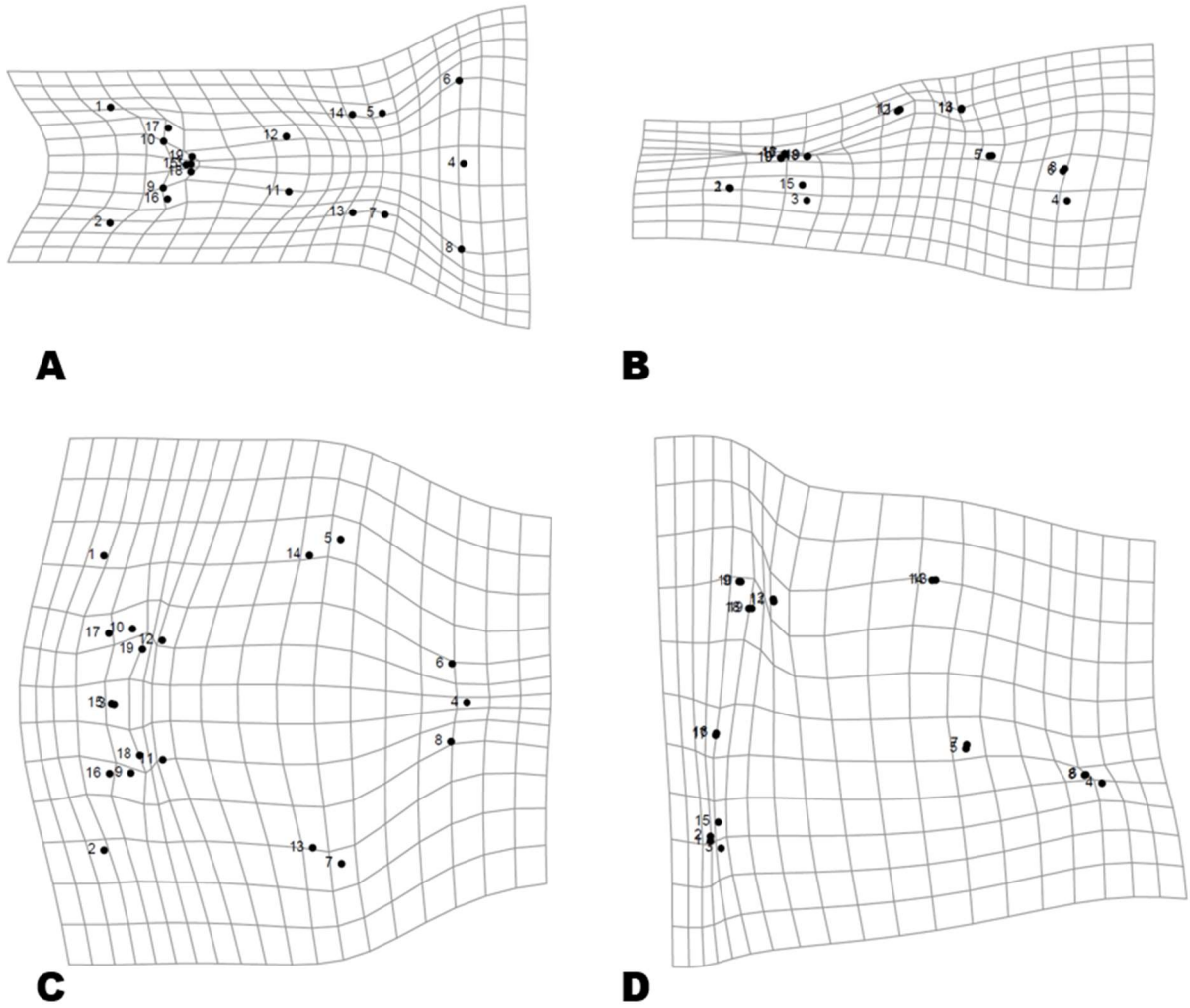

Figure 6. Warp grids for extremes of principal component 1. A) *Anilius scytale*, xy warp, B) *Anilius scytale,* yz warp. C) *Pseudaspis cana,* xy warp, D) *Pseudaspis cana*, yz warp.

In comparison, the warp for PC1 of *Pseudaspis cana*, representing the extreme positive extent of PC1 is wider overall. Landmarks 1 and 2 cluster with landmarks 3 and 15 in the Y,Z dimension, which represents how the anterior end of the parietal of *P. cana* is more horizontally oriented, with a straight frontoparietal suture. Additionally there is a distinct narrowing of the posterior shelf, with landmarks 6 and 8 more medially positioned at the positive extreme of PC1. The parietal is also wider in the Y, Z dimension, which corresponds to a shorter parietal in these taxa.

Principal component 2 (PC2) accounts for 11.3% of the total variance in parietal shape. PC2 corresponds to the narrowing of the posterior parietal shelf, as well as narrowing of the anterior end. Comparison of the warps of *Vermicella annulata* (lowest value of PC2

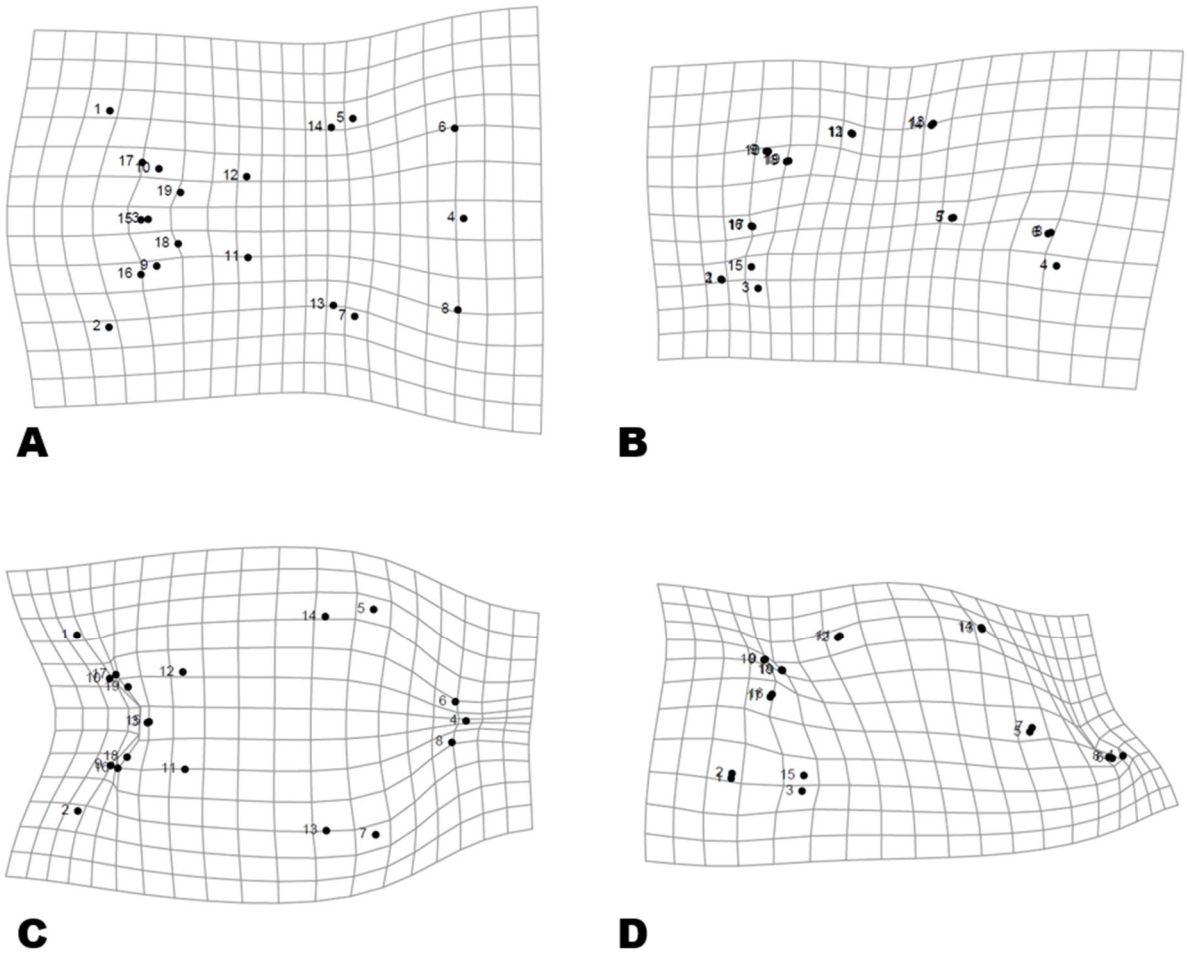

Figure 7. Warp grids for extremes of principal component 2. A) *Xenopeltis unicolor*, xy warp, B) *Xenopeltis unicolor,* yz warp. C) *Vermicella annulata*, xy warp, D) *Vermicella annulata*, yz warp.

-0.165251584) and *Xenopeltis unicolor* (highest value of PC2 0.123326921) also reveals specific morphological characters that are represented by this principal component (See Figure 7). Relative to mean shape, at the lowest value of PC2 the parietal is narrower at the anterior end. This principal component also captures part of the u or v-shaped anterior end. The negative extreme of PC2 also corresponds to a significant narrowing of the posterior shelf, as those taxa with these values often have a u or triangular shaped posterior shelf. In the Y,Z dimension, the landmarks 11-14 are more ventrally positioned, resulting in a more bulbous shape to the lateral walls of the parietal. In comparison, the positive extremes of PC2 are not markedly different to the mean shape. There is an expansion of the posterior shelf, representing the wide and rectangular parietal shelf seen in taxa with positive PC2 values.

In general, fossorial taxa occupy the negative values of PC1 and terrestrial taxa occupy the positive values, with a few exceptions. Of all terrestrial taxa, only 4 species possess PC1 values less than fossorial taxa, these are the pythons *Aspidites melanocephalus* and *Morelia*

spilota (2), and the two booids *Exiliboa placata* and *Casarea dussumieri*, but all four of these taxa possess positive PC2 values, whereas the fossorial taxa with comparable PC1 values possess negative PC2 values. This position of these four terrestrial taxa is likely due to landmarks capturing an overall more elongate parietal with a particularly prominent posterior shelf. This is likely due to the landmark scheme being unable to capture the lateral postorbital processes which form a distinct part of the anatomy of pythonids and booids.

Dinilysia patagonica appears in the negative half of PC1, with a PC1 value of -0.1046 (See Figure 5). The closest extant taxa are the two fossorial species *Xenopeltis unicolor*, and *Loxocemus bicolor*. The position of *Dinilysia* in the morphospace reflects the overall elongated parietal that *Dinilysia* shares with these two taxa, as well as the overall wide frontoparietal suture and large rectangular posterior shelf. However, *Dinilysia* falls outside of the crown group for PC2. This reflects the very wide posterior shelf in this taxa, which expands laterally relative to the anterior end of the parietal to an extent not seen in any of the examined extant taxa. PC2 also captures the more anteriorly projecting midline of the frontoparietal suture present in *Dinilysia*, due to the interdigitation present in this taxa.

Phylogenetically corrected principal component analysis also delineated fossorial from terrestrial taxa for both the molecular data hypothesis and the morphological data hypothesis (See Appendix 6), confirming that the morphological differences seen between fossorial and terrestrial taxa are not simply an artefact of phylogenetic relatedness for either hypotheses. *Dinilysia* appears in the fossorial portion of the morphospace even when data is phylogenetically corrected for both phylogenetic hypotheses.

3.3 Ecology as a predictor variable

A two sample t-test of PC1 and ecological designation rejected the null hypothesis that the two means for fossorial and terrestrial taxa was equal to 0 with high significance (t=-11.166, df=71, p-value < 2.2e-16; 95% CI[-0.26,-0.18). This supports the hypothesis that PC1 values varies for taxa on the basis of ecology. None of the other first 10 principal components were significantly associated with ecology (See Table 4).

Linear discriminant analysis clearly delineated parietals of fossorial taxa from terrestrial taxa, with 100% accuracy and no overlap of values (See Figure 8). The model predicted fossorial and terrestrial ecology for the 72 extant taxa with 100% accuracy. The linear discriminant model trained on extant taxa predicted the ecology of *Dinilysia* to be fossorial (posterior fossorial probability=1, posterior terrestrial probability= 8.24e-91, LD1=-22.701).

Table 4. Results of t-test for each of first ten principal components with ecology. % variation – percentage variation of morphology that the principal component represents.

PC	T Value	P-Value	95 percent confidence interval	% Variation
PC1	-11.121	<2.2e-16 ***	-0.2609, -0.1816	43.52
PC2	-1.4785	0.1437	-0.0543, 0.0081	11.25
PC3	-1.0771	0.2851	-0.0466, 0.0139	9.29
PC4	-2.3854	0.01973	-0.0607, -0.0054	8.24
PC5	0.86483	0.39	-0.0122, 0.0310	4.81
PC6	-2.0591	0.04315	-0.0413, -0.0007	4.38
PC7	-0.51363	0.6091	-0.0202, 0.0120	3.13
PC8	-0.961	0.3398	-0.0227, 0.0079	2.41
PC9	-0.00909	0.9928	-0.0133, 0.0132	2.07
PC10	-0.82826	0.4103	-0.0199, 0.0082	2

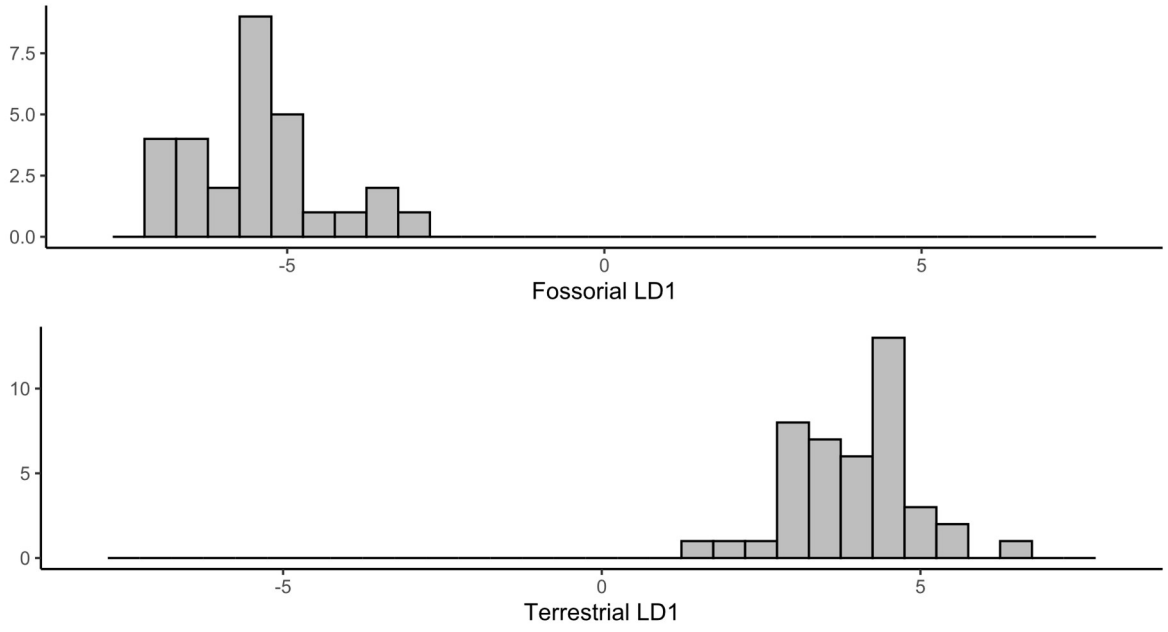

Figure 8. Histogram of linear discriminant function per ecological category for extant taxa. No overlap of histogram extents indicates that categories are clearly delineated by linear discriminant.

4. Discussion

4.1 Parietal shape and ecology in alethinophidian snakes

This study finds clear morphological correlates with ecology, particularly for distinguishing fossorial taxa from terrestrial taxa. Linear discriminant analysis of the principal components found two clear groups of parietal shape concordant with ecology. This finding supports the hypotheses that adaptation to a fossorial ecology results in homoplastic characters in the parietal.

In general, the parietals of fossorial taxa share a number of morphological features. These include the distinct u or v-shaped frontoparietal suture, which is potentially a way to strengthen the braincase when subjected to the larger forces present when pushing the skull through a dense substrate. The parietals of fossorial taxa are also more elongate than those of terrestrial taxa. This is concordant with observations made by Cundall & Irish (2008) in their discussion on the morphological differences between the fossorial colubrids and non-fossorial colubrids that fossorial taxa tend to have shortened orbits and long postorbital braincases (Cundall and Irish, 2008), both of which are features that relate to the elongation of the parietal. Relative to terrestrial members of their clades, both fossorial dipsadines and fossorial elapids have more elongate parietals, with a more distinct u-shaped frontoparietal suture, showing that these characters are not only found in the fossorial taxa *Anilius* and *Cylindrophis*. In particular, the dipsadine *Phalotris mertensi* has distinct anterolaterally projecting supraorbital processes that distinguishes it from other dipsadines, forming a very clearly u-shaped frontoparietal suture. This u-shaped frontoparietal suture is often used as morphological character in phylogenetic analyses of relatedness, and therefore the correlation between this feature and fossoriality calls into question whether this character is informative (see Section 4.4 for further discussion).

Another morphological feature of the parietal that correlates with fossoriality is a prominent posterior shelf. In the fossorial dipsadines and fossorial elapids this posterior shelf is u-shaped, but projects considerably more posteriorly relative to terrestrial members of these clades. This prominently projecting u-shaped posterior shelf is also seen in most uropeltids. In contrast, in *Anilius*, *Cylindrophis*, *Xenopeltis,* and *Loxocemus*, the posterior shelf forms a broad contact with the back of the braincase. The posterior shelf of these clades is distinguished from terrestrial taxa with prominent parietal shelves by the extent of the lateral projections of the posterior edges. In fossorial taxa, these edges project laterally, usually passed the width of the body of the parietal. By contrast, in terrestrial taxa such as *Morelia spilota*, the long parietal shelf projects posteriorly from the body of the parietal with no corresponding lateral projections.

Again the biomechanical function of this feature is not clear, but it may be due to the relative narrowing of the snout seen in fossorial taxa that use the skull to burrow through the substrate (Wake, 1993), in addition to the need to maintain the morphology of the otic region at the back of the skull.

Narrowing of the skull may also be responsible for the observed dorsoventral and mediolateral narrowing in examined fossorial taxa. Previous studies in fossorial lizards have shown that narrower bodies are significantly correlated with burrow use in *Egernia* skinks (Wu et al., 2015), and narrower heads correlates with faster burrowing speeds in *Calyptommatus* microteiid lizards (de Barros et al., 2021). Differences in the extent of narrowing if fossorial snakes may be due to differences in substrate density and in the forces required to push through such substrates.

4.2 Categorising snake ecology

Although many studies interested in the ecological origin of snakes have focussed on whether the ancestral snake was aquatic, fossorial, or another ecological designation (Lee, 1997; Caldwell, 1999; Hsiang et al., 2015; Yi and Norell, 2015; Da Silva et al., 2018; Watanabe et al., 2019), there is still a lack of primary data on the ecology of extant snakes, as well as clear definitions to what these ecological categories mean when relating to actual activity patterns of living organisms. While this is not uncommon for many vertebrate clades, it is a particular issue for snakes as they are often found in cryptic habitats (such as under leaflitter or logs) and exist in low population densities, and as such are unlikely to be the focus of long-term ecological studies. It is also difficult to categorise activity patterns when they are predominantly underground, as researchers only encounter individuals during their above ground excursions. Snakes in general also possess a body type that allows easy transition between environments, as the elongate limbless body is well suited for terrestrial, aquatic, and subterranean locomotion (Lillywhite, 2014). As such, any attempt to place a single categorical ecology onto a snake species is difficult.

For example, I have included the species *Exiliboa placata* in the analysis. Little is known about the ecology of this species, only that the holotype and subsequent specimens were found beneath rocks and the reluctance of captive specimens to eat unless in the dark, suggesting nocturnality (O'Shea, 2018). Yi & Norrell (2015) classed *E. placata* as fossorial, although gave no reasoning in the text or supplementary material. Likewise, the bolyeriid *Casarea dussumieri*, was classed as terrestrial in this analysis. There is not much ecological information in the literature about this species, which is only found on Round Island, north of Mauritius (O'Shea,

2018). This species is nocturnal, usually found inactive under leaf litter during the day (Bullock, 1986). A closely related species, the possibly extinct *Bolyeria multocarinata* purportedly exhibits a fossorial ecology (O'Shea, 2018), which perhaps helps explain the position of *C. dussumieri* in the current PCA. It is also possible that *C. dussumieri* possesses a more fossorial ecology than previously understood. Interestingly, when correcting for phylogenetic non-independence, both of these taxa appear within the fossorial cluster, supporting the hypothesis of fossoriality for both *C. dussumieri* and *E. placata* (see Appendix 6). Further field studies focused on these taxa will help clarify the ecology of both of these species.

The coral snakes, species belonging to the genera *Calliophis, Micruroides,* and *Micrurus* were classed as fossorial in the current analysis. This was deemed appropriate due to the diet of these species largely consisting of fossorial amphisbaenians and caecilians, suggesting at least an ability to hunt or excavate these prey items (O'Shea, 2018). The genus *Micrurus* has been considered semi-fossorial by previous researchers (Jackson and Franz, 1981). This is also supported by the similarity in morphology (elongation and u-shaped frontoparietal suture) shared between coral snakes and other fossorial taxa in the current analysis. While preliminary analysis has compared the burrowing forces of scolecophidian clades compared to alethinophidians (Herrel et al., 2021), information about the burrowing mechanics of many clades, including elapids, remains sparse. Further studies into the active burrowing forces in elapids may help elucidate how the morphology identified here correlates with increased burrowing ability. For example, the u-shaped frontoparietal suture may act as a biomechanical brace to the snout, particularly when the bones of the snout are used to push through the substrate in burrowing behaviours. The need to form a stronger structure to

4.3 Morphology of the parietal of *Dinilysia patagonica* supports a fossorial ecology

The ecology of *Dinilysia patagonica* has considerable implications for the understanding of the ecological origins of snakes. If this taxa is interpreted as a stem snake (Scanlon and Lee, 2000; Gauthier et al., 2012; Zaher and Scanferla, 2012; Caldwell et al., 2015), a predicted fossorial ecology would provide support the hypothesis that the elongate limbless snake body plan evolved in a fossorial environment. Fossorial ecology has been previously suggested for *Dinilysia* based on morphological observations. Initial description of the skull noted similarities between *Dinilysia* and *Anilius scytale* such as the non-projecting supratemporal and the small, robust quadrate (Smith-Woodward, 1901). Other similarities between fossorial taxa and *Dinilysia* have been documented, including the shape of the supraoccipital, the broad attachment of the quadrate bone, and the wide cultriform process of the basisphenoid that

resembles *Cylindrophis* (Estes et al., 1970). Further studies on a natural endocast of *Dinilysia* observed a similar morphology to the fossorial genus *Uropeltis*, including a large spherical vestibule of the inner ear (Triviño et al., 2018), and similarity to the fossorial species *Anilius scytale* with an elongated shape (Scanferla, 2022).

Previous work attempting to investigate the ecology of *Dinilysia* using geometric morphometric techniques focused on this inner ear morphology, however the interpretation of this ecology was not as clear, with Yi & Norrell (2015) reporting a fossorial ecology for *Dinilysia* and Palci et al (2017) reporting a semi-fossorial/semi-aquatic ecology. In contrast, this current study provides independent morphological evidence supporting a fossorial ecology for *Dinilysia*. Using linear discriminant analysis, the parietal of *Dinilysia* was strongly predicted to be fossorial. This is concordant with the position of the parietal of *Dinilysia* in the PCA analysis, where the fossil appears closest to *Loxocemus bicolor* and *Xenopeltis unicolor*, two fossorial taxa (See Figure 5). Both of these analyses are concordant with Yi & Norrell's (2015) study on inner ear morphology that suggested *Dinilysia* was a large-bodied burrower due to similarities in the morphology of the vestibule and semi-circular canals and the results of a principal component analysis (Yi and Norell, 2015)

The current result of *Dinilysia* as a fossorial species has considerable implications for our understanding of early snake evolution. In phylogenetic analyses, *Dinilysia* is usually recovered as a stem snake (Gauthier et al., 2012) or a stem-alethinophidian (Conrad, 2008). The presence of adaptation to fossoriality early on in snake evolution provides considerable support that adaptation to fossoriality was facilitated by the elongate limbless snake body plan, as seen in other limbless squamates.

4.4 Homoplasy has the potential to confuse morphological phylogenetics

The presence of a strong relationship between parietal morphology and ecological habitat is particularly important to consider when using parietal characters in data for phylogenetic reconstruction. The problem of convergence of morphology related to a fossorial ecology is well-documented in squamates in general and snakes in particular (Lee, 1998, 2005; Wiens et al., 2006). The influence of such homoplastic features has been hypothesised to have resulted in the lack of congruence between phylogenetic hypotheses of relatedness constructed with either morphological or molecular data. Characters concerning parietal morphology are present in the character lists of many recent phylogenetic hypotheses of the relatedness of snakes (Tchernov et al., 2000; Lee and Scanlon, 2002; Scanlon, 2006; Conrad, 2008; Gauthier et al., 2012).

In the Tchernov et al (2000) analysis, which aimed to place the newly described limbed snake *Haasiophis terrasanctus* in context of extant taxa, of the 89 characters included 7 characters correspond to parietal morphology. Several of these characters correlate with ecology in the current analysis. These include character 32 (Frontoparietal suture relatively straight (0), or distinct supraorbital process of parietal extends along at least 50% of the length of dorsal margin of orbit (1)), character 34 (Supratemporal processes of parietal distinctly developed (0), or not distinctly developed (1)), and character 35 (Parietal not expanded laterally at anterior end (below postorbital) (0) or distinctly expanded (1)) (Tchernov et al., 2000). All of these characters are shown to correlate with PC1 in the current analysis, and therefore correlate with ecology rather than providing information about relatedness independent from ecology. This is especially the case for character 32, which corresponds to the morphology of the frontoparietal suture. This analysis also provides a list of apomorphies for clades, which reveals that these parietal characters are informative for the relationships recovered between extant clades. This includes an apomorphy of the Alethinophidia as character 32 (1), an apomorphy of the Macrostomata as character 34 (0), and an apomorphy of Macrostomata without *Xenopeltis, Loxocemus, Haasiophis,* and *Pachyrhachis* as character 32 (0). Given the correlation between these traits and ecology, their ability to inform about phylogenetic relatedness should be under consideration.

In the Scanlon (2006) analysis, which aimed to place the madtsoiid *Yurlunggur* in context of extant taxa, of the 209 characters included, 10 characters correspond to parietal morphology. This character list was based on Lee & Scanlon (2002), which contains 212 characters. Several characters in this list correspond to the morphology that correlates with ecology in the current analysis. These include character 54 (Frontal-parietal contact (dorsal aspect). Mostly straight and transverse, slight median notch in frontals at most (0), anteriorly concave, ie. frontals extending posteriorly into broad median embayment in parietals (1), complex W or M shape (2)), character 63 (Anterior (supraorbital) processes of parietal. Absent or poorly developed (0), enlarged, extending along at least 40% of the lateral margin of frontal (1)), and character 66 (Posterolateral (supratemporal or suspensorial) process of parietal. Well developed, posterolateral margin of parietal with a distinct flange (0), reduced, posterolateral margin of parietal with a triangular corner (1), absent, posterolateral margin of parietal rounded (2)). Character states 54 (1), 63 (1), and 66 (1) appear to relate to fossorial ecology based on the current morphometric analysis.

Both Conrad (2008) and Gauthier et al (2012) analyses are focused on the systematics of Squamata. In the Conrad (2008) character list, of the 363 characters included, 16 relate to parietal morphology. The characters included that relate to the morphology examined in the current analysis include character 70 (Frontoparietal suture, dorsal view. U-shaped, anteriorly

arched (0), transverse (1), W-shaped (2), U-shaped, posteriorly arched (3)), character 79 (Parietal, posterior flange (not associated with a sagittal, jaw adductor, crest) absent (0), present (1)) and character 80 (Parietal, supratemporal processes length from the level of the parietal notch compared to the parietal anterior to that point. Greater than one half (0), less than one half (1), absent (2). In particular, character state 70 (3) correlates with ecology in snakes.

In the Gauthier et al (2012) character list, of the 610 characters included, 26 relate to parietal morphology. In particular, these include character 57 (Frontoparietal suture dorsal outline. Bowed anteriorly/inverted U (0), roughly transverse (1), shallow U or W bowed posteriorly (2), deeply bowed U or W (3) frontal postero-dorsolateral corner protrudes posterolaterally (4)), character 101 (Parietal supratemporal process length. Well-developed (0), reduced, less than 25% of parietal width (1), absent (2)), and character 106 (Parietal supraorbital process. Absent (0), present (1), deeply clasping frontal orbital margin (2)). Parietal characters reported as synapomorphies for crown Serpentes in the Gauthier et al (2012) analysis include 101 (1), and 106 (1), both of which are shown to correlate with ecology in the current analysis. Additionally crown Alethinophidia is supported by parietal characters 57 (3) and 106 (2). All of these character states correlate with ecology in the current analysis.

These four examples of morphological character lists used to reconstruct both the relationships between snake clades and the relationships of snakes to other squamates show the importance of understanding morphological characters likely to be affected by homoplasy. The u-shaped frontoparietal suture is present in most character lists, and the current study shows that this character correlates with a fossorial ecology across snakes, and therefore may not represent close phylogenetic relatedness. The inclusion of this character, and others that correlate with ecology, may explain why clades such as Macrostomata and Anilioidea are not recovered in hypotheses of phylogenetic relatedness based on molecular data despite being regularly recovered when using morphological data.

5. Conclusion

This study has shown that the morphology of the parietal of snakes clearly correlates with adaptation to a fossorial ecology in multiple instances across the snake total clade. Given the importance of fossoriality in discussions both of snake origins and snake phylogenetics, understanding homoplasy as it relates to different ecologies is particularly important. Specifically, this current study shows that an overall elongate parietal with a deep u-shaped frontoparietal suture, prominent supraorbital processes, and a large posterior shelf are morphological features more likely to be observed in fossorial taxa. The inclusion of these characters may be the cause of the well-documented incongruences between phylogenetic hypotheses for snakes based on either morphological or molecular data, and future works should attempt to address the effect of removing these characters on hypothesis of phylogenetic relatedness based on morphological data..

This analysis also highlights the potential for homoplastic characters to help decipher the ecology of extinct organisms. Previous geometric morphometric work on the inner ear of snakes found conflicting predictions for the ecology of *Dinilysia patagonica*, either fossorial (Yi and Norell, 2015) or semi-aquatic/semi-fossorial (Palci et al., 2017). My findings here provide independent morphometric evidence for a fossorial ecology for *Dinilysia.* Due to similarities in both body size and parietal morphology, the ecology of *Dinilysia* was likely similar to that of the fossorial *Xenopeltis unicolor* and *Loxocemus bicolor. Dinilysia* was therefore likely a large-bodied fossorial snake. As most phylogenetic analysis recover *Dinilysia patagonica* as a stem snake, this finding provides strong support for the hypothesis that the early evolution of the elongate limbless snake body plan, as well as the distinctive snake skull, involved adaptation to a fossorial habitat.

Bibliography

Adams, D.C., and Otárola-Castillo, E., 2013, Geomorph: An r package for the collection and analysis of geometric morphometric shape data: Methods in Ecology and Evolution, v. 4, p. 393–399.

Apesteguía, S., and Zaher, H., 2006, A Cretaceous terrestrial snake with robust hindlimbs and a sacrum: Nature, v. 440, p. 1037–1040.

Baken, E.K., Collyer, M.L., Kaliontzopoulou, A., and Adams, D.C., 2021, geomorph v4.0 and gmShiny: Enhanced analytics and a new graphical interface for a comprehensive morphometric experience: Methods in Ecology and Evolution, v. 2021, p. 1–9.

de Barros, F.C., Grizante, M.B., Zampieri, F.A.M., and Kohlsdorf, T., 2021, Peculiar relationships among morphology, burrowing performance and sand type in two fossorial microteiid lizards: Zoology, v. 144.

Bullock, D.J., 1986, The ecology and conservation of reptiles on Round Island and Gunner's Quion, Mauritius: Biological Conservation, v. 37, p. 135–156.

Caldwell, M.W., 1999, Squamate phylogeny and the relationships of snakes and mosasauroids: Zoological Journal of the Linnean Society, v. 125, p. 115–147.

Caldwell, M.W., and Albino, A., 2003, Exceptionally Preserved Skeletons of the Cretaceous Snake Dinilysia patagonica Woodward, 1901: Journal of Vertebrate Paleontology, v. 22, p. 861–866.

Caldwell, M.W., Nydam, R.L., Palci, A., and Apesteguía, S., 2015, The oldest known snakes from the Middle Jurassic-Lower Cretaceous provide insights on snake evolution.: Nature Communications, v. 6, p. 5996.

Conrad, J.L., 2008, Phylogeny and systematics of Squamata (Reptilia) based on morphology: Bulletin American Museum of Natural History, v. 310, p. 182.

Cundall, D., and Irish, F., 2008, The Snake Skull; p. 352–692. *In* C. Gans, A.S. Gaunt, and K. Adlre (eds.), Biology of the Reptilia. Volume 20. Morphology H. The Skull of Lepidosauria. Society for the Study of Amphibians and Reptiles.

Currie, A., 2013, Convergence as evidence: British Journal for the Philosophy of Science, v. 64, p. 763–786.

Estes, R., Frazetta, T.H., and Williams, E.E., 1970, Studies on the fossil snake Dinilysia patagonica Woodward: Part I. Cranial Morphology: Bulletin of the Museum of Comparative Zoology at Harvard College, v. 140, p. 25–74.

Gans, C., 1961, The feeding mechanism of snakes and its possible evolution: American Zoologist, v. 1, p. 217–227.

Gans, C., 1975, Tetrapod Limblessness: Evolution and Functional Corollaries: American

Zoologist, v. 15, p. 455–467.

Gauthier, J.A., Kearney, M., Maisano, J.A., Rieppel, O., and Behlke, A.D.B., 2012, Assembling the squamate tree of life : Perspectives from the phenotype and the fossil record: Bulletin of the Peabody Museum of Natural History, v. 53, p. 3–308.

Gower, D.J., Vidal, N., Spinks, J.N., and McCarthy, C.J., 2005, The phylogenetic position of Anomochilidae (Reptilia: Serpentes): first evidence from DNA sequences: Journal of Zoological Systematics and Evolutionary Research, v. 43, p. 315–320.

Greenlees, M.J., Webb, J.K., and Shine, R., 2005, Led by the Blind : Bandy-Bandy Snakes Vermicella annulata (Elapidae) Follow Blindsnake Chemical Trails: Copeia, v. 2005, p. 184–187.

Greer, A.E., 1991, Limb reduction in squamates: Identification of the lineages and discussion of the trends: Journal of Herpetology, v. 25, p. 166–173.

Hanken, J., and Wake, D.B., 1993, Miniaturization of body size: Organismal consequences and evolutionary significance: Annual Review of Ecology and Systematics, v. 24, p. 501–519.

Herrel, A., Lowie, A., Miralles, A., Gaucher, P., Kley, N.J., Measey, J., and Tolley, K.A., 2021, Burrowing in blindsnakes: A preliminary analysis of burrowing forces and consequences for the evolution of morphology: Anatomical Record, v. 304, p. 2292–2302.

How, R.A., and Shine, R., 1999, Ecological traits and conservation biology of five fossorial "sand-swimming" snake species (Simoselaps: Elapidae) in south-western Australia: Journal of Zoology, v. 249, p. 269–282.

Hsiang, A.Y., Field, D.J., Webster, T.H., Behlke, A.D.B., Davis, M.B., Racicot, R.A., and Gauthier, J.A., 2015, The origin of snakes: revealing the ecology, behavior, and evolutionary history of early snakes using genomics, phenomics, and the fossil record.: BMC Evolutionary Biology, v. 15, p. 87.

Jackson, D.R., and Franz, R., 1981, Ecology of the Eastern Coral Snake (Micrurus fulvius) in Northern Peninsular Florida: Herpetologica, v. 37, p. 213–228.

Jayne, B.C., Voris, H.K., and Ng, P.K.L., 2018, How big is too big? Using crustacean-eating snakes (Homalopsidae) to test how anatomy and behaviour affect prey size and feeding performance: Biological Journal of the Linnean Society, v. 123, p. 636–650.

Kley, N.J., and Brainerd, E.L., 1999, Feeding by mandibular raking in a snake: Nature, v. 402, p. 369–370.

Lee, M.S.Y., 1997, The phylogeny of varanoid lizards and the affinities of snakes: Philosophical Transactions of the Royal Society B: Biological Sciences, v. 352, p. 53–91.

Lee, M.S.Y., 1998, Convergent evolution and character correlation in burrowing reptiles: towards a resolution of squamate relationships: Biological Journal of the Linnean Society, v. 65, p. 369–453.

Lee, M.S.Y., 2005, Squamate phylogeny, taxon sampling, and data congruence: Organisms Diversity and Evolution, v. 5, p. 25–45.

Lee, M.S.Y., and Scanlon, J.D., 2002, Snake phylogeny based on osteology, soft anatomy and ecology: Biological Reviews of the Cambridge Philosophical Society, v. 77, p. 333–401.

Li, M., Fry, B.G., and Kini, R.M., 2005, Eggs-only diet: Its implications for the toxin profile changes and ecology of the marbled sea snake (Aipysurus eydouxii): Journal of Molecular Evolution, v. 60, p. 81–89.

Lillywhite, H.B., 2014, Locomotion: How snakes move; p. 77–102. *In* How Snakes Work: Structure, Function and Behavior of the World's Snakes. Oxford University Press, New York.

Maritz, B., and Alexander, G.J., 2009, Breaking ground: Quantitative fossorial herpetofaunal ecology in South Africa: African Journal of Herpetology, v. 58, p. 1–14.

McDowell, S.B., 1975, A Catalogue of the Snakes of New Guinea and the Solomons, with Special Reference to Those in the Bernice P. Bishop Museum. Part II. Anilioidea and Pythoninae: Journal of Herpetology, v. 9, p. 1–79.

Mizuno, T., and Kojima, Y., 2015, A blindsnake that decapitates its termite prey: Journal of Zoology, v. 297, p. 220–224.

O'Shea, M., 2018, The Book of Snakes: A Life-Size Guide to Six Hundred Species from around the World: Ivy Press, London, p.

Olori, J.C., and Bell, C.J., 2012, Comparative skull morphology of uropeltid snakes (Alethinophidia: Uropeltidae) with special reference to disarticulated elements and variation: PloS ONE, v. 7, p. e32450.

Palci, A., Lee, M.S.Y., and Hutchinson, M.N., 2016, Patterns of postnatal ontogeny of the skull and lower jaw of snakes as revealed by micro-CT scan data and three-dimensional geometric morphometrics: Journal of Anatomy, v. 229, p. 723–754.

Palci, A., Hutchinson, M.N., Caldwell, M.W., and Lee, M.S.Y., 2017, The morphology of the inner ear of squamate reptiles and its bearing on the origin of snakes: Royal Society Open Science, v. 4, p. 170685.

Revell, L.J., 2009, Size-correction and principal components for interspecific comparative studies: Evolution, v. 63, p. 3258–3268.

Romer, A.S., 1956, Osteology of the Reptiles: University of Chicago Press, Chicago, 772 p.

Scanferla, A., 2022, A Glimpse into the Evolution of the Ophidian Brain; p. 294–315. *In* D.J. Gower and H. Zaher (eds.), The Origin and Early Evolutionary History of Snakes. Cambridge University Press, Cambridge.

Scanlon, J.D., 2005, Cranial morphology of the Plio-Pleistocene giant madtsoiid snake Wonambi naracoortensis: Palaeontologica Polonica, v. 50, p. 139–180.

Scanlon, J.D., 2006, Skull of the large non-macrostomatan snake Yurlunggur from the Australian Oligo-Miocene: Nature, v. 439, p. 839–842.

Scanlon, J.D., and Lee, M.S.Y., 2000, The Pleistocene serpent *Wonambi* and the early evolution of snakes: Nature, v. 403, p. 416–420.

Shine, R., 1980, Reproduction , Feeding and Growth in the Australian Burrowing Snake Vermicella annulata: Journal of Herpetology, v. 14, p. 71–77.

Da Silva, F.O., Fabre, A.-C., Savriama, Y., Ollonen, J., Mahlow, K., Herrel, A., Müller, J., and Di-Poï, N., 2018, The ecological origins of snakes as revealed by skull evolution: Nature Communications, v. 9, p. 376.

Simões, B.F., Sampaio, F.L., Jared, C., Antoniazzi, M.M., Loew, E.R., Bowmaker, J.K., Rodriguez, A., Hart, N.S., Hunt, D.M., Partridge, J.C., and Gower, D.J., 2015, Visual system evolution and the nature of the ancestral snake: Journal of Evolutionary Biology, v. 28, p. 1309–1320.

Smith-Woodward, A., 1901, On some Extinct Reptiles from Patagonia, of the Genera Miolania, Dinilysia, and Genyodectes: Proceedings of the Zoological Society of London, v. 70, p. 169–184.

Stayton, C.T., 2015, What does convergent evolution mean? The interpretation of convergence and its implications in the search for limits to evolution: Interface Focus, v. 5.

Tchernov, E., Rieppel, O., Zaher, H., Polcyn, M.J., and Jacobs, L.L., 2000, A Fossil Snake with Limbs: Science, v. 287, p. 2010–2012.

Triviño, L.N., Albino, A.M., Dozo, M.T., and Williams, J.D., 2018, First natural endocranial cast of a fossil snake (Cretaceous of Patagonia, Argentina): The Anatomical Record, v. 301, p. 9–20.

Underwood, G., 1967, A Contribution to the Classification of Snakes: British Museum, London, 179 p.

Voris, H.K., and Voris, H.H., 1983, Feeding strategies in marine snakes: An analysis of evolutionary, morphological, behavioral and ecological relationships: Integrative and Comparative Biology, v. 23, p. 411–425.

Wake, M.H., 1993, The skull as a locomotor organ; p. *In* J. Hanken and B.K. Hall (eds.), The Skull: Functional and Evolutionary Mechanics. University of Chicago Press, Chicago.

Watanabe, A., Fabre, A.-C., Felice, R.N., Maisano, J.A., Müller, J., Herrel, A., and Goswami, A., 2019, Ecomorphological diversification in squamates from conserved pattern of cranial integration: Proceedings of National Academy of Sciences, v. July, p. e201820967.

Wiens, J.J., Brandley, M.C., and Reeder, T.W., 2006, Why does a trait evolve multiple times within a clade? Repeated evolution of snakelike body form in squamate reptiles: Evolution, v. 60, p. 123–141.

Wiens, J.J., Kuczynski, C.A., Townsend, T., Reeder, T.W., Mulcahy, D.G., and Sites, J.W., 2010, Combining phylogenomics and fossils in higher-level squamate reptile phylogeny:

Molecular data change the placement of fossil taxa: Systematic Biology, v. 59, p. 674–688.

Wilson, J.A., Mohabey, D.M., Peters, S.E., and Head, J.J., 2010, Predation upon hatchling dinosaurs by a new snake from the Late Cretaceous of India: PLoS Biology, v. 8.

Wu, N.C., Alton, L.A., Clemente, C.J., Kearney, M.R., and White, C.R., 2015, Morphology and burrowing energetics of semi-fossorial skinks (Liopholis spp.): Journal of Experimental Biology, v. 218, p. 2416–2426.

Yi, H., and Norell, M.A., 2015, The burrowing origin of modern snakes: Science Advances, v. 1, p. e1500743–e1500743.

Zaher, H., and Rieppel, O., 2002, On the phylogenetic relationships of the Cretaceous snakes with legs, with special reference to Pachyrhachis problematicus (Squamata, Serpentes): Journal of Vertebrate Paleontology, v. 22, p. 104–109.

Zaher, H., and Scanferla, C.A., 2012, The skull of the Upper Cretaceous snake *Dinilysia patagonica* Smith-Woodward, 1901, and its phylogenetic position revisited: Zoological Journal of the Linnean Society, v. 164, p. 194–238.

Zheng, Y., and Wiens, J.J., 2016, Combining phylogenomic and supermatrix approaches, and a time-calibrated phylogeny for squamate reptiles (lizards and snakes) based on 52 genes and 4162 species: Molecular Phylogenetics and Evolution, v. 94, p. 537–547.

Appendix 1 – Specimens list with ecological designation

No.	*Species*	Taxonomy	Specimen Number	Institution	Ecology
1	*Anilius scytale*	Aniliidae	BMNH 1855.5.28.23	Natural History Museum, London	Fossorial
2	*Anilius scytale*	Aniliidae	BMNH 1923.11.7.6	Natural History Museum, London	Fossorial
3	*Anomochilus leonardi*	Anomochilidae	frim:0026	Forest Research Institute Malaysia	Fossorial
4	*Candoia bibroni*	Boidae	BMNH 1967.771	Natural History Museum, London	Terrestrial
5	*Casarea dussumieri*	Boidae	ummz:herps:190285	University of Michigan, Museum of Zoology, Division of Reptiles & Amphibians	Terrestrial
6	*Epicrates cenchria*	Boidae	UMZC R3.51-1	University Museum of Zoology, Cambridge	Terrestrial
7	*Exiliboa placata*	Boidae	MVZ 137126	Museum of Vertebrate Zoology, Berkeley	Terrestrial
8	*Sanzinia madagascariensis*	Boidae	ku:kuh:183837	KUBI Herpetology Collection	Terrestrial
9	*Boiga irregularis*	Colubridae: Colubrinae	ummz:herps:170417	University of Michigan, Museum of Zoology, Division of Reptiles & Amphibians	Terrestrial
10	*Coluber constrictor*	Colubridae: Colubrinae	ummz:herps:225480	University of Michigan, Museum of Zoology, Division of Reptiles & Amphibians	Terrestrial
11	*Dasypeltis gansi*	Colubridae: Colubrinae	ummz:herps:FS1352	University of Michigan, Museum of Zoology, Division of Reptiles & Amphibians	Terrestrial
12	*Drymarchon corais*	Colubridae: Colubrinae	ku:kuh:289805	KUBI Herpetology Collection	Terrestrial
13	*Lampropeltis getula*	Colubridae: Colubrinae	ummz:herps:218638	University of Michigan, Museum of Zoology, Division of Reptiles & Amphibians	Terrestrial

14	*Oligodon arnensis*	Colubridae: Colubrinae	ummz:herps:65634	University of Michigan, Museum of Zoology, Division of Reptiles & Amphibians	Terrestrial
15	*Pantherophis guttatus*	Colubridae: Colubrinae	lsumz:herps:88802	LSUMZ Herps Collection	Terrestrial
16	*Platyceps najadum*	Colubridae: Colubrinae	ummz:herps:127487	University of Michigan, Museum of Zoology, Division of Reptiles & Amphibians	Terrestrial
17	*Ptyas mucosa*	Colubridae: Colubrinae	ummz:herps169877	University of Michigan, Museum of Zoology, Division of Reptiles & Amphibians	Terrestrial
18	*Senticolis triaspis*	Colubridae: Colubrinae	ummz:herps:111096	University of Michigan, Museum of Zoology, Division of Reptiles & Amphibians	Terrestrial
19	*Carphophis amoenus*	Colubridae: Dipsadinae	ummz:herps:209970	University of Michigan, Museum of Zoology, Division of Reptiles & Amphibians	Terrestrial
20	*Elapomorphus quinquelineatus*	Colubridae: Dipsadinae	ummz:herps:65879	University of Michigan, Museum of Zoology, Division of Reptiles & Amphibians	Fossorial
21	*Phalotris mertensi*	Colubridae: Dipsadinae	ummz:herps:63022	University of Michigan, Museum of Zoology, Division of Reptiles & Amphibians	Fossorial
22	*Philodryas patagoniensis*	Colubridae: Dipsadinae	ummz:herps:108987	University of Michigan, Museum of Zoology, Division of Reptiles & Amphibians	Terrestrial
23	*Pseudoboa coronata*	Colubridae: Dipsadinae	ummz:herps:246839	University of Michigan, Museum of Zoology, Division of Reptiles & Amphibians	Terrestrial
24	*Xenodon neuwiedii*	Colubridae: Dipsadinae	ummz:herps:63002	University of Michigan, Museum of Zoology, Division of Reptiles & Amphibians	Terrestrial
25	*Natrix natrix*	Colubridae: Natricinae	ummz:herps:65465	University of Michigan, Museum of Zoology, Division of Reptiles & Amphibians	Terrestrial

26	*Nerodia sipedon*	Colubridae: Natricinae	ummz:herps:205025	University of Michigan, Museum of Zoology, Division of Reptiles & Amphibians	Terrestrial
27	*Thamnophis rufipunctatus*	Colubridae: Natricinae	ummz:herps:172510	University of Michigan, Museum of Zoology, Division of Reptiles & Amphibians	Terrestrial
28	*Cylindrophis lineatus*	Cylindrophiidae	BMNH 1901.5.17-1	Natural History Museum, London	Fossorial
29	*Cylindrophis melanotus*	Cylindrophiidae	BMNH 1872.4.6.123	Natural History Museum, London	Fossorial
30	*Cylindrophis ruffus*	Cylindrophiidae	UMZC R4.12-1	University Museum of Zoology, Cambridge	Fossorial
31	*Cylindrophis ruffus*	Cylindrophiidae	UMZC R4.12-2	University Museum of Zoology, Cambridge	Fossorial
32	*Cylindrophis ruffus*	Cylindrophiidae	UMZC R4.12-3	University Museum of Zoology, Cambridge	Fossorial
33	*Bungarus fasciatus*	Elapidae	ummz:herps:201916	University of Michigan, Museum of Zoology, Division of Reptiles & Amphibians	Terrestrial
34	*Calliophis maculiceps*	Elapidae	UMZC R9.221-1	University Museum of Zoology, Cambridge	Fossorial
35	*Furina diadema*	Elapidae	ummz:herps:83498	University of Michigan, Museum of Zoology, Division of Reptiles & Amphibians	Terrestrial
36	*Micruroides euryxanthus*	Elapidae	ummz:herps:200295	University of Michigan, Museum of Zoology, Division of Reptiles & Amphibians	Fossorial
37	*Micrurus fulvius*	Elapidae	fmnh:amphibians and reptiles:39479	The Field Museum of Natural History	Fossorial
38	*Micrurus nigrocinctus*	Elapidae	ummz:herps:131984	University of Michigan, Museum of Zoology, Division of Reptiles & Amphibians	Fossorial
39	*Naja naja*	Elapidae	UMZC R9.177-3	University Museum of Zoology, Cambridge	Terrestrial
40	*Notechis scutatus*	Elapidae	ummz:herps:65874	University of Michigan, Museum of Zoology, Division of Reptiles & Amphibians	Terrestrial

41	*Oxyuranus scutellatus*	Elapidae	lsumz:herps:94344	LSUMZ Herps Collection	Terrestrial
42	*Simoselaps bertholdi*	Elapidae	ummz:herps:244197	University of Michigan, Museum of Zoology, Division of Reptiles & Amphibians	Fossorial
43	*Vermicella annulata*	Elapidae	UMZC R9.239-1	University Museum of Zoology, Cambridge	Fossorial
44	*Amblyodipsas polylepis hildebrantii*	Lamprophiidae: Aparallactinae	cas:herp:173555	California Academy of Sciences Herpetology Collection	Fossorial
45	*Aparallactus capensis*	Lamprophiidae: Aparallactinae	cas:herp:11683	California Academy of Sciences Herpetology Collection	Fossorial
46	*Aparallactus modestus*	Lamprophiidae: Aparallactinae	cas:herp:111865	California Academy of Sciences Herpetology Collection	Fossorial
47	*Aparallactus niger*	Lamprophiidae: Aparallactinae	amnh:herpetology:r-142406	AMNH Herpetology Collections	Fossorial
48	*Polemon christyi*	Lamprophiidae: Aparallactinae	cas:herp:147905	California Academy of Sciences Herpetology Collection	Fossorial
49	*Homoroselaps lacteus*	Lamprophiidae: Atractaspidinae	cas:herp:173258	California Academy of Sciences Herpetology Collection	Fossorial
50	*Boaedon fuliginosus*	Lamprophiidae: Lamprophiinae	cas:herp:85747	California Academy of Sciences Herpetology Collection	Terrestrial
51	*Psammophylax variabilis*	Lamprophiidae: Psammophiinae	ummz:herps:61233	University of Michigan, Museum of Zoology, Division of Reptiles & Amphibians	Terrestrial
52	*Pseudaspis cana*	Lamprophiidae: Pseudaspidinae	lsumz:herps:54361	LSUMZ Herps Collection	Terrestrial

53	*Duberria lutrix*	Lamprophiidae: Pseudoxyrhophiinae	cas:herp:201763	California Academy of Sciences Herpetology Collection	Terrestrial
54	*Heteroliodon occipitalis*	Lamprophiidae: Pseudoxyrhophiinae	ummz:herps:229038	University of Michigan, Museum of Zoology, Division of Reptiles & Amphibians	Terrestrial
55	*Langaha madagascariensis*	Lamprophiidae: Pseudoxyrhophiinae	ummz:herps:209371	University of Michigan, Museum of Zoology, Division of Reptiles & Amphibians	Terrestrial
56	*Lycodryas granuliceps*	Lamprophiidae: Pseudoxyrhophiinae	ummz:herps:209566	University of Michigan, Museum of Zoology, Division of Reptiles & Amphibians	Terrestrial
57	*Loxocemus bicolor*	Loxocemidae	BMNH 1988.354	Natural History Museum, London	Fossorial
58	*Loxocemus bicolor*	Loxocemidae	BMNH 1988.355	Natural History Museum, London	Fossorial
59	*Aspidites melanocephalus*	Pythonidae	fmnh:amphibians and reptiles:97055	The Field Museum of Natural History	Terrestrial
60	*Malayopython reticulatus*	Pythonidae	UMZC R3.24-4	University Museum of Zoology, Cambridge	Terrestrial
61	*Morelia spilota*	Pythonidae	UMZC R3.22-4	University Museum of Zoology, Cambridge	Terrestrial
62	*Morelia spilota*	Pythonidae	ummz:herps:227833	University of Michigan, Museum of Zoology, Division of Reptiles & Amphibians	Terrestrial
63	*Python molurus*	Pythonidae	UMZC R3.25-7	University Museum of Zoology, Cambridge	Terrestrial
64	*Trachyboa boulengeri*	Tropidophiidae	BMNH 1923.10.12.9	Natural History Museum, London	Terrestrial
65	*Tropidophis melanurus*	Tropidophiidae	BMNH 1932.11.11.33	Natural History Museum, London	Terrestrial
66	*Plectrurus perroteti*	Uropeltidae	UMZC R5.56-1	University Museum of Zoology, Cambridge	Fossorial
67	*Rhinophis philippinus*	Uropeltidae	UMZC R5.7-1	University Museum of Zoology, Cambridge	Fossorial

68	*Teretrurus sanguineus*	Uropeltidae	cas:herp:244362	California Academy of Sciences Herpetology Collection	Fossorial
69	*Uropeltis melanogaster*	Uropeltidae	ummz:herps:96275	University of Michigan, Museum of Zoology, Division of Reptiles & Amphibians	Fossorial
70	*Crotalus atrox*	Viperidae	ummz:herps:11004	University of Michigan, Museum of Zoology, Division of Reptiles & Amphibians	Terrestrial
71	*Vipera aspis*	Viperidae	ummz:herps:116957	University of Michigan, Museum of Zoology, Division of Reptiles & Amphibians	Terrestrial
72	*Xenopeltis unicolor*	Xenopeltidae	BMNH 1912.6.26.3	Natural History Museum, London	Fossorial
73	*Xenopeltis unicolor*	Xenopeltidae	UMZC R6.1-2	University Museum of Zoology, Cambridge	Fossorial
74	*Dinilysia patagonica*	Fossil	MACN RN-1013	Museo Argentino de Ciencias Naturales	Fossil

Appendix 2 – MorphoSource Specimen Details

No.	Species	Specimen Number	Ark	Funding	Attribution
3	*Anomochilus leonardi*	frim:0026	ark:/87602/m4/M114921	EF-0334961, DBI-1902242	oUTCT provided access to these dataoriginally appearing in Gauthier et al., 2012, with data collection funded by NSF EF-0334961 and data upload to MorphoSource funded by DBI-1902242. The files were downloaded from www.MorphoSource.org, Duke University.
5	*Casarea dussumieri*	ummz:herps:190285	ark:/87602/m4/M98459	DBI-1902242	oUTCT provided access to these dataoriginally appearing in Maisano and Rieppel, 2007, with data collection fundwith data upload to MorphoSource funded by DBI-1902242. The files were downloaded from www.MorphoSource.org, Duke University.
8	*Sanzinia madagascariensis*	ku:kuh:183837	ark:/87602/m4/M75029	oVert TCN; NSF DBI-1701714; NSF DBI-1701713; NSF DBI-1701932	University of Kansas Center for Research Inc provided access to these data , the collection of which was funded by oVert TCN. The files were downloaded from www.MorphoSource.org, Duke University.
9	*Boiga irregularis*	ummz:herps:170417	ark:/87602/m4/M57278	NSF DBI-1701714; NSF DBI-1701713; oVert TCN	University of Michigan Museum of Zoology provided access to these data , the collection of which was funded by oVert TCN. The files were downloaded from www.MorphoSource.org, Duke University.
10	*Coluber constrictor*	ummz:herps:225480	ark:/87602/m4/M33604	Funding provided by the University of Michigan	
11	*Dasypeltis gansi*	ummz:herps:FS1352	ark:/87602/m4/M43757	Funding provided by the University of Michigan	
12	*Drymarchon corais*	ku:kuh:289805	ark:/87602/m4/M82903	NSF DBI-1701714; NSF DBI-1701713; NSF DBI-1701932; oVert TCN	University of Kansas Center for Research Inc provided access to these data , the collection of which was funded by oVert TCN. The files were downloaded from www.MorphoSource.org, Duke University.

13	*Lampropeltis getula*	ummz:herps: 218638	ark:/87602/m4/ M70100	NSF DBI-1701714; NSF DBI-1701713; oVert TCN	University of Michigan Museum of Zoology provided access to these data , the collection of which was funded by oVert TCN. The files were downloaded from www.MorphoSource.org, Duke University.
14	*Oligodon arnensis*	ummz:herps: 65634	ark:/87602/m4/ M43771	Funding provided by the University of Michigan	
15	*Pantherophis guttatus*	lsumz:herps:8 8802	ark:/87602/m4/ M73956	NSF DBI-1701714; NSF DBI-1701402; oVert TCN	Louisiana State University & Agricultural and Mechanical College provided access to these data provided access to these data , the collection of which was funded by oVert TCN. The files were downloaded from www.MorphoSource.org, Duke University.
16	*Platyceps najadum*	ummz:herps: 127487	ark:/87602/m4/ M55963	Funding provided by the University of Michigan	
17	*Ptyas mucosa*	ummz:herps1 69877	ark:/87602/m4/ M43427	Funding provided by the University of Michigan	
18	*Senticolis triaspis*	ummz:herps: 111096	ark:/87602/m4/ M33705	Funding provided by the University of Michigan	
19	*Carphophis amoenus*	ummz:herps: 209970	ark:/87602/m4/ M68474	NSF DBI-1701714; NSF DBI-1701713; oVert TCN	University of Michigan Museum of Zoology provided access to these data provided access to these data , the collection of which was funded by oVert TCN. The files were downloaded from www.MorphoSource.org, Duke University.
20	*Elapomorphus quinquelineatus*	ummz:herps: 65879	ark:/87602/m4/ M55973	Funding provided by the University of Michigan	
21	*Phalotris mertensi*	ummz:herps: 63022	ark:/87602/m4/ M68506	NSF DBI-1701714; NSF DBI-1701713; oVert TCN	University of Michigan Museum of Zoology provided access to these data provided access to these data , the collection of which was funded by oVert TCN. The files were downloaded from www.MorphoSource.org, Duke University.

22	*Philodryas patagoniensis*	ummz:herps: 108987	ark:/87602/m4/ M68369	NSF DBI-1701714; NSF DBI-1701713; oVert TCN	University of Michigan Museum of Zoology provided access to these data provided access to these data , the collection of which was funded by oVert TCN. The files were downloaded from www.MorphoSource.org, Duke University.
23	*Pseudoboa coronata*	ummz:herps: 246839	ark:/87602/m4/ M59223	Funding provided by the University of Michigan	
24	*Xenodon neuwiedii*	ummz:herps: 63002	ark:/87602/m4/ M43791	Funding provided by the University of Michigan	
25	*Natrix natrix*	ummz:herps: 65465	ark:/87602/m4/ M84258	NSF DBI-1701714; NSF DBI-1701713; oVert TCN	University of Michigan Museum of Zoology provided access to these data , the collection of which was funded by oVert TCN. The files were downloaded from www.MorphoSource.org, Duke University.
26	*Nerodia sipedon*	ummz:herps: 205025	ark:/87602/m4/ M70079	NSF DBI-1701714; NSF DBI-1701713; oVert TCN	University of Michigan Museum of Zoology provided access to these data , the collection of which was funded by oVert TCN. The files were downloaded from www.MorphoSource.org, Duke University.
27	*Thamnophis rufipunctatus*	ummz:herps: 172510	ark:/87602/m4/ M48400	NSF DBI-1701714; oVert TCN	
33	*Bungarus fasciatus*	ummz:herps: 201916	ark:/87602/m4/ M68445	NSF DBI-1701714; NSF DBI-1701713; oVert TCN	University of Michigan Museum of Zoology provided access to these data provided access to these data , the collection of which was funded by oVert TCN. The files were downloaded from www.MorphoSource.org, Duke University.
35	*Furina diadema*	ummz:herps: 83498	ark:/87602/m4/ M76271	NSF DBI-1701714; NSF DBI-1701713; oVert TCN	University of Michigan Museum of Zoology provided access to these data , the collection of which was funded by oVert TCN. The files were downloaded from www.MorphoSource.org, Duke University.
36	*Micruroides euryxanthus*	ummz:herps: 200295	ark:/87602/m4/ M68436	NSF DBI-1701714; NSF DBI-1701713; oVert TCN	University of Michigan Museum of Zoology provided access to these data provided access to these data , the collection of which was funded by oVert TCN. The files

					were downloaded from www.MorphoSource.org, Duke University.
37	*Micrurus fulvius*	fmnh:amphibians and reptiles:39479	ark:/87602/m4/M98579	EF-0334961, DBI-1902242	oUTCT provided access to these dataoriginally appearing in Gauthier et al., 2012, with data collection funded by NSF EF-0334961 and data upload to MorphoSource funded by DBI-1902242. The files were downloaded from www.MorphoSource.org, Duke University.
38	*Micrurus nigrocinctus*	ummz:herps:131984	ark:/87602/m4/M30224	Funding provided by the University of Michigan	
40	*Notechis scutatus*	ummz:herps:65874	ark:/87602/m4/M57930	Funding provided by the University of Michigan	
41	*Oxyuranus scutellatus*	lsumz:herps:94344	ark:/87602/m4/M78560	NSF DBI-1701714; NSF DBI-1701402; oVert TCN	Louisiana State University & Agricultural and Mechanical College provided access to these data , the collection of which was funded by oVert TCN. The files were downloaded from www.MorphoSource.org, Duke University.
42	*Simoselaps bertholdi*	ummz:herps:244197	ark:/87602/m4/M71019	NSF DBI-1701714; oVert TCN; NSF DBI-1701713	University of Michigan Museum of Zoology provided access to these data , the collection of which was funded by oVert TCN. The files were downloaded from www.MorphoSource.org, Duke University.
44	*Amblyodipsas polylepis hildebrantii*	cas:herp:173555	ark:/87602/m4/M25805	University of Florida	
45	*Aparallactus capensis*	cas:herp:11683	ark:/87602/m4/M25787	University of Florida	
46	*Aparallactus modestus*	cas:herp:111865	ark:/87602/m4/M37554		
47	*Aparallactus niger*	amnh:herpetology:r-142406	ark:/87602/m4/M25784		
48	*Polemon christyi*	cas:herp:147905	ark:/87602/m4/M25802	University of Florida	

49	*Homoroselaps lacteus*	cas:herp:173258	ark:/87602/m4/M25796	University of Florida	
50	*Boaedon fuliginosus*	cas:herp:85747	ark:/87602/m4/M37559		
51	*Psammophylax variabilis*	ummz:herps:61233	ark:/87602/m4/M55969	Funding provided by the University of Michigan	
52	*Pseudaspis cana*	lsumz:herps:54361	ark:/87602/m4/M78508	oVert TCN; NSF DBI-1701402; NSF DBI-1701714	Louisiana State University & Agricultural and Mechanical College provided access to these data , the collection of which was funded by oVert TCN. The files were downloaded from www.MorphoSource.org, Duke University.
53	*Duberria lutrix*	cas:herp:201763	ark:/87602/m4/M63821	NSF DBI-1701714; NSF DBI-1701783; oVert TCN	
54	*Heteroliodon occipitalis*	ummz:herps:229038	ark:/87602/m4/M70112	NSF DBI-1701714; NSF DBI-1701713; oVert TCN	University of Michigan Museum of Zoology provided access to these data , the collection of which was funded by oVert TCN. The files were downloaded from www.MorphoSource.org, Duke University.
55	*Langaha madagascariensis*	ummz:herps:209371	ark:/87602/m4/M70088	NSF DBI-1701714; NSF DBI-1701713; oVert TCN	University of Michigan Museum of Zoology provided access to these data , the collection of which was funded by oVert TCN. The files were downloaded from www.MorphoSource.org, Duke University.
56	*Lycodryas granuliceps*	ummz:herps:209566	ark:/87602/m4/M75098	NSF DBI-1701714; NSF DBI-1701713; oVert TCN	University of Michigan Museum of Zoology provided access to these data , the collection of which was funded by oVert TCN. The files were downloaded from www.MorphoSource.org, Duke University.
59	*Aspidites melanocephalus*	fmnh:amphibians and reptiles:97055	ark:/87602/m4/M98387	EF-0334961, DBI-1902242	oUTCT provided access to these dataoriginally appearing in Gauthier et al., 2012, with data collection funded by NSF EF-0334961 and data upload to MorphoSource funded by DBI-1902242. The files were downloaded from www.MorphoSource.org, Duke University.

62	*Morelia spilota*	ummz:herps:227833	ark:/87602/m4/M68478	oVert TCN; NSF DBI-1701714; NSF DBI-1701713	University of Michigan Museum of Zoology provided access to these data provided access to these data , the collection of which was funded by oVert TCN. The files were downloaded from www.MorphoSource.org, Duke University.
68	*Teretrurus sanguineus*	cas:herp:244362	ark:/87602/m4/M74711	NSF DBI-1701714; NSF DBI-1701713; oVert TCN; NSF DBI-1701870	California Academy of Sciences provided access to these data , the collection of which was funded by oVert TCN. The files were downloaded from www.MorphoSource.org, Duke University.
69	*Uropeltis melanogaster*	ummz:herps:96275	ark:/87602/m4/M39128	Funding provided by the University of Michigan	
70	*Crotalus atrox*	ummz:herps:11004	ark:/87602/m4/M44009	Funding provided by the University of Michigan	
71	*Vipera aspis*	ummz:herps:116957	ark:/87602/m4/M57865	Funding provided by the University of Michigan	
74	*Dinilysia patagonica*	MACN RN-1013	ark:/87602/m4/M114982	EF-0334961, DBI-1902242	oUTCT provided access to these dataoriginally appearing in Gauthier et al., 2012, with data collection funded by NSF EF-0334961 and data upload to MorphoSource funded by DBI-1902242. The files were downloaded from www.MorphoSource.org, Duke University.

Appendix 3 – Scores of first two principal components

No.	Species	PC1 (43.27 %)	PC2 (11.35%)
1	*Anilius scytale*	-0.275903894	0.07464883
2	*Anilius scytale*	-0.308727108	0.039711386
3	*Anomochilus leonardi*	-0.094795697	0.031149643
4	*Candoia bibroni*	-0.011164918	0.045284711
5	*Casarea dussumieri*	-0.066083252	0.006950633
6	*Epicrates cenchria*	-0.009453745	-0.088623157
7	*Exiliboa placata*	-0.060550105	0.028528359
8	*Sanzinia madagascariensis*	-0.013563712	0.080279668
9	*Boiga irregularis*	0.179173394	-0.02976544
10	*Coluber constrictor*	0.193552789	0.020396933
11	*Dasypeltis gansi*	0.110219922	0.012277029
12	*Drymarchon corais*	0.193299979	0.008637171
13	*Lampropeltis getula*	0.110158556	-0.044454415
14	*Oligodon arnensis*	0.115641303	-0.059654056
15	*Pantherophis guttatus*	0.138734662	-0.063200191
16	*Platyceps najadum*	0.173824384	-0.049336882
17	*Ptyas mucosa*	0.215460096	0.100287124
18	*Senticolis triaspis*	0.10071782	0.025120796
19	*Carphophis amoenus*	0.12857838	0.014178359
20	*Elapomorphus quinquelineatus*	-0.168369821	-0.095048165
21	*Phalotris mertensi*	-0.262747006	-0.040635498
22	*Philodryas patagoniensis*	0.207416932	-0.05009096
23	*Pseudoboa coronata*	0.054252668	-0.066440462
24	*Xenodon neuwiedii*	0.168103623	0.054780816
25	*Natrix natrix*	0.18364778	0.025374688
26	*Nerodia sipedon*	0.145453675	0.043200394
27	*Thamnophis rufipunctatus*	0.041907033	-0.007718762
28	*Cylindrophis lineatus*	-0.21124512	0.022628766
29	*Cylindrophis melanotus*	-0.218627555	0.031732557
30	*Cylindrophis ruffus*	-0.252828516	0.051679244
31	*Cylindrophis ruffus*	-0.17862556	0.049382201
32	*Cylindrophis ruffus*	-0.219940454	0.033203745
33	*Bungarus fasciatus*	0.022382519	-0.009847621
34	*Calliophis maculiceps*	-0.046598144	-0.053365387
35	*Furina diadema*	0.019389422	-0.027145512
36	*Micruroides euryxanthus*	-0.02558044	-0.118794001
37	*Micrurus fulvius*	-0.139134154	-0.14039769
38	*Micrurus nigrocinctus*	-0.039853328	-0.108460575
39	*Naja naja*	0.037260423	0.032681844
40	*Notechis scutatus*	0.059325369	-0.005862325
41	*Oxyuranus scutellatus*	0.042094683	-0.016318973
42	*Simoselaps bertholdi*	-0.059503023	-0.045980897

43	*Vermicella annulata*	-0.089967998	-0.165251584
44	*Amblyodipsas polylepis hildebrantii*	-0.102106254	-0.063562661
45	*Aparallactus capensis*	-0.035839009	-0.081128428
46	*Aparallactus modestus*	-0.029550965	-0.063482785
47	*Aparallactus niger*	-0.048023696	-0.015736119
48	*Polemon christyi*	-0.161753829	-0.119349212
49	*Homoroselaps lacteus*	-0.154597466	-0.147219242
50	*Boaedon fuliginosus*	0.110782279	0.015362185
51	*Psammophylax variabilis*	0.210555963	-0.007752907
52	*Pseudaspis cana*	0.256885143	0.099641148
53	*Duberria lutrix*	0.117579761	0.057114949
54	*Heteroliodon occipitalis*	0.10172898	-0.0429536
55	*Langaha madagascariensis*	0.073502046	0.032433817
56	*Lycodryas granuliceps*	0.174060332	-0.014664086
57	*Loxocemus bicolor*	-0.095797061	0.08288117
58	*Loxocemus bicolor*	-0.066876775	0.102741149
59	*Aspidites melanocephalus*	-0.049992321	0.07879295
60	*Malayopython reticulatus*	0.001103163	0.063938108
61	*Morelia spilota*	0.013336654	0.028025505
62	*Morelia spilota*	-0.048253401	0.056070947
63	*Python molurus*	0.0910388	0.083342425
64	*Trachyboa boulengeri*	0.0959234	-0.046217587
65	*Tropidophis melanurus*	0.069635714	-0.069495126
66	*Plectrurus perroteti*	-0.139923157	0.053322151
67	*Rhinophis philippinus*	-0.034936618	-0.042446854
68	*Teretrurus sanguineus*	-0.157837082	0.047714167
69	*Uropeltis melanogaster*	-0.039597291	-0.041249083
70	*Crotalus atrox*	0.162407275	0.047129202
71	*Vipera aspis*	0.111391845	-0.068168792
72	*Xenopeltis unicolor*	-0.072302306	0.108829439
73	*Xenopeltis unicolor*	-0.135276886	0.123326921
74	*Dinilysia patagonica*	-0.104599102	0.197037905

Appendix 4 – Scores of first two phylogenetically corrected principal components Zheng & Wiens (2016) molecular phylogenetic hypothesis

No.	Species	PC1 (42.44 %)	PC2 (15.49%)
1	*Anilius scytale*	0.015883112	-0.021682232
2	*Anilius scytale*	0.028752343	-0.107126626
3	*Anomochilus leonardi*	0.113154887	-0.117759122
4	*Candoia bibroni*	-0.034120032	0.034430351
5	*Casarea dussumieri*	-0.003116555	0.009853828
6	*Epicrates cenchria*	0.047924155	-0.027311441
7	*Exiliboa placata*	-0.121345424	-0.172829615
8	*Sanzinia madagascariensis*	-0.160415966	-0.199506422
9	*Boiga irregularis*	0.071496712	0.02791553
10	*Coluber constrictor*	0.092330983	0.1286852
11	*Dasypeltis gansi*	0.042149696	0.21382474
12	*Drymarchon corais*	0.148354948	0.111280965
13	*Lampropeltis getula*	0.118191781	0.163397874
14	*Oligodon arnensis*	-0.009813085	0.058395261
15	*Pantherophis guttatus*	0.100006149	0.207446892
16	*Platyceps najadum*	-0.012841702	-0.011295602
17	*Ptyas mucosa*	-0.058850632	-0.151498176
18	*Senticolis triaspis*	0.002554769	-0.016294247
19	*Carphophis amoenus*	-0.04095601	-0.158622807
20	*Elapomorphus quinquelineatus*	-0.090144037	-0.172568903
21	*Phalotris mertensi*	-0.006412515	-0.133105231
22	*Philodryas patagoniensis*	-0.080881117	-0.141914514
23	*Pseudoboa coronata*	0.074212397	0.210908563
24	*Xenodon neuwiedii*	0.105125368	0.100711294
25	*Natrix natrix*	0.119926431	0.121899948
26	*Nerodia sipedon*	-0.098116251	-0.002316708
27	*Thamnophis rufipunctatus*	-0.060737225	0.063585661
28	*Cylindrophis lineatus*	0.032975549	-0.035209922
29	*Cylindrophis melanotus*	-0.106425003	-0.115407238
30	*Cylindrophis ruffus*	0.082586554	0.018184904
31	*Cylindrophis ruffus*	-0.061383152	-0.130512028
32	*Cylindrophis ruffus*	0.137455487	0.070682839
33	*Bungarus fasciatus*	0.000778663	-0.025284206
34	*Calliophis maculiceps*	0.026363564	0.000408889
35	*Furina diadema*	0.079523332	0.108975631
36	*Micruroides euryxanthus*	0.121692343	0.161029122
37	*Micrurus fulvius*	0.057079412	0.093788045
38	*Micrurus nigrocinctus*	0.056724753	-0.044701584
39	*Naja naja*	-0.143723248	-0.05522153
40	*Notechis scutatus*	-0.008070314	-0.01184194
41	*Oxyuranus scutellatus*	-0.004935688	0.077449185

42	*Simoselaps bertholdi*	0.032474201	0.048568996
43	*Vermicella annulata*	-0.045511393	0.045072649
44	*Amblyodipsas polylepis hildebrantii*	-0.028344061	0.112727351
45	*Aparallactus capensis*	0.084386883	0.20512115
46	*Aparallactus modestus*	0.049601564	0.083299508
47	*Aparallactus niger*	0.129766286	0.146815025
48	*Polemon christyi*	0.100135239	0.101197002
49	*Homoroselaps lacteus*	-0.062021456	0.125317093
50	*Boaedon fuliginosus*	0.200247007	0.246311793
51	*Psammophylax variabilis*	-0.200063411	-0.053517659
52	*Pseudaspis cana*	0.054306276	0.062239663
53	*Duberria lutrix*	0.010793303	0.177818063
54	*Heteroliodon occipitalis*	-0.176493802	-0.17318939
55	*Langaha madagascariensis*	0.113730699	0.111004854
56	*Lycodryas granuliceps*	0.108447148	0.242684559
57	*Loxocemus bicolor*	0.084063449	0.174520218
58	*Loxocemus bicolor*	0.011008884	0.265964332
59	*Aspidites melanocephalus*	0.041307832	-0.104538857
60	*Malayopython reticulatus*	0.10178784	0.223702623
61	*Morelia spilota*	0.050450357	-0.012268994
62	*Morelia spilota*	-0.036912211	-0.005658435
63	*Python molurus*	-0.006926498	0.057605679
64	*Trachyboa boulengeri*	0.072002837	0.112593102
65	*Tropidophis melanurus*	0.146772609	0.062031911
66	*Plectrurus perroteti*	0.090311816	0.056123979
67	*Rhinophis philippinus*	0.015292352	0.069263629
68	*Teretrurus sanguineus*	0.003325563	-0.112278992
69	*Uropeltis melanogaster*	0.04789368	-0.009005969
70	*Crotalus atrox*	-0.015095555	-0.090278612
71	*Vipera aspis*	0.054167152	0.109639272
72	*Xenopeltis unicolor*	0.087356468	0.184409284
73	*Xenopeltis unicolor*	0.074411693	-0.036305691
74	*Dinilysia patagonica*	0.004909897	-0.068743777

Appendix 5 – Scores of first two phylogenetically corrected principal components Gauthier et al (2012) morphological phylogenetic hypothesis

No.	Species	PC1 (26.51 %)	PC2 (15.11%)
1	*Anilius scytale*	-0.014048273	0.007380449
2	*Anilius scytale*	0.05142084	-0.027899806
3	*Anomochilus leonardi*	0.0070641	-0.129972293
4	*Candoia bibroni*	-0.020864213	0.092029219
5	*Casarea dussumieri*	-0.032382486	0.049805755
6	*Epicrates cenchria*	-0.032583473	-0.008346432
7	*Exiliboa placata*	0.198858068	0.021380126
8	*Sanzinia madagascariensis*	0.2441564	0.029851914
9	*Boiga irregularis*	-0.076603812	-0.046947497
10	*Coluber constrictor*	-0.16700922	0.020261398
11	*Dasypeltis gansi*	-0.206410383	0.159145245
12	*Drymarchon corais*	-0.197395775	0.014898804
13	*Lampropeltis getula*	-0.222185112	0.068208137
14	*Oligodon arnensis*	-0.048760512	0.076635216
15	*Pantherophis guttatus*	-0.223814721	0.020129474
16	*Platyceps najadum*	-0.011654578	0.053762807
17	*Ptyas mucosa*	0.141264924	-0.039368785
18	*Senticolis triaspis*	-0.005805688	0.004495313
19	*Carphophis amoenus*	0.135204849	-0.035064355
20	*Elapomorphus quinquelineatus*	0.181081172	-0.008319963
21	*Phalotris mertensi*	0.101052107	-0.071107679
22	*Philodryas patagoniensis*	0.143833396	-0.012390388
23	*Pseudoboa coronata*	-0.214957424	0.088542696
24	*Xenodon neuwiedii*	-0.148142901	-0.012897512
25	*Natrix natrix*	-0.180229783	0.006386737
26	*Nerodia sipedon*	0.064640706	0.066640205
27	*Thamnophis rufipunctatus*	-0.031422498	0.130277685
28	*Cylindrophis lineatus*	-0.011503089	-0.0207229
29	*Cylindrophis melanotus*	0.144207396	0.021739167
30	*Cylindrophis ruffus*	-0.081773613	-0.019796136
31	*Cylindrophis ruffus*	0.126379896	-0.049223921
32	*Cylindrophis ruffus*	-0.15920804	-0.027122916
33	*Bungarus fasciatus*	-0.001144276	0.035431956
34	*Calliophis maculiceps*	-0.041088625	0.037191043
35	*Furina diadema*	-0.153263994	0.024842645
36	*Micruroides euryxanthus*	-0.210988245	0.031354817
37	*Micrurus fulvius*	-0.106091029	-0.004676228
38	*Micrurus nigrocinctus*	-0.023898586	-0.065892123
39	*Naja naja*	0.108311488	0.124411903
40	*Notechis scutatus*	-0.008918647	0.015033999
41	*Oxyuranus scutellatus*	-0.065629669	0.072094924

42	*Simoselaps bertholdi*	-0.075644725	0.051513793
43	*Vermicella annulata*	-0.027488697	0.128637075
44	*Amblyodipsas polylepis hildebrantii*	-0.075284488	0.103974639
45	*Aparallactus capensis*	-0.218532934	0.052646808
46	*Aparallactus modestus*	-0.112001366	0.035179421
47	*Aparallactus niger*	-0.199472789	-0.028768988
48	*Polemon christyi*	-0.156730012	0.007699826
49	*Homoroselaps lacteus*	-0.064281869	0.138466603
50	*Boaedon fuliginosus*	-0.326274806	0.013551013
51	*Psammophylax variabilis*	0.15414798	0.148774735
52	*Pseudaspis cana*	-0.108094795	0.061212027
53	*Duberria lutrix*	-0.164173349	0.133451735
54	*Heteroliodon occipitalis*	0.249147448	0.058267194
55	*Langaha madagascariensis*	-0.166488175	-0.001243082
56	*Lycodryas granuliceps*	-0.24753185	0.032916291
57	*Loxocemus bicolor*	-0.194621248	0.026714721
58	*Loxocemus bicolor*	-0.223053318	0.158257518
59	*Aspidites melanocephalus*	0.033906996	-0.072136401
60	*Malayopython reticulatus*	-0.247221328	0.059528651
61	*Morelia spilota*	-0.055443248	0.00019308
62	*Morelia spilota*	0.006437601	0.050624914
63	*Python molurus*	-0.052917209	0.097495811
64	*Trachyboa boulengeri*	-0.138795921	0.025326925
65	*Tropidophis melanurus*	-0.16342701	-0.024680219
66	*Plectrurus perroteti*	-0.116670558	0.01150454
67	*Rhinophis philippinus*	-0.059556423	0.003545514
68	*Teretrurus sanguineus*	0.066740018	-0.054737428
69	*Uropeltis melanogaster*	-0.05509006	0.002147831
70	*Crotalus atrox*	0.057328175	-0.029812545
71	*Vipera aspis*	-0.129098305	0.031363071
72	*Xenopeltis unicolor*	-0.195391054	0.033044303
73	*Xenopeltis unicolor*	-0.034099781	-0.052567652
74	*Dinilysia patagonica*	0.038877054	0.001702387

Appendix 6 – Phylogenetically corrected principal component analysis

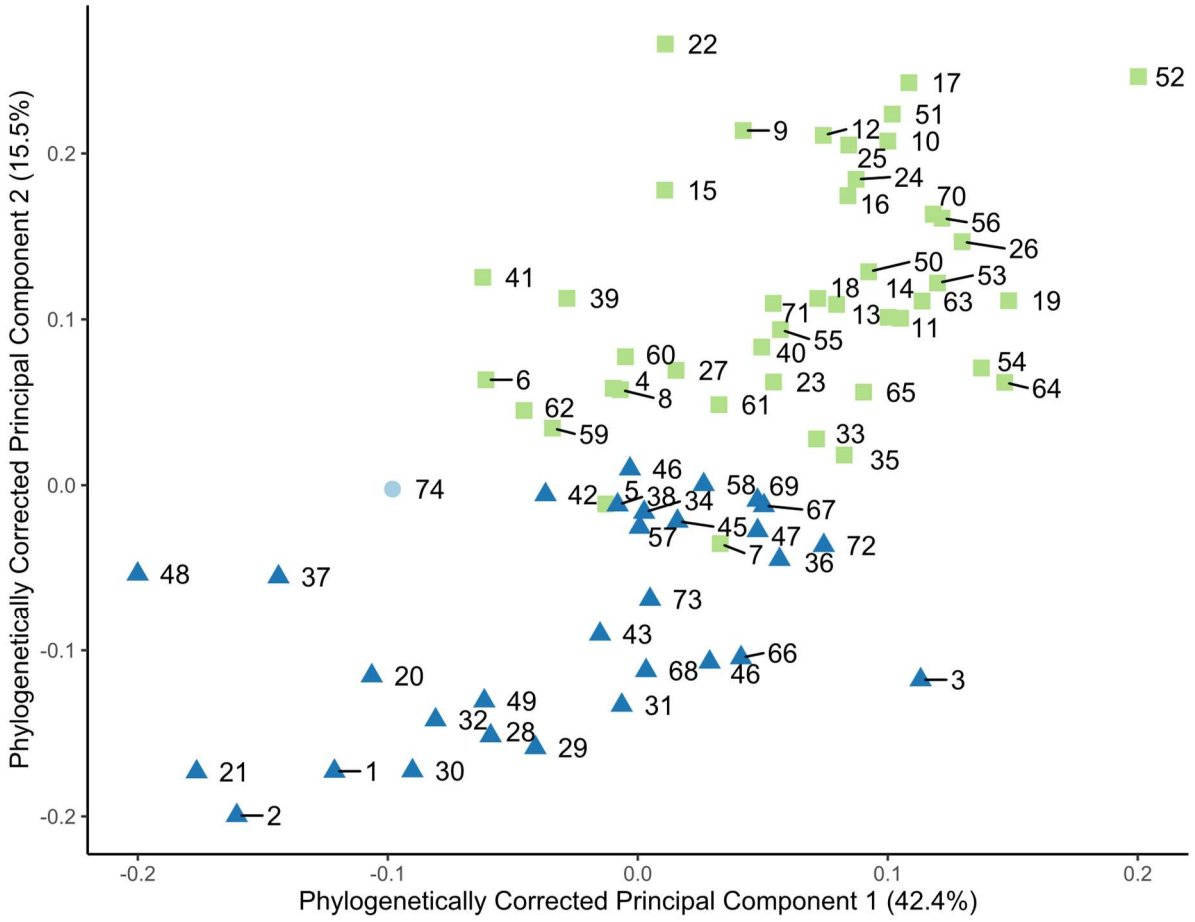

Figure. Phylogenetically corrected principal component analysis for molecular phylogenetic hypothesis. Colours and shapes by ecological category: Dark blue triangles – Fossorial, Light green squares – Terrestrial, Light blue circle - Fossil.

Specimen numbers: 1 Anilius scytale, 2 Anilius scytale, 3 Anomochilus leonardi, 4 Candoia bibroni, 5 Casarea dussumieri, 6 Epicrates cenchria, 7 Exiliboa placata, 8 Sanzinia madagascariensis, 9 Boiga irregularis, 10 Coluber constrictor, 11 Dasypeltis gansi, 12 Drymarchon corais, 13 Lampropeltis getula, 14 Oligodon arnensis, 15 Pantherophis guttatus, 16 Platyceps najadum, 17 Ptyas mucosa, 18 Senticolis triaspis, 19 Carphophis amoenus, 20 Elapomorphus quinquelineatus, 21 Phalotris mertensi, 22 Philodryas patagoniensis, 23 Pseudoboa coronate, 24 Xenodon neuwiedii, 25 Natrix natrix, 26 Nerodia sipedon, 27 Thamnophis rufipunctatus, 28 Cylindrophis lineatus, 29 Cylindrophis melanotus, 30 Cylindrophis ruffus, 31 Cylindrophis ruffus, 32 Cylindrophis ruffus, 33 Bungarus fasciatus, 34 Calliophis maculiceps, 35 Furina diadema, 36 Micruroides euryxanthus, 37 Micrurus fulvius, 38 Micrurus nigrocinctus. 39 Naja naja, 40 Notechis scutatus, 41 Oxyuranus scutellatus, 42 Simoselaps bertholdi, 43 Vermicella annulata, 44 Amblyodipsas polylepis hildebrantii, 45 Aparallactus capensis, 46 Aparallactus modestus, 47 Aparallactus niger, 48 Polemon christyi, 49 Homoroselaps lacteus, 50 Boaedon fuliginosus, 51 Psammophylax variabilis, 52 Pseudaspis cana, 53 Duberria lutrix, 54 Heteroliodon occipitalis, 55 Langaha madagascariensis, 56 Lycodryas granuliceps, 57 Loxocemus bicolor, 58 Loxocemus bicolor, 59 Aspidites melanocephalus, 60 Malayopython reticulatus, 61 Morelia spilota, 62 Morelia spilota, 63 Python molurus, 64 Trachyboa boulengeri, 65 Tropidophis melanurus, 66 Plectrurus perroteti, 67 Rhinophis philippinus, 68 Teretrurus sanguineus, 69 Uropeltis melanogaster, 70 Crotalus atrox, 71 Vipera aspis, 72 Xenopeltis unicolor, 73 Xenopeltis unicolor, 74 Dinilysia patagonica

Figure. Phylogenetically corrected principal component analysis for morphological phylogenetic hypothesis. Colours and shapes by ecological category: Dark blue triangles – Fossorial, Light green squares – Terrestrial, Light blue circle - Fossil.

Specimen numbers: 1 Anilius scytale, 2 Anilius scytale, 3 Anomochilus leonardi, 4 Candoia bibroni, 5 Casarea dussumieri, 6 Epicrates cenchria, 7 Exiliboa placata, 8 Sanzinia madagascariensis, 9 Boiga irregularis, 10 Coluber constrictor, 11 Dasypeltis gansi, 12 Drymarchon corais, 13 Lampropeltis getula, 14 Oligodon arnensis, 15 Pantherophis guttatus, 16 Platyceps najadum, 17 Ptyas mucosa, 18 Senticolis triaspis, 19 Carphophis amoenus, 20 Elapomorphus quinquelineatus, 21 Phalotris mertensi, 22 Philodryas patagoniensis, 23 Pseudoboa coronate, 24 Xenodon neuwiedii, 25 Natrix natrix, 26 Nerodia sipedon, 27 Thamnophis rufipunctatus, 28 Cylindrophis lineatus, 29 Cylindrophis melanotus, 30 Cylindrophis ruffus, 31 Cylindrophis ruffus, 32 Cylindrophis ruffus, 33 Bungarus fasciatus, 34 Calliophis maculiceps, 35 Furina diadema, 36 Micruroides euryxanthus, 37 Micrurus fulvius, 38 Micrurus nigrocinctus. 39 Naja naja, 40 Notechis scutatus, 41 Oxyuranus scutellatus, 42 Simoselaps bertholdi, 43 Vermicella annulata, 44 Amblyodipsas polylepis hildebrantii, 45 Aparallactus capensis, 46 Aparallactus modestus, 47 Aparallactus niger, 48 Polemon christyi, 49 Homoroselaps lacteus, 50 Boaedon fuliginosus, 51 Psammophylax variabilis, 52 Pseudaspis cana, 53 Duberria lutrix, 54 Heteroliodon occipitalis, 55 Langaha madagascariensis, 56 Lycodryas granuliceps, 57 Loxocemus bicolor, 58 Loxocemus bicolor, 59 Aspidites melanocephalus, 60 Malayopython reticulatus, 61 Morelia spilota, 62 Morelia spilota, 63 Python molurus, 64 Trachyboa boulengeri, 65 Tropidophis melanurus, 66 Plectrurus perroteti, 67 Rhinophis philippinus, 68 Teretrurus sanguineus, 69 Uropeltis melanogaster, 70 Crotalus atrox, 71 Vipera aspis, 72 Xenopeltis unicolor, 73 Xenopeltis unicolor, 74 Dinilysia patagonica

Appendix 7. CT Scans of Parietals

Pg 254-255 *Anilius scytale*

Pg 256-257 Tropidophiidae

Pg 258-262 Cylindrophiidae

Pg 263 *Anomochilus leonardi*

Pg 264-267 Uropeltidae

Pg 268-269 *Xenopeltis unicolor*

Pg 270-271 *Loxocemus bicolor*

Pg 272-276 Pythonidae

Pg 277-281 Boidae

Pg 282-291 Colubridae: Colubrinae

Pg 292-297 Colubridae: Dipsadinae

Pg 298-300 Colubridae: Natricinae

Pg 301-311 Elapidae

Pg 312-324 Lamprophiidae

Pg 325-326 Viperidae

Pg 327 *Dinilysia patagonica*

Figure 1. *Anilius scytale* BMNH 1855.5.28.23

A) Dorsal, B) Ventral, C) Left Lateral, D) Right Lateral, E) Anterior, F) Posterior. Scale bar = 1mm.

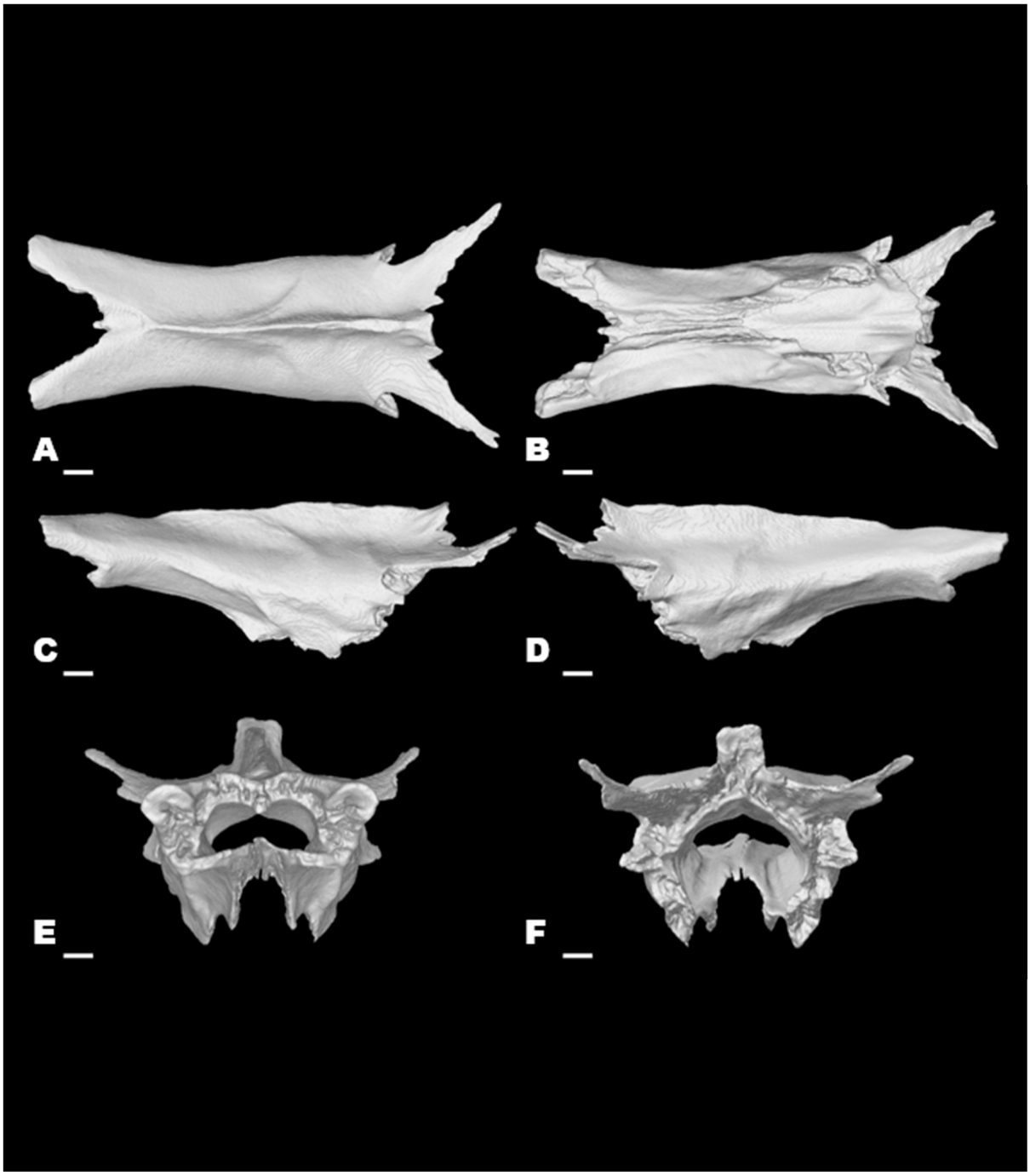

Figure 2. *Anilius scytale* BMNH 1923.11.7.6

A) Dorsal, B) Ventral, C) Left Lateral, D) Right Lateral, E) Anterior, F) Posterior. Scale bar = 1mm.

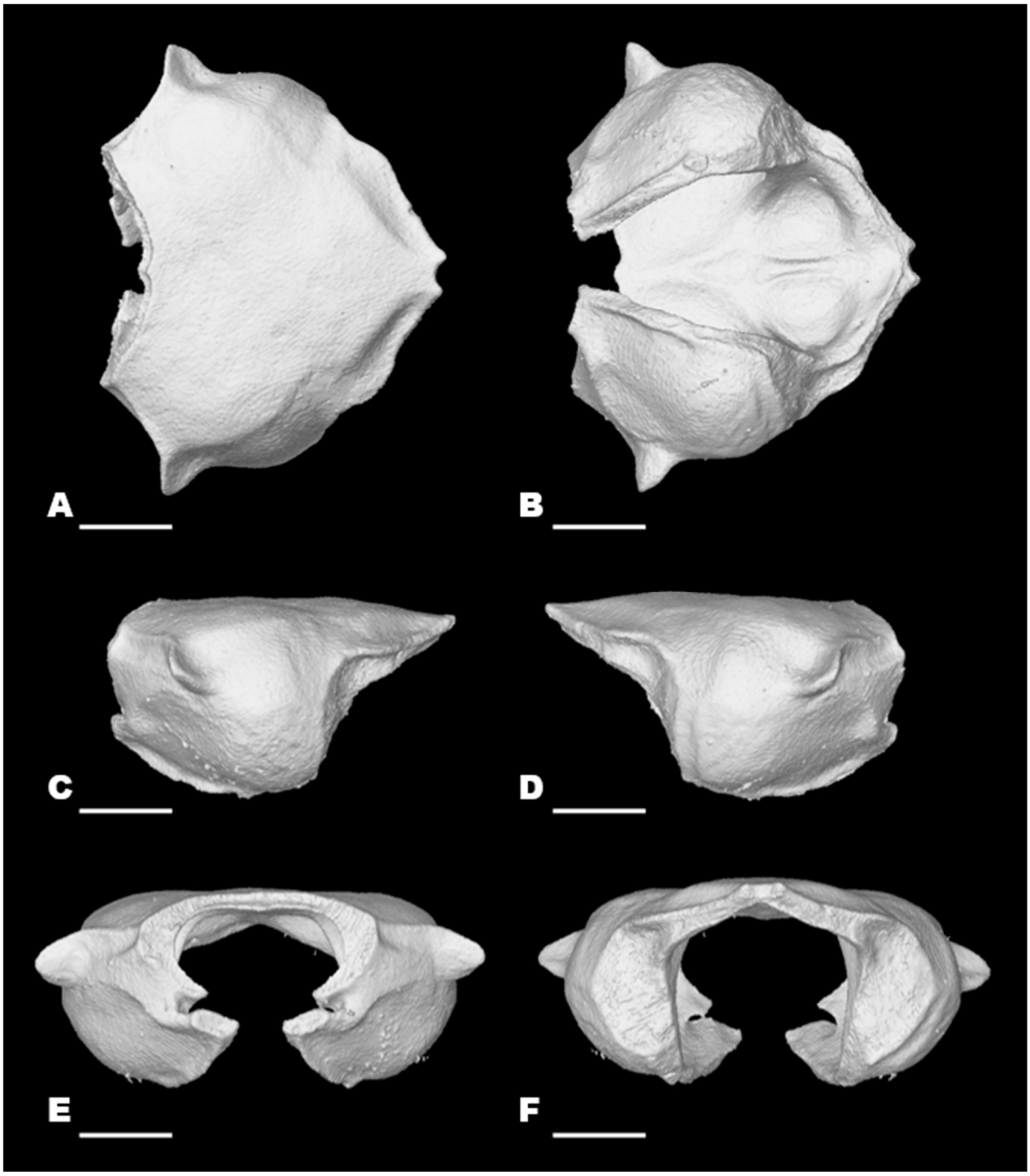

Figure 3. *Trachyboa boulengeri* BMNH 1923.10.12.9
A) Dorsal, B) Ventral, C) Left Lateral, D) Right Lateral, E) Anterior, F) Posterior. Scale bar = 1mm.

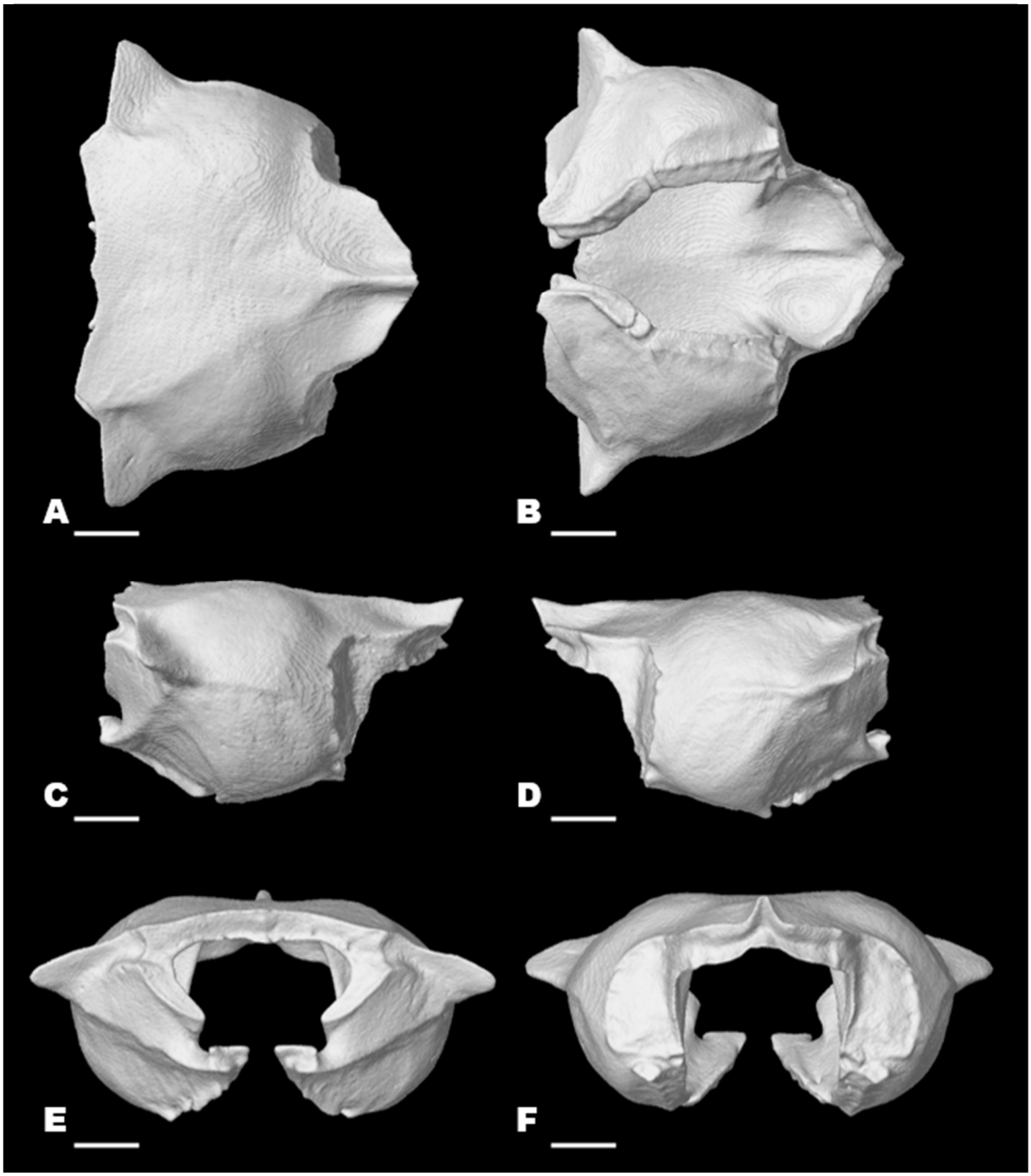

Figure 4. *Tropidophis melanurus* BMNH 1932.11.11.33

A) Dorsal, B) Ventral, C) Left Lateral, D) Right Lateral, E) Anterior, F) Posterior. Scale bar = 1mm.

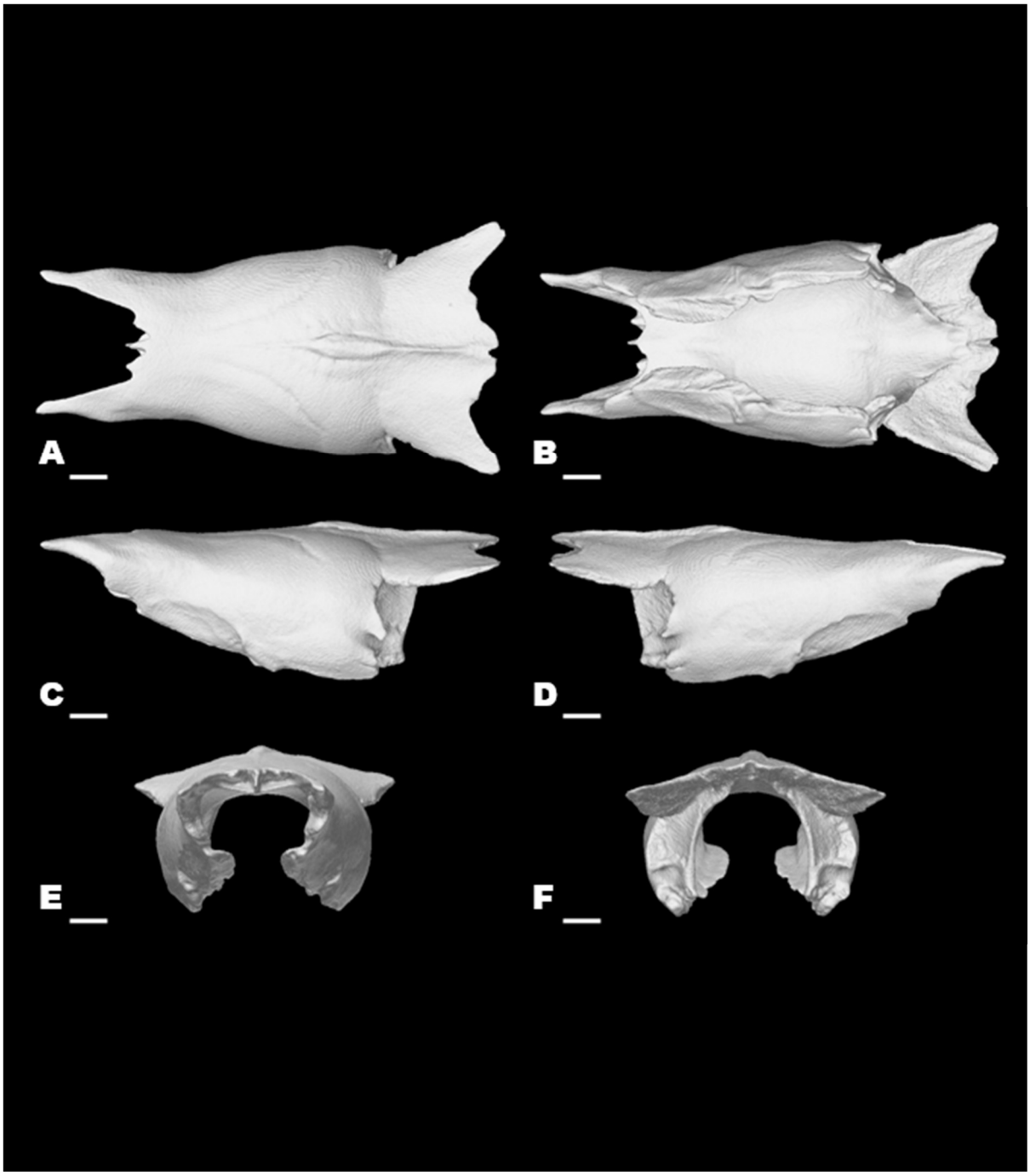

Figure 5. *Cylindrophis lineatus* BMNH 1901.5.17-1

A) Dorsal, B) Ventral, C) Left Lateral, D) Right Lateral, E) Anterior, F) Posterior. Scale bar = 1mm.

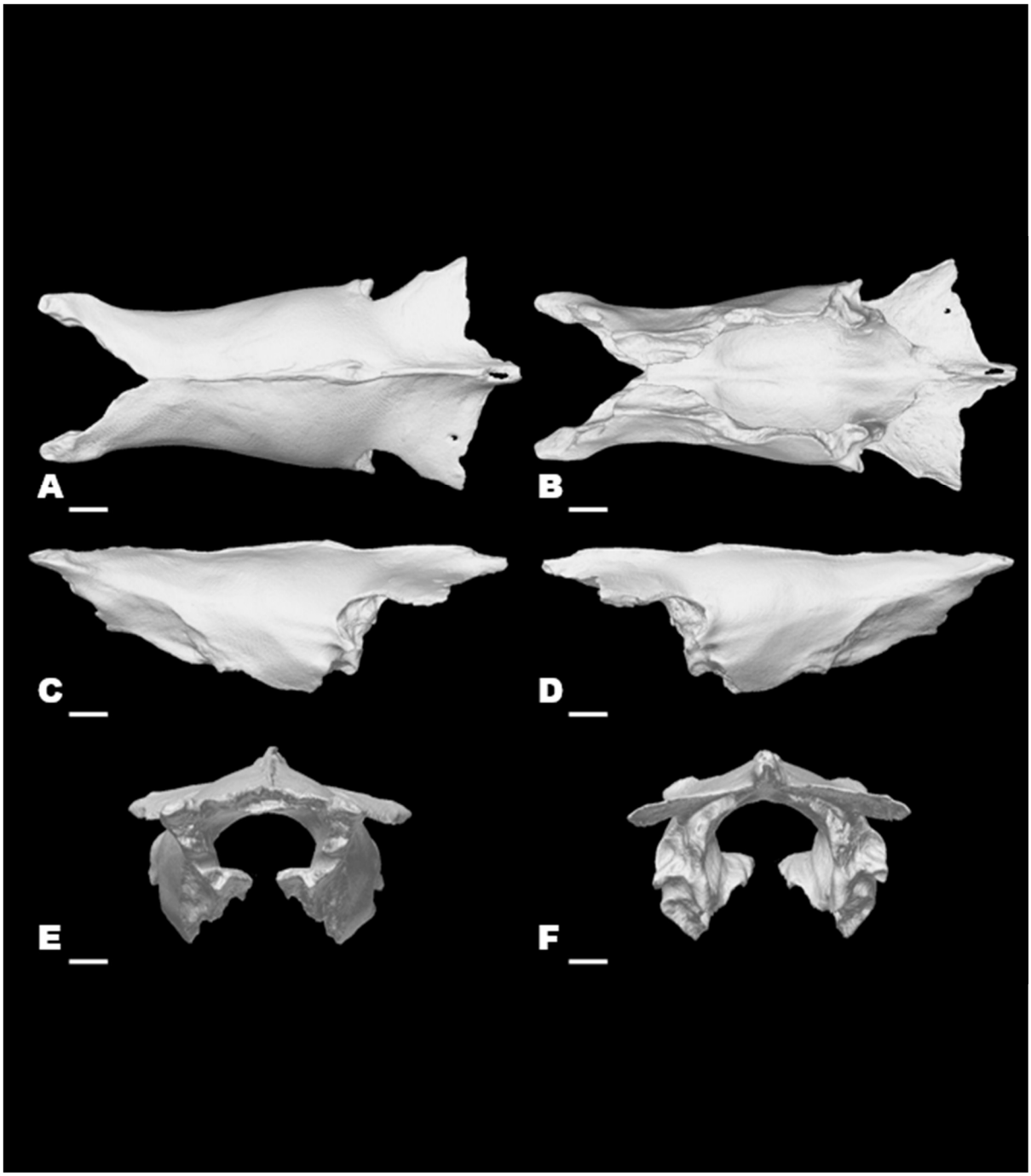

Figure 6. *Cylindrophis melanotus* BMNH 1872.4.6.123

A) Dorsal, B) Ventral, C) Left Lateral, D) Right Lateral, E) Anterior, F) Posterior. Scale bar = 1mm.

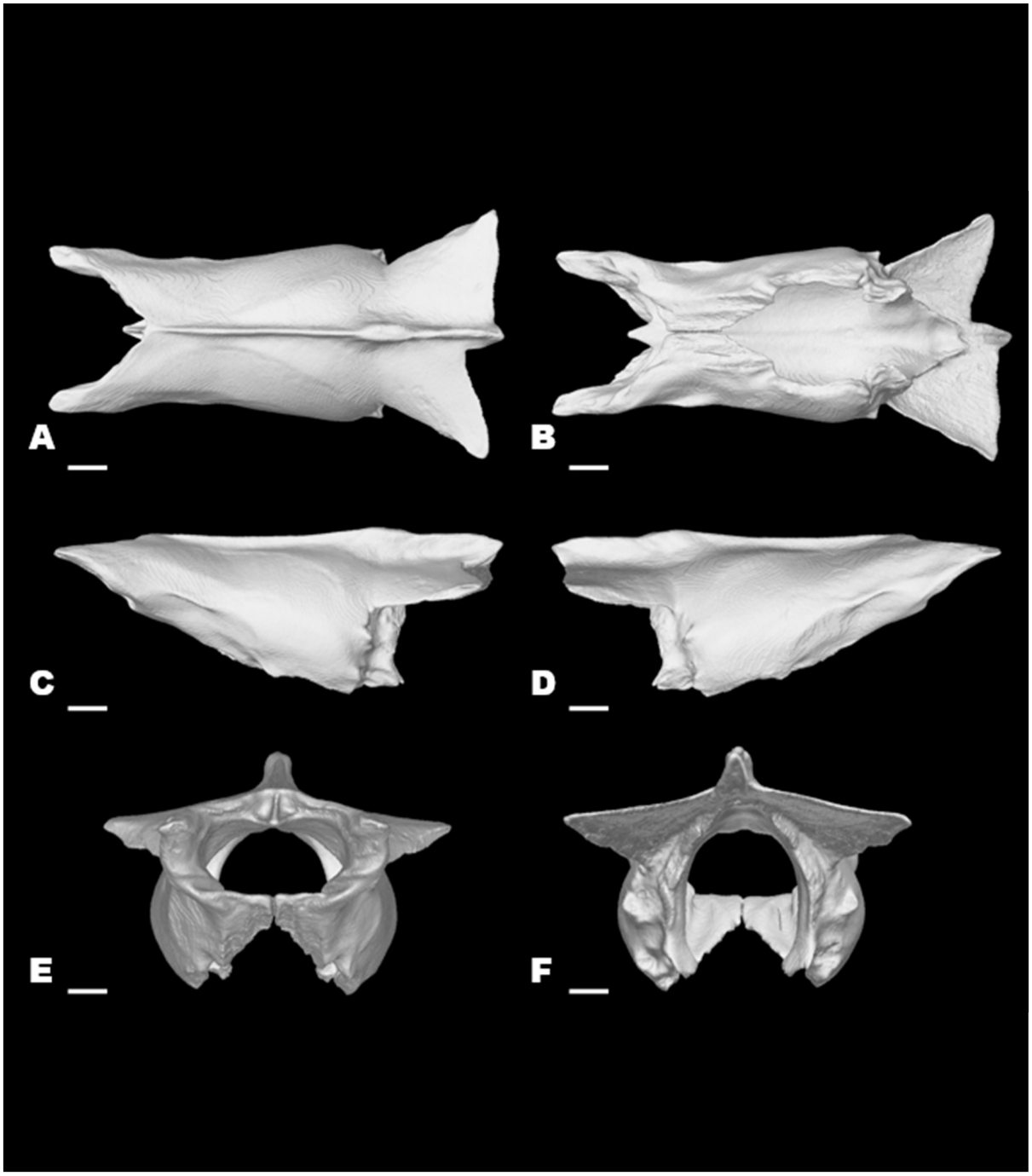

Figure 7. *Cylindrophis ruffus* UMZC R4.12-1

A) Dorsal, B) Ventral, C) Left Lateral, D) Right Lateral, E) Anterior, F) Posterior. Scale bar = 1mm.

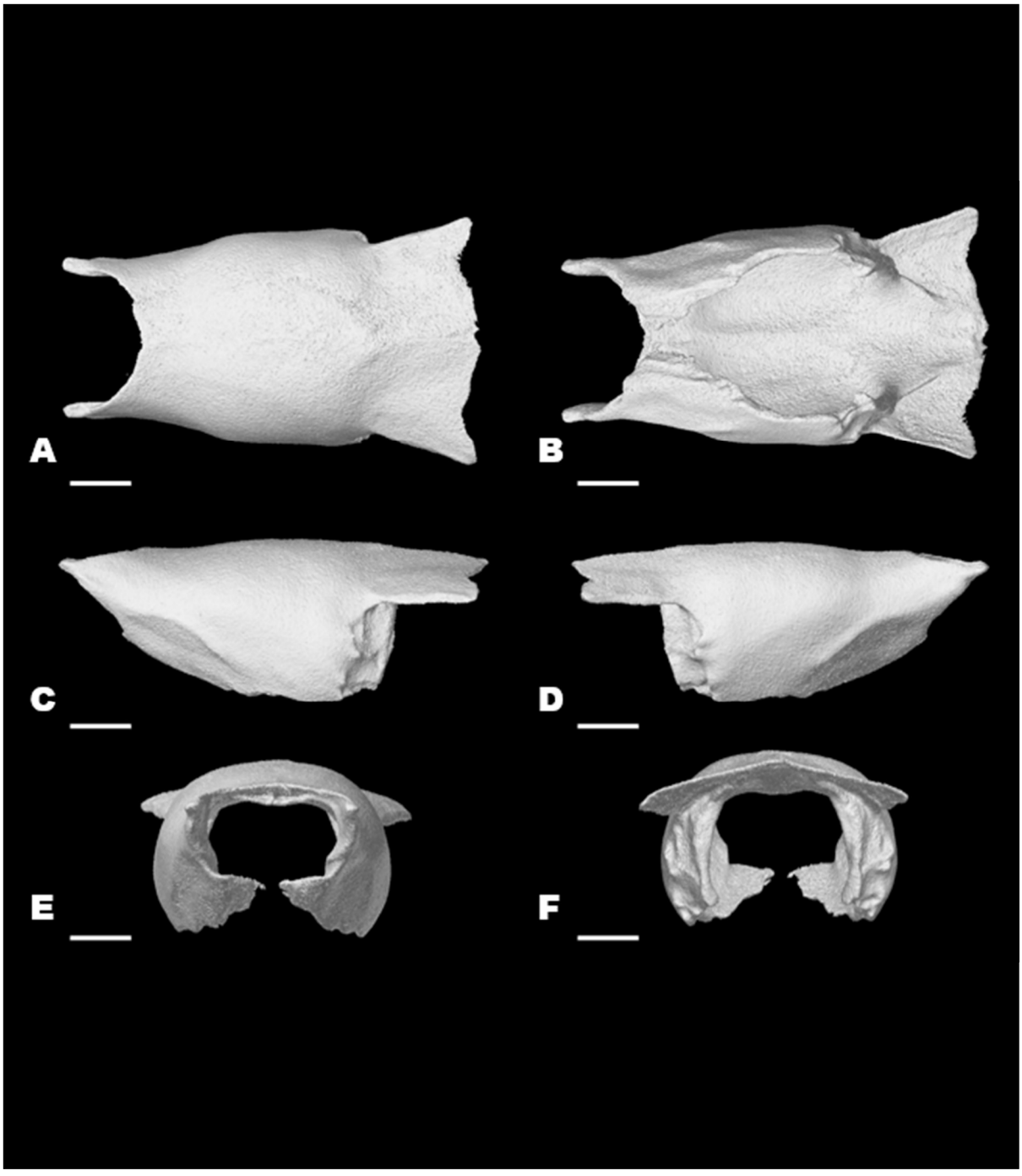

Figure 8. *Cylindrophis ruffus* UMZC R4.12-2

A) Dorsal, B) Ventral, C) Left Lateral, D) Right Lateral, E) Anterior, F) Posterior. Scale bar = 1mm.

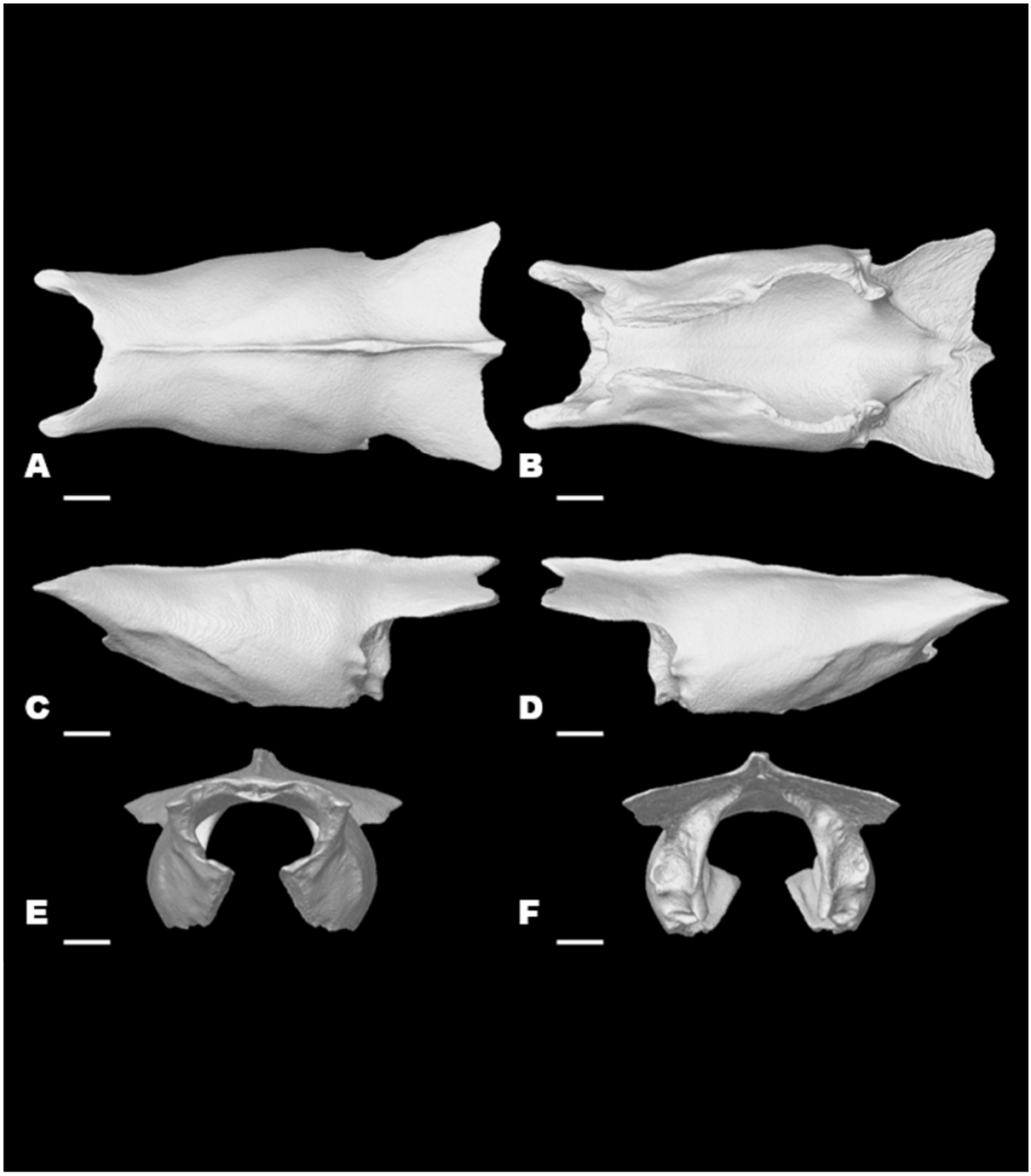

Figure 9. *Cylindrophis ruffus* UMZC R4.12-3

A) Dorsal, B) Ventral, C) Left Lateral, D) Right Lateral, E) Anterior, F) Posterior. Scale bar = 1mm.

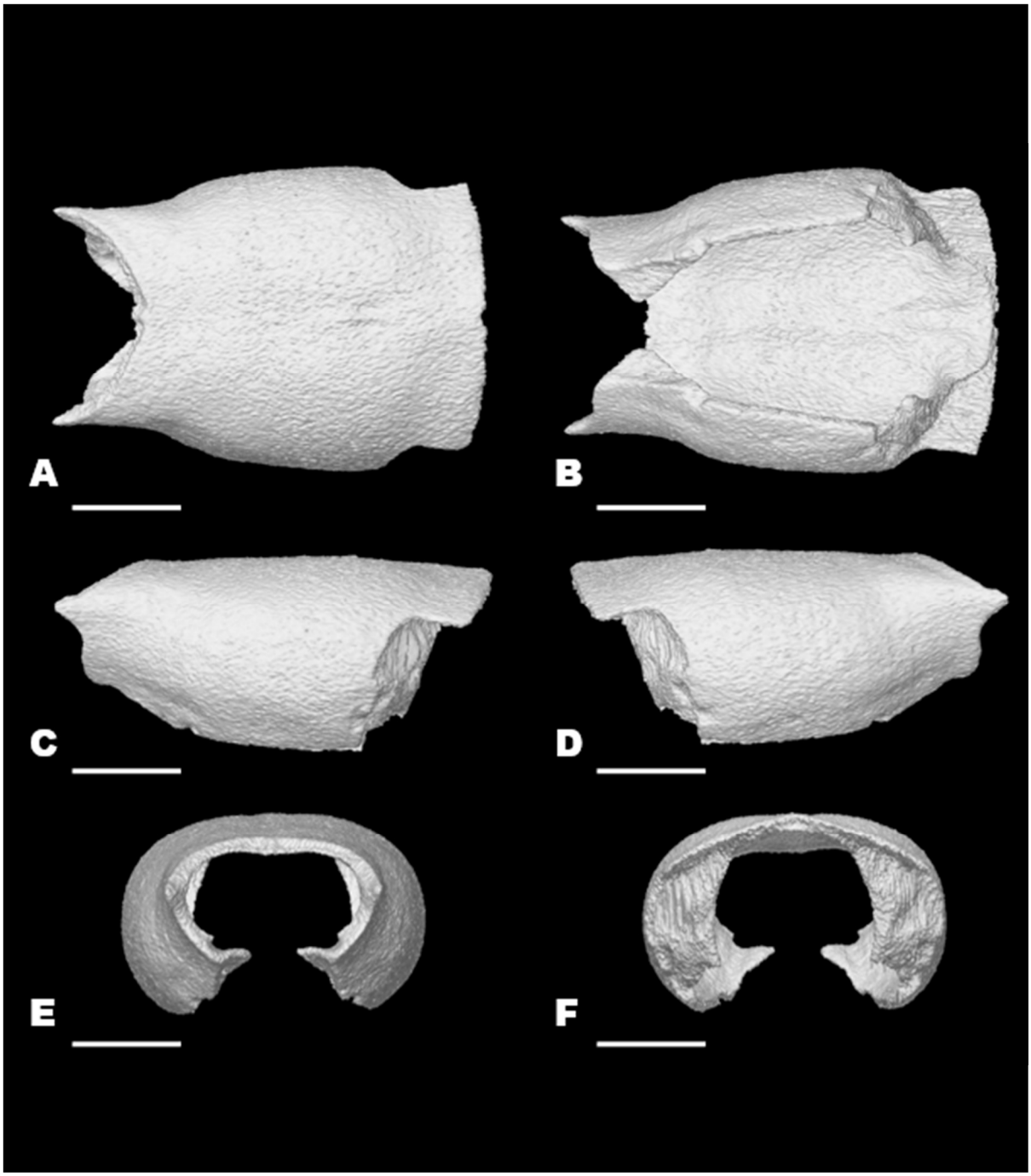

Figure 10. *Anomochilus leonardi* FRIM 0026

A) Dorsal, B) Ventral, C) Left Lateral, D) Right Lateral, E) Anterior, F) Posterior. Scale bar = 1mm.

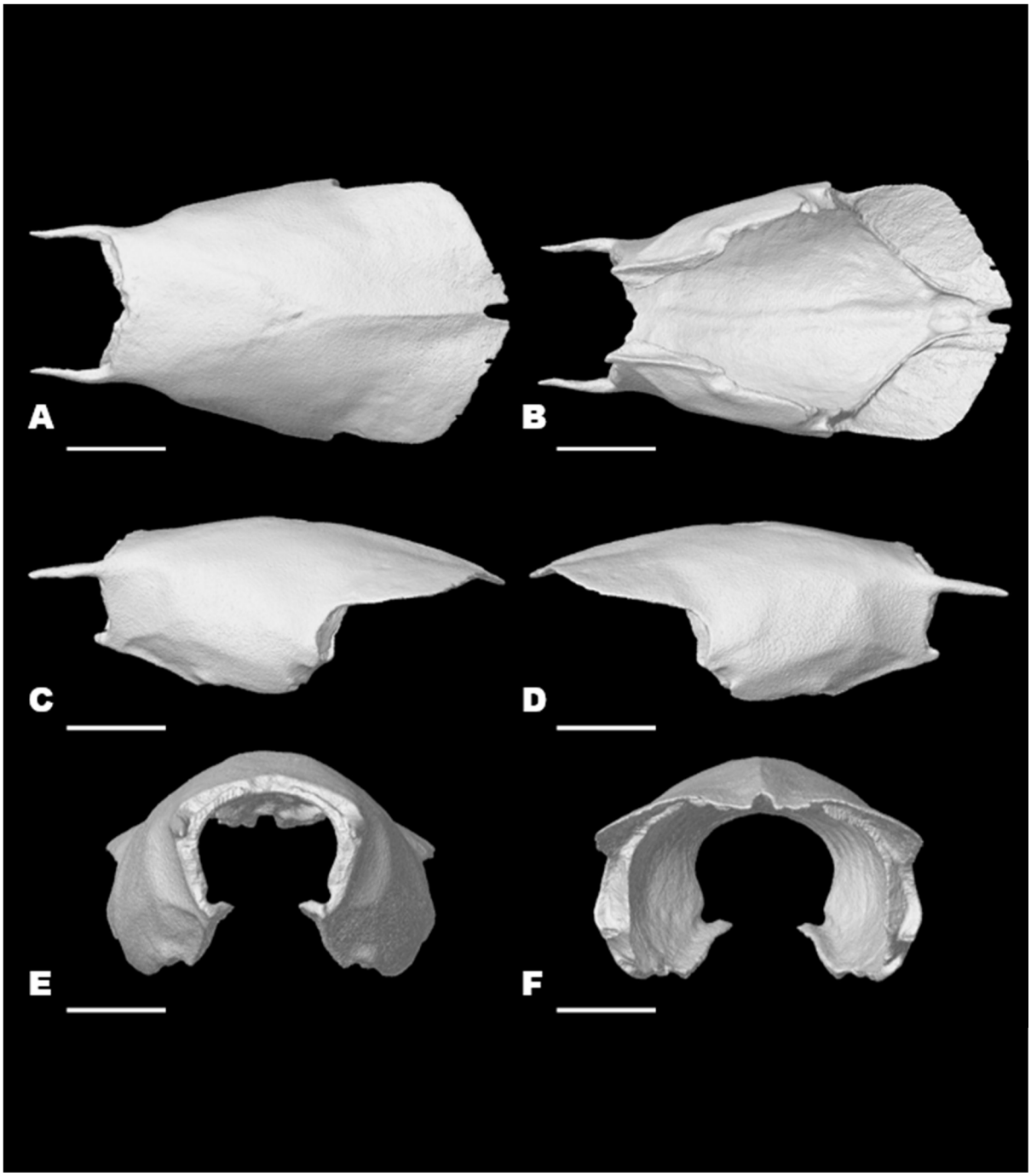

Figure 11. *Plectrurus perroteti* UMZC R5.56-1

A) Dorsal, B) Ventral, C) Left Lateral, D) Right Lateral, E) Anterior, F) Posterior. Scale bar = 1mm.

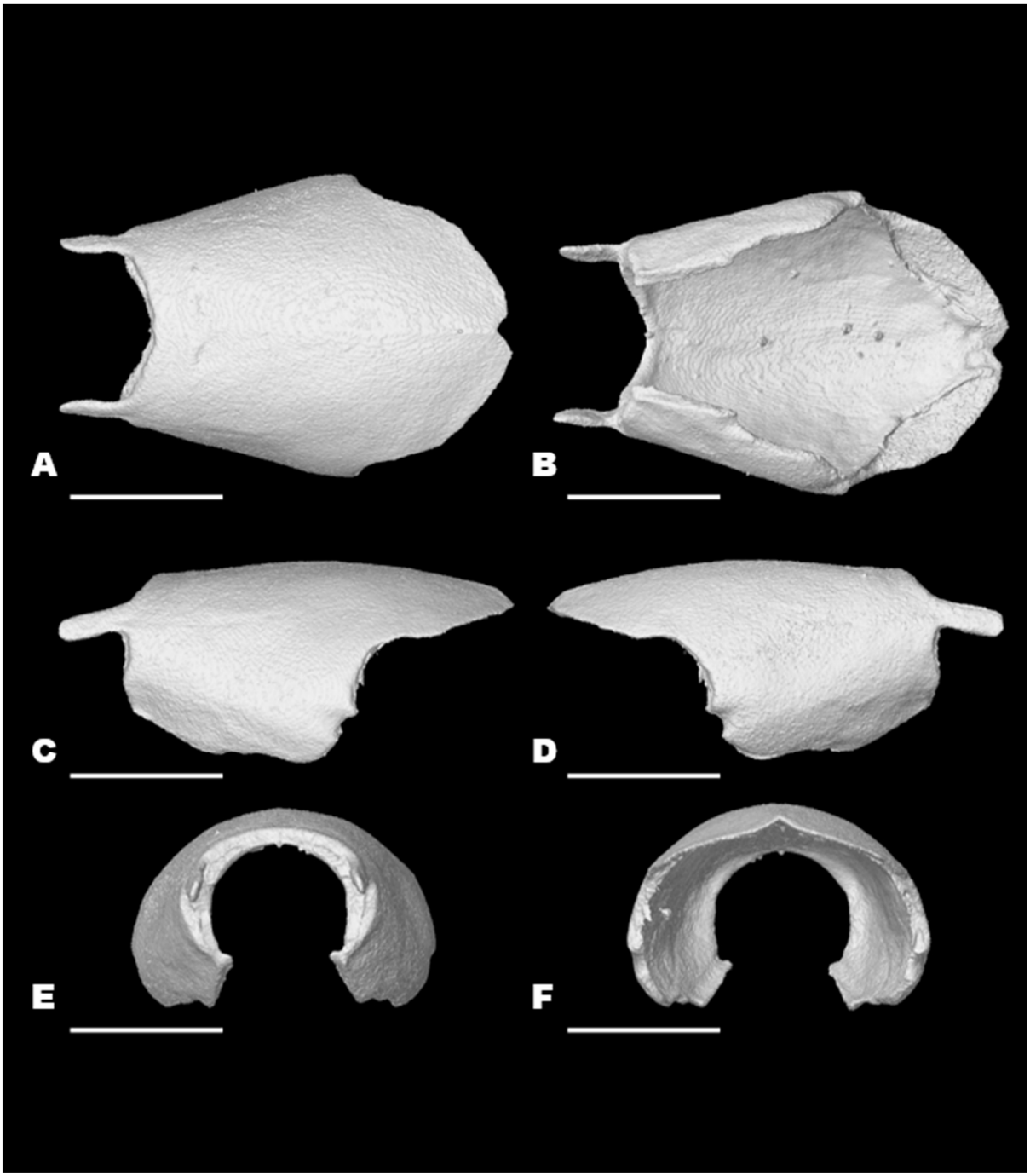

Figure 12. *Rhinophis philippinus* UMZC R5.7-1

A) Dorsal, B) Ventral, C) Left Lateral, D) Right Lateral, E) Anterior, F) Posterior. Scale bar = 1mm.

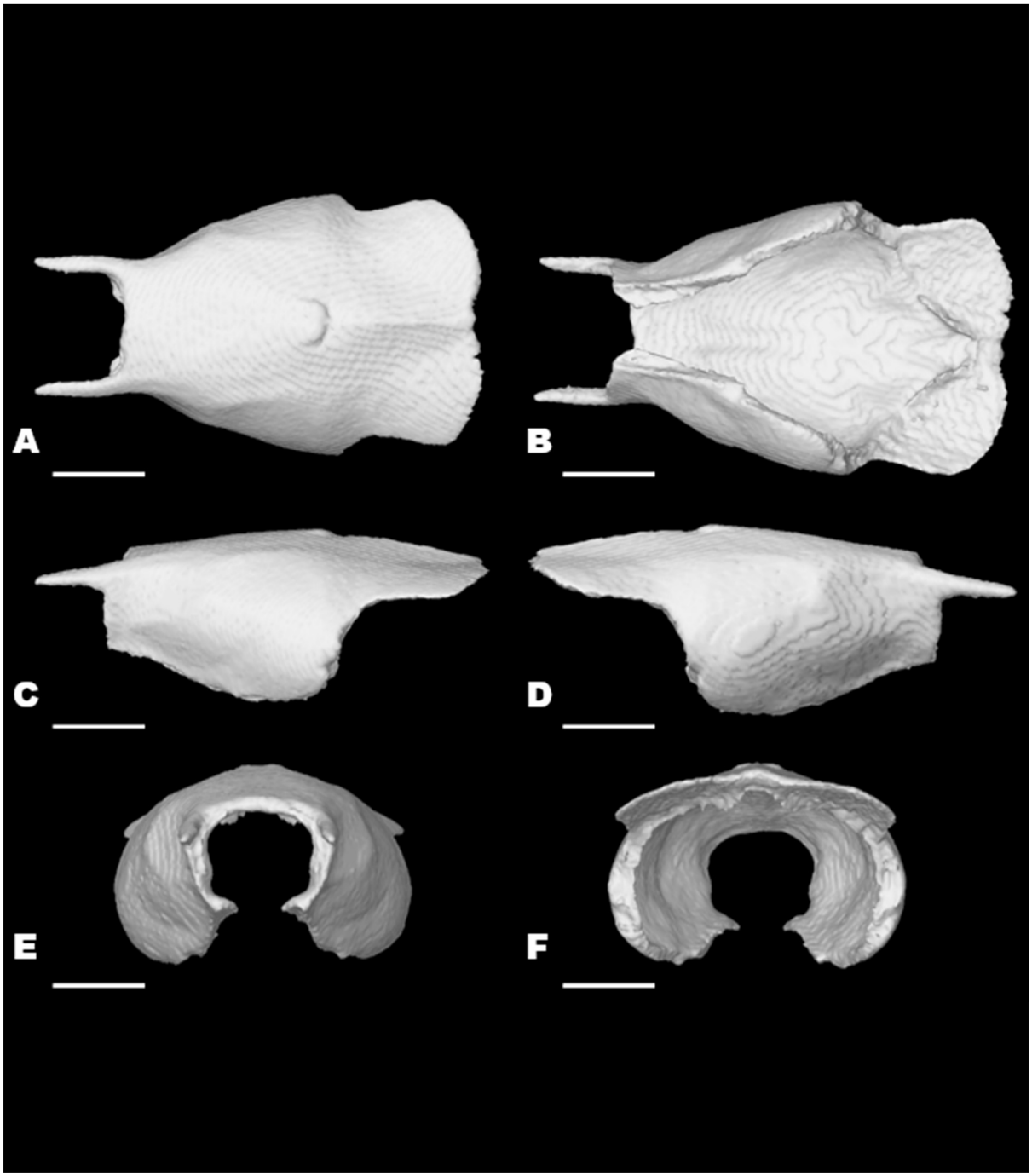

Figure 13. *Teretrurus sanguineus* CAS:HERP:244362

A) Dorsal, B) Ventral, C) Left Lateral, D) Right Lateral, E) Anterior, F) Posterior. Scale bar = 1mm.

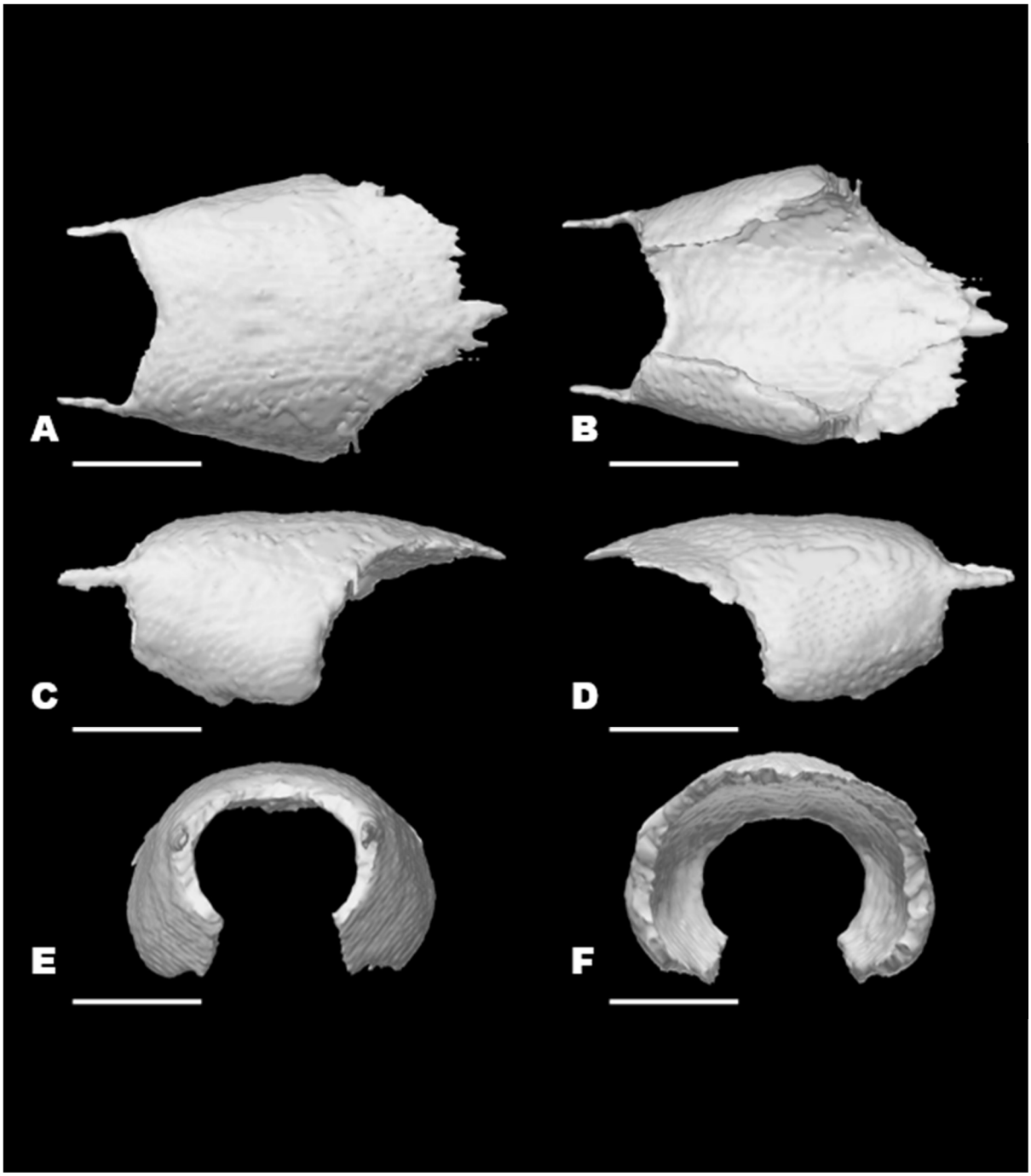

Figure 14. *Uropeltis melanogaster* UMMZ:HERPS:96275

A) Dorsal, B) Ventral, C) Left Lateral, D) Right Lateral, E) Anterior, F) Posterior. Scale bar = 1mm.

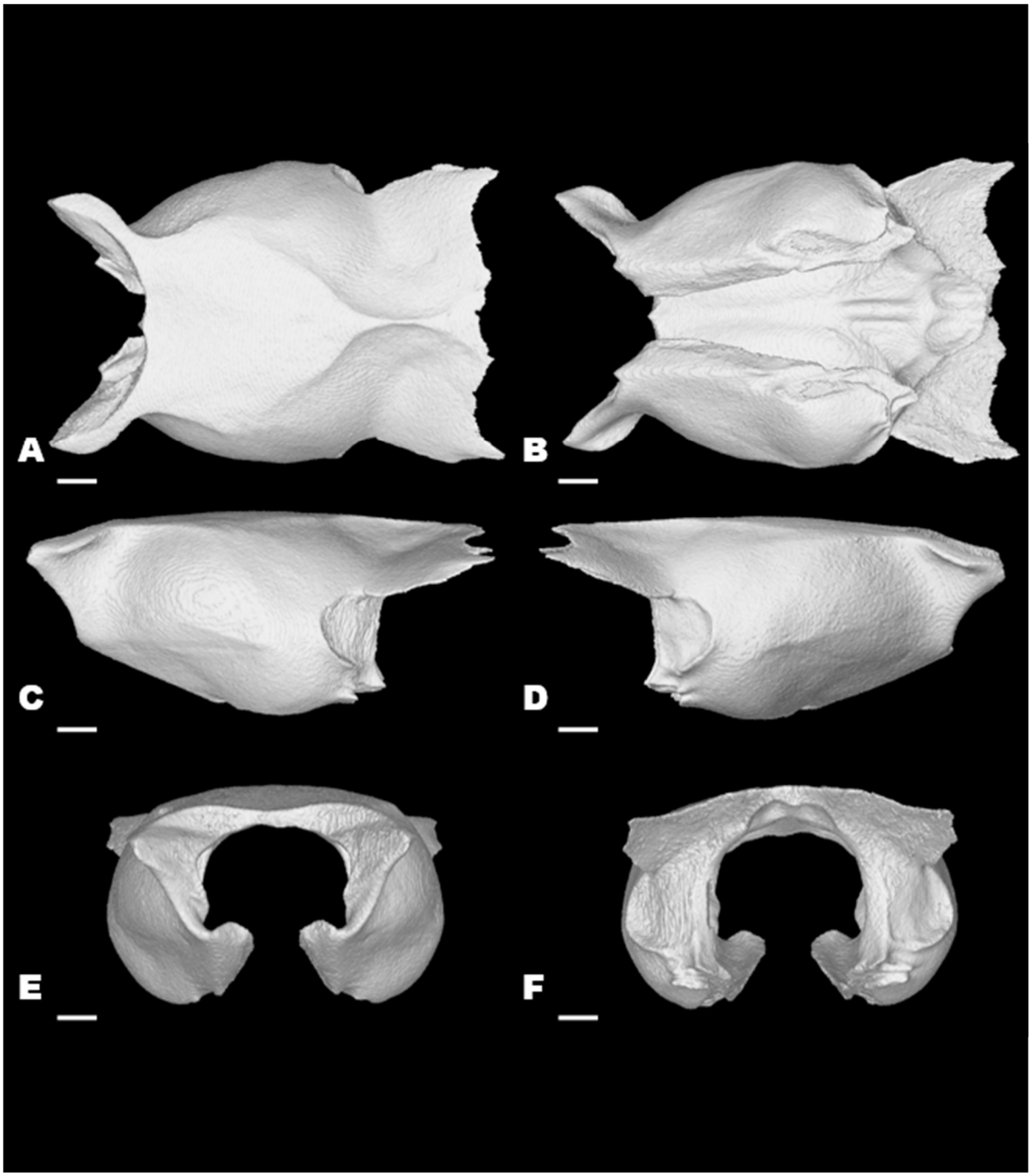

Figure 15 *Xenopeltis unicolor* BMNH 1912.6.26.3

A) Dorsal, B) Ventral, C) Left Lateral, D) Right Lateral, E) Anterior, F) Posterior. Scale bar = 1mm.

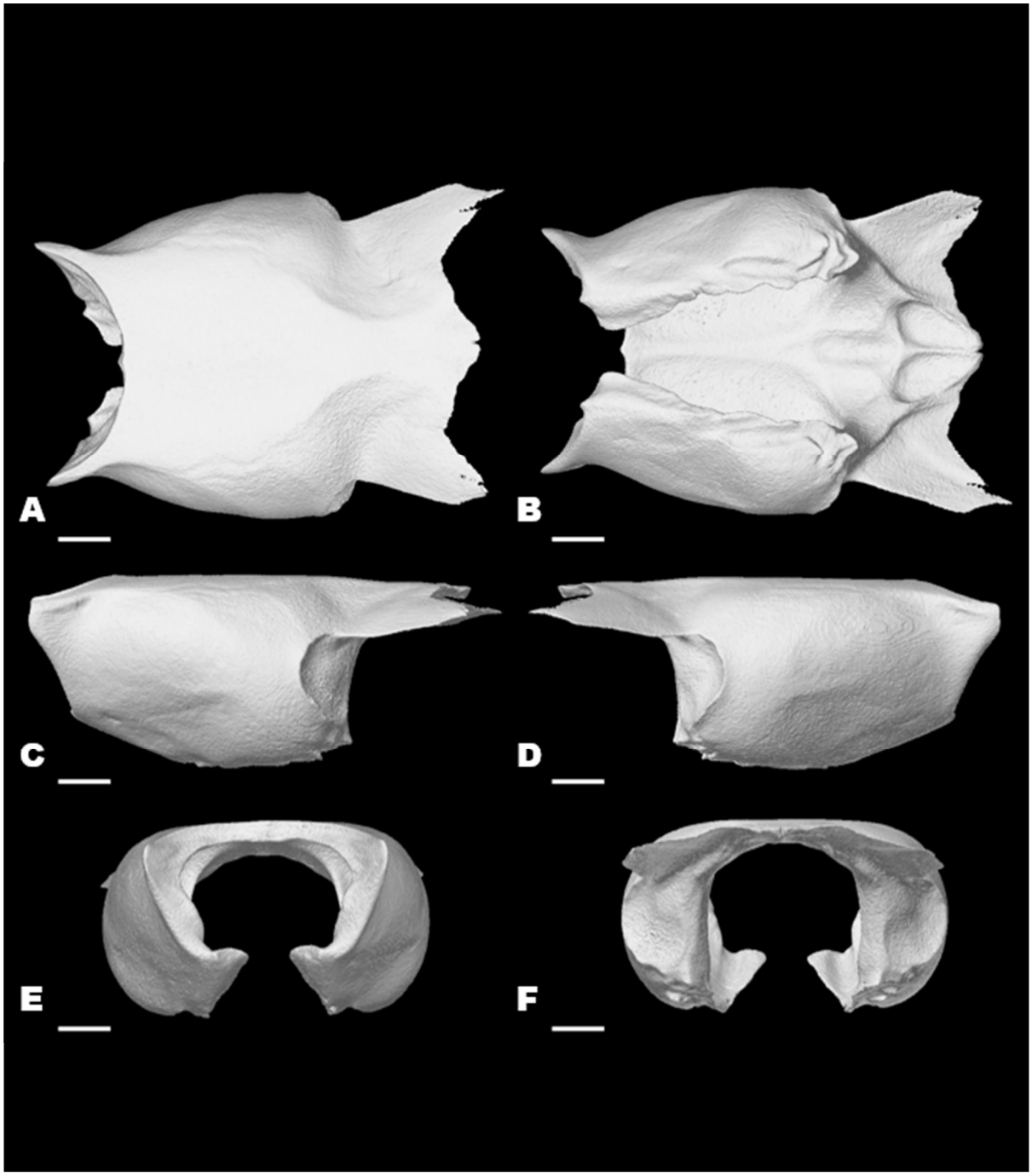

Figure 16. *Xenopeltis unicolor* UMZC R6.1-2

A) Dorsal, B) Ventral, C) Left Lateral, D) Right Lateral, E) Anterior, F) Posterior. Scale bar = 1mm.

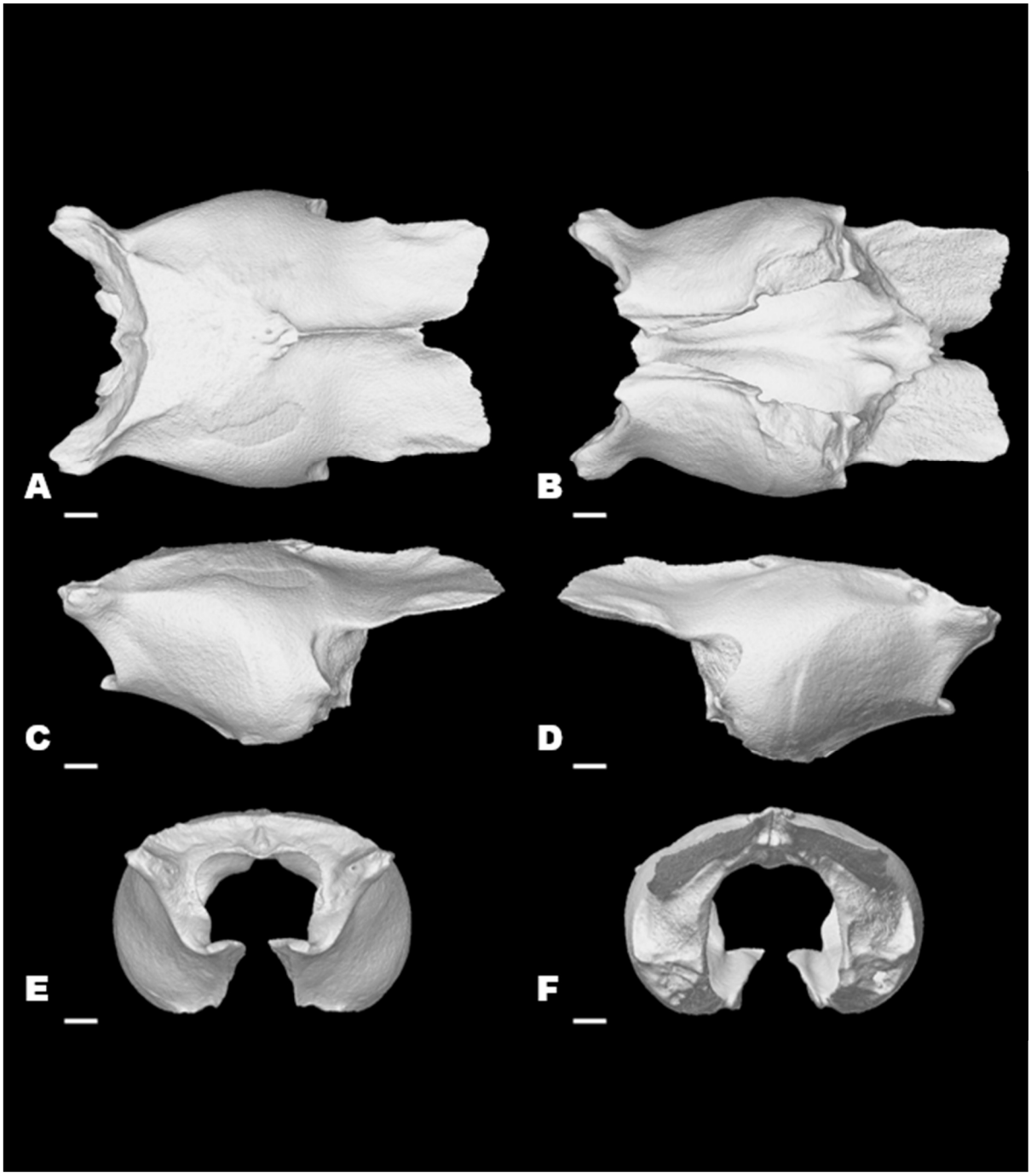

Figure 17. *Loxocemus bicolor* BMNH 1988.354

A) Dorsal, B) Ventral, C) Left Lateral, D) Right Lateral, E) Anterior, F) Posterior. Scale bar = 1mm.

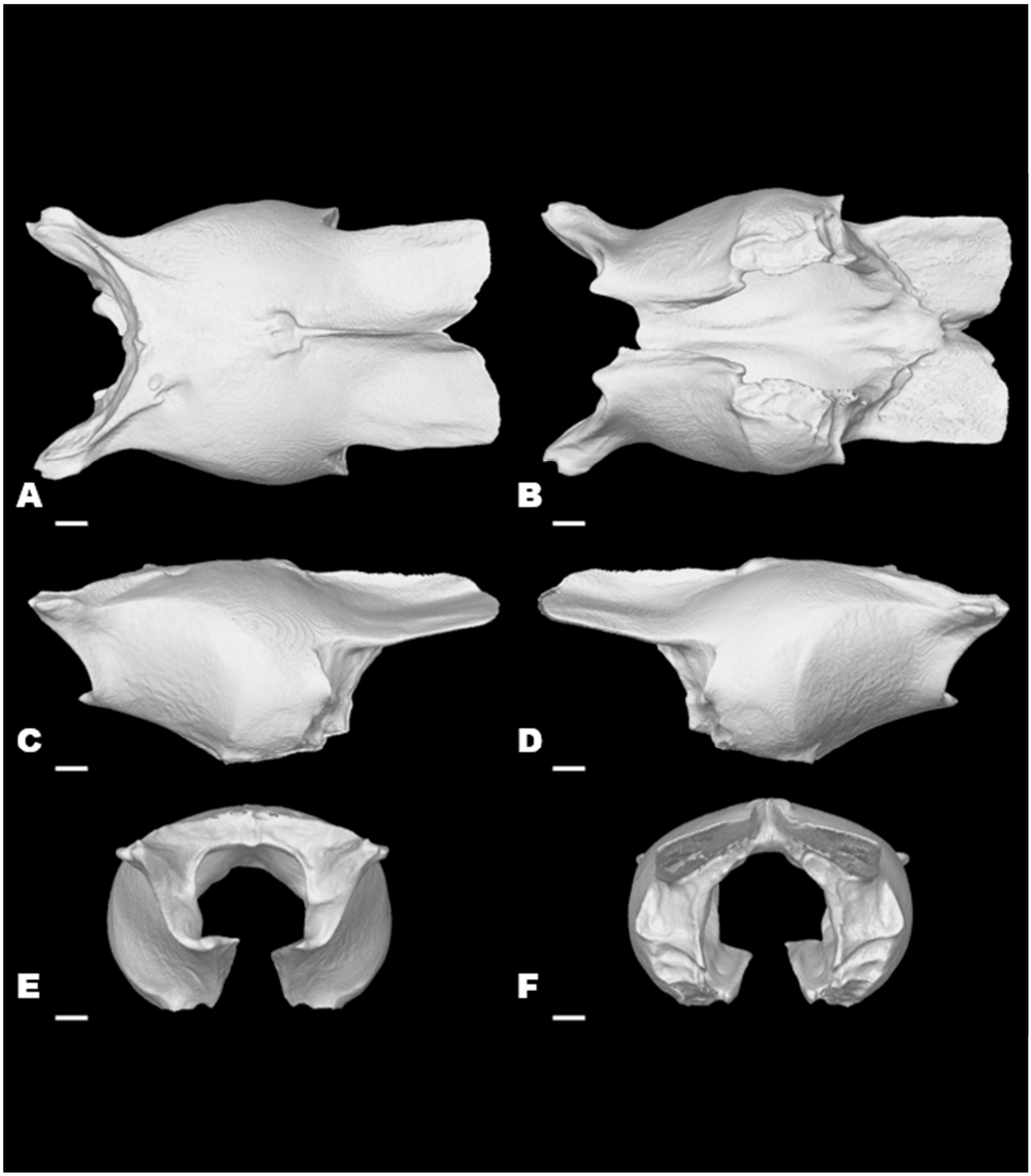

Figure 18. *Loxocemus bicolor* BMNH 1988.355

A) Dorsal, B) Ventral, C) Left Lateral, D) Right Lateral, E) Anterior, F) Posterior. Scale bar = 1mm.

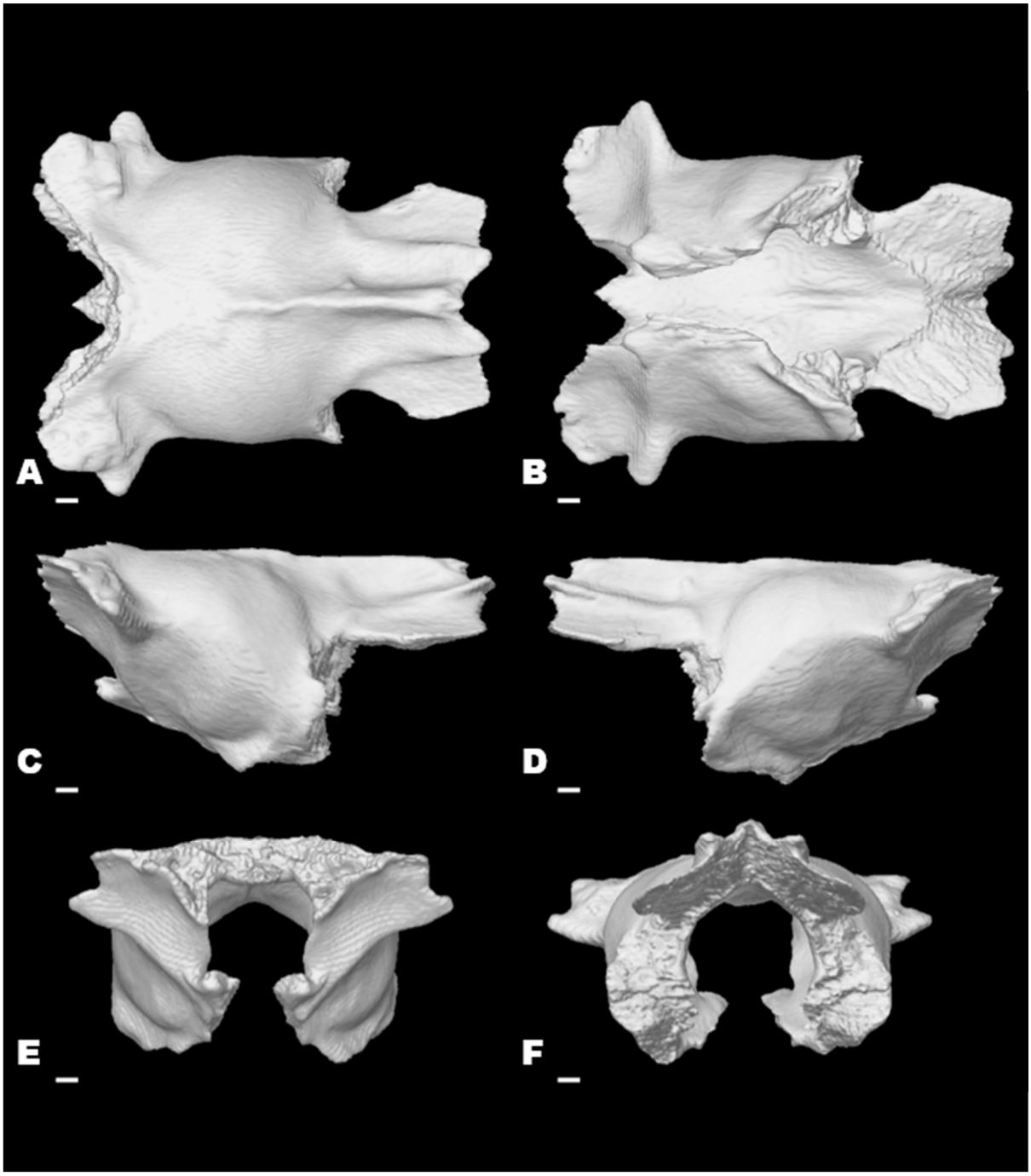

Figure 19. *Aspidites melanocephalus* FMNH:AMPHIBIANS AND REPTILES:97055

A) Dorsal, B) Ventral, C) Left Lateral, D) Right Lateral, E) Anterior, F) Posterior. Scale bar = 1mm.

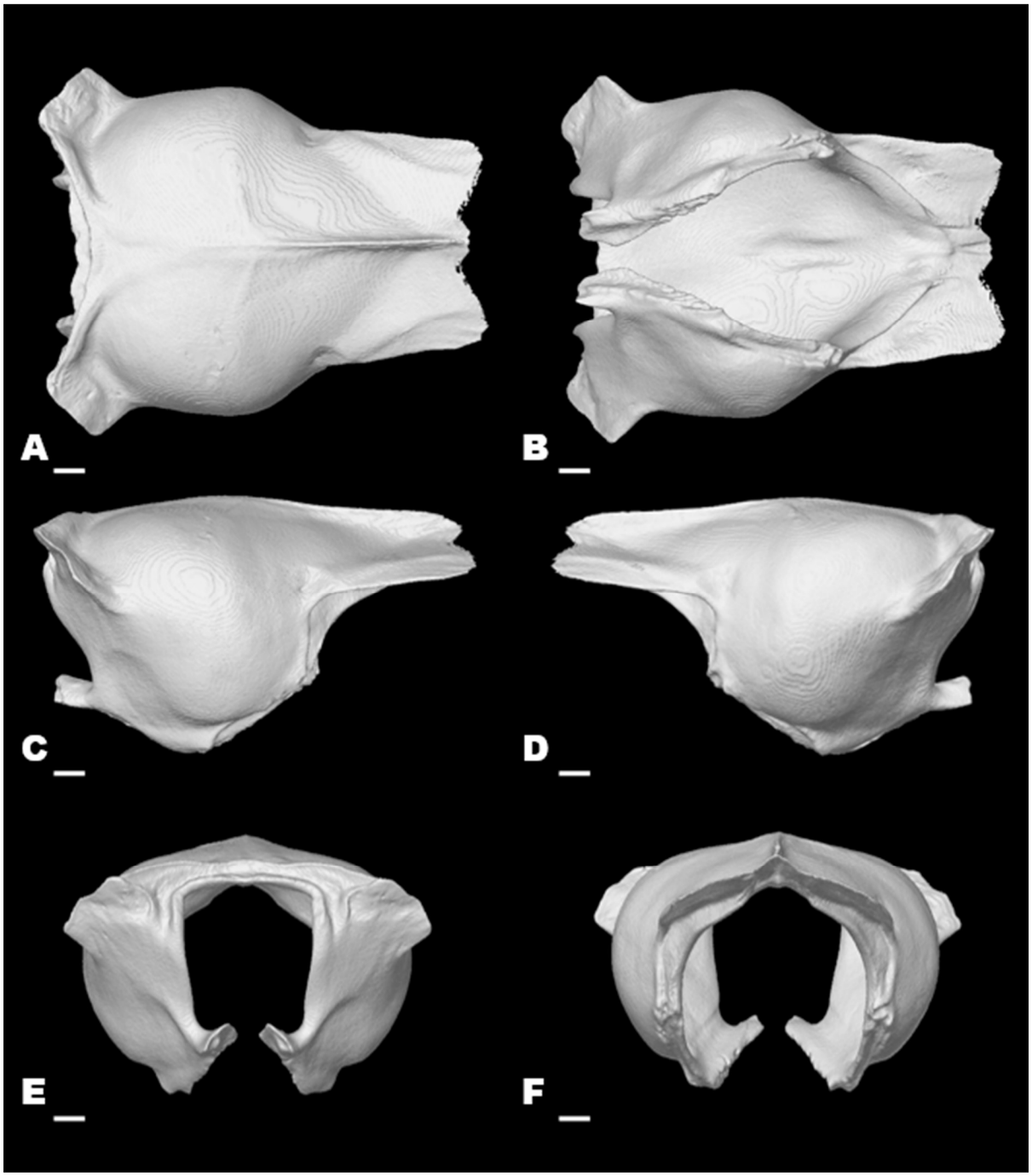

Figure 20. *Malayopython reticulatus* UMZC R3.24-4

A) Dorsal, B) Ventral, C) Left Lateral, D) Right Lateral, E) Anterior, F) Posterior. Scale bar = 1mm.

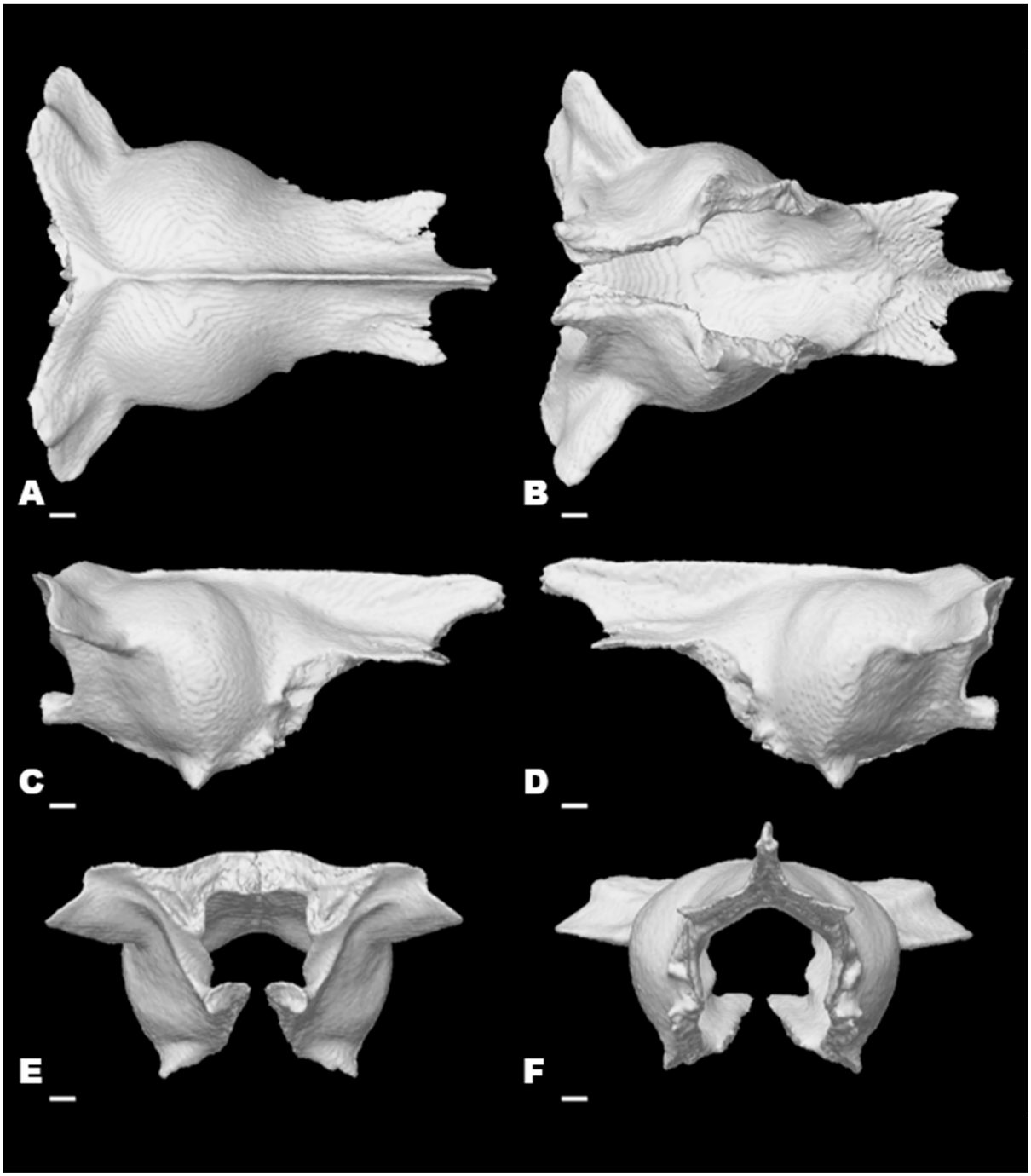

Figure 21. *Morelia spilota* UMMZ:HERPS:227833

A) Dorsal, B) Ventral, C) Left Lateral, D) Right Lateral, E) Anterior, F) Posterior. Scale bar = 1mm.

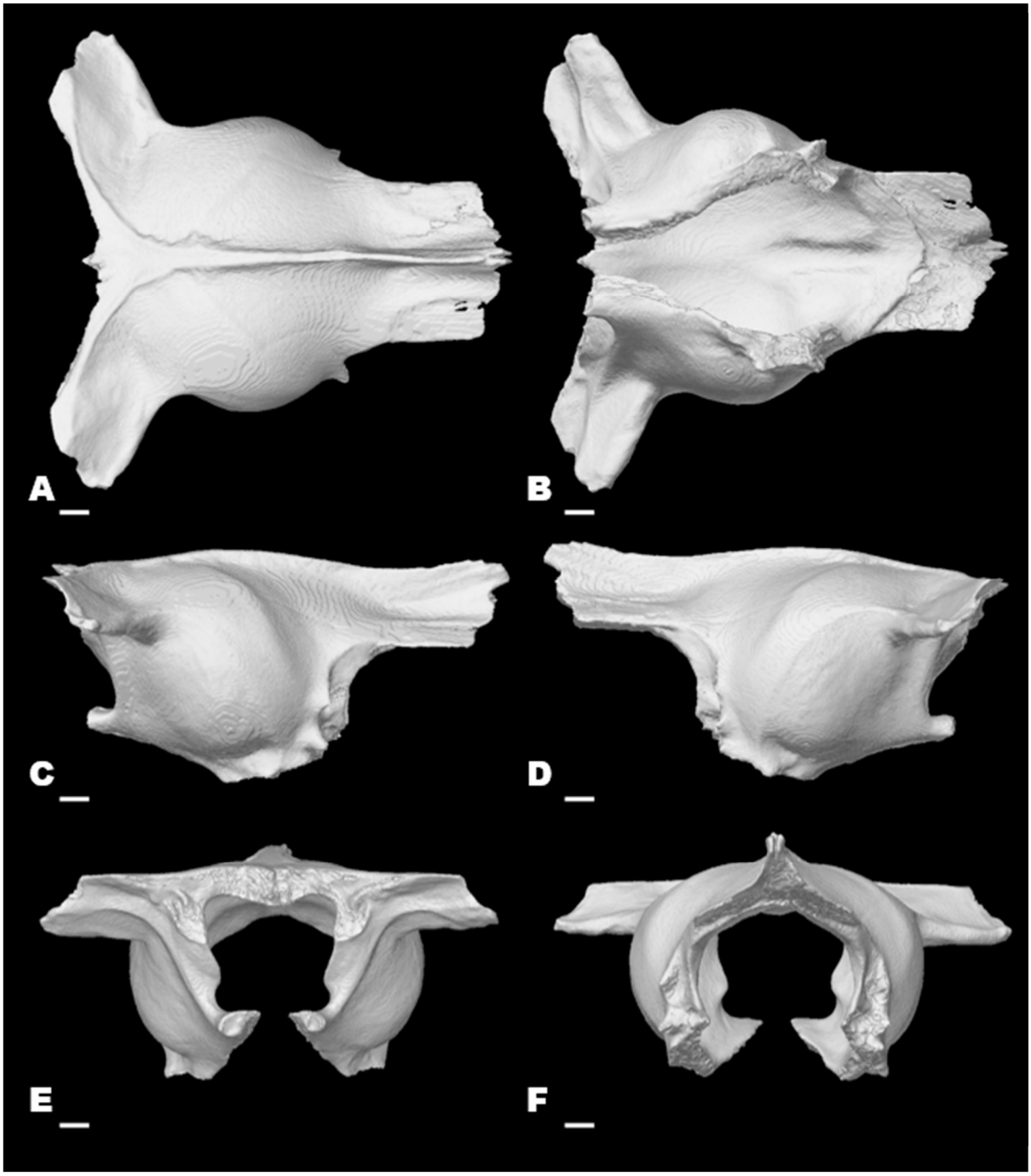

Figure 22. *Morelia spilota* UMZC R3.22-4

A) Dorsal, B) Ventral, C) Left Lateral, D) Right Lateral, E) Anterior, F) Posterior. Scale bar = 1mm.

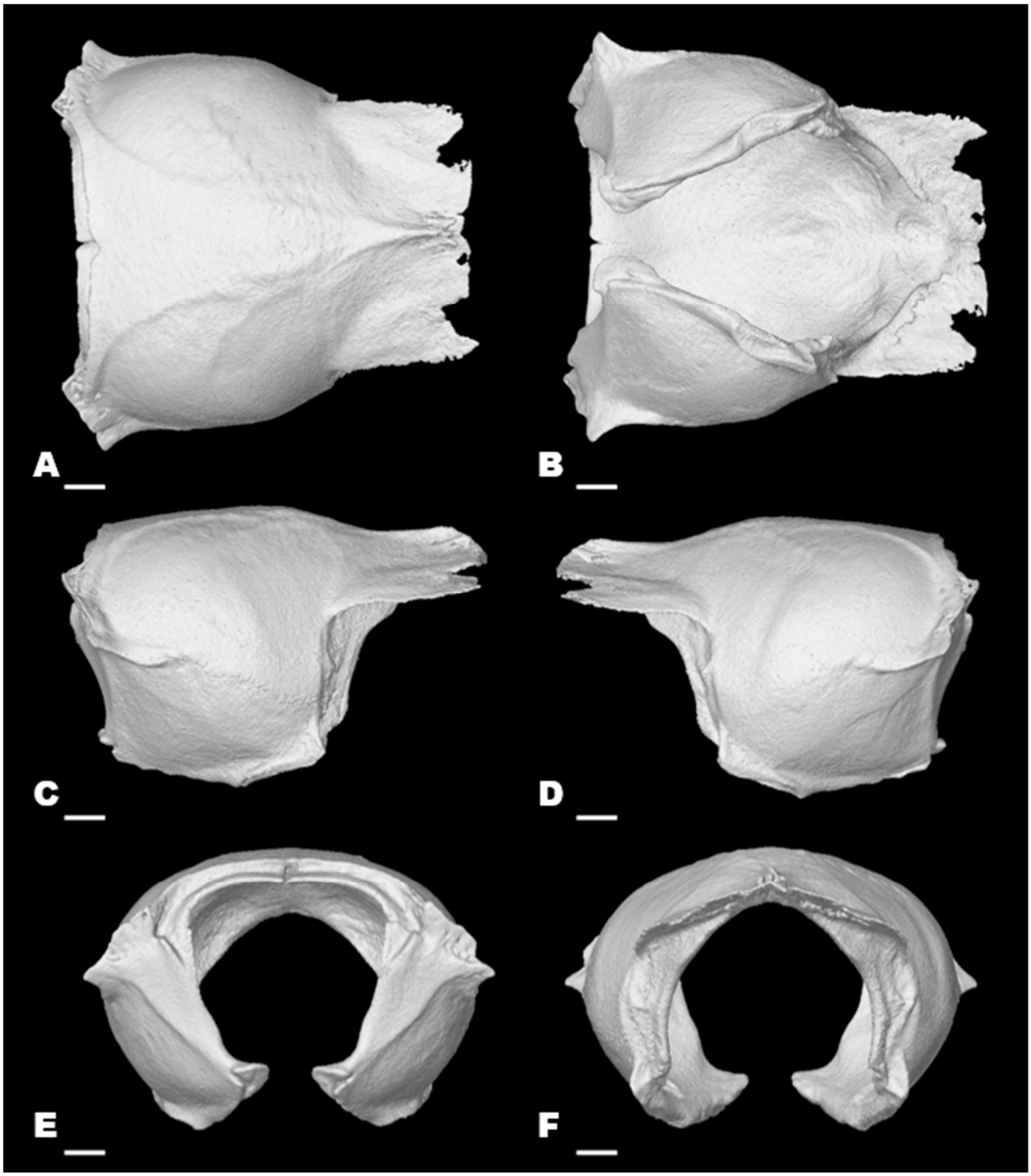

Figure 23. *Python molurus* UMZC R3.25-7

A) Dorsal, B) Ventral, C) Left Lateral, D) Right Lateral, E) Anterior, F) Posterior. Scale bar = 1mm.

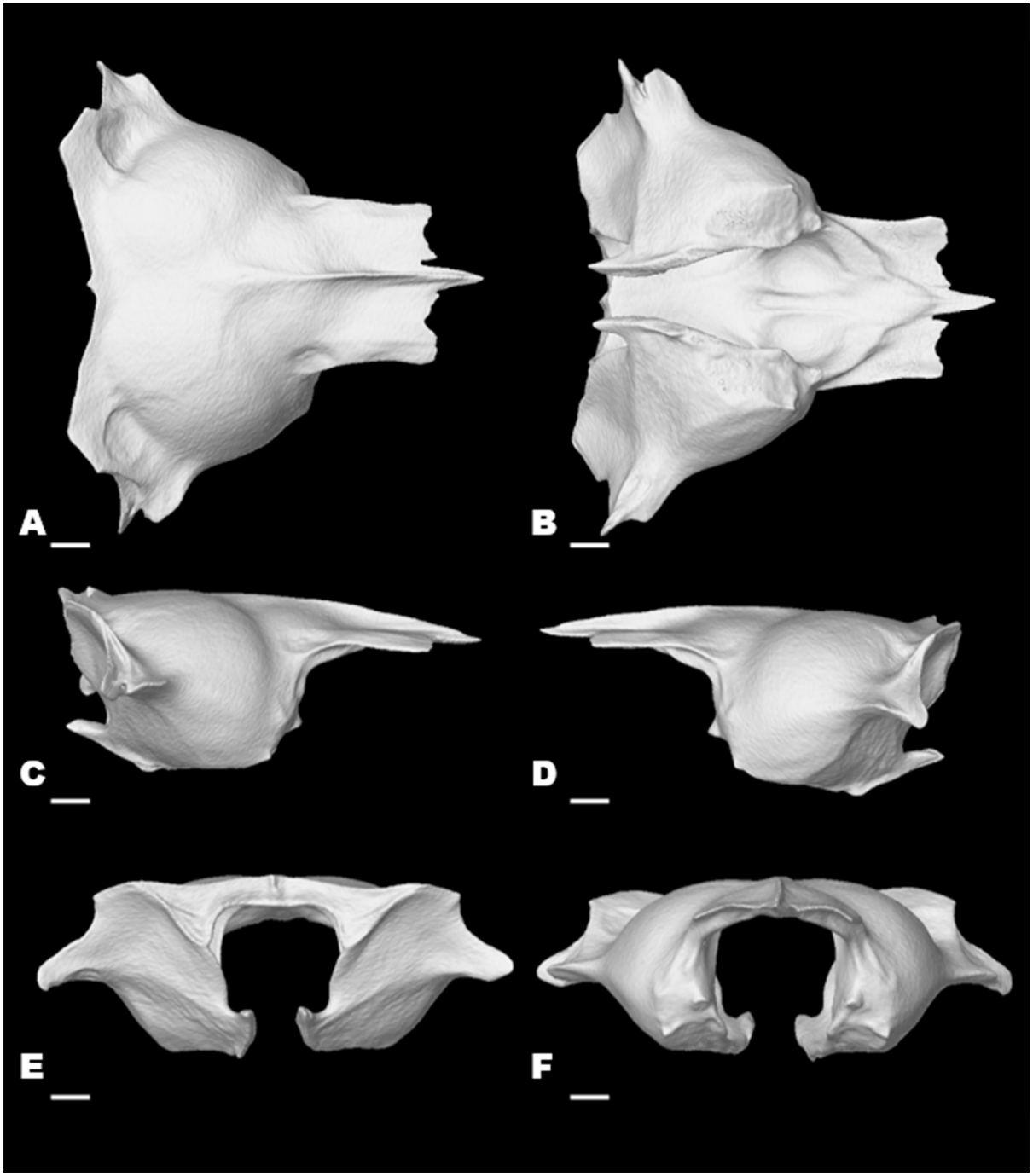

Figure 24. *Candoia bibroni* BMNH 1967.771

A) Dorsal, B) Ventral, C) Left Lateral, D) Right Lateral, E) Anterior, F) Posterior. Scale bar = 1mm.

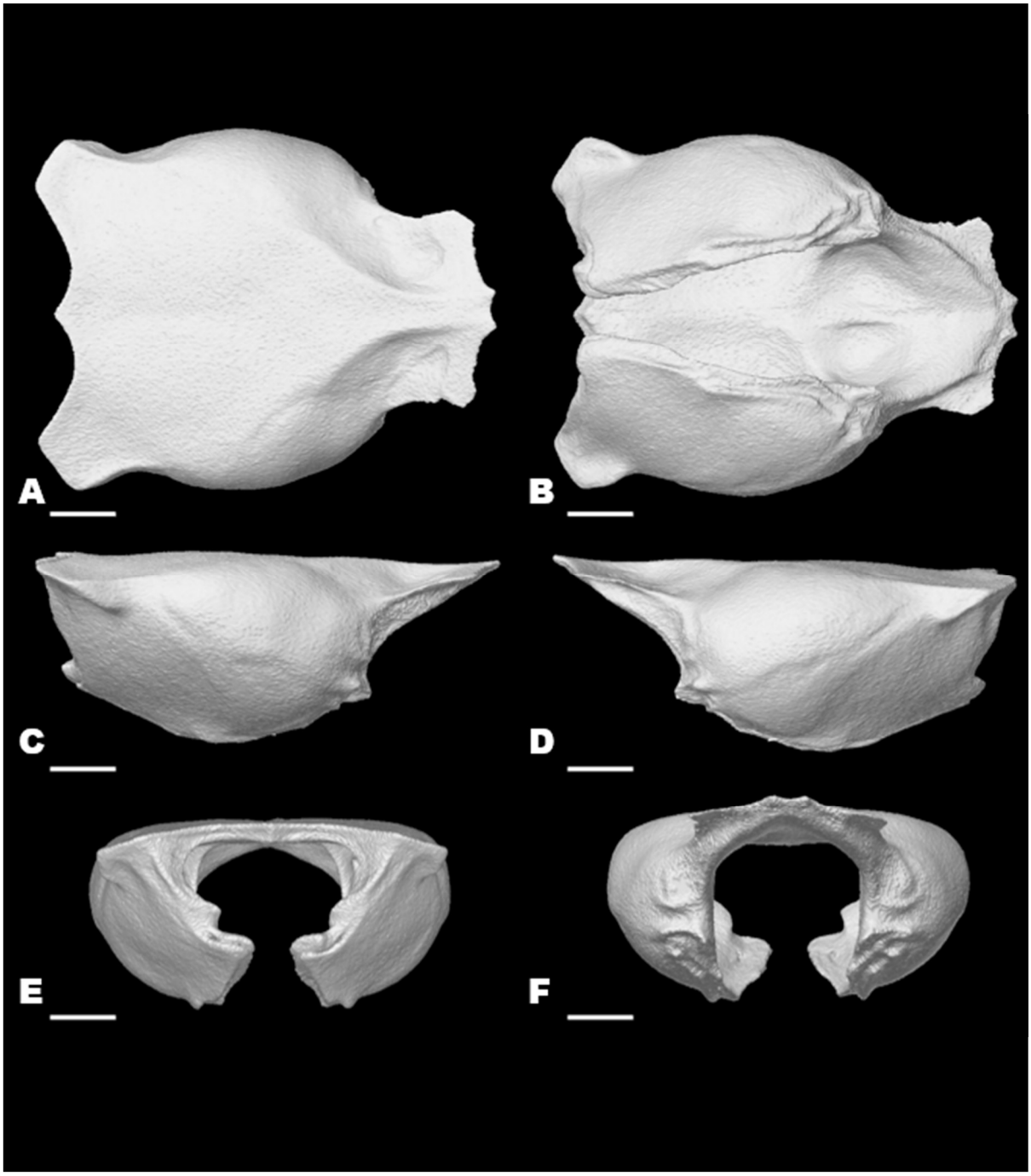

Figure 25. *Casarea dussumieri* UMMZ:HERPS:190285

A) Dorsal, B) Ventral, C) Left Lateral, D) Right Lateral, E) Anterior, F) Posterior. Scale bar = 1mm.

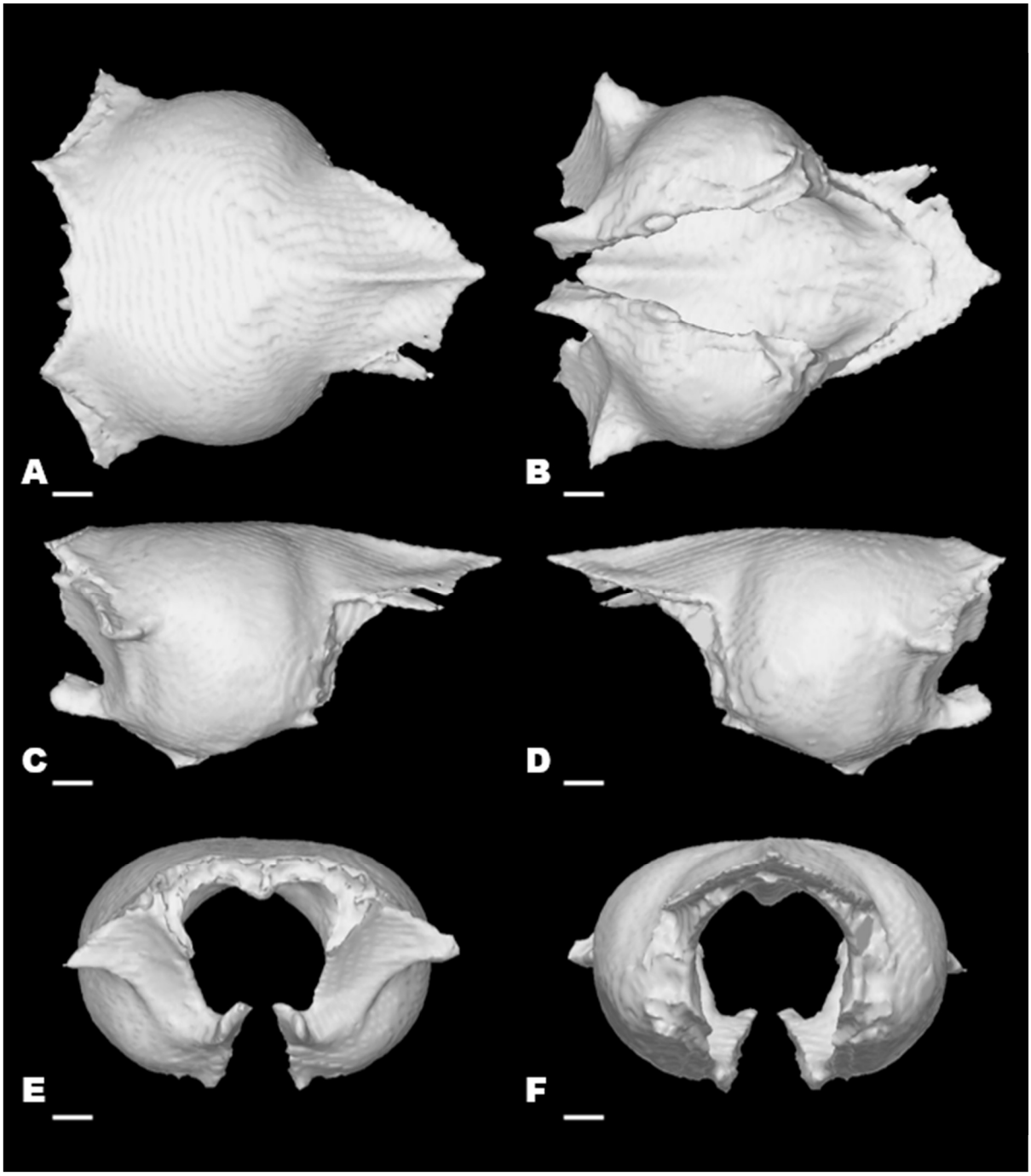

Figure 26. *Epicrates cenchria* UMZC R3.51-1

A) Dorsal, B) Ventral, C) Left Lateral, D) Right Lateral, E) Anterior, F) Posterior. Scale bar = 1mm.

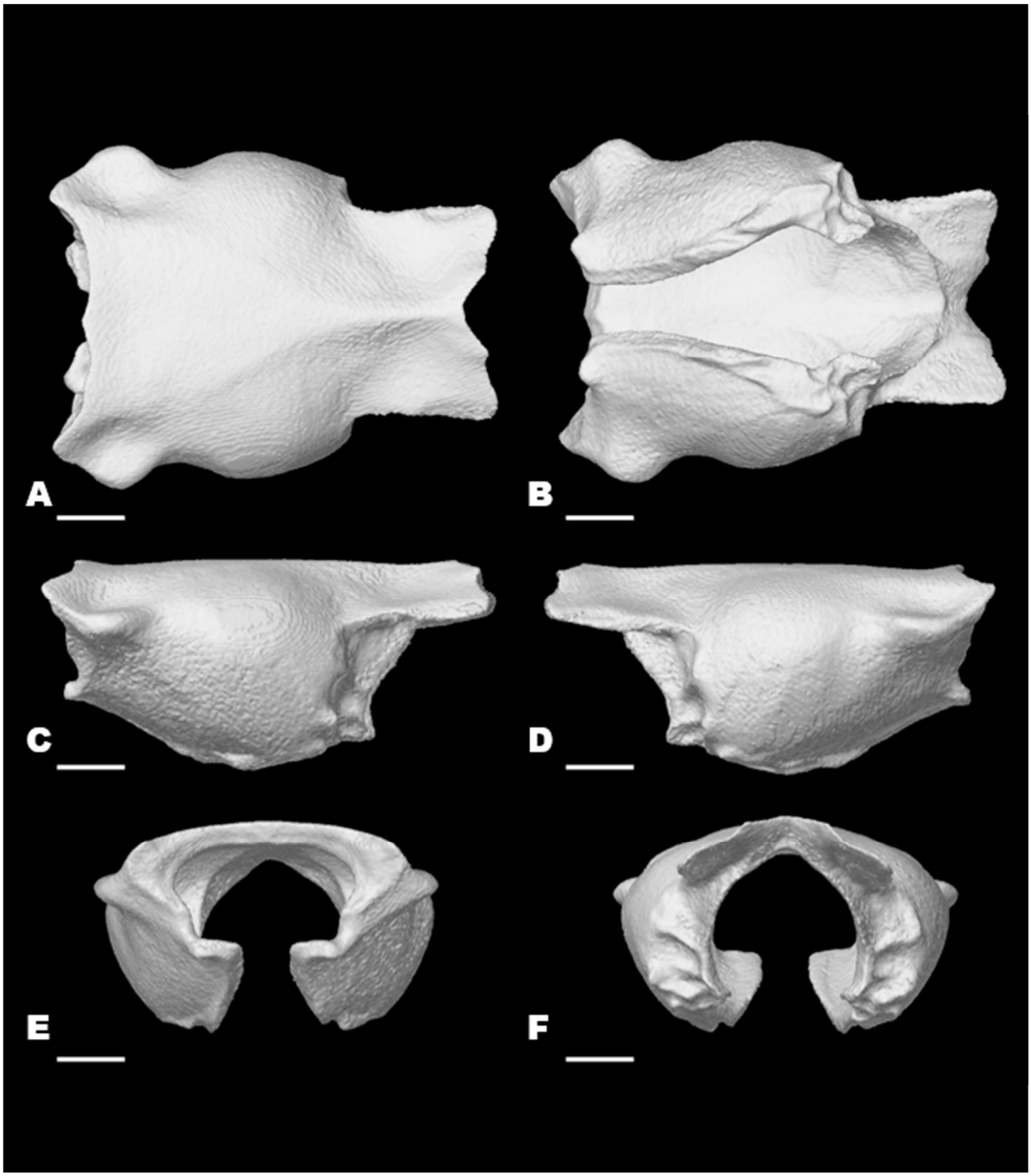

Figure 27. *Exiliboa placata* MVZ 137126

A) Dorsal, B) Ventral, C) Left Lateral, D) Right Lateral, E) Anterior, F) Posterior. Scale bar = 1mm.

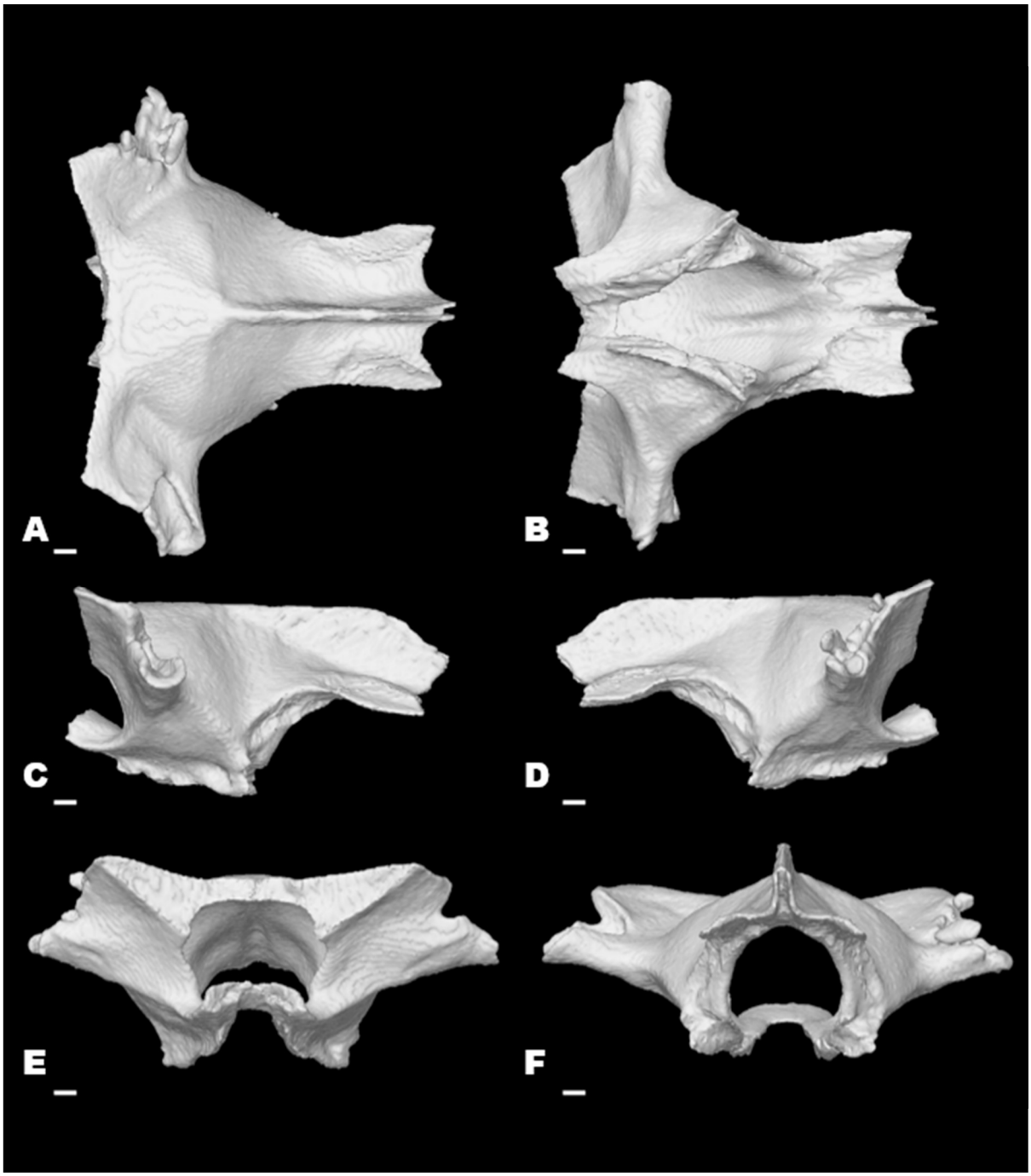

Figure 28. *Sanzinia madagascariensis* KU:KUH:183837

A) Dorsal, B) Ventral, C) Left Lateral, D) Right Lateral, E) Anterior, F) Posterior. Scale bar = 1mm.

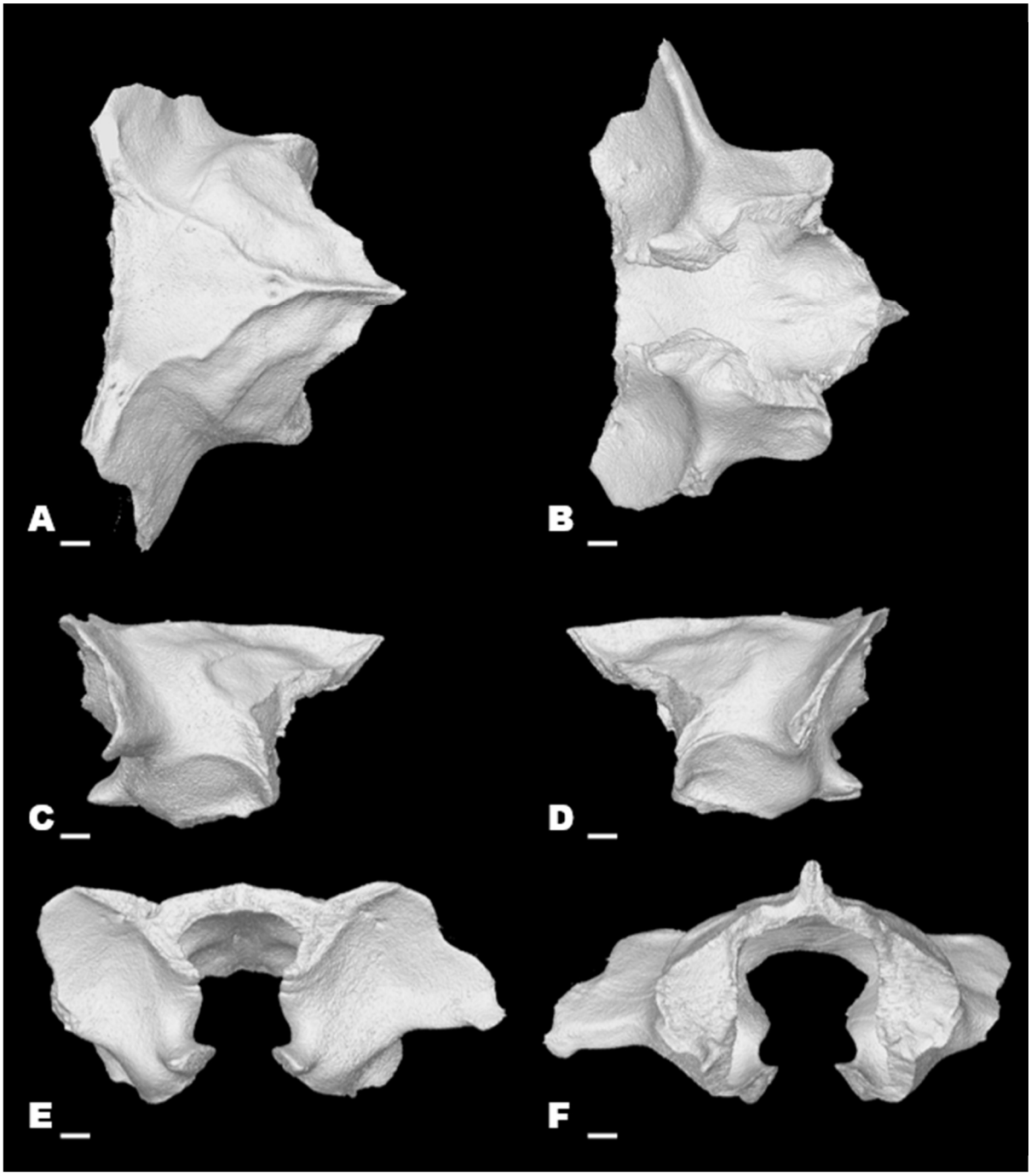

Figure 29. *Boiga irregularis* UMMZ:HERPS:170417

A) Dorsal, B) Ventral, C) Left Lateral, D) Right Lateral, E) Anterior, F) Posterior. Scale bar = 1mm.

Figure 30. *Coluber constrictor* UMMZ:HERPS:225480

A) Dorsal, B) Ventral, C) Left Lateral, D) Right Lateral, E) Anterior, F) Posterior. Scale bar = 1mm.

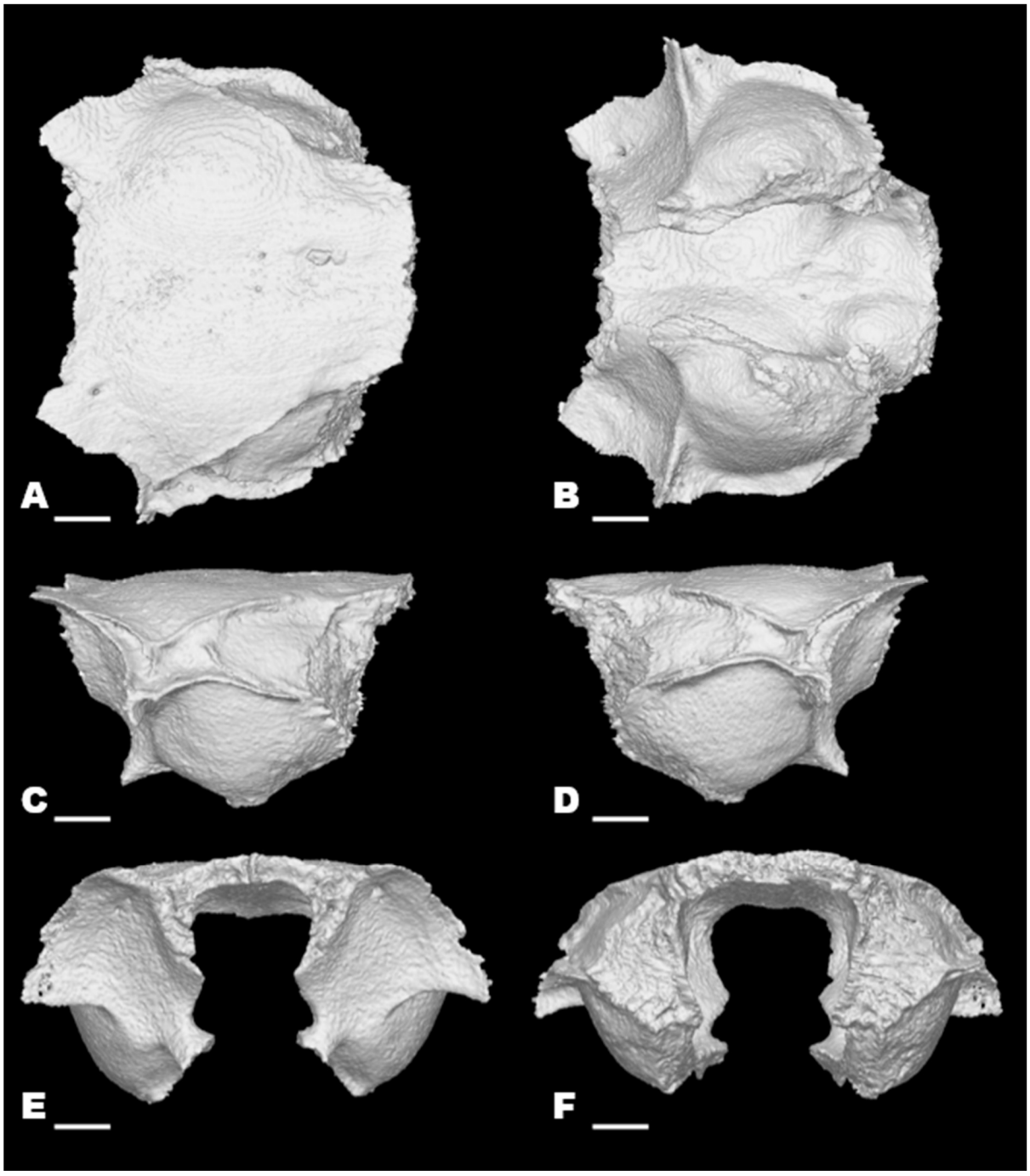

Figure 31. *Dasypeltis gansi* UMMZ:HERPS:FS1352

A) Dorsal, B) Ventral, C) Left Lateral, D) Right Lateral, E) Anterior, F) Posterior. Scale bar = 1mm.

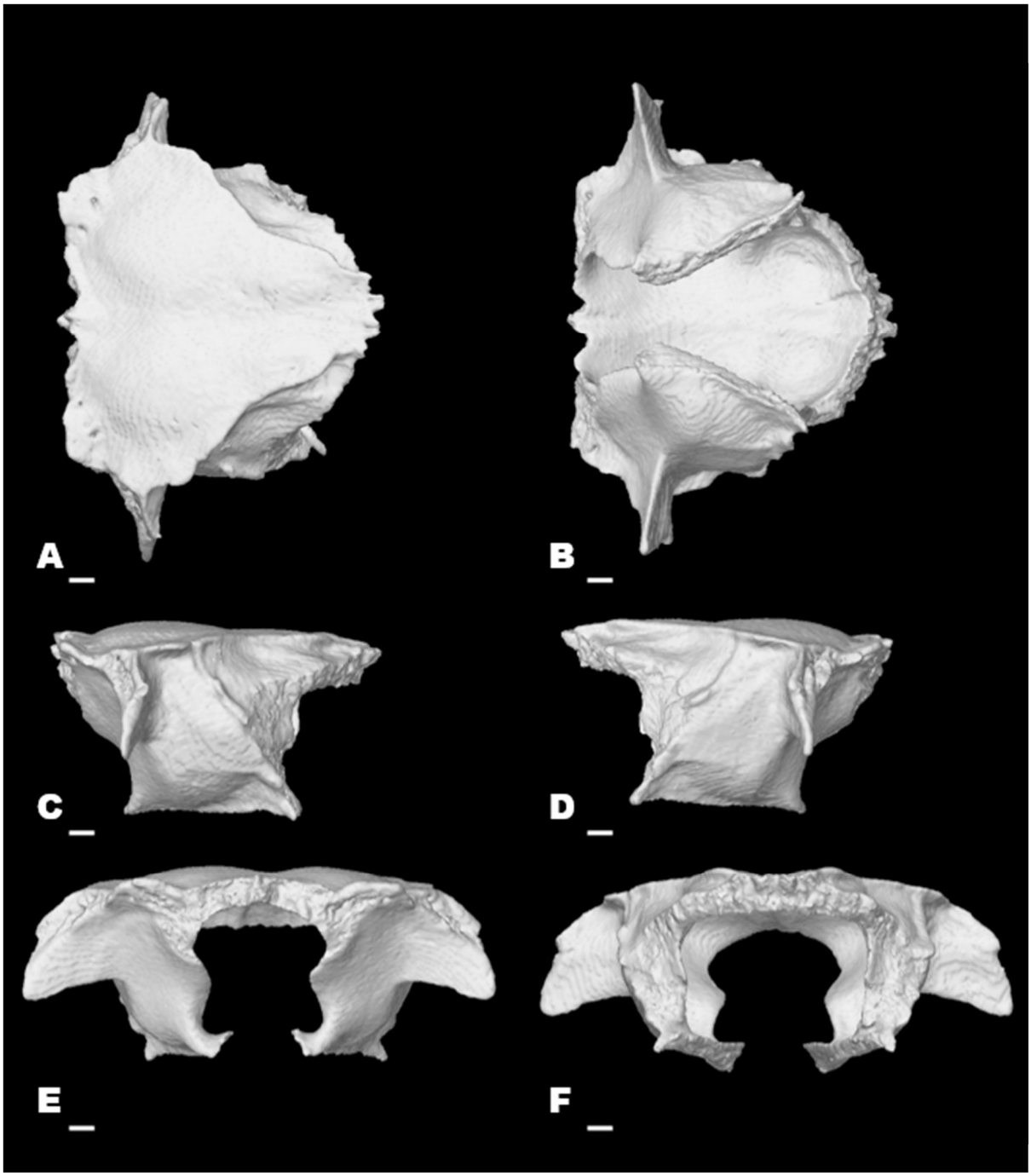

Figure 32. *Drymarchon corais* KU:KUH:289805

A) Dorsal, B) Ventral, C) Left Lateral, D) Right Lateral, E) Anterior, F) Posterior. Scale bar = 1mm.

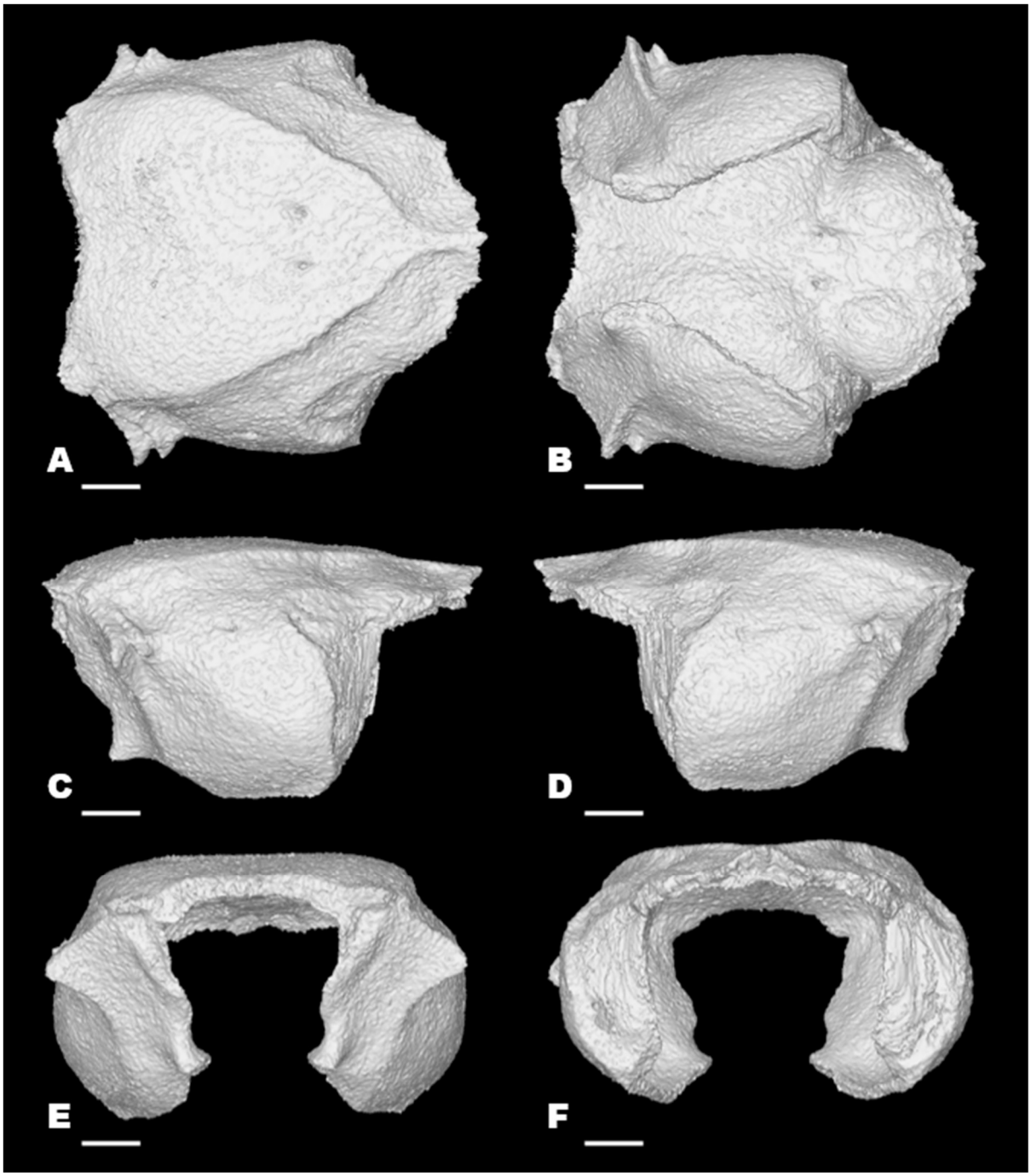

Figure 33. *Lampropeltis getula* UMMZ:HERPS:218638

A) Dorsal, B) Ventral, C) Left Lateral, D) Right Lateral, E) Anterior, F) Posterior. Scale bar = 1mm.

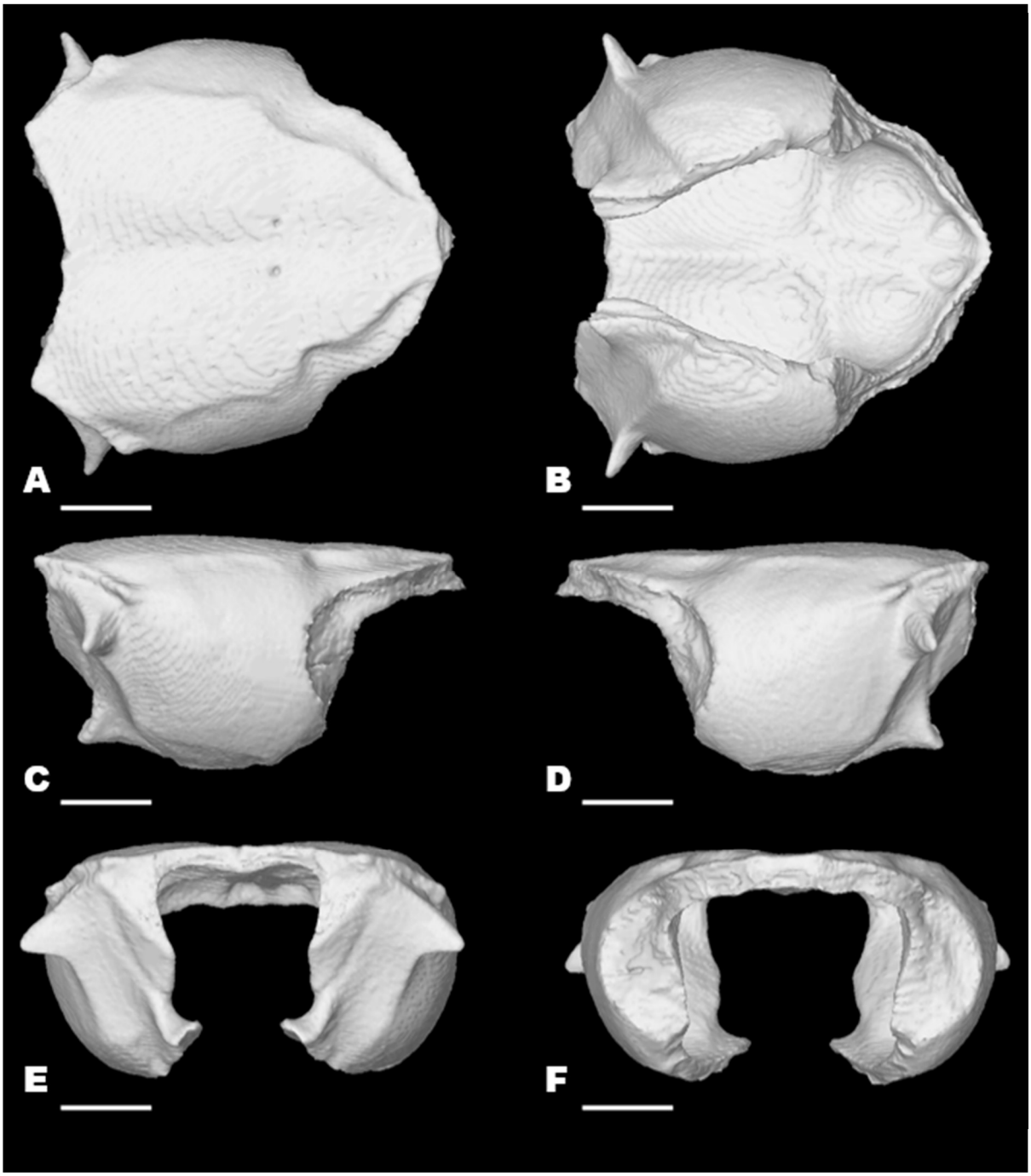

Figure 34. *Oligodon arnensis* UMMZ:HERPS:65634

A) Dorsal, B) Ventral, C) Left Lateral, D) Right Lateral, E) Anterior, F) Posterior. Scale bar = 1mm.

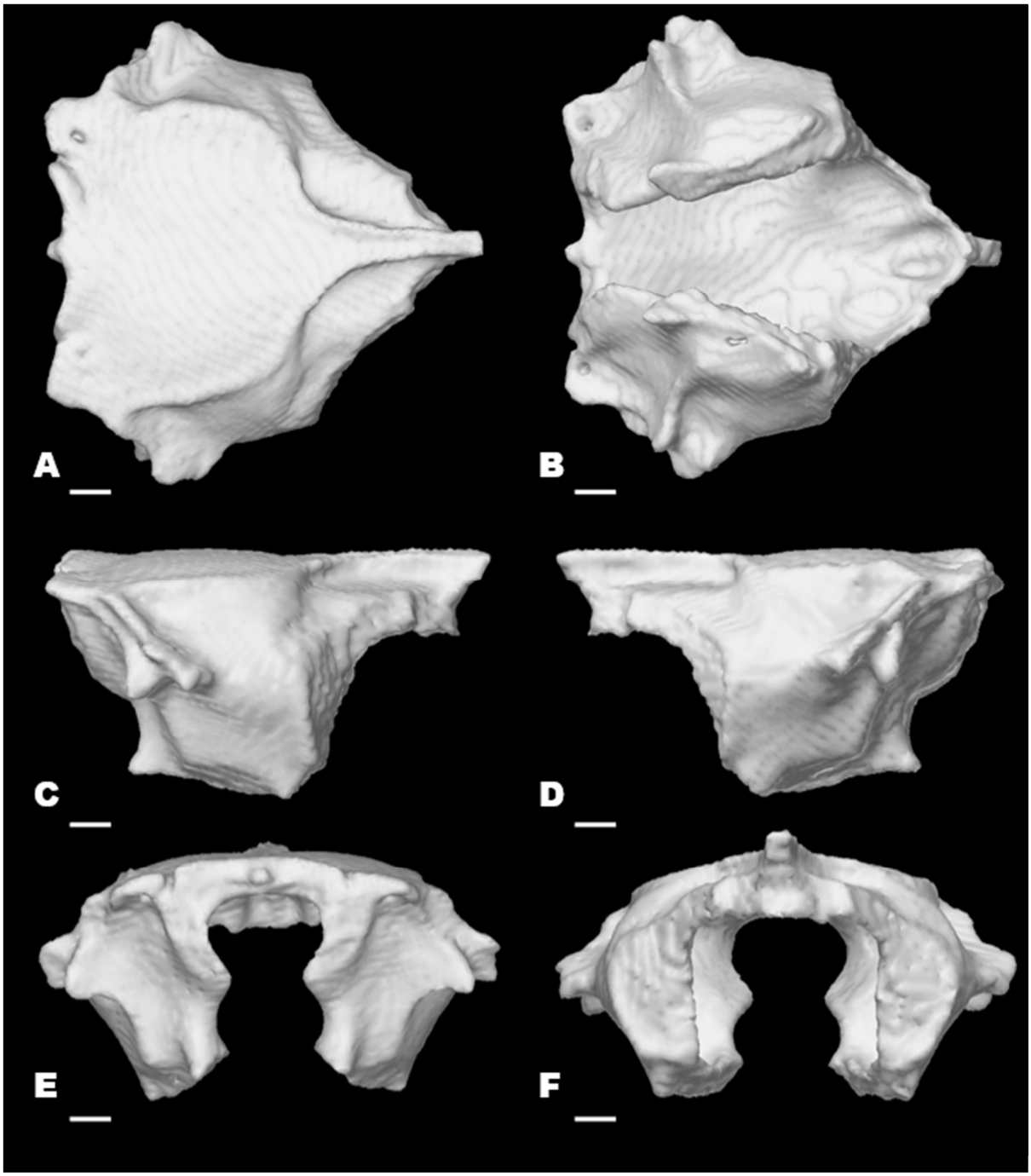

Figure 35. *Pantherophis guttatus* LSUMZ:HERPS:88802

A) Dorsal, B) Ventral, C) Left Lateral, D) Right Lateral, E) Anterior, F) Posterior. Scale bar = 1mm.

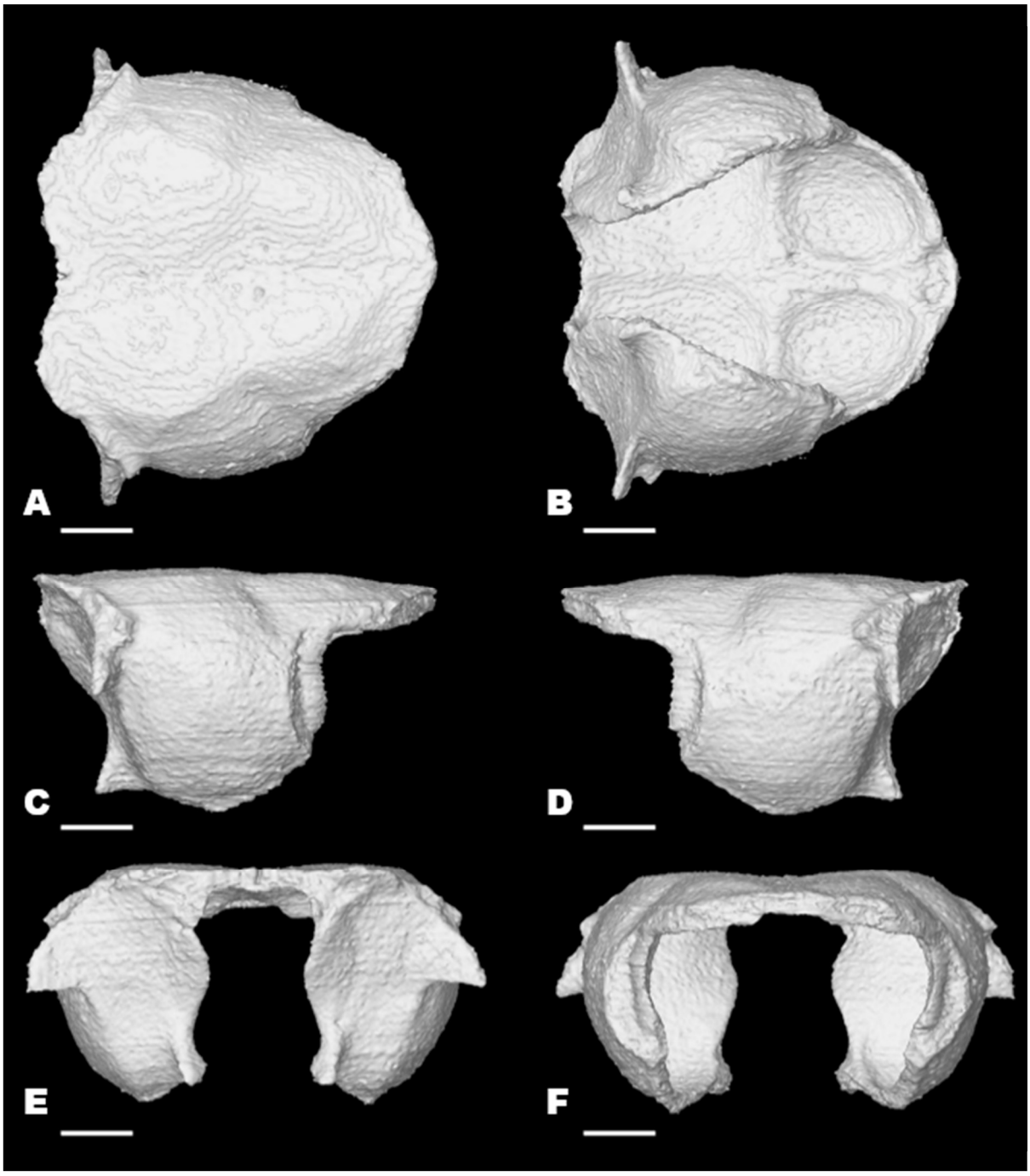

Figure 35. *Platyceps najadum* UMMZ:HERPS:127487

A) Dorsal, B) Ventral, C) Left Lateral, D) Right Lateral, E) Anterior, F) Posterior. Scale bar = 1mm.

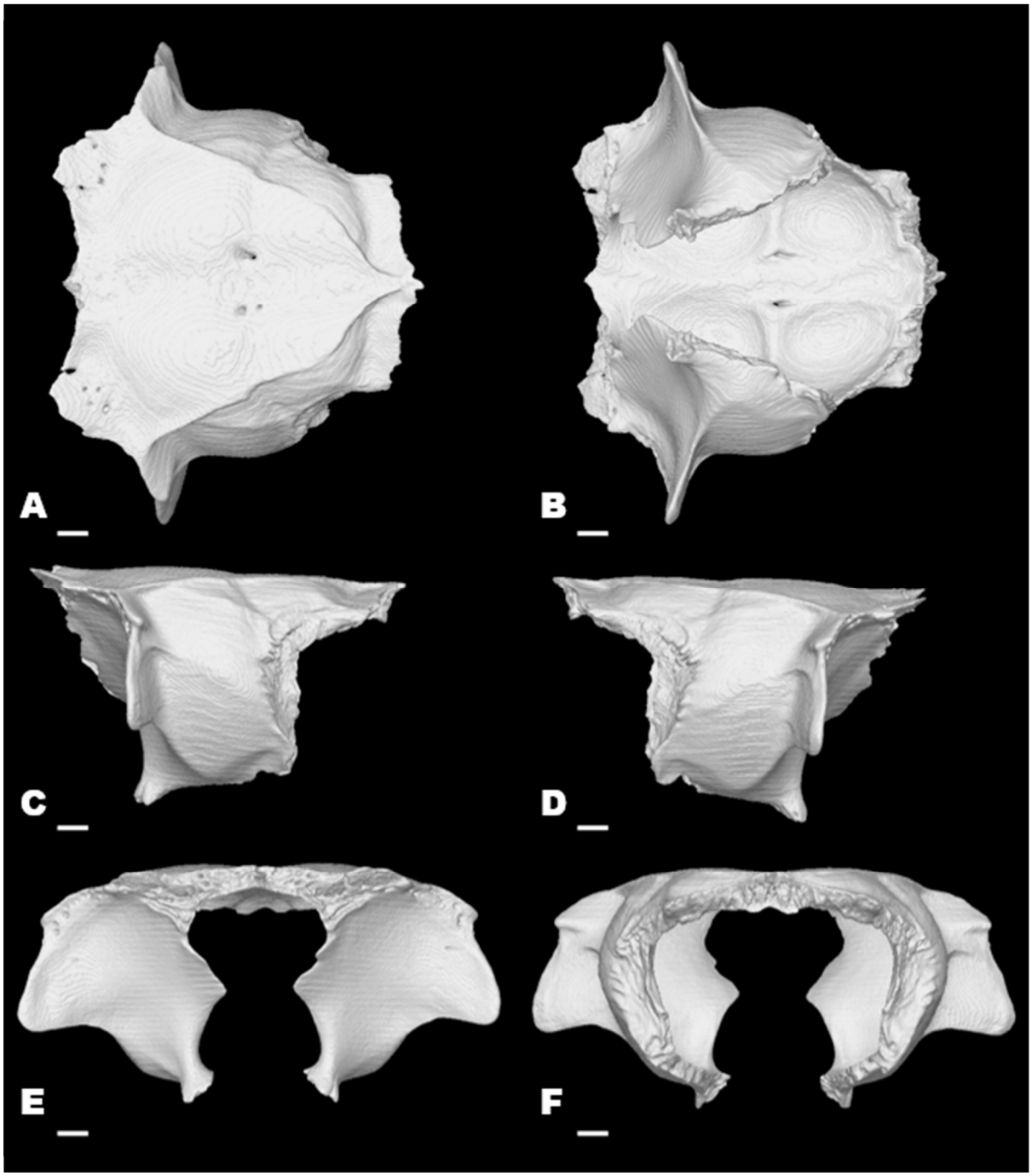

Figure 37. *Ptyas mucosa* UMMZ:HERPS:169877

A) Dorsal, B) Ventral, C) Left Lateral, D) Right Lateral, E) Anterior, F) Posterior. Scale bar = 1mm.

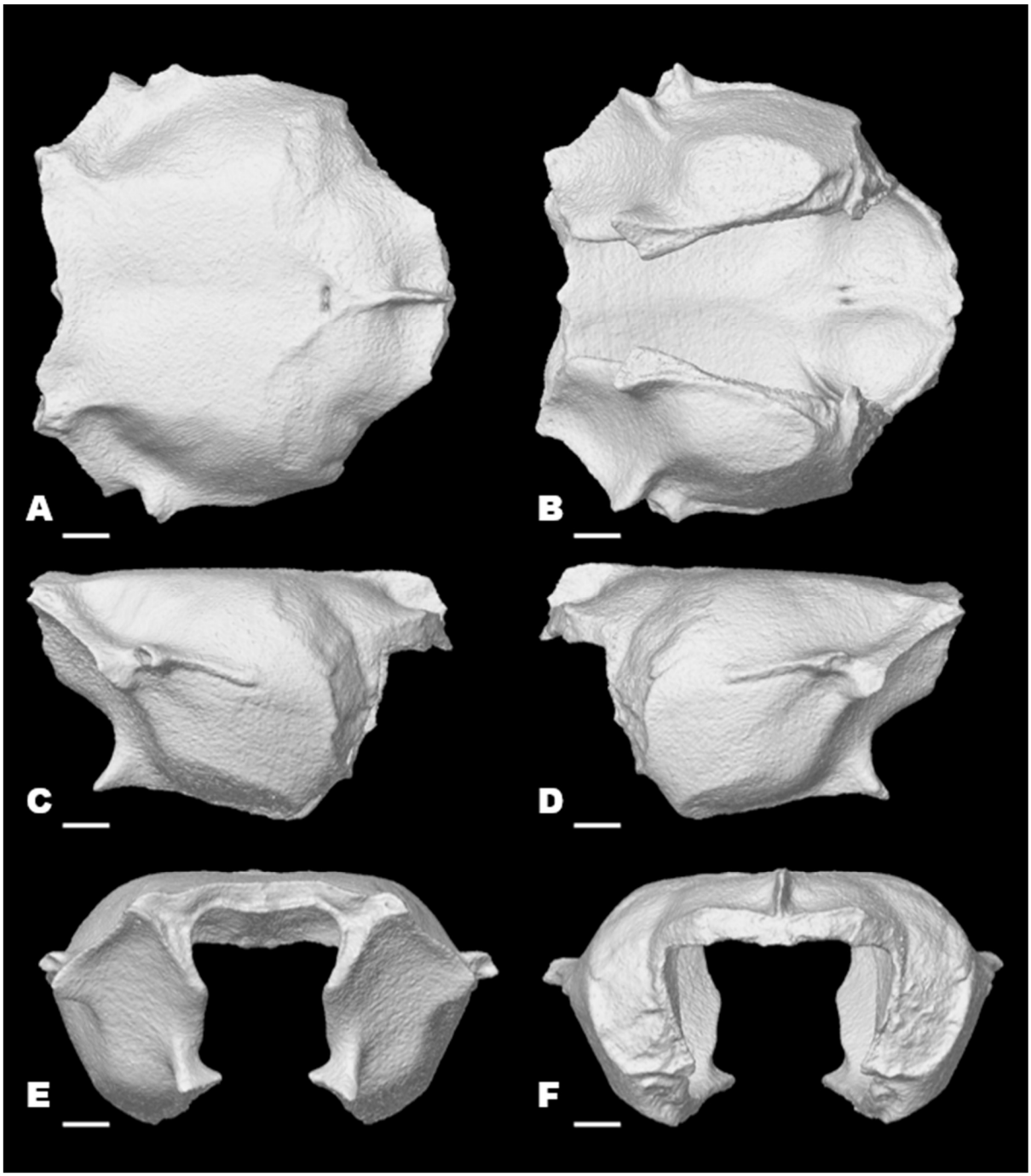

Figure 38. *Senticolis triaspis* UMMZ:HERPS:209970

A) Dorsal, B) Ventral, C) Left Lateral, D) Right Lateral, E) Anterior, F) Posterior. Scale bar = 1mm.

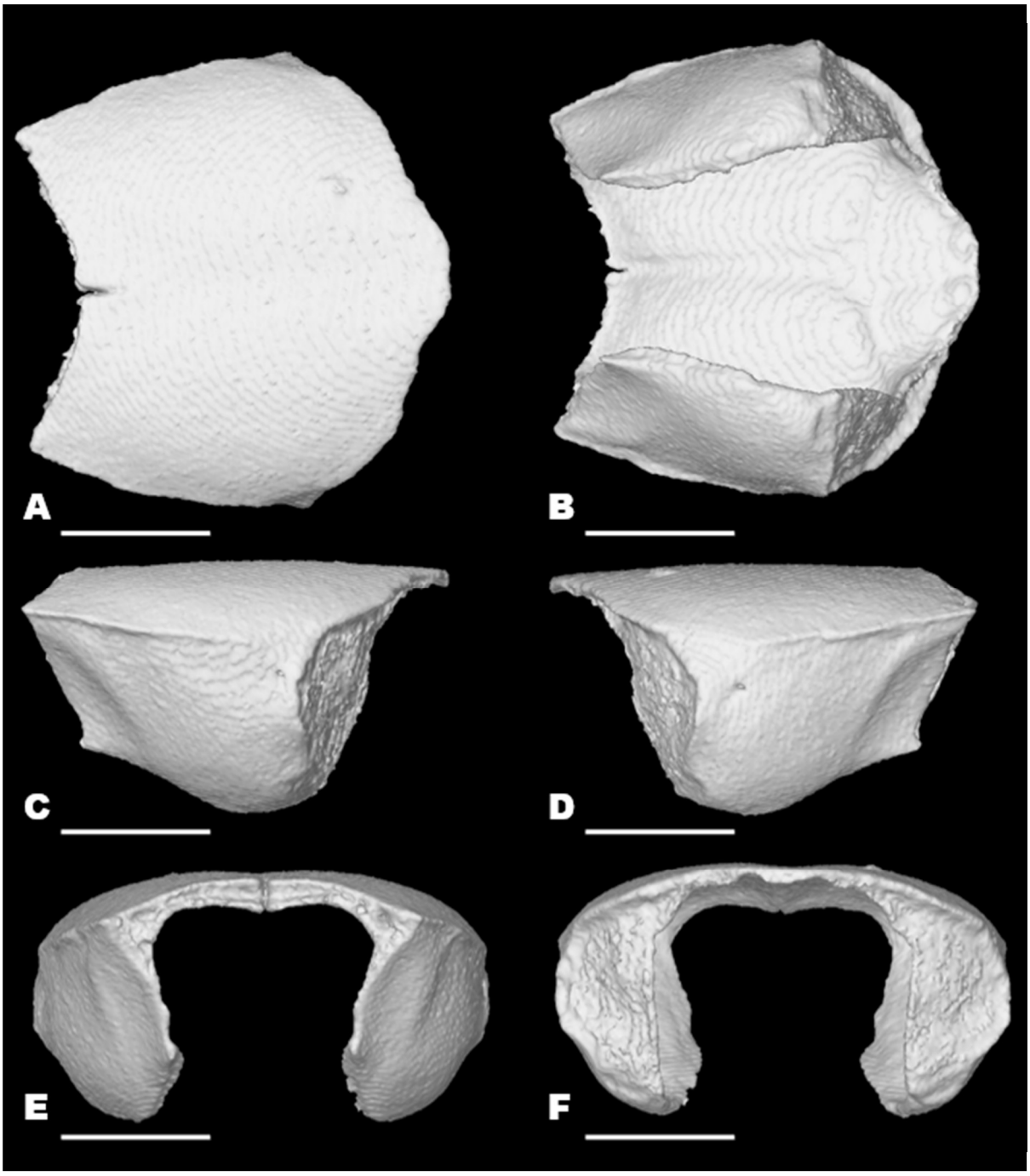

Figure 39. *Carphophis amoenus* UMMZ:HERPS:209970

A) Dorsal, B) Ventral, C) Left Lateral, D) Right Lateral, E) Anterior, F) Posterior. Scale bar = 1mm.

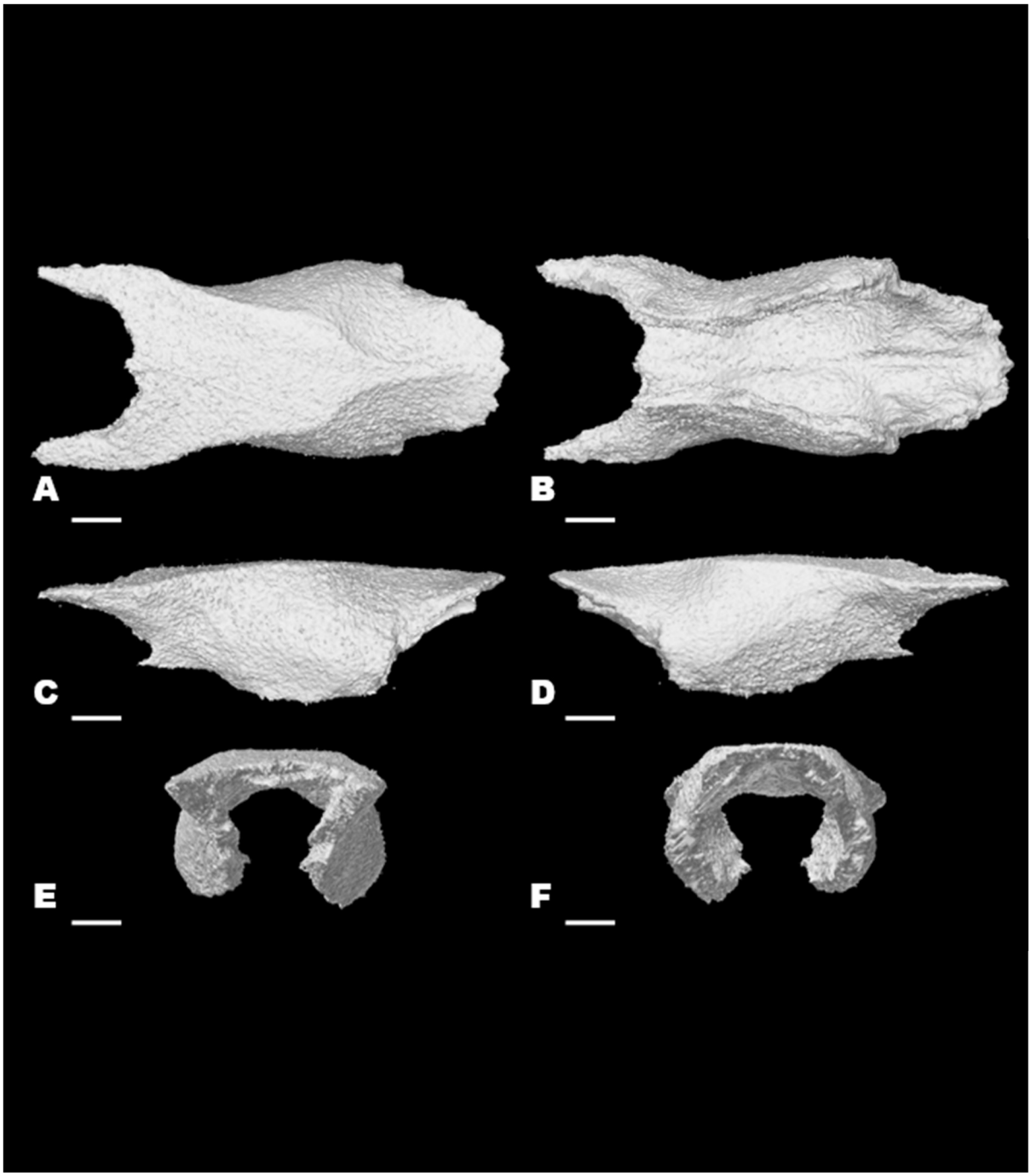

Figure 40. *Elapomorphus quinquelineatus* UMMZ:HERPS:65879

A) Dorsal, B) Ventral, C) Left Lateral, D) Right Lateral, E) Anterior, F) Posterior. Scale bar = 1mm.

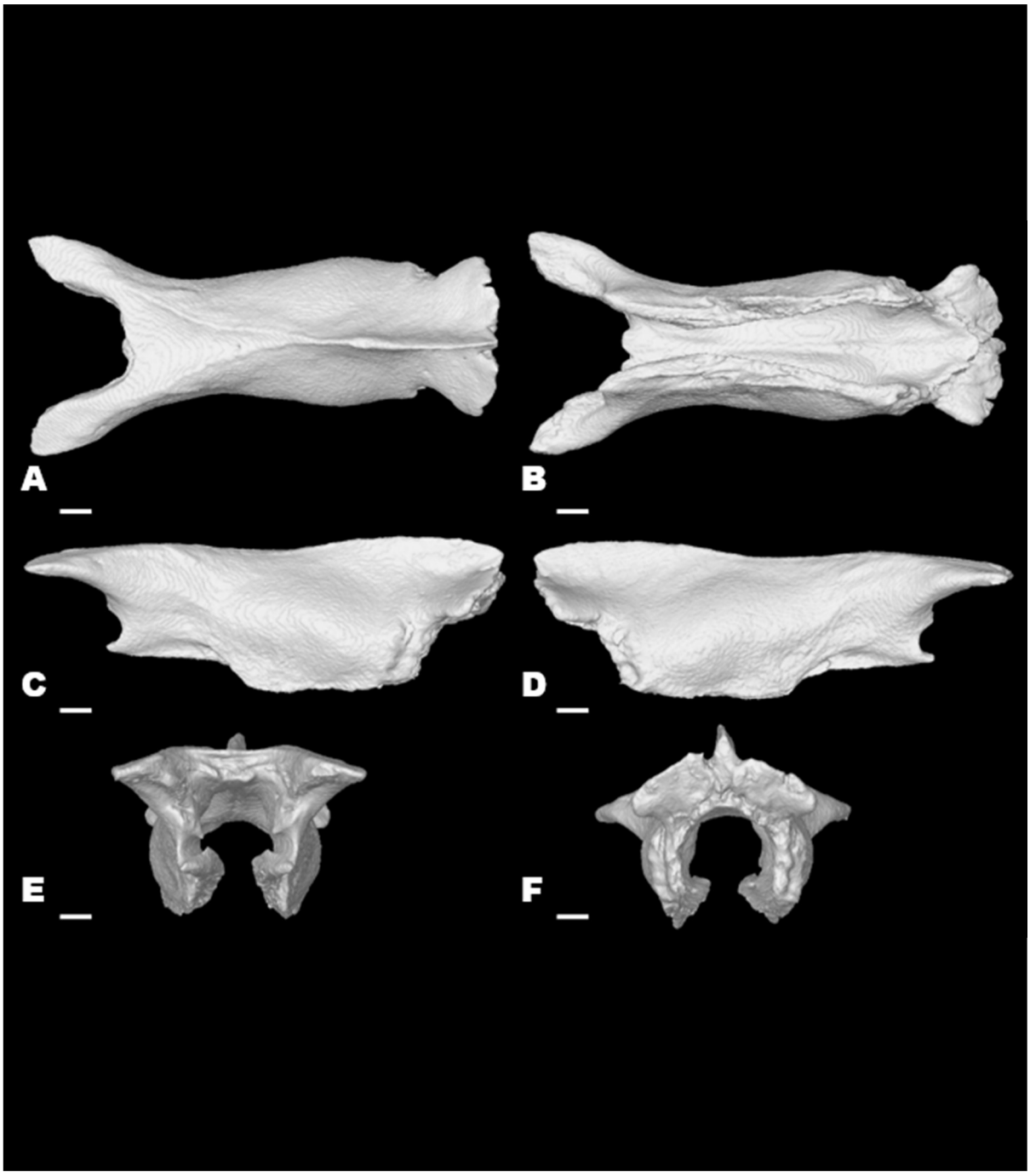

Figure 41. *Phalotris mertensi* UMMZ:HERPS:63022

A) Dorsal, B) Ventral, C) Left Lateral, D) Right Lateral, E) Anterior, F) Posterior. Scale bar = 1mm.

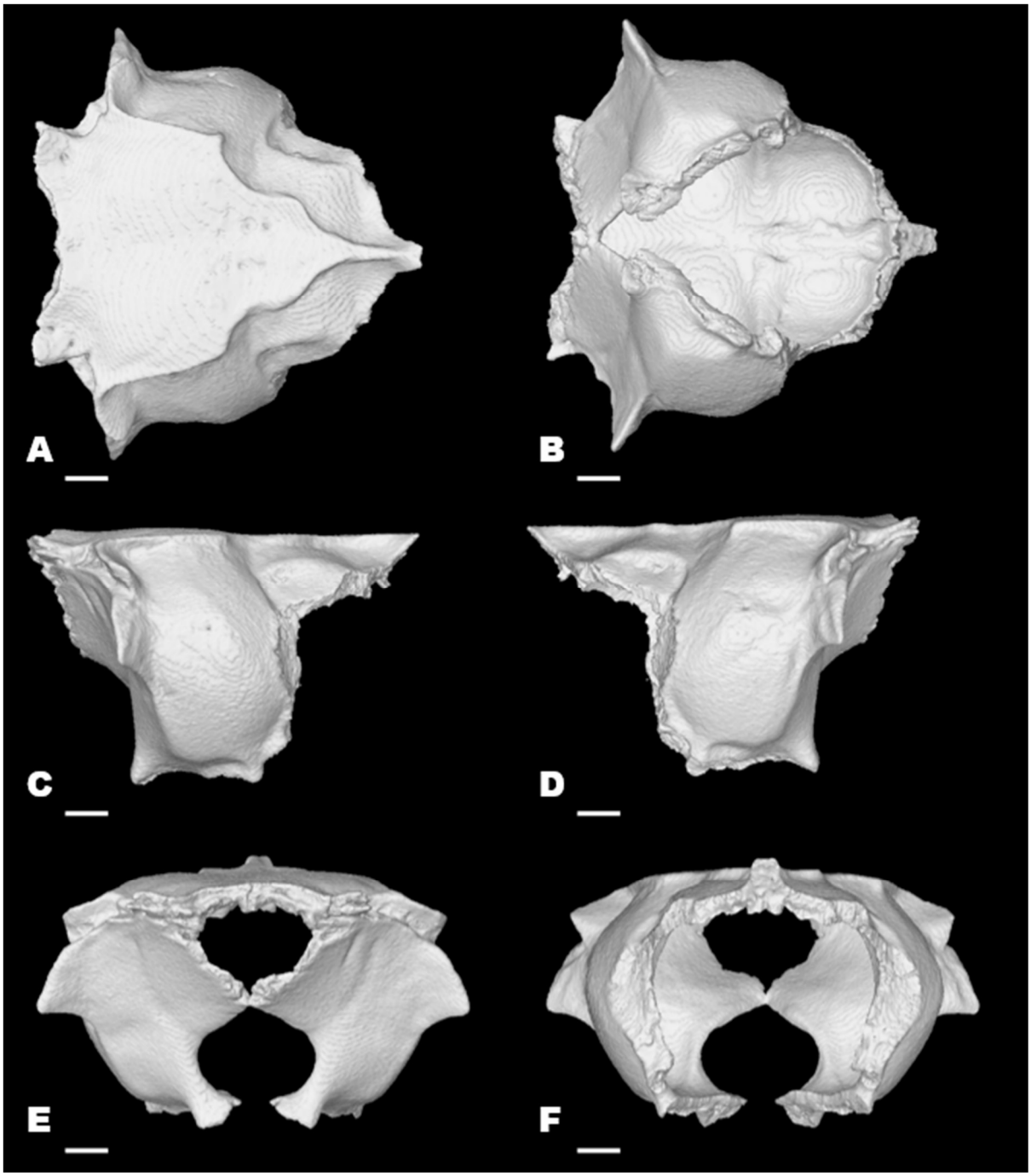

Figure 42. *Philodryas patagoniensis* UMMZ:HERPS:108987

A) Dorsal, B) Ventral, C) Left Lateral, D) Right Lateral, E) Anterior, F) Posterior. Scale bar = 1mm.

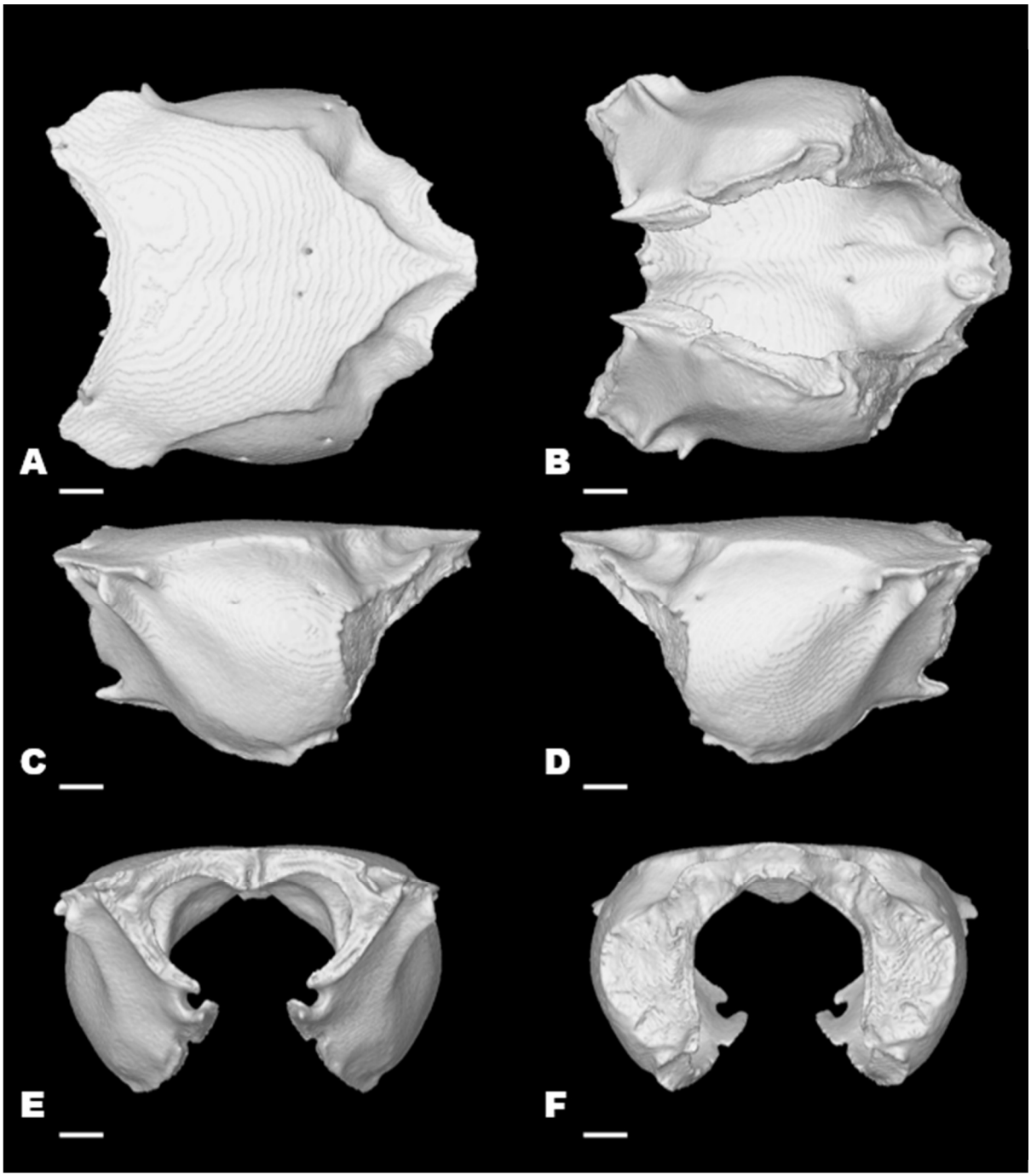

Figure 43. *Pseudoboa coronata* UMMZ:HERPS:246839

A) Dorsal, B) Ventral, C) Left Lateral, D) Right Lateral, E) Anterior, F) Posterior. Scale bar = 1mm.

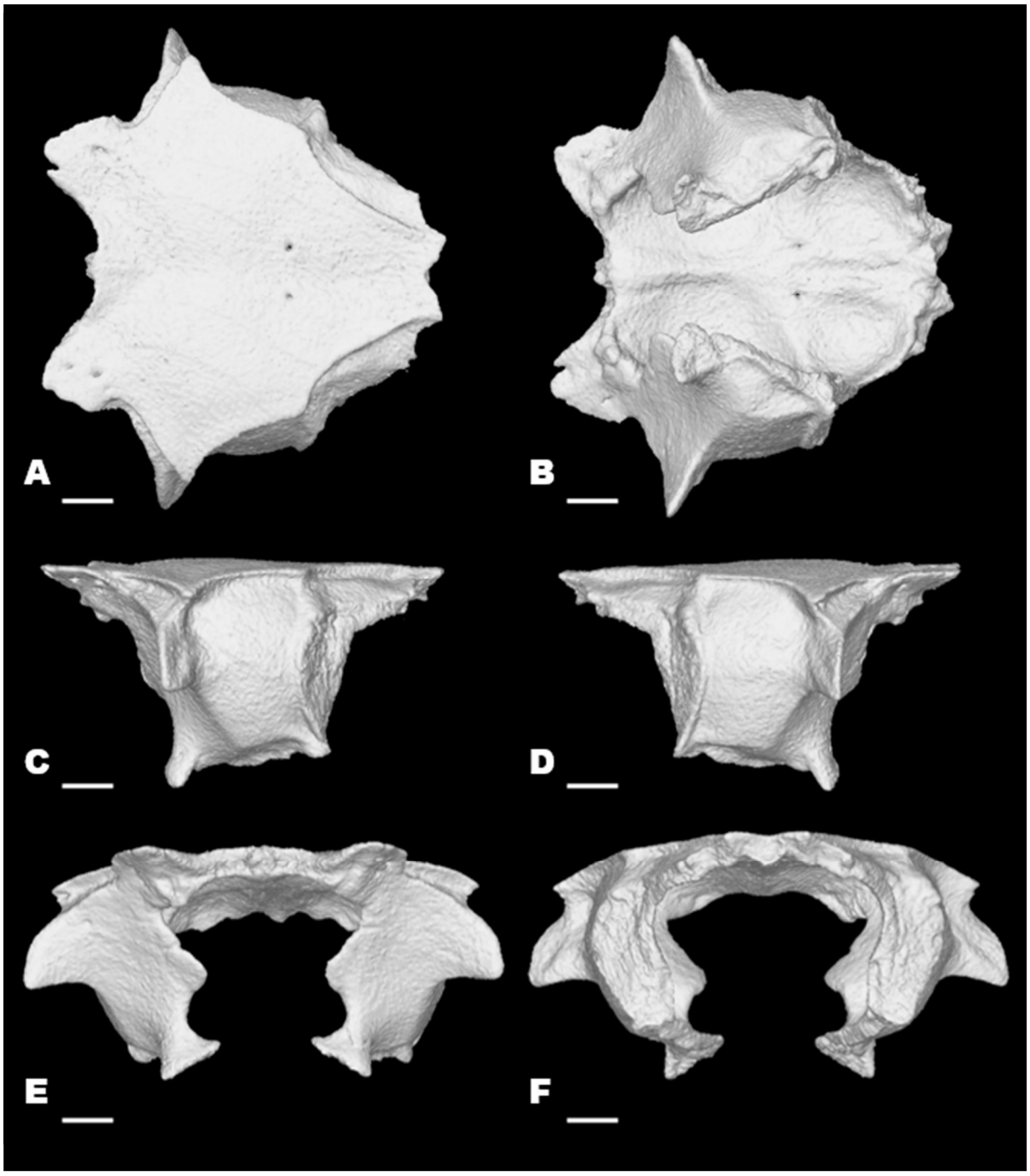

Figure 44. *Xenodon neuwiedii* UMMZ:HERPS:63002
A) Dorsal, B) Ventral, C) Left Lateral, D) Right Lateral, E) Anterior, F) Posterior. Scale bar = 1mm.

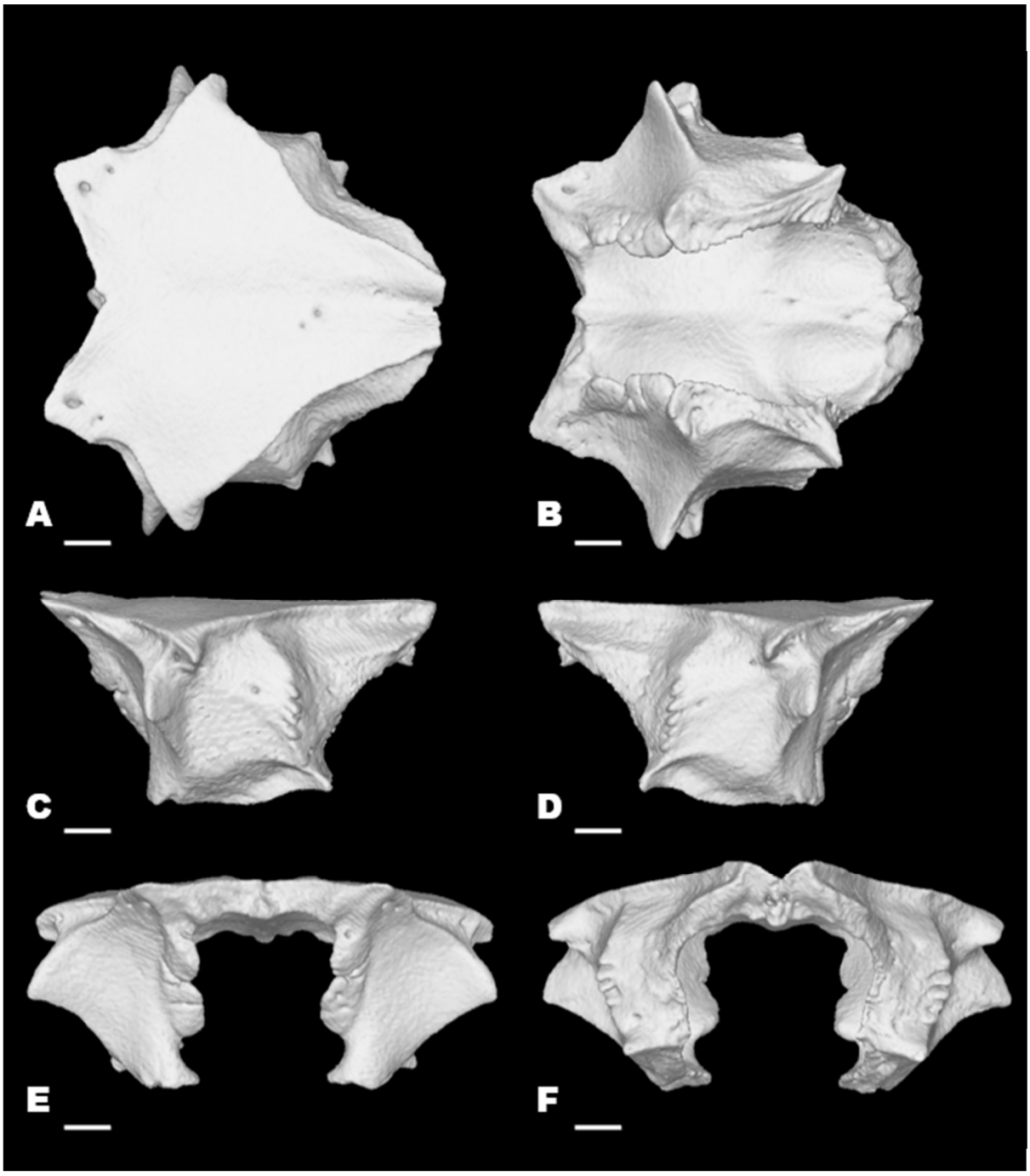

Figure 45. *Natrix natrix* UMMZ:HERPS:65465

A) Dorsal, B) Ventral, C) Left Lateral, D) Right Lateral, E) Anterior, F) Posterior. Scale bar = 1mm.

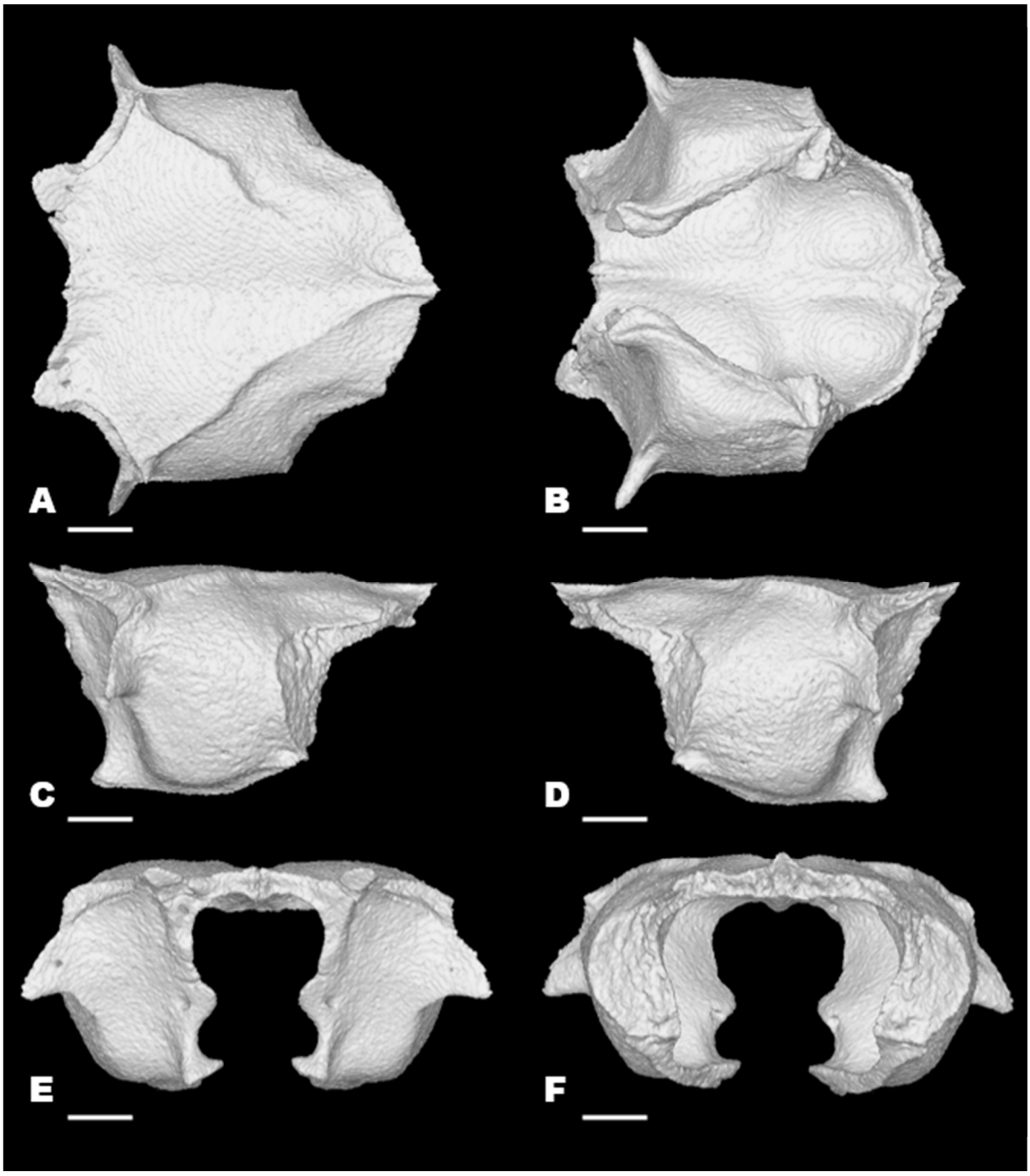

Figure 46. *Nerodia sipedon* UMMZ:HERPS:205025

A) Dorsal, B) Ventral, C) Left Lateral, D) Right Lateral, E) Anterior, F) Posterior. Scale bar = 1mm.

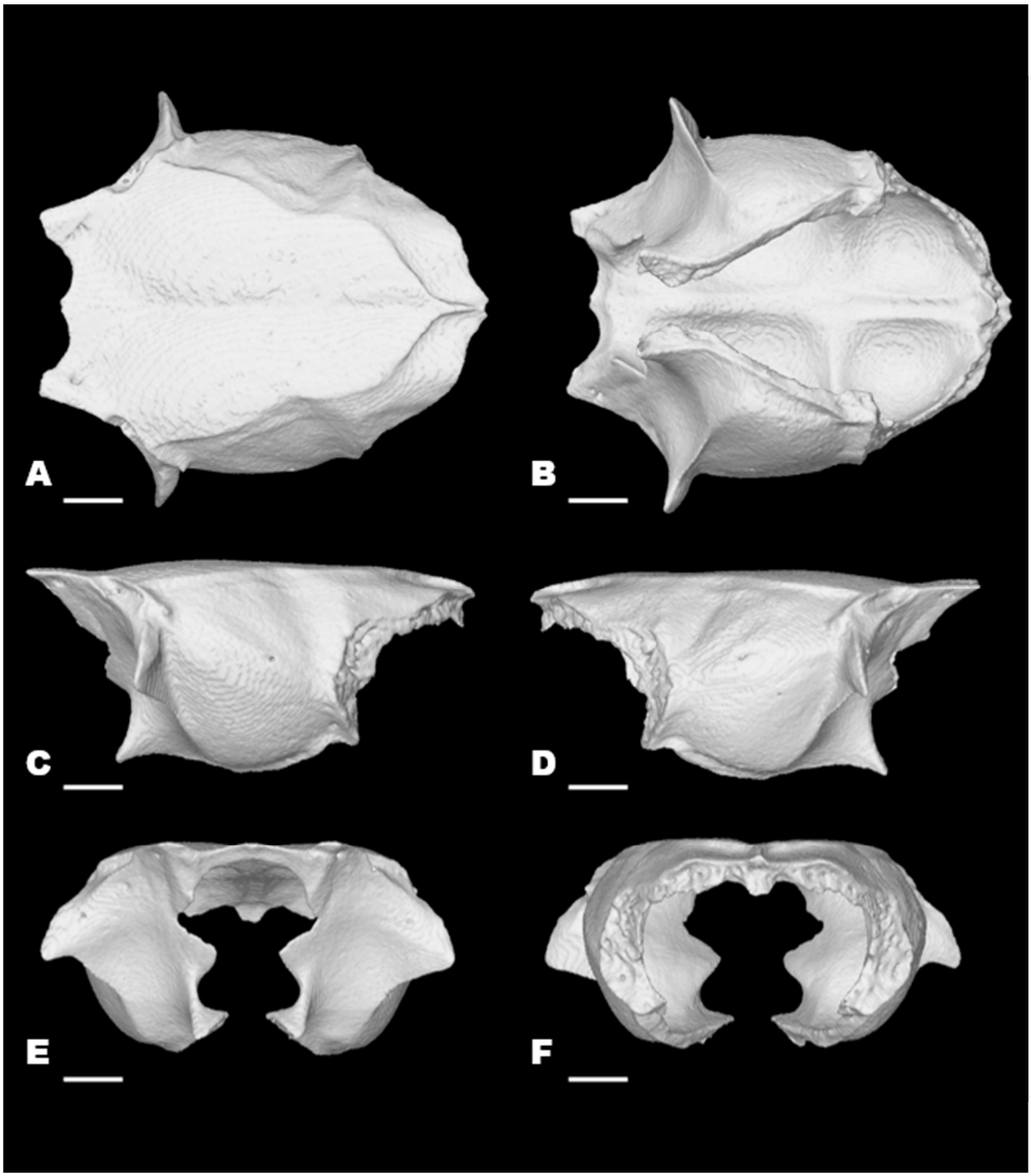

Figure 47. *Thamnophis rufipunctatus* UMMZ:HERPS:172510

A) Dorsal, B) Ventral, C) Left Lateral, D) Right Lateral, E) Anterior, F) Posterior. Scale bar = 1mm.

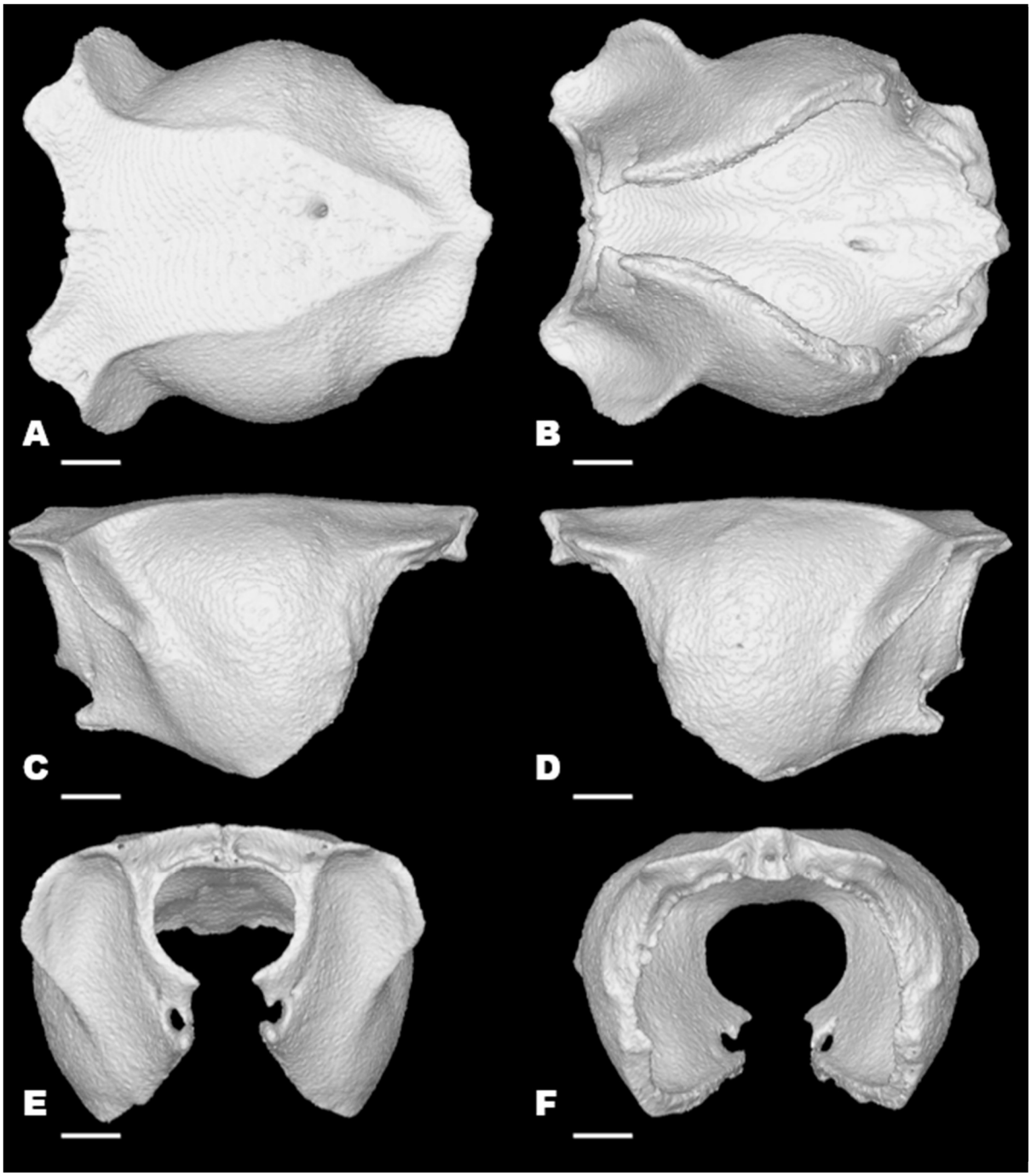

Figure 48. *Bungarus fasciatus* UMMZ:HERPS:201916

A) Dorsal, B) Ventral, C) Left Lateral, D) Right Lateral, E) Anterior, F) Posterior. Scale bar = 1mm.

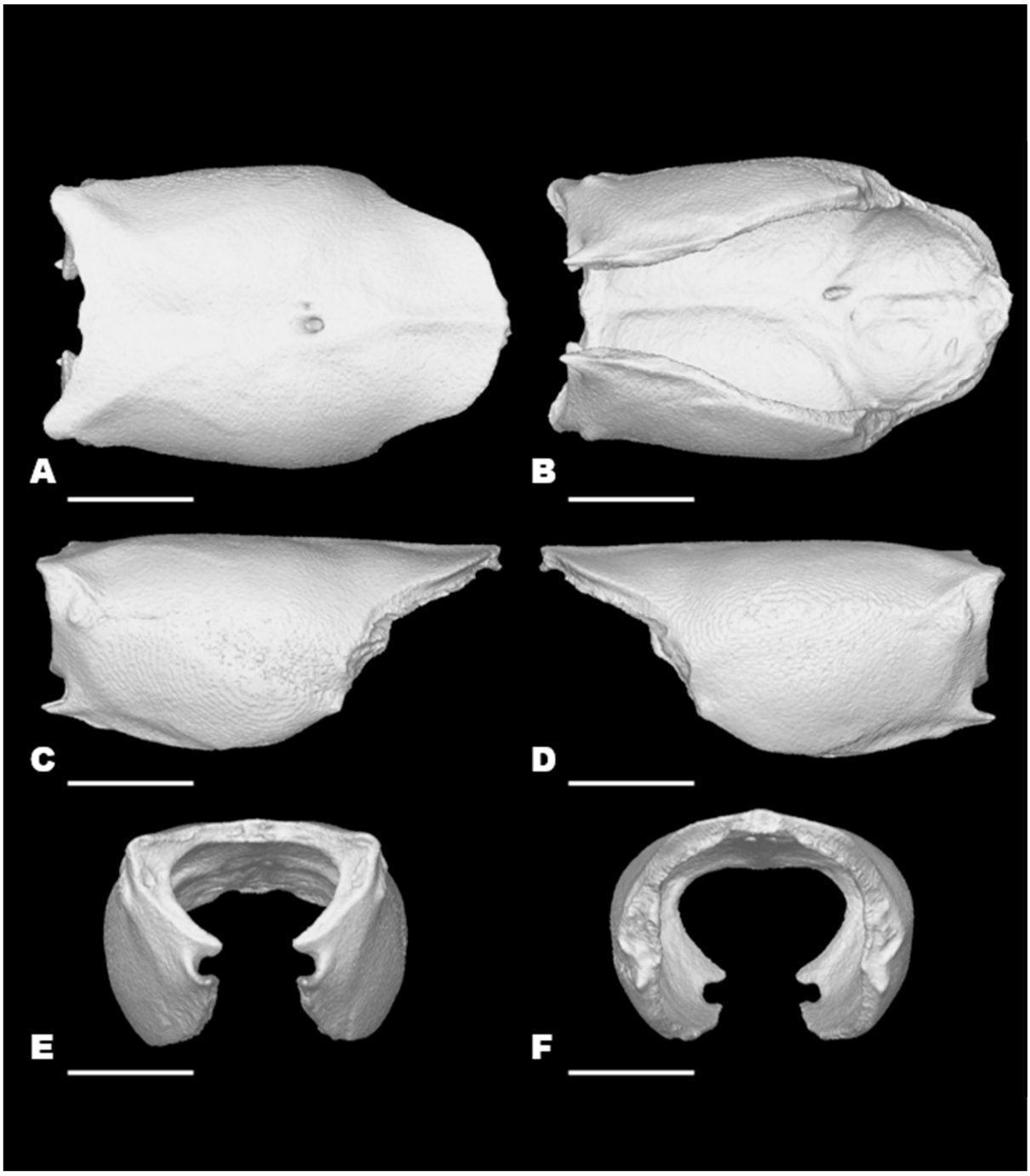

Figure 49. *Calliophis maculiceps* UMZC R9.221-1

A) Dorsal, B) Ventral, C) Left Lateral, D) Right Lateral, E) Anterior, F) Posterior. Scale bar = 1mm.

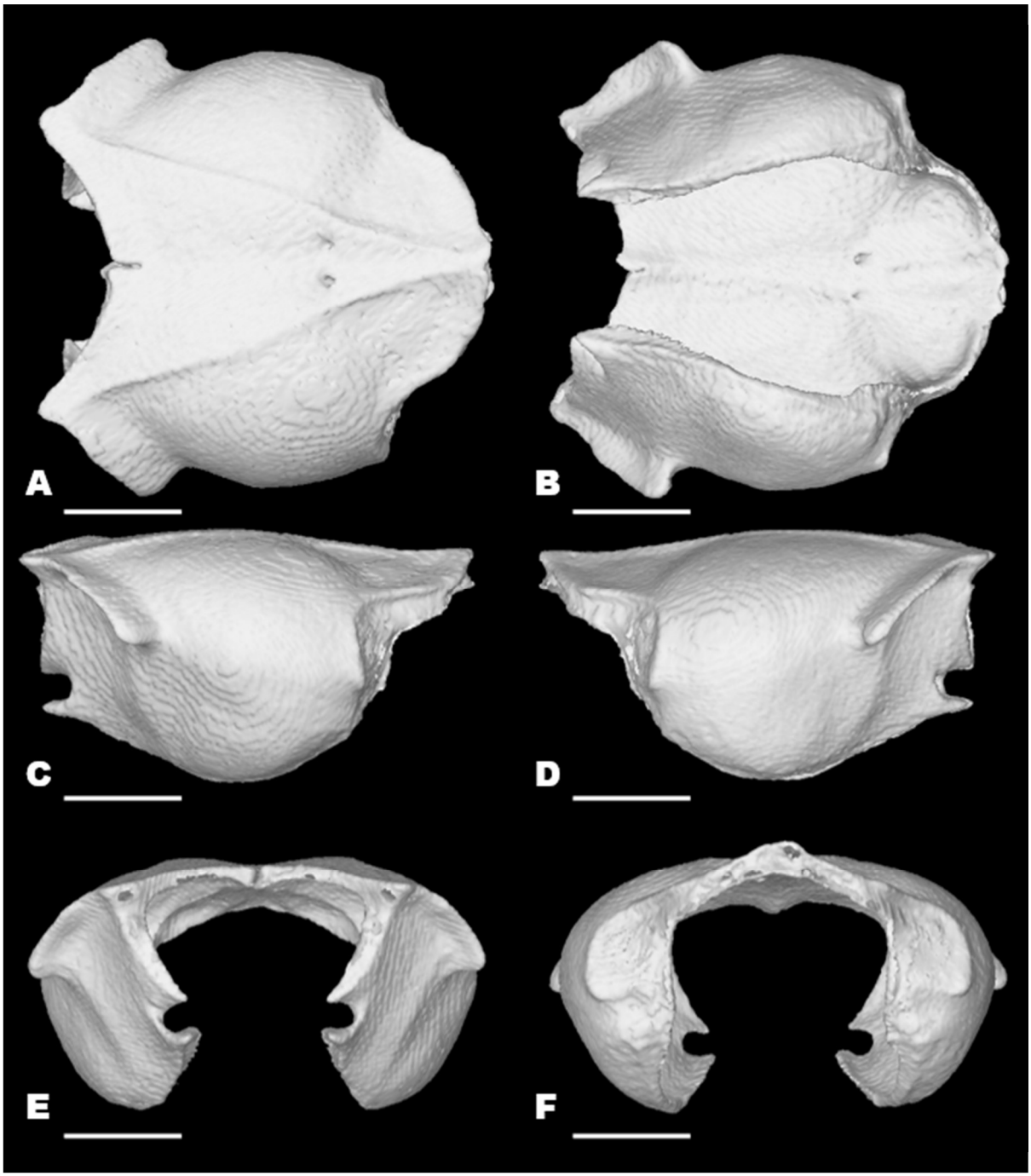

Figure 50. *Furina diadema* UMMZ:HERPS:83498

A) Dorsal, B) Ventral, C) Left Lateral, D) Right Lateral, E) Anterior, F) Posterior. Scale bar = 1mm.

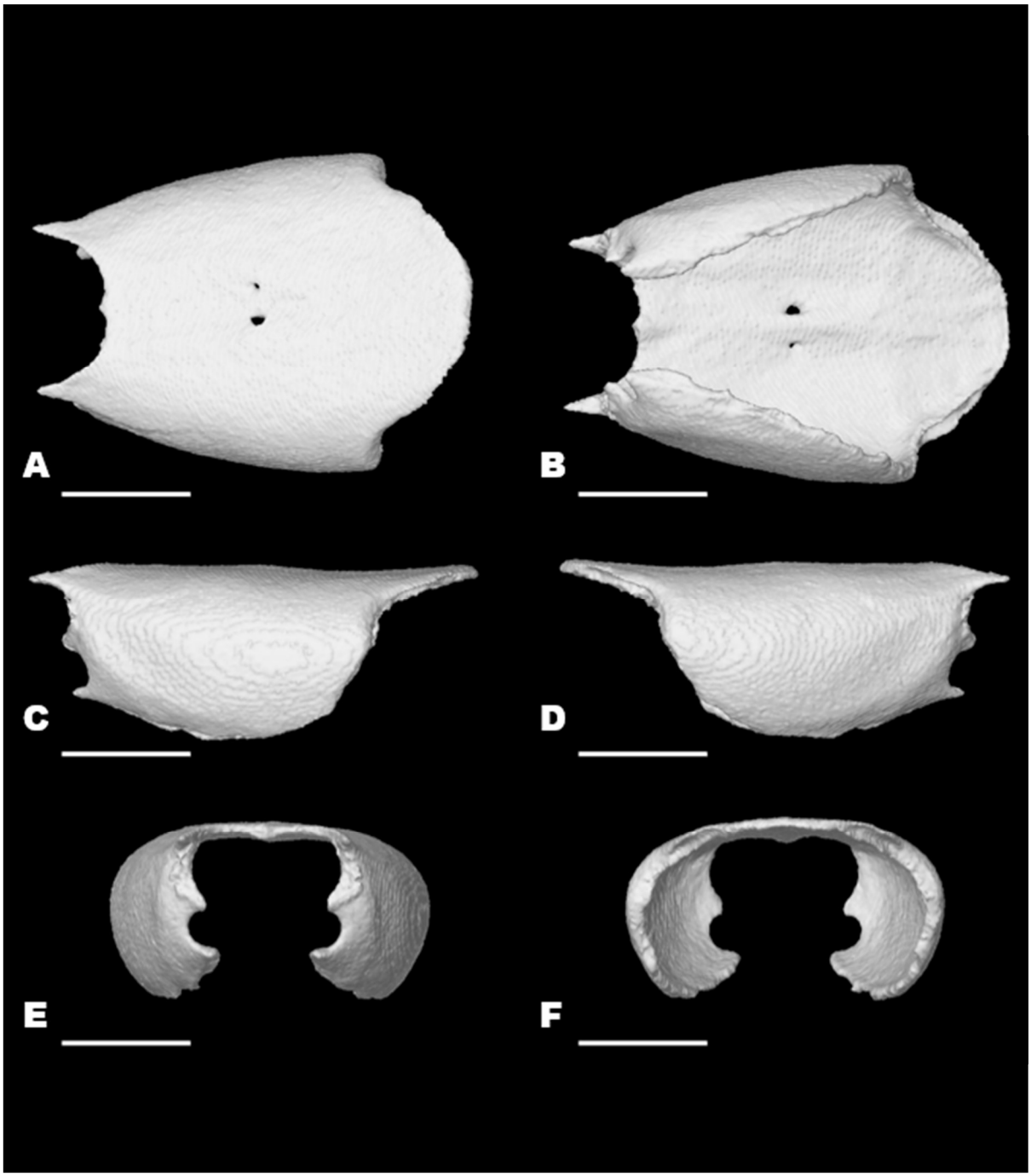

Figure 51. *Micruroides euryxanthus* UMMZ:HERPS:200295

A) Dorsal, B) Ventral, C) Left Lateral, D) Right Lateral, E) Anterior, F) Posterior. Scale bar = 1mm.

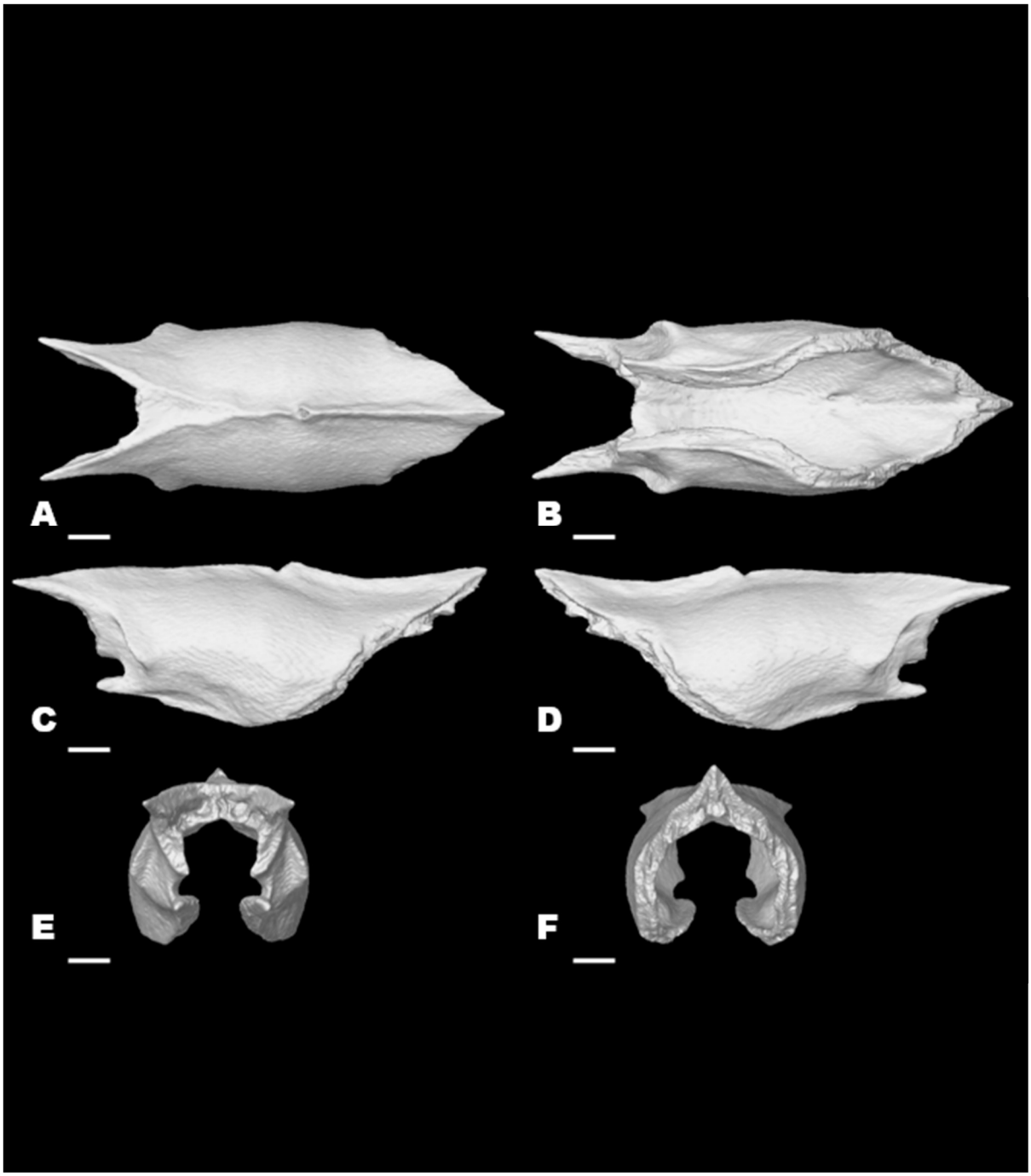

Figure 52. *Micrurus fulvius* FMNH:AMPHIBIANS AND REPTILES:39479

A) Dorsal, B) Ventral, C) Left Lateral, D) Right Lateral, E) Anterior, F) Posterior. Scale bar = 1mm.

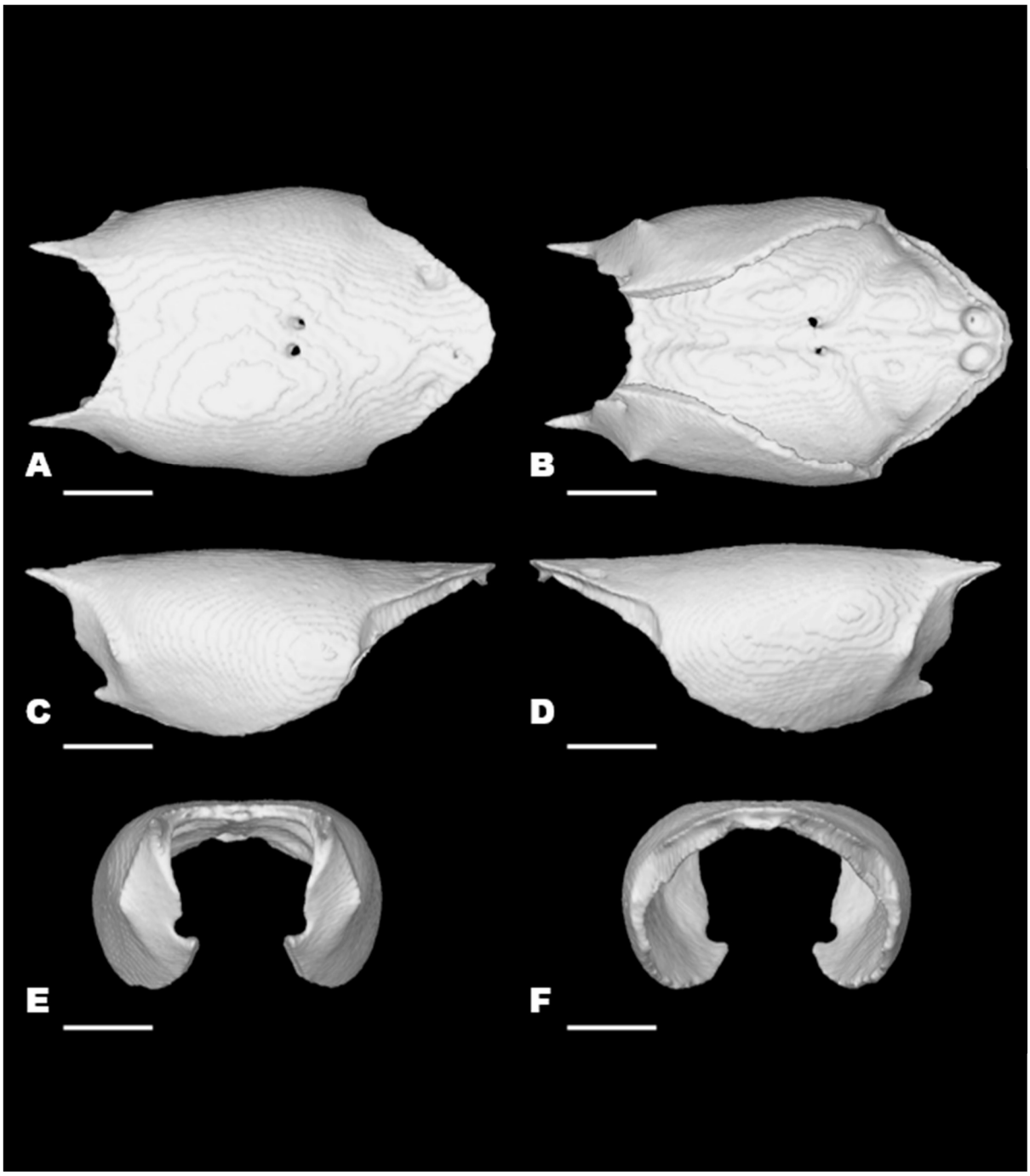

Figure 53. *Micrurus nigrocinctus* UMMZ:HERPS:131984

A) Dorsal, B) Ventral, C) Left Lateral, D) Right Lateral, E) Anterior, F) Posterior. Scale bar = 1mm.

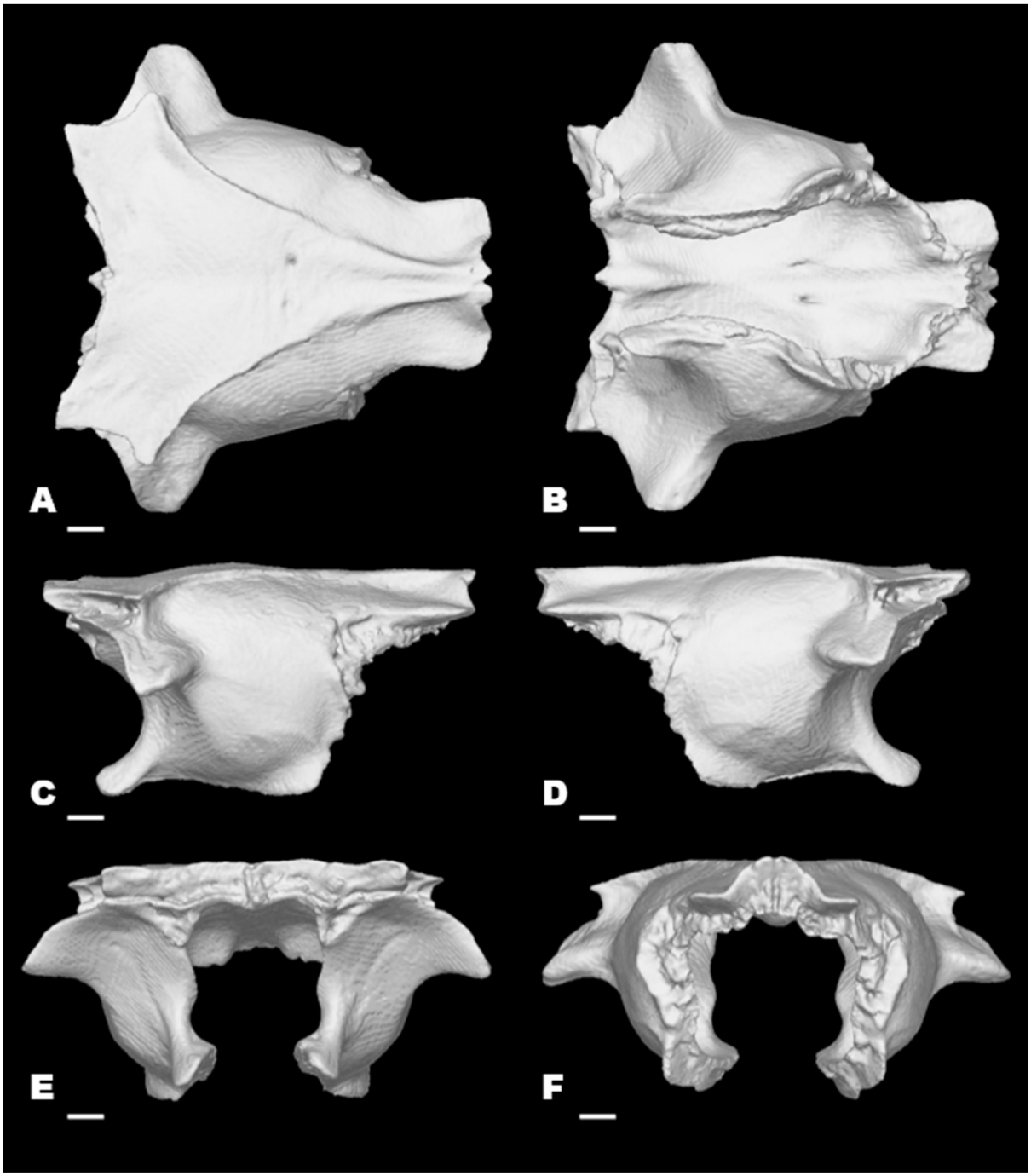

Figure 54. *Naja naja* UMZC R9.177-3

A) Dorsal, B) Ventral, C) Left Lateral, D) Right Lateral, E) Anterior, F) Posterior. Scale bar = 1mm.

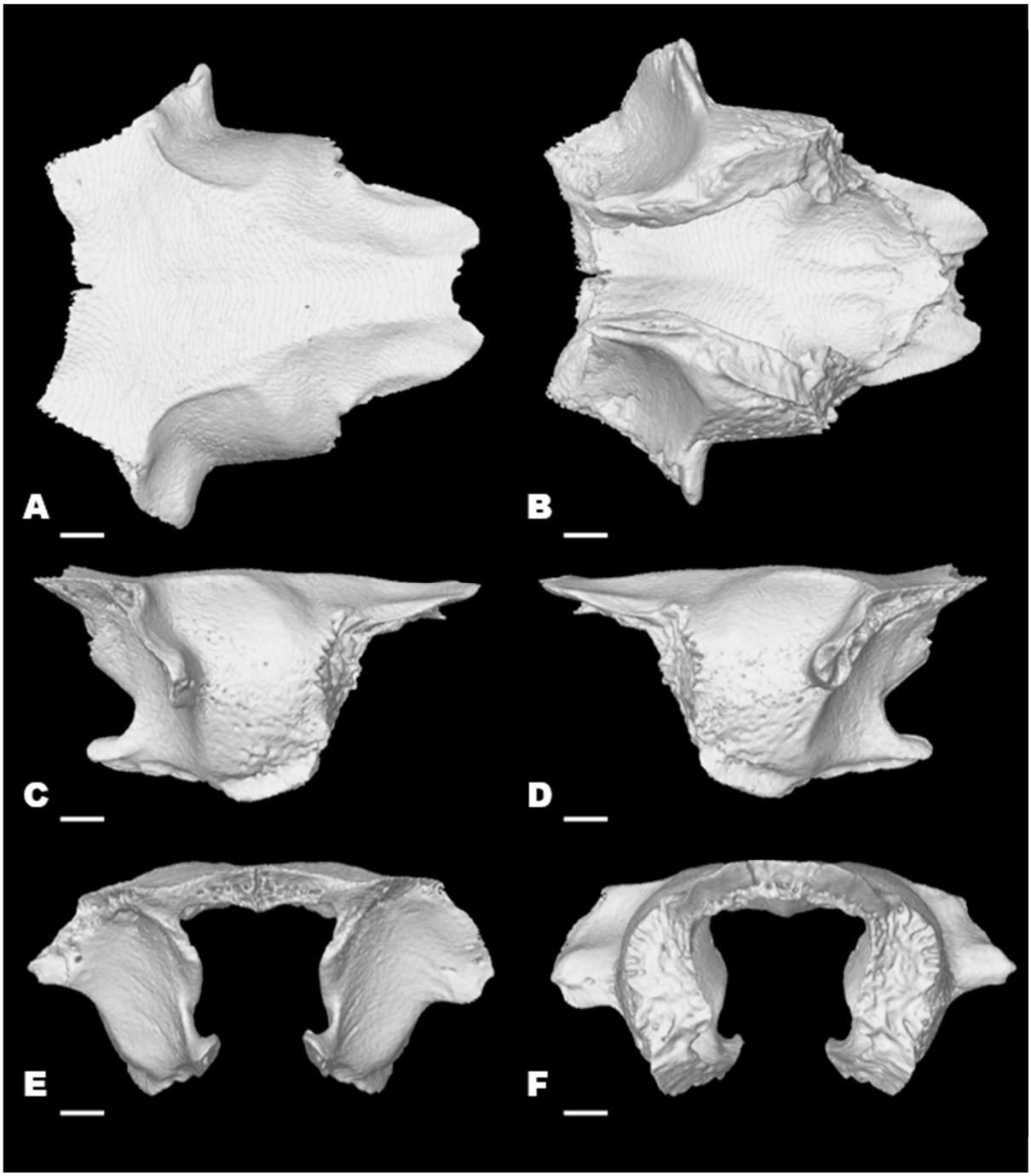

Figure 55. *Notechis scutatus* UMMZ:HERPS:65874

A) Dorsal, B) Ventral, C) Left Lateral, D) Right Lateral, E) Anterior, F) Posterior. Scale bar = 1mm.

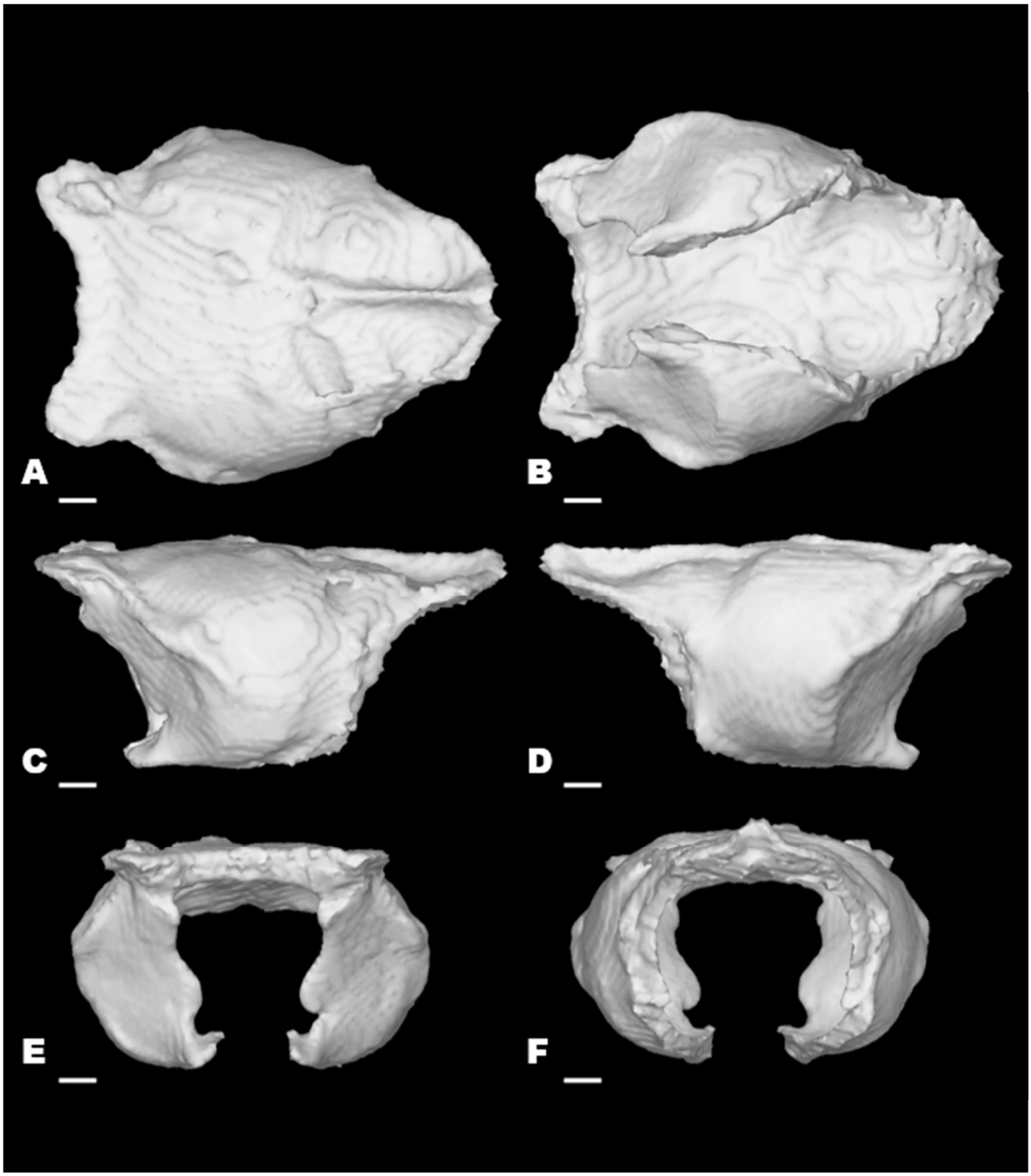

Figure 56. *Oxyuranus scutellatus* LSUMZ:HERPS:94344

A) Dorsal, B) Ventral, C) Left Lateral, D) Right Lateral, E) Anterior, F) Posterior. Scale bar = 1mm.

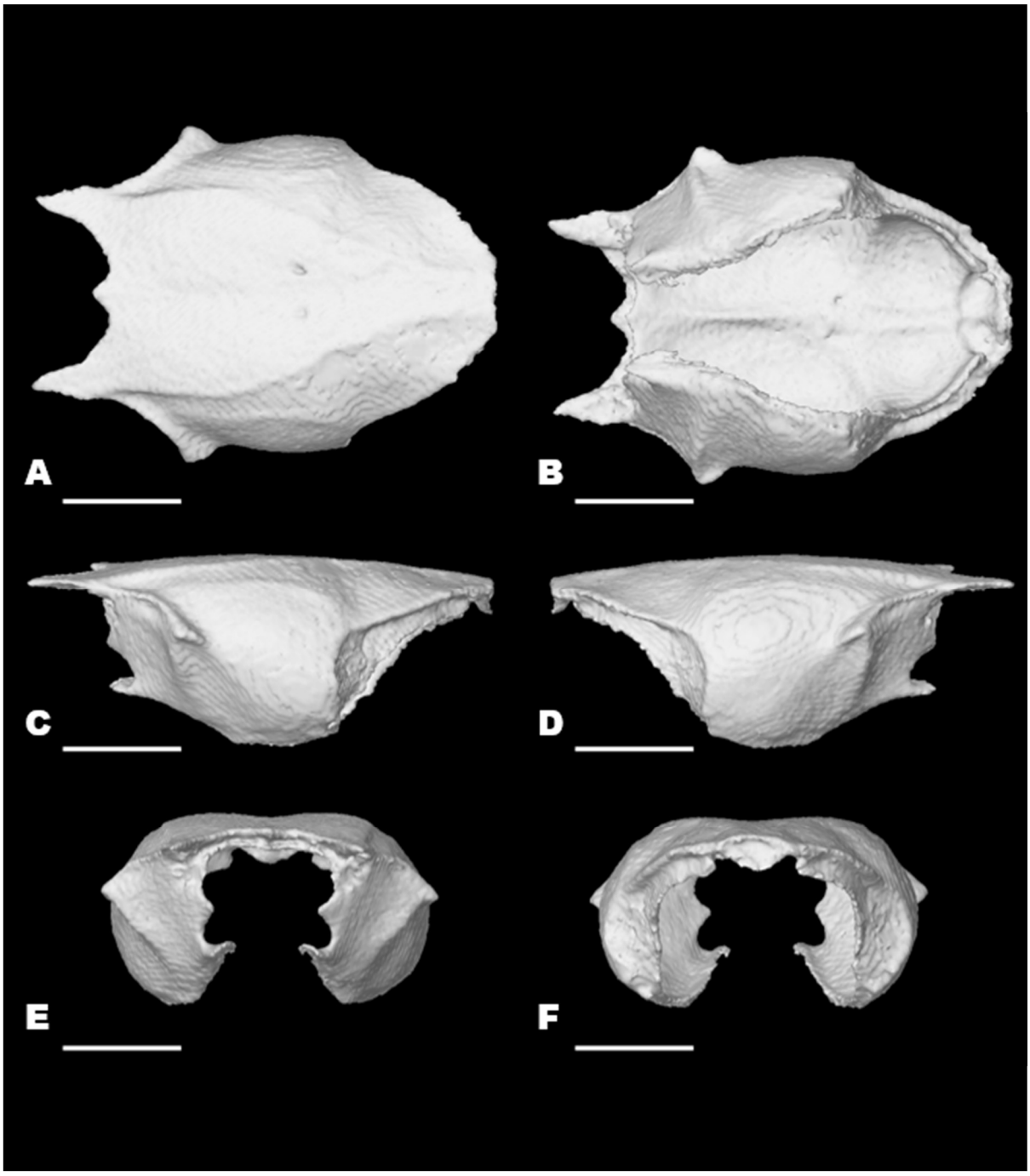

Figure 57. *Simoselaps bertholdi* UMMZ:HERPS:244197

A) Dorsal, B) Ventral, C) Left Lateral, D) Right Lateral, E) Anterior, F) Posterior. Scale bar = 1mm.

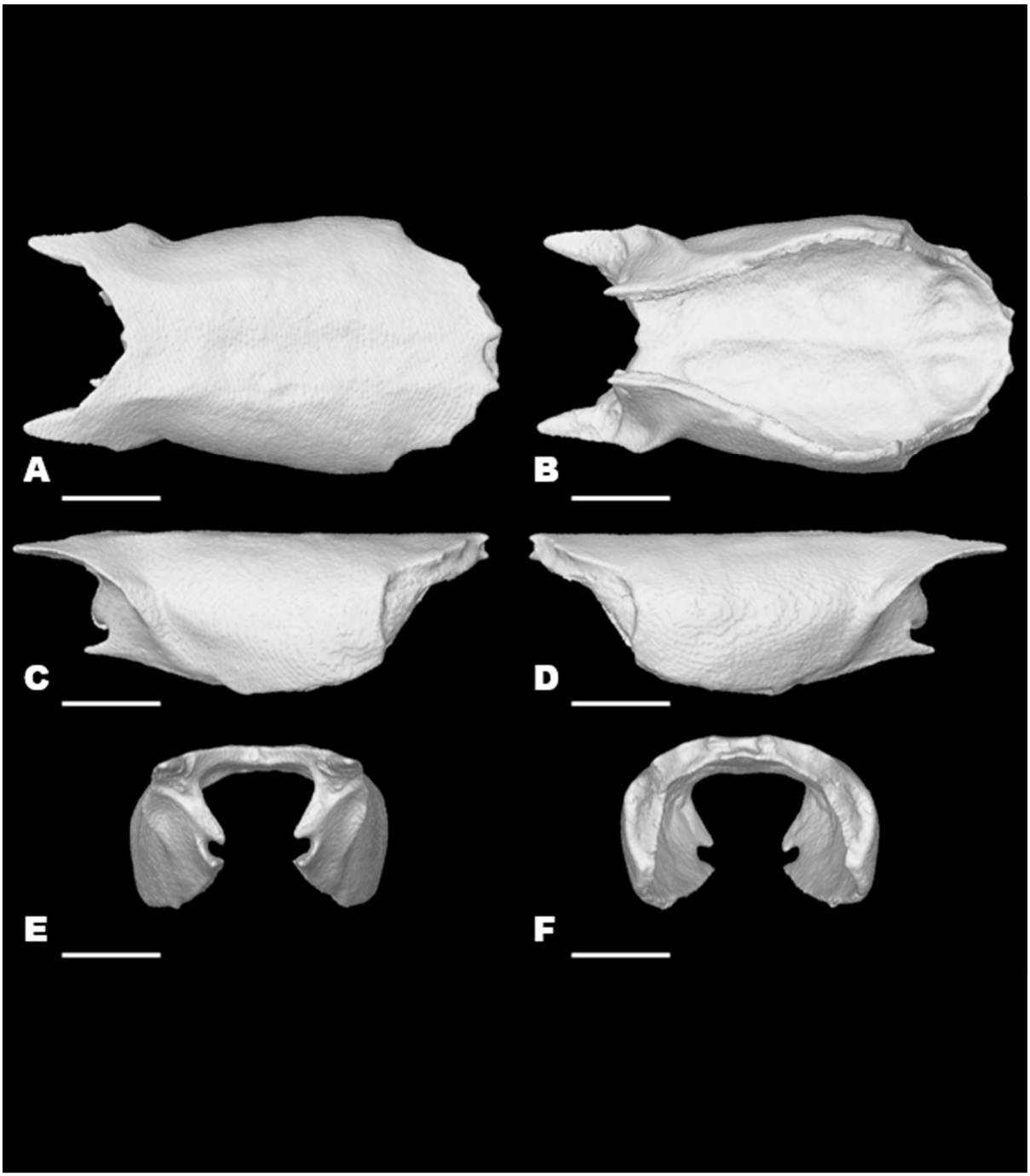

Figure 58. *Vermicella annulate* UMZC R9.239-1

A) Dorsal, B) Ventral, C) Left Lateral, D) Right Lateral, E) Anterior, F) Posterior. Scale bar = 1mm.

Figure 59. *Amblyodipsas polylepis hildebrantii* CAS:HERP:173555

A) Dorsal, B) Ventral, C) Left Lateral, D) Right Lateral, E) Anterior, F) Posterior. Scale bar = 1mm.

Figure 60. *Aparallactus capensis* CAS:HERP:11683

A) Dorsal, B) Ventral, C) Left Lateral, D) Right Lateral, E) Anterior, F) Posterior. Scale bar = 1mm.

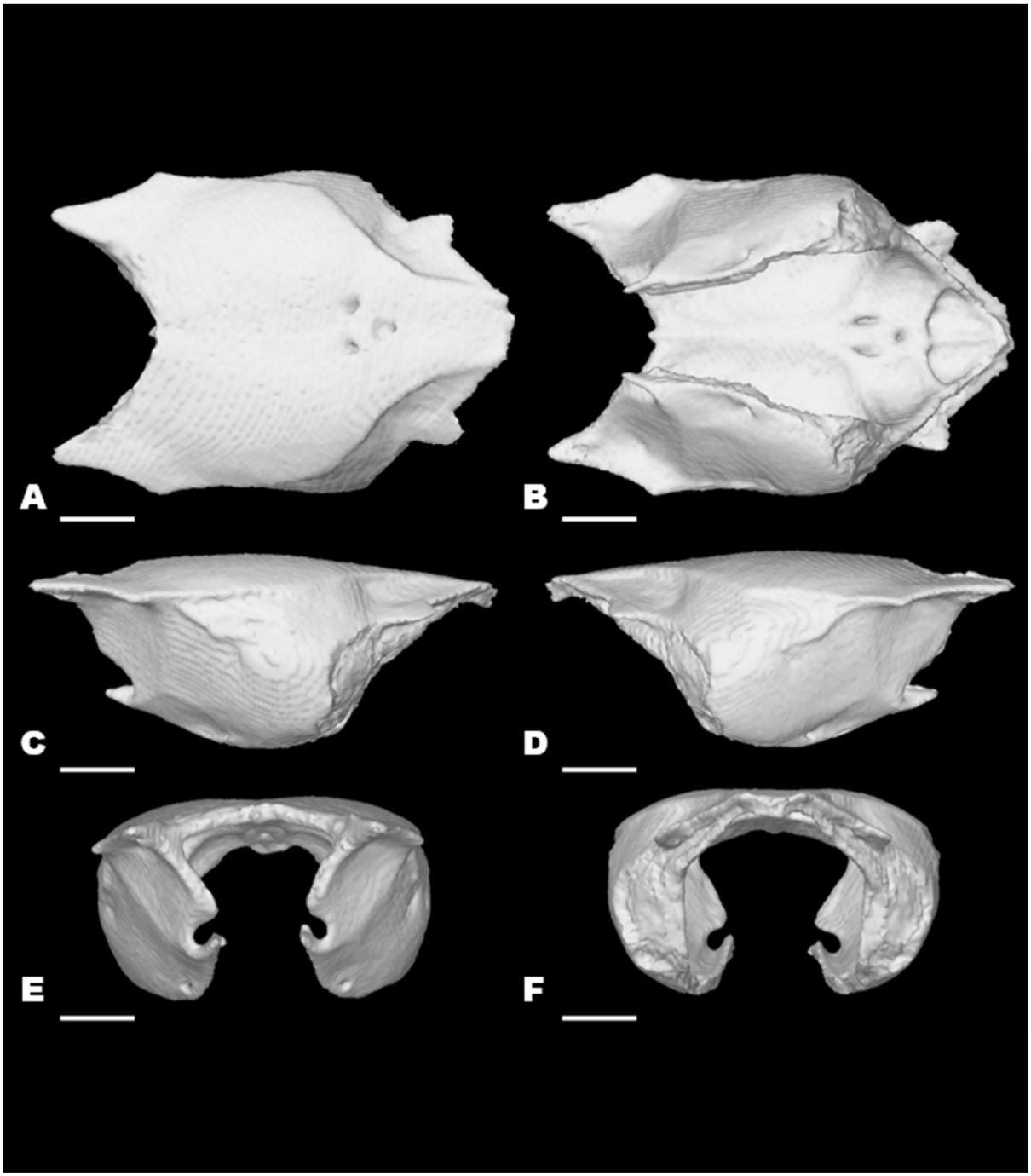

Figure 61. *Aparallactus modestus* CAS:HERP:111865

A) Dorsal, B) Ventral, C) Left Lateral, D) Right Lateral, E) Anterior, F) Posterior. Scale bar = 1mm.

Figure 62. *Aparallactus niger* AMNH:HERPETOLOGY:R-142406

A) Dorsal, B) Ventral, C) Left Lateral, D) Right Lateral, E) Anterior, F) Posterior. Scale bar = 1mm.

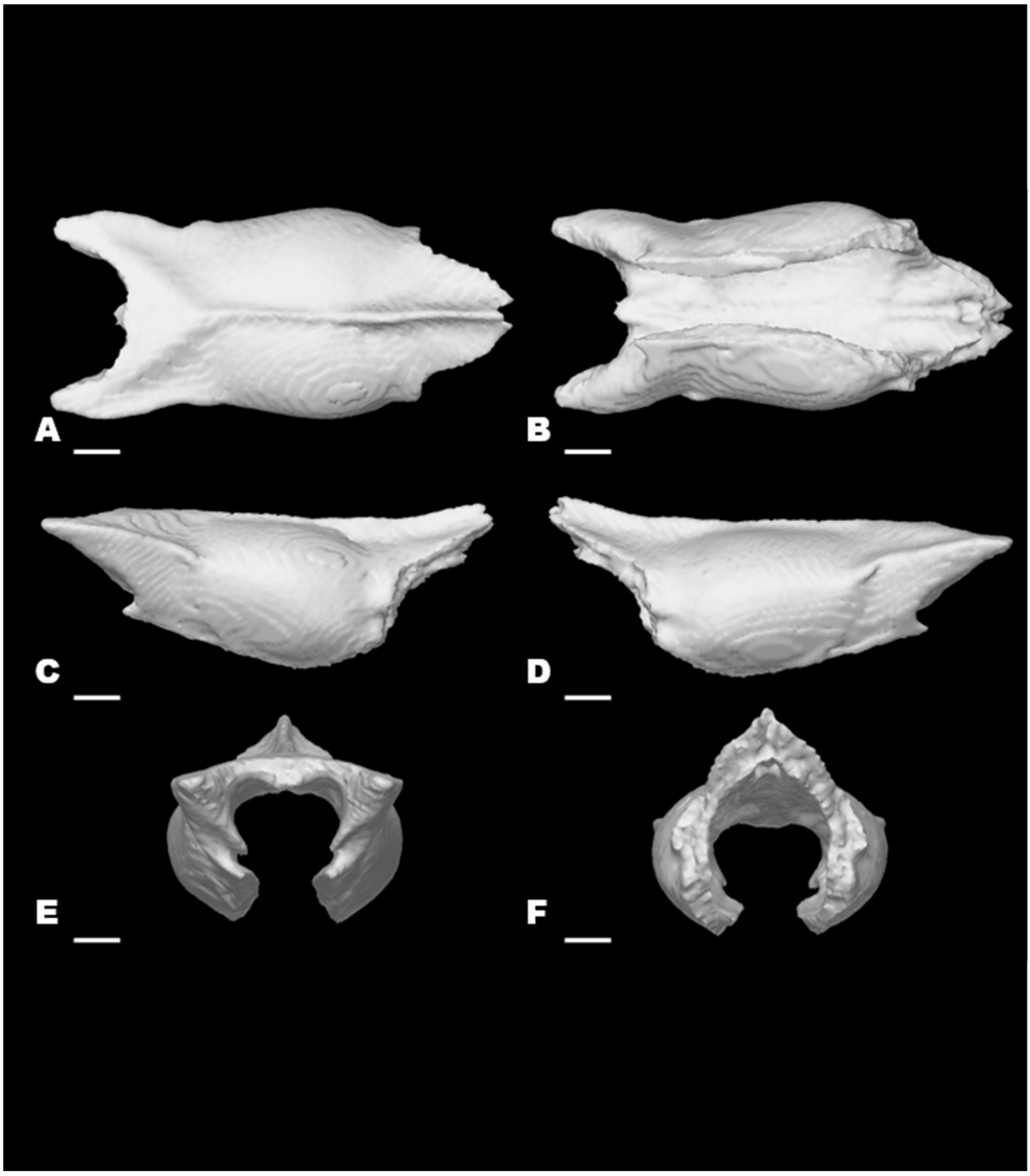

Figure 63. *Polemon christyi* CAS:HERP:147905

A) Dorsal, B) Ventral, C) Left Lateral, D) Right Lateral, E) Anterior, F) Posterior. Scale bar = 1mm.

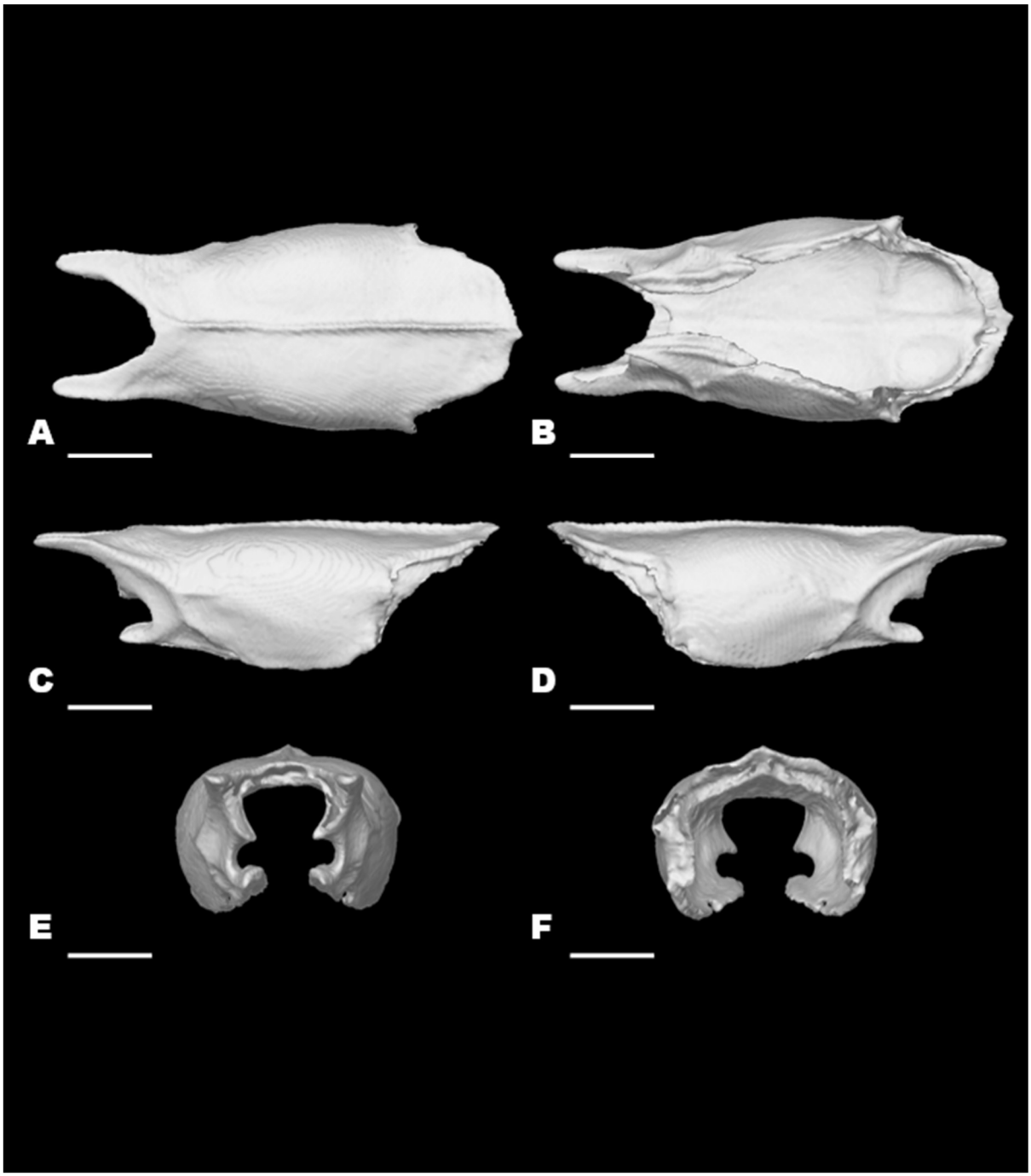

Figure 64. *Homoroselaps lacteus* CAS:HERP:173258

A) Dorsal, B) Ventral, C) Left Lateral, D) Right Lateral, E) Anterior, F) Posterior. Scale bar = 1mm.

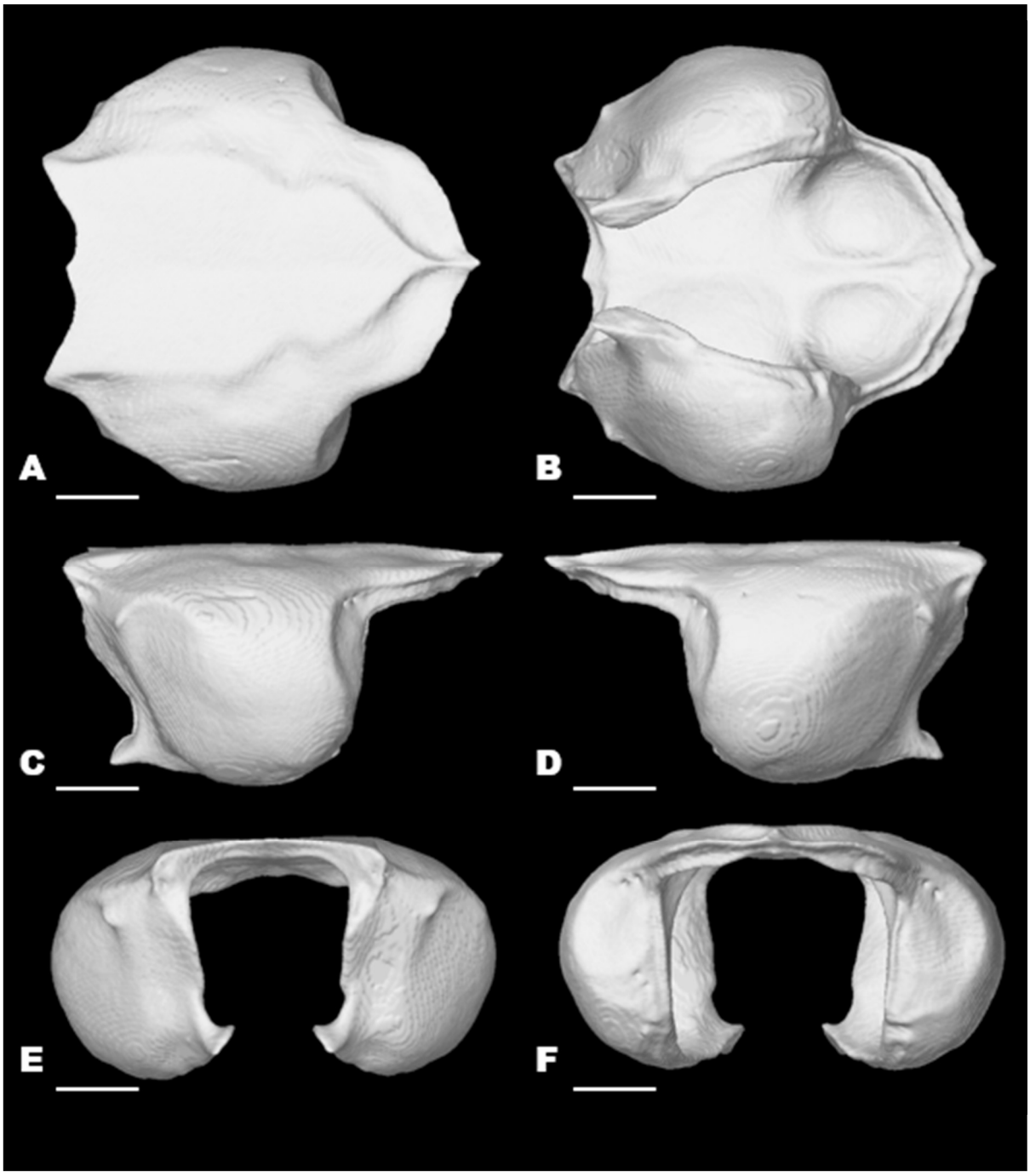

Figure 65. *Boaedon fulginosus* CAS:HERP:85747

A) Dorsal, B) Ventral, C) Left Lateral, D) Right Lateral, E) Anterior, F) Posterior. Scale bar = 1mm.

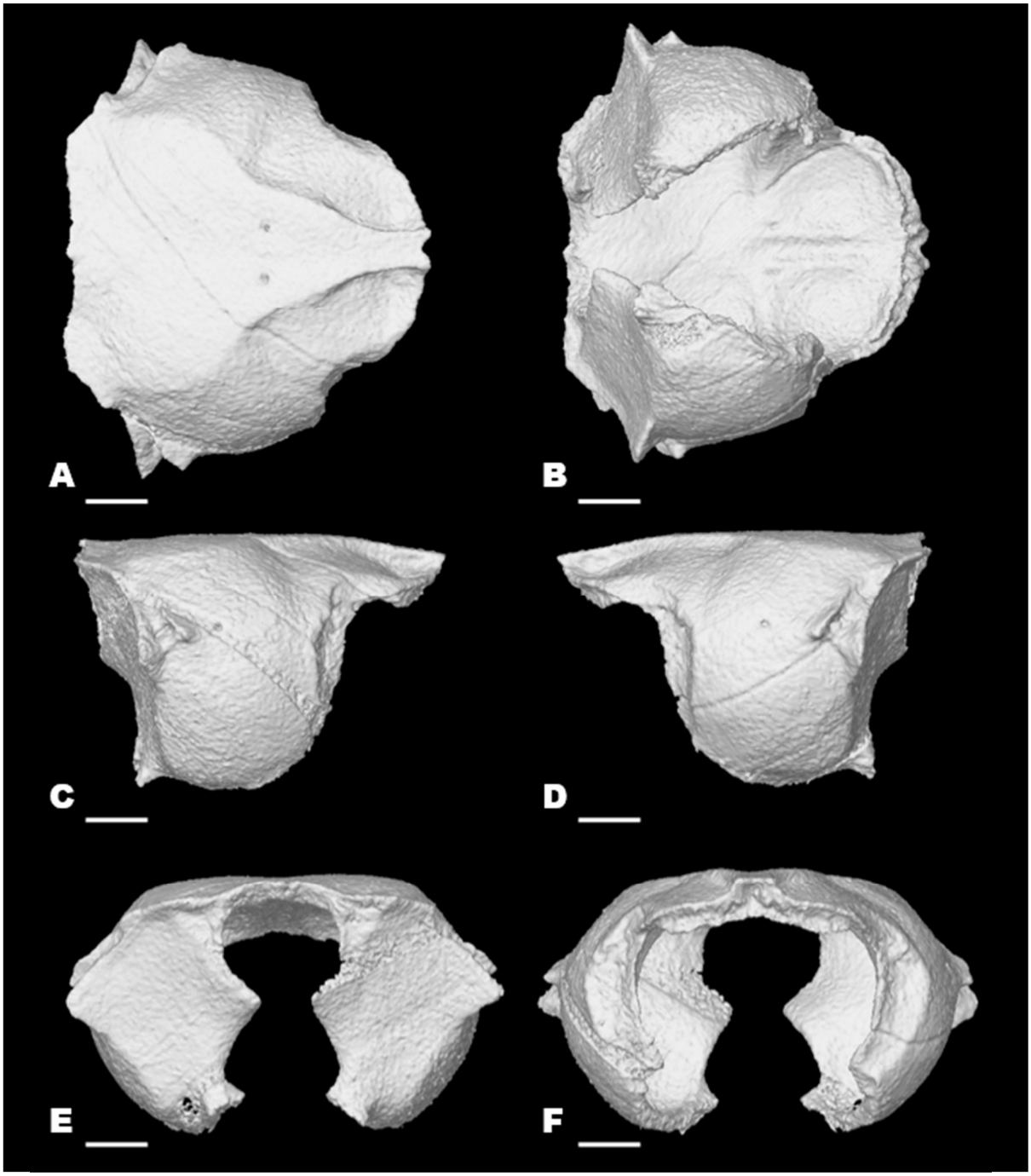

Figure 66. *Psammophylax variabilis* UMMZ:HERPS:61233

A) Dorsal, B) Ventral, C) Left Lateral, D) Right Lateral, E) Anterior, F) Posterior. Scale bar = 1mm.

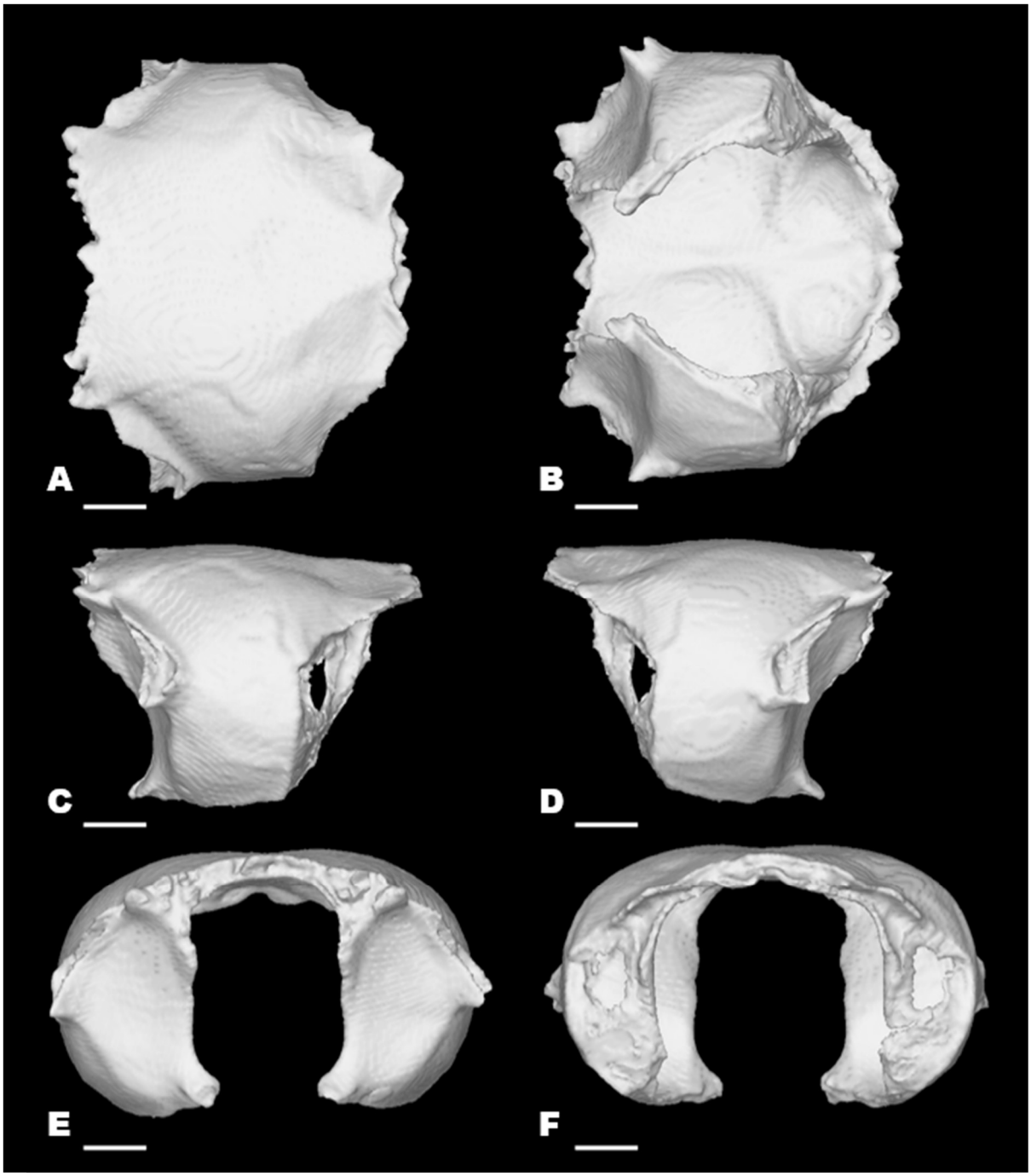

Figure 67. *Pseudaspis cana* LSUMZ:HERPS:54361

A) Dorsal, B) Ventral, C) Left Lateral, D) Right Lateral, E) Anterior, F) Posterior. Scale bar = 1mm.

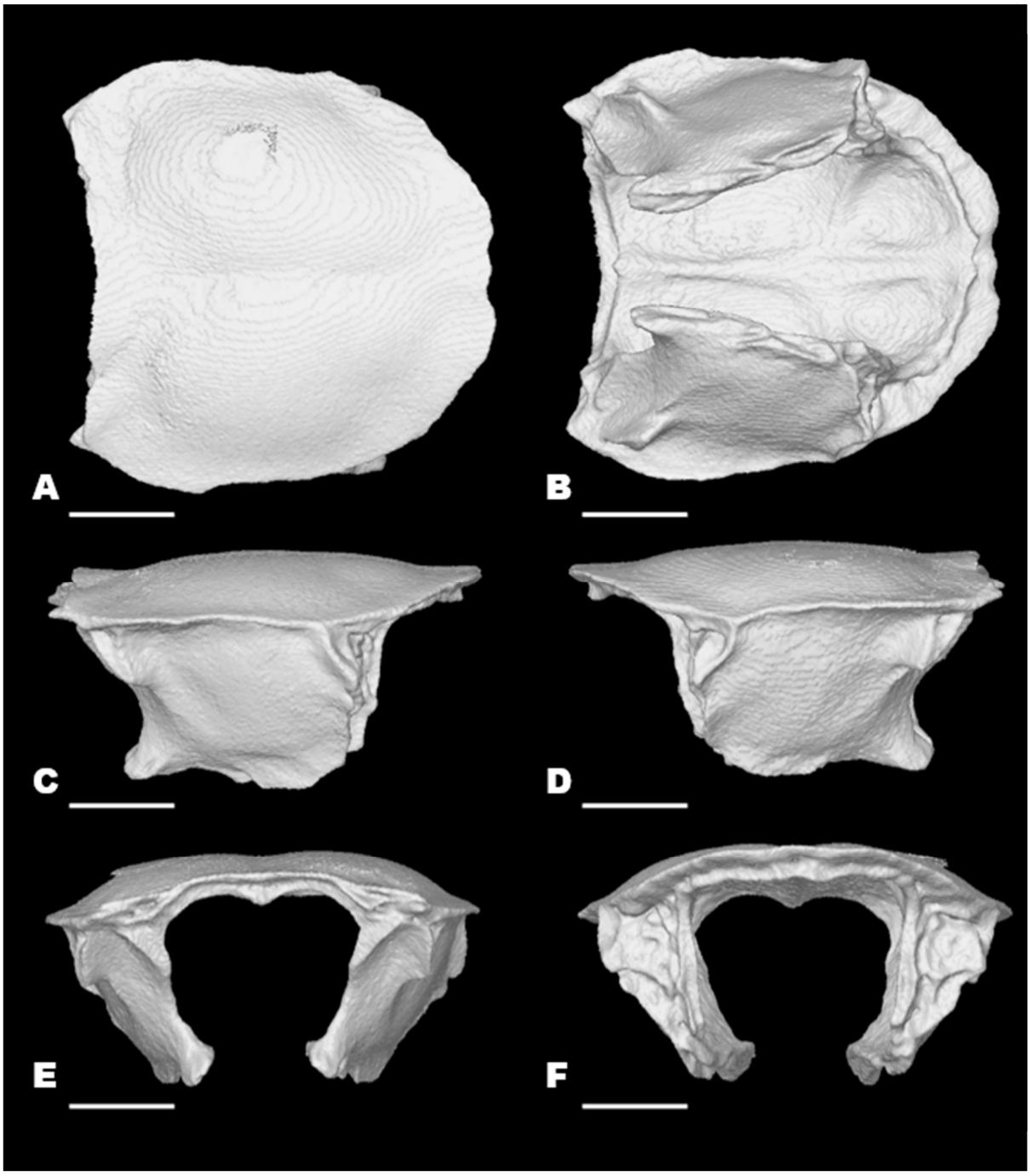

Figure 68. *Duberria lutrix* CAS:HERP:201763

A) Dorsal, B) Ventral, C) Left Lateral, D) Right Lateral, E) Anterior, F) Posterior. Scale bar = 1mm.

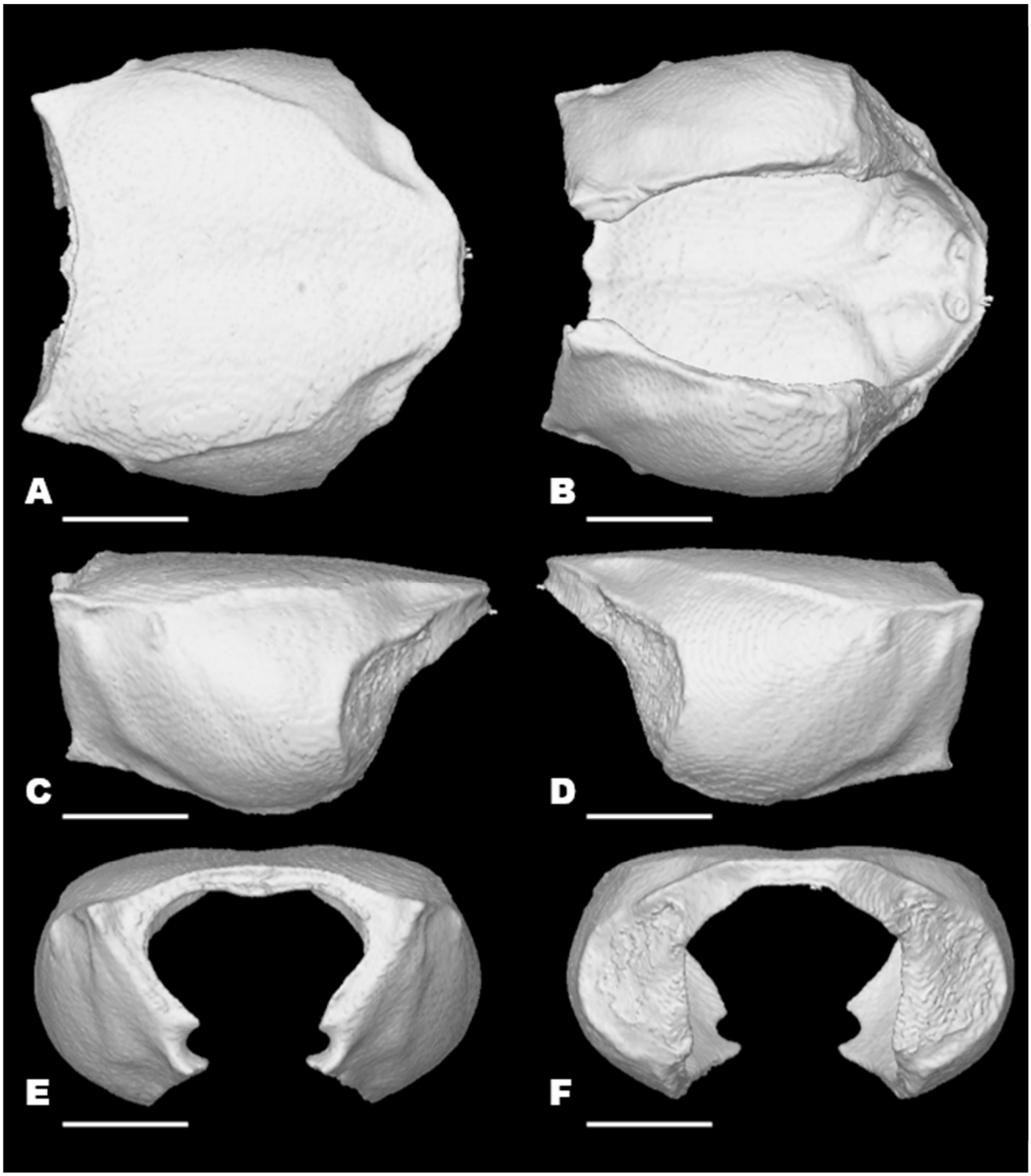

Figure 69. *Heteroliodon occipitalis* UMMZ:HERPS:229038

A) Dorsal, B) Ventral, C) Left Lateral, D) Right Lateral, E) Anterior, F) Posterior. Scale bar = 1mm.

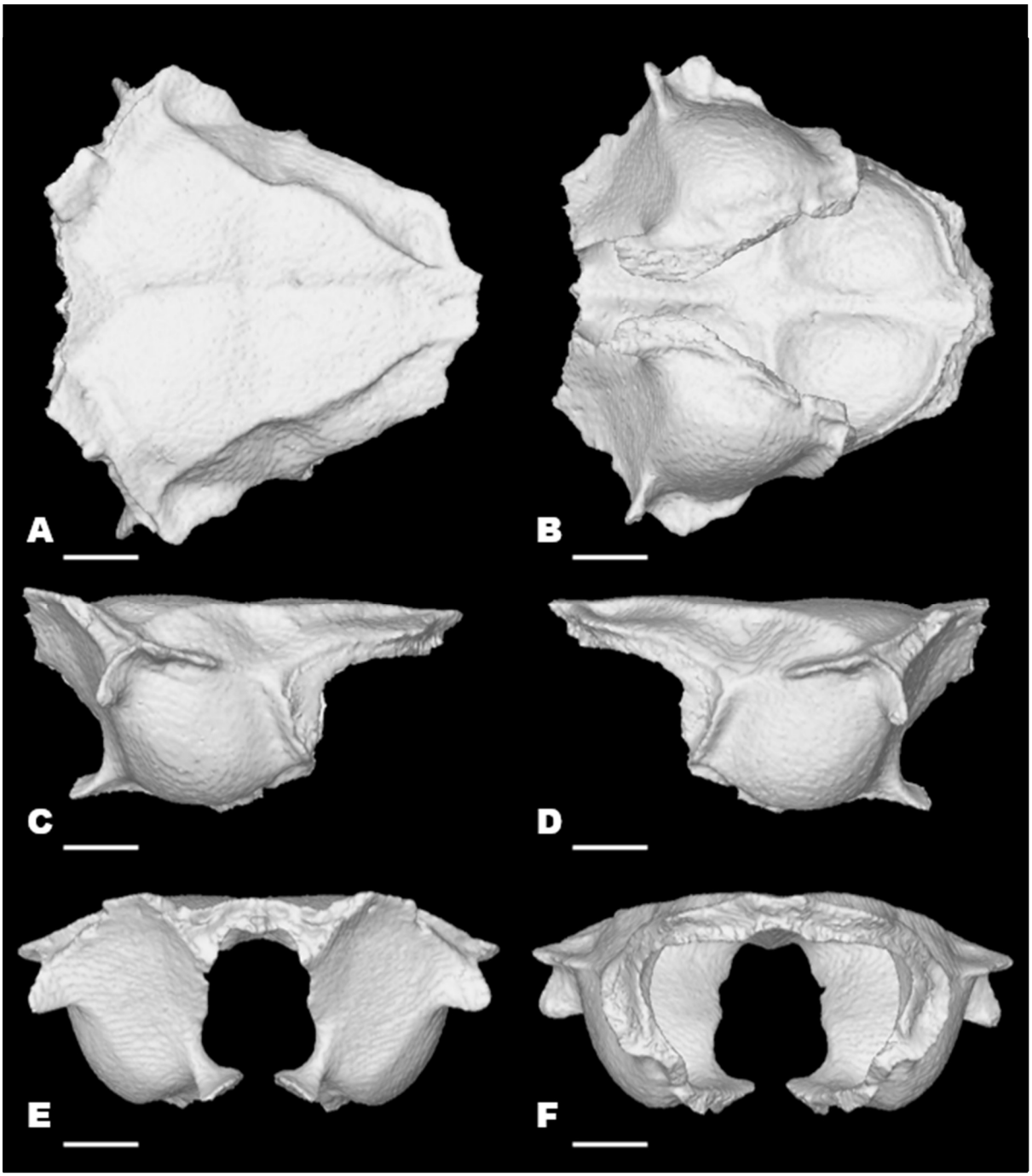

Figure 70. *Langaha madagascariensis* UMMZ:HERPS:209371

A) Dorsal, B) Ventral, C) Left Lateral, D) Right Lateral, E) Anterior, F) Posterior. Scale bar = 1mm.

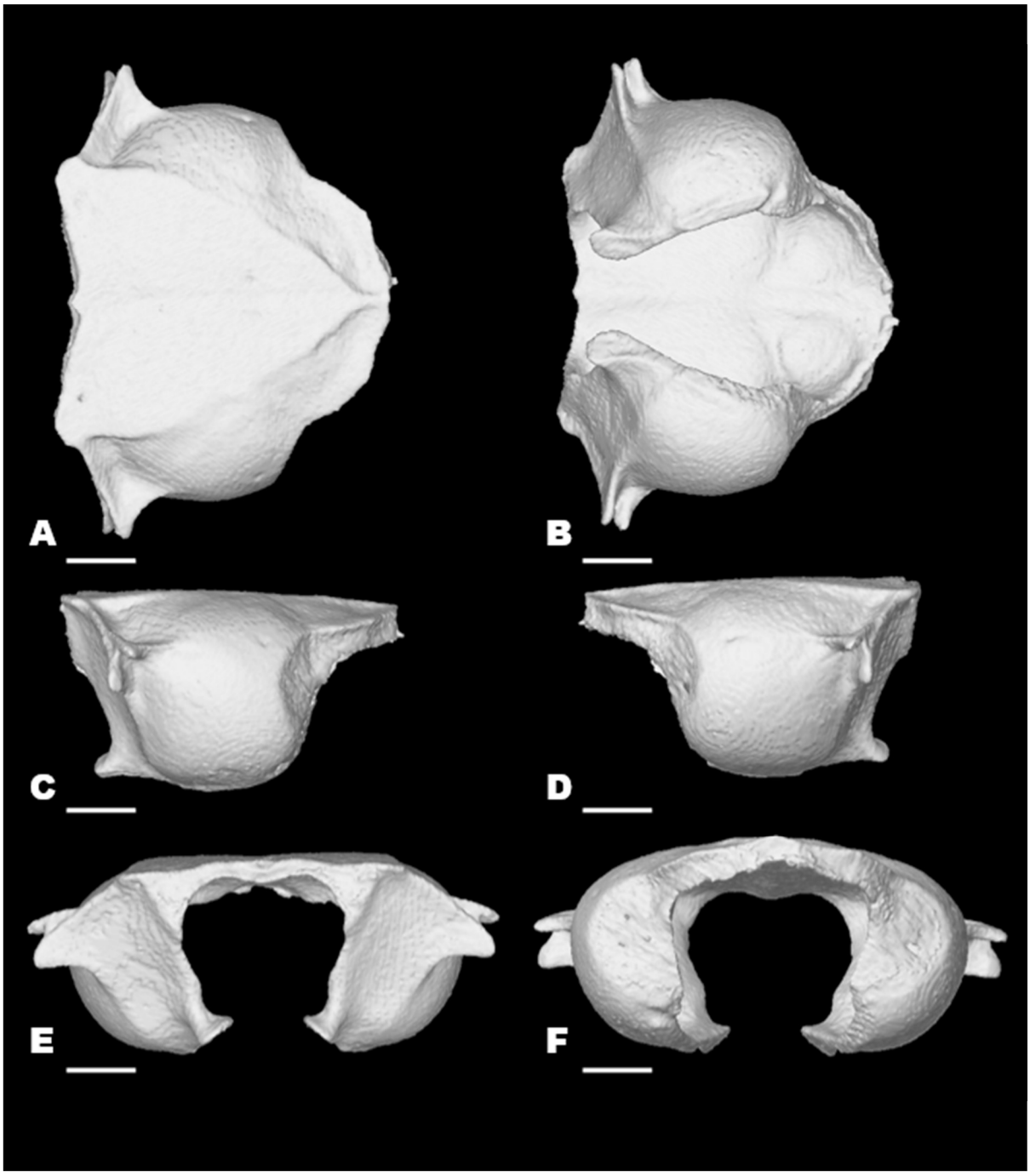

Figure 71. *Lycodryas granuliceps* UMMZ:HERPS:209566

A) Dorsal, B) Ventral, C) Left Lateral, D) Right Lateral, E) Anterior, F) Posterior. Scale bar = 1mm.

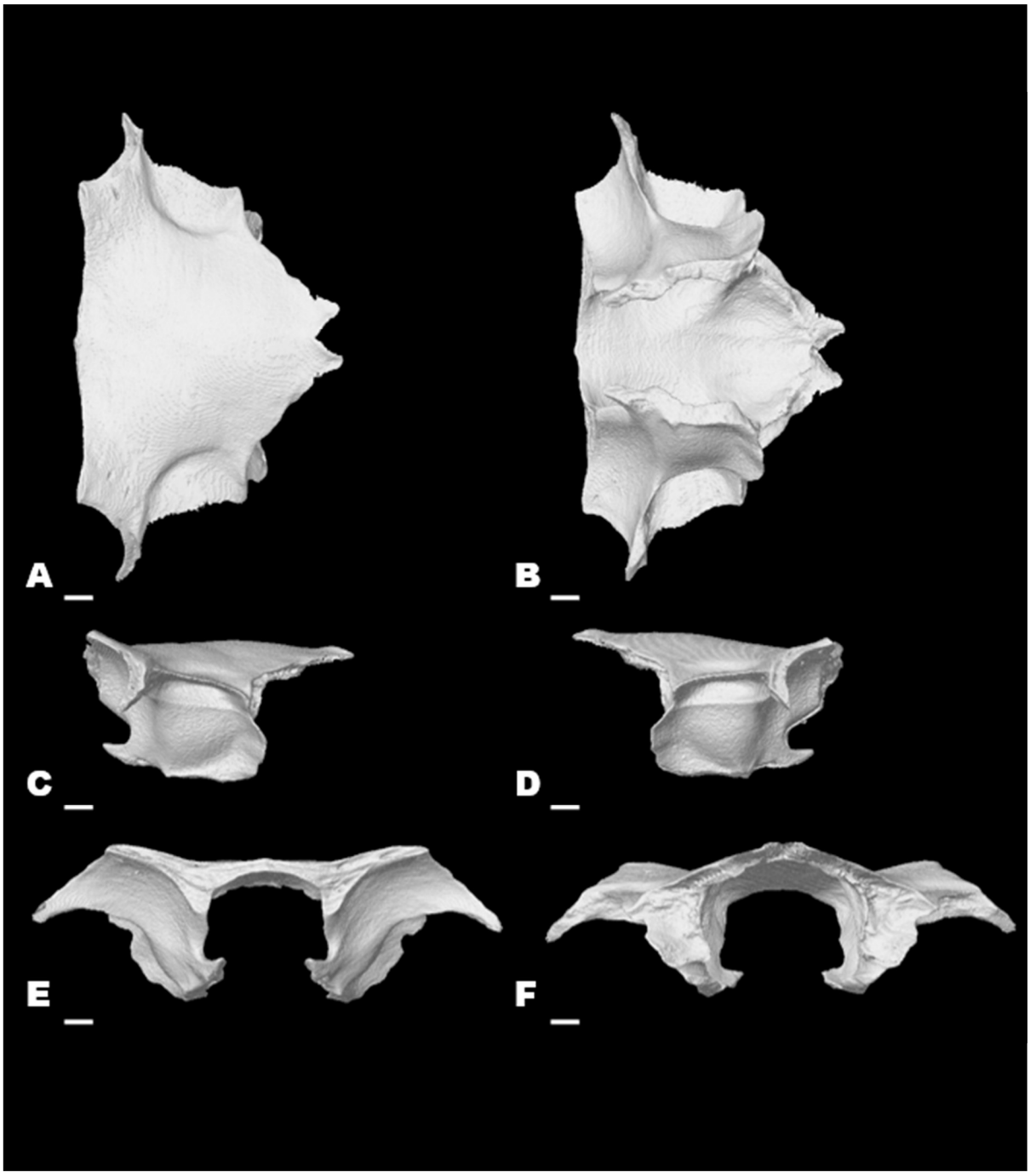

Figure 72. *Crotalus atrox* UMMZ:HERPS:11004

A) Dorsal, B) Ventral, C) Left Lateral, D) Right Lateral, E) Anterior, F) Posterior. Scale bar = 1mm.

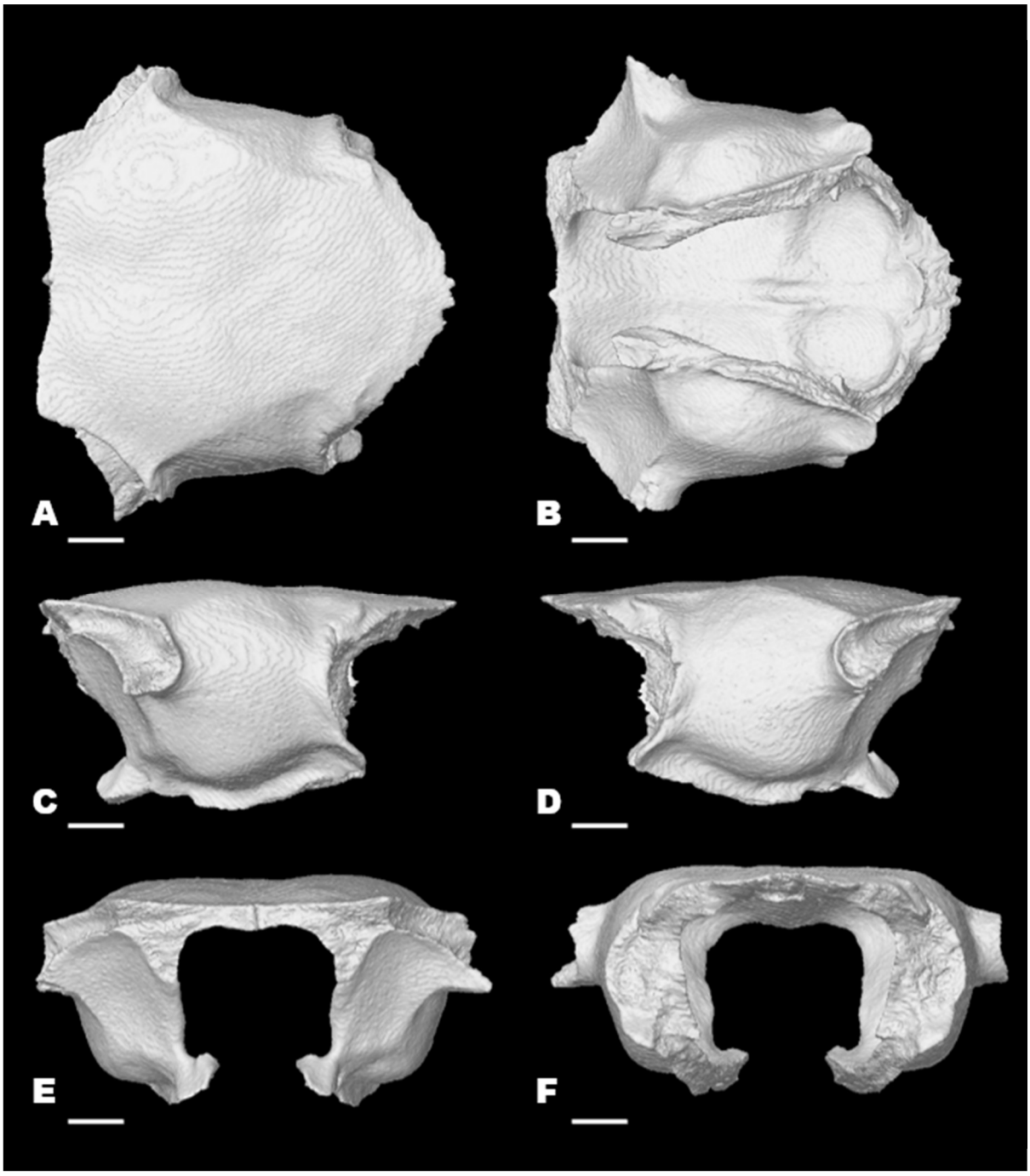

Figure 73. *Vipera aspis* UMMZ:HERPS:116957

A) Dorsal, B) Ventral, C) Left Lateral, D) Right Lateral, E) Anterior, F) Posterior. Scale bar = 1mm.

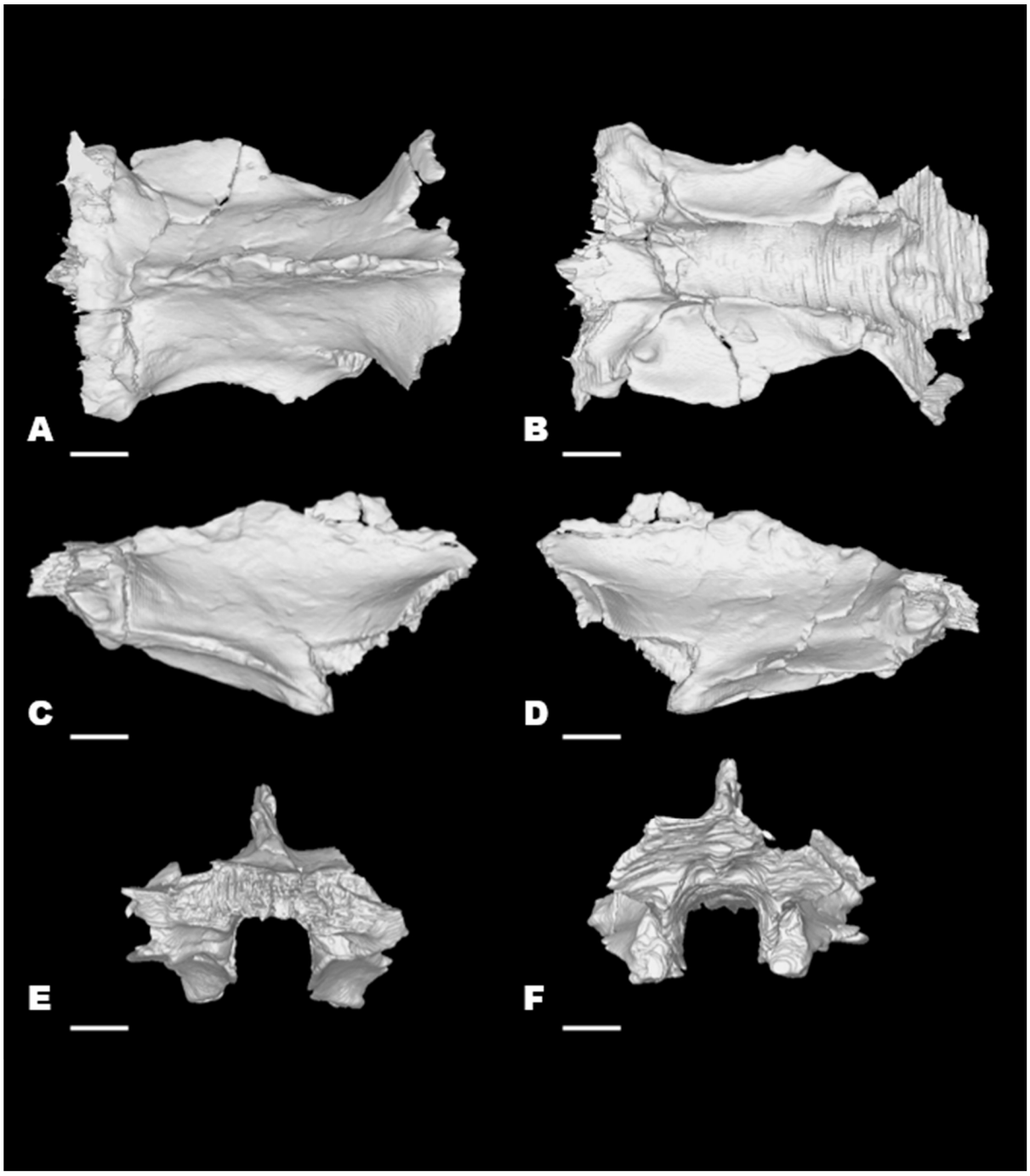

Figure 74. *Dinilysia patagonica* MACN-RN1013

A) Dorsal, B) Ventral, C) Left Lateral, D) Right Lateral, E) Anterior, F) Posterior. Scale bar = 5mm.

Chapter 5. The implications of fossoriality to early snake evolution

1. Body size ancestral state reconstructions reveal patterns of early evolution

The sparsity of the fossil record poses several problems when attempting to derive information about large scale evolution across clades with long evolutionary histories. These problems are related not just to lack of preservation, but also incomplete or biased sampling methods. Therefore, there is considerable benefit to finding techniques that are still able to provide informative results about deep time processes despite the apparent challenges posed by the incompleteness of the fossil record. Ancestral state reconstructions have the benefit of both wide application and low computational requirements, which has lead to their widespread use in reconstructing information about deep time evolutionary events.

However, as with all analytical techniques that rely on large amounts of input data, the results can vary considerably depending on the quality and amount of data used in these analyses. This current study has showed that the inclusion of fossils near to the age of the nodes of interest has the potential to greatly affect estimates of body size at ancestral nodes, a pattern previously seen in mammals (Finarelli and Goswami, 2013). The inclusion of fossils not only changes the estimate of body size the ancestral snake, but also nodes within the phylogeny.

My study examining body size evolution has revealed several interesting patterns in the evolution of snakes not previously appreciated. The first being support for independent reductions in body size in the three clades of Scolecophidia (Typhlopoidea, Leptotyphlopidae, and Anomalepididae). While there are considerable morphological similarities between these three clades, there are also differences, particularly in the disparate jaw architectures despite a similar diet across all taxa. These different jaw architectures support the hypothesis that all three clades adapted to fossoriality and insectivory independently from one another, although possibly from a fossorial ancestor. My estimates of body size at ancestral nodes support this hypothesis, and highlight the importance of further research into the early evolution of this enigmatic clade.

One potential argument against the inclusion of fossils is the uncertainty of fossil placement in extant phylogenetic trees. However, my study showed how patterns of body size increase in snakes can be detected for multiple different placements of fossil taxa. An increase in body size at the ancestral node of snakes was detected when fossils were added in multiple different phylogenetic positions. This finding highlights the importance of including fossils even when their phylogenetic position relative to extant clades is uncertain.

A benefit of the elongate body plan of snakes means that body size of fossil taxa is easily estimated from vertebral measurements by simple regression models based on extant taxa

(McCartney et al., 2018). My study has showed how these methods can reveal previously unappreciated patterns of body size evolution in the Cretaceous. By the end of the Cretaceous, snakes have already achieved large body sizes, such as *Madtsoia madagascariensis* that reaches over 8m in length in the Maastrichtian (Laduke et al., 2010). Such an increase in body size so early on in snake evolution is not detected by ancestral state reconstruction models that use only extant data. Additionally, my study has shown how the inclusion of a small number of fossils in key positions can help detect patterns of body size evolution that are reflected in the fossil record, such as a body size of 4m in the Coniacian-Santonian, and a body size of over 5m in the Campanian that are detected when fossils are included as stem alethinophidians.

These findings show that by the Late Cretaceous snakes have already achieved a wide variety of body lengths. This diversification of body sizes likely also reflects adaptation to a number of different habitats and diets. Large body sizes possibly allow snakes to consume larger prey, and presumably also allows a greater number of prey species to be targeted (Slip and Shine, 1988; Boback, 2003). Conversely, reduction in body size is a well understood adaptive trait for fossorial organisms, and the smallest extant snakes are all fossorial (Hanken and Wake, 1993; Lee, 1998; Hedges, 2008). The Cretaceous also likely had a number of fossorial species, in particular it has been suggested that the diagnostic characters for *Coniophis* species may in fact represent adaptations to fossoriality (Fox, 1975; Rage, 1991; Rage et al., 2004). The repeated occurrence of small *Coniophis* throughout the Cretaceous in my study supports this hypothesis for the uncertain affinities of *Coniophis*.

Finally, my study has shown how the combination of data from both the fossil record and analytical techniques such as ancestral state reconstructions can be combined to understand the evolution of clades. Results of ancestral state reconstructions that include Madtsoiidae and Simoliophiidae as stem alethinophidians, and *Najash rionegrina* and *Dinilysia patagonica* as either stem snakes or stem alethinophidians, are more concordant with the pattern of body size evolution seen in the fossil record. This therefore does not support the phylogenetic placement of Simoliophiidae as stem snakes, or the hypothesis that the marine ecology typical of Simoliophiidae is representative of the ancestral snake. Instead, it supports either a fossorial or terrestrial origin for snakes, depending on interpretations of the ecology of *Dinilysia* or *Najash*.

2. Previously unknown morphological diversity in Typhlopidae

Before the advent of molecular DNA extraction and analytical techniques, deciphering the relationships between individual species relied on the accurate assessment of shared morphological characters. This is more difficult for miniaturised clades, where bones are often less than a millimetre in length. Recent advances in micro-CT techniques has allowed comparative anatomy of these clades. Despite being universally considered to all share a similar skeletal and soft-tissue morphology, the use of micro-CT techniques has allowed more detailed analysis into the complex morphology of Scolecophidia, the most basally diverging lineages of snakes. Due to the small size of most scolecophidians, traditional dissection methods have proved difficult, given the high likelihood of bones being broken or lost during preparation (List, 1966; Bell et al., 2021). Micro-CT techniques however, have the benefit of preserving bone-to-bone relationships as would have been seen in the living animal, as well as allowing the identification of miniscule bones and foramina for the passage of cranial nerves that would be invisible to the naked eye.

Understanding the morphology of Scolecophidia is important for constructing phylogenetic hypothesis of relatedness between snakes clades. High morphological similarities result in the recovery of the three clades of Scolecophidia (Leptotyphlopidae, Typhlopoidea, and Anomalepididae) as a monophyletic clade in phylogenetic trees constructed with morphological data (Conrad, 2008; Gauthier et al., 2012). However, molecular data constructed phylogenies continue to recover Scolecophidia as a paraphyletic grade, usually recovering the Typhlopoidea and Leptotyphlopidae as sister clades, with the Anomalepididae closer to Alethinophidia (Zheng and Wiens, 2016). The potential paraphyly of this morphologically distinct clade has led researchers to more closely examined the apparent conserved morphology shared by these snakes. My study contributes to this body of work that aims to challenge the conception that all Scolecophidia are morphologically similar.

My study has shown revealed unappreciated diversity within Typhlopidae, the most speciose clade of Scolecophidia. This includes variation in fusion of the bones that comprise the otic complex and the presence of either a paired or singular parietal bone. I have also identified features in the giant blindsnakes, *Afrotyphlops mucruso* and *Afrotyphlops schlegelii*, previously thought to be found only in Alethinophidia. The dorsally projecting lateral wings of the basisphenoid are considered to be diagnostic of Alethinophidia, however they are present in the largest blindsnakes. This highlights the importance of investigating the diversity of morphology present in extant clades when assigning diagnostic morphological characters. The presence of dorsally projecting lateral wings in both *A. mucruso* and *A. schlegelii* suggests that the absence of this character in Scolecophidia is due to reduction in body size, although as these two species

are sister taxa, further examination of morphology within *Afrotyphlops* is needed. Other features that appear in *Afrotyphlops* that vary with size include the laterally projecting processes of the parietal and distinct adductor ridges. This is especially prevalent when comparing my specimen of *Afrotyphlops punctatus* with a smaller specimen from a previous study, as this specimen lacked these features (Deolindo et al., 2021).

Conversely, in the smallest Typhlopidae, there is also considerable morphological diversity. Paired parietals were observed in both *Indotyphlops braminus* and *Madatyphlops arenarius*, a feature which is known in snakes to be linked to ontogeny (Palci et al., 2016). By contrast, while *I. braminus* possesses a fused otic region, *M. arenarius* has all three bones present. This finding indicates that while miniaturised taxa can possess features usually only found in juveniles, this is not a strict relationship, and not all miniaturised taxa possess these characters. Future analysis that concentrate on morphological correlates with ontogeny in Typhlopidae will help identify diagnostic characters, particularly in the context of which characters are influenced by age, small body size, or close relatedness.

3. Homoplasy in parietal morphology

As homoplastic characters have the potential to hinder reconstructing the relationships between taxa using morphology, geometric morphometrics provides a quantitative technique to understand differences in shapes between different species. Once shape change is understood quantifiably, then questions about morphological correlates with ecology can be addressed. Geometric morphometrics on a single bone, rather than whole skull specimens, is beneficial in that it allows comparison of a large number of specimens, as well as the inclusion of fossil specimens that may not be complete. In the case of snakes, the problem of convergence associated with a fossorial ecology has long been considered to confuse attempts to reconstruct not only relationships of snakes to other squamate clades, but also relationships between clades within snakes.

My study has identified clear morphological differences between the parietal of fossorial and terrestrial snakes, confirmed statistically both with standard t-tests and linear discriminant analysis. These morphological changes appear to concur with previous studies that have noted certain morphological features shared by fossorial snakes, such as enlarged supraorbital processes that enclose the posterior ends of the paired frontals, forming a u-shaped frontoparietal suture. The next step after identifying these morphological correlates is to

identify and assess the biomechanical benefit that these morphologies provide. Presumably the high amount of morphological convergence seen among fossorial snakes is due to adaptation to a habitat and locomotion method that result in more forces being concentrated onto the skull. The typical snake skull is characterised by loosely joined cranial elements, and so cranial consolidation is likely to occur when organisms adapt to using the skull to push through the substrate.

I have identified several features of the parietal that correlate with fossoriality, including a deep u-shaped frontoparietal suture and an elongate posterior shelf. These two characters in particular are probably due to the need to strengthen the skull to prevent distortion when burrowing. It is important to identify characters that correlate with ecology as these are often used in character lists for morphological phylogenetic analyses. I have identified several different morphological character lists, aimed at deciphering the relationships between snakes and between snakes and other squamates, that include the shape of the frontoparietal suture as a diagnostic character (Tchernov et al., 2000; Lee and Scanlon, 2002; Scanlon, 2006; Conrad, 2008; Gauthier et al., 2012). Understanding the relationship between morphology and ecology is of vital importance for snakes, particularly in context of the well documented incongruence between phylogenetic hypotheses constructed with either morphological or molecular data.

Finally, the presence of these homoplastic characters that have a clear relationship with ecology means that the ecology of extinct organisms can be predicted. Using the correlation between morphology of the parietal and a fossorial ecology, I have predicted the ecology of the Cretaceous snake *Dinilysia patagonica* to be fossorial. Previous work attempting to decipher the ecology of *Dinilysia* based on the morphology of the inner ear has disagreed, either predicting fossorial (Yi and Norell, 2015) or semi-aquatic/semi-fossorial (Palci et al., 2017). My finding of *Dinilysia* as sharing a parietal morphology seen only in extant fossorial snakes supports the initial finding of Yi and Norell (2015) of a fossorial ecology of *Dinilysia*. This also supports early descriptions of this fossil, that noted similarities of the skull of that with the fossorial pipe snake *Anilius scytale* (Smith-Woodward, 1901), although this may be due to relatedness between the two taxa. My study shows how the identification of homoplastic characters in extant organisms can inform ecological understanding of fossils. Additionally, the recovery of a fossorial ecology for *Dinilysia*, although representing just one species, supports the hypothesis that the elongate limbless body plan of snakes was facilitated by or allowed adaptation to fossoriality. *Dinilysia* is often recovered as a stem snake in phylogenetic hypothesis, and therefore possibly represents the early ecology of snakes before they diversified into the numerous habitats that they are found today.

4. Conclusion

Fossoriality is a widespread ecology in snakes, that has clear consequences for morphological evolution. This is seen in body size evolution, where the presence of fossorial taxa at the base of the extant snake tree biases ancestral state reconstructions of body size. This is also seen in the distinctive morphology of Typhlopidae, a miniaturised clade of fossorial snakes. And finally, the effects of adaptation to fossoriality is seen across Alethinophidia, with the repeated acquisition of a similar parietal morphology in numerous clades of extant snakes. I have shown that examining an ecology such as fossoriality from multiple perspectives can help decipher the vast diversity of snakes.

Bibliography

Bell, C.J., Daza, J.D., Stanley, E.L., and Laver, R.J., 2021, Unveiling the elusive: X-rays bring scolecophidian snakes out of the dark: The Anatomical Record, p. 1–8.

Boback, S.M., 2003, Body Size Evolution in Snakes : Evidence from Island Populations: Copeia, v. 2003, p. 81–94.

Conrad, J.L., 2008, Phylogeny and systematics of Squamata (Reptilia) based on morphology: Bulletin American Museum of Natural History, v. 310, p. 182.

Deolindo, V., Koch, C., and Joshi, M., 2021, To move or not to move ? Skull and lower jaw morphology of the blindsnake Afrotyphlops punctatus (Leach, 1819) (Serpentes, Typhlopoidea, Typhlopidae) with comments on its previously advocated cranial kinesis: The Anatomical Record, p. 1–13.

Finarelli, J.A., and Goswami, A., 2013, Potential pitfalls of reconstructing deep time evolutionary history with only extant data, a case study using the canidae (mammalia, carnivora): Evolution, v. 67, p. 3678–3685.

Fox, R.C., 1975, Fossil snakes from the Upper Milk River Formation (Upper Cretaceous), Alberta: Canadian Journal of Earth Sciences, v. 12, p. 1557–1563.

Gauthier, J.A., Kearney, M., Maisano, J.A., Rieppel, O., and Behlke, A.D.B., 2012, Assembling the squamate tree of life : Perspectives from the phenotype and the fossil record: Bulletin of the Peabody Museum of Natural History, v. 53, p. 3–308.

Hanken, J., and Wake, D.B., 1993, Miniaturization of body size: Organismal consequences and evolutionary significance: Annual Review of Ecology and Systematics, v. 24, p. 501–519.

Hedges, S.B., 2008, At the lower size limit in snakes: two new species of threadsnakes (Squamata: Leptotyphlopidae: *Leptotyphlops*) from the Lesser Antilles: Zootaxa, v. 30, p. 1–30.

Laduke, T.C., Krause, D.W., Scanlon, J.D., and Kley, N.J., 2010, A Late Cretaceous (Maastrichtian) Snake Assemblage from the Maevarano Formation, Mahajanga Basin, Madagascar: Journal of Vertebrate Paleontology, v. 30, p. 109–138.

Lee, M.S.Y., 1998, Convergent evolution and character correlation in burrowing reptiles: towards a resolution of squamate relationships: Biological Journal of the Linnean Society, v. 65, p. 369–453.

Lee, M.S.Y., and Scanlon, J.D., 2002, Snake phylogeny based on osteology, soft anatomy and ecology: Biological Reviews of the Cambridge Philosophical Society, v. 77, p. 333–401.

List, J.C., 1966, Comparative osteology of the snake families Typhlopidae and Leptotyphlopidae: Illinois Biological Monographs, v. 36, p. 1–112.

McCartney, J.A., Roberts, E.M., Tapanila, L., and O'Leary, M.A., 2018, Large palaeophiid and

nigerophiid snakes from Paleogene Trans-Saharan Seaway deposits of Mali: Acta Palaeontologica Polonica, v. 63, p. 207–220.

Palci, A., Lee, M.S.Y., and Hutchinson, M.N., 2016, Patterns of postnatal ontogeny of the skull and lower jaw of snakes as revealed by micro-CT scan data and three-dimensional geometric morphometrics: Journal of Anatomy, v. 229, p. 723–754.

Palci, A., Hutchinson, M.N., Caldwell, M.W., and Lee, M.S.Y., 2017, The morphology of the inner ear of squamate reptiles and its bearing on the origin of snakes: Royal Society Open Science, v. 4, p. 170685.

Rage, J.-C., Prasad, G.V.R., and Bajpai, S., 2004, Additional snakes from the uppermost Cretaceous (Maastrichtian) of India: Cretaceous Research, v. 25, p. 425–434.

Rage, J.C., 1991, Squamate Reptiles from the Early Paleocene of the Tiupampa Area (Santa Lucia Formation), Bolivia: Fosiles y Facies de Bolivia - Vol. 1 Vertebrados, p. 503–508.

Scanlon, J.D., 2006, Skull of the large non-macrostomatan snake Yurlunggur from the Australian Oligo-Miocene: Nature, v. 439, p. 839–842.

Slip, D.J., and Shine, R., 1988, Feeding habits of the Diamond Python, *Morelia s. spilota*: Ambush predation by a boid snake: Journal of Herpetology, v. 22, p. 323–330.

Smith-Woodward, A., 1901, On some Extinct Reptiles from Patagonia, of the Genera Miolania, Dinilysia, and Genyodectes: Proceedings of the Zoological Society of London, v. 70, p. 169–184.

Tchernov, E., Rieppel, O., Zaher, H., Polcyn, M.J., and Jacobs, L.L., 2000, A Fossil Snake with Limbs: Science, v. 287, p. 2010–2012.

Yi, H., and Norell, M.A., 2015, The burrowing origin of modern snakes: Science Advances, v. 1, p. e1500743–e1500743.

Zheng, Y., and Wiens, J.J., 2016, Combining phylogenomic and supermatrix approaches, and a time-calibrated phylogeny for squamate reptiles (lizards and snakes) based on 52 genes and 4162 species: Molecular Phylogenetics and Evolution, v. 94, p. 537–547.